MEDICAL RADIOLOGY

Diagnostic Imaging

A. L. Baert
M. Knauth
K. Sartor

Radiation Dose from Adult and Pediatric Multidetector Computed Tomography

D. Tack
P. A. Gevenois
Editors

Springer

MEDICAL RADIOLOGY

Diagnostic Imaging

D. Tack · P. A. Gevenois (Eds.)

Radiation Dose from Adult and Pediatric Multidetector Computed Tomography

With Contributions by

H. T. Abada · T. Batch · P. Bellinck · A. Blum · N. Buls · K. H. Chadwick · E. Coche
B. Cohen · J. de Mey · G. Ferquel · P. A. Gevenois · S. Golding · M. K. Kalra · C. Keyzer
H. P. Leenhouts · T. Ludig · T. Mulkens · H.-D. Nagel · A. Noël · R. Patel · J.-F. Paul
B. Sauer · R. Salgado · G. Stamm · J. Stoker · D. Tack · T. L. Toth · H. W. Venema
P. Vock · R. E. Van Gelder · D. Winninger · R. Wolf

Foreword by

A. L. Baert

With 148 Figures in 273 Separate Illustrations, 58 in Color and 47 Tables

Springer

Denis Tack, MD, PhD
Clinic of Cardiac Imaging
Department of Radiology
Hôpital Erasme
Université libre de Bruxelles
Route de Lennik 808
1070 Brussels
Belgium

Pierre Alain Gevenois, MD, PhD
Professor of Radiology
Clinic of Chest Imaging
Department of Radiology
Hôpital Erasme
Université libre de Bruxelles
Route de Lennik 808
1070 Brussels
Belgium

Medical Radiology · Diagnostic Imaging and Radiation Oncology
Series Editors: A. L. Baert · L. W. Brady · H.-P. Heilmann · M. Knauth · M. Molls · K. Sartor

Continuation of Handbuch der medizinischen Radiologie
Encyclopedia of Medical Radiology

Library of Congress Control Number: 2006925265

ISBN 10 3-540-28888-0 Springer Berlin Heidelberg New York
ISBN 13 978-3-540-28888-6 Springer Berlin Heidelberg New York

Springer is part of Springer Science+Business Media

http//www.springer.com

Printed in Germany

Medical Editor: Dr. Ute Heilmann, Heidelberg
Desk Editor: Ursula N. Davis, Heidelberg
Production Editor: Kurt Teichmann, Mauer
Cover-Design and Typesetting: Verlagsservice Teichmann, Mauer

Printed on acid-free paper – 21/3151xq – 5 4 3 2 1 0

Foreword

A major portion of the total irradiation dose applied for medical purposes now derives from the use of computed tomography. Indeed, over the past two decades a steady increase in the use of this high-performance, non-invasive diagnostic modality has been observed in the developed world. This trend in medical practice is a source of major concern to public health authorities and clinicians.

This highly topical and serious problem is addressed and comprehensively covered in this new volume of our Medical Radiology series.

The first part provides the theoretical basis for our understanding of radiation issues and the risks involved in the clinical applications of multidetector CT. The second part deals with the various anatomic body areas and offers detailed guidelines on how to conduct multidetector CT studies of specific organs under optimal circumstances of dose reduction. A separate chapter is devoted to CT studies in children, an age group for which radiologists should make maximal efforts in dose reduction due to the greater risk of long-term harmful effects.

All contributors are internationally renowned experts. They have provided us with a well balanced and highly informative text which will undoubtedly be very helpful for all radiologists in training, certified radiologists, as well as for all referring general practitioners and specialists.

I am very much indebted to the editors, D. Tack and P.A. Gevenois, for this interesting and outstanding volume.

Leuven

Albert L. Baert

Introduction

The use of computed tomography (CT) has seen enormous growth over the past decade. In the US, approximately 63 million examinations were performed in 2005 (Niagara Health Quality Coalition 2004) compared to 35 million in 2000. The increased number of clinical applications (e.g., in emergency and trauma, paediatric, cardiac, and vascular disorders) made possible by the fast scanning capabilities of multidetector CT (MDCT) will drive even greater growth.

CT is already the main cause of radiation dose to the US population (Wiest et al. 2002; Mettler et al. 2000), and this will surely increase as the number of examinations per patient increases. This is a serious concern with which the radiology community is now confronted. The significant uncertainty associated with radiation risk estimates, long delays between exposure and cancer manifestation, and the fact that carcinogenesis is proved by statistical inference rather than by direct observation tend to reduce the perceived urgency to reduce radiation dose delivered by CT. However, the radiology community needs to be made aware that the small but acceptable risk–benefit decisions made at the individual patient level are amplified by the huge number of CT procedures performed each year. In a recent report on the biological effects of ionizing radiation (Beir 2005), the overall probability of death due to a solid tumor induced by a single 10-mGy CT examination is estimated to be approximately 0.00041. This apparently very low risk – multiplied by the 63 million CT examinations performed each year – suggests in fact that 25,420 fatal cancers are induced by CT every year.

This calculation, however, has a number of major flaws. The most important flaw is the fact that the risk factors were derived for generally healthy individuals in the population of Japanese A-bomb survivors, whereas patients who undergo CT are usually older and have a lower life expectancy than those in the general population. Moreover, the health benefit of CT-derived diagnostic information is immediate, whereas the risk of induced cancer is decades away. Nevertheless, this mathematical calculation was meant to underscore the importance of restraint in the use of MDCT.

Given these figures, what are radiologists supposed to do? Should they refuse to perform CT examinations on the patients referred to them? Conservative estimates of the benefit-to-risk ratios for CT are 100:1 and even higher. This discussion does suggest, however, that CT should not be performed for dubious or trivial clinical indications. Appropriateness criteria need to be vigilantly applied for all patients referred for a CT examination. Appropriate medical training in radiation risk management would be helpful in reducing the number of inappropriate requests for CT examinations. Academic radiologists should push for this training and organize dedicated lectures in medical schools. In training hospitals, CT examinations requested by young residents should be approved by senior physicians.

MDCT has the potential to revolutionize cross-sectional imaging. However, substantial improvements are necessary for maximal diagnostic utility. Radiologists need to revise the CT protocols, change viewing strategies, and develop new visualization skills to use these scanners to their full potential. The excellent temporal resolution of most modern MDCT will be used for rapid imaging of the heart and elsewhere, generating a new appreciation of the functional capabilities of dynamic CT.

As radiation doses delivered to patients will increase further still with these modern MDCT scanners, the radiology community needs to develop and adhere to updated appropriateness criteria for routine MDCT examinations. There is also a need for evidence-based benefit–risk analyses. Such analyses should include patient age and parameters related to his or her health status. The increase in clinical applications and in image quality that permit MDCT scanners will induce strong modifications in disease assessment and diagnostic medicine. To remain masters of this technology, radiologists need to know when to use or not to use this technique, to be conversant and knowledgeable about radiation risk issues, to be aware of the CT parameters that influence the radiation dose delivered to the patient, and to optimize MDCT acquisition and reconstruction parameters suited for the clinical indication, as well as for individual risk factors depending on the underlying disease, gender, and age. Radiologists will then be able to develop radically new acquisition and interpretation practices that will improve the diagnostic accuracy of MDCT examinations at a substantially lower radiation risk.

References

Niagara Health Quality Coalition (2004) CT scanner services in Western New York. Finger Lakes Health Systems Agency, Rochester, NY

Wiest PW, Locken JA, Heintz PH et al. (2002) CT scanning: a major source of radiation exposure. Semin Ultrasound CT MR 23:402–410

Mettler FA Jr, Wiest PW, Locken JA et al. (2000) CT scanning: patterns of use and dose. J Radiol Prot 20:353–359

BEIR VII phase 2 (2005) Health risks from exposure to low levels of ionizing radiation. National Academies Press, Washington, DC

Contents

Clinical Expansion of CT and Radiation Dose

1

Rajesh Patel and Stephen Golding

CONTENTS

1.1 Introduction

The principles of protecting the subject undergoing investigation by radiation are clear and well known: it is the responsibility of all radiological services to ensure the information required for the clinical management of the patient is obtained with the lowest practicable exposure to radiation. Within this clear objective, however, medical investigation operates in a constantly changing scenario influenced by increasing knowledge of disease processes and advancing technological development. This syndrome ensures that as time passes differing objectives and concerns come to the fore. Over the past few years the emergence of multidetector computed tomography (MDCT) has posed new challenges in radiological protection, to the extent that some now claim that this represents today's greatest single challenge in clinical radiation protection. This book expounds the challenges posed by MDCT to scientists and physicians and in this chapter we provide an introduction to the main themes which are of concern.

Since its inception in 1973 (Hounsfield 1973) the development of computed tomography (CT) has been dramatic and the technique continues to mature. Twenty-five years ago a typical study consisted of 10-mm sections, a 20-s exposure time and a 60-s image reconstruction time. Technical developments including the development of slip rings, increased X-ray tube heat capacity, advances in detector technology and improvement in computers now permit rapid sub-second exposures for acquiring sub-millimetre sections and almost instantaneous image reconstruction. These improvements have brought benefits in clinical examination, extending the applications of CT into new areas and facilitating difficult or demanding examinations in all applications. The major development in technology has been multidetector CT (MDCT), which has dramatically increased the performance capability of CT. Successive generations of systems capable of acquiring 4, 8 or 16 sections simultaneously have been introduced (Berland and Smith 1998; Hu et al. 2000; Kalender 2000). Even greater configurations are now becoming available, with the latest cone beam systems capable of simultaneously acquiring 256 sections (Mori et al. 2006).

The incorporation of slip ring technology into the design of scanners in the late 1980s removed the need for rigid mechanical linkage between the power cables and the X-ray tube. The ability to rotate the tube continuously in one direction allowed the development of helical CT and re-established CT as a front-line imaging modality. Helical CT allows a volume of tissue rather than individual slices to be scanned as the table supporting the patient also moves continuously while the tube is rotating; the data are reformatted automatically to display the images as axial slices. Furthermore, whereas conventional and spiral scanners use a single row of detectors, MDCT scanners currently have up to

R. Patel, MD
S. Golding, MD
Radiology Research Group, Nuffield Department of Surgery, University of Oxford, MRI Centre, John Radcliffe Hospital, Oxford, OX3 9DU, UK

eight active rows of detectors. The increased number of detectors combined with sub-second tube rotation times have increased the speed and the ability to cover large body areas without anatomical misregistration (Garney and Hanlon 2002). Whole CT examinations may now be carried out within a single breathhold (e.g. thorax, abdomen and pelvis in a trauma patient in 20 s) (Kalender et al. 1990). As well as increased speed and volume coverage, MDCT offers excellent opportunities for dedicated 2D and 3D visualization and post processing. Continuous data acquisition also means lesions can be evaluated during different phases of contrast enhancement and small lesions which may be missed with conventional CT can now be detected (Scheck et al. 1998).

Thus, modern CT scanners now offer clinical tools of almost unlimited flexibility. However, these benefits have not been without a price and it is arguable that MDCT has become radiology's major radiation protection problem.

1.2 Clinical Expansion

The development of MDCT seems likely to increase the challenge of patient protection, owing to increased use in established applications and the introduction of a wide range of new applications, many of which are more extensive than the traditional uses of CT. MDCT has made multiphase enhancement studies feasible (Zoetelief and Geleijns 1998), has enabled CT angiography (Makayama et al. 2001) and CT urography (Anderson and Cowan 2004), and has contributed significantly to much greater potential in 3D imaging and virtual reality (Caramella and Bartolozzi 2002). For example, in the case of a neoplasm of the pancreas, it is possible to outline the primary neoplasm at an optimal phase of enhancement while at the same time gathering images of the liver in different phases of enhancement in order to examine for metastatic disease (Johnson 2001). Where the investigation is justified, completing it in one sitting is clearly of benefit in terms of facilitating treatment planning and for the patient.

It is recognized that the effective dose from CT scans of the head and neck is considerably lower than that from CT examinations of the abdomen or chest. However, head and neck CT examinations for well established clinical indications (such as sinusitis, unilateral conductive hearing loss and acute stroke) are more common and the collective dose to the population from cranial examinations is therefore higher. Scan parameters for head and neck CT examination protocols are generally chosen to obtain the best image quality and meet the highest diagnostic criteria. Radiation dose from head CT scans may vary considerably as a result of inherent differences in equipment and because of variations in exposure technique and scanning protocol. Previous studies where systematic changes in scanning parameters were analysed with respect to resulting image quality have reported dose reductions of up to 40% in CT scans of the head without loss of relevant information or diagnostic image quality (Cohnen et al. 2000; Smith et al. 1998).

Well established clinical indications for CT of the chest include bronchiectasis and the evaluation of interstitial lung disease. Chest CT is also commonly used to detect pulmonary metastases. A relatively new use of helical CT is the diagnosis of pulmonary embolism and some authors have even suggested that MSCT could replace pulmonary scintigraphy or angiography as a first-line investigation for pulmonary embolism (Mayo 1997). While traditional angiography will continue to be used for various treatment options (such as the placement of stents or angioplasty) the diagnostic role of angiography is increasingly being carried out using the noninvasive procedure of CT angiography and this method may now be the examination of choice for suspected pulmonary embolism. A meta-analysis of this technique has demonstrated sensitivities of 53%–100% and specificities of 83%–100%, wide ranges which are partly explained by technologic improvements over time (Rathburn et al. 2000; Wittram et al. 2004). At present there is no consensus on the optimal tube current setting for chest CT (Mayo et al. 1997) and surveys of radiation exposure from chest CT have reported tube currents from 200 mAs to 533 mAs (Nishizawa et al. 1991).

The introduction of multi-slice cardiac CT has reduced scan times to a few seconds allowing patients to be scanned with very high resolution. Also, patients with severe pulmonary disease and congestive heart failure can be examined in a single breathold.

Fast acquisition of narrow slices combined with ECG gating permits scans with greater temporal resolution. The main use of these images is for the visualization of the coronary arteries and calcium

scoring for assessment of stenoses. The evaluation of the effect of ECG-controlled tube current modulation on radiation exposure in retrospectively ECG-gated multi-slice CT of the heart has been shown to reduce dose by between 37% and 44% (Poll et al. 2002).

Established indications for CT of the abdomen include ruling out abscess, and detection of retroperitoneal lymphadenopathy or liver metastases from neoplasms. A relatively new clinical indication is urolithiasis. CT urography is a promising diagnostic examination that allows comprehensive evaluation of the urinary tracts. It is becoming the primary imaging study for evaluation of patients with hematuria and other genitourinary conditions and has become an established technique for patients with acute renal colic (Kawashima et al. 2004; Wells et al. 1998). The sensitivity and accuracy of non-contrast CT in assessing ureteral calculi has been reported to be as high as 97% (Smith et al. 1996). Both CT angiography and CT urography cover large body areas with several hundred sections. The field of 3D imaging and virtual reality is too large to cover here but MSCT has made these studies remarkably easy, e.g. facilitating the development of CT colonography (Iannaccone et al. 2003). The technique of virtual colonoscopy was first introduced in the mid 1990s as a non-invasive technique to image the colon (Vining 1997). Thin axial slices through the abdomen are obtained in supine and prone positions and may be reconstructed into 3D (surface rendered) images giving the impression of viewing the large bowel via an endoscope.

A further development has been CT fluoroscopy which enables real-time monitoring for image-guided biopsy procedures. Improved needle manipulation has made previously difficult procedures easier. However, careful use of this technique is essential as there is potential for large skin doses to both patient and operator (Olerud et al. 2002). The use of tube currents as low as 10–30 mA have been shown to give significantly lower patient skin doses whilst still providing sufficient image quality in order to control the difficult steps of the procedure. In addition, lead protection has been shown to reduce the scattered dose to the operator by more than 90% (Irie et al. 2001).

CT screening is an emerging concept targeting early detection of disease entities such as lung cancer, colon cancer and coronary artery disease. The issue of screening for disease by CT is a difficult area, as clinical benefit has to be demonstrated conclusively to justify irradiation of a large number of normal individuals. One American study of the detection of pulmonary nodules found a primary neoplasm rate of only 0.03% (Benjamin et al. 2003).

In situations where the diagnostic yield of CT is expected to be so low, alternative, safer examinations should always be considered. Contrary to the general expectation that, with the advent of magnetic resonance imaging (MRI) and its widespread use, the use of x-ray computed tomography would decline rapidly, MDCT has continued to gain in importance (Kalender 2000). However, MRI is an imaging modality that is considerably safer than CT on the basis of a number of factors, of which radiation dose is perhaps the most significant. It therefore provides the main "competition" for MDCT in clinical practice. A recent article has shown that screening MRI of the entire body may be more accurate than individual "gold standard" diagnostic investigations of individual organ systems (Lauenstein et al. 2004). There are important differences between MDCT and MRI, not least in availability and cost. However, the present high use of MDCT suggests powerfully that whether MRI can replace CT for various indications should be continuously reevaluated, even in circumstances where MDCT may be diagnostically more accurate (Semelka 2005).

The extension of CT into new areas continues. Several studies have already demonstrated that CT is ideally suited to the challenges posed by patients with suspected appendicitis. Raptopoulos et al. (2003) have reported the use of CT for selecting patients for management of acute appendicitis, finding that with increased use of CT there were less severe imaging findings, a significant decrease in surgical-pathologic severity and shortened hospital stay. These would seem to be clinical benefits but the routine use of a high radiation dose in a relatively benign process requires careful study of costs and benefits, especially as most patients with acute appendicitis, of whatever stage, are managed effectively without specialized investigation.

1.3 The Dose Problem

The fact that CT is a modality giving significant exposure is well known. In the past this was seen as permissible as in areas of its greatest applica-

tion, such as the investigation of malignancy, its diagnostic value was greater than its inherent risk. However, CT is now used extensively in benign disease and in the young in whom cumulative dose considerations are of the utmost importance. This issue of radiation dose from CT has received much attention in both the popular media and scientific literature, due in part to the fact that the dose levels from CT typically exceed those from conventional radiography and fluoroscopy, and that the use of CT continues to grow. CT contributes a significant portion of the total collective dose from ionizing radiation delivered to the public from medical procedures. The United Nations Scientific Committee on the Effects of Atomic Radiation (UNSCEAR) has highlighted that worldwide there about 93 million CT examinations performed annually at a rate of about 57 examinations per 1000 persons. UNSCEAR also estimated that CT constitutes about 5% of all X-ray examinations worldwide while accounting for about 34% of the resultant collective dose. In the countries that were identified as having the highest levels of healthcare, the corresponding figures were 6% and 41% respectively (UNSCEAR 2000).

In a frequently cited study performed by the Federal Bureau on Radiation Protection in Germany, it was found that between 1990 and 1992 only 4% of all X-ray examinations were performed on CT scanners, yet CT accounted for 35% of the collective effective dose (BMU 1996). In the United Kingdom, in 1991 the National Radiological Protection Board (NRPB) pointed out that CT makes a disproportionately large contribution to dose, at that time representing only 2.5% of examinations but constituting 25% of the collective dose to the population from diagnostic use (Shrimpton et al. 1991). Subsequent studies indicate that this proportion has increased; in 1998 Shrimpton and Edyvean (1998) suggested that the cumulative radiation dose was closer to 40%. Mettler et al. (2000) have indicated that in their department CT comprises 11% of examinations and 67% of the collective dose, 11% of these examinations being carried out in children, in whom radiation protection considerations are paramount.

Whereas there is still a paucity of published data available on the trends in patient doses following the introduction of MDCT, an increased contribution to patient dose may be expected due to reduced geometric efficiency and the more prominent impact of the additional tube rotations necessary before and after data acquisition over the planned scan range. When scanning in helical mode, all CT scanners acquire additional rotations at each end of the scan length in order to obtain sufficient data to reconstruct the full imaged volume. Two recent studies have reported significant increases in effective dose per patient of 10% and 34% for multislice compared with single-slice CT (Brix et al. 2003; Yates et al. 2004). Reconstruction methods on multidetector systems sometimes require a greater number of additional rotations. This together with greater X-ray beam widths used can result in a significant increase in effective dose, particularly for short scan lengths (Nicholson and Fetherston 2002). Recently published results from the 2003 UK CT dose survey (Shrimpton et al. 2005) show that there has been a reduction in average patient doses from CT examinations since the last national UK CT dose survey published in 1991. However they also show that doses from MDCT are consistently slightly higher than current dose levels from single-slice CT scanners.

Of particular concern is the fact that many of the new applications are especially applicable to young patients and those with benign disease. However this challenge is not the only problem facing radiation protection in CT. The short scanning time of MDCT means there is a danger of uncritical use being made of the technique and previous studies have shown that there are large variations in the scanning protocols employed for the use of CT (Lewis and Edyvean 2005). The risk is that the flexibility of MDCT in terms of long scan lengths and use of narrow imaged slices with high mAs values can lead to unnecessarily high doses if diagnostic requirements are not adequately considered (Shrimpton et al. 2005).

Controlling technique variations may be problematic. Recommendations of CT manufacturers vary with regard to clinical protocols and cannot really be compared because of different scanner makes and models (Scheck et al. 1998). Institutions may also change protocols according to their needs. Further, different CT scanners employ specific detector geometry and filtration characteristics. As a result it has been shown that even identical scanning parameters can result in considerable dose differences in the patient (Scheck et al. 1998). Consequently, there is a worrying level of variation in exposure for examinations carried out for identical purposes.

Shrimpton et al. (2005) reported that effective dose could differ by a factor between 10 and 40 in examinations for the same application and Olerud (1997) has reported variations between 8

and 20 times. These differences seem to relate principally to variations in examination technique. In our experience (unpublished data) a tenfold variation in the number of sections and exposure factors is found across the work of one general department. It is inevitable that some complex cases will require a larger number of CT sections and multiple phases, but the disparity occurring between apparently similar applications is of serious concern.

It is now widely accepted that unoptimized CT examination protocols are a significant contributor of unnecessary radiation dose. There appears to be much scope for dose optimization through use of appropriate protocols (Lewis and Edyvean 2005). Efforts and measures to reduce dose can be initiated by the examiner by critically considering the indication and the choice of scanning protocols and parameters for CT examination.

There may be justifiable reasons for some variability in practice, of which the most important one is the difference in clinical indication. Furthermore, as techniques develop there is a period of learning during which the examination technique should develop to a mature level. This difference is greater if operators and practitioners are insufficiently educated in newly emerging technology. Further, increasing demand in radiology may induce radiologists to use over-intense protocols for CT, for viability to supervise the examination directly while engaged in other work. It is perceived that this is more likely to occur with relatively inexperienced workers and it is also possible that some examinations are carried out more intensively than needed as a means of clinical risk limitations. These factors indicate strongly against measures to provide effective radiation protection.

One of the critical questions to ask is to what extent developments in technology should alter the technique (Berland and Smith 1998). There is a natural tendency for changes in the examination technique to be driven by advances in technology but the person carrying out the examination has to ask if there is added benefit in intensifying the examination and therefore the radiation exposure. It has to be accepted that clinical demand and workload pressures currently motivate against protection measures and that optimization of practice is one of the greatest challenges facing dose constraint in CT (Golding and Shrimpton 2002).

Unfortunately, despite the development of exposure-reducing technology, the evidence base for practice is limited (Kalra et al. 2004). A dose reduction of 90% has been reported in high-resolution CT of the face in patients with orbital trauma (Jackson and Whitehouse 1993), and in CT of the chest minimizing tube current has been reported to reduce the dose by 50% (Mayo et al. 1995). Starck et al. (1998) reported that in very specialized circumstances a 96% reduction in dose can be achieved and similar levels of reduction may be possible in CT colonography (Iannaccone et al. 2003). Our own studies in this area (publication forthcoming) bear out this experience. These studies related to areas of high natural contrast and high resolution imaging, where large exposure latitude may be expected. However, research is needed in the main areas of application of CT, where detection of low contrast lesions is paramount. It is necessary to establish the minimum exposure threshold that will deliver adequate image quality in each application, preferably expressed in terms of clinical effectiveness (Mini et al. 1995).

1.4 Approaches to the Problem

The answers to the challenges facing the use of MDCT must come both from technological development and from the clinical practice. On the industrial side the significant developments that have already been achieved in dose-constraint technology must continue and must impact on the way that MDCT operates in practice, as described in the following chapters. These advances in practice must be based upon a clear perception of the factors important in protecting the patient in MDCT, as outlined below.

1.4.1 The ALARA Principle

The ALARA principle states that all medicinal exposure for diagnostic purposes shall be kept as low as reasonably achievable. It is based on the radiation assurance recommendations of various international expert committees and organizations and forms the cornerstone of radiation protection. Based on the assumption that there is no lower threshold for carcinogenesis (i.e. that there is no dose that can be considered completely safe or harmless), the reduction of radiation exposure to ALARA remains an ongoing challenge.

1.4.2 The Role of the Referrer: Justification

It is a sine qua non of investigational medicine that the risk of the procedure is outweighed by the putative benefit to the patient. Although simple in essence, this principle may be difficult to put into practice. In many areas of established use of CT the potential benefit to the patient is clear and its application therefore well justified. However, patients are all individuals and in other areas it may be difficult to quantify accurately the potential benefit to the patient; in many instances, it is accepted, clinicians may tend to refer patients for examination in order to give themselves reassurance concerning their intended management regime; in such cases benefit is difficult to demonstrate.

The aims of radiation protection – and of effective justification and the ALARA Principle – may best be met by encouraging referring clinicians to adopt a critical appraisal of their own referral practice. The clinician needs to ask, before referring a patient for MDCT, "do I really need this investigation? Will it change what I do?" If the answer to these questions is positive, the next critical question is to ask whether the information that is needed could be obtained without the use of ionizing radiation. In many abdominal and pelvic applications ultrasound and MRI provide acceptable alternatives to MDCT, and MRI is also an effective competitor elsewhere in the body. Even where these two techniques may not be as sensitive as MDCT, there may be a case for employing them first, especially in young patients, on the basis that if they yield the required information then exposure of the patient to radiation may not be required. In our own practice the investigation of some cases of orbital fracture – an application usually regarded as exclusively a requirement for CT – has been successfully achieved using MRI. In such clinical decisions referral guidelines such as those issued by the Royal College of Radiologists (2006) in the UK (reference) have an established value.

1.4.3 The Role of the Operator: Optimization

It should be a given principle that all MDCT equipment is operated at optimum technical performance and subject to regular quality assurance. However, the objectives of optimization of the examination go beyond this. As indicated above, there are current technological advances which may be used to constrain exposure and, in appropriate circumstances, image quality can be manipulated to reduce exposure, provided that the resulting examination does not fall below an acceptable threshold of image quality and therefore of sensitivity appropriate to the clinical application. All departments should have in place local guidelines, based on the best evidence to date, to ensure that these objectives are met.

1.4.4 The Role of Guidelines in MDCT

As indicated above, the evidence base for dose constraint in CT is not strong and in these circumstances practice guidelines may be important. In 1994 the European Commission set up a working group on image quality and dose in CT, resulting in publication in 2000 of the European Guidelines on Quality Criteria for Computed Tomography (European Commission 2000). This group has continued and is currently producing a second edition of the guidelines (ref), which concentrates on MDCT. The second edition of the guidelines surveys technical and clinical principles in MSCT and make recommendations on good technique in 26 common areas of application, together with the guidelines on dose measurement and audit. Particular attention is paid to paediatrics. The group has also been active in promoting research studies to generate an evidence basis, principally a European field survey.

One problem that the group has had to face is the variation in the performance of individual CT scanners. Whereas in the first edition it was possible to make specific recommendations on slice thickness and pitch, only ranges can now be specified. As in the first edition, the guidelines recommend quality criteria that enable examinations to be assessed. However, the key issue of diagnostic effectiveness and exposure still needs to be addressed by robust research studies.

1.4.5 The Role of Evidence: Vigilance

Overall, experience indicates that the dramatic rise in applications of CT has not yet reached a plateau. This is despite the fact that both technically and clinically, MSCT may be used in a way to aid dose constraint (Olerud 1997; Kalender 2004; Yates

et al. 2004). A number of factors actually offer the potential of dose reduction if taken into consideration by clinicians. For example, repeat scans which were frequently required if the patient moved significantly or breathed between single scans have been practically eliminated by MDCT. Overlapping scans which were often selected for good multiplanar or 3D displays and led to corresponding increases in dose are no longer a necessity because overlapping images are routinely available in helical CT with no additional exposure. Also, the selection of pitch factors greater than 1 results in a reduction in dose corresponding to the pitch factor (Kalender 2000). Significant reduction of dose can also be obtained through attenuation-dependent tube current modulation which allows constant image quality to be maintained regardless of patient attenuation characteristics and is now widely available on most MSCT systems (Yates at al. 2004).

It is important that all practitioners in CT continue to review emerging evidence and adapt their practice accordingly. For the present dose audit remains mandatory and further surveys of practice are required. Departments must ensure that their justification criteria are soundly applied, and that examinations are carefully targeted to clinical applications and do not exceed the clinical requirements. Where evidence supports the approach, exposure should be adjusted to the lowest threshold that delivers the required clinical sensitivity. It is necessary to follow published guidelines and observe all updates in these.

Overall, the challenge of patient exposure in MDCT will best be served by continuing vigilance; from the manufacturers towards new dose-soaring developments and advice to their uses, from clinical referrers to ensure that over-demand is avoided, and from radiology department staff to ensure that the principles of best practice are always applied. This is, therefore, a field in which understanding of the balance between risks and benefit is most likely to be served by effective inter-disciplinary communication and education.

References

Anderson K, Cowan NC (2004) Multidetector CT urography. Radiol Now 21:4–6

Benjamin MS, Drucker EA, McLoud TC, Shepherd J (2003) Small pulmonary nodules: detection at chest CT and outcome. Radiology 226:489–493

Berland LL, Smith JK (1998) Multidetector-array CT: once again, technology creates new opportunities. Radiology 209:327–329

BMU (1996) (Bundesministerium fur Umwelt, Naturschutz und Reaktorsicherheit). Umweltradioaktivitat und Strahlenbelastung im Jahre. Deutscher Bundestag 13. Wahlperiode; Drucksache 13/8630

Brix G, Nagel HD, Stamm G et al (2003) Radiation exposure in multi-slice versus single slice spiral CT: results of a nationwide survey. Eur Radiol 13:1979–1991

Caramella D, Bartolozzi C (eds) (2002) 3D image processing: techniques and applications. Springer, Berlin Heidelberg New York

Cohnen M, Fischer H, Hamacher J et al (2000) CT of the head by use of reduced current and kilovoltage: relationship between image quality and dose reduction. Am J Neuroradiol 21:1654–1660

European Commission. European Guidelines on quality criteria for computed tomography (2000). EUR 16262EN (Luxembourg: EC)

Garney CJ, Hanlon R (2002) Computed tomography in clinical practice. BMJ 324:1077–1080

Golding SJ, Shrimpton PC (2002) Radiation dose in CT: are we meeting the challenge? Br J Radiol 75:1–4

Hounsfield GN (1973) Computerised transverse axial scanning (tomography). Br J Radiol 46:1016

Hu H, He HD, Foley WD, Fox SH (2000) Four multidetector-row helical CT: image quality and volume coverage speed. Radiology 215:55–62

Iannaccone R, Laghi A, Catalano C et al (2003) Feasibility of ultra-low dose multislice CT colonography for the detection of colorectal lesions: preliminary experience. Eur Radiol 13:1297–1302

International Commission on Radiological Protection (2001) Managing patient dose in computed tomography. ICRP Publication 87. Ann ICRP 30(4). Pergamon, Oxford

Irie T, Kajitani M, Itai Y (2001) CT fluoroscopy-guided intervention: marked reduction of scattered radiation dose to the physicians hand by use of a lead plate and an improved I-I device. J Vasc Interv Radiol 12:1417–1421

Jackson A, Whitehouse RW (1993) Low-dose computed tomographic imaging in orbital trauma. Br J Radiol 66:655–661

Johnson CD (2001) Pancreatic carcinoma: developing a protocol for multidetector row CT. Radiology 220:3–4

Kalender WA (2000) Computed tomography. Publicis MCD, Munich

Kalender W (2004) Dose management in multislice spiral computed tomography. Eur Radiol Syllabus 14:40–49

Kalender WA, Seissler W, Klotz E, Vock P (1990) Spiral volumetric CT with single-breath-hold technique, continuous transport, and continuous scanner rotation. Radiology 176:181–183

Kalra KM, Maher M, Toth TL et al (2004) Techniques and applications of automatic tube current modulation. Radiology 233:649–657

Kawashima A, Vrtiska TJ, LeRoy AJ et al (2004) CT urography. RadioGraphics 24:S35–S54

Lauenstein TC, Goehde SC, Herborn CU et al (2004) Whole-body MR imaging: evaluation of patients for metastases. Radiology 233:139–148

Lewis MA, Edyvean S (2005) Patient dose reduction in CT. Br J Radiol 78:880–883

Makayama Y, Yamashita Y, Takahahi M (2001) CT of the aorta and its major branches. In: Reiser M, Takahashi M, Modic M, Bruening R (eds) Multislice CT. Springer, Berlin Heidelberg New York

Mayo JR (1997) Opinion response to acute pulmonary embolism: the role of computed tomographic imaging. J Thoracic Imaging 12:95–97

Mayo JR, Hartman, TE, Lee KS et al (1995) CT of the chest: minimal tube current required for good image quality with the least radiation dose. Am J Roentgenol 164:603–607

Mayo JR, Whittall KP, Leung AN et al (1997) Simulated dose reduction in conventional chest CT: validation study. Radiology 202:453–457

Mettler FA, Wiest PW, Locken JA, Kelsey CA (2000) CT scanning: patterns of use and dose. J Radiol Prot 20:353–359

Mini RL, Vock P, Mury R, Schneeberger PP (1995) Radiation exposure of patients who undergo CT of the Trunk. Radiology 195:557–562

Mori S, Endo M, Nishizawa K et al (2006) Comparison of patient doses in 256-slice CT and 16-slice CT scanners. Br J Radiol 79:56–61

Nicholson R, Fetherston S (2002) Primary radiation outside the imaged volume. Br J Radiol 75:518–522

Nishizawa K, Maruyama T, Takayama M et al (1991) Determinations of organ doses and effective dose equivalents from computed tomographic examinations. Br J Radiol 64:20–28

Olerud HM (1997) Analysis of factors influencing patient doses from CT in Norway. Radiat Prot Dosim 71:123–133

Olerud HM, Obberg S, Widmark A, Hauser M (2002) Physician and patient radiation dose in various CT guided biopsy protocols. Sixth European ALARA Network on "Occupational Exposure Optimisation in the Medical Field and Radiopharmaceutical Industry". Madrid, Spain, 23–25 October 2002

Poll LW, Cohnen M, Brachten S, Ewen K, Modder U (2002) Dose reduction in multi-slice CT of the heart by use of ECG-controlled tube current modulation ("ECG pulsing"): phantom measurements. Rofo 174:1500–1505

Raptopoulos V, Katson G, Rosen P et al (2003) Acute appendicitis: effect of increased use of CT on selecting patients earlier. Radiology 226:521–526

Rathburn SW, Raskob GE, Whitsett TL (2000) Sensitivity and specificity of helical computed tomography in the diagnosis of pulmonary embolism: a systematic review. Ann Int Med 132:227–232

Royal College of Radiologists (2006) Making the Best Use of a Department of Clinical Radiology Guidelines for Doctors. Fifth Edition. On line publication at http://www.rcr.ac.uk/index.asp?PageID=310&PublicationID=71 (access on May 26, 2006)

Scheck RJ, Coppenrath EM, Kellner MW et al (1998) Radiation dose and image quality in spiral computed tomography: multicentre evaluation at six institutions. Br J Radiol 71:734–744

Semelka RC (2005) Radiation risks from CT scans: a call for patient-focused imaging. Medscape Radiology 6(1)

Shrimpton PC, Edyvean S (1998) CT scanner dosimetry. Br J Radiol 71:1–3

Shrimpton PC, Jones DG, Hillier MC et al (1991) Survey of CT practice in the UK. Part 2: dosimetric aspects. NRPB Report R249. NRPB, Chilton, UK

Shrimpton PC, Hillier MC, Lewis MA, Dunn M (2005) Doses from computed tomography (CT). Examinations in the UK – 2003 Review. NRPB-W67

Smith RC, Verga M, McCarthy S, Rosenfield AT (1996) Diagnosis of acute flank pain: value of unenhanced helical CT. Am J Roentgenol 166:97–101

Smith A, Shah GA, Kron T (1998) Variation of patient dose in head CT. Br J Radiol 71:1296–1301

Starck G, Lonn L, Cederblad A et al. (1998) Radiation dose reduction in CT: application to tissue area and volume determination. Radiology 209:397–403

United Nations Scientific Committee on the Effects of Atomic Radiation (2000) Sources and effects of ionising radiation. UNSCEAR Vol I

Vining DJ (1997) Virtual colonoscopy. Gastrointest Endosc Clin N Am 7:285–291

Wells ES, Ginsberg JS, Anderson DR et al (1998) Use of a clinical model for safe management of patients with suspected pulmonary embolism. Ann Intern Med 129:997–1005

Wittram C, Maher MM, Yoo AJ et al (2004) CT angiography of pulmonary embolism: diagnosis criteria and causes of misdiagnosis. RadioGraphics 24:1219–1238

Yates SJ, Pike LC, Goldstone KE (2004) Effect of multislice scanners on patient dose from routine CT examinations in East Anglia. Br J Radiol 77:472–478

Zoetelief J, Geleijns J (1998) Patient dose in spiral CT. Br J Radiol 71:584–586

Part I
Radiation Risks in Multidetector CT

Risks from Ionising Radiation

2

Kenneth H. Chadwick and Hendrik P. Leenhouts

CONTENTS

K. H. Chadwick, PhD, Retired
3 Ellerbank, Cowan Head, Kendal, Cumbria LA8 9HX, UK
H. P. Leenhouts, PhD, Retired
FredBantinglaan 6, 6721 BC Bennekom, The Netherlands

2.1 Introduction

2.1.1 Preamble

The radiation doses received by patients undergoing diagnostic radiological examinations by means of computed tomography (CT) are generally in the order of 1–24 mSv (milliSieverts) per examination for adults (UNSCEAR 2000) and 2–6.5 mSv for children (Shrimpton 2003). These effective doses can be classified as low, although they are invariably larger than those observed using conventional diagnostic radiology. The immediate question that comes to mind is whether these low doses carry any risk for the patient.

Deleterious health effects induced by ionising radiation have conventionally been separated into two different categories: deterministic effects and stochastic effects.

Exposures to high acute doses in excess of one or two gray (Gy) or sievert (Sv) cause substantial levels of cell killing, which is expressed as organ and tissue damage and, soon after exposure, as deleterious clinical effects. These effects are called deterministic, and the dose–effect relationships exhibit a long threshold dose, with no observable effect, after which the effect increases in severity as the radiation dose increases. The possibility of deterministic health effects, such as radiation sickness, arising after the low doses used with computed tomography can be dismissed.

At lower doses, deleterious health effects, such as cancer or hereditary disease which may take years to be revealed, can occur as a consequence of molecular damage to the nucleus of a single cell. These effects are called stochastic effects, and the probability for their occurrence increases as the dose increases, but the severity of the effect is unrelated to the dose. The potential for stochastic health effects to occur as a result of computed tomogra-

phy examinations cannot be so easily dismissed because the shape of the dose–effect relationship at low doses is not known.

2.1.2 Threshold or Linear No-Threshold

Estimation of the risk of radiation-induced cancer relies on the analyses of epidemiological data from exposed populations, most notably the atomic bomb survivors. All the epidemiological data sets show that cancer levels found in populations exposed to low doses are not significantly different from those in unexposed populations; thus, the dose–effect relationship at low doses is not well defined. There are basically two different opinions about the shape of the dose–effect relationship for stochastic effects at low doses. There are those who believe that very low doses of radiation carry no risk and that a threshold dose has to be exceeded before an effect will be induced. Others support the concept of radiation risk increasing linearly with dose from zero dose up, i.e. the linear no-threshold (LNT) concept.

The LNT concept of radiation risk has been the subject of much debate (Academie des Sciences 1997; Clarke 1998; Tubiana 1998; Kellerer 2000; Kellerer and Nekolla 2000), and supporters of the "threshold" concept (Bond et al. 1996; Becker 1997; Tubiana 2000) include some who support the idea that low doses can have a beneficial health effect, i.e. "radiation hormesis" (Calabrese 2002; Luckey 1997; Sagan 1992; Kesavan and Sugahara 1992). Those who support the LNT concept include some who claim that it underestimates the risk of low dose radiation (Gofman and Tamplin 1971; Stewart and Kneale 1990; Edwards 1997). However, it is important to note that, following extensive reviews, both the United Nations Scientific Committee on the Effects of Atomic Radiation (UNSCEAR 2000) and the National Council on Radiation Protection and Measurements of the United States of America (NCRP 2001) have concluded that the LNT extrapolation provides the interpretation of low dose radiation effects that is most consistent with current scientific data and developing knowledge. UNSCEAR qualifies this by adding that a strictly linear dose response should not be expected in all circumstances.

Even more important is the fact that the Recommendations of the International Commission on Radiological Protection (ICRP), as outlined in its Publication 60 (ICRP 1991), implicitly adopt the LNT concept and the ICRP itself considers that the risks estimated using the concept are probably conservative. The concept has formed the basis for the development of an extremely useful radiological protection philosophy, including the valuable ALARA [As Low As Readily Achievable] principle and Collective Dose, which is a parameter that, while useful, is also open to abuse. In this context, it is worth noting that there are indications that the ICRP might adopt a different strategy in the future (Clarke 1999; ICRP 2003).

However, the ICRP has, in its current recommendations dating from 1991, adopted the LNT concept and estimated low dose-rate radiation risk, essentially using an interpretation of the data on cancer induction in the atomic bomb survivors. The ICRP uses a dose and dose-rate reduction factor (DDREF) of two to convert from high dose-rate risk to low dose, low dose-rate risk taking into account the sparing effect of low dose rate which is commonly found in radiation biology. The ICRP quantified radiation risk in 1991 by adopting a value of 5% for the nominal lifetime excess absolute risk (EAR) per sievert of fatal cancer for a general population exposed to low doses. For a population of working age, a value of 4% was adopted.

More recently, UNSCEAR (UNSCEAR 2000) derived a quantification of radiation risk in a somewhat different way. Starting from an assessment of lifetime risk estimates for solid cancer mortality in a population of all ages after an acute dose of 1 Sv (9% for men, 13% for women), UNSCEAR applied a 50% reduction to estimate risk from chronic exposures but suggested that risks of solid cancer incidence are about twice those of mortality. Compared with adults, children are thought to have twice the level of risk. The lifetime risk of developing leukaemia is taken as 1% for both men and women following an acute dose of 1 Sv, but the non-linearity of the acute dose response is expected to lead to a 20-fold reduction in risk if the acute dose is reduced from 1 Sv to 0.1 Sv.

2.1.3 What the Data Tell

The debate about the LNT concept continues to rage because the extrapolation of epidemiological and experimental radiation biological data measured at higher doses down to zero is open to several interpretations and has important economic and policy implications for radiological protection and medical

radiology as well as energy production and nuclear decommissioning. The discussion about the different interpretations of the shape of the dose–effect relationship at low doses continues to be unresolved because the statistical and systematic variations inherently associated with the zero dose effect make it impossible to measure a significant increase at very low doses.

This problem is unavoidable in experimental radiation biology (Pohl-Ruhling et al. 1983, 1986; Lloyd et al. 1988, 1992; Mill et al. 1998) as well as in epidemiology (Brenner et al. 2003). In a multilaboratory exercise, the lowest dose at which a significant effect of radiation on the induction of dicentric chromosome aberrations in human lymphocytes could be measured was 20 mGy (Lloyd et al. 1992). The lowest dose at which a statistically significant excess of cancer can be detected in the atomic bomb survivors has been estimated to be 50 mSv (Pierce et al. 1996), although others have claimed that the value should be 200 mSv (Heidenreich et al. 1997a, 1997b; Pierce and Preston 1997). The data on the occurrence of leukaemia in children following prenatal exposure to diagnostic X-rays indicates a risk from accumulated doses of a few tens of millisieverts (Stewart et al. 1956; 1958; Bithell and Stiller 1988; Doll and Darby 1991; Wakeford et al. 1997). Other epidemiological data on chronically exposed nuclear workers (Muirhead et al. 1999; Cardis et al. 2005), while being interpreted in terms of a linear dose–effect relationship and showing general agreement with the ICRP risk estimate within the statistical limits of the studies (Wakeford 2005), illustrate the problem of detecting statistically significant effects at low dose and the difficulties of defining the shape of the dose–effect relationship at low doses. This can be seen in Figure 2.1, in which the data reveal no statistically significant radiation effect in the range 0–100 mSv, which is of greatest relevance to computed tomography.

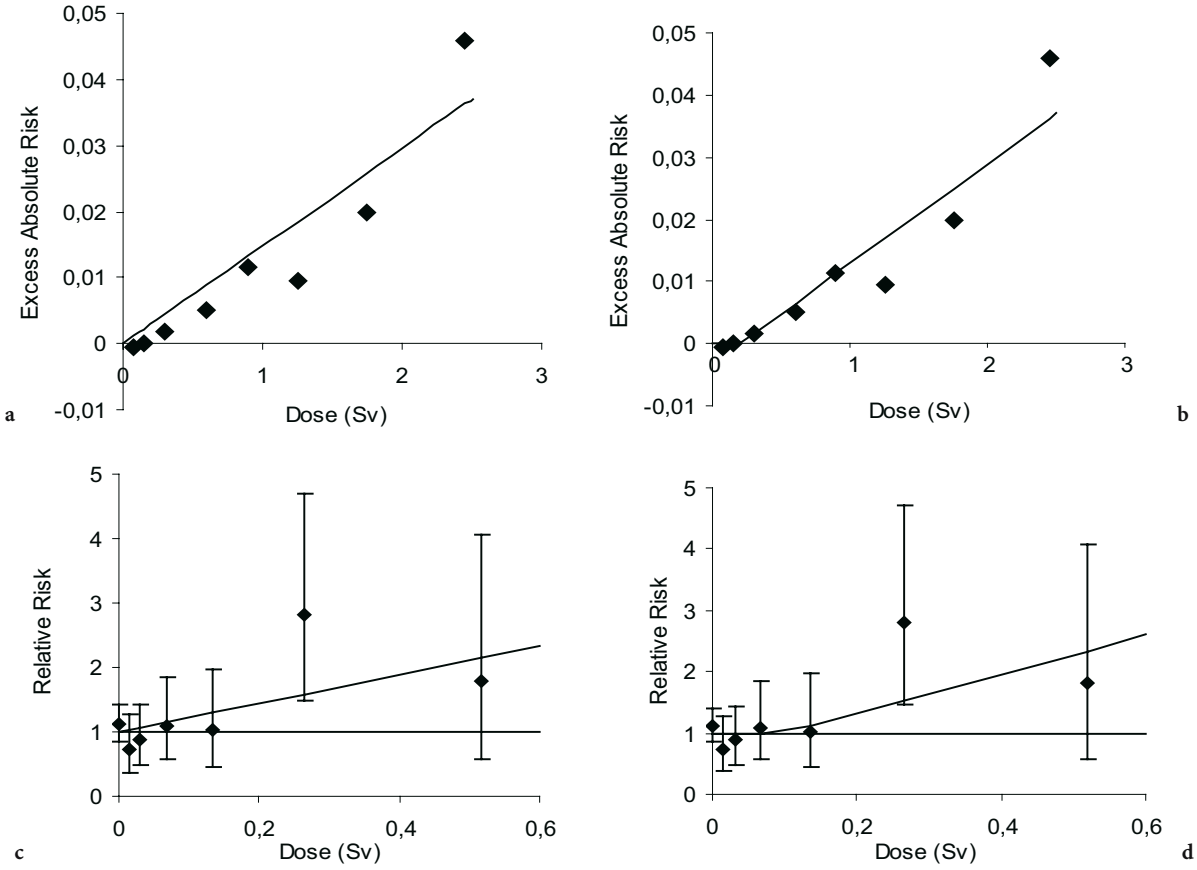

Fig. 2.1a–d. Two examples illustrating the difficulty of determining the shape of the dose–effect relationship at low doses. The upper graphs (**a**,**b**) present atomic bomb survivor data (Pierce et al. 1996) with a straight line from the origin through the data (**a**) and a straight line from a threshold dose through the data (**b**). The lower graphs (**c**,**d**) present similar extrapolations through data for the UK nuclear workers (Muirhead et al. 1999)

2.1.4 The Way Forward

The unavoidable conclusion is that it will never be possible to determine the real shape of the dose–effect relationship at the low doses relevant for radiological protection and computed tomography using experimental and epidemiological studies. It is clear that the only way for progress to be made in defining the real shape of this relationship is by understanding the mechanism of radiation action at the molecular level and developing a credible model approach that provides a coherent interpretation of the higher dose, statistically significant, experimental and epidemiological data (Brenner et al. 2003; Chadwick et al. 2003). The model must take account of the biophysics of radiation action, induction and repair of molecular damage, occurrence of effects at the cellular level and the influence of cellular effects on the development of cancer.

In the following sections, we present the outline of a model that can be used to derive the pathway from radiation-induced molecular damage to radiation-induced cancer. We also provide evidence to support the various links in the chain required to complete the pathway. The model is based on a mechanism of radiation action at the molecular level that results in different cellular end-points and provides a quantifiable description of the dose response for a variety of radiation effects.

2.2 Model Development

The pathway from radiation energy deposition through cellular effects to the induction of cancer is described here in two parts. The first describes a model that provides an explanation of the cellular effects of radiation in terms of a basic lesion and mathematical expressions for the dose–effect relationships. The second part incorporates the cellular–effects model into a biologically based cancer model in order to deduce the implications that the pathway has for radiation risk at low doses.

The cellular effects model is presented in a series of stages that closely follow its historical development, starting from the fitting of dose–effect relationships for cell killing, through the choice of lesion with all its implications, to the inter-relationship of different cellular end-points. The features of the cancer model are discussed in a qualitative way to show how the incorporation of the cellular model can be envisaged and to derive some important conclusions for radiological protection.

We have been using and developing the cellular model for 30 years and have benefited from the insight into radiation biological effects that the model has given us. All models represent a simplification of reality and the one presented here is but one of many, although we are not aware of another radiobiological model that is as far-reaching and comprehensive. We commend it for its straight-forward simplicity but warn that, in some aspects, it contradicts some current radiobiological dogma. It provides a logical explanation of experimental and epidemiological findings and, although the model is supported by fits to cellular and cancer data, it has not yet been proven.

2.2.1 Dose–Effect Relationships

The development of the model started when we noticed that different cell survival curves could all be very closely fitted using a linear-quadratic dose–effect relationship of the type:

$$S = \exp[-p(\alpha D + \beta D^2)] \qquad (2.1)$$

Where S is cell survival, D is radiation dose and $p\alpha$ and $p\beta$ are values derived from fitting the data (Chadwick and Leenhouts 1973).

Sinclair (1966) had already found that the linear-quadratic relationship gave the best fit by analysing cell survival data using various possible mathematical functions although he did not have a mechanistic interpretation for the equation. Later Gillespie et al. (1975a;b) showed, in a series of elegant experiments, that the linear-quadratic function fitted cell survival as well as could be statistically expected and Skarsgard et al. (1993) showed, in equally elegant experiments, that the survival of synchronised cells was accurately described by the equation down to low doses.

The equation suggests that cell killing is a result of "things" induced in a single radiation event ($p\alpha D$) and "things" arising from a combination of two radiation events ($p\beta D^2$). Our analysis of several sets of cell survival data revealed consistent results and indicated that the equation could provide straight

forward explanations for known radiation biological phenomena, such as dose rate and fractionation effects, and radiation quality effects, in terms of changes in the values of the curve-fitting coefficients pα and pβ. For example, decreasing the dose rate of exposure leads to a sparing effect and increased cell survival, and this is expressed in the linear-quadratic equation by a decrease in the quadratic coefficient pβ, which goes to zero at very low dose rates, while the linear coefficient pα does not change (Wells and Bedford 1983; Metting et al. 1985). This effect is often referred to as the repair of sub-lethal damage. Another example is the effect of radiation quality, which is revealed in a change in the value of the pα coefficient. In general, pα increases as the radiation becomes more densely ionising. Alpha particles, for example, which are more densely ionising than gamma radiation, induce a virtually linear survival curve because pα dominates and is substantially larger than the pα found following gamma radiation (Barendsen 1964; Todd 1967) (Fig. 2.2).

An additional indication of the consistency of the curve fitting was revealed by analysis of the survival of cells synchronised in different phases of the cell cycle. This showed that the linear-quadratic equation fitted all the different survival curves and, in addition, it was found that the linear and quadratic coefficients varied through the cell cycle in a typical way independent of the type or strain of cell line examined (Chadwick and Leenhouts 1975).

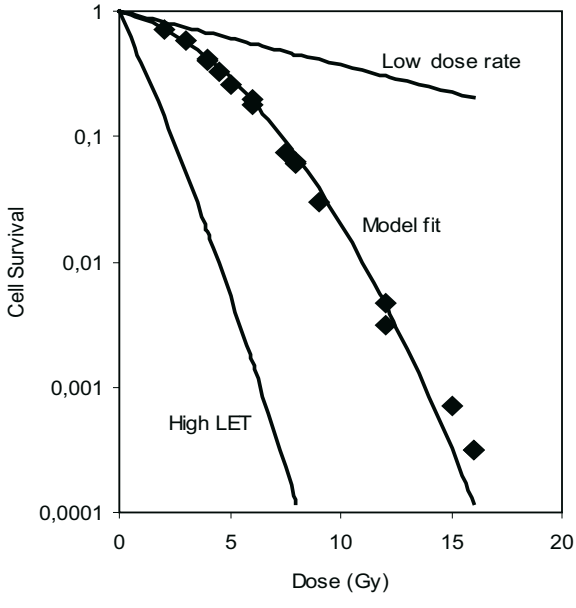

Fig. 2.2. An example of the fitting of the linear-quadratic dose–effect equation (2.3) to the survival of stationary CHO cells after acute gamma ray exposure ($p\alpha = 0.0992\ Gy^{-1}$; $p\beta = 0.0291\ Gy^{-2}$). The figure also shows the expected low dose rate curve when $p\beta = 0$ and a typical survival curve after exposure to densely ionising radiation with $p\alpha = 0.9\ Gy^{-1}$; $p\beta = 0.029\ Gy^{-2}$

The linear-quadratic equation for cell killing provides a first indication of the shape of dose-effect relationships at low doses. It is important to note that the quadratic term only starts to influence the response at acutely delivered doses above about 2 Gy and that the linear term, which is dependent on radiation quality but not on dose rate, is the term defining cell killing at very low doses.

Although comparable effects of dose rate and radiation quality were known for other end-points, such as the induction of chromosomal aberrations and somatic mutations, and the dose–effect relationship for these end-points had been found to be linear-quadratic, it was only when we decided on the nature of the radiation-induced "thing" responsible for cell killing that we found real insight into radiation effects and a whole panoply of explanations offered themselves.

2.2.2 The Choice of Lesion–DNA Double-Strand Breaks

There are several reasons why a DNA double-strand break is a suitable choice for the crucial radiation-induced lesion.

- The DNA helix is a large, important, structured target molecule in the nucleus of the cell.
- Cells with a reduced ability to repair double-strand breaks are very sensitive to ionising radiation.
- In the unineme concept of chromosome structure, where the chromosome backbone is a single DNA helix, a double-strand break is the same as a chromosome break.
- Permanent damage to DNA can cause mutations.
- The error free repair of single-strand breaks can be ascribed to sub-lethal damage repair to explain dose rate and fractionation effects.
- The repair of double-strand breaks, which is unlikely to be completely error free, can be ascribed to potentially lethal damage repair to explain changes in survival that occur on post-irradiation storage of non-cycling cells.
- The interaction of radiation with the two strands of the DNA helix offers an explanation for the increased effectiveness of densely ionising radiation.

2.2.2.1 Modes of Radiation Action

The DNA helix can, at least hypothetically, be disrupted in two modes of radiation action as illustrated in Figure 2.3.

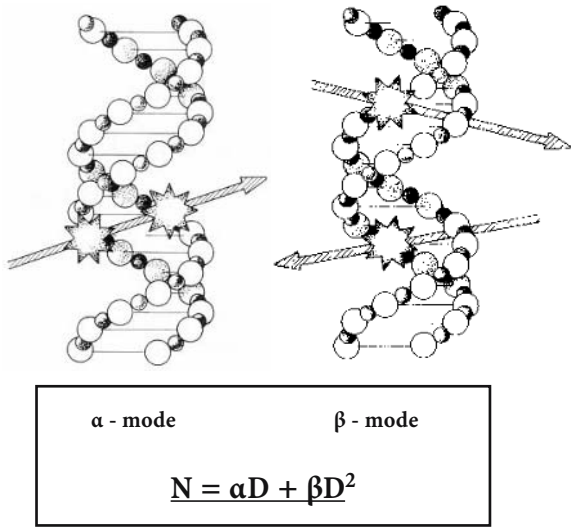

Fig. 2.3. A schematic representation of the possible modes of radiation action for the induction of DNA double-strand breaks. In the α-mode, a single particle track causes two spatially and temporally correlated ionisation events close to the two strands of the DNA helix. In the β-mode, two separate particle tracks each induce a single-strand break in the two strands of the DNA helix. N represents the number of DNA double-strand breaks induced by a dose (*D*) of radiation

The two strands of the helix can be broken during the passage of a single ionising particle if two energy depositions, closely associated in time and space, occur along the particle track close to, or on, the two strands. A double-strand break also results if two independent ionising particles cause single-strand breaks in each strand of the helix. Thus, the equation for the number (N) of DNA double-strand breaks induced by a dose (D) of radiation is given as:

$$N = (\alpha D + \beta D^2) \qquad (2.2)$$

so that if f_p is the proportion of unrestored double-strand breaks and p_0 is the probability of an unrestored double-strand break causing cell killing, then cell survival (S) is given by:

$$S = \exp[-pN] = \exp[-p(\alpha D + \beta D^2)] \qquad (2.3)$$

where $p = p_0 f_p$.

In fuller derivations of this equation (Chadwick and Leenhouts 1973; 1981), the α and β coefficients are made up of several parameters that take the effects of radiation quality and repair into account. A parameter (f_1) is included in the β-coefficient to take account of the repair of single-strand breaks so that $f_1 = 1$ for acute exposure but decreases to $f_1 = 0$ for chronic exposure where β becomes zero. This essentially reflects the probability that a single-strand break can be repaired during exposure before a second single-strand break converts it to a double-strand break and provides a mechanistic explanation for the dose-rate effect and fractionation.

A consideration of the α-mode of double-strand break induction should, intuitively, lead to the understanding that more densely ionising particle tracks have a higher probability of causing two energy deposition events close to the two strands of the helix than sparsely ionising particle tracks and should, therefore, be more effective per unit dose. This provides a mechanistic understanding of the effect of radiation quality.

The association of the double-strand break with cell killing, chromosome arm breakage and mutations, and the knowledge that similar effects of dose rate and radiation quality had been found in aberration and mutation studies (Lloyd et al. 1984; Iliakis 1984; Vivek Kumar et al. 2006; Furuno-Fukushi et al. 1996; Leenhouts and Chadwick 1990; Lloyd et al. 1976; Goodhead et al. 1979; Albertini et al. 1997) led us to propose that each of the three cellular end-points derive from the same type of molecular damage, namely DNA double-strand breaks. In this case, the yield of chromosomal aberrations (Y) can be described by the equation:

$$Y = cN = c(\alpha D + \beta D^2) \qquad (2.4)$$

where c relates induced double-strand breaks to chromosomal aberrations, and the mutation frequency (M) can be described (to a first approximation) by the equation:

$$M = qN = q(\alpha D + \beta D^2) \qquad (2.5)$$

where q relates induced double-strand breaks to mutations.

2.2.2.2 Correlations

Comparison of equations 2.4 and 2.5 with 2.3 leads to the following equations which correlate cell killing with the yield of chromosomal aberrations:

$$\ln S = -(p/c)Y \quad (2.6)$$

and cell killing with mutation frequency:

$$\ln S = -(p/q)M \quad (2.7)$$

Equations 2.6 and 2.7 predict that the logarithm of cell survival should correlate as a linear function of chromosomal aberration yield or mutation frequency when the end-points are measured in the same experiment, irrespective of the non-linear shape of the dose–effect relationships. Several examples of these correlations have been measured (Dewey et al. 1970; 1971a; b; 1978; Bhambhani et al. 1973; Franken et al. 1990; Richold and Holt 1974; Thacker and Cox 1975; Thacker et al. 1977; Rao and Hopwood 1982; Iliakis 1984). Examples of these correlations are presented in Figure 2.4 and Figure 2.5.

In accordance with the model, our interpretation of these correlations is not that aberrations or mutations cause cell killing but that each end-point arises from the same type of molecular lesion–the DNA double-strand break. In this respect, equation 2.3 predicts that the logarithm of cell survival should be linearly related to the number (N) of DNA double-strand breaks measured in the same experiment, irrespective of the non-linear shape of the dose–effect relationships. The development of sensitive neutral filter elution techniques to measure DNA double-strand breaks in the 1980s enabled these correlations to be measured (Radford 1985; 1986; Prise et al. 1987; Murray et al. 1989; 1990). An example of this correlation is presented in Figure 2.6.

These correlations create a linkage chain between DNA double-strand breaks and all three cellular end-points.

2.2.2.3 Implications for Low Dose Effects

The association of cell killing, chromosomal aberrations and mutations with DNA double-strand breaks permits an understanding of the shape of the dose–effect relationships for these end-points down to very low doses. This is not achieved by extrapolating the data to lower and lower doses but by considering the modes of radiation action in the production of double-strand breaks. At low doses, the α-mode (Fig. 2.3) is obviously dominant, even for acute exposure, and the biophysics of radiation energy deposition suggests that two energy depositions close to, or on, each of the DNA strands in one radiation track are needed to cause the double-strand break (Brenner and Ward 1992; Nikjoo et al. 1994, 1999; Friedland et al. 1998, 1999). This has been confirmed by experiments that have shown the role of pairs of hydroxyl radicals in the induction of

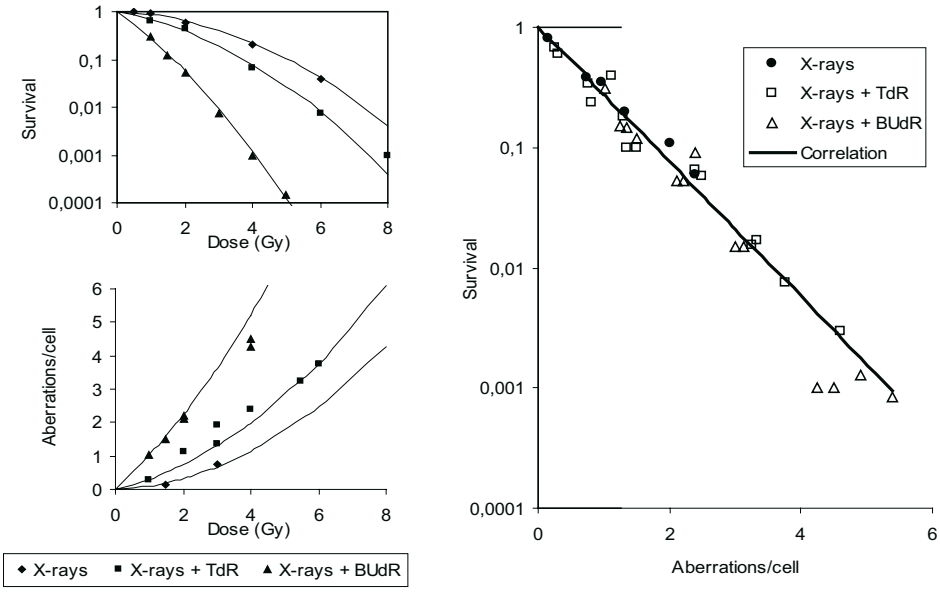

Fig. 2.4. The correlation between the induction of chromosomal aberrations and cell survival in accordance with equation 2.6 predicted by the model (data taken from Dewey et al. 1970; 1971a,b). The correlation shows data from nine different non-linear survival and aberration yield dose–effect curves of which three are shown in the graphs on the left of the figure

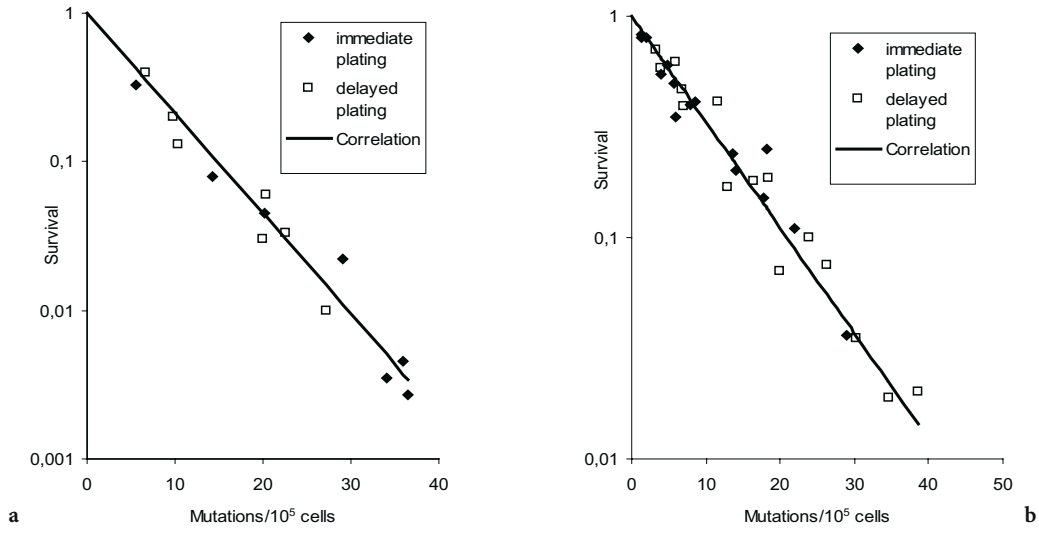

Fig. 2.5a,b. Two examples of the correlation between mutation frequency and cell survival in accordance with equation 2.7 predicted by the model [data taken from Rao and Hopwood 1982 (**a**) and Iliakis 1984 (**b**)]

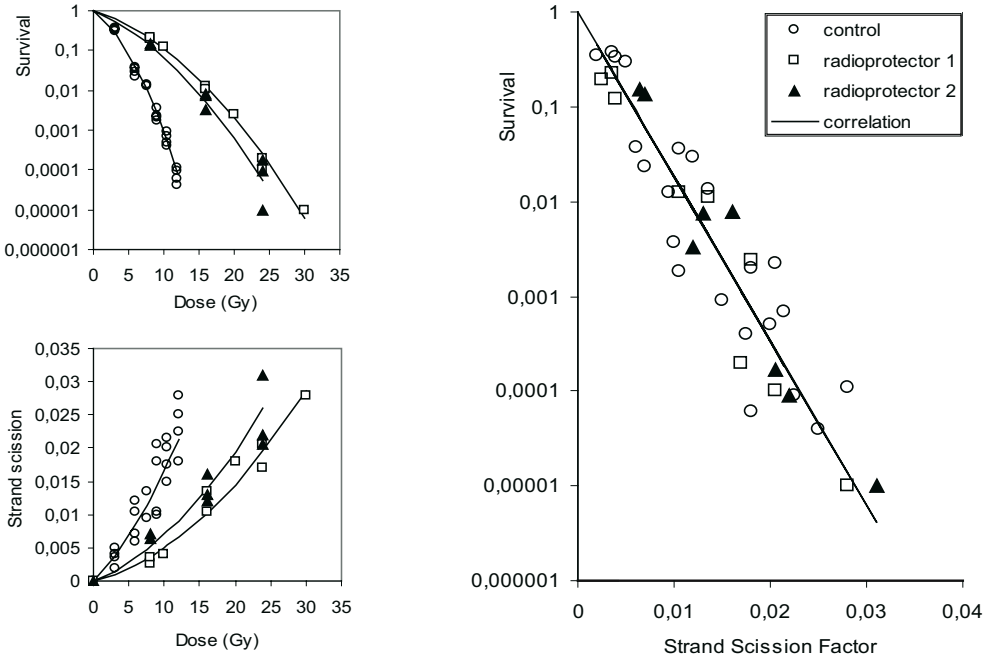

Fig. 2.6. An example of the correlation between the induction of DNA double-strand breaks and cell survival in accordance with equation 2.3 predicted by the model (data taken from Murray et al. 1989)

DNA double-strand breaks (Prise et al. 1993, 1999; Milligan et al. 1995, 2000). The three-dimensional molecular structure and the 2-nm distance between the two strands of the DNA helix impose the requirement that a single radiation track must have energy deposition events occurring every couple of nanometers along its path in order to induce a double-strand break. It is not difficult to understand that the densely ionising tracks produced by α-particles, for example, will have the required ionisation clustering to cause double-strand breaks efficiently. Although it is less intuitive, sparsely ionising radiation, such as X-rays, which lose energy by electron scattering, produce electron tracks with a sufficiently high ioni-

sation clustering, especially at the track ends, to induce double-strand breaks. Indeed, Goodhead and his colleagues (Goodhead et al. 1979; Thacker et al. 1986) have shown that 0.3-keV carbon ultrasoft X-rays creating electron tracks of only 7 nm in length have a high efficiency for inducing cell killing, aberrations and mutations. These results put an upper limit on the size of the "target" for the effects and also suggest that each of the cellular end-points arises from the same type of damage.

The important conclusion from this is that all types of ionising radiation from the very sparsely ionising high-energy gamma rays to the most densely ionising energetic heavy particles are able to induce DNA double-strand breaks in a single radiation track. This means that the dose–effect relationship for DNA double strand breaks and for the three cellular end-points must be linear at low doses from zero dose up. So the risk of hereditary mutations deriving from cellular effects in germ cells must also be linear at low doses from zero dose up.

An important corollary from this is that the effectiveness of different sparsely ionising radiations, in terms of the α-coefficient, will not be the same, and softer X-rays will be more effective than harder X-rays and gamma rays. In other words, the relative biological effectiveness (RBE) or Radiation Weighting Factor for all sparsely ionising radiation will not be 1, even though the ICRP has chosen this value for practical purposes.

2.2.2.4 The Formation of Chromosomal Aberrations

One major problem that arose during the development of the model was the clash that it created with the Classical and Exchange Theories for the formation of chromosomal aberrations (Sax 1940; Lea and Catcheside 1942; Lea 1946; Revell 1963, 1974). Briefly, both of these theories generate linear-quadratic equations for the yield of aberrations. The Classical Theory assumes that radiation induces chromosome arm breaks in proportion to dose so that exchange aberrations, requiring two breaks, have a linear-quadratic yield with dose while deletions are linear with dose. The Exchange Theory assumes that primary events, not breaks, in chromosome arms are induced in proportion to dose and that two primary events interact to produce both exchange aberrations and deletions.

The major difference between the classical and exchange theories and the model presented here is that we propose that the chromosome arm break, which is a DNA double-strand break, is induced by radiation with linear-quadratic dose kinetics. Thus, while our model predicts linear-quadratic dose–effect relationships for all types of chromosomal aberrations, except complex aberrations, we are left to explain the origin of the second break which is so clearly evident in exchange aberrations, such as dicentrics or reciprocal exchanges.

The explanation that we have proposed derives from the work of Resnick (1976) who devised a model for the repair of DNA double-strand breaks via a recombinational exchange process. In this process, the broken DNA helix pairs with a homologous undamaged DNA helix, DNA strands are exchanged which allows copying of the homologous DNA at the site of the break, and a Holliday junction is formed which can be resolved to give either perfect repair or misrepair involving the reciprocal exchange of DNA strands (Fig. 2.7). In terms of the unineme concept of chromosome structure, the reciprocal exchange of DNA strands represents the reciprocal exchange of chromosome arms (Fig. 2.7). In other words, the second break, so clearly visible in exchange chromosome aberrations, is not radiation-induced but arises as a consequence of the repair of the radiation-induced double-strand break.

We expanded on the proposals of Resnick by suggesting that complete homology between the broken and unbroken helices might not be needed and that the recombination repair process would also occur in regions of short-range homology on either side of the double-strand break. In this case, the short-range homologous association at the break can be developed between the broken DNA and the undamaged DNA from any other chromosome, not just the homologous chromosome. The large proportion of repetitive and closely homologous DNA sequences in eukaryotic chromosomes provides a multitude of regions on all the chromosomes for the short-range, homologous association to occur. This, in turn, means that the recombinational repair of a radiation-induced DNA double-strand break can lead to the exchange of chromosome arms between different chromosomes as well as regions on the same chromosome with the result that all the different chromosomal aberration configurations can be derived in this way (Chadwick and Leenhouts 1978, 1981).

Our proposals for the formation of chromosome aberrations from one radiation-induced chromosome arm break contradicted the accepted conven-

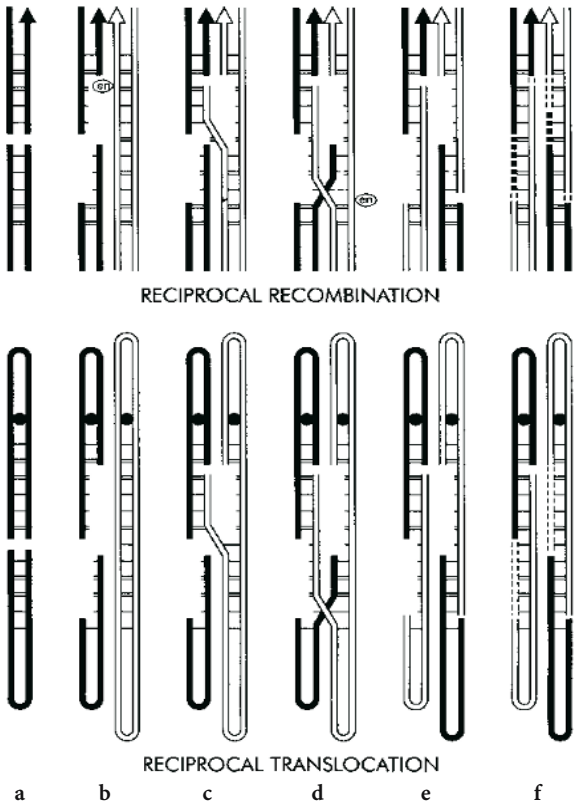

Fig. 2.7a–f. A schematic representation of how homologous recombinational repair of a DNA double-strand break can lead to the formation of a chromosomal aberration. The upper part of the drawing presents the repair of the DNA while the lower part presents the same repair at the level of the chromosome. The broken ends of the helix (**a**) are trimmed by endonuclease, and an undamaged stretch of homologous DNA aligns with the break (**b**). Strand exchange (**c**) leads to the formation of a Holliday junction (**d**) which can be resolved to give either perfect repair (not shown) or the complete exchange of the DNA helices (**e**) and (**f**). The misrepair of the DNA double-strand break leads to the exchange of chromosome arms and the formation of exchange aberrations. A reciprocal translocation is illustrated

tional cytological wisdom, and there were no experimental data that could be interpreted to resolve this. There are now some results that appear to suggest we may be correct.

The experiments of Goodhead and his colleagues, using the ultrasoft X-rays with radiation tracks of only a few nanometers, were expected to induce chromosome aberrations with an almost completely quadratic dose–effect relationship according to traditional cytological theory. Such short tracks were not expected to break more than one chromosome arm so that there would be no α-mode of radiation action. In fact, several workers (Virsik et al. 1980; Goodhead et al. 1980; Thacker et al. 1986; Simpson and Savage 1996; Griffin et al. 1996; 1998) found that the ultrasoft X-rays with tracks as short as 7 nm induced chromosomal aberrations efficiently with a yield that was closely linear with dose, i.e. a strong α-mode of radiation action.

Another piece of evidence in favour of the model comes from the experiments of Aten and his colleagues (Ludwików et al. 2002) who were able to induce double-strand breaks in one chromosome and show that exchange chromosome aberrations were formed between the damaged chromosome and other undamaged chromosomes in the cells. The double-strand breaks could be induced in only one chromosome because it was unusually late replicating so that, by adding iodine-125 labelled iododeoxyuridine (IUdR) to the medium after the other chromosomes had replicated, only the late-replicating chromosome carried the iodine-125 which emits very short-range Auger-electrons. This experiment provides an extremely clear indication of the formation of exchange aberrations by the interaction of the damaged chromosome with the other undamaged chromosomes.

Further support for the interaction of damaged and undamaged chromosomes to create exchange aberrations comes from experiments studying aberrations formed after the fusion of irradiated and unirradiated cells. The first experiment of this type appeared to show no interaction between the irradiated and un-irradiated chromosomes (Cornforth 1990), but more recent work contradicts this (Darroudi et al. 2001).

In addition, the molecular biology, biochemistry and genetics of DNA double-strand break repair has advanced considerably in recent years, and a gene (*RAD54*) controlling homologous recombinational repair (HR) in mammalian cells has been identified and cells deficient in this repair process are sensitive to ionising radiation (Essers et al. 1997).

We remain confident that the problem of the mechanisms involved in the formation of chromosomal aberrations will be resolved in the near future.

2.2.2.5 The β-Mode of Radiation Action

Another problem that has dogged the development of the model is the β-mode of radiation action where the model proposes that two independently induced

DNA single-strand breaks can combine to produce a double-strand break. It is a particularly attractive process because it is known that the repair of single-strand breaks is correct, and thus error free, and because the repair process explains very straight forwardly the dose rate and fractionation effects which also appear to be error free.

The problem arises because calculations based purely on the physics of energy deposition predict that two, independently induced, single-strand breaks will only occur close enough together to produce a double-strand break at much larger doses than those at which the quadratic component of dose–effect relationships becomes apparent. We assume that what happens in the cell is not just physics but that chemistry and biology must also be involved, and we believe that there are certain extenuating circumstances that need to be taken into account, although we acknowledge that our arguments are more conjectural than established.

The first point to be made is that the β-coefficient measured for cell survival in synchronous cells is maximum at the start of the S-phase when the DNA starts to replicate and is at a minimum, often close to zero, during the G_2-phase and mitosis. In other words, when the DNA and chromosomes are tightly bound during mitosis, the cell may be behaving more or less in accordance with the physics. However, there are indications that the DNA 'relaxes' and unwinds as it begins the replication process and it might even form regions or 'microbubbles' of single-stranded DNA (Gaudette and Benbow 1982; Benbow et al. 1985; Chadwick and Leenhouts 1994). These extended regions of single-stranded DNA would increase the distance along DNA over which two single-strand breaks could combine to form a double-strand break.

In addition, it has been shown that the sensitivity of DNA to hydroxyl attack increases by some 100-fold as the proteins surrounding cellular DNA are stripped away (Ljungman 1991; Ljungman et al. 1991; Nygren et al. 1995). If a first single-strand break led to an uncoiling of the DNA helix–as a result of the relaxation of the strain normally experienced by the helix–and the DNA spiralled away from the histones, which coil it into the chromosomes, this region of single-stranded DNA might be more susceptible to the induction of a second single-strand break by hydroxyl radical attack.

We have also made calculations which show that, in the α-mode, the two breaks are induced by radicals induced within about 0.5 nm of the helix. In the β-mode, if the first single-strand break is caused by hydroxyl radical attack from within about 0.5 nm of the helix, then the second independently induced break would need to be caused by radical attack from within about 5 nm of the second strand to comply with the values found for the β-coefficient in radiation biology (Leenhouts and Chadwick 1976; Chadwick and Leenhouts 1981). The radical scavenging experiments of Chapman et al. (1975) support our conclusion that the radiation chemistry of the α- and β-modes should be different.

One other completely different piece of evidence which, we think, supports our ideas on the combination of two single-strand breaks to form a double-strand break comes from the fact that we were able to extend our model to describe the cell-killing effects of UV light as well as cytotoxic chemicals (Chadwick and Leenhouts 1983; Leenhouts and Chadwick 1984). A photon of UV light cannot interact with both strands of the DNA helix but can induce a pyrimidine dimer on one strand. Monofunctional cytotoxic chemicals only interact with a single strand of the DNA. In both cases, the extension of our model predicted a purely quadratic cell survival curve, i.e. no α-mode action, in good agreement with experimental data. We were also able to derive a mathematical expression to describe the synergistic interaction of cytotoxic chemicals or UV light with ionising radiation based on the combination of a radiation-induced single-strand break with single-strand damage induced by the chemical or UV light (Leenhouts and Chadwick 1978).

Thus, although there is no definite proof for our interpretation of the β-mode of radiation action, there is enough conjectural evidence in support of this interpretation for us to continue with our approach and maintain the implications we derive from it.

2.2.3 Conclusions from the Cellular Model

At this stage we conclude that:

- the linear-quadratic equation provides an accurate description of the dose–effect relationships of cellular end-points;
- the DNA double-strand break is the crucial radiation-induced lesion causing each of the end-points;
- the α-mode of radiation action is responsible for low-dose effects, even after an acute exposure;

- all ionising radiation is capable of inducing a DNA double-strand break in the α-mode;
- not all DNA double-strand breaks will be repaired perfectly;
- the induction of DNA double-strand breaks and, consequently, of chromosomal aberrations, mutations and cell killing, will be initially linear with radiation dose from zero dose up.

In other words, cellular end-points, including hereditary mutations, will be induced at low doses in direct proportion to the radiation dose, in accordance with the LNT concept.

2.3 Radiation-Induced Cancer

Insight can be gained into the induction of cancer by radiation and the shape of the dose–effect relationship at low doses by incorporating the cellular model into a multi-step model of carcinogenesis. A "two-mutation step with clonal expansion of intermediate cells" model for cancer was derived by Moolgavkar and Knudson (1981). The cancer model has a firm biological basis because it was developed from conclusions drawn by Knudson from a study of the occurrence of retinoblastoma in children (Knudson 1971, 1985, 1991). The conclusions have been subsequently confirmed by molecular biological analysis.

2.3.1 A Multi-Step Cancer Model

Figure 2.8 presents, schematically, a two-mutation model for carcinogenesis.

A population of normal stem cells in an organ is at risk of a mutation (μ_1), 'initiation', to an intermediate state. A cell in the intermediate state can divide and undergo clonal expansion (ε), 'promotion', to form, as time passes, an increasing population of cells at risk of a second mutation (μ_2), 'conversion', which creates a malignant cell. The malignant cell divides, 'progression', and produces a detectable tumour after a certain lag time (t_0).

There have been some criticisms levelled at the model because mutational and cytological analyses of tumour cells appear to show more than two mutational changes, although there may be several explanations for this. First, many of these changes might occur during the progression of the malignant cells to tumour formation. Then, the recent findings that only certain cells in a tumour are able to divide continuously and act as "cancer stem cells" (Beachy et al. 2004) seem to suggest that not all cells in a tumour will be informative for the malignant process. Alternatively, the two mutations may be rate limiting for the process, i.e. other steps occur quickly and do not affect the mathematics of the model.

We have used a slightly modified version of the Moolgavkar model which allows us to calculate, simultaneously, the age-dependent increase in cancer incidence and the dose–effect relationships and we have been able to apply the modified version of

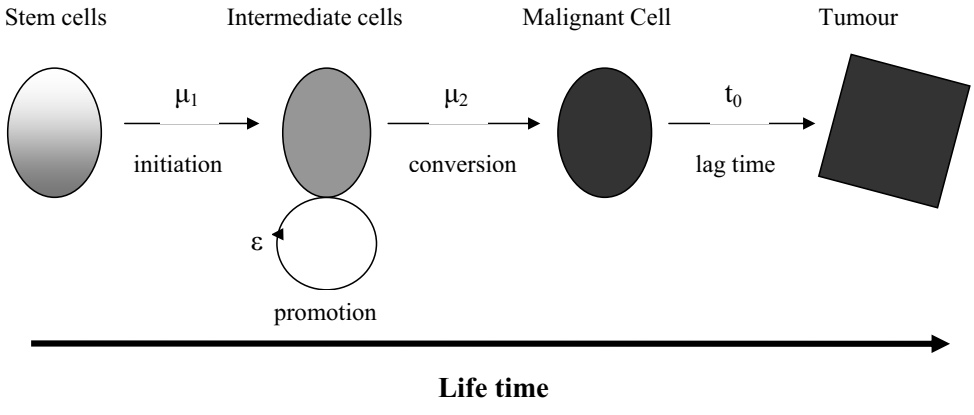

Fig. 2.8. A schematic representation of the two-mutation cancer model showing the development from normal stem cells via an intermediate state to the malignant cell which can grow out to form a detectable tumour. The intermediate cell population expands exponentially in time. Note the important role that time plays in the model

the model to the analysis of animal radiation biological data and epidemiological data from exposed human populations (Leenhouts and Chadwick 1994a; 1994b; Leenhouts 1999; Leenhouts and Brugmans 2000; 2001; Leenhouts et al. 2000).

It is not necessary to go into the complicated mathematics associated with the model but it is useful to form a basic understanding of how the model functions especially because the model has some important implications for the shape of the dose–effect relationship at low doses and for levels of radiation risk.

2.3.1.1 Spontaneous Cancers

Consider first the case of spontaneous cancer which, according to the model, must arise as a consequence of spontaneous mutations (μ_{b1}, μ_{b2}). The probability that one of the normal organ stem cells mutates to an intermediate cell increases proportionally with time as long as the spontaneous mutation rate (μ_{b1}) remains approximately constant. The intermediate cell divides and, by population doubling at each division, produces an exponentially increasing population of intermediate cells, all of which are targets for a second spontaneous mutation (μ_{b2}) to create a malignant cell. Time, a significant part of lifetime, plays a major role in the model and it is important to realise that, while the mutation probabilities are proportional to time, the cellular expansion of the intermediate cells is exponential with time. The model has been shown to describe the rapidly increasing incidence of several spontaneous cancers in older people (Moolgavkar and Venzon 1979) (Fig. 2.9a).

2.3.1.2 Cancers Induced by an Acute Exposure

If we now consider an acute exposure to radiation, the mutations it causes can only be taken into account in the model together with the spontaneous mutations. In this case, there are two possibilities: (1) the radiation affects the first mutational step, e.g. if the person exposed is young and has none or very few intermediate cells, ($\mu_1 \rightarrow \{\mu_b + f(D)\}_1$) and an intermediate cell derived from a radiation-induced mutation will need a spontaneous mutation (μ_{b2}) to convert it to malignancy (Fig. 2.9b) or (2) if the person exposed is older and already has many intermediate cells, radiation is more likely to affect the second mutation ($\mu_2 \rightarrow \{\mu_b + f(D)\}_2$) and convert an intermediate cell deriving from a spontaneous mutation (μ_{b1}) to a malignant state (Fig. 2.9b). $f(D)$ is a function of dose (D), normally linear-quadratic, which represents the contribution of the acute exposure to the mutations in the initiation step or the conversion step, although $f(D)_1$ is not necessarily the same as $f(D)_2$.

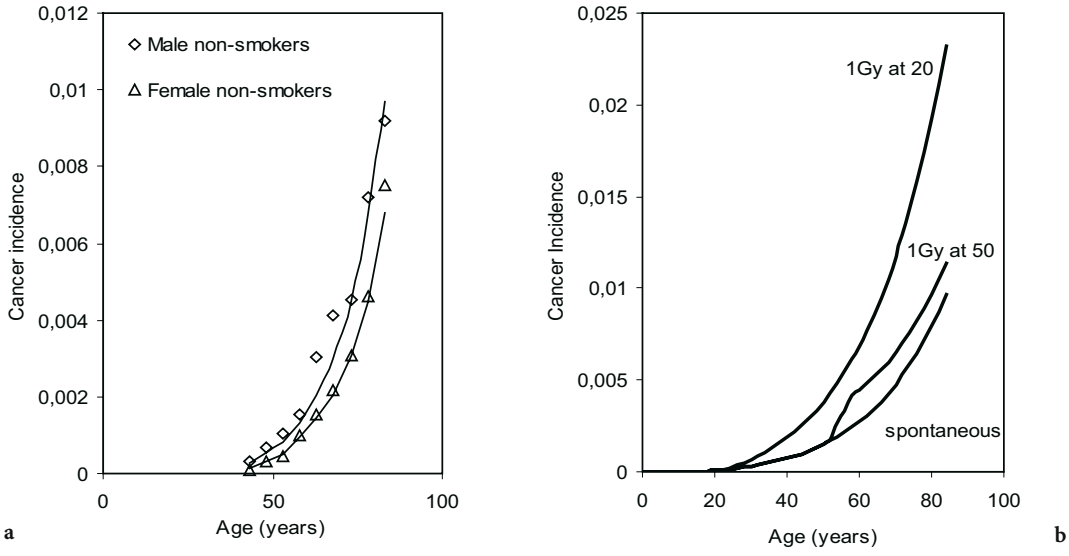

Fig. 2.9a,b. a The fitting of the model to the occurrence of lung cancers in non-smoking males and females as a function of age (data from Hammond 1966). The fitting of the model to spontaneous cancers is used to define values for the basic parameters, e.g. μ_{b1}, μ_{b2}, ε, t_0. **b** A model simulation showing the effect of 1 Gy at 20 years and 50 years of age on the increasing incidence of cancer as a function of age after exposure

In each case, the radiation-induced mutation in one step relies on a spontaneous mutation in the other step to complete the path from a normal to a malignant state, and radiation may be seen to be a co-factor in the induction of cancer.

2.3.1.3 Implications and Consequences

Several important implications derive from the fact that the radiation-induced mutations cannot be treated separately from the spontaneous mutations.

- The spontaneous mutation rates in the stem and intermediate cells define the spontaneous incidence of a specific cancer and, in general, the higher the spontaneous mutation rates the higher the spontaneous incidence of the cancer.
- The effect of radiation is irrevocably inter-woven with the spontaneous mutations and, consequently, with the spontaneous cancer incidence.
- The effect of radiation on cancer incidence, i.e. the radiation risk, depends on the level of the spontaneous mutation rates and will be different for different cancers.
- In general, the effect of radiation, or radiation risk, will be greater for cancers with higher specific incidence levels (Fig. 2.10).
- The shape of the dose–effect relationship for cancer is defined by the dose–effect relationship for cellular mutation frequency, or aberration yield, so that at low to moderate doses $f(D)$ can be approximated to $f(D) = k(\alpha D + \beta D^2)$ which is linear with dose at very low doses.

All of this means:

- each specific cancer will have its own level of radiation risk dependent on its spontaneous incidence;
- the radiation risk of a specific cancer in populations with different spontaneous incidences of that cancer (cf. Japanese atomic bomb survivors with a European population) will not be the same, although the model offers a way of extrapolating risk across populations;
- the shape of the dose–effect curve for radiation-induced cancer in animals or man will resemble the shape of the dose–effect curve for cellular mutation and show, at least qualitatively, the same dose rate and radiation quality effects;
- at very low doses, the shape of the dose–effect curve is linear;
- the slope of the linear dose–effect curve, which defines radiation risk for a specific cancer, is dependent on the cellular sensitivity ($k\alpha$) and the spontaneous mutation rates μ_b.

2.3.1.4 Age-Dependent Risk

Using the modified cancer model to calculate the age-dependent increase in cancer incidence for spontaneous cancers and cancers after exposure at different ages (Fig. 2.9) has allowed a simulation of the dependence of risk in adults on age at exposure, although the model has not been used to consider the case of babies and infants. Briefly, the pattern of the relative risk, the induced cancer incidence divided by the spontaneous cancer incidence, is similar for an adult acutely exposed at age 20 years to that for one exposed at age 50 years (Fig. 2.11a). The relative risk increases rapidly after the lag period, peaks and then drops gradually over time. At the same exposure level, and using the same cellular radiation sensitivity, the increase is larger following exposure at the younger age but it should be borne in mind that the rapid increase in relative risk results because a small induced effect is divided by a very

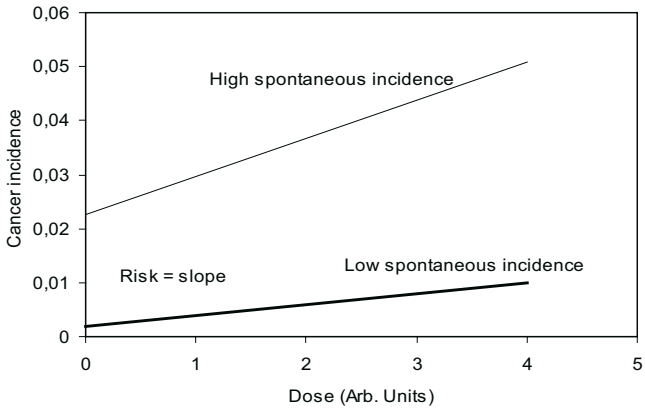

Fig. 2.10. A model simulation showing the effect of spontaneous cancer incidence on the radiation risk, i.e. the slope of the line, even when the cellular radiation sensitivities are held constant

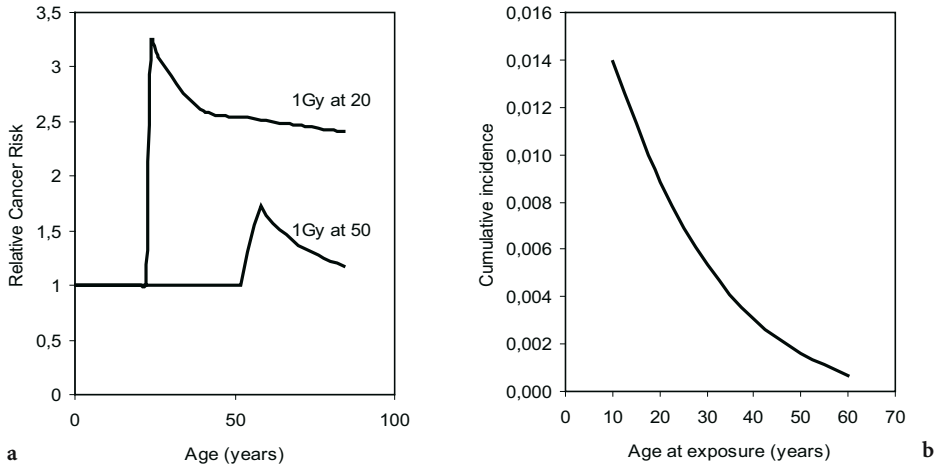

Fig. 2.11a,b. a A model simulation of the relative cancer risk after exposure at 20 years and 50 years of age as a function of time after exposure. **b** A model simulation of the cumulative cancer incidence as a function of age-at-exposure showing an increasing risk following exposure at younger ages

small spontaneous incidence that is much smaller at age 20 years than at 50 years. Figure 2.11b presents the cumulative risk as a function of age-at-exposure and reveals that the risk is higher in those exposed at younger ages. This, to some extent, reflects the 'amplification' resulting from a longer period for the exponential clonal expansion of intermediate cells. We think it prudent to assume that the risk in babies and children would be greater than that in young adults although the model has not been used to simulate these risks.

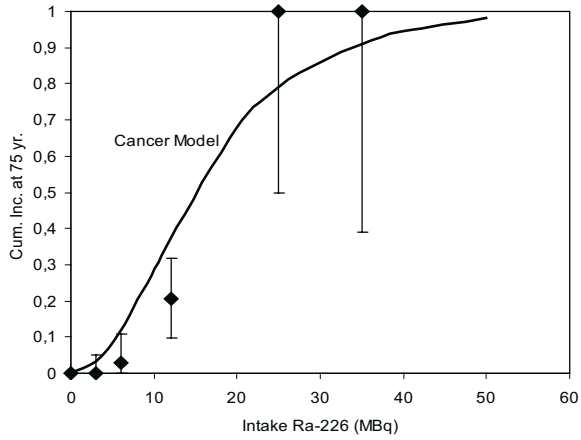

Fig. 2.12. The model fitting to the cumulative bone cancer incidence at 75 years of age in radium dial painters illustrating the strongly curved risk resulting from a combination of the very low spontaneous incidence of bone cancer and the radiation-induced mutations in both steps of the cancer pathway. The incidence has been interpreted as indicating a threshold, but the model provides an alternative explanation

2.3.2 Some Additional Considerations

Some additional points need to be made even though they are of lesser relevance to the dose levels and practices associated with computed tomography.

2.3.2.1 Protracted Exposure

The complementation of a radiation-induced mutation in one step by a spontaneous mutation in the other, which is rather intuitive for an acute exposure, also applies to the case of an exposure protracted over a major part of lifetime, as long as the spontaneous mutation rate is comparable to the radiation-induced mutation rate. One interesting exception to this rule occurs when the spontaneous mutation rates are very low and, consequently, the spontaneous cancer incidence is very low. In this case, a long-term radiation exposure may induce mutations in both steps of the pathway and the radiation risk curve becomes much more quadratic with accumulated dose. An example of this is to be found in the bone cancers occurring in the radium dial painters who ingested high levels of the bone seeking α-particle emitters radium-226 and radium-228 (Rowland 1994). Primary bone cancer has a very low sponta-

neous incidence, and bone cancer incidence in the dial painters appears to show a threshold dose type of response (Fig. 2.12). However, the model offers an explanation based on the induction of both mutations by the α-particle radiation and suggests that the incidence is more likely to be closely quadratic. Even so, there will be a very small low dose linear component because the spontaneous bone cancer incidence, and thus the spontaneous mutation rate, is low but not completely zero (Leenhouts and Brugmans 2000).

2.3.2.2 The Role of Cell Killing

At high acute doses, the effect of cell killing has to be taken into account because a mutated cell that fails to survive cannot express the mutation. Cellular studies score mutations per surviving cell but, in an organ, the mutations expressed are per irradiated cell. This means that the approximate function $f(D)$, which is accurate enough for low doses, must be modified by a term for survival and:

$$f(D) \rightarrow \{1-\exp[-k(\alpha D+\beta D^2)]\}\exp[-p(\alpha D+\beta D^2)] \quad (2.8)$$

This equation is linear-quadratic at lower doses, flattens to a peak and then decreases at high doses where cell killing dominates. This is illustrated in Figure 2.13, which also shows how the data for leukaemia in the atomic bomb survivors (presented in Fig. 2.1a) might be described by the equation.

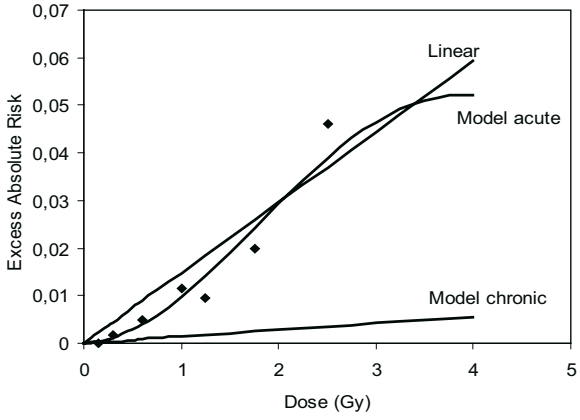

Fig. 2.13. An illustration of how a linear-quadratic model might be fitted to the data (shown in Fig. 2.1) for the acute exposure of the atomic bomb survivors compared with a linear interpretation. The lower straight line shows the risk that would be predicted by the model for chronic exposure

2.3.2.3 Different Mutations to the Same Cancer

The schematic diagram of the multi-step cancer model (see Fig 2.8) suggests that there is one mutation (μ_1) that changes an organ stem cell into an intermediate cell and one mutation (μ_2) that changes an intermediate cell into a malignant cell which divides to produce a tumour. This is a simplified way of looking at the cancer process, and we are convinced that there are several different mutations that can change an organ stem cell into an intermediate cell and yet others that can change an intermediate cell into a malignant cell, even though the tumours eventually formed are classified pathologically in the same type. However, with different mutagenic pathways leading to the same pathological tumour, it is reasonable to expect that the tumours would express different molecular signatures and possibly exhibit different levels of virulence. Despite these considerations, the model calculations and simulations remain useful as the mutation rates used (μ_1, μ_2) will represent average values for the spectrum of mutations involved in each step of the pathway to a specifically classified tumour.

The situation is different when different types of tumours are considered because the stem cells of one organ, for example, the kidney, need not necessarily have the same radiation sensitivity to cellular mutation as the stem cells of, for example, the brain, and the rate of cell expansion (ε) of the intermediate cells and the lag time (t_0) might differ from one organ to the next. This means that, especially in the case of acute exposure when the dose–effect curve is likely to be non-linear, each type of tumour needs to be analysed individually. Consequently, the grouping of all solid tumours arising in the atomic bomb survivors (Pierce et al. 1996) is unlikely to provide much useful information about the dose–effect relationship or radiation risk for radiation-induced cancer. This situation is probably less critical for populations exposed to low acute or to protracted irradiation where the dose–effect curve is likely to be linear.

2.4 Discussion and Conclusions

We have established a link from a radiation-induced molecular lesion in the nucleus of the cell to the development of cancer. The molecular lesion, the DNA double-strand break, is known to be a critical lesion which cannot always be perfectly repaired and which is strongly associated with sensitivity to ionising radiation. The cellular model provides a link from the molecular lesion to chromosomal aberrations, mutations and cell killing, and evidence has been presented supporting these links and associations. The biophysics of energy deposition clearly reveals that all forms of ionising radiation are able to induce DNA double-strand breaks directly in proportion to radiation dose and that this mode of radiation action will dominate at low doses down to zero. This means the dose–effect relationship for cellular effects must be linear at such doses. Biophysics also reveals that the induction of double-strand breaks by a single particle traversal of the DNA helix will depend on radiation quality so that different energy X-rays will have different efficiencies in the production of breaks, and the relative effectiveness for sparsely ionising radiation will not always be the same.

The multi-step cancer model allows the radiation biology of cellular effects to be applied to the induction of cancer and suggests that, in general, radiation will only affect one of the mutational steps on the pathway to cancer. Spontaneous mutations, responsible for spontaneous cancers, will be needed to complement the radiation-induced mutation and produce a malignant cell. This means that the dose–effect relationship for the induction of cancer is linear at low doses from zero dose up and that the slope of that straight line, the radiation risk, depends on the spontaneous incidence of the cancer and will be larger for cancers with a high spontaneous incidence. This argument is valid even if more than two mutational steps are involved in cancer development.

In conclusion, if we accept that the DNA double-strand break is the critical radiation-induced lesion which can, ultimately, lead to cancer, we must accept that the dose–effect relationship for radiation-induced cancer, the main radiation risk, is linear with dose from zero dose up because:

- the lowest dose imaginable is a single electron track through one of a population of cells;
- the track has a small positive probability of causing a DNA double-strand break in the nucleus of that cell;
- the double-strand break has a small positive probability of causing a mutation;
- the mutation has a small positive probability of being involved in a pathway to cancer.

The arguments presented here are based on a mechanism of radiation action at the level of the DNA in the nucleus of the cell. The conclusions are in accordance with a Linear No-Threshold concept of radiation risk at low acute or protracted exposures, although we stress that our approach to such a LNT concept is different from that applied by ICRP. The modelling does not provide any values for the slope of the dose–effect relationship which quantifies the radiation risk but does imply that it will vary from cancer type to cancer type. Further analysis of epidemiological data using the model is required to obtain quantified estimates of risk.

A LNT concept of radiation risk implies that each increment of dose carries a concomitant increase in radiation risk so the ALARA principle remains valid and the development of improvements in computed tomography, which lead to a reduction of the dose to the patient, continues to be worthwhile.

References

Académie des Sciences (1997) Problems associated with the effects of low doses of ionising radiations Académie des Sciences, Rapport No 38 (Technique and Documentation, Paris)

Albertini RJ, Clark LS, Nicklas JA et al (1997) Radiation quality affects the efficiency of induction and the molecular spectrum of *HPRT* mutations in human T cells. Radiat Res 148[Suppl]:S76–S86

Barendsen GW (1964) Impairment of the proliferative capacity of human cells in culture by α-particles with different linear energy transfer. Int J Radiat Biol 8:453–466

Beachy PA, Karhadkar SS, Berman DM (2004) Tissue repair and stem cell renewal in carcinogenesis. Nature 432:324–331

Becker K (1997) Threshold or no threshold, that is the question. Radiat Prot Dosim 71:3–5

Benbow RM, Gaudette MF, Hines PJ et al (1985) Initiation of DNA replication in eukaryotes. In: Boynton AL, Leffert HL (eds) Control of animal cell proliferation Vol 1. Academic Press, New York, pp 449–483

Bhambhani R, Kuspira J, Giblak RE (1973) A comparison of cell survival and chromosomal damage using CHO cells

synchronised with and without colcemid. Can J Genet Cytol 15:605–618
Bithell JF, Stiller CA (1988) A new calculation of the carcinogenic risk of obstetric X-raying. Stat Med 7:857–864
Bond VP, Wielopolski L, Shani G (1996) Current misinterpretations of the linear no-threshold hypothesis. Health Phys 70:877–882
Brenner DJ, Ward JF (1992) Constraints on energy deposition and target size of multiply damaged sites associated with DNA double-strand breaks. Int J Radiat Biol 61:737–748
Brenner DJ, Doll R, Goodhead DT et al (2003) Cancer risks attributable to low doses of ionizing radiation: Assessing what we really know. Proc Natl Acad Sci USA 100:13761–13766
Calabrese EJ (2002) Hormesis: changing view of the dose-response, a personal account of the history and current status. Mutat Res 511:181–189
Cardis E, Vrijheid M, Blettner M et al (2005) Risk of cancer after low doses of ionising radiation: retrospective cohort study in 15 countries. BMJ 331:77–83
Chadwick KH, Leenhouts HP (1973) A molecular theory of cell survival. Phys Med Biol 18:78–87
Chadwick KH, Leenhouts HP (1975) The effect of an asynchronous population of cells on the initial slope of dose-effect curves. In: Alper T (ed) Cell survival after low doses of radiation: Theoretical and clinical implications. The Institute of Physics and John Wiley and Sons, London, pp 57–63
Chadwick KH, Leenhouts HP (1978) The rejoining of DNA double-strand breaks and a model for the formation of chromosomal rearrangements. Int J Radiat Biol 33:517–529
Chadwick KH, Leenhouts HP (1981) The molecular theory of radiation biology. Springer Verlag, Berlin Heidelberg New York
Chadwick KH, Leenhouts HP (1983) A quantitative analysis of UV-induced cell killing. Phys Med Biol 28:1369–1383
Chadwick KH, Leenhouts HP (1994) DNA double strand breaks from two single strand breaks and cell cycle radiation sensitivity. Radiat Prot Dosim 52:363–366
Chadwick KH, Leenhouts HP, Brugmans MJP (2003) A contribution to the linear no-threshold discussion. J Radiol Prot 23:53–78
Chapman JD, Gillespie CJ, Reuvers AP et al (1975) The inactivation of Chinese hamster cells by X-rays: the effects of chemical modifiers on single- and double-events. Radiat Res 64:365–375
Clarke R (1998) Conflicting scientific views on the health risks of low-level ionising radiation. J Radiol Prot 18:159–160
Clarke R (1999) Control of low-level radiation exposure: time for a change? J Radiol Prot 19:107–115
Cornforth MN (1990) Testing the notion of the one-hit exchange. Radiat Res 121:21–27
Darroudi F, Natarajan AT, Savage JRK et al (2001) Induction of chromosomal aberrations by low and high LET radiations: mechanisms and spectra. In: Proceedings European Radiation Research, Dresden 2001, (ISBN 3-00-007790-1)
Dewey WC, Furman SC, Miller HH (1970) Comparison of lethality and chromosomal damage induced by X-rays in synchronised Chinese hamster cell in vitro. Radiat Res 43:561–581
Dewey WC, Stone LE, Miller HH et al (1971a) Radiosensitization with 5-bromodeoxyuridine of Chinese hamster cells irradiated during different phases of the cell cycle. Radiat Res 47:672–688
Dewey WC, Miller HH, Leeper DB (1971b) Chromosomal aberrations and mortality of X-irradiated mammalian cells: emphasis on repair. Proc Natl Acad Sci USA 68:667–671
Dewey WC, Saparetto SA, Betten DA (1978) Hyperthermic radiosensitization of synchronised Chinese hamster cells: relationship between lethality and chromosomal aberrations. Radiat Res 76:48–59
Doll R, Darby S (1991) Leukaemia: some unsolved problems. Br Inst Radiol Rep 22:1–6
Edwards R (1997) Radiation roulette. New Scientist (11 October) pp36–40
Essers J, Hendriks RW, Swagemakers SMA et al (1997) Disruption of mouse RAD54 reduces ionizing radiation resistance and homologous recombination. Cell 89:195–204
Franken NAP, Ruurs P, Ludwikow G et al (1999) Correlation between cell reproductive death and chromosome aberrations assessed by FISH for low and high doses of radiation and sensitization by iodo-deoxyuridine in human SW-1573 cells. Int J Radiat Biol 75:293–299
Friedland W, Jacob P, Paretzke HG et al (1998) Monte Carlo simulation of the production of short DNA fragments by low-linear energy transfer radiation using high-order DNA models. Radiat Res 150:170–182
Friedland W, Jacob P, Paretzke HG et al (1999) Simulation of DNA-fragment distribution after irradiation with photons. Radiat Environ Biophys 38:39–47
Gaudette MF, Benbow RM (1986) Replication forks are under-represented in chromosomal DNA of *Xenopus laevis* embryos. Proc Natl Acad Sci USA 83:5953–5957
Gillespie CJ, Chapman JD, Reuvers AP et al (1975a) The inactivation of Chinese hamster cells by X-rays: synchronized and exponential cell populations. Radiat Res 64:353–364
Gillespie CJ, Chapman JD, Reuvers AP et al (1975b) Survival of X-irradiated hamster cells: analysis in terms of the Chadwick-Leenhouts model. In: Alper T (ed) Cell survival after low doses of radiation: theoretical and clinical implications. The Institute of Physics and John Wiley and Sons, London, pp 25–31
Gofman JW, Tamplin AR (1971) The question of safe radiation thresholds for alpha-emitting bone seekers in man. Health Phys 21:47–51
Goodhead DT, Thacker J, Cox R (1979) Effectiveness of 0.3 keV carbon ultrasoft X-rays for the inactivation and mutation of cultured mammalian cells. Int J Radiat Biol 36:101–114
Goodhead DT, Virsik RP, Harder D et al (1980) Ultrasoft X-rays as a tool to investigate radiation-induced dicentric chromosome aberrations. In: Booz J, Ebert, HG, Hartfield HD (eds) Proceedings of the Seventh Symposium on Microdosimetry. Harewood Academic Press, London, EUR 7147 pp 1275–1285
Griffin CS, Stevens DL, Savage JRK (1996) Ultrasoft 1.5 keV aluminium X-rays are efficient producers of complex chromosome exchange aberrations revealed by fluorescence in situ hybridization. Radiat Res 146:144–150
Griffin CS, Hill MA, Papworth DG et al (1998) Effectiveness of 0.28 keV carbon K ultrasoft X-rays at producing simple and complex chromosome exchanges in human

fibroblasts *in vitro* detected using FISH. Int J Radiat Biol 73:591–598
Hammond EC (1966) Smoking in relation to the death rates of one million men and women. In: Epidemiological study of cancer and other chronic diseases. National Cancer Institute Monograph 19 pp 127–204
Heidenreich WF, Paretzke HG, Jacob P (1997a) No evidence for increased tumor rates below 200 mSv in the atomic bomb survivors data. Radiat Environ Biophys 36:205–207
Heidenreich WF, Paretzke HG, Jacob P (1997b) Reply to the 'Commentary' by DA Pierce and DL Preston. Radiat Environ Biophys 36:211–212
ICRP 1991 (1990) Recommendations of the International Commission on Radiological Protection. ICRP Publication 60. Annals of the ICRP 21:1–3
ICRP (2003) The evolution of the current system of radiological protection: the justification for new ICRP recommendations (a memorandum from the International Commission on Radiological Protection). J Radiol Prot 23:129–142
Iliakis G (1984) The influence of conditions affecting repair and fixation of potentially lethal damage on the induction of 6-thioguanine resistance after exposure of mammalian cells to X-rays. Mutat Res 126:215–225
Kellerer AM (2000) Risk estimates for radiation-induced cancer - the epidemiological evidence. Radiat Environ Biophys 39:17–24
Kellerer AM, Nekolla EA (2000) The LNT-controversy and the concept of "Controllable Dose". Health Phys 74:412–418
Kesavan PC, Sugahara T (1992) Perspectives in mechanistic considerations of biological effects of low dose radiations. In: Sugahara T, Sagan L, Aoyama T (eds) Low dose irradiation and biological defence mechanisms. Excerpta Medica International Congress Series 1013, Elsevier, Amsterdam, pp 439–443
Knudson AG (1971) Mutation and cancer: statistical study of retinoblastoma gene. Proc Natl Acad Sci USA 68:620–623
Knudson AG (1985) Hereditary cancer, oncogenes and antioncogenes. Cancer Res 45:1437–1443
Knudson AG (1991) Overview: genes that predispose to cancer. Mutat Res 247:185–190
Lea DE (1946) Actions of radiations on living cells. University Press, Cambridge
Lea DE, Catcheside DG (1942) The mechanism of induction by radiation of chromosome aberrations in *Tradescantia*. J Genet 44:216–245
Leenhouts HP (1999) Radon-induced lung cancer in smokers and non-smokers: risk implications using a two mutation carcinogenesis model. Radiat Environ Biophys 38:57–71
Leenhouts HP, Chadwick KH (1976) Stopping power and the radiobiological effects of electrons, gamma rays and ions. In: Booz J, Ebert HG, Smith BGR (eds) Fifth Symposium on Microdosimetry, Commission of the European Communities, Luxembourg, EUR 5452, pp 289–308
Leenhouts HP, Chadwick KH (1978) An analysis of synergistic sensitization. Br J Cancer 37 Suppl III, pp 198–201
Leenhouts HP, Chadwick KH (1984) A quantitative analysis of the cytotoxic action of chemical mutagens. Mutat Res 129:345–357
Leenhouts HP, Chadwick KH (1990) The influence of dose rate on the dose-effect relationship. J Radiat Prot 10:95–102
Leenhouts HP, Chadwick KH (1994a) A two-mutation model of radiation carcinogenesis: applications to lung tumours in rodents and implications for risk evaluations. J Radiol Prot 14:115–130
Leenhouts HP, Chadwick KH (1994b) Analysis of radiation induced carcinogenesis using a two stage carcinogenesis model: Implications for dose-effect relationships. Radiat Protect Dosim 52:465–469
Leenhouts HP, Brugmans MJP (2000) An analysis of bone and head sinus cancers in radium dial painters using a two-mutation carcinogenesis model. J Radiol Prot 20:169–188
Leenhouts HP, Brugmans MJP (2001) Calculation of the 1995 lung cancer incidence in the Netherlands and Sweden caused by smoking and radon: risk implications for radon. Radiat Environ Biophys 40:11–21
Leenhouts HP, Brugmans MJP, Chadwick KH (2000) Analysis of thyroid cancer data from the Ukraine after 'Chernobyl' using a two-mutation carcinogenesis model. Radiat Environ Biophys 39:89–98
Ljungman M (1991) The influence of chromatin structure on the frequency of radiation-induced DNA breaks: a study using nuclear and nucleoid monolayers. Radiat Res 126:58–64
Ljungman M, Nyberg S, Nygren J et al (1991) DNA-bound proteins contribute much more than soluble intracellular compounds to the intrinsic protection against radiation-induced DNA strand breaks in human cells. Radiat Res 127:171–176
Lloyd DC, Purrott RJ, Dolphin GW et al (1976) Chromosome aberrations induced in human lymphocytes by neutron irradiation. Int J Radiat Biol 29:169–182
Lloyd DC, Edwards AA, Prosser JS et al (1984) The dose response relationship obtained at constant irradiation times for the induction of chromosome aberrations in human lymphocytes by cobalt-60 gamma rays. Radiat Environ Biophys 23:179–189
Lloyd DC, Edwards AA, Leonard A et al (1988) Frequencies of chromosomal aberrations induced in human blood lymphocytes by low doses of X-rays. Int J Radiat Biol 53:49–55
Lloyd DC, Edwards AA, Leonard A et al (1992) Chromosomal aberrations in human lymphocytes induced *in vitro* by very low doses of X-rays. Int J Radiat Biol 61:335–343
Luckey TD (1997) Low-dose irradiation reduces cancer deaths. Radiation Protection Management 14(6):58–64
Ludwików G, Xiao Y, Hoebe RA et al (2002) Induction of chromosome aberrations in unirradiated chromatin after partial irradiation of a cell nucleus. Int J Radiat Biol 78:239–247
Metting NF, Braby LA, Roesch WC et al (1985) Dose-rate evidence for two kinds of radiation damage in stationary-phase mammalian cells. Radiat Res 103:204–212
Mill AJ, Frankenberg D, Bettega D et al (1998) Transformation of C3H 10T1/2 cells by low doses of ionising radiation: a collaborative study by six European laboratories strongly supporting a linear dose-response relationship. J Radiol Prot 18:79–100
Milligan JR, Ng JY-Y, Wu CCL et al (1995) DNA repair by thiols in air shows two radicals make a double-strand break. Radiat Res 143:273–280

Milligan JR, Aguilera JA, Nguyen T-TD et al (2000) DNA strand-break yields after post-irradiation incubation with base excision repair endonucleases implicate hydroxyl radical pairs in double-strand break formation. Int J Radiat Biol 76:1475–1483

Moolgavkar SH, Venzon D (1979) Two-event models for carcinogenesis. Incidence curves for childhood and adult tumors. Math Biosci 47:55–77

Moolgavkar SH, Knudson AG (1981) Mutation and cancer: a model for human carcinogenesis. J Natl Cancer Inst 68:1037–1052

Muirhead CR, Goodill AA, Haylock RGE et al (1999) Occupational radiation exposure and mortality: second analysis of the National Registry for Radiation Workers. J Radiol Prot 19:3–26

Murray D, Prager A, Milas L (1989) Radioprotection of cultured mammalian cells by amniothiols WR-1065 and WR-255591: correlation between protection against DNA double-strand breaks and cell killing after γ-radiation. Radiat Res 120:154–163

Murray D, Prager A, Vanankeren SC (1990) Comparative effect of the thiols dithiothreitol, cysteamine and WR-151326 on survival and on the induction of DNA damage in cultured Chinese hamster ovary cells exposed to γ-radiation. Int J Radiat Biol 58:71–91

NCRP (2001) Evaluation of the linear-nonthreshold dose-response model for ionizing radiation. NCRP Report No. 136. National Council on Radiation Protection and Measurements, Washington

Nikjoo H, O'Neill P, Terrisol M et al (1994) Modelling of radiation-induced DNA damage: the early physical and chemical events. Int J Radiat Biol 66:453–457

Nikjoo H, O'Neill P, Terrissol M et al (1999) Quantitative modelling of DNA damage using Monte Carlo track structure method. Radiat Environ Biophys 37:1–8

Nygren J, Ljungman L, Ahnstrom G (1995) Chromatin structure and radiation-induced DNA strand breaks in human cells: Soluble scavengers and DNA-bound proteins offer a better protection against single- than double-strand breaks. Int J Radiat Biol 68:11–18

Pierce DA, Shimuzu Y, Preston DL et al (1996) Studies of the mortality of atomic bomb survivors. Report 12, Part I. Cancer: 1950-1990. Radiat Res 146:1–27

Pierce DA, Preston DL (1997) On 'No evidence for increased tumor rates below 200 mSv in the atomic bomb survivors data'. Radiat Environ Biophys 36:209–210

Pohl-Ruhling J, Fischer P, Haas O et al (1983) Effects of low-dose acute X-irradiation on the frequencies of chromosomal aberrations in human peripheral lymphocytes *in vitro*. Mutat Res 110:71–82

Pohl-Ruling J, Fischer P, Lloyd DC et al (1986) Chromosomal damage induced in human lymphocytes by low doses of D-T neutrons. Mutat Res 173:267–272

Prise KM, Davies S, Michael BD (1987) The relationship between radiation-induced DNA double-strand breaks and cell kill in hamster V79 fibroblasts irradiated with 250 kVp X-rays, 2.3 MeV neutrons or ^{238}Pu α-particles. Int J Radiat Biol 52:893–902

Prise KM, Davies S, Michael BD (1993) Evidence for induction of DNA double-strand breaks at paired radical sites. Radiat Res 134:102–106

Prise KM, Gillies NE, Michael BD (1999) Further evidence for double-strand breaks originating from a paired radical precursor from studies of oxygen fixation processes. Radiat Res 151:635–641

Radford IR (1985) The level of induced DNA double-strand breakage correlates with cell killing after X-irradiation. Int J Radiat Biol 48:45–54

Radford IR (1986) Evidence for a general relationship between the induced level of DNA double-strand breakage and cell killing after X-irradiation of mammalian cells. Int J Radiat Biol 49:611–620

Rao BS, Hopwood LE (1982) Modification of mutation frequency in plateau Chinese hamster ovary cells exposed to gamma radiation during recovery from potentially lethal damage. Int J Radiat Biol 42:501–508

Revell SH (1963) Chromatid aberrations–the general theory. In: Wolff S (ed) Radiation induced chromosome aberrations. Columbia University Press, New York, pp 41–72

Revell SH (1974) The breakage-and-reunion theory and the exchange theory for chromosomal aberrations induced by ionizing radiation: a short history. Adv Radiat Biol 4:367–416

Resnick MA (1976) The repair of double-strand breaks in DNA: a model involving recombination. J Theor Biol 59:97–106

Richold M, Holt PD (1974) The effect of differing neutron energies on mutagenesis in cultured Chinese hamster cells. In: Biological effects of neutron irradiation (IAEA, Vienna) pp 237–244

Rowland RE (1994) Radium in humans: a review of U.S. studies. US Department of Commerce, Technology Administration, National Technical Information Service, Springfield

Sagan L (1992) It's time to re-think the radiation paradigm. In: Sugahara T, Sagan L, Aoyama T (eds) Low dose irradiation and biological defence mechanisms. Excerpta Medica International Congress Series 1013. Elsevier, Amsterdam pp 3–12

Sax K (1940) X-ray-induced chromosomal aberrations in *Tradescantia*. Genetics 25:41–68

Shrimpton PC, Hillier MC, Lewis MA et al (2003) Data from computed tomography (CT) examinations in the UK–2003 Review. NRPB – 67, National Radiological Protection Board, Chilton

Simpson P, Savage JRK (1996) Dose–response curves for simple and complex chromosome aberrations induced by X-rays and detected using fluorescence *in situ* hybridization. Int J Radiat Biol 69:429–436

Sinclair WK (1966) The shape of radiation survival curves of mammalian cells cultured *in vitro*. In: Biophysical aspects of radiation quality, Technical Reports Series 58, International Atomic Energy Agency, Vienna, pp 21–43

Skarsgard LD, Wilson DJ, Durrand RE (1993) Survival at low dose in asynchronous and partially synchronized Chinese hamster V79-171 cells. Radiat Res 133:102–107

Sternglass EJ (1963) Cancer: relation of prenatal radiation to development of the disease in childhood. Science 140:1102–1104

Sternglass EJ (1968) Evidence for leukemogenic effects of radiation in man at low dose rates. Health Physics 15:202

Stewart AM, Webb J, Giles D et al (1956) Malignant disease in childhood and diagnostic radiation *in utero*. Lancet 2:447

Stewart AM, Webb J, Hewitt D (1958) A survey of childhood malignancies. BMJ 1:1495–1508

Stewart AM, Kneale GW (1990) A-bomb radiation and evidence of late effects other than cancer. Health Physics 58:729–735

Thacker J, Cox R (1975) Mutation induction and inactivation in mammalian cells exposed to ionizing radiation. Nature 258:429–431

Thacker J, Stretch A, Stephens MA (1977) The induction of thioguanine-resistant mutants of Chinese hamster cells by γ-rays. Mutat Res 42:313–326

Thacker J, Wilkinson RE, Goodhead DT (1986) The induction of chromosome exchange aberrations by carbon ultrasoft X-rays in V79 hamster cells. Int J Radiat Biol 49:645–656

Todd P (1967) Heavy-ion irradiation of cultured human cells. Radiat Res Suppl 7:196–207

Tubiana M (1998) The report of the French Academy of Science: 'Problems associated with the effects of low doses of ionising radiations'. J Radiat Prot 18:243–248

Tubiana M (2000) Radiation risks in perspective: radiation-induced cancer among cancer risks. Radiat Environ Biophys 39:3–16

UNSCEAR (2000) Sources and effects of ionizing radiation. United Nations Scientific Committee on the Effects of Atomic Radiation Report to the General Assembly. United Nations, New York

Virsik RP, Schafer CH, Harder D et al (1980) Chromosome aberrations induced in human lymphocytes by ultrasoft Al-K and Cu X-rays. Int J Radiat Biol 38:545–557

Vivek Kumar PR, Mohankumar MN, Zareena Hamza V et al (2006) Dose-rate effect on the induction of *HPRT* mutants in Human G_0 lymphocytes exposed *in vitro* to gamma radiation. Radiat Res 165:43–50

Wakeford R, Doll R, Bithell JF (1997) Childhood cancer and intrauterine irradiation. In: Health effects of low dose radiation: challenges of the 21st century. British Nuclear Energy Society, London pp 114–119

Wakeford R (2005) Cancer risk among nuclear workers. J Radiat Prot 25:225–228

Wells RL, Bedford JS (1983) Dose-rate effects in mammalian cells IV: repairable and non-repairable damage in non-cycling C3H 10T1/2 cells. Radiat Res 94:105–134

The Cancer Risk from Low-Level Radiation

3

Bernard L. Cohen

CONTENTS

3.1 Introduction

It is commonly stated that "any radiation dose, no matter how small, can cause cancer." The basis for that statement is the linear no-threshold theory (LNT) of radiation carcinogenesis. According to LNT, if 1 Gy (100 rad) of exposure gives a cancer risk R, the risk from 0.01 Gy (1 rad) of exposure is $R/100$, the risk from 0.00001 Gy (1 mrad) is $R/100{,}000$, and so on. Thus the cancer risk is not zero regardless of how small the exposure.However, in recent years, a strong sentiment has developed in the community of radiation health scientists to regard risk estimates in the low-dose region based on LNT as being grossly exaggerated or completely negligible. For example, the 6000-member Health Physics Society, the principal organization for radiation protection scientists, issued a position paper (Health Physics Society 1996) stating "Below 10 rad … risks of health effects are either too small to be observed or are non-existent." A similar position statement was issued by American Nuclear Society. When the Health Physics Society Newsletter asked for submission of comments on the validity of LNT, there were about 20 negative comments submitted and only a single comment supportive of LNT. In a worldwide poll conducted by the principal on-line discussion group of radiation protection professionals (RADSAFE), the vote was 118 to 12 against LNT. A 2001 report by the French Academy of Medicine concluded that LNT is "without any scientific validity," and an elaborate joint study by the French Academy of Medicine and the French Academy of Sciences (Aurengo et al. 2005) strongly condemned the use of LNT. While U.S. official agencies have been slower to accept this position, the U.S. National Council on Radiation Protection and Measurements (NCRP) stated, in NCRP Publication No. 121 (NCRP 1995), "Few experimental studies and essentially no human data can be said to prove or even provide direct support for the [LNT] concept," and in NCRP Publication No.136 (NCRP 2001) it stated "It is important to note that the rates of cancer in most populations exposed to low level radiation have not been found to be detectably increased, and in most cases the rates appear to be decreased." A group of scientists opposing use of LNT (Radiation Science and Health) submitted several hundred papers supporting their position to National Research Council.

Beyond failure of LNT, there is substantial evidence that low-level radiation may be *protective* against cancer; a view known as "hormesis." There is an International Hormesis Society, which sponsors an annual International Scientific Conference

B. L. Cohen, MD
Department of Physics, University of Pittsburgh, 201-B Old Engineering Hall, Pittsburgh, PA 15260, USA

and publishes a peer-reviewed scientific journal and a regular newsletter.

The purpose of this paper is to review the basis for LNT and to present some of the mostly recent information that has caused this strong shift in sentiment. Other recent reviews have been published with somewhat different approaches to similar objectives (Feinendegen 2005a, 2005b; Tubiana and Aurengo 2005).

3.2 Problems with the Basis of the Linear No-Threshold Theory

The original basis of LNT, as that theory emerged in the mid twentieth century, was theoretical and very simple. A single particle of radiation hitting a single deoxyribonucleic acid (DNA) molecule in a single cell nucleus of the human body can initiate a cancer. The probability of such a cancer initiation is therefore proportional to the number of such hits, which is proportional to the number of particles of radiation, which is proportional to the dose. Thus the risk is proportional to the dose – this is linear no-threshold theory.

An important problem with this simple argument is that factors other than initiating events affect the cancer risk. Human bodies have biological defense mechanisms which prevent the vast majority of initiating events from developing into a fatal cancer (Pollycove and Feinendagen 2001). A list of some of the most important examples, including how they are affected by low-level radiation, follows (Feinendegen 2005a):

- Our bodies produce repair enzymes which repair DNA damage with high efficiency, and low-level radiation stimulates production of these repair enzymes.
- Apoptosis, a process by which damaged cells "commit suicide" to avoid extending the effects of the damage, is stimulated by low-level radiation. A similar effect is achieved by premature differentiation and maturation to senescence.
- The immune system is important for preventing mutations from developing into a cancer; there is abundant evidence that low-level radiation stimulates the immune system, but high radiation levels depress it.
- Corrosive chemicals are the overwhelmingly most important cause of DNA damage (reactive oxygen species, ROS); there are processes for scavenging these out of cells, and low-level radiation stimulates these scavenging processes (Kondo 1993). Elevated ROS levels have been shown to initiate a broad array of biochemical reactions that are stress responses, leading to the conclusion that "the best protection against stress is stress itself" (Finkel and Holbrook 2000).
- Radiation can alter cell cycle timing. This can extend the time before the next cell division (mitosis). Damage repair is most effective before the next mitosis, so changing this available time can be important (M Elkind, personal communication). Altered cell timing can also affect DNA repair processes in many ways by changing chemical processes (Boothman et al. 1996).
- Various other effects of low-level radiation on cell survival have been observed and are referred to as "low dose hypersensitivity," "increased radiation radioresistance," and "death-inducing effects" (Bonner 2004).

It is now recognized that development of cancer is a much more complex process than was originally envisioned. The role of "bystander effects," signaling between neighboring cells relevant to their radiation experiences, is now recognized to be an important, albeit poorly understood, factor. In fact it seems that the tissue response, and even the whole organ response, rather than just the cellular response, must be considered (Aurengo et al. 2005).

There is also apparently obvious evidence for the failure of the original simple model. For example, the number of initiating events is roughly proportional to the mass of the animal – more DNA targets mean more hits. Thus the simple theory predicts that the cancer risk should be approximately proportional to the mass of the animal. But the cancer risk in a given radiation field for a 30-g mouse is similar to that for a 70,000-g human. As another example, our very definition of dose (based on the energy absorbed per unit mass of tissue, which is proportional to the number of radiation hits per unit target mass) would be misleading if only the total number of hits (which is proportional to the number of initiating events) were relevant regardless of the target mass.

A detailed theoretical approach to evaluating the validity of LNT is based on the commonly accepted idea that double strand breaks (DSB) in DNA molecules are the principal initiating event in causing cancer. But DSB are also caused by endogenous

corrosive chemicals, ROS. In fact the DNA damage caused by radiation is mostly due to the production of ROS by the ionizing effects of the radiation on omnipresent water. It is estimated that endogenous ROS causes about 0.1 DSB per cell per day, whereas 100 mSv (10 rem) of radiation, which is close to the upper limit of what is normally called low-level radiation, causes about 4 DSB per cell (Feinendegen 2005a). Assuming that the number of cancers is proportional to the number of DSB, a 100-mSv dose of radiation would increase the lifetime (28,000 days × 0.1 DSB/day) risk of cancer by only about (4/2800=) 0.14%, whereas LNT predicts an increase of 1%. From this it is concluded that the underlying assumption of LNT, namely that cancer-initiating events are the controlling factor in determining the dose–response relationship for radiation, is a serious over-simplification.

Sophisticated experimental techniques have been developed for observing the effects of a single alpha particle hitting a single cell. It was found (Miller et al. 1999) that the probability for transformation to malignancy from *N* particle hits on a cell is much greater than *N* times the probability for transformation to malignancy from a single hit. This is a direct violation of LNT, indicating that estimated effects based on extrapolating the risk from high exposure, represented by *N* hits, greatly exaggerates the risk from low-level exposure as represented by a single hit.

A very clear demonstration of a threshold response, in contrast to LNT, was found in tumor induction by irradiation of mouse skin throughout life (Tanooka 2001). For irradiation rates of 1.5 Gy/week, 2.2 Gy/week, and 3 Gy/week, the percentages of mice that developed tumors were 0%, 35%, and 100% respectively.

3.3 Direct Experimental Challenges to the Basis for LNT

A direct demonstration of the failure of the basis for LNT derives from microarray studies determining which genes are upregulated and which are downregulated by radiation. It is found that generally low-level radiation affects a different set of genes than high-level radiation. For example, in one study of mouse brain (Yin et al. 2003), 191 genes were affected by a dose of 0.1 Sv but not by a dose of 2.0 Sv, 213 genes were affected by 2.0 Sv but not by 0.1 Sv, while 299 genes were affected by both doses. The 0.1-Sv dose induced the expression of genes involved in protective and repair functions while down-modulating genes involved in unrelated processes.

A similar study with even lower doses on human fibroblast cells (Golder-Novoselsky et al. 2002) found that a dose of 0.02 Sv caused more than 100 genes to change their expression, and these were generally different than the genes affected by 0.5 Sv. The former group was heavily weighted by stress response genes.

Several other microarray studies have shown that high radiation doses, which serve as the calibration for application of LNT, are not equivalent to an accumulation of low radiation doses (Tubiana and Aurengo 2005).

3.4 Effects of Low-Level Radiation on Biological Defense Mechanisms

3.4.1 Adaptive Response

An important type of biological defense mechanism is known as the "adaptive response" (UNSCEAR 1994) – exposing a cell to a stress such as radiation stimulates the natural defense against such stresses and hence protects against subsequent further stresses. On an experimental basis, this is most easily studied by exposing cells to a low dose to prime the adaptive response, and then later, upon exposing it to a high radiation "challenge dose," the adaptive response is observed as a reduced effect of the challenge dose in comparison with a similar challenge exposure without the priming dose.

The most widely studied examples have involved observations on chromosome aberrations, perhaps the simplest tool for detecting genetic damage. It has long been recognized that radiation increases the number of these aberrations. However, an in vitro study on human lymphocyte cells (Shadley and Dai 1992) shows, in Table 3.1, how that process is affected if the high dose is preceded a few hours before by a low dose. We see that the number of chromosome aberrations caused by the high dose

Table 3.1. Effects of pre-exposure to 5 cGy on two types of chromosome aberrations in human lymphocyte cells, induced by 400 cGy of X-rays 6 h later (Shadley and Dai

	Dicentrics and rings		Deletions	
Donor	400 cGy	(5 + 400) cGy	400 cGy	(5+400) cGy
1	136	92	52	51
2	178	120	62	46
3	79	50	39	15
4	172	42	46	34
5	134	106	58	41

is substantially reduced. This is an example of the adaptive response.

As an example of an in vivo experiment (Cai and Liu 1990), it was found that exposure of mouse cells to 65 cGy (65 rad) caused chromosome aberrations in 38% of bone marrow cells and in 12.6% of spermatocytes, but if these exposures are preceded 3 h earlier by an exposure to 0.2 cGy, these percentages are reduced to 19.5% and 8.4% respectively. There are many other examples of such experiments, both in vitro and in vivo (UNSCEAR 1994), and the results are usually explained as stimulated production of repair enzymes by low-level radiation.

The effects of the adaptive response in protecting against chromosome aberrations were observed for in-vivo human exposures in comparing residents of a high background radiation area (1 cGy/year) and a normal background radiation area (0.1 cGy/year) in Iran (Ghiassi-nejad et al. 2002). When lymphocytes from these groups were exposed to 1.5 Gy (150 rad), the mean frequency of chromosome aberrations per cell was 0.098±0.012 for the high background area versus 0.176±0.017 for the low background area, a difference of 4 standard deviations. Presumably the adaptive response induced by radiation in the high background area protected its citizens against chromosome aberrations induced by the 1.5-Gy dose.

A microarray study on human lymphoblastoid cells (Coleman et al. 2005) was carried out to investigate the processes involved in the adaptive response. A 0.05-Sv priming dose was followed by a 2.0-Sv challenge dose, and adaptive response was measured by the reduction of chromosome aberrations; the goal was to identify genes involved in the adaptive response and determine how their states of activation are affected by the priming dose. It reported that 145 genes were affected by the priming dose, generally upregulated for protein synthesis – a key element in DNA repair – and downregulated for metabolic and signal transduction, perhaps as a means to conserve resources for devotion to DNA repair. Many genes associated with DNA repair, stress response, cell cycle control, and apoptosis were strongly affected by the priming dose. The specifics of the process were found to be highly complex and sometimes pointing in different directions; for example, the TP53 gene, which can act as either a tumor promoter or a tumor suppressor, plays an important but not clearly defined role.

Apart from studies using chromosome aberrations, another type of experiment that reveals the effects of the "adaptive response" involves detection of genetic mutations. As an example of an in vitro experiment (Kelsey et al. 1991), it was found that an X-ray exposure of human lymphocytes to 300 cGy induced a frequency of mutations at the *hprt* locus of 15.5×10^{-6}, but if this large exposure was preceded 16 h earlier by an exposure of 1 cGy, this frequency was reduced to 5.2×10^{-6}.

As an in vivo example (Fritz-Niggli and Schaeppi-Buechi 1991), it was found that the percentage of dominant lethal mutations in offspring resulting from exposures of female *Drosophila* to 200 cGy of X-rays before mating was substantially reduced by preceding this high dose with an exposure to 2 cGy; for different strains of *Drosophila* and different oocyte maturities these percentages were reduced from 42% to 27%, from 11% to 4.5%, from 40% to 36%, from 32% to 12.5%, from 42% to 30%, and from 51% to 22%.

A technique has been developed for directly observing repair of DNA base damage (Le et al. 1998). It was found that preceding an exposure to 2 Gy of gamma radiation with 0.25 Gy 4 h beforehand reduced the time for 50% DNA lesion removal from 100 min to 50 min. The progression of the repair over time is shown in Figure 3.1 with and without the 0.25-Gy priming dose.

From the types of data discussed above, one might consider the possibility that the adaptive response is only effective in protecting against damage caused by subsequent large doses of radiation. But there are data on its effectiveness against spontaneous transformation to malignancy in cells with a predisposition to such transformation. This was shown (Azzam et al. 1996) for exposures of C3H 10T1/2 mouse cells, where 1 day after exposure to low doses of radiation the rate of *spontaneous* neoplastic transformation was reduced by 78%. In a similar experiment (Redpath and Antoniono 1998) with human HeLa

x skin fibroblast cells, the reduction was by 55%. The dependence on dose for this cell type is shown in Figure 3.2 (Redpath et al. 2003) with error bars indicating 95% confidence intervals. We see there that the effect is statistically indisputable even at very low doses, below 1 cGy.

The question has been raised as to how long the adaptive response persists following a priming dose. In one in vivo experiment (Zaichkina et al. 2003) measuring chromosome damage in bone marrow cells of mice, both spontaneously and by a challenge dose, the adaptive response was found after 1, 3, 6, 9, and 12 months following priming doses of 0.1 and 0.2 Gy, and the protection against spontaneous damage persisted to the end of life (20 months).

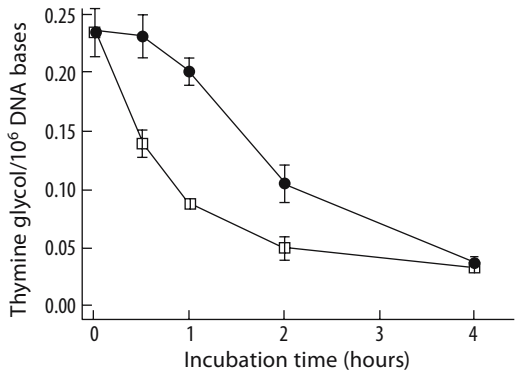

Fig. 3.1. Comparison of removal of thymine glycol by A549 cells after 2 Gy irradiation, with (*open squares*) or without (*shaded circles*) a 0.25-Gy priming dose given 4 h before (Le et al. 1998)

This adaptive response protection against spontaneous development of cancer may be understood from the effects of radiation on corrosive chemicals (ROS). Since ROS is the dominant cause of spontaneous cancers through initiating DNA damage, reducing the amount of ROS and increasing the amount of antioxidants that scavenge them out of cells is protective against development of spontaneous cancers. The results of a study of these on rat cells (Yamaoka 1991) are shown in Figure 3.3. We see there that 50 cGy of X-ray exposure decreases the amount of the oxidant lipid peroxide by about 20%, and increases the amount of the antioxidant superoxide dismutase (SOD) by about 25%, and that these beneficial effects are appreciable over the entire dose range up to above 100 cGy. Many other studies with similar results have been summarized and extended in a recent report (Yukawa et al. 2005).

3.4.2 Stimulation of the Immune System

Since the immune system destroys cells with persistent DNA damage and is thus important in protecting against the development of cancer, the effects of low-level radiation on it are relevant here. Such effects on several different measures of the immune response (Liu 1992) are listed in Table 3.2. We see that by each of these measures, the immune response is increased by low-level radiation, and increasingly so at least up to 7.5 cSv.

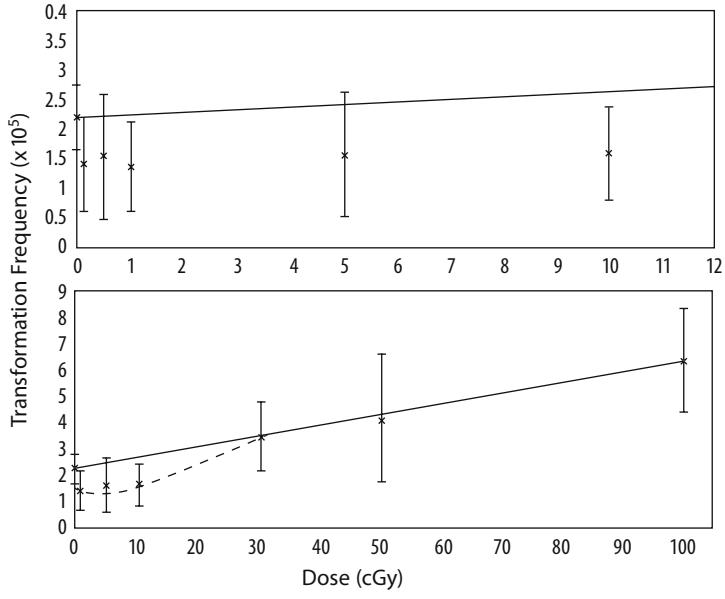

Fig. 3.2. Transformations per surviving cell as a function of dose for HeLa x skin fibroblast human hybrid cells irradiated with gamma rays (Redpath et al. 2003). Upper plot is of same data on an expanded scale. *Error bars* represent 95% confidence limits

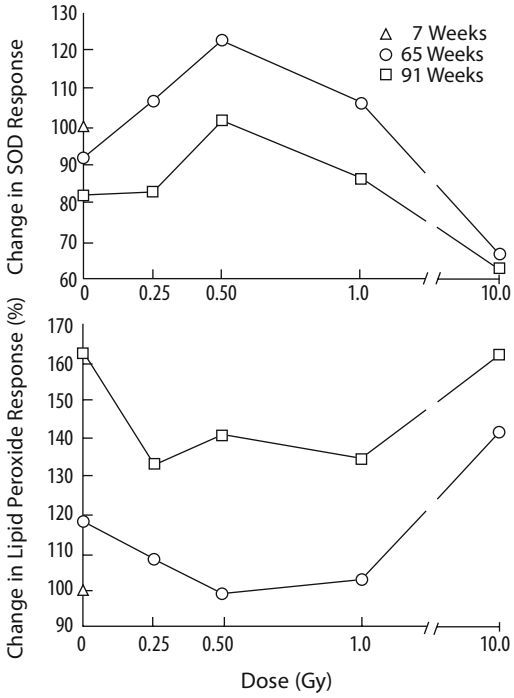

Fig. 3.3. Antioxidant superoxide dismutase (SOD) and lipid peroxide response to age and radiation of rat brain cortex (Yamaoka 1991)

Table 3.2. Effects of radiation on immune response. Different columns give the percentage response to various tests in unexposed mice, to response in mice exposed as indicated (Liu 1992). (*ADCC*, Antibody-dependent cell-mediated cytotoxicity, which assists NK activity; *Con A*, concanavalin-A, lectin that stimulates T-lymphocytes; *MLC*, mixed lymphocyte culture, used as a test of T-cell function; *NK*, natural killer cells which recognize and kill tumor cells; *PFC*, plaque-forming cell)

Test	Dose (cGy)		
	2.5	5	7.5
PFC reaction	110	143	174
MLC reaction	109	133	122
Reaction to Con A	191	155	530
NK activity	112	109	119
ADCC activity	109	128	132

The results of one study of this effect over a wide range of radiation doses (Makinodan and James 1990) is shown in Figure 3.4. We see there increases in the immune response by 80% in vitro and by 40% in vivo at about 20 cGy followed by a rapid decrease to well below the unirradiated level at doses above 50 cGy.

In a review (Liu 2003) of extensive mouse studies utilizing about 10 levels of whole-body radiation exposure, the effects on 52 immunologic parameters were analyzed to determine dose–response curves for 2 categories of these parameters. The first category included 20 parameters that would lead to decreased immune system activity, for which the results are shown in the upper part of Figure 3.5; the second category included the remaining 32 parameters that would lead to increased immune system activity, for which the results are shown in the lower part of Figure 3.5. We see from Figure 3.5 that low doses downregulate the parameters indicative of decreased immune system activity, and that these low doses upregulate parameters indicative of increased immune activity. In both cases, these effects are reversed for high-level radiation exposure. The conclusion is that low-level radiation increases immune system activity and high-level exposures reduce immune system activity, in agreement with what is seen in Figure 3.4.

Contrary to expectations from the basic assumption of LNT that the cancer risk depends only on total dose, effects on the immune system are very different for the same total dose given at a low dose rate versus a high dose rate. In a study of effects on various indicators of the immune response in several wild-type mouse strains (Ina and Sakai 2005), continuous whole-body irradiation at 1.2 mGy per hour stimulated the immune response as shown for a few example indicators in Figure 3.6, but the same doses given at a high rate had the opposite effect.

Further information on the dose rate dependence was reported in a mouse study of thymic lymphomas (Ina et al. 2005). Acute challenge doses totaling 7.2 Gy induced tumors in 90% of the mice, but if the mice were previously exposed at a rate of 1.2 mGy per hour for 258 days (a total of 7.2 Gy) prior to the 7.2-Gy challenging dose, only 43% developed such tumors – this may seem like an extreme case of adaptive response, although the priming dose is equal to the challenge dose and doubling the total dose resulted in far fewer tumors. But most significantly for the present discussion, the low dose rate exposure, even extended to 450 days for a total exposure of 12.6 Gy, resulted in no tumors without a challenging dose. Various indicators of immune response were significantly increased by the continuous whole-body radiation, and the authors attribute their observations to stimulation of the immune system by this radiation.

Several studies have shown that the immune system provides resistance to metastasis of tumors; one

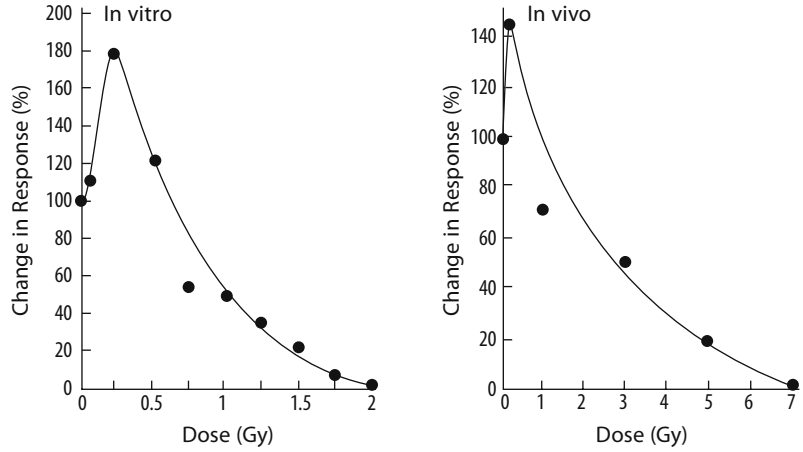

Fig. 3.4. Immune system response to radiation. Mouse splenic cells primed with antigenic sheep red blood cells (Makinodan and James 1996)

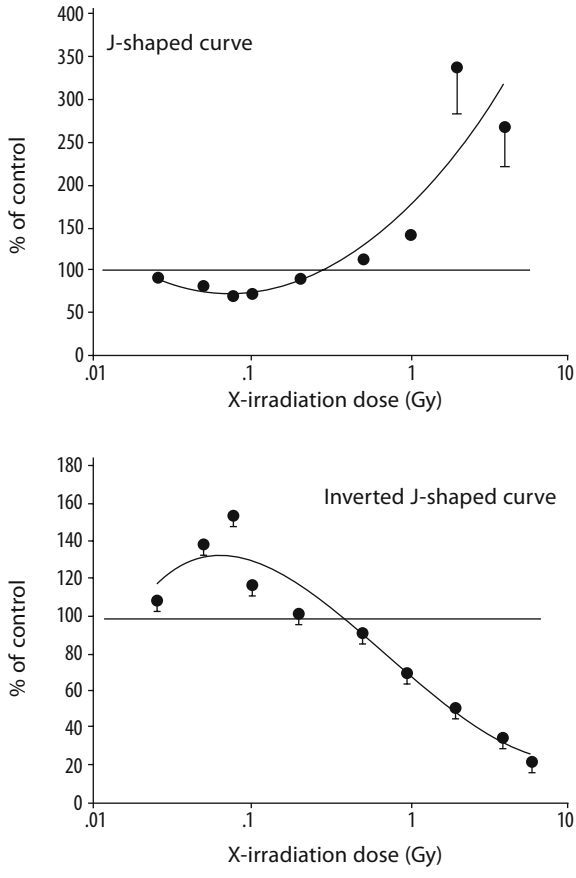

Fig. 3.5. Dose–response curves constructed from multiple parameters of the immune system following whole body irradiation of C57BL/6 and Kunming mice (Liu 2003). *Upper figure* is for 20 parameters that lead to decreased immune system activity, and *lower figure* is for 32 parameters that lead to increased immune system activity

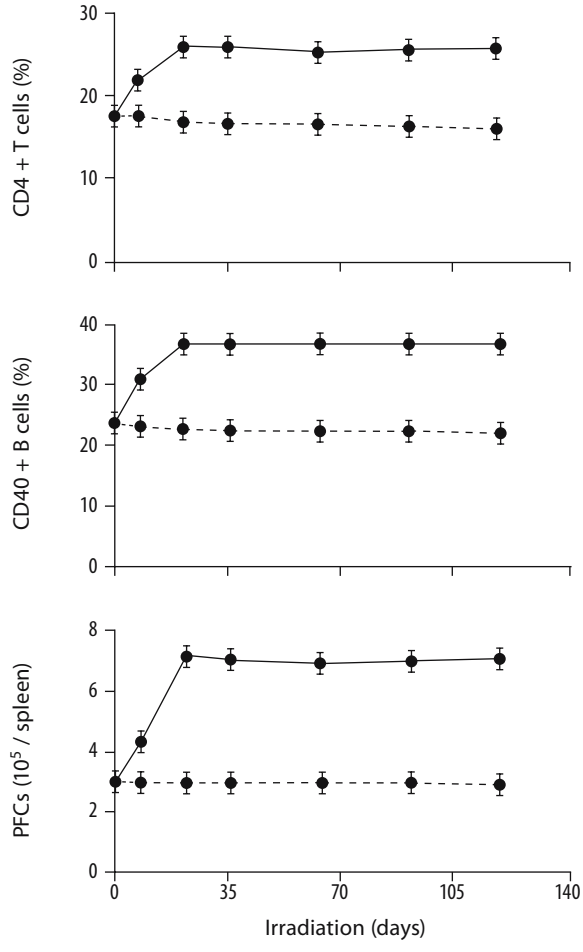

Fig. 3.6. Solid lines show activation by continuous low-dose-rate γ irradiation at 1.2 mGy h^{-1} from 5 weeks of age, of three different immune cell populations in the spleens of C57BL/6 mice challenged intraperitoneally by SRBC; data are plotted as a function of irradiation time. *Dashed lines* are the same for un-irradiated control mice (Ina and Sakai 2005)

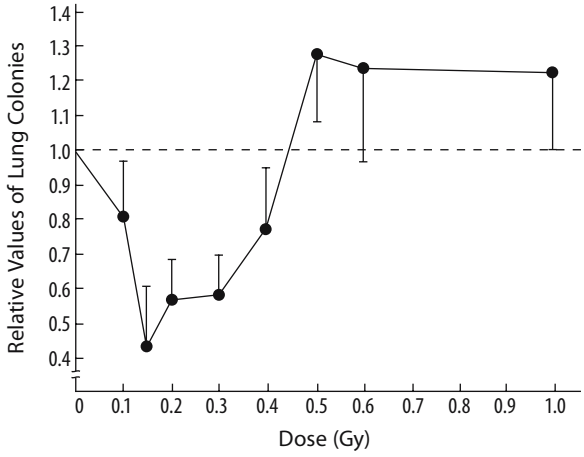

Fig. 3.7. Spontaneous lung metastases after total body irradiation of mice, given 12 days after tumor transplantation into the groin (Sakamoto et al. 1997)

example is shown in Figure 3.7. When tumor cells are transplanted into the groin of mice, the rate of their metastasis into the lung is cut about in half by total body irradiation with 15–30 cGy 12 days after the transplantation (Sakamoto et al. 1997). Doses above 50 cGy, on the other hand, reduce the immune response, leading to increased rates of metastasis. A study in rats (Hashimoto et al. 1999) showed that total body irradiation – but not tumor irradiation – with low-level radiation reduces the rate of metastasis and increases infiltration into the tumor of immune system agents (Makinodan and James 1990).

Studies on naturally cancer-prone mice (Mitchel et al. 2003) found that, while low-level radiation exposure does not prevent the eventual development of cancer, it delays the process substantially. Total body irradiation with low-level radiation has also been shown to reduce tumor size (Anderson 1992; Makinodan 1992). The only reasonable explanation for such effects of total body low-level radiation would seem to be stimulation of the body's immune system.

3.5 Cancer Risk Versus Dose in Animal Experiments

There have been numerous direct studies of cancer risk versus dose, testing the validity of LNT, with animals exposed to various radiation doses. An example was a series of external gamma ray exposure studies at Oak Ridge National Laboratory, for which one result (Ullrich and Storer 1979) is shown in Figure 3.8; we see there clear evidence for failure of LNT in the low dose region. In those experiments, exposed animals lived considerably longer (up to 40%) than their controls. Another example was a series of animal studies at Argonne National Laboratory in the 1950s and 1960s with injection of radioactive materials; these are reviewed by Finkel and Biskis (1962, 1969). The results of one of these studies, for bone cancers in mice injected with radioactive isotopes of calcium and strontium (Finkel and Biskis 1968), are shown in Figure 3.9. Nearly all of these studies indicate, with high statistical significance, that LNT theory overestimates the cancer risk from low-level radiation, generally suggesting a threshold.

A review of over 100 such experiments (Duport 2001) involved a total of 85,000 exposed animals with their 45,000 corresponding controls, with a total of 60,000 and 12,000 cancers in exposed and control animals, respectively. In cases where cancers were observed in control animals, either no effect or an apparent reduction in cancer risk was observed in 40% of the data sets for neutron exposure, 50% of the data sets for X-rays, 53% of the data sets for gamma rays, and 61% of the data sets for alpha particles.

3.6 Cancer Risk Versus Dose: Data from Human Exposures

3.6.1 Data Cited as Supportive of LNT

The principal data that have been cited by those in influential positions to support LNT are those for solid tumors (all cancers except leukemia) among the Japanese A-bomb survivors. The data up to 1990 (Pierce et al. 1996) are shown in Figure 3.10, where the error bars represent 95% confidence limits (2 standard deviations). If error bars are ignored, the points do indeed suggest a linear relationship with intercept near zero dose.

But the data themselves give no statistically significant indication of excess cancers for doses below about 25 cSv. This conclusion applies to the incidence data as well as to the mortality data (Heidenreich

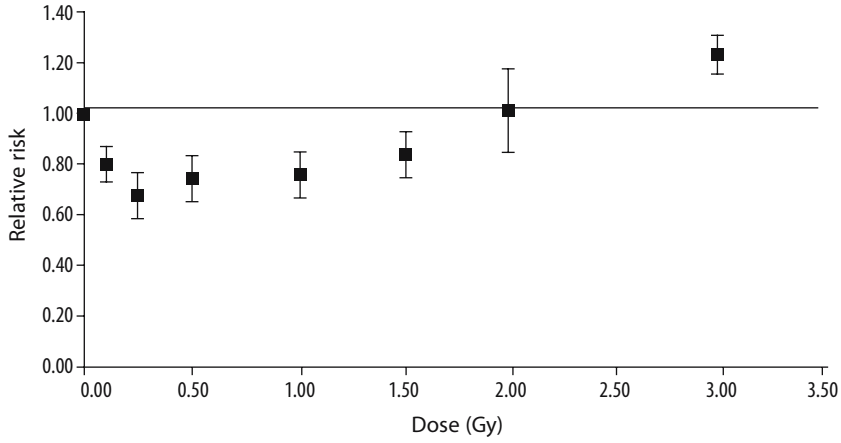

Fig. 3.8. Relative risk of lung cancer in mice following gamma ray exposure (Ullrich and Storer 1979)

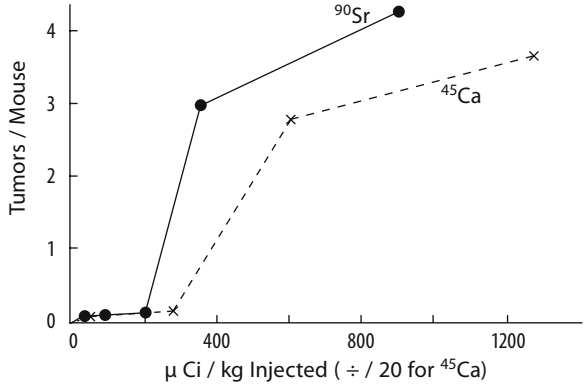

Fig. 3.9. Osteogenic sarcomas produced in CF1 female mice by injection of ^{90}Sr and ^{45}Ca at age 70 days (Finkel and Biskis 1968). ^{90}Sr experiments used 810 mice and 150 controls; results for 1.3, 4.5, and 20 μCi/kg, not shown on the plot, had ordinate values zero

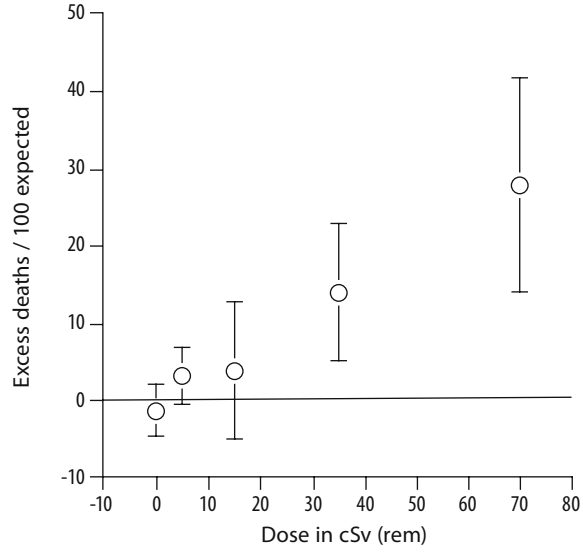

Fig. 3.10. Excess deaths from solid tumors per 100 "expected" among Japanese A-bomb survivors (1950–1990) versus their dose (Pierce et al. 1996). *Error bars* are 95% confidence limits

et al. 1997). In fact, it was shown (Cohen 1998) that considering the three lowest dose points alone (i.e., up to 20 cSv), the slope of the dose–response curve has a 20% probability of being negative (risk decreasing with increasing dose). A recent update (Preston et al. 2004) of the data on A-bomb survivors has been published but with insufficient detail to repeat the above analysis. A crude preliminary analysis indicates that the above conclusions will not be appreciably changed.

The data on leukemia among A-bomb survivors (Pierce et al. 1996) are shown in Figure 3.11, with error bars indicating 95% confidence limits. These data strongly suggest a threshold above 20 cSv, and this difference from LNT expectations is recognized by the authors and by all widely recognized reviews.

The IARC (International Association for Research on Cancer) studies of monitored radiation workers provide the principal other evidence that has been widely cited as supporting LNT. The first and most fully reported (Cardis et al. 1995) was a study of 95,673 monitored radiation workers in US, UK, and Canada. For all cancers except leukemia, there were 3,830 deaths but *no excess* over the number expected. The risk is reported as –0.07/Sv with 90% confidence limits (–04 , +0.3). There is surely no support for LNT here.

However, for the 146 leukemia deaths, they did report a positive risk versus dose relationship and

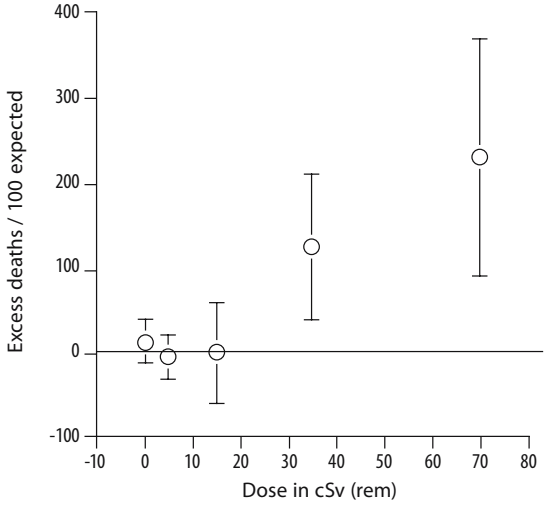

Fig. 3.11. Excess deaths from leukemia per 100 "expected" among Japanese A-bomb survivors (1950–1990) versus their dose (Pierce et al. 1996). *Error bars* are 95% confidence limits

Table 3.3. Leukemia deaths from International Association for Research on Cancer (IARC) Study (Cardis et al. 1995). The *final column* is the ratio of observed to expected, *O/E*

Dose (cSv)	Observed	Expected	O/E
0–1	72	75.7	0.95
1–2	23	21.2	1.08
2–5	20	21.8	0.92
5–10	12	11.3	1.06
10–20	9	7.8	1.15
20–40	4	5.5	0.73
>40	6	2.6	2.3

vociferously claimed that this supports LNT. Their data are listed in Table 3.3. It is obvious from those data that there is no indication of any excess risk below 40 cSv (even the excess for >40 cSv is by only 1.4 standard deviations). The conclusion by the authors that this supports LNT is based on an analysis which arbitrarily discards the data in Table 3.3 for which o/e (observed/expected) is less than unity! They thus arbitrarily discard three of the seven data points.

A follow-up study by the same group involved 407,000 monitored workers in 154 facilities spread through 15 countries, and reported results only as excess risk per Sv, assuming LNT. Thus a data display similar to that in Table 3.3 cannot be given here, but since the lead author is the same, it seems reasonable to assume that similar questionable procedures were used. No information on smoking status, an important risk factor for cancer, was collected. There was no consideration given to non-occupational exposure; the average occupational exposure was 2 cSv and 90% were below 5 cSv, whereas the average person is exposed throughout life to about 25 cSv of non-occupational radiation with large variations, typically at least 10 cSv, depending on geography and medical treatment. Thus the "signal" is very much smaller than the noise, making any conclusions about validity of LNT highly debatable. Another weakness is that most of the data were derived from photographic film badges which are sensitive to humidity and temperature; the films were handled differently in the 15 different countries (and also frequently by different organizations in the same country) which reduces the reliability of the results. There are other inherent problems in combining data from many different sources such as differences in ethnicity and socioeconomic status. If the data from just one of the 15 countries, Canada, are excluded, the excess risk is no longer statistically different from zero.

Many other studies have been reported on cancer risk versus dose for such normal occupational exposures. In response to heavy media coverage of some non-scientific reporting, a $10 million study (Matanoski 1991) was sponsored by the US Center for Disease Control and Prevention of workers in eight US Navy shipyards involved in servicing nuclear-propelled ships. The study included 28,000 exposed workers and 33,000 age- and job-matched controls who worked on non-nuclear ships. The former group all had exposures above 0.5 cSv and average exposures of 5 cSv. The cancer mortality rate for the exposed was only 85% of that for the unexposed, a difference of nearly two standard deviations. Hiring procedures, medical surveillance, job type, and other factors were the same for both groups, so the often used explanation of "healthy worker effect" does not apply here – the study was specifically designed to eliminate that factor. The issue of non-occupational exposure was not addressed, but there was a high degree of homogeneity among the different worker groups being compared.

More discussion of "healthy worker effect" may be appropriate here. In studies comparing mortality rates among employed workers with those for the general population, it is invariably found that employed workers have lower mortality, and it is widely understood that this results from the fact that unemployed persons may be unemployed because of

health problems which lead to their earlier demise. However it has been pointed out (Monson 1986) that healthy worker effect should not apply to cancers occurring long after their initial employment because health problems leading to such cancers would not be apparent in a pre-employment medical exam. A direct test of this in Sweden (Gridley et al. 1999) comparing 545,000 employed women with 1,600,000 unemployed women found that the standardized cancer incidence rate for employed women was 1.05 (1.04–1.06) times higher than for the unemployed women. This would certainly seem to eliminate healthy worker effects for cancer.

Several other studies of cancer rates among people whose employment involves radiation exposure have been published:

- Studies of British radiologists compared with other British medical practitioners (Berrington et al. 2001) found that radiologists who began work in earlier years, when radiation exposure restrictions were much looser than recent standards, did experience excess cancers. But among the most recent cohort, radiologists who began work between 1955 and 1979, cancer mortality was only 0.71 (95% confidence limits, 0.49–1.00) times that of other medical practitioners who presumably had considerably lower radiation exposures.
- A study of medical X-ray workers in China (Wang et al. 2002) used cancer incidence rather than mortality, and a comparison group of workers in the same hospitals who were not involved with X-rays. The relative risks for earlier workers whose average exposure was 55 cGy were 2.4 for leukemias and 1.2 for solid cancers, while for the more recent workers whose average exposure was only 8.2 cGy, these risks were 1.73 for leukemias (based on 11 cases) and 1.06 (based on 232 cases) for solid cancers. For the recent workers, the differences from 1.0 are not statistically significant.
- A US study of 146,000 radiologic technologists (Mohan et al. 2003) used only the total US population as a comparison group and reported an SMR of 0.82 for all cancers, but a statistically significant increase among those first employed before 1940 as compared with those who began work after 1960.
- A review of studies of 8 cohorts of radiologists and radiological technologists in various countries, comprising 270,000 monitored radiation workers (Yoshinaga et al. 2004), concluded that there was good evidence for excess cancers among the early workers, but no such evidence among more recent workers.
- A study of 22,000 monitored workers in the French nuclear power industry (Rogel et al. 2005) found that the cancer mortality rate was only 0.58 (90% confidence interval 0.49–0.68) times that for the general population of France. The authors attribute this to healthy worker effect, but such an explanation seems to be an extreme "stretch" for explaining such a large effect. There was no evidence for increased cancer as a function of increasing radiation exposure.

Perhaps the most reasonable conclusion from studies of normally exposed radiation workers is that they give no conclusive information on effects of low-level radiation. There is as much information suggesting zero or negative risk as information indicating the increased risk claimed by the IARC study. In any case, the fact that the monitored radiation received by the subjects was much lower than their non-occupational unmonitored exposures, make these data inherently of marginal significance.

3.6.2 Data Contradictory to LNT

There are substantial statistically robust human data contradictory to LNT. One example is for breast cancer among Canadian women exposed to frequent X-ray fluoroscopic examinations in a tuberculosis sanatorium (Miller et al. 1989); the data for them are shown in Figure 3.12. While the

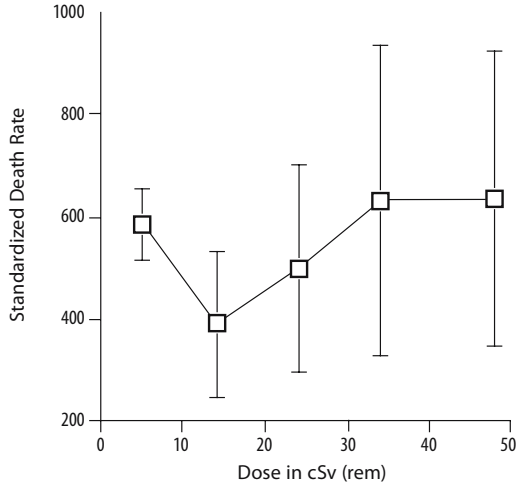

Fig. 3.12. Standardized death rates per million person-years from breast cancer among Canadian women after irradiation in fluoroscopic examinations versus their radiation dose (Miller et al. 1989). *Error bars* are 95% confidence limits

statistical uncertainties are substantial, there seems to be a decrease in risk with increasing dose at least up to about 25 cSv.

The data on lung cancer among these Canadian women (Howe 1995), and also a one point study of 10,000 individuals in Massachusetts (Davis et al. 1989) are shown in Figure 3.13. Here again we see a decrease in the low dose region, in this case extending at least up to 100 cSv. In Figure 3.13, these data are compared with lung cancer data for the Japanese A-bomb survivors, and we see there a difference between the two data sets that is clearly statistically significant: the A-bomb survivor data give a much higher risk at all doses. This is probably explained by the difference between the very high dose rate to the A-bomb survivors and the low dose rate from protracted fluoroscopic exams extending over many weeks. In any case, Figure 3.13 must make one pause before accepting the widely practiced approach of using A-bomb survivor data to predict risks from low dose rate low-level radiation. Other arguments confirming the importance of dose rate, rather than only of total dose, have been expounded elsewhere (Tubiana and Aurengo 2005).

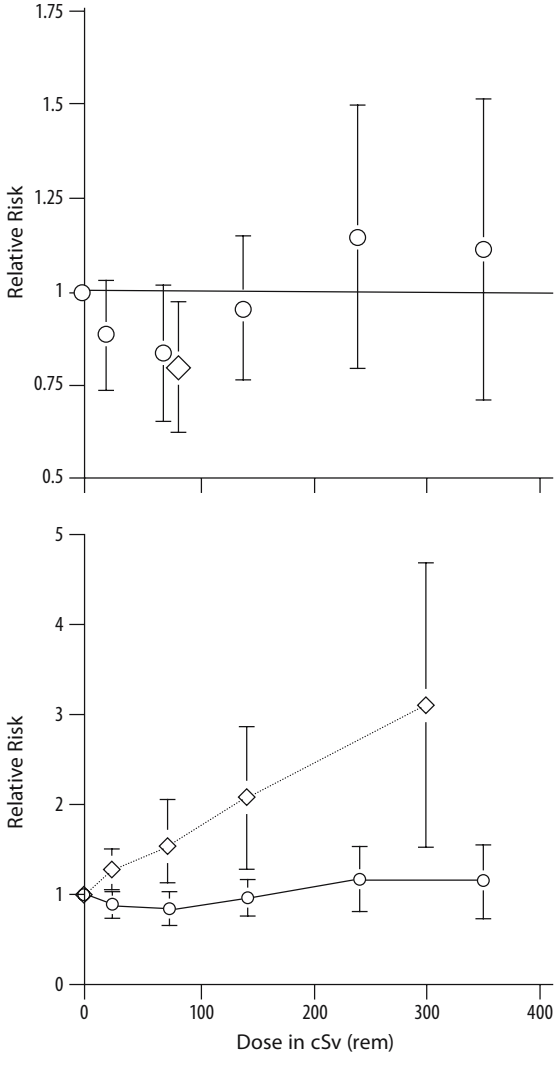

Fig. 3.13. Relative risk of mortality from lung cancer versus dose to lung, with 95% confidence limits. In *upper figure* with *expanded vertical scale*, *circles* are from Howe (1995) and *diamond* is from Davis et al. (1989). In the *lower figure* (Howe 1995), the *solid line* connects data from Canadian fluoroscopy patients, and the *dotted line* connects data from A-bomb survivors

In 1957, there was an explosion in an incredibly mismanaged radioactive waste storage facility at the former USSR Mayak nuclear weapons complex in the Eastern Urals of Siberia, causing large radiation exposures to people in nearby villages. A follow-up on 7852 of these villagers (Kostyuchenko and Krestina 1994) found that the rate of subsequent cancer mortality was much lower among these than among unexposed villagers in the same area. The ratio for exposed to unexposed was 0.73±0.07 for 4 cGy, 0.61±0.07 for 12 cGy, and 0.72±0.12 for 50 cGy (here, ± indicates one standard deviation).

Studies are underway on the workers at this Mayak complex (Koshurnikova et al. 2002), among whom there have been many excess cancers, but exposures were generally quite high and the data reported give little information on the dose–response relationship in the low-dose region.

Stimulation of the immune system by low-level radiation is being used on an experimental basis for medical treatment of non-Hodgkin's lymphoma with total body and half body (trunk only) irradiation. This radiation was administered to one group of patients ("irradiated" group), but not to an otherwise similar "control" group, before both groups were given similar other standard treatments such as chemotherapy with or without accompanying high radiation doses to tumors. In one such study (Sakamoto et al. 1997), after 9 years, 50% of the control group, but only 16% of the irradiated group had died. In a 25-year-old study (Chaffey et al. 1976) with different standard treatment, 4-year survival was 70% for the irradiated group versus 40% for the controls. In another study in that time period (Choi et al. 1979) with a more advanced chemotherapy, 4-year survival was 74% for the irradiated group versus 52% for the control group. The information in the scientific literature is very supportive of using whole body or half body low-level radiation

to stimulate the immune system. US physicians have not utilized it but further applications are underway in Japan.

The above described data deal with radiation by X-rays and gamma rays (and some neutrons for the A-bomb survivors). There are also impressive relevant data from radiation with alpha particles. One such study is of bone and head cancers among dial painters, chemists, and others occupationally exposed to ingested radium (Evans 1974). There were no tumors among those with exposures below 1,000 cGy, but for dose ranges centered about 1800, 3500, 7500, and 20,000 cGy, 25%–38% in each category developed tumors. Elaborate analyses of these data show that a linear no-threshold fit is statistically unsupportable and a threshold behavior is strongly suggested.

Several studies have reported that workers who inhaled plutonium, resulting in sizable radiation exposures to their lungs, have equal or lower lung cancer mortality rates than those not so-exposed (Tokarskaya et al. 1997; Voelt et al. 1983; Gilbert et al. 1989).

Very strong evidence against LNT is provided by a very extensive study of lung cancer mortality rates, *m*, versus average radon exposure in homes for 1729 US counties – more than half of all US counties, and including 90% of the US population (Cohen 1995, 2006). Plots of age-adjusted rates are shown in Figure 3.14a, c, where, rather than showing individual points for each county, these are grouped into intervals of radon exposure (shown on the baseline along with the number of counties in each group) and plotted as the mean value of *m* for each group, its standard deviation indicated by the error bars, and the first and third quartiles of the distribution. Figure 3.14b, d shows these data corrected for prevalence of cigarette smoking. Note that when there is a large number of counties in an interval, the standard deviation of the mean is quite small. We see, in Figure 3.14, a clear tendency for lung cancer rates, with or without correction for smoking prevalence, to *de*crease with increasing radon exposure, in sharp contrast to the *in*crease expected from LNT, shown by the lines labeled "Theory." These data have been analyzed for over 500 possible confounding factors, including socioeconomic, geographic, environmental, and ethnic associations (Cohen 2000), and the possible effects of an unrecognized confounding factor were investigated (Cohen 2005), but the conclusion remains firm that LNT fails very badly by grossly overestimating the cancer risk from low-level radiation.

What has been interpreted as conflicting results were derived from a pooled study of seven case–control studies (Krewski et al. 2005); shown in Table 3.4. We see there that none of the data points give a very statistically significant excess lung cancer risk, but the pattern suggests an excess risk from radon exposures, although not necessarily increasing with exposure at least for the four lowest points which comprise the region of significance in Figure 3.14. A pooled study includes many complicated adjustments for differences among the different studies in the pool, and potential confounding factors with the adjustments for the few of them that are recognized might be a problem. If there is a conflict with Figure 3.14, each of the several attempts to explain it as a problem with the latter have been shown to be completely implausible (Cohen 2005). Actually it is not clear that there is a conflict, because Figure 3.14 is not a dose–response relationship for individuals exposed to radon, but rather is an experimental observation with extremely high statistical significance, to be compared with the prediction from LNT. That comparison indicates that the theory fails very badly, grossly overestimating the risk from low-level exposure. The results in Table 3.4 can hardly be interpreted as a test of LNT.

Table 3.4. Odds ratios for lung cancer versus residential radon exposure from seven pooled case–control studies (Krewski et al. 2005)

Radon level (Bq/m^3)	Odds ratio (95% C.I.)
<25	1.00
25–49	1.13 (0.95–1.35)
50–74	1.09 (0.89–1.34)
75–99	1.16 (0.91–1.48)
100–149	1.24 (0.96–1.60)
150–199	1.22 (0.87–1.71)
>199	1.37 (0.98–1.92)

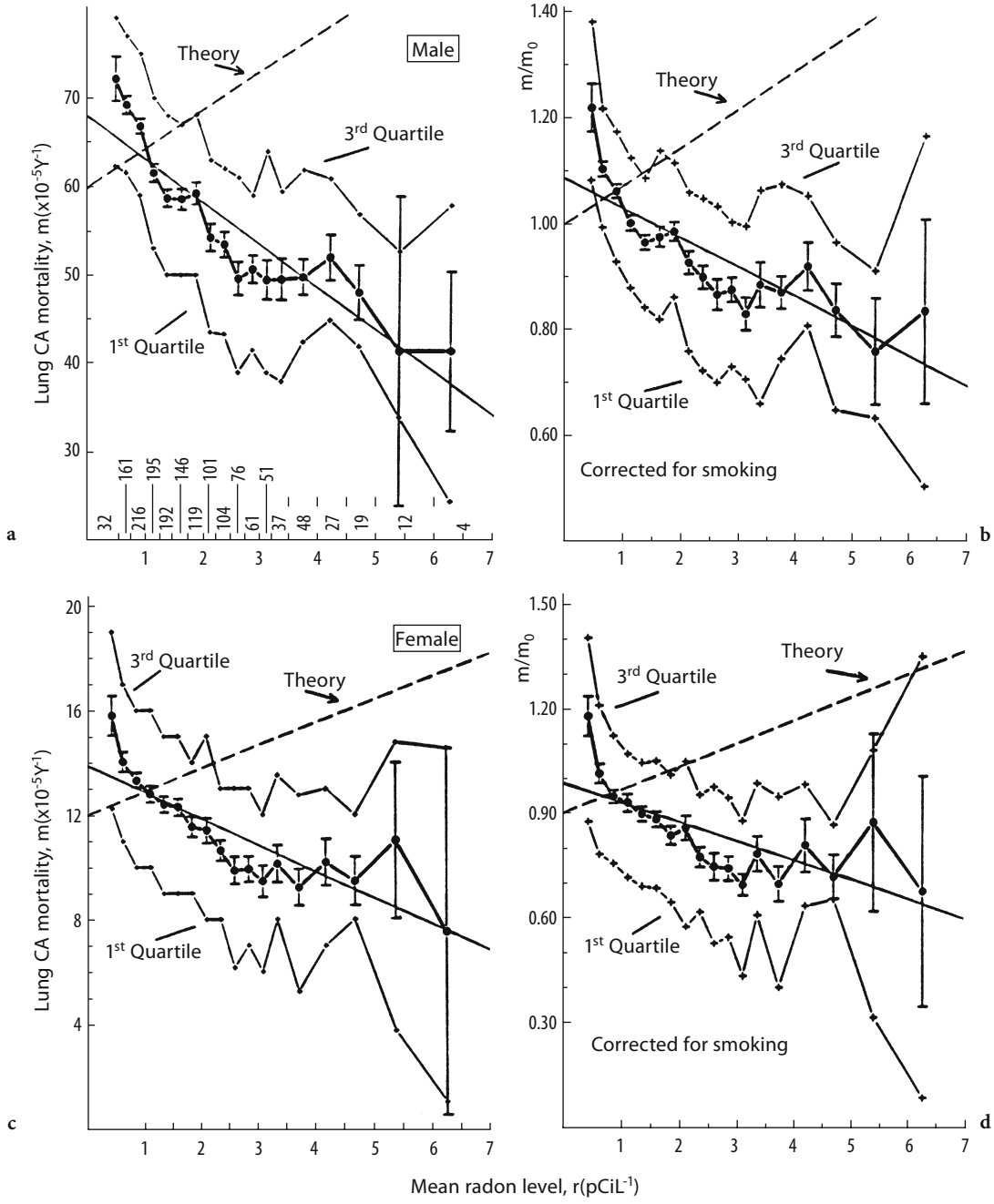

Fig. 3.14a–d. Age-adjusted lung cancer mortality rates, with and without correction for smoking prevalence, versus average radon level in homes for US counties (Cohen 1995). See explanations in text. **a, c** Without smoking correction, for males and females respectively. **b, d** With smoking correction for males and females respectively

3.7 Dependence of Latent Period on Dose

There is a substantial body of data, both on animals and on humans, indicating that the latent period between radiation exposure and cancer death increases with decreasing exposure; these have been reviewed by Cohen (1980) and by Raabe (1994). An example of results for dogs injected with alpha particle emitters (Dougherty and Mays 1969) is shown in Figure 3.15. These observations lead to the obvious conclusion that for low enough exposures, the latent period exceeds the normal life span, so no actual cancers develop. Thus there is an effective threshold.

This effect alone, even in the absence of all considerations discussed previously, would invalidate LNT as applied to low-level radiation.

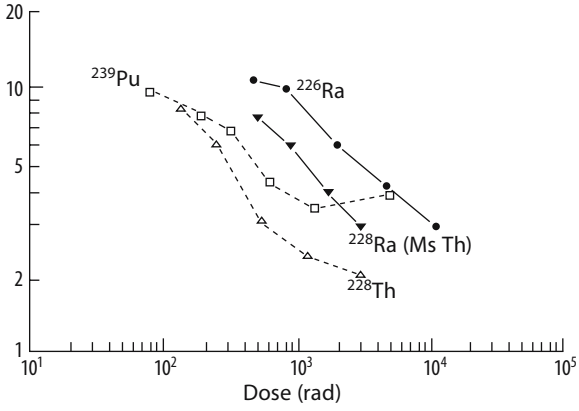

Fig. 3.15. Survival time for beagle dogs who developed bone cancer from injections of various alpha-emitting radioactive isotopes, versus dose to their bone at 1 year before death (Dougherty and Mays 1969)

3.8 Conclusion

The conclusion from the evidence reviewed in this paper is that LNT theory fails very badly in the low dose region, grossly overestimating the risk from low-level radiation. This means that the cancer risk from the vast majority of normally encountered radiation exposures is much lower than given by usual estimates, and may well be zero or even negative.

Acknowledgement

The author acknowledges a great debt to Myron Pollycove and James Muckerheide for help in pointing out references involved in this paper.

References

Anderson RE (1992) Effects of low dose radiation on the immune response. In: Calabrese EJ (ed) Biological effects of low level exposures to chemicals and radiation. Lewis, Chelsea, Mich., pp 95–112

Aurengo A et al (2005) Dose-effect relationship and estimation of the carcinogenic effects of low dose ionizing radiation. Available at http://cnts.wpi.edu/rsh/docs/FrenchAcads-EN-FINAL.pdf

Azzam EI, de Toledo SM, Raaphorst GP, Mitchel REJ (1996) Low dose ionizing radiation decreases the frequency of neoplastic transformation to a level below spontaneous rate in C3H 10T1/2 cells. Radiat Res 146:369–373

Berrington A, Darby SC, Weiss HA, Doll R (2001) 100 years of observation on British radiologists; mortality from cancer and other causes, 1897–1997. Br J Radiol 74:507–519

Bonner WN (2004) Phenomena leading to cell survival values which deviate from linear-quadratic models. Mutat Res 568:33–39

Boothman DA et al (1996) Altered G1 checkpoint control determines adaptive survival responses to ionizing radiation. Mutat Res 358:143–153

Cai L, Liu SZ (1990) Induction of cytogenic adaptive response of somatic and germ cells in vivo and in vitro by low dose X-irradiation. Int J Radiat Biol 58:187–194

Cardis E et al (1995) Effects of low dose and low dose rates of external ionizing radiation: cancer mortality among nuclear industry workers in three countries. Radiat Res 142:117–132

Cardis E et al (2005) Risk of cancer after low doses of ionizing radiation: retrospective cohort study in 15 countries. Br Med J 331:77–90

Chaffey JT, Rosenthal DS, Moloney WC, Hellman S (1976) Total body radiation as treatment for lymphosarcoma. Int J Radiat Oncol Biol Phys 1:399–405

Choi NC, Timothy AR, Kaufman SD, Carey RW, Aisenberg AC (1979) Low dose fractionated whole body irradiation in the treatment of advanced non-Hodgkin's lymphoma. Cancer 43:1636–1642

Cohen BL (1980) The cancer risk from low level radiation. Health Phys 39:659–678

Cohen BL (1995) Test of the linear-no threshold theory of radiation carcinogenesis for inhaled radon decay products. Health Phys 68:157–174

Cohen BL (1998) The cancer risk from low level radiation. Radiat Res 149:525–526

Cohen BL (2000) Updates and extensions to tests of the linear-no threshold theory. Technology 7:657–672

Cohen BL (2006) Test of the linear-no threshold theory; rationale for procedures. Dose-Response 3:369–390

Coleman MA et al (2005) Low dose irradiation alters the transcript profiles of human lymphoblastoid cells including genes associated with cytogenic radioadaptive response. Radiat Res 164:369–382
Davis HG, Boice JD, Hrubec Z, Monson RR (1989) Cancer mortality in a radiation-exposed cohort of Massachusetts tuberculosis patients. Cancer Res 49:6130–6136
Dougherty TF, Mays CW (1969) In: Radiation induced cancer. International Atomic Energy Agency, Vienna, p 361ff
Duport P (2001) A data base of cancer induction by low-dose radiation in mammals: overview and initial observations. Second Conference of the World Council of Nuclear Workers (WUNOC), Dublin, 2001
Evans RD (1974) Radium in Man. Health Phys 27:497–510
Feinendegen LE (2005a) Evidence for beneficial low level radiation effects and radiation hormesis. Brit J Radiol 78:3–7
Feinendegen LE (2005b) Low doses of ionizing radiation: relationship between biological benefit and damage induction, a synopsis. World J Nucl Med 4:21–34
Feinendegen LE, Loken MK, Booz J, Muhlensiepen H, Sondhaus CA, Bond VP (1995) Cellular mechanisms of production and repair induced by radiation exposure and their consequences for cell system responses. Stem Cells Suppl 13:7–20
Finkel MP, Biskis BO (1962) Toxicity of plutonium in mice. Health Phys 8:565–579
Finkel MP, Biskis BO (1968) Prog Exp Tumor Res 10:72ff
Finkel MP, Biskis BO (1969) Pathological consequences of radiostrontium administered to fetal and infant dogs. Radiation biology of the fetal and juvenile mammal. AEC Symposium Series, vol. 17, Proceedings of the 9th Hanford Biology Symposium, pp 543–565
Finkel T, Holbrook NJ (2000) Oxidants, oxidative stress, and the biology of aging. Nature 408:239–247
Fritz-Niggli H, Schaeppi-Buechi C (1991) Adaptive response to dominant lethality of mature and immature oocytes of *D. melanogaster* to low doses of ionizing radiation: effects in repair-proficient and repair deficient strains. Int J Radiat Biol 59:175–184
Ghiassi-nejad M, Mortazavi SMJ, Beitollahi M, Cameron JR et al (2002) Very high background radiation areas of Ramsar, Iran: preliminary biological studies and possible implications. Health Phys 82:87–93
Gilbert ES, Petersen GR, Buchanan JA (1989) Mortality of workers at the Hanford site: 1945–1981. Health Phys 56:11–25
Golder-Novoselsky E, Ding LH, Chen F, Chen DJ (2002) Radiation response in HSF cDNA microarray analysis. DOE Low dose radiation research program Workshop III, US Deptartment of Energy, Washington, DC
Gridley G et al (1999) Is there a healthy worker effect for cancer incidence among women in Sweden? Am J Ind Med 36:193–199
Hashimoto S, Shirato H, Hosokawa M et al (1999) The suppression of metastases and the change in host immune response after low-dose total body irradiation in tumor bearing rats. Radiat Res 151:717–724
Health Physics Society (HPS) (1996) Radiation risk in perspective: position statement of the Health Physics Society (adopted January 1996). Health Physics Society directory and handbook, 1998–1999, p 238 (also at www.hps.org)
Heidenreich WF, Paretzke HG, Jacob B (1997) No evidence for increased tumor risk below 200 mSv in the atomic bomb survivor data. Radiat Environ Biophys 36:205–207
Howe GR (1995) Lung cancer mortality between 1950 and 1987 after exposure to fractionated moderate dose rate ionizing radiation in the Canadian fluoroscopy cohort study and a comparison with lung cancer mortality in the atomic bomb survivors study. Radiat Res 142:295–304
Ina Y, Sakai K (2005) Activation of immunological network by chronic low dose rate irradiation in wild type mouse strains: analysis of immune cell populations and surface molecules. Int J Radiat Biol 81:721–729
Ina Y et al (2005) Suppression of thymic lymphoma induction by life-long low dose rate irradiation accompanied by immune activation of C57BL/6 mice. Radiat Res 163:153–158
Kelsey KT, Memisoglu A, Frenkel A, Liber HL (1991) Human lymphocytes exposed to low doses of X-rays are less susceptible to radiation induced mutagenesis. Mutat Res 263:197–201
Ko M, Lao X-Y, Kapadia R, Elmore E, Redpath JL (2006) Neoplastic transformation in vitro by low doses of ionizing radiation: role of adaptive response and bystander effects. Mutat Res 597:11–17
Kondo S (1993) Health effects of low level radiation. Medical Physics, Madison, Wis., pp 85–89
Koshurnikova NA et al (2002) Studies of the Mayak nuclear workers: health effects. Radiat Environ Biophys 41:29–31
Kostyuchenko VA, Krestina LY (1994) Long term irradiation effects in the population evacuated from the East-Urals radioactive trace area. Sci Total Environ 142:119–125
Krewski D et al (2005) Residential radon and risk of lung cancer: a combined analysis of 7 North American case-control studies. Epidemiology 16:137–145
Le XC, Xing JZ, Lee J, Leadon SA, Weinfeld M (1998) Inducible repair of thymine glycol detected by an ultrasensitive assay for DNA damage. Science: 280:1066–1069
Liu SJ (1992) Multilevel mechanisms of stimulatory effect of low dose radiation on immunity. In: Sugahara T, Sagan LA, Aoyama T (eds) Low dose irradiation and biological defense mechanisms. Elsevier, Amsterdam, pp 225–232
Liu SZ (2003) Non-linear dose-response relationship in the immune system following exposure to ionizing radiation: mechanisms and implications. Nonlinear Biol Toxicol Med 1:71–92
Makinodan T (1992) Cellular and sub-cellular alteration in immune cells induced by chronic intermittent exposure in vivo to very low dose of ionizing radiation and its ameliorating effects on progression of autoimmune disease and mammary tumor growth. In: Sugahara T, Sagan LA, Aoyama T (eds) Low dose irradiation and biological defense mechanisms. Elsevier, Amsterdam, pp 233–237
Makinodan T, James SJ (1990) T cell potentiation by low dose ionizing radiation: possible mechanisms. Health Phys 59:29–34
Matanoski GM (1991) Health effect of low level radiation in shipyard workers, Final report. Report No. DOE DE-AC02-79 EV10095; U.S. Dept. of Energy. See Tables 3.6B and 3.6D
Miller AB, Howe GR, Sherman GJ et al (1989) Mortality from breast cancer after irradiation during fluoroscopic examinations in patients being treated for tuberculosis. N Engl J Med 321:1285–1289

Miller RC, Randers-Pehrson G, Geard CR, Hall EJ, Brenner DJ (1999) The oncogenic transforming potential of the passage of single alpha particles through mammalian cell nuclei. Proc Natl Acad Sci USA 96:19–22

Mitchel REJ et al (2003) Low doses of radiation increase the latency of spontaneous lymphomas and spinal osteosarcomas in cancer prone, radiation sensitive Trp53 heterozygous mice. Radiat Res 159:320–327

Mohan AK et al (2003) Cancer and other causes of mortality among radiologic technicians in the United States. Int J Cancer 103:259–267

Monson RR (1986) Observations on the healthy worker effect. J Occup Med 28:425-433

NCRP (National Council on Radiation Protection and Measurements) (1995) Principles and application of collective dose to radiation protection, NCRP Publication 121, Bethesda, Md.

NCRP (2001) Evaluation of the linear nonthreshold dose-response model for ionizing radiation, NCRP Publication 136, Bethesda, Md.

Pierce DA, Shimizu Y, Preston DL, Vaeth M, Mabuchi K (1996) Studies of the mortality of atomic bomb survivors, Report 12, Part 1, Cancer: 1950–1990. Radiat Res 146:1–27

Pollycove M, Feinendagen L (2001) Biologic responses to low doses of ionizing radiation: detriment vs hormesis; Part 1. J Nucl Med 42:17N–27N

Preston DL et al (2004) Effect of recent changes in atomic bomb survivor dosimetry on cancer mortality risk estimates. Radiat Res 162:377–389

Raabe OG (1994) Three dimensional models of risk from internally deposited radionuclides. In: Raabe OG (ed) Internal radiation dosimetry. Medical Physics, Madison, Wis., pp 633–656

Redpath JL, Antoniono RJ (1998) Induction of a rapid response against spontaneous neoplastic transformation in vitro by low dose gamma radiation. Radiatr Res 149:517–520

Redpath JL, Liang D, Taylor TH, Christie C, Elmore E (2001) The shape of the dose–response curve for radiation-induced neoplastic transformation *in vitro*: evidence for an adaptive response against neoplastic transformation at low doses of low-LET radiation. Radiat Res 156:700–707

Redpath JL, Lu Q, Lao X, Molloi S, Elmore E (2003) Low doses of diagnostic X-rays protect against neoplastic transformation in vitro. Int J Radiat Biol 79:235–240

Rogel A et al (2005) Mortality of workers exposed to ionizing radiation at the French National Electricity company. Am J Ind Med 47:72–82

Sakamoto K, Myogin M, Hosoi Y et al (1997) Fundamental and clinical studied on cancer control with total and upper half body irradiation. J Jpn Soc Ther Radiol Oncol 9:161–175

Shadley JD, Dai GQ (1992) Cytogenic and survival adaptive responses in G-1 phase human lymphocytes. Mutat Res 265:273–281

Tanooka H (2001)Threshold dose-response in radiation carcinogenesis: an approach from chronic beta-irradiation experiments and a review of non-tumor doses. Int J Radiat Biol 77:541–551

Tokarskaya ZB, Okladlnikova ND, Belyaeva ZD, Drozhko EG (1997) Multifactorial analysis of lung cancer dose-response relationships for workers at the Mayak Nuclear Enterprise. Health Phys 73:899–905

Tubiana M, Aurengo A (2005) Dose effect relationship and estimation of the carcinogenic effects of low doses of ionizing radiation. Int J Low Radiat 2:1–19

Ullrich RL, Storer JB (1979) Influence of gamma radiation on the development of neoplastic diseases in mice: II solid tumors. Radiat Res 80:317–324

UNSCEAR (United Nations Scientific Committee on Effects of Atomic Radiation) (1994) Report to the General Assembly, Annex B: Adaptive response. United Nations, New York

Voelz GL, Wilkinson CS, Acquavelle JF (1983) An update of epidemiologic studies of plutonium workers. Health Phys [Suppl 1] 44:493–503

Wang JX et al (2002) Cancer incidence and risk estimation among medical X-ray workers in China, 1950–1995. Health Phys 82:455–466

Yamaoka K (1991) Increased SOD activities and decreased lipid peroxide in rat organs induced by low X-irradiation. Free Radic Biol Med 11:3–7

Yin E et al (2005) Gene expression changes in mouse brain after exposure to low-dose ionizing radiation. Int J Radiat Biol 79:759–775

Yoshinaga S et al (2004) Cancer risks among radiologists and radiologic technologists: review of epidemiologic studies. Radiology 233:313–321

Yukawa O et al (2005) Induction of radical scavenging ability and suppression of lipid peroxidation in rat liver microsomes following whole body low dose X-irradiation. J Radiat Biol 81:681–688

Zaichkina SI et al (2003) Low doses of radiation decrease the level of spontaneous and gamma induced chromosomal mutagenesis in bone marrow cells of mice in vivo. Radiat Biol Radioecol 43:153–155

CT Parameters that Influence the Radiation Dose

4

Hans Dieter Nagel

CONTENTS

H. D. Nagel, PhD
Science and Technology Group, Philips Medical Systems, Roentgenstr. 24, 22335 Hamburg, Germany

The exposure to radiation of patients undergoing computed tomography (CT) examinations is determined by two factors: equipment-related factors, i.e., design of the scanner with respect to dose efficiency, and application-related factors, i.e., the way in which the radiologist or the radiographer makes use of the scanner. In this chapter, the features and parameters influencing patient dose are outlined. First, however, a brief introduction on the dose descriptors applicable to CT is given.

4.1 CT Dose Descriptors

The dose quantities used in projection radiography are not applicable to CT for three reasons:

- First, the dose distribution inside the patient is completely different from that for a conventional radiogram, where the dose decreases continuously from the entrance of the X-ray beam to its exit, with a ratio of between 100 and 1000 to 1. In the case of CT, as a consequence of the scanning procedure that equally irradiates the patient from all directions, the dose is almost equally distributed in the scanning plane. A dose comparison of CT with conventional projection radiography in terms of skin dose therefore does not make any sense.
- Second, the scanning procedure using narrow beams along the longitudinal z-axis of the patient implies that a significant portion of the radiation energy is deposited outside the nominal beam width. This is mainly due to penumbra effects and scattered radiation produced inside the beam.
- Third, the situation with CT–unlike with conventional projection radiography–is further complicated by the circumstances in which the volume to be imaged is not irradiated simultaneously. This often leads to confusion about what the dose from a complete series of, for example, 15 slices might be compared with the dose from a single slice.

As a consequence, dedicated dose quantities that account for these peculiarities are needed: the 'computed tomography dose index (CTDI)', which is a measure of the local dose, and the 'dose–length product (DLP)', representing the integral radiation exposure associated with a CT examination. Fortunately, a bridge exists that enables comparison of CT with radiation exposure from other modalities and sources; this can be achieved by the effective dose (E). So, there are three dose descriptors in all, which everyone dealing with CT should be familiar with.

4.1.1 Computed Tomography Dose Index

The CTDI is the fundamental CT dose descriptor. By making use of this quantity, the first two peculiarities of CT scanning are taken into account: The CTDI [unit: milligray (mGy)] is derived from the dose distribution along a line that is parallel to the axis of rotation for the scanner (= z-axis) and is recorded for a single rotation of the X-ray source. Figure 4.1 illustrates the meaning of this term: CTDI is the equivalent of the dose value inside the irradiated slice (beam) that would result if the absorbed radiation dose profile were entirely concentrated to a rectangular profile of width equal to the nominal beam width $N \cdot h_{col}$, with N being the number of independent (i.e., non-overlapping) slices that are acquired simultaneously. Accordingly, all dose contributions from outside the nominal beam width, i.e., the areas under the tails of the dose profile, are added to the area inside the slice.

The corresponding mathematical definition of CTDI therefore describes the summation of all dose contributions along the z-axis:

$$CTDI = \frac{1}{N \cdot h_{col}} \cdot \int_{-\infty}^{+\infty} D(z) \cdot dz \qquad (4.1)$$

where D(z) is the value of the dose at a given location, z, and $N \cdot h_{col}$ is the nominal value of the total collimation (beam width) that is used for data acquisition. CTDI is therefore equal to the area of the dose profile (the 'dose–profile integral') divided by the nominal beam width. In practice, the dose profile is accumulated in a range of -50 mm to +50 mm relative to the center of the beam, i.e., over a distance of 100 mm.

The relevance of CTDI becomes obvious from the total dose profile of a scan series with, for example, $n = 15$ subsequent rotations (Fig. 4.2). The average level of the total dose profile, which is called 'multiple scan average dose (MSAD)' (Shope 1981), is higher than the peak value of each single dose profile. This increase results from the tails of the single dose profiles for a scan series. Obviously, MSAD and CTDI are exactly equal if the table feed (TF) is equal

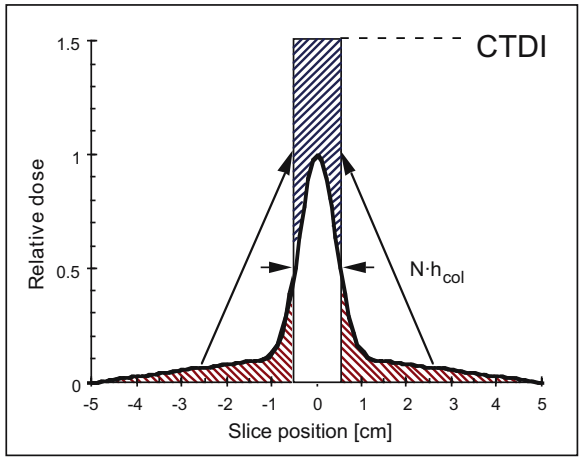

Fig. 4.1. Illustration of the term 'Computed Tomography Dose Index (CTDI)': CTDI is the equivalent of the dose value inside the irradiated slice (beam) that would result if the absorbed radiation dose profile were entirely concentrated to a rectangular profile of width equal to the nominal beam width $N \cdot h_{col}$

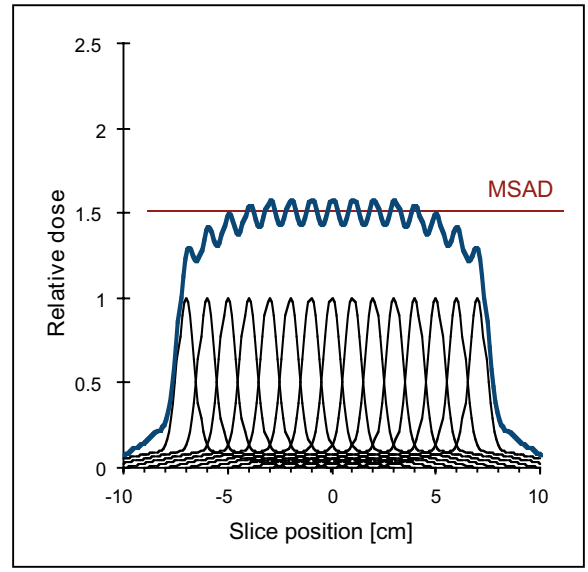

Fig. 4.2. Total dose profile of a scan series with n=15 subsequent rotations. The average level of the total dose profile, which is called 'Multiple Scan Average Dose (MSAD)', is equal to the computed tomography dose index (CTDI) if the table feed (TF) is equal to the nominal beam width $N \cdot h_{col}$ (i.e., pitch p = 1)

to the nominal beam width $N \cdot h_{col}$, i.e., if the pitch factor

$$p = \frac{TF}{N \cdot h_{col}} \tag{4.2}$$

is equal to 1. In general (i.e., if the pitch is not equal to 1, Fig. 4.3), the relationship between CTDI and MSAD is given by

$$MSAD = \frac{1}{p} \cdot CTDI \tag{4.3}$$

The practical implication of Equation 4.3 is that, in order to obtain the average dose for a scan series, it is not necessary to carry out all the scans. Instead, it is sufficient to obtain the CTDI from a single scan by acquiring the entire dose profile according to Equation 4.1. This is achieved with dose measurements using long, pencil-like detectors, with an active length of 10 cm (Fig. 4.4). These detectors accumulate the dose profile integral (DPI; unit: mGy·cm), i.e., the area under the dose profile shown in Figure 4.1. The CTDI is then obtained according to Equation 4.1 by dividing by the nominal beam width $N \cdot h_{col}$.

In order to obtain estimates of the dose to organs located in the scan range, the CTDI generally refers to standard dosimetry phantoms with patient-like diameters. In the standard measuring procedure for CTDI, which utilizes two cylindrical Perspex (PMMA) phantoms of different diameter (Fig. 4.4), dose is measured at the center and near the periphery of the phantom (Fig. 4.5). The larger phantom, being 32 cm in diameter, represents the absorption that is typical for the trunk region of adults. The smaller phantom (16 cm in diameter) represents the patient in head examinations. The smaller phantom is also used for dose assessment in pediatric examinations (Shrimpton 2000). The dose values thus obtained are denoted as:

$$CTDI_{H,c} \text{ and } CTDI_{H,p} \tag{4.4a}$$

and

$$CTDI_{B,c} \text{ and } CTDI_{B,p} \tag{4.4b}$$

with H = head, B = body, c = center, p = periphery.

To make life easier, each pair of CTDI values (central and peripheral) can be combined into a single one named 'weighted CTDI ($CTDI_w$)', which represents the CTDI averaged over the cross section of the pertaining phantom:

$$CTDI_W = \frac{1}{3} \cdot CTDI_{XYZ,c} + \frac{2}{3} \cdot CTDI_{XYZ,p} \tag{4.5}$$

where the subscript XYZ stands for either H(ead) or B(ody). In daily practice, $CTDI_w$ is used as one

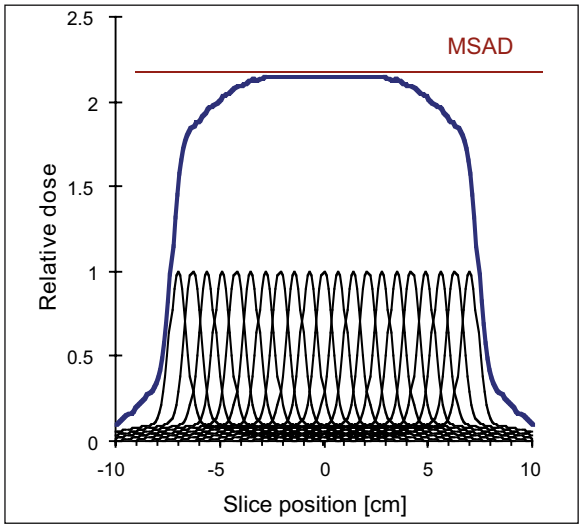

Fig. 4.3. Total dose profile of a scan series with $n = 15$ subsequent rotations, although scanned with pitch = 0.7. Due to the larger overlap, multiple scan average dose (MSAD) is higher than that in Fig. 4.2 and amounts to computed tomography dose index (CTDI) divided by pitch

Fig. 4.4. Cylindrical standard computed tomography (CT) dosimetry phantoms (16 cm and 32 cm in diameter) made from Perspex for representative measurements of the computed tomography dose index (CTDI) in regions of the head and the trunk, and a pencil-like detector for measurements of the dose-profile integral

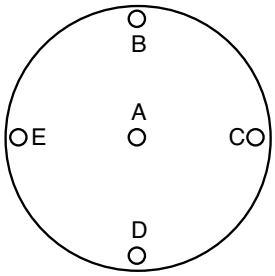

Fig. 4.5. Arrangement of the locations A–E for the determination of the computed tomography dose index (CTDI) in a standard CT dosimetry phantom

of two dose descriptors for dose recommendations ('reference values') that have been introduced by the European Commission (1999a).

If pitch-related effects on the radiation exposure have already been taken into account at the level of local dose (i.e., CTDI), a quantity named 'volume CTDI ($CTDI_{vol}$)' is defined (IEC 2001):

$$CTDI_{vol} = \frac{CTDI_W}{p} \tag{4.6}$$

So $CTDI_{vol}$ is the pitch-corrected $CTDI_w$. Apart from the integration length, which is limited to 100 mm, $CTDI_{vol}$ is practically identical to MSAD based on $CTDI_w$ (i.e., $MSAD_w$). Since averaging includes both the cross section and the scan length, $CTDI_{vol}$ therefore represents the average dose for a given scan volume. $CTDI_{vol}$ is used as the dose quantity that is displayed at the operator's console of newer scanners. This also holds true even if the display is labeled as '$CTDI_w$' due to faulty definition in the first edition of the particular IEC standard for CT (IEC 1999), or simply as 'CTDI'.

Attention is required if the dose displayed as $CTDI_{vol}$ shall be used for comparison with reference values given in terms of $CTDI_w$. For this purpose, the pitch correction introduced in Equation 4.6 needs to be reversed by multiplying the $CTDI_{vol}$ value by the pitch factor. Care is also required if the $CTDI_{vol}$ displayed is used to assess pediatric radiation exposure: whether head or body CTDI values are displayed depends only on the scan mode (head or body), not on the patient size. Consequently, the dose to children and infants undergoing CT examinations of the trunk region, which for the same scan parameter settings depends on the patient diameter, is currently underestimated with the dose displayed at the operator's console by a factor two to three.

CTDI statements in scanner specification sheets are given for the head phantom as well as for the body phantom and often apply to a current–time product of 100 mAs or 1 mAs. In this case, it must be recognized that a quantity named 'normalized CTDI' is used, which is labeled '$_nCTDI$ (unit: mGy/mAs)' in order to avoid confusion. The normalized CTDI is obtained by dividing the CTDI value by the mAs product Q that was used to measure CTDI:

$$_nCTDI = \frac{CTDI}{Q} \tag{4.7}$$

It is worthwhile (and indeed necessary) to note that the normalized CTDI is a characteristic quantity for a scanner (dose rate coefficient), which simply represents the capacity of a scanner in terms of output and conveys absolutely nothing about patient dose. Very often it is assumed that scanners with a high value of $_nCTDI$ are more 'dangerous' than other models with lower $_nCTDI$ values. This is not necessarily the case. Reference to patient dose cannot be made unless the normalized CTDI has been multiplied by the tube current–time product Q that is required in order to produce images of diagnostic quality with the type of scanner under consideration. Only after having carried out this step is it possible to decide whether a particular scanner needs more or less dose than another model for a specified type of examination.

4.1.2 Dose–Length Product

The third peculiarity of CT, i.e., the question of what the dose from a complete series of, for example, 15 slices might be compared with that from a single slice, is solved by introducing a dose descriptor named 'dose–length product (DLP; unit: mGy·cm)'. DLP takes both the 'intensity' (represented by the $CTDI_{vol}$) and the extension (represented by the scan length L) of an irradiation into account (Fig. 4.6):

$$DLP = CTDI_{vol} \cdot L \tag{4.8}$$

So the DLP increases with the number of slices (correctly: with the length of the irradiated body section), while the dose (i.e., $CTDI_{vol}$) remains the same regardless of the number of slices or length. In Figure 4.6, the area of the total dose profile of the scan series represents the DLP. DLP is the equivalent of the dose–area product (DAP) in projection radiography, a quantity that also combines both aspects (intensity and extension) of patient exposure.

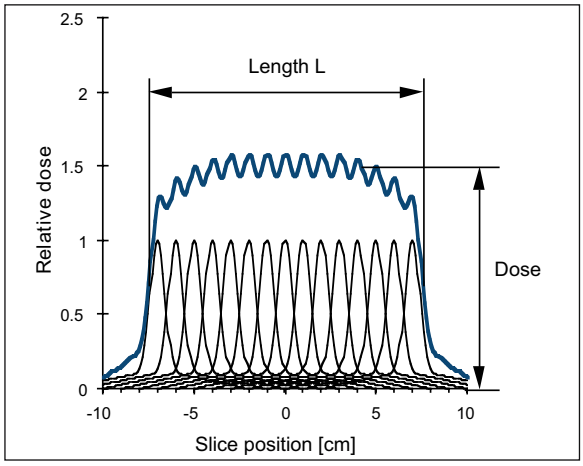

Fig. 4.6. Total dose profile of a scan series with n=15 subsequent rotations. The dose–length product (DLP) is the product of the height ($CTDI_{vol}$) and the width (scan length L) of the total dose profile and is equal to the area under the curve

In sequential scanning, the scan length is determined by the beam width $N \cdot h_{col}$ and the number (n) of table feeds TF):

$$L = n \cdot TF + N \cdot h_{col} \tag{4.9}$$

while in spiral scanning the scan length only depends on the number (n) of rotations and the table feed (TF):

$$L = n \cdot TF = \frac{T}{t_{rot}} \cdot p \cdot N \cdot h_{col} \tag{4.10}$$

where T is the total scan time, t_{rot} is the rotation time, and p is the pitch factor. While in sequential scanning the scan length L is equal to the range from the beginning of the first slice until the end of the last, the (gross) scan length for spiral scanning not only comprises the (net) length of the imaged body section but also includes the additional rotations at the beginning and the end of the scan ('overranging') which are required for data interpolation.

If an examination consists of several sequential scan series or spiral scans, the DLP of the complete examination (DLP_{exam}) is the sum of the DLPs of each single series or spiral scan:

$$DLP_{exam} = \sum_i DLP_i \tag{4.11}$$

In daily practice, the DLP is used as the second (and most important) of the two dose descriptors for dose recommendations ('reference values') that have been introduced by the European Commission (1999a).

4.1.3 Effective Dose

CTDI and DLP are CT-specific dose descriptors that do not allow for comparisons with radiation exposures from other sources, e.g., projection radiography, nuclear medicine or natural background radiation. The only common denominator to achieve this goal is the 'effective dose'. With effective dose, the organ doses from a partial irradiation of the body are converted into an equivalent uniform dose to the entire body.

Effective dose E [unit: millisievert (mSv)] according to ICRP 60 (ICRP 1991) is defined as the weighted average of organ dose values H_T for a number of specified organs:

$$E = \sum_i w_i \cdot H_{T,i} \tag{4.12}$$

How much a particular organ contributes to calculation of effective dose depends on its relative sensitivity to radiation-induced effects, as represented by the tissue-weighting factor w_i attributed to the organ:

- 0.20 for gonads
- 0.12 for each of lungs, colon, red bone marrow and stomach wall
- 0.05 for each of breast, urinary bladder, liver, thyroid and esophagus
- 0.01 for each of skeleton and skin
- 0.05 for the 'remainder'

The 'remainder' consists of a group of additional organs and tissues with a lower sensitivity to radiation-induced effects for which the average dose must be used: small intestine, brain, spleen, muscle tissue, adrenals, kidneys, pancreas, thymus and uterus. The sum of all tissue-weighting factors w_i is equal to 1.

Effective dose cannot as such be measured directly in vivo. Measurements in anthropomorphic phantoms with thermo-luminescent dosemeters (TLDs) are very time-consuming and therefore not well suited for daily practice. Effective dose, however, can be assessed in various ways using conversion factors. For coarse estimates, it is sufficient to multiply the DLP with mean conversion factors, depending on which one of three body regions has been scanned and whether that scan was made in head or body scanning mode:

$$E \approx DLP \cdot f_{mean} \tag{4.13}$$

For adults of standard size, the following generic mean conversion factors f_{mean} apply:

1. 0.025 mSv/mGy·cm for the head region
2. 0.060 mSv/mGy·cm for the neck region, scanned in head mode
3. 0.100 mSv/mGy·cm for the neck region, scanned in body mode
4. 0.175 mSv/mGy·cm for the trunk region

Similar factors ('E_{DLP}'), which additionally distinguish between chest, abdomen and pelvis, but do not account for differences in scan mode, are given in report EUR 16262 (European Commission 1999b).

In order to apply Equation 4.13, the DLP or at least the $CTDI_{vol}$ and the (gross) scan length L, from which the DLP can be calculated according to Equation 4.8, must be available. If the scanner is not equipped with a dose display, or if a more detailed assessment of effective dose is desired (e.g., to be more specific for the scanned region of the body, to distinguish between males and females, to assess pediatric doses, or to take differences between scanners into account), dedicated CT dose calculation software should be used. These programs make use of more detailed conversion factors and also allow for calculation of organ doses. Currently, five different programs are in general use. They are available either commercially or as freeware and differ significantly in specifications, performance, and price.

Typical tolerances in effective dose assessment with these programs are in the order of ±20–30%. Similar uncertainties also apply to effective dose assessment with TLD measurements in Alderson phantoms. This should always be borne in mind when comparing doses from different scanners in terms of effective dose. Care is also needed not to mix up effective dose with organ doses, as both are expressed in millisieverts. Nevertheless, effective dose is of great value, e.g., to answer questions raised by patients. For this purpose, the annual natural background radiation, which is between 2 mSv and 3 mSv in most countries, can be used as a scale.

A comprehensive compilation of dose-relevant scanner data and other useful information required for CT dose assessment can be found in a textbook by Nagel et al. (2002). The data given there apply to most of the scanners currently in use, except the most recent. However, data for these new scanners can be found in the CT-Expo software package (Stamm and Nagel 2001), which is based on the data and formalism outlined in this book and is updated regularly.

4.2 Equipment-Related Factors

4.2.1 Beam Filtration

In conventional projection radiography, beam filtration is a well-known means to reduce those portions of the radiation spectrum with no or little contribution to image formation. In the early years of CT history, beam filtration was comparatively large in order to compensate for beam-hardening artifacts. Filters made from 0.5 mm of copper, with filtering properties equivalent to approximately 18 mm of aluminum (quality equivalent filtration, Nagel 1986), were not unusual at that time. The present generation of scanners typically employs a beam filtration for the X-ray tube assembly of between 1 mm and 3 mm aluminum and an additional filtration (flat filter) of 0.1 mm copper, giving a total beam filtration of between 5 mm and 6 mm aluminum.

Apart from this, there are a number of older and also newer scanners that operate with an added filtration of approximately 0.2 mm copper, resulting in a total beam filtration of between 8 mm and 9 mm aluminum, and sometimes even more (currently up to 12 mm aluminum quality-equivalent filtration). Likewise, there are also scanners that employ less filtration. Consequently, the normalized dose values for these scanners ($_nCTDI$ in terms of mGy/mAs) differ significantly. Very often these lower or higher values are misunderstood as being an indicator that the equipment is more or less dose efficient compared with other scanners. This might not necessarily be the case in reality.

Apart from dose, the consequences on image quality arising from the beam hardening and beam attenuating properties of filtration have also to be considered (Nagel 1989). The use of additional filtration impairs primary contrast and increases noise due to reduced beam intensity per mAs, as experienced by the detectors. Without compensating for these adverse effects (e.g., by increasing tube current–time product), the contrast-to-noise ratio (CNR), which affects the detectability of small or low-contrast details, is reduced. Unpublished studies by the author show that, in order to maintain the CNR (i.e., for constant image quality), the net reduction in terms of effective dose achieved by increasing the standard beam filtration (1 mm Al + 0.1 mm Cu = 4.5 mm Al quality equivalent) by 0.2 mm Cu

amounts to not more than 10%, even in favorable situations (soft tissue imaging, Fig. 4.7). Conversely, the same added filtration leads to higher patient doses (up to 15%) in examinations with administration of contrast agents (iodine). At the same time, tube loading must be increased by 20% in order to compensate for reduced beam intensity.

Newer surveys on CT practice (Galanski et al. 2001) revealed that scanners of comparable age, but with largely differing beam filtration, are operated at almost similar dose levels. Similar results in terms of dose efficiency have been found in comparative tests on scanners with differing beam filtration conducted by ImPACT (2004). Contrary to projection radiography, which operates at comparatively lower tube potentials, beam filtration plays only a minor role in CT, where higher tube potentials are applied. A return to increased beam filtration–as sometimes recommended or practiced–is less advantageous than expected and should only be made if sufficient X-ray tube loading capacity is available or if other important aspects exist (e.g., improved performance of reconstruction filters).

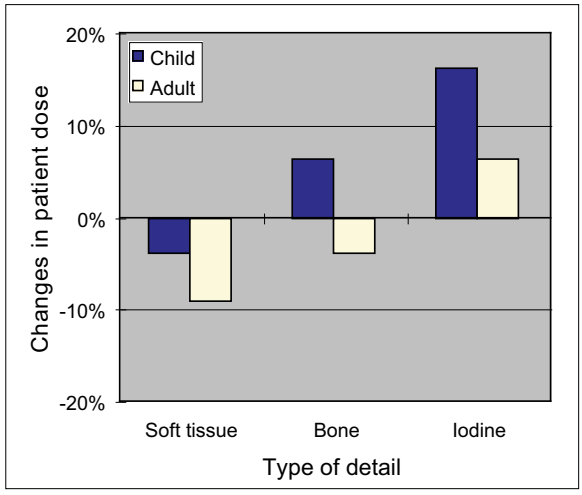

Fig. 4.7. Changes in patient dose due to increased beam filtration at constant contrast-to-noise ratio for different types of detail. Standard filtration: 1 mm Al + 0.1 mm Cu (= 4.5 mm Al quality equivalent); added filtration: 0.2 mm Cu (= 7 mm Al quality equivalent)

4.2.2 Beam Shaper

Most scanners are equipped with a dedicated filter device, named 'beam shaper' or 'bow-tie filter', that modifies the spatial distribution of radiation emitted within the fan beam. The purpose of this kind of filter (which is characterized by increasing thickness toward its outer edges) is to adapt the beam intensity to match the reduced attenuation of objects in the outer portions of the fan beam. Dynamic range requirements for the detector system can thus be reduced. Simultaneously, beam-hardening effects are also less likely.

In order to provide attenuating properties that are almost tissue equivalent, beam shapers should be made from materials containing only elements with a low atomic number Z. However, this is not always the case in practice. Beam shapers preferentially affect the dose in the outer portions of an object, thereby reducing the peripheral $CTDI_p$ values. But, as the dose at the center is mainly caused by scattered radiation from the periphery of the object, the central $CTDI_c$ value is also somewhat reduced. The ratio of dose at the periphery to that at the center therefore decreases, making the dose distribution inside an object more homogeneous and so improving the uniformity of noise in the image. Contrary to the flat filter, the beam shaper has a much greater impact on the dose properties of a scanner.

The beam shapers found in practice not only differ by the material from which they are made. They also differ by their shape, thus producing more or less compensation. A prominent example is the beam shaper of the Elscint CT Twin, which was modified in 1998 to produce more compensation. In addition, different types of beam shapers can be selected on some scanners, depending on the nature and diameter of the object (e.g., for head and body scanning mode).

4.2.3 Beam Collimation

The beam collimation for defining the thickness of the slice to be imaged is made in the first instance close to the X-ray source (primary collimation). The shape of the dose profile is determined by the aperture of the collimator, its distance from the focal spot, and the size and shape (i.e., the intensity distribution) of the focal spot. Due to the narrow width of collimation, penumbral effects occur. These effects become more and more pronounced as collimation is further narrowed.

In addition, there is a secondary collimation close to the detector ('post-patient collimation') that primarily serves to remove scattered radiation. On some single-slice and dual-slice scanners, this secondary

collimation is further narrowed in order to improve the shape of the slice profile ('restrictive post-patient collimation', Fig. 4.8a,b). For multi-slice scanners with more than two detector rows, the primary collimation must necessarily be made wider than N_{times} the selected slice collimation in order to avoid (or at least to reduce) penumbral effects in the outer portions of the detector array (Fig. 4.8c). In both cases, the dose profile is wider than the slice profile or the nominal beam width, and the patient is exposed to a larger extent ('overbeaming'), as becomes obvious from normalized CTDI values that increase with reduced beam width.

Overbeaming can be expressed by a single parameter, the 'overbeaming parameter' dz, which is equal to the combined width of the portion of the dose profile not used for detection (Fig. 4.8c). Overbeaming itself, i.e., the percentage increase in CTDI due to the unused portion of the dose profile, is then given by

$$\Delta CTDI_{rel} = \frac{dz}{N \cdot h_{col}} \cdot 100 \qquad (4.14)$$

The overbeaming parameter dz typically amounts to 1 mm for single- and dual-slice scanners that employ restrictive post-patient collimation, and to 3 mm for multi-slice scanners with $N=4$ and more slices that are acquired simultaneously, although this may vary depending on the type of scanner. For narrow beam-width settings, the increase in dose that results from overbeaming can be 100% and more.

In practice, overbeaming is no real issue for single- and dual-slice scanners, as the limited coverage restricts the use of narrow beam width to a few examinations with a short scan range (e.g., inner ear). With multi-slice scanners, however, overbeaming effects have to be taken seriously, as multi-slice computed tomography (MSCT) technology aims to provide improved resolution along the z-axis, which requires reduced slice collimation. Overbeaming, i.e., the increase in CTDI that results from beam-width settings that are typical for each type of scanner, is shown in Figure 4.9 for a number of scanners from different manufacturers. As indicated by the trend line, overbeaming is most pronounced with quad-slice scanners and is diminished with an increasing beam width $N \cdot h_{col}$ provided by scanners with more slices (Nagel 2005).

4.2.4 Detector Array

In contrast to single-slice scanners, multi-slice scanners are equipped with a detector array that consists of more than a single row of detectors. Gas detectors or fourth-generation stationary detector rings are no longer compatible with multi-slice requirements. Consequently, only third-generation detector arcs with solid-state detectors have remained. In general, solid-state detectors are more dose efficient than gas

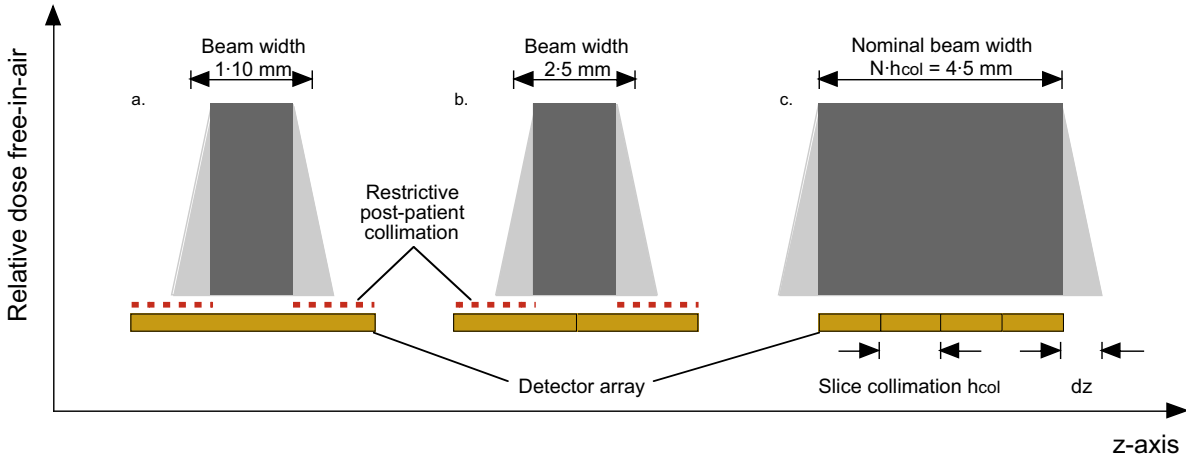

Fig. 4.8a–c. Dose profiles free-in-air with umbra (*dark gray*) and penumbra (*light gray*) portions for a single-slice scanner (**a**), a dual-slice scanner (**b**), and a quad-slice scanner (**c**). With single- and dual-slice scanners, the width of the active detector rows is sufficient to capture the entire dose profile, penumbra included (except for some scanners that employ restrictive post-patient collimation). For scanners with four and more slices acquired simultaneously, penumbra is excluded from detection in order to serve all detector channels equally well. The combined width of the penumbra triangles at both sides is characterized by the overbeaming parameter dz

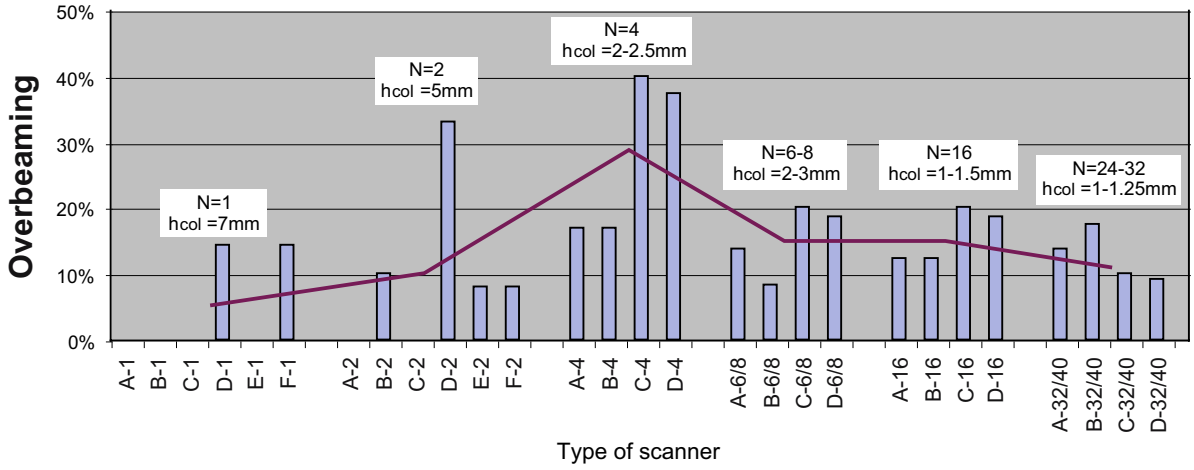

Fig. 4.9. Overbeaming, i.e., the percentage increase in the computed tomography dose index (CTDI), for single-slice ($N=1$), dual-slice ($N=2$), quad-slice ($N=4$), 6 to 8-slice ($N=6$–8), 16-slice ($N=16$) and 32 to 40-slice ($N=32$–40) scanners from different manufacturers (A–F) for the slice collimations h_{col} typically employed. The *red trend line* indicates that overbeaming is most pronounced with quad-slice scanners in practice and is diminished with an increasing beam width $N \cdot h_{col}$

detectors (van der Haar et al. 1998), but require additional means to suppress scattered radiation (anti-scatter-grids) that inevitably cause a certain loss of primary radiation, too.

The single detectors in a multi-row, solid-state detector array are separated by narrow strips ('septa') which are not sensitive to radiation and therefore do not contribute to detector signal. Due to the large number of additional strips, these inactive zones result in minor or major geometrical losses, depending on the design of the detector array. In addition, further losses occur due to a decrease in sensitivity at the edges of each row that results from cutting the scintillator crystal. In contrast to a single-row detector array, the width of which can be larger than the maximum slice thickness (Fig. 4.10), the edges of the rows in a multi-row detector array are located inside the beam. Due to both these effects–separating strips and decreased sensitivity–the net efficiency of a solid-state detector array, which is typically 85% for single-slice scanners, is further decreased, typically to 70%.

When 4-slice scanners were introduced in 1998, very different detector designs were used (Fig. 4.11), with variations in the number of rows (between 8 and 34) and the smallest detector size (between 0.5 mm and 1.25 mm). The large number of rows (much larger than the number of slices that can be acquired simultaneously) was necessary to enable the use of different slice collimations (between 4×0.5 mm and 4×8 mm). Slice collimations wider than the detector size were achieved by electronically combining several adjacent detector rows [e.g., 4×1.25 mm = 5 mm (GE) or 1+1.5+2.5 = 5 mm (Philips/Siemens)]. Each detector design had its specific advantages and drawbacks: Toshiba's hybrid arrangement offered the largest coverage (32 mm) and the acquisition of four sub-millimeter slices, but had the largest number of septa (1 per mm) and the smallest detector size (0.5 mm). The progressive design, commonly used by Philips and Siemens, had the smallest number of septa (0.35 per mm), but was restricted to two sub-millimeter slices only. GE's matrix arrangement was a compromise (0.75 per mm) that, however, facilitated the next technology step toward eight simultaneously acquired slices with the same detector array.

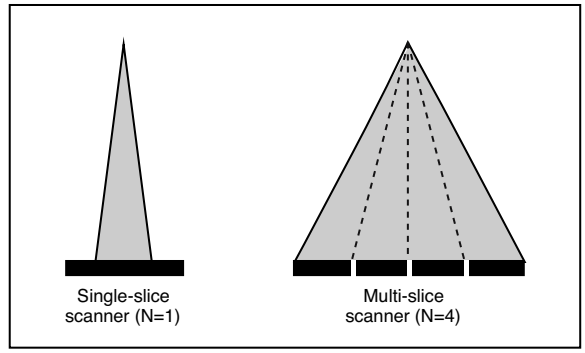

Fig. 4.10. A multi-slice computed tomography (MSCT) scanner, with simultaneous scanning of four slices, compared with a conventional single-slice scanner. Due to the additional septa between the detector rows, the geometric efficiency of MSCT detector arrays is comparatively lower by 10–20%

All 16-slice scanners introduced in 2001 now made use of the same hybrid design, with 16 smaller central detectors, accompanied by a number of larger detectors at both sides (Fig. 4.12). Apart from the number of detector rows (between 24 and 40) and array width (between 20 mm and 32 mm), there were differences in the size of the detectors (between 0.5 mm and 1.5 mm), and each manufacturer claimed his solution to be the best. As in real life, there are a number of conflicting needs (spatial resolution, dose efficiency, coverage) that must be met, especially with respect to cardiac imaging where scan times below 20 s (one breathhold) are mandatory. Consequently, any design that emphasized only one of these criteria was definitely not the best compromise. Due to the increased number of septa [from 0.6 per mm (4-slice) to 1.1 per mm (16-slice) on average], the geometric efficiency of 16-slice detector arrays is somewhat lower.

In the latest generation of 64-slice scanners, matrix arrangements that allow for simultaneous acquisition of 64 sub-millimeter slices are employed by the majority of manufacturers (Fig. 4.13). By electronically combining several adjacent rows, thicker slices can also be acquired, but this results in a reduced number of slices (e.g., 32×1.25 mm, 16×2.5 mm, etc.). Once again, the number of septa was increased (to 1.6 per mm on average), resulting in an additional loss in geometric efficiency.

The hybrid detector design exclusively used by Siemens for its Sensation 64 scanner is uncommon, insofar as the number of simultaneous slices claimed by the manufacturer (64) is much larger than the number of rows (32×0.6 mm or 24×1.2 mm). The claim is based on a special acquisition mode that employs two alternating focal spot positions to simultaneously produce 64 data sets per rotation with 50% overlap in order to achieve a somewhat

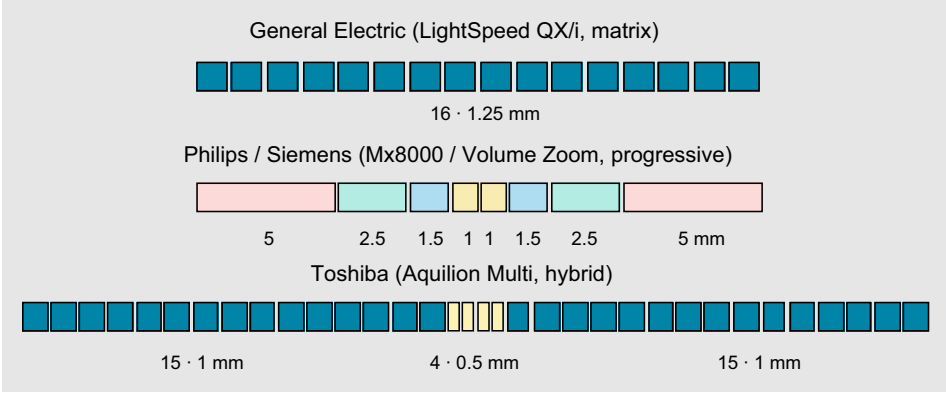

Fig. 4.11. Detector arrangement of four-slice scanners with significant differences in design (number of rows, detector size, array width). Most are optimized for simultaneous acquisition of four slices

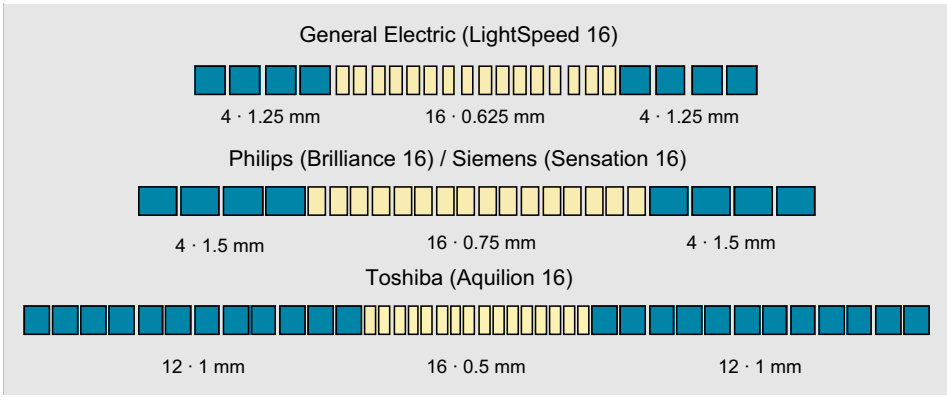

Fig. 4.12. Detector arrangement of 16-slice scanners, all of which employ a hybrid design, but with differences in the number of rows, detector size, and array width

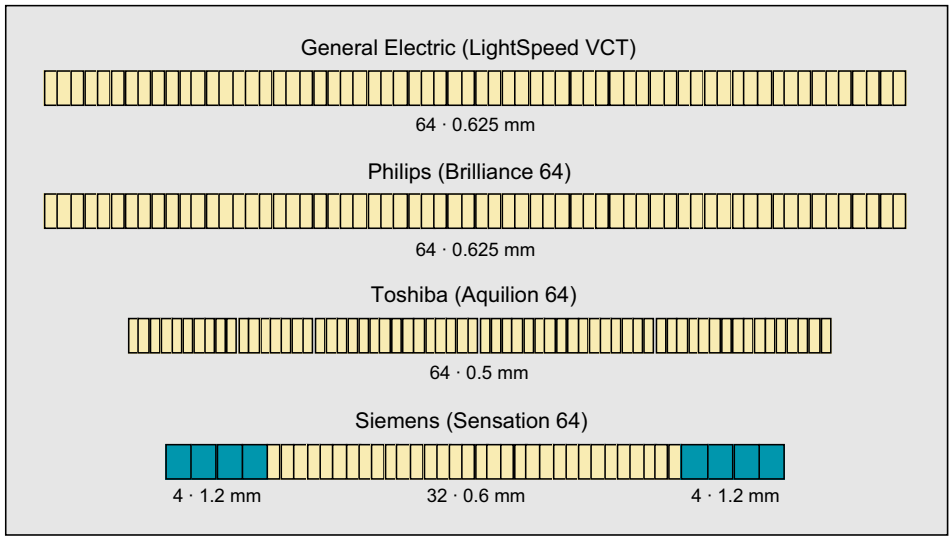

Fig. 4.13. Detector arrangement of 64-slice scanners, most of which employ a matrix design with 64 rows of uniform size. The Siemens design refers to a 32-slice scanner that makes use of a particular acquisition mode (alternating focal spot) with 64 overlapping (i.e. non-independent) slices

improved spatial resolution in the z-direction. With respect to all other important features (collimation, coverage, overbeaming effects, etc.), however, this model behaves as a 32-slice scanner in submillimeter mode and a 24-slice scanner in all other modes at maximum. In addition, the thickness of the smallest slice that can be reconstructed (relevant for partial volume effects) is at least equal to the smallest slice collimation, i.e., 0.6 mm (Flohr et al. 2004), not lower.

4.2.5 Data Acquisition System

The data acquisition system (DAS) serves to collect the detector signals, to convert them into digital information and to transfer the data to the image reconstruction system. The number of DAS channels, not the number of detector rows, is the decisive parameter that limits the number of independent slices that can be acquired simultaneously. Consequently, the term 'MDCT (multi-detector-row CT)' is somewhat misleading, as has recently happened to the term 'MSCT (multi-slice CT)', too. Thus, 'multi-channel CT (MCCT)' would be the most unequivocal notation.

With the advent of 16-slice scanners at the latest, the spatial requirements of an increased number of detector rows and the exorbitantly increased data rate no longer allow use of traditional circuit boards. Instead, application-specific integrated circuits (ASICs) have been developed, with significantly reduced dimensions (Fig. 4.14) and drastically increased data transfer capabilities. As these ASICs operate with reduced electronic noise, they are advantageous with respect to the dose efficiency of the detector assembly. This is demonstrated in Figure 4.15 where the dose that is necessary to obtain images of equal image noise at equal slice thickness was reduced by 25% with the introduction of this advanced DAS chip (Vlassenbroek 2004).

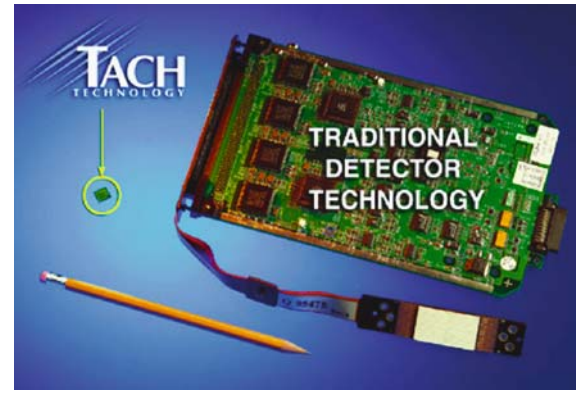

Fig. 4.14. The spatial requirements of an increased number of detector rows and the exorbitantly increased data rate necessitated the development of data acquisition systems with tiny application-specific integrated circuits (ASICs) that replaced the traditional circuit boards (courtesy: Philips Medical Systems)

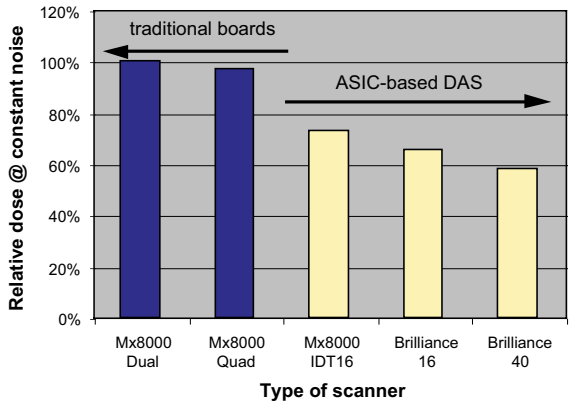

Fig. 4.15. As a side effect, the lower electronic noise of ASIC-based data acquisition systems introduced with 16-slice scanners allows for a 25% dose reduction at constant noise (beam width for all scanners: $N \cdot h_{col} = 10$ mm)

4.2.6 Spiral Interpolation

Data acquisition in spiral scanning mode requires an additional interpolation step to obtain axial slices. The interpolation scheme of single-slice scanners employs two data points for each projection angle only, thus producing a bell-shaped slice profile. Depending on whether only true data (360° linear interpolation (LI), Fig. 4.16a) or also virtual data (180° LI, Fig. 4.16b) are used, the width of the slice profile is significantly broadened with increasing pitch (Fig. 4.18a). The relative noise, however, remains independent from pitch and amounts to 83% (360° LI) and 117% (180° LI) compared with sequential scanning.

Most multi-slice scanners make use of a different interpolation scheme with more than two data points ('z-filtering', Taguchi and Aradate 1998). Depending on the slice thickness h_{rec} to be reconstructed, interpolation is made using all data points that are located inside the pre-selected filter width (FW; $= h_{rec}$, Fig. 4.17). Contrary to single-slice scanners, the width of the slice profile thus remains unaffected from changes in pitch settings of up to $p = 2$ (Fig. 4.18b).

However, as the number of data points inside FW is reduced, the noise will increase with pitch unless corrective actions are taken. This can be accomplished by adjusting the (electrical) tube current I_{el} proportional to the change in pitch p. This adjustment is automatically made for all MSCT scanners from Elscint, Philips and Siemens, thereby using a different mAs notation (Q_{eff}) named 'effective mAs' or 'mAs per slice', which is different from the traditional electric mAs product Q_{el}:

$$Q_{eff} = \frac{I_{el} \cdot t_{rot}}{p} = \frac{Q_{el}}{p} \qquad (4.15)$$

As a result, pitch has no longer any influence on slice profile width, image noise and average dose ($CTDI_{vol}$) if Q_{eff} is held constant. This does not hold for MSCT scanners manufactured by General Electric and Toshiba, which do not automatically correct the tube current for pitch and do not use effective mAs notation.

4.2.7 Adaptive Filtration

Adaptive filtration (AF) is a dedicated data processing technique for projections that are subject to strong attenuation. Without AF, images, e.g., from the pelvis region, often exhibit inhomogeneous noise patterns due to 'photon starvation' (Fig. 4.19, left). The noise statistics of these projections are improved by making use of additional data close to the position of the reconstructed slice, i.e., by increasing the FW at the level of image reconstruction. However, as indicated in Figure 4.20, this is made only for those projections that suffer from excessive attenuation. Thus, the spatial resolution in the z-direction is only slightly impaired. As a result, images processed with AF show a reduced and more homogeneous noise pattern (Fig. 4.19, right). This can be used either to improve the image quality or to lower the dose settings.

4.2.8 Overranging

'Overranging' is the increase in DLP due to the additional rotations at the beginning and at the end of a spiral scan required for data interpolation to reconstruct the first and the last slice of the imaged body region. With single-slice scanners, the theory requires that $\Delta n = 1$ additional rotation is usually made in total (Kalender 2000). For multi-slice scanners, the situation is much less obvious, as will be seen from the results presented below.

Overranging effects can be expressed in terms of both the additional number Δn of rotations and the increase ΔL in scan length. ΔL depends primarily on two factors: the beam width $N \cdot h_{col}$ and the pitch fac-

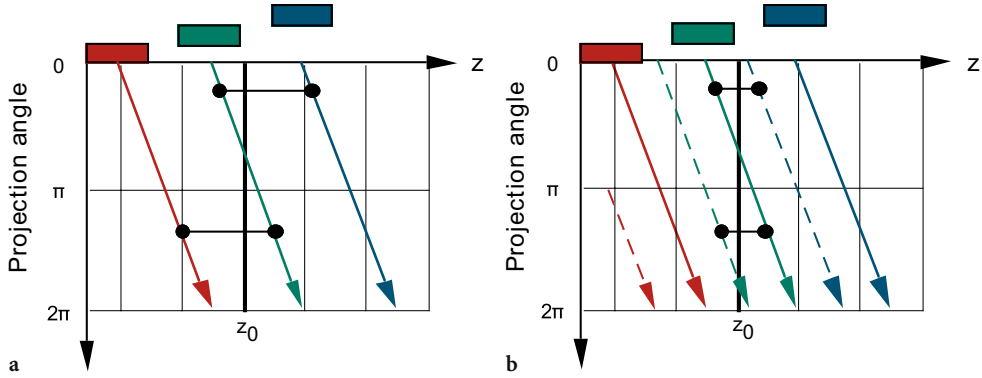

Fig. 4.16a,b. The most common interpolation schemes for single-slice scanners are either 360° LI (**a**) or 180° LI (**b**). Both schemes employ two data points closest to the position z_0 of the reconstructed slice for each projection angle. Making use of the virtual (*complementary*) data (*dashed lines*), a shorter interpolation distance is achieved with 180° LI, resulting in a narrower slice profile

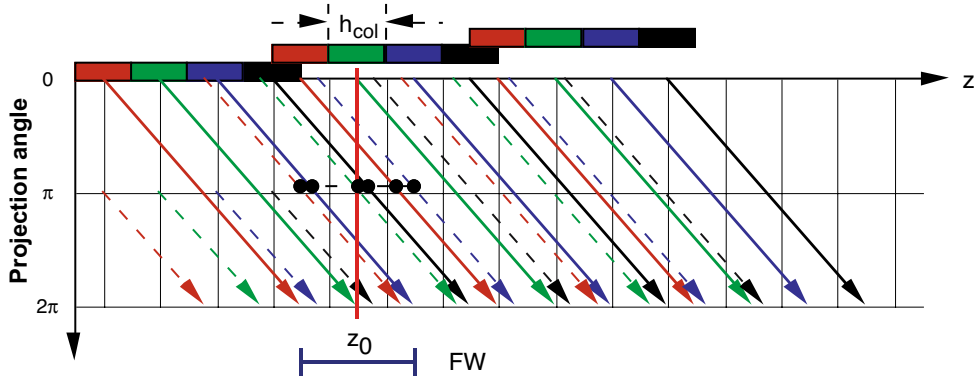

Fig. 4.17. Most multi-slice computed tomography (MSCT) makes use of a filtered multi-point data interpolation scheme (z-filtering). All data points (true and virtual) lying inside a pre-selected filter width (FW) contribute to the slice reconstructed at position z_0, with slice thickness $h_{rec} = FW$. In this example, the interpolation scheme for a 4-slice scanner at pitch 0.875 is shown ($FW = 2 \cdot h_{col}$)

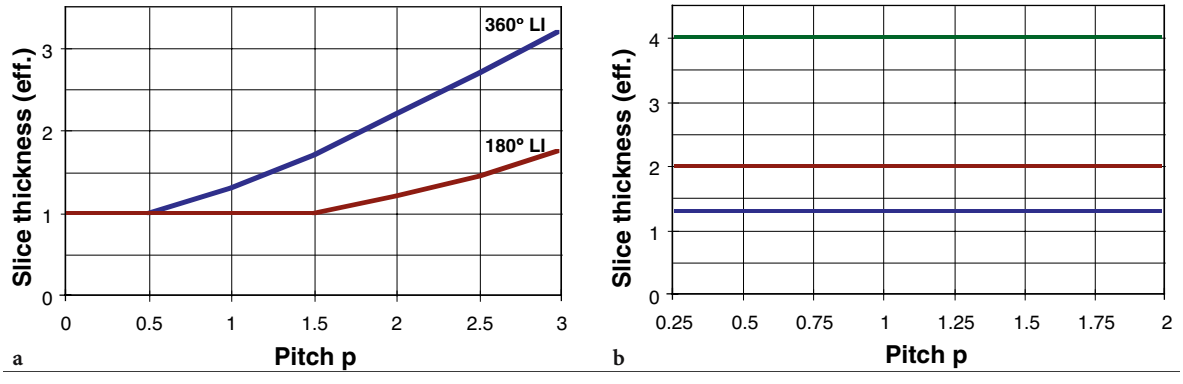

Fig. 4.18a,b. With single-slice scanner, two-point data interpolation results in a significant broadening of the effective slice thickness with increasing pitch, depending on the selected interpolation scheme (**a**). The multi-point data interpolation used for most multi-slice scanners ensures a constant effective slice thickness regardless of the pitch setting that depends only on the selected filter width and holds up to $p = 2$ (**b**)

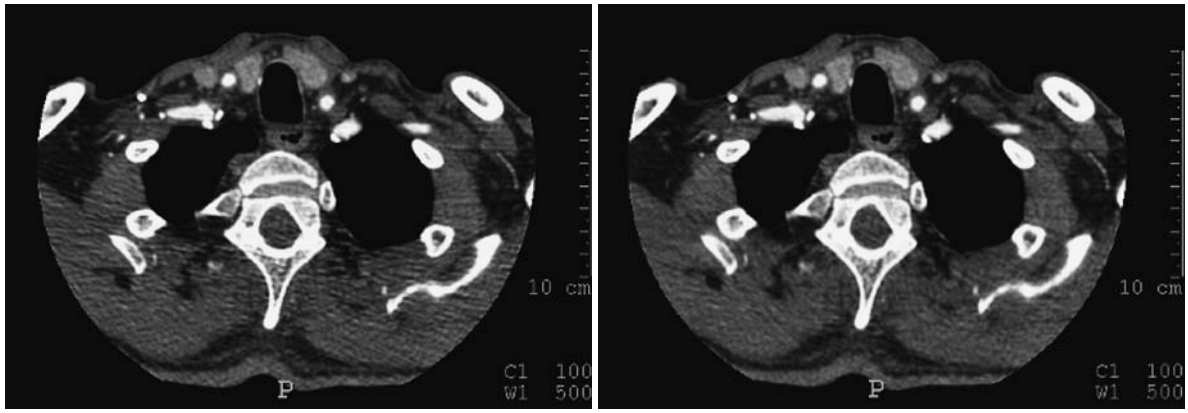

Fig. 4.19. Projections suffering from excessive attenuation result in images with unisotropic noise patterns (*left*); images processed with adaptive filtration show a reduced and more homogeneous noise pattern (*right*)

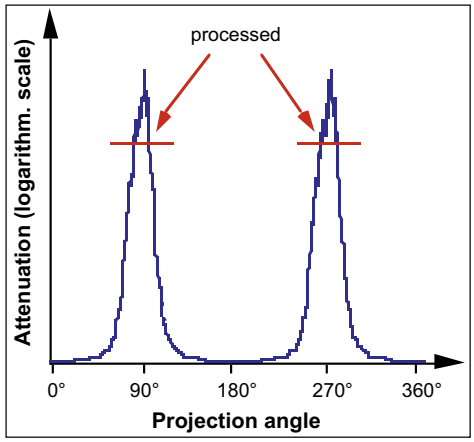

Fig. 4.20. Adaptive filtration affects only those projections where the attenuation exceeds a pre-selected level

tor p. This can be fairly well described by a linear relationship (Nagel 2005):

$$\Delta L = (m_{OR} \cdot p + b_{OR}) \cdot N \cdot h_{col} \tag{4.16}$$

While single-slice scanners behave as expected from theory, the characteristics of typical MSCT scanners differ markedly. The number Δn of additional rotations (Fig. 4.21a) is strongly pitch dependent, while the normalized elongation of the scan range, $\Delta L/N{\cdot}h_{col}$, is almost independent of pitch (Fig. 4.21b) and amounts to approximately 1.5, i.e., ΔL is typically 1.5 times the total beam width $N{\cdot}h_{col}$. For most single-slice scanners, the overranging parameters m_{OR} and b_{OR} are equal to 2 and –1, respectively. For the majority of MSCT scanners, typical values for m_{OR} and b_{OR} are 1 and 0.5, respectively.

The implications of overranging effects for the radiation exposure to the patient, i.e., the DLP, depend not only on ΔL, but also on the length L_{net} of the imaged body region. The percentage increase in DLP is given by

$$\Delta DLP_{rel} = \frac{\Delta L}{L_{net}} \cdot 100 \tag{4.17}$$

and will be largest if ΔL is large and L_{net} is small.

The extent of overranging is shown in Figure 4.22 for a representative selection of single and multi-slice scanners from different manufacturers for typical scan parameter settings and a typical scan length of 20 cm. Overranging effects are normally almost negligible for single-slice and the majority of dual- and quad-slice scanners. Contrary to overbeaming, overranging becomes larger with an increasing number of slices acquired simultaneously due to the enlarged beam width. Even greater values might occur for beam widths larger than the typical ones assumed here and scan ranges shorter than 20 cm.

4.2.9 Devices for Automatic Dose Control

Newer scanners are equipped with means that automatically adapt the mAs settings to the individual size and shape of the patient. As this matter is discussed in detail in Chapter 6, only a brief overview shall be given here.

Automatic dose control systems offer up to four different functionalities, that can be used either alone or in combination:

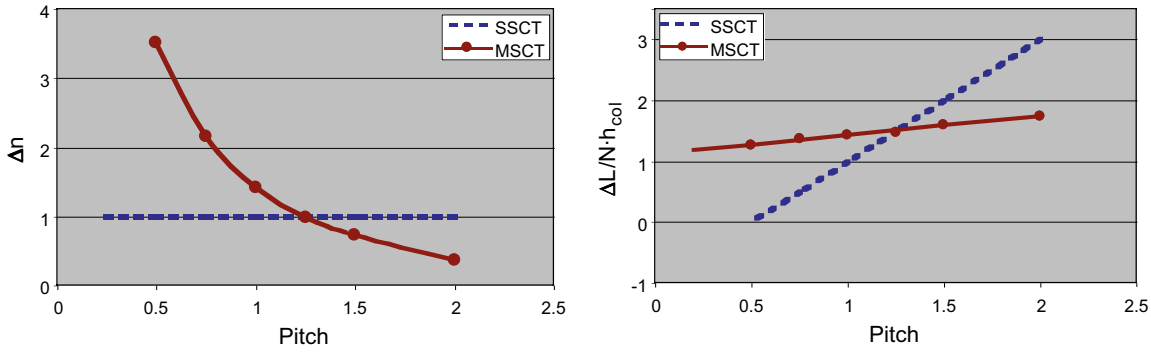

Fig. 4.21. While single-slice computed tomography scanners (SSCTs) usually require only one additional rotation Δn in spiral scanning mode, multi-slice computed tomography scanners (MSCTs) show a pronounced pitch dependence. Conversely, the normalized elongation of the scan range, $\Delta L/N \cdot h_{col}$, is almost constant for most MSCT scanners, but increases linearly with pitch for SSCT scanners

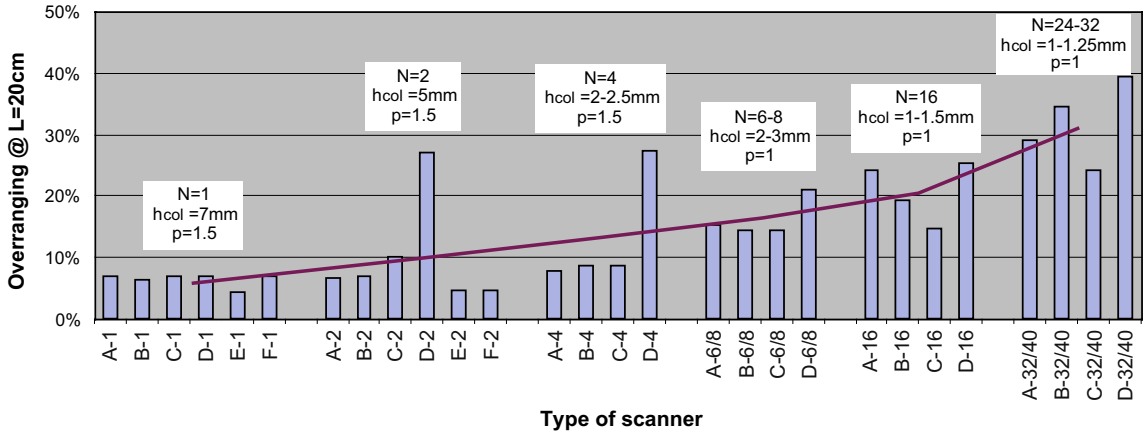

Fig. 4.22. Overranging, i.e., the percentage increase in dose–length product (DLP), for single-slice ($n=1$), dual-slice ($n=2$), quad-slice ($n=4$), 6 to 8-slice ($n=6$–8), 16-slice ($n=16$) and 32 to 40-slice ($n=32$–40) scanners from different manufacturers (A–F) for a scan length L of 20 cm and the slice collimations and pitch settings typically employed. The *red trend line* indicates that overranging becomes more pronounced with scanners that allow for a wider beam width $N \cdot h_{col}$

- Automatic exposure control (AEC, Fig. 4.23), which accounts for the average attenuation of the patient's body region that is to be scanned. Information on the patient's attenuation properties is derived from the scan projection radiogram (SPR) usually recorded prior to the scan for planning purposes.
- Longitudinal dose modulation (LDM, Fig. 4.24), which is a refinement of AEC by adapting the mAs settings locally, i.e., slice-by-slice or rotation by rotation.
- Angular dose modulation (ADM, Fig. 4.25), another refinement of AEC that adapts the tube current to the varying attenuation at different projection angles. Information on the patient's attenuation properties is derived either from two SPR or in real-time from the preceding rotation.
- Temporal dose modulation (TDM, Fig. 4.26), which reduces the tube current in cardiac CT (or other ECG-gated CT examinations) during those phases of the cardiac cycle that are not suited for image reconstruction due to excessive object motion.

The common denominator of these functionalities is that the user no longer needs to select his parameter settings with respect to the 'worst case',

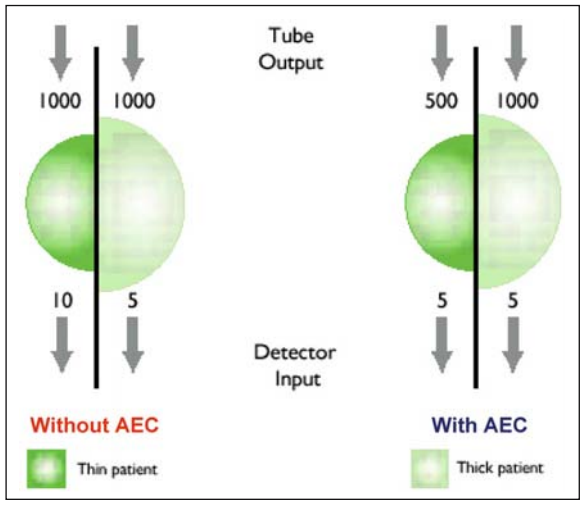

Fig. 4.23. Automatic exposure control (AEC) accounts for the average attenuation of the patient's body region that is to be scanned. For slim patients, mAs is reduced to a level that ensures constant image quality

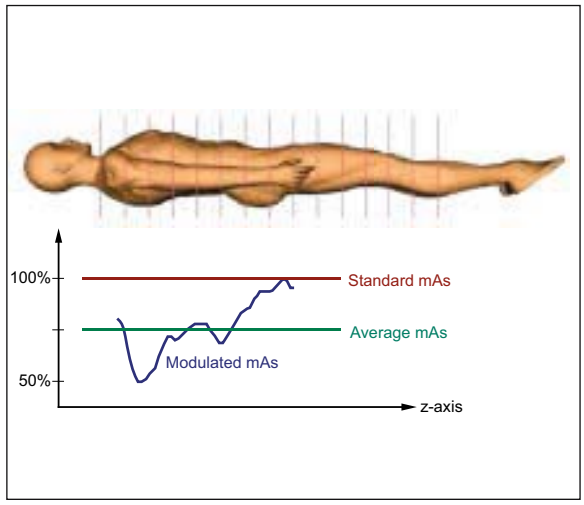

Fig. 4.24. Longitudinal dose modulation (LDM) is a refinement of AEC that adapts the mAs settings slice-by-slice or rotation by rotation. Those parts of the scan range with reduced attenuation will be less exposed

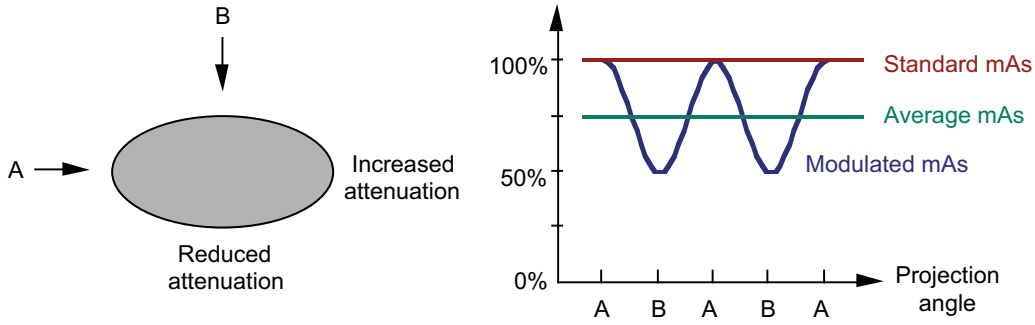

Fig. 4.25. Angular dose modulation (ADM) is an other refinement of AEC that adapts the tube current to the varying attenuation at different projection angles. Those projections with reduced attenuation will be less exposed

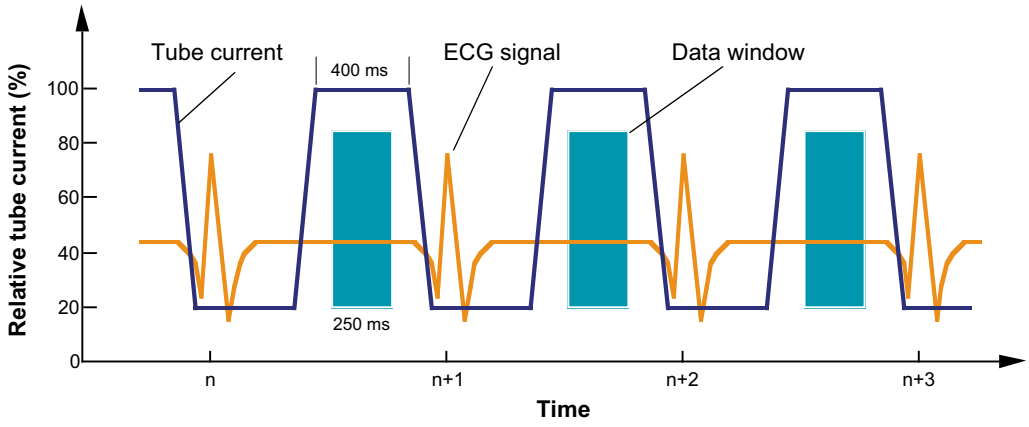

Fig. 4.26. In cardiac computed tomography (CT; or other ECG-gated CT examinations), temporal dose modulation (TDM) reduces the tube current during those phases of the cardiac cycle that are not suited for image reconstruction due to excessive object motion

i.e., obese patients, the part of the scan range with the highest attenuation (e.g., shoulder in chest exams), the projection with the highest attenuation (lateral), etc. Consequently, a significant dose reduction from the application of these devices can be expected.

All major CT manufacturers now offer some or all of these functionalities with their latest scanners. A comprehensive report on the current status of automatic dose control systems has been published by ImPACT (2005). However, there are significant differences in how these devices operate and perform. At present, some of these systems are not sufficiently user-friendly and make adjustments in a way that seems to be theoretically sound, but does not comply with other, more comprehensive aspects of image quality. Some of these shortcomings will be discussed in the following section.

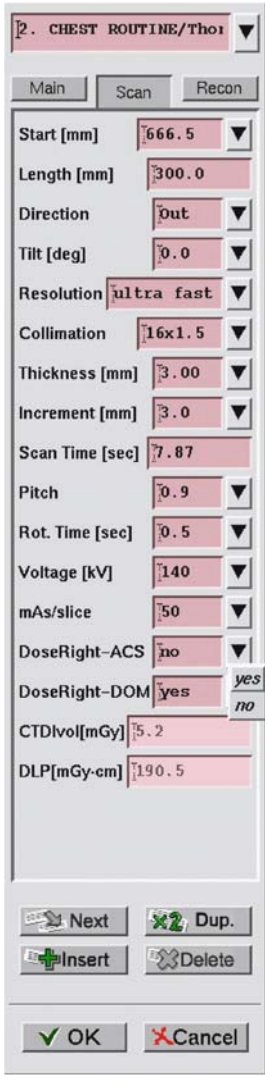

Fig. 4.27. Scan protocol window of a Philips Mx8000 IDT scanner with dose display ($CTDI_{vol}$ and DLP per scan series) at the bottom

4.2.10 Dose Display

Newer scanners must be equipped with a dose display. At present, only the display of $CTDI_{vol}$ is mandatory (IEC 2001). However, many scanners already also show the DLP, either just per scan series or both per scan series and per exam. An example with display of $CTDI_{vol}$ and DLP per scan series is shown in Figure 4.27.

With the dose display, dose is not saved per se, but feedback is provided that may help to achieve this goal, e.g., by comparison of the displayed dose values with dose recommendations. In addition, changes in scan parameter settings and their implications for patient exposure are made immediately obvious. Thus, the dose display can be used for purposes of dose optimization. Finally, $CTDI_{vol}$ can be used as a fair estimate for the dose to organs that are entirely located in the scan range.

The interpretation of the dose values displayed at the scanner's console needs special attention in the following situations:

- Many dose recommendations are given in terms of weighted CTDI ($CTDI_w$); in order to allow for comparisons, the pitch correction involved in $CTDI_{vol}$ must be reverted by multiplying $CTDI_{vol}$ by the pitch factor.
- Until now, the dose values for examinations carried out in body scanning mode have always been based on body-CTDI regardless of patient size. In pediatric CT examinations, the displayed figures should be multiplied by 2 for children and by 3 for infants in order to give a realistic estimate of patient dose.

4.3 Application-Related Factors

Although the scanner design is of some importance, surveys on CT practice have regularly shown that the way that the scanner is used has the largest impact on the doses applied in a CT examination. The application-related factors on which patient exposure depends can be grouped into:

- Scan parameters, i.e., those factors that directly determine the local dose level ($CTDI_{vol}$) and that are often pre-installed or recommended by the manufacturer (e.g., in application guides)

- Examination parameter, i.e., those factors that–in combination with $CTDI_{vol}$–determine the integral exposure (i.e., DLP) and depend on the preferences of the user
- Reconstruction and viewing parameters, which implicitly influence the dose settings

First, however, the principal inter-dependence between dose settings and image quality shall be outlined

4.3.1 Brooks' Formula

As in conventional projection radiography, aspects of dose and image quality are linked. For CT, Brooks and DiChiro (1976) have formulated the correlation between these two opposed quantities:

$$D \propto \frac{B}{\sigma^2 \cdot a^2 \cdot b \cdot h} \text{ with } B = \exp^{-\mu \cdot d} \quad (4.18)$$

where

D = patient dose
B = attenuation factor of the object
μ = mean attenuation coefficient of the object
d = diameter of the object
σ = standard deviation of CT numbers (noise)
a = sample increment
b = sample width
h = slice thickness

This fundamental equation–commonly known as the 'Brooks' formula'–describes what happens with respect to patient dose if one of the parameters is changed while image noise remains constant:

- Dose must be doubled if slice thickness is cut by half
- Dose must be doubled if object diameter increases by 4 cm
- An eightfold increase in dose is required if spatial resolution is doubled (by cutting sample width and sample increment by half)

In this context, the term 'dose' is applicable to each of the dose quantities that are appropriate for CT. Dose and noise are inversely related to each other in such a way that a fourfold increase in dose is required if noise is to be cut by half.

It should be noted, however, that the Brooks' formula is incomplete, in that image quality is only considered in terms of quantum noise and spatial resolution. Other important influences, such as contrast, electronic noise and artifacts, are not taken into account and will therefore modify optimization strategies under particular circumstances.

4.3.2 Scan Parameters

4.3.2.1 Tube Current–Time Product (Q)

As in conventional radiology, a linear relationship exists between the tube current–time product and dose; i.e., all dose quantities will change by the same amount as the applied mAs. The mAs product Q for a single sequential scan is obtained by multiplying the tube current I and exposure time t; in spiral scanning mode, Q is the product of the tube current I and rotation time t_{rot} .This should not be mixed up with the total mAs product of the scan which is the product of tube current I and (total) scan time T.

The consequences on image quality resulting from variations in the tube current–time product are relatively simple to understand. The only aspect of image quality so affected is image noise, which is–as indicated in Equation 4.18–inversely proportional to the square root of dose (i.e., mAs).

The tube current–time product is often used as a surrogate for the patient dose (i.e., CTDI). However, this is highly misleading, as the normalized CTDI values and thus the dose that results for the same mAs setting can vary by up to a factor of six between different scanners. So it makes absolutely no sense to communicate dose information or recommendations on the basis of mAs. Instead, only $CTDI_{vol}$ (and DLP) should be used for this purpose.

With the advent of multi-slice scanners, additional confusion arose due to the introduction of a different, pitch-corrected mAs notation ('effective mAs' or 'mAs per slice', Eq. 4.15) by Elscint, Philips and Siemens. As most multi-slice scanners make use of a multi-point spiral interpolation scheme as outlined in section 4.2.6, effective mAs is the most appropriate notation for MSCT. Nevertheless, General Electric and Toshiba still prefer the traditional electrical mAs notation, which further makes it difficult to compare mAs settings among different scanners. This particularly holds for cardiac CT where very low pitch settings are used.

Recommendation:
The settings for the tube current–time product should be adapted to the characteristics of the scanner, the size of the patient (see section 4.3.2.5), and the dose requirements of each type of examination. Examinations with high inherent contrast, such as for chest or skeleton, that are characterized by viewing with wide window settings, can regularly be conducted at significantly reduced mAs settings.

4.3.2.2 Tube Potential (U)

When the tube potential is increased, both the tube output and the penetrating power of the beam are improved, while image contrast is adversely affected. In conventional projection radiography, increased tube potentials are applied in order to ensure short exposure times for obese patients, to equalize large differences in object transmission (e.g., during chest examinations) or to reduce patient dose. In the latter case, automatic exposure control devices guarantees that the improved penetrating power of the beam is exclusively for the benefit of the patient.

In CT, increased tube voltages are used preferentially for improvements in tube loading and image quality. Contrary to the case for mAs, the consequences of variations in kV cannot easily be assessed. The relationship between dose and tube potential U is not linear, but rather of an exponential nature which varies according to the specific circumstances. The intensity of the radiation beam at the detector array, for example, varies with U to the power of 3.5. If the tube potential is increased, e.g., from 120 kV to 140 kV, the electrical signal obtained from the detectors therefore changes by a factor 1.7 (Fig. 4.28).

The decrease in primary contrast which normally results from this action is largely overcompensated by the associated decrease in noise, i.e., the higher the tube potential, the better the CNR (except for the application of iodine as contrast agent). The only reason why this analysis generally holds true is the absence of any kind of automatic exposure control devices in the majority of scanners which might prevent unnecessary increases in the detector signal. This clearly demonstrates that dose is not reduced by applying higher kilovolt settings, but merely increased as long as mAs settings are not changed: weighted CTDI and effective dose increase with U to the power of 2.5 (Fig. 4.28), which means that both are increased by approximately 50% if kilovolt settings are changed from 120 kV to 140 kV.

Therefore the question of whether and when it might be reasonable to deviate from the 120-kV setting usually applied is justified. As can be seen from Figure 4.29, this depends on the attenuation characteristics of the detail that is diagnostically relevant. The figures are given in terms of contrast-to-noise ratio squared (CNR^2) at constant patient dose; this notation allows direct conversion of the percentage differences into dose differences. For soft tissue contrast (e.g., differences in tissue density), higher tube potentials perform slightly better than lower ones, but the differences are quite small. The opposite holds true for bone contrast (i.e., bone versus tissue). For iodine contrast, however, there is a strong dependence on tube potential that is much in favor of lower kilovolt settings. Thus, 80 kV instead of 120 kV would allow reduction of the patient dose

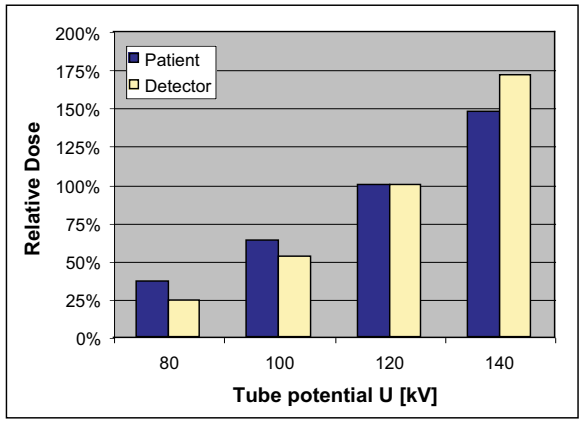

Fig. 4.28. Voltage dependence of patient dose ($CTDI_w$) and detector signal (reference: 120 kV)

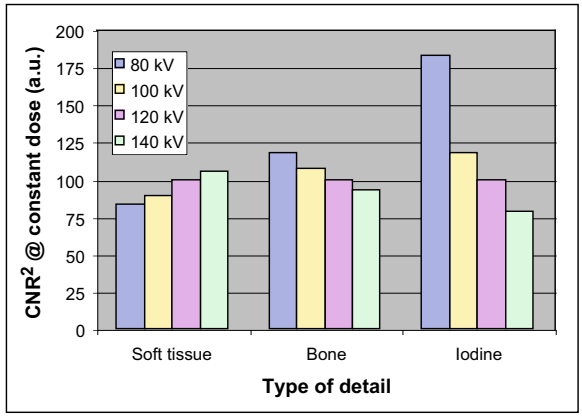

Fig. 4.29. Voltage dependence of contrast-to noise ratio squared (CNR^2) at constant patient dose ($CTDI_w$) for different types of detail. While CNR^2 is almost constant for imaging of soft tissue and bone, imaging performance is significantly improved for iodine at lower voltages

by almost a factor of two without sacrificing image quality.

Recommendation:

Tube potentials other than 120 kV should be considered only in the case of:

- Obese patients in whom mAs cannot be further increased: use higher kilovolt settings
- Slim patients and pediatric CT, where mAs cannot be further reduced: use lower kilovolt settings
- CT angiography with iodine: use lower kilovolt settings

Variations in tube potential should not be considered for pure dose reduction purposes except in the case of CT angiography. Due to the complexity involved, adaptation of mAs settings should not be left to AEC systems, as these do not account for changes in contrast. Dose settings in CT angiography should not be higher than in unenhanced scans of the same body section and should be lowered if performed at reduced kilovolt settings.

4.3.2.3 Slice Collimation (h_{col}) and Slice Thickness (h_{rec})

With single-slice CT (SSCT), the slice collimation h_{col} used for data acquisition and the reconstructed slice thickness h_{rec} used for viewing purposes were identical (except for slice profile broadening in spiral scans with increased pitch, as discussed in section 4.2.6). So there was no need to distinguish between them. With MSCT, the slice collimation (e.g., 0.75 mm) and the reconstructed slice thickness h_{rec} (e.g., 5 mm) are usually different. Frequently, the selection of the reconstructed slice thickness is made with respect to multi-planar reformatting (MPR) purposes (e.g., 1 mm), thus creating a so-called 'secondary raw data set', i.e., a stack of thin slices from which MPR slabs with larger thickness (e.g., 5 mm) can be made for viewing purposes.

The ability to acquire longer body sections with thin slices in order to achieve an almost isotropic spatial resolution is the most important achievement of multi-slice technology. As reduced slice thickness is associated with increased image noise, this may have a significant impact on patient dose as expressed by the Brooks' formula (Eq. 4.18). Therefore, it is worthwhile to treat this matter in a somewhat more detailed fashion.

A narrow slice collimation is a precondition for a narrow slice thickness, but its impact on patient dose is restricted to aspects of overbeaming and overranging only. As these show opposed dependence on beam width, as outlined in sections 4.2.3 and 4.2.8, the question arises as to the optimized beam-width settings. As demonstrated in Figure 4.30 for a typical MSCT scanner, dose performance is almost equal with beam-width settings greater than 10 mm (a), except at short scan ranges (spine, pediatrics) where a beam width of between 10 mm and 20 mm is more appropriate (b). Beam-width settings below 10 mm should be avoided due to increased overbeaming effects unless there are other important aspects to justify overriding this recommendation.

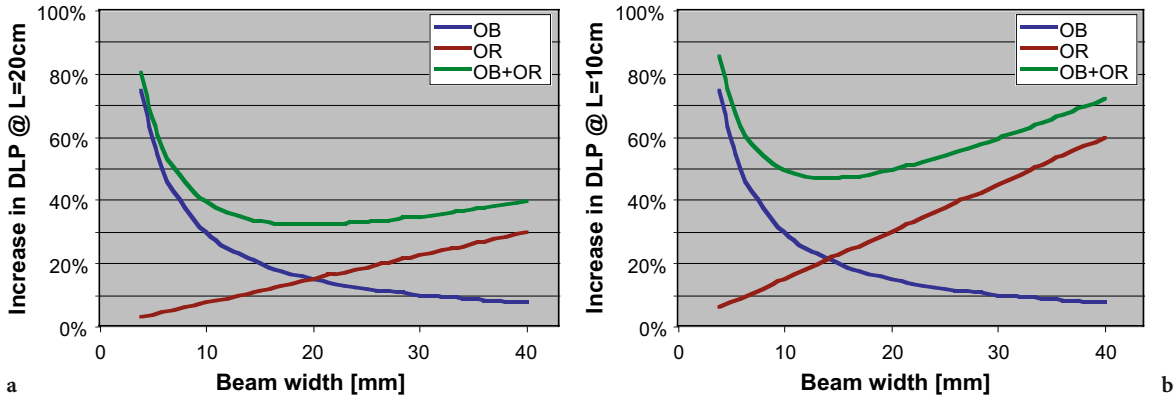

Fig. 4.30a,b. Increased dose–length product due to overbeaming (*OB*) and overranging (*OR*) effects for a typical multi-slice computed tomography (MSCT) scanner. For average to long scan ranges (L = 20 cm and more, **a**), all beam-width settings above 10 mm perform almost equally well. For short scan ranges (L = 10 cm, as in pediatric and spine exams, **b**), beam-width settings between 10 mm and 20 mm are preferred

The decisive determinant with respect to image noise and its implications for patient dose, however, is the slice thickness h_{rec} used for viewing purposes. The relationship among slice thickness, noise and dose expressed in the Brooks' formula attempts to correct any reduction in slice thickness by a corresponding increase in dose to ensure a constant image noise, and some AEC systems exactly do so. However, any variation in slice thickness also affects image contrast due to a modification in partial volume effect, which is not taken into account by the Brooks' formula. As shown in Figure 4.31, image noise and image contrast of small details will react in a different fashion on reduction of the slice thickness: while image quality in terms of noise is impaired proportionally to the square root of the change in slice thickness only, the contrast is improved in proportion to the slice thickness. As a result, there is a net gain in image quality in terms of CNR without any increase in dose whenever partial volume effect is of importance.

This is clearly demonstrated by the clinical example given in Figure 4.32, where the visibility of a liver lesion (approximately 3 mm in size) diminishes continually with increasing slice thickness, despite reduced image noise. In addition, a detailed analysis of the results of the German survey on CT practice in 1999 (Galanski et al. 2001) has revealed that slice thickness has only minor or no influence on clinical dose settings. This is shown in Figure 4.33 for liver examinations with slice thicknesses of between 3 mm and 10 mm that were used in practice. Therefore, it is essential to understand that the selection of a narrow slice collimation is only a means to an end: to enable MPR images without or with reduced step artifacts, and, if necessary, to overcome partial volume effects.

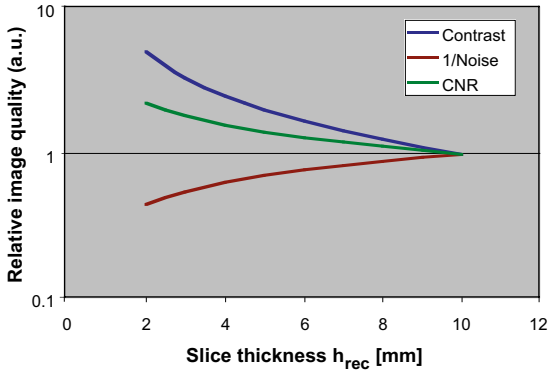

Fig. 4.31. Dependence of relative image quality on the slice thickness h_{rec}. Improvements in image quality (better detail contrast due to reduced partial volume effects) outweigh the deterioration caused by increased noise. As a result there is a net gain in contrast-to-noise ratio (CNR) at reduced slice thickness without any increase in dose

Recommendation:

The slice collimation should be selected as small as compatible with aspects of overbeaming/overranging, total scan time and tube power. Viewing should preferentially be made with thicker slabs (e.g., 3–8 mm), thereby reducing image noise and other artifacts. Thinner slabs should only be used if partial volume effect is of importance. This should preferentially be done in conjunction with workstations that allow one to change the slab thickness in real-time. Except for very narrow slices, there should be no need for any increase in dose settings on reduction of slice thickness.

4.3.2.4 Pitch (p)

With SSCT scanners, scanning at increased pitch settings primarily serves to increase the speed of data acquisition. As a side effect, however, patient dose is reduced accordingly, at the expense of impaired slice profile width, i.e., z-resolution. As already outlined in section 4.2.6, MSCT scanners make use of a spiral interpolation scheme that is different from SSCT. Thus, the slice profile width remains unaffected from changes in pitch settings. Instead, image noise changes with pitch (Fig. 4.34a) unless the tube current is adapted accordingly.

Scanners that make use of the effective mAs (mAs per slice) concept not only keep slice profile width, but also image noise constant when pitch changes (Fig. 4.34a). To achieve this goal, the electrical mAs product supplied to the X-ray tube automatically changes linearly with pitch (Fig. 4.34b). As a consequence, patient dose ($CTDI_{vol}$) is no longer reduced at increased pitch settings in contrast with SSCT scanners; neither will dose increase at reduced pitch settings. MSCT scanners without automatic adaptation of mAs will still save dose at increased pitch setting, but this will happen at impaired image quality (more noise) as long as mAs is not adapted manually.

Frequently, image quality in terms of artifacts depends on pitch settings. In general, spiral artifacts are reduced at lower pitch settings. For similar reasons, some scanners allow the setting of a limited

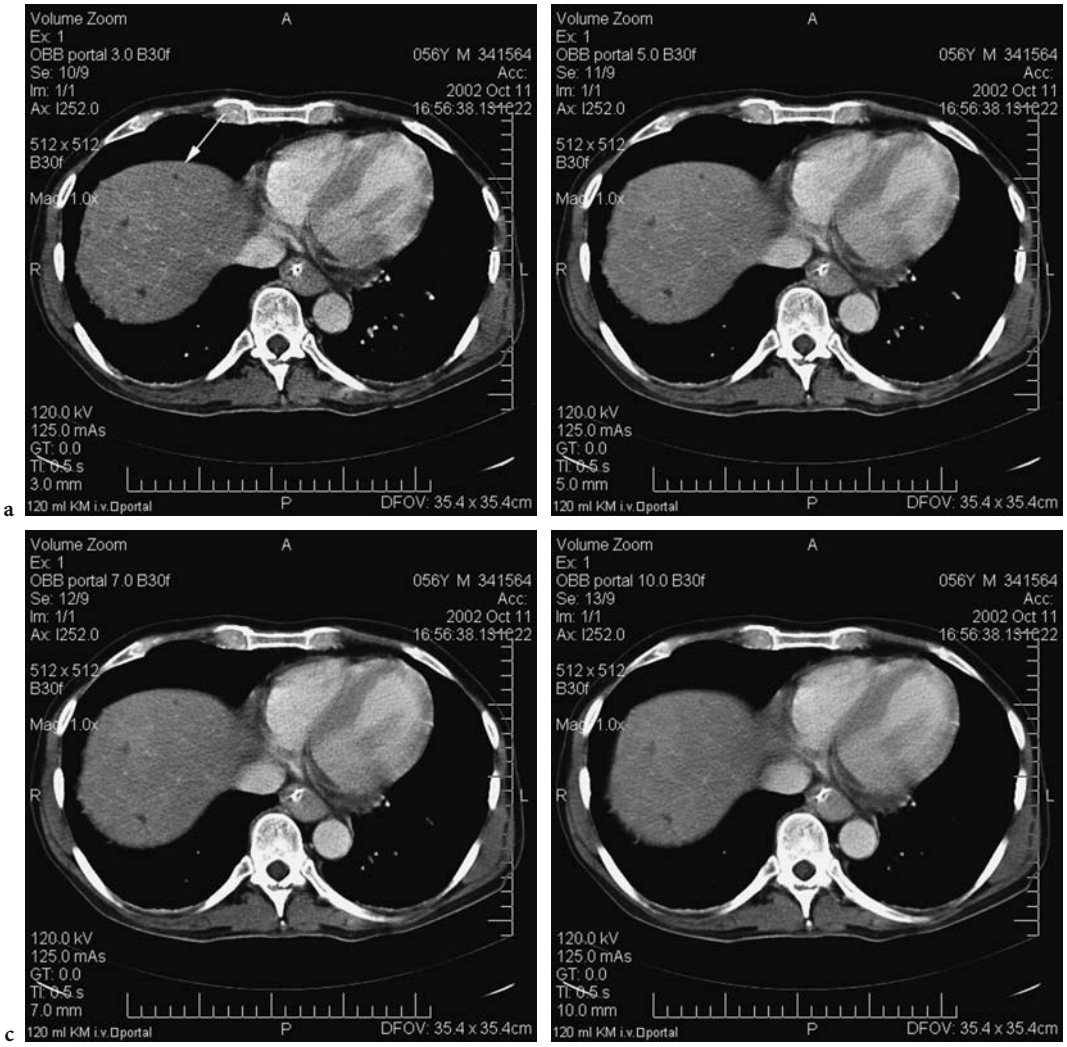

Fig. 4.32a–d. Multi-slice computed tomography (MSCT) examination of the liver performed on a MSCT scanner (Siemens Somatom Volume Zoom) at 120 kV, 4×2.5 mm slice collimation and 125 mAs_{eff} ($CTDI_{vol}$ = 11 mGy). From the same raw data set, slices of different thickness [3 mm (**a**), 5 mm (**b**), 7 mm (**c**), and 10 mm (**d**)] were reconstructed at the same central position z_0. Despite the increased noise pertaining to thinner slices, the visibility of small lesions improves remarkably owing to reduced partial volume effects. This is clearly demonstrated by a lesion approximately 3 mm in size (*arrow*) (courtesy Dr. Wedegaertner, University Hospital Eppendorf, Hamburg, Germany)

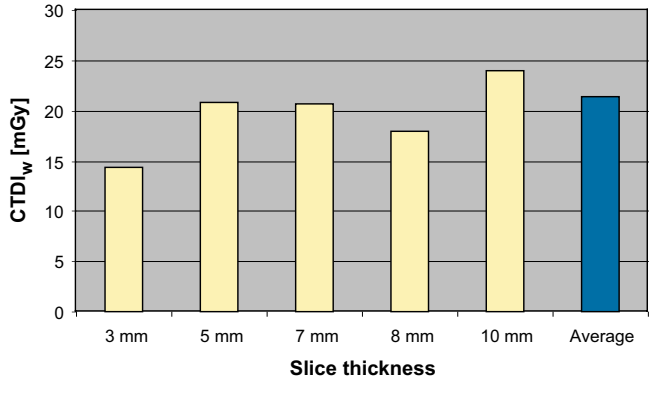

Fig. 4.33. The patient dose ($CTDI_w$) applied by the participants of the German CT survey, 1999, for liver examinations was almost constant despite the selection of different slice thickness

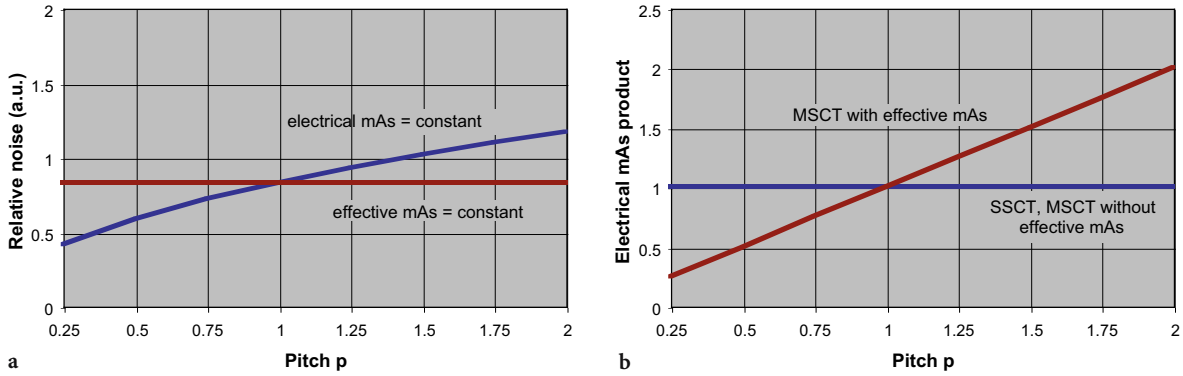

Fig. 4.34a,b. For multi-slice computed tomography (MSCT) systems that employ multi-point spiral data interpolation (z-filtering), image noise changes with pitch unless the effective current–time product (mAs_{eff}) is held constant (**a**). This implies that the electrical current–time product (mAs_{el}) supplied to the tube changes with pitch (**b**). Contrary to single-slice computed tomography (SSCT), changes in pitch settings therefore no longer have any influence on patient dose in terms of $CTDI_{vol}$

number of 'preferred' pitches only. Reduced pitch settings can also be applied to enhance the effective tube power, however, at the expense of reduced scanning speed.

Recommendation:

Pitch settings with MSCT scanners should be made exclusively with respect to scan speed, spiral artifacts and tube power. Dose considerations no longer play a role if scanners that employ effective mAs are used or if (electrical) mAs is adapted to pitch to achieve constant image noise.

4.3.2.5 Object Diameter (d) or Patient Weight (m)

Patient size, although not a parameter to be selected at the scanner's console, represents an important influencing parameter that needs to be considered in this context. Considerable reductions in mAs settings are appropriate whenever slim patients, and particularly children, are examined. In order to avoid unnecessary over-exposure, the mAs must be intentionally adapted by the operator unless AEC-like devices are available. Due to the decreased attenuation for the smaller object, image quality will not be impaired if mAs is selected appropriately. This means that the image quality will be at least as good as for patients of normal size, although the dose has been reduced.

The two questions to be solved in this context are:

- To which degree shall mAs settings be adapted in dependence of the object diameter d?
- Which diameter is typical for a standard patient to whom the standard protocol settings refer to?

From theoretical considerations (half-value thickness for CT beam qualities), mAs should be altered by a factor of two for each change in patient diameter of 4 cm tissue-equivalent thickness. However, dedicated studies (Wilting et al. 2001) have shown that this algorithm does not work well in practice: although objective (i.e., measured) noise was almost constant for patient diameters of between 24 cm and 36 cm, it was found that the subjective (i.e., perceived) image quality continually decreased with the patient diameter and vice versa. This is most likely due to the circumstance that adipose patients have more fatty tissue around their organs. Thus, the inherent contrast is better, and more noise can be tolerated. The opposite holds true with slim patients.

Consequently, a more gentle adaptation of mAs with patient diameter (factor of two in mAs per 8-cm change in patient diameter) will better comply with clinical needs. Among the AEC systems currently in use, those from Philips and Siemens already make use of this modified algorithm that ensures a constant 'adequate' image quality, while those implemented by General Electric and Toshiba simply attempt to ensure a constant noise level. As already outlined in sections 4.3.2.2 for tube potential and 4.3.2.3 for slice thickness, strategies for automatic dose control that do not account for image contrast will fall short with respect to clinical needs. Similar considerations apply to the longitudinal dose modulation functionality: in

examinations comprising several consecutive body sections with differing attenuation properties (e.g., in tumor staging of chest, abdomen and pelvis in a single spiral acquisition), mAs adjustment is often made in a way that ensures constant image noise, thus producing the highest settings in the pelvis region. However, inherent contrast in the pelvis region is much better than in the upper abdomen; consequently, reduced mAs settings would be more appropriate, as recommended in ICRP publication 88 (ICRP 2001).

Although not specified explicitly, standard protocol settings implemented by the manufacturers are usually tailored to satisfy the vast majority of clinical situations except for obese patients in whom higher mAs or kilovolt settings must be applied. So, there is good reason to refer these standard settings to patients of about 80–85 kg body weight, which is also the average weight of European males. This corresponds to a lateral diameter of 33 cm, according to a detailed analysis of patient data from a large children's hospital in Germany (Schneider 2003; Fig. 4.35a.). The following formula can be used to convert from lateral patient diameter d_{lat} (in cm) to patient weight m (in kg) and vice versa:

$$d_{lat} = 6.5 + 3 \cdot \sqrt{m} \tag{4.19}$$

In current literature, numerous differing recommendations can be found on how to reduce mAs settings with patient weight or diameter. In Fig. 4.35b, three examples are shown, which are representative of weak (Donelly et al. 2001), moderate (Rogalla 2004) and strong (Huda et al. 2000) adaptations of mAs to patient weight. As indicated by the dashed lines, mAs adaptation by a factor of two per 8-cm change in patient diameter is almost perfectly met by Rogalla's recommendation, which follows a very simple relationship:

$$\textit{Relative mAs} \propto \textit{body weight} + 5\ \textit{kg} \tag{4.20}$$

A similar relationship has been proposed by another research group (Honnef et al. 2004). This formula can be used to create a set of standard protocols for different weight classes (e.g., 0–5 kg, 6–10 kg, 11–20 kg, 21–40 kg, 41–60 kg, 61–80 kg, etc.), which can easily be applied in daily practice.

Recommendation:

mAs settings should be adapted to patient size in a more gentle way (factor of two per 8-cm change in diameter) than predicted by theoretical considerations that only account for image noise. In addition, body regions with better inherent contrast should be scanned at reduced mAs settings. Preferentially, AEC systems that measure rather than estimate patient absorption should be used, provided that their algorithm makes use of this more gentle mAs adjustment. Failing this, manual adjustment using a set of patient-weight-adapted protocols based on Rogalla's formula (4.20) should be applied instead. For head examinations, mAs adaptation should not be made with respect to patient weight, but to patient age.

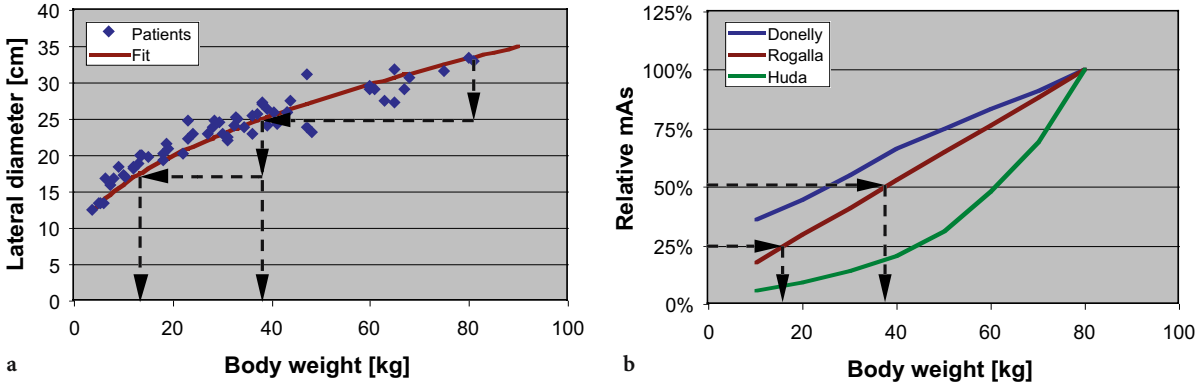

Fig. 4.35a,b. Relationship between patient weight and lateral diameter according to a detailed analysis of patient data from a big children's hospital (**a**) and dependence of patient weight on relative current–time product (mAs) settings, as recommended by three representative authors (**b**). As indicated by the *dashed lines*, adaptation of the current–time product by a factor of 2 per 8-cm change in patient diameter is almost perfectly met by Rogalla's recommendation

4.3.3 Examination Parameters

4.3.3.1 Scan Length (L)

As already pointed out in section 4.1, the local dose, i.e., CTDI, is almost independent of the length of the scanned body section. The same does not hold, however, for the integral dose quantities, i.e., DLP and effective dose. Both increase in proportion to the length of the body section. Therefore, limiting the scan length according to the clinical needs is essential.

On most scanners, the scan length, L, is usually not indicated explicitly. Instead, the positions of the first and the last slice are stated only; the same holds for the information that is documented on the images or in the DICOM data file. The net scan length, L_{net}, i.e., the length of the imaged body section, is calculated by:

$$L_{net} = \left| pos.\ first\ sl. - pos.\ last\ sl. \right| + h_{rec} \tag{4.21}$$

while the gross scan length, L_{gross}, i.e., the length of the irradiated body section, is:

$$L_{gross} = L_{net} + \Delta L \tag{4.22}$$

where ΔL is the increase in scan length due to overranging as described in Equation 4.16. As a rule of thumb that holds for the majority of MSCT scanners, the actual scan range, overranging included, is extended at each side of the planned scan range by approximately $0.75 \cdot N \cdot h_{col} + 0.5\ h_{rec}$. This amounts to approximately 2 cm for a 16-slice scanner with 20-mm beam width and 5-mm slice thickness.

Recommendation:

For each patient, the scan length should be selected individually, based on the scan projection radiograph that is generally made prior to scanning for the purposes of localization, and should be kept as short as necessary. Moreover, a reduction in the scan range should be considered in multi-phase examinations and follow-up studies. Whenever feasible, critical organs, such as the eye lenses or the male gonads, should be excluded from the scan range. This may be difficult for MSCT scanners that allow for large beam-width settings due to increased overranging effects.

4.3.3.2 Number of Scan Series (n_{Ser})

In CT terminology, a scan series is usually referred to as a series of consecutive sequential scans or one complete spiral scan. With the limited tube power available for many SSCT scanners, CT examinations of long body sections (e.g., tumor staging of the entire trunk) had to be separated into several consecutive subsections. If the same protocol settings are applied to each series, the local dose will always be the same, while the integral dose is the sum of the DLP or effective dose values of each series. So it would not make a difference whether the body section is scanned as a whole or in several shorter subsections, except for overranging effects that will increase proportionally to the number of subjections. However, mAs settings can be adapted to the particular needs of each subsection, e.g., lower settings for the chest, higher settings for the upper abdomen and reduced settings for the pelvis, as indicated in section 4.3.2.5.

If the same body section (or parts of it) is scanned more than once, this is usually denoted as 'multiphasic'. However, this not only applies to examinations with administration of contrast agents, but also to examinations where the same body section is scanned with different orientation (such as in facial bone exams) or with different slice collimation settings (e.g., chest standard plus high resolution). Although more than one scan is made at the same position, the length of each single scan of a multiphasic exam does not necessarily have to be the same. While it is meaningful to sum up the integral doses (DLP, effective dose) of each phase, this is not true for the local doses (i.e., $CTDI_{vol}$). Nevertheless, multi-phasic exams result in an increase in integral radiation exposure that is roughly proportional to the number of phases.

Recommendation:

The number of scan series (phases) should be kept as low as necessary. This holds true particularly for liver examinations, where studies with up to six different phases are sometimes recommended in literature.

4.3.3.3 Number of Rotations in Dynamic CT Studies (n)

In dynamic CT studies, e.g., in CT fluoroscopy or in perfusion studies, a multiple number of scans is

made at the same position. Therefore, it is meaningful to sum up the local doses, also. For this particular situation, the main issue is the avoidance of deterministic radiation effects. Local doses can be quite high if the scans are made with the standard dose settings used for that body region. Integral doses are normally comparable to the values encountered in standard examinations of the same region. However, with the advent of wider detector arrays, which may become even larger in future, integral dose will also be significantly increased.

The doses applied in dynamic CT studies depend on two factors: the dose, i.e., the $CTDI_w$, per rotation, and the number of rotations. As perfusion studies are regularly made with administration of contrast agents, the benefits of reduced kilovolt settings as described in section 4.3.2.2 should be used to reduce the dose settings. The number of rotations can be kept low by limiting the total length of the study, by reducing the image acquisition rate or by intermitting the procedure (in CT fluoroscopy) whenever possible.

Recommendations:

Dynamic CT studies should be made with the lowest dose settings, the most narrow beam width, the shortest length and the smallest image rate that is compatible with the clinical needs of the examination.

4.3.4 Reconstruction and Viewing Parameters

4.3.4.1 Filter Kernel (FK)

CT images are reconstructed from sets of attenuation measurements using dedicated mathematical procedures (algorithms) known as 'reconstruction filters' or 'filter kernels'. These algorithms are characterized as having quite different properties with regard to image quality: with highly resolving filter kernels, spatial resolution is improved but noise is increased. The opposite happens with smoothing kernels, which reduce noise at the expense of spatial resolution.

The properties of reconstruction filters are not subject to standardization. Therefore, kernels of equal or similar designation may vary considerably from one brand of scanner to the next. Equally,

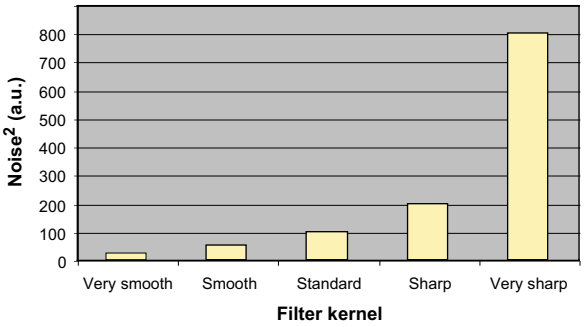

Fig. 4.36. Typical noise characteristics of different filter kernels. Relative figures are given in terms of noise squared, so the percentage differences can be translated directly into dose differences that would be necessary for constant image noise

reconstruction filters used for head or body scans carrying the same name are by no means identical. Labels such as 'smooth' or 'sharp' can only be used as coarse indicators of the balance between spatial resolution and image noise.

The compromise between spatial resolution and contrast resolution for a particular clinical indication must be found by appropriate selection of the reconstruction filter. The better the spatial resolution, the higher the noise, as indicated in Figure 4.36. Image noise, however, strongly affects contrast resolution. Due to the relationship between dose and noise given by the Brooks' formula (Eq. 4.18), the decision to use a particular filter kernel may directly affect the amount of dose required.

There are two practical sets of circumstances in which dose can be saved by proper selection of the reconstruction filter. The first is where spatial resolution is more than sufficient for a given clinical indication. Contrary to the manufacturer's recommendations, a smoother filter kernel can therefore be selected. The improvements resulting from this choice can then be used to reduce dose instead of noise, as indicated in Figure 4.37. The second is where the CNR for high-contrast structures (e.g., lungs, skeleton) is more than sufficient, even though a highly resolving filter kernel was used. In this case, increased noise can be tolerated, even if dose is reduced. So it turns out once again that the Brooks' formula is somewhat misleading as it does not account for image contrast. Nevertheless, the automatic exposure control system from one particular manufacturer also attempts to compensate for changes in noise that result from the selection of the filter kernel.

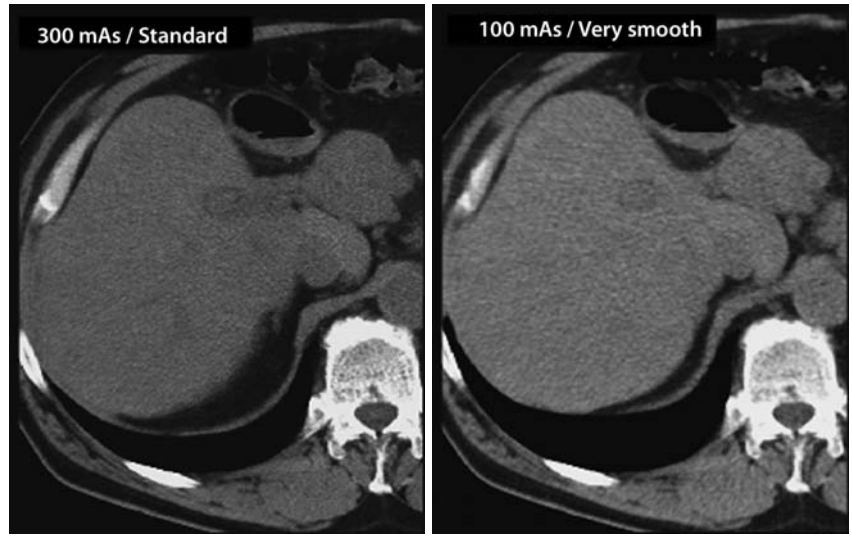

Fig. 4.37. Comparison of two images that were scanned and reconstructed with different current–time product (mAs) and filter kernel settings but result in similar image noise

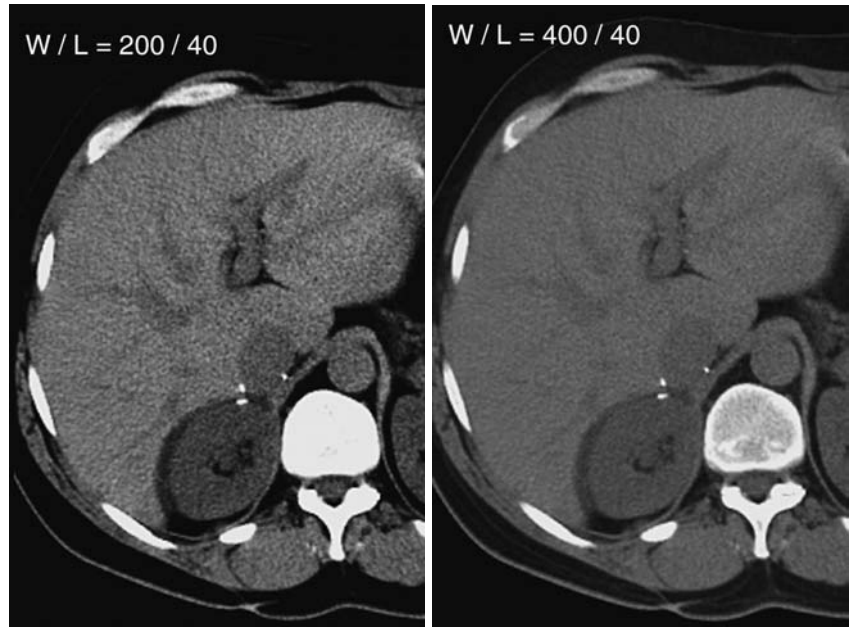

Fig. 4.38. Comparison of two images with different settings of the window width W. Wider window settings result in smoother images, thus allowing for reduced dose settings, provided that the inherent contrast is sufficiently high

Recommendation:

The selection of the filter kernel should be made with respect to the inherent contrast and as smooth as compatible with the clinical needs, thereby reducing the dose to that noise level that is appropriate. High-resolution kernels should only be used for high-contrast structures without adaptation of mAs settings.

4.3.4.2 Window Width (W)

The window width is often not regarded as a relevant factor influencing dose, since it is assumed that the width of the window is a parameter only related to image presentation. However, the visual perception of image noise strongly depends on the choice of window width setting. Using a wide window set-

ting, noise perception can be reduced, as shown in Figure 4.38. The reduction is inversely correlated to window width (Prokop 1998). However, image contrast is also decreased, of course, because the number of gray scale values is simultaneously reduced.

Therefore, a prerequisite for dose reduction using wider window settings is the sufficiency of CNR. Due to the non-linear relationship between dose and noise, even a relatively small increase in window width is profitable: if a setting of 350 HU is used instead of 300 HU, dose can be reduced by 26% while noise perception remains the same. It is therefore worthwhile finding out whether wider settings than those recommended by the manufacturer might also be appropriate. This holds particularly for high-contrast structures; by doubling the window width, the dose can be cut to one-quarter.

Recommendation:

The window width should be selected as wide as tolerable. With high-contrast structures, the improvement in noise thus achieved should be used to reduce the dose settings.

References

Brooks RA, DiChiro G (1976) Statistical limitations in X-ray reconstructive tomography. Med. Phys. 3:237–240

Donnelly LF, Emery KH, Brody AS, Laor T, Gylys-Morin VM, Anton CG, Thomas SR, Frush DP (2001) Minimizing radiation dose for pediatric body applications of single-detector helical CT: strategies at a large children's hospital. AJR 176:303–306

European Commission (1999a) Guidance on diagnostic reference levels (DRLs) for medical exposures. Radiation Protection 109. Office for Official Publications of the European Communities, Luxembourg

European Commission (1999b) European guidelines on quality criteria for computed tomography. Report EUR 16262 EN. Office for Official Publications of the European Communities, Luxembourg, pp 69–78

Flohr T, Stierstorferr K, Raupach R, Ulzheimer S, Bruder H (2004) Performance evaluation of a 64-slice CT system with z-flying focal spot. Fortschr Roentgenstr 176:1803–1810

Galanski M, Nagel HD, Stamm G (2001) CT-Expositionspraxis in der Bundesrepublik Deutschland - Ergebnisse einer bundesweiten Umfrage im Jahre 1999. Fortschr Roentgenstr 173:R1–R66

Honnef D, Wildberger JE, Stargardt A, Hohl C, Barker M, Günther RW, Staatz G (2004) Multislice spiral CT (MSCT) in pediatric radiology: dose reduction for chest and abdomen examinations (in German). Fortschr Roentgenstr 176:1021–1030

Huda W, Scalzetti EM, Levin G (2000) Technique factors and image quality as functions of patient weight at abdominal CT. Radiology 217:430–435

ICRP (International Commission on Radiological Protection) (1991) 1990 recommendations of the ICRP. Publication 60. Pergamon Press, Oxford

ICRP (International Commission on Radiological Protection) (2001) Managing patient dose in computed tomography. Publication 88, Annals of the ICRP Vol 31, No 2. Pergamon Press, Oxford

IEC (International Electrotechnical Commission) (1999) Medical electrical equipment – Part 2: Particular requirements for the safety of X-ray equipment for computed tomography. IEC standard 60601-2-44. IEC, Geneva

IEC (International Electrotechnical Commission) (2001) Medical Electrical Equipment – Part 2: Particular requirements for the safety of X-ray equipment for computed tomography. IEC-Standard 60601-2-44 Ed. 2.0. IEC, Geneva

ImPACT (2004) Evaluation Report MHRA 04048: Sixteen slice CT scanner comparison report version 12. Medicine and Healthcare Products Regulatory Agency, London, pp 7–9

ImPACT (2005) Report 05016: CT scanner automatic exposure control systems. Medicine and Healthcare Products Regulatory Agency, London

Kalender WA (2000) Computertomographie – Grundlagen, Gerätetechnologie, Bildqualität, Anwendungen. Publicis MCD-Verlag, München, pp 127–128

Nagel HD (1986) Aluminium equivalence of materials used in diagnostic radiology and its dependence on beam quality. Phys. Med. Biol. 31:1381–1399

Nagel HD (1989) Comparison of performance characteristics of conventional and K-edge filters in general diagnostic radiology. Phys. Med. Biol. 34:1269–1287

Nagel HD (2005) Significance of overbeaming and overranging effects of single- and multi-slice CT scanners. In: Proc. 14th International Conference of Medical Physics, Nuremberg, pp 395–396

Nagel HD (ed), Galanski M, Hidajat N, Schmidt T, Maier W (2002) Radiation exposure in computed tomography – fundamentals, influencing parameters, dose assessment, optimisation, scanner data, terminology, 4th revised and updated edition. CTB-Publications, Hamburg (contact: ctb-publications@gmx.de)

Prokop M, Schäfer-Prokop CM, Galanski M (1998) Dose reduction vs. image quality in spiral CT: How far down can we go in clinical practice? In: Krestin GP, Glazer GM (eds.). Advances in CT IV. Springer Verlag, Berlin: pp 16–26

Rogalla P (2004) Personal communication

Schneider K (2004) Personal communication

Shope TB, Gagne RM, Johnson GC (1981) A method for describing the doses delivered by transmission X-ray computed tomography. Med. Phys. 8:488–495

Shrimpton PC and Wall B (2000) Reference doses for paediatric computed tomography. Radiation Protection Dosimetry 90:249–252

Stamm G, Nagel HD (2002) CT-Expo – a novel program for dose evaluation in CT (in German). Fortschr Roentgenstr 174:1570–1576

Tack D, Gevenois PA (2006) Comparison of the performance characteristics of five programs for patient dose assessment in computed tomography. Submitted to Eur. Radiol.

Taguchi K, Aradate H (1998) Algorithm for image reconstruction in multi-slice helical CT. Med. Phys. 25:550–561

van der Haar T, Klingenbeck-Regn K, Hupke R (1998) Improvement of CT performance by UFC detector technology. In: Krestin GP, Glazer GM (eds). Advances in CT IV. Springer Verlag, Berlin, pp 9–15

Vlassenbroek A (2004) Dose management in pediatric examinations. In: Proc. 2nd Philips CT user meeting, Barcelona, pp 39–44

Wilting JE, Zwartkruis A, van Leeuwen MS, Timmer J, Kamphuis AGA, Feldberg M (2001) A rational approach to dose reduction in CT: individualized scan protocols. Eur Radiol 11:2627–2632

Collective Radiation Dose from MDCT: Critical Review of Surveys Studies

5

Georg Stamm

CONTENTS

5.1 Introduction

Over the years a lot of surveys have been carried out trying to estimate not only the collective dose of computed tomography (CT) examinations but also the effective dose for specific scan regions. Only a few surveys of large sample size have been carried out [UK 1999, 2001 and 2003 (National Radiological Protection Board 1999; Hart and Wall 2001; Shrimpton et al. 2003); Germany 1992–1995, 1999, 2002 (Bernhardt et al. 1995; Galanski et al. 2001; Brix et al. 2003); Switzerland 1998 (Aroua et al. 1998); and Austria 2000 (Nowotny)] while a larger number of surveys with smaller sample sizes can be found in the literature. The later ones were often focused on either a limited number of scanners or a small number of scanner sites (e.g. Greece, Italy, Wales, USA). These small surveys will always contain biased data because they are not representative of all scanners and sites (Szendrö et al. 1995; Olerud 1997, 2003; van Unnik et al. 1997; Scheck et al. 1998; Shrimpton et al. 1998; Goddard and Al-Farsi 1999; Einarsson and Magnusson 2001; Hiles et al. 2001; Olerud et al. 2001; Tsapaki et al. 2001; Hatziioannou et al. 2003; Papadimitriou et al. 2003; Origgi et al. 2006).

Large-scale surveys are necessary to take into account the considerable variations in patient size and differences in scan parameters and settings even within the various sites.

NEXT (Nationwide Evaluation of X-ray Trends) surveys in the US (see for example Conway et al. 1992) are carried out nearly every year and are mostly focused on a defined body region. Although this seems to be a very promising approach for obtaining reliable data, the spectrum of typical examinations is very limited; a broad overview will be available only after several years, when the first surveys are already out of date.

Surveys with small sample size, showing only a snapshot of the current situation using scanners of only one or two vendors, can be found more frequently in medical journals. The larger surveys are all carried out on behalf of national authorities such as National Radiological Protection Board (NRPB) in UK, Bundesamt für Strahlenschutz (BfS) in Germany and Bundesministerium für soziale Sicherheit und Gesundheit (BMSG) in Austria with a typical time frame of 5–15 years between updates.

The aim of this chapter is to compare the results of the different surveys to stress on local or national specialities. It is a critical review of current trends and will help interested readers to interpret the results of those surveys more carefully.

The chapter focuses on European surveys and compares methods, results, outcomes and conclusions. Whenever possible a comparison of differ-

G. Stamm, PhD
Medizinische Hochschule Hannover, Diagnostische Radiologie/AB Exp. Radiologie, Carl-Neuberg-Strasse 1, 30625 Hannover, Germany

ent national surveys will also be made. Publications from the United States and Australia will be included as examples and do not necessarily meet the requirements of completeness. Also the mentioned small-sized surveys may not show up as a complete list.

The large-sized surveys were used as a reference for establishing guidelines for scan techniques and parameter settings; but what is more important for future work is to introduce guidelines for optimization. The German survey from 1999, for example, was used to produce reliable data on patient dose from CT examinations to set up national reference dose levels for CT. However, it also guided and provided hints on how to optimize scan protocols, which will be discussed later on.

Another main aim for future tasks should be to define acceptable image quality in relation to patient dose. The manufacturers have already shown the possibility for automatic exposure control (AEC) in CT, but the procedures to achieve this aim vary. The definition of acceptable image quality should be uniform and applicable to all different scanner models. This is especially important because the relationship between peak kilovoltage (kVp), image quality and dose is very complex. Defining image quality only in terms of image noise (standard deviation of HU values) does not meet all requirements. A more sophisticated approach in terms of contrast-to-noise ratios (CNR) defined for the various body regions is needed, in particular for low contrast examinations such as liver and abdomen.

5.2 Reference Dose Levels (RDL)

Looking at the frequencies of CT examinations and their contribution to the annual collective dose (Tables 5.1–5.3, Figs. 5.1, 5.2) it is necessary to introduce so-called reference dose levels (RDL) to clearly define thresholds which can be exceeded in individual cases but should not be exceeded in general.

A lot of surveys have been carried out in the past either to establish national RDL according the

Table 5.1. Number of CT examination per year and 1000 people (values from UNSCEAR 2000 report if not mentioned otherwise)

UNSCEAR Heath Level 1	57
UNSCEAR Heath Level 2	1.5
Germany	64
Germany (1990–92)	55
Germany (1999)	90
UK	21
USA	91
Sweden	39
Sweden (1991)	24
Australia (1994)	60
Austria (2000)	76
Switzerland (1998)	46

Table 5.2. Frequencies of different CT procedures in percent (%), total number of exams per year and scanner and number of installed CT bases (see also Fig. 5.1)

	Germany (1999)[a]	UK (1997/98)[b]	Austria (2000)[c]	Italy (2006)[d]	Switzerland (1998)[e]	Netherlands (1998)[f]	Sweden (1991)[g]	Australia (1994)[h]
Brain	37	44.5	34.9	39	24	39	53	30.4
Chest	15	13.8	15.3	17	14.6	19	–	8.1
Abdomen	25	21.4	26.1	20	20.4	28	25[i]	14.6
Lumbar spine	–	4.5	–	10	11.5	10	9.6	12.4
Pelvis	–	10	–	10	–	3	–	5.9
No. of exams per scanner and	3600	–	4560	–	–	–	–	–
Installed bases	2000	–	227	1328	–	–	90	–

[a] Galanski et al. (2001)
[b] National Radiological Protection Board (1999)
[c] Nowotny R. (http://www.bmgf.gv.at/cms/site/detail.htm?thema=CH0343&doc=CMS1065194276970)
[d] Origgi et al. (2006)
[e] Aroua et al. (1998)
[f] Meeuwsen and Brugmans (2003)
[g] Szendrö et al. (1995)
[h] Thomson and Tingey (1997)
[i] Sweden examination of the trunk

Table 5.3. Comparison of percentage of total collective dose delivered by CT examination (see also Fig. 5.1)

	Germany (1990–92)[a]	Germany (1999)[b]	UK (1997/98)[c]	Austria (2000)[d]	UNSCEAR (2000) HL1[e]	UNSCEAR (2000) HL2[e]	Switzerland (1998)[f]	Netherlands (1998)[g]	Iceland (1998)[h]
% Collective dose	35	40	39.7	40.4	41	5	27.8	42	54
% No. of exams	4	6	3.3	4.2	6	1	3.4	5.8	13.6
No. of exams/year	–	$7.2 \cdot 10^6$	$1.39 \cdot 10^6$	620,000	–	–	328,000	494,000	25,762

[a] Bernhardt et al. (1995)
[b] Galanski et al. (2001)
[c] National Radiological Protection Board (1999)
[d] Nowotny R. (http://www.bmgf.gv.at/cms/site/detail.htm?thema=CH0343&doc=CMS1065194276970)
[e] UNSCEAR Report 2000 Annex D, Medical Radiation Exposure, New York (2000)
[f] Aroua et al. (1998)
[g] Meeuwsen and Brugmans (2002)
[h] Einarsson and Magnusson (2001)

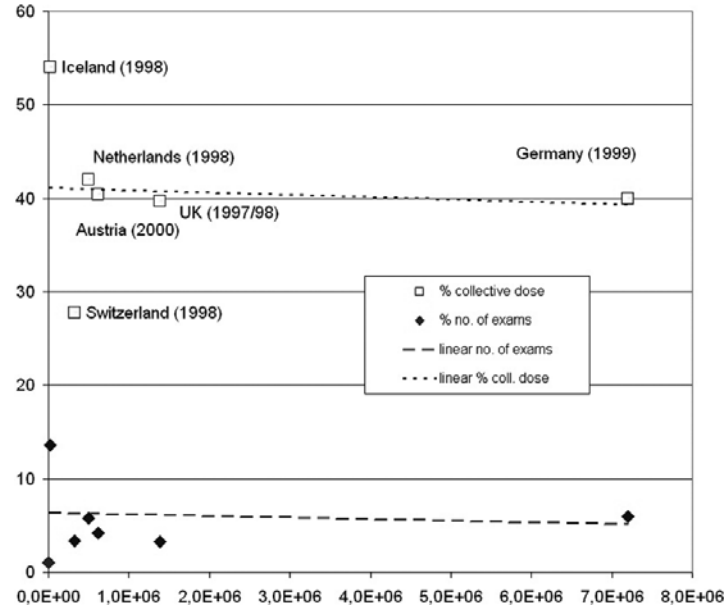

Fig. 5.1. Contribution to total number of radiographic procedures and contribution to collective effective dose as a function of the total number of CT examination per year. Independent of total number of CT examinations the relative contribution to total number of radiographic procedures is about 6% while the relative contribution to collective effective dose is about 40% (see Table 5.2 for detail)

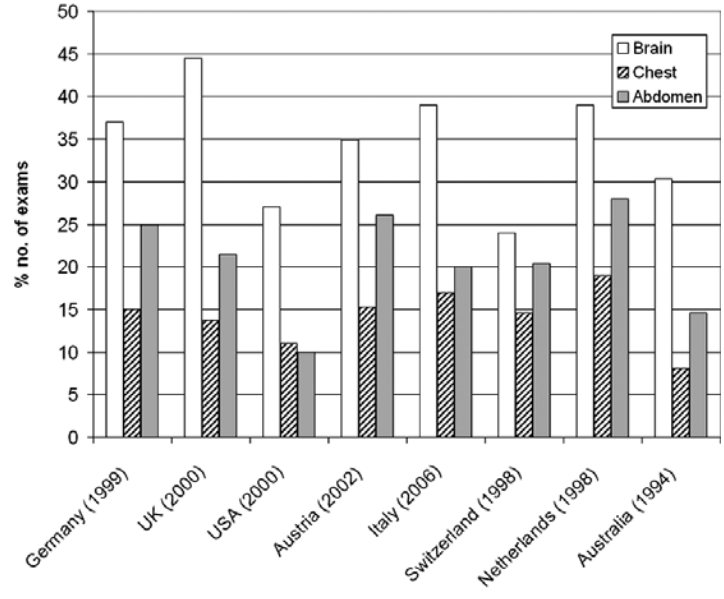

Fig. 5.2. Relative distribution of the CT procedures on the brain, chest and abdomen in different countries

EU quality criteria for CT (EUR16262, European Commission 1999) or to check if CT procedures in the different member states comply with the EU RDL. RDL can and should be included in guidelines for scanning techniques. While using projection radiography the consistency between the actual dose values and the RDL can only be checked after the examination, whereas with CT it is possible to check compliance beforehand. Although RDL do not represent an individual patient's exposure they are an estimation of the mean collective dose to the patient for the corresponding body regions.

Three major dose quantities can serve as RDL: first we have the two local dose values, namely weighted computed tomography dose index ($CTDI_w$) and volume CTDI ($CTDI_{vol}$). The latter can be regarded as a measure of the mean dose within an examination region and is dependent on mAs product, kV settings and the distance focus-to-axis-of-rotation. The third quantity is the dose length product (DLP), which is an integral dose value and depends on the correct choice of scan length. A comparison of the estimated RDL of several different surveys is in Tables 5.4 and 5.5.

Table 5.4. Comparison of reference dose levels (*RDL*) in terms of weighted computed tomography dose index ($CTDI_w$, mGy) in different European countries compared with the EU directive EUR16262

	Germany (1999)[a, f]	Germany (2002)[b]	UK (2003) SSCT[c]	UK (2003) MSCT[c]	Austria (2000)[d, g]	EUR 16262[e]
Routine head (brain)	45	60	70	110	68.9	60
Face and sinuses	25	35	–	–		35
Routine chest	13	22	13	18	18.9	30
Chest HR	–	–	22	50	28	35
Routine abdomen	15	24	20	20	19.8	35
Liver and spleen	15	25	–	–	20.6	35
Lumbar spine	30	47	–	–	40.7	–
Routine pelvis	18	28	17	20	23.5	35

[a] Galanski et al. (2001)
[b] Brix et al. (2003)
[c] Shrimpton et al. (2003)
[d] Nowotny R. (http://www.bmgf.gv.at/cms/site/detail.htm?thema=CH0343&doc=CMS1065194276970)
[e] European Commission (1999)
[f] 1st quartile of the 1999 survey for comparison
[g] 3rd quartile of the 2000 survey

Table 5.5. Comparison of reference dose levels (*RDL*) in terms of dose length product (*DLP*, mGy·cm) in different European countries compared with the EU directive EUR16262

	Germany (1999)[a]	Germany (2002)	UK (2003) SSCT	UK (2003) MSCT	Austria (2000)[b]	EUR 16262
Routine head (brain)	520	1175	760	930	1275	1050
Face and sinuses	190		–	–		
Routine chest	250	650	430	580	484	650
Chest HR	–	–	80	170	76	280
Routine abdomen	490	1500	510	560	1109	780
Liver and spleen	210	770	460	470	763	900
Lumbar spine	170	280	–	–	495	800
Routine pelvis	300	750	–	–	589	570

[a] 1st quartile of the 1999 survey for comparison
[b] 3rd quartile of the 2000 survey

5.3 Statistical Values and their Meanings

The surveys provide a lot of data on examination or scan parameters. $CTDI_w$, $CTDI_{vol}$ and DLP can be interpreted and compared in different ways. Mean values of common or often-used procedures may serve to rank each scanner site in comparison with the results of the survey. Median values can be used to evaluate the distribution (for example the skewness or asymmetry) of the data. The results of the German 1999 (Galanski et al. 2001) survey showed that there is not a big difference between mean and median values. Of common interest in particular are the 3rd quartile values, which can serve as a threshold that should not be exceeded in general. These values also provide a well established base for defining RDL. The 3rd quartile value means that 75% of the participating institutes and scanner sites conform to these values while only 25% have to change their protocols or procedures.

Some examples of mean dose values for the different surveys as well as 3rd quartile values are presented in Tables 5.6 and 5.7.

Interpreting the data from the German 1999 survey in more detail, we have found that the 1st quartile values are a good measure for an optimization process especially for new scanners. This has often been neglected in the past. Surveys should not only

Table 5.6. Mean dose values. Comparison of different surveys [$CTDI_w$ (mGy), DLP (mGy·cm) and effective dose *E* (mSv) for whole examination; DLP and *E* are mean values for male and female]

	Germany (1999)[a]			Germany (2002)[b]			Greece (2002)[d]			Italy (2002)[d]			Italy (2006)[e]	
Region	$CTDI_w$	DLP	*E*	$CTDI_w$	DLP	*E*	$CTDI_w$	DLP	*E*	$CTDI_w$	DLP	*E*	$CTDI_w$	*E*
Brain	57	676	1.8	58.4	1016	2.8	68	919	2.1	59	707	1.6	59.6	1.7
Upper abdomen	21	–	–	–	–	–	23	493	7.4	23	632	8.3	24.3	7.8
Abdomen and pelvis	21	770	13	15.6	790	14.4	–	–	–	–	–	–	–	–
Pelvis	23	480	8	17.1	398	7.2	27	540	10.3	24	434	8.2	24.9	8.9
Chest	18	420	6.5	14.8	350	5.7	21	430	7.3	21	480	6.2	19.7	8.0
Lumbar spine	39	230[f]	2.8	30.3	445[g]	8.1	39	470[g]	–	36	303[h]	4.7	34.1	4.5
Sample size (sites)	850	113	14	32	56									
% of inst. bases	45	50	–	–	–									

	UK (2003)[c]			Austria (2000)			Switzerland (1998)[i]	Oman (1999)[j]	Iceland (1998)[k]	Australia (1994)[l]
Region	$CTDI_w$	DLP	*E*	$CTDI_w$	DLP	*E*	*E*	*E*	*E*	*E*
Brain	57	690	1.5	57.7	1036	2.25	2.4	2.4	1.3	2.4
Upper abdomen	16	350	5.3	17.5	877	14.7	10.3	9.5	13.2	–
Abdomen and pelvis	16	470	7.1	–	–	–	–	–	–	16.7
Pelvis	–	–	–	20.2	487	8.0	7.3	–	6.1.	11.2
Chest	14	400	5.8	16.2	400	6.7	9.0	3.4	8.5	10.4
Lumbar spine	–	–	–	35.5	407	6.2	9.4	–		12.4
Sample size (sites)	118	130	–	6	4	182				
% of inst. bases	25	57	–	–	80	55				

[a] Galanski et al. (2001)
[b] Brix et al. (2003)
[c] Shrimpton et al. (2003)
[d] Papadimitriou et al. (2003)
[e] Origgi et al. (2006)
[f] Only one segment (= 6 cm scan length)
[g] Multiple segments
[h] Mean scan length 8.6 cm
[i] Aroua et al. (1998)
[j] Hiles et al. (2001)
[k] Einarsson and Magnusson (2001)
[l] Thomson and Tingey (1997)
[m] Olerud et al. (2001)
[n] Olerud (1997)
[o] Szendrö et al. (1995)
[p] Sweden examination of the trunk

Table 5.6. Mean dose values (continued). Comparison of different surveys

	Wales (1999)[j]		Nordic Pilot survey (2001)[m]			Norway (1993)[n]	Sweden (1991)[o]
Region	$CTDI_w$	DLP	$CTDI_w$	DLP	*E*	*E*	*E*
Brain	46	731	60	740	1.7	2.0	2.1
Upper abdomen	22	745	–	–	–	12.8	
Abdomen and pelvis	–	–	–	–	–	–	10[p]
Pelvis	23	646	–	–	–	9.8	–
Chest	17	663	10.8	420	7.1	11.5	–
Lumbar spine	–	–	40	420	7.9	4.6	6
Sample size (sites)	18	25	49	90			
% of inst. bases	–	–	50	100			

[i] Aroua et al. (1998)
[j] Hiles et al. (2001)
[k] Einarsson and Magnusson (2001)
[l] Thomson and Tingey (1997)
[m] Olerud et al. (2001)
[n] Olerud (1997)
[o] Szendrö et al. (1995)
[p] Sweden examination of the trunk

Table 5.7. The 3rd quartile dose values. Comparison of different surveys ($CTDI_w$, DLP and effective dose *E* for whole examination; DLP and *E* are mean values for male and female)

	Germany (1999)			Germany MSCT (2002)			Italy (2006)			UK (2003)[c]		Austria (2000)		
Region	$CTDI_w$	DLP	*E*	$CTDI_w$	DLP	*E*	$CTDI_w$	DLP	*E*	$CTDI_w$	DLP	$CTDI_w$	DLP	*E*
Brain	66	783	2.2	76	1149	3.3	68.7	915	2.1	66	784	57.7	1036	2.25
Upper abdomen	–	–	–	–	–	–	25.6	602	9.1	20	477	17.5	877	14.7
Abdomen and pelvis	24	941	15.7	18	1029	18.9	–	–	–	19	534	–	–	–
Pelvis	28	603	10.3	20	455	8.3	28.9	501	9.5	–	–	20.2	487	8.0
Chest	22	540	8.2	20	442	7.2	25	627	10.7	15	488	16.2	400	6.7
Lumbar spine	47	319[a]	3.1	39	575[b]	10.3	41.7	367	6.2	–	–	35.5	407	6.2
Sample size (sites)	850			113			29			118		130		
% of inst. bases	45			50						25		57		

[a] Only one segment (= 6 cm scan length)
[b] Multiple segments
[c] Values are for all scanners (SSCT and MSCT)

delineate the present state but also show possible improvements and ameliorations.

Boxplots are an expressive and convincing representation of data from surveys. Within only one figure, they show not only the sometimes large variation between minimum and maximum values but also the important statistical parameters such as mean and median values and the two quartile values (see Fig. 5.3). There can be a large variation between minimum and maximum values: sometimes the outliers in both directions are separated by a factor of up to 30, as can be seen in Table 5.8, showing the range and ratios of dose values found in different surveys. This should not cause alarm because the majority of data are distributed within a factor of 2 or 3 of the mean value; for example, Figure 5.4 shows a histogram plot of the effective dose deduced for the examination of the abdomen/pelvis in the German 1999 survey.

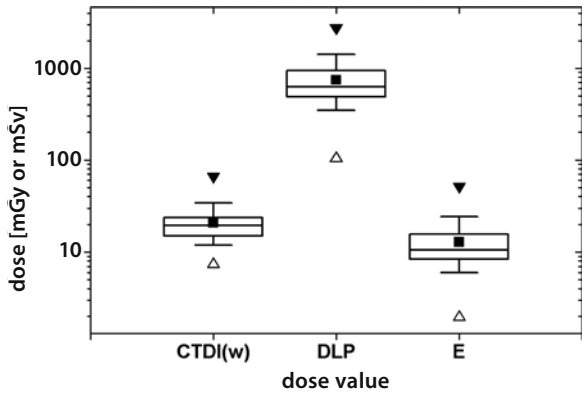

Fig. 5.3. Boxplot of estimated dose values for examination "abdomen and pelvis". Reported values show a range of 30. Figure taken from the results of the German 1999 survey (Galanski et al. 2001)

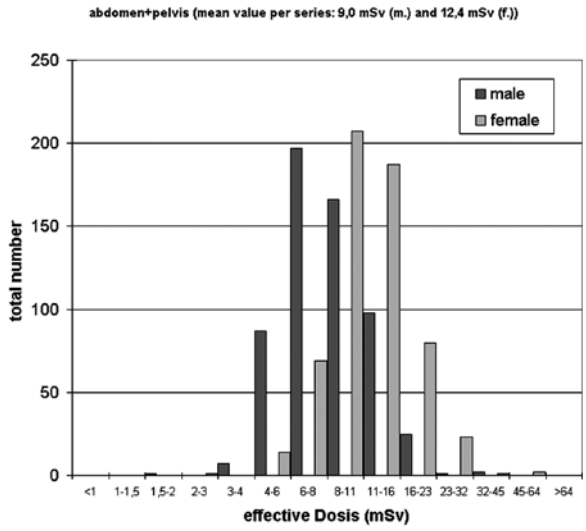

Fig. 5.4. Distribution of effective dose for examination "abdomen and pelvis". Mean values were 9.0 mSv for male and 12.4 mSv for female. Figure taken from the results of the German 1999 survey (Galanski et al. 2001)

Table 5.8. Range and ratios of dose values found in serveral surveys, which indicates that there are possibilities of remarquable dose reductions

	Germany (1999)[a]				UK[f] (1998)[b]		EU 2004 QC[c]		Norway (1993)[d]	Australia (1994)[e]
	$CTDI_w$ (mGy) Min (Max)	DLP (mGy·cm) Min (Max)	*E* (mSv) Min (Max)	E^g	$CTDI_w$ (mGy) Min (Max)	DLP (mGy·cm) Min (Max)	DLP[h] (mGy·cm)	E^g	E^g	E^g
Head	14 (199)	173 (2384)	0.4 (14.5)	36	21 (130)	231 (2087)	204 (2805)	11.7	8	29
Chest	5.5 (66)	100 (1766)	1.35 (26.4)	21	4 (46.4)	72 (1304)	61 (1322)	14.4	19.5	64
Abdomen and pelvis	7.4 (66)	105 (2767)	2 (51.1)	26	6.8 (46.4)	115 (1874)	140 (1475)	10.6	13.3	25
Pelvis	6.9 (56.2)	90 (1349)	1.6 (23)	14	6.8 (55.2)	68 (1324)	–	–	17.2	18
Lumbar Spine	9.4 (94.1)	29 (821)	0.35 (10.4)	30	–	–	–	–	–	–

[a] Galanski et al. (2001)
[b] National Radiological Protection Board (1999)
[c] CT Quality Criteria (2004)
[d] Olerud (1997)
[e] Thomson and Tingey (1997)
[f] Values were used for the European EU16262EN quality criteria
[g] Min/max ratio
[h] Head/cranium: acute stroke, chest: pulmonary embolism, abdomen/pelvis: rule out abscess

5.4 Interpretation of Data and Pitfalls

Most surveys are only local rather than nationwide studies. Sometimes they are restricted also to only a few radiological centres; therefore, the collected data may include an unbalanced bias which can lead to misinterpretation. For example, using data just from selected institutes with good radiological practice will not produce the mean of all institutes. Including only a few scanners will cause a bias based on the specialties of those scanners, i.e. the focus-axis distance, filtration and limited pitch values. Other scanners which do not meet those technical parameters will show up as "dose slingshots". Looking at

the values of the normalized $CTDI_w$ ($_nCTDI_w$) of the example in Table 5.9, scanner A seems to deliver a sixfold higher dose to the patient than scanner B. After estimating the corresponding effective dose we can conclude that they are nearly the same, which can be explained by taking into account the mAs settings for both scanners: scanner A needs only one-sixth of the mAs settings compared with scanner B. This is also a convincing example of the statement: "mAs is **not** dose".

Table 5.9. Comparison of normalized $CTDI_w$, resulting effective dose and corresponding mAs settings for a male patient undergoing a CT examination of the abdomen

Scanner	$_nCTDI_w$ (mGy/mAs)	*E* (mSv)	mAs
A	0.25	7.3	74
B	0.043	7.9	267

The survey in 1999 was the first study in Germany in which data for all scanners from all manufacturers were collected. The quota for returned questionnaires was more than 50%, enabling a reasonable analysis concerning the age of the scanners and the distribution among university hospitals and private practice; it was also possible to take into account the features of the new scanners.

The German survey of multidetector CT (MDCT) scanners in 2002 (Brix et al. 2003) resulted in a snapshot of the present situation. It showed that the change from single-detector CT (SDCT) to MDCT was not smooth but resulted in an increase in dose. The main reason was an inadequate use of the new technique and a lack of intensive training of the users. For the future an additional survey should be carried out, with a broader base and including those scanners with $N>8$ (aquiring more than 8 slices simultaneously).

RDL are indicated in terms of weighted CTDI ($CTDI_w$), which is a local dose value (dose per slice) given in terms of DLP, which is an integral dose value (dose to the patient). The 2003 UK survey (Shrimpton et al. 2003) and the EU 2004 survey on MDCT (CT Quality Criteria 2004; Shrimpton 2004) suggested specifying RDL in terms of volume CTDI ($CTDI_{vol}$) in order to take into account new scanner technologies and the introduction and use of so-called effective mAs settings. The main aim of this concept, introduced by the vendors in the early stages of MDCT starting with 4-slice scanners, is to keep image quality constant and independent of the chosen pitch or table feed.

This has caused some irritation among users, who were accustomed to noticing a dose reduction when using pitch values greater than 1. This was a common and well known rule when dealing with SDCT scanners but is not applicable to most MDCT scanners. Thus the introduction of a direct dose indicator to solve this problem was almost mandatory. More recent scanner models display the $CTDI_{vol}$ directly at the operator window according to the IEC Standard 60601-2-44 (IEC International Electrotechnical Commission 2001). This would allow a direct comparison to RDL prior to starting the examination if the RDL were defined in terms of $CTDI_{vol}$. Unfortunately RDL are defined in terms of $CTDI_w$ which means that the user has to multiply the displayed value by the corresponding pitch. This simple task will become complicated if this pitch value is not displayed numerically but in descriptive terms such as "high quality" or "high speed". This behaviour has been abandoned by the vendors, as has calling the displayed $CTDI_{vol}$ weighted CTDI. However, those scanners are still in operation and the user must know about these possible pitfalls.

A revision of the EU RDL is necessary because they were established before the introduction of MDCT. The update should include the new dose value $CTDI_{vol}$ to enable a direct comparison with the displayed value at the operator console. First values for RDL in terms of $CTDI_{vol}$ reported in the EU 2004 survey can be found in Tables 5.10 and 5.11.

A result of the Swiss 1998 survey (Aroua et al. 1998) was the suggestion of an update every 5 years in a so-called mini survey covering only about 10% of the volume of a complete survey. This should be sufficient for reliable data on examination frequencies and trends in dosimetric values. When looking at the rapid evolution of scanner techniques this seems to be mandatory, although it should be remembered that a mini survey may produce only a snapshot of a rapidly changing technique and usage which cannot be applied in general. The Swiss survey proposed a complete re-evaluation with the same sample size every 20 years, which is a rather long time period. Only if the mini surveys produce reliable data and are focused on rapid evolving techniques a re-evaluation can be successfull.

With regard to CT examinations, the characteristic features of the CT scanners and the optimization of examination protocols are important (number of passages, scanned volume, thickness and spacing of slices, etc.). They enable a significant reduction of the doses given (see the proposals of the recent German study; Sect. 5.8).

Table 5.10. Median results of the 2004 survey on MSCT (CT Quality Criteria 2004) compared with the initial EUR16262 values (European Commission 1999)

	$CTDI_{vol}$ (mGy)	DLP (mGy·cm)	*E* (mSv)	QC criterion $CTDI_{vol}$	EUR16262 $CTDI_w$	EUR16262 DLP
Cranium[a]	53	746	1.7	60	60	1050
Chest, HR	3	117	2.5	10	15	280
Chest, pulmonary embolism	11	302	5.9	10	30	650
Abdomen, rule out abscess	11	551	9.3	15	35	780
Abdomen, liver metastases	13	643	9.5	25	35	900

[a] Cranium: acute stroke

Table 5.11. 2004 Quality Criteria MSCT vs. SSCT (www.msct.info) (Quality Criteria 2004)

	$SSCT/CTDI_w$ (mGy)	$MSCT/CTDI_{vol}$ (mGy)	Remarks
Cranium (acute stroke)	60	60	Pitch 1 or contiguous scan
Chest HR	35	10	
Chest (pulmonary embolism and pulmonary metastases)	30	10	Pitch >1
Abdomen/pelvis (rule out abscess)	35	15	
– Liver metastases	35	25	
– Urolithiasis	35	10	

5.5 Comparison of Different Surveys

The annual frequency of examinations, the contribution to collective dose as well as the corresponding relative numbers of examinations are presented in Tables 5.1–5.3 and compared with the findings of the UNSCEAR Report (2000).The different surveys are listed in Tables 5.4–5.7, which compare the findings concerning RDL in terms of $CTDI_w$ and DLP (Tables 5.4 and 5.5). In Table 5.6 the mean of the different dose values including effective dose is compared, while Table 5.7 shows the 3rd quartile which is commonly used as a reference level.

The EUR16262 document introduced normalized dose values with respect to dose length product [conversion factor f = mSv/(mGy×cm)] to enable a quick and robust estimate of effective dose values. As can be seen from the figures in Table 5.12 these conversion factors only differ by about 10%–20% among the different surveys. These differences may be caused by different scan lengths for the listed procedures. As can be seen by looking for example at the data from Shrimpton (whole trunk 0.015; chest 0.014; abdomen and pelvis 0.015) normalized values can be used for three anatomical regions: head, neck and body. The conversion factors should be based on the phantom values of DLP and not on DLP free in air. With DLP on display at the operator console, this value can be used for a quick evaluation of the effective dose and hence radiation exposure of the patient. Although the listed values suggest that these conversion factors may serve as a robust estimate, one has always to bear in mind that they were derived from mean values. This means that they were averaged for all scanners and all different scan parameter settings (such as kVp, mAs, scan length, slice and section thickness, pitch). So these values should and can be used whenever a quick estimate of effective dose is necessary, but one has to remember that this is only a rough estimate and does not take into account the gonads. For the neck region two values have to be considered, depending on whether body or head mode is used during the scan. They should never be used to compare different scanners, because even if scan parameters are nearly identical other dose-influencing factors may

Table 5.12. Normalized values of effective dose per dose length product [$f = E/\mathrm{DLP}$ in mSv/(mGy·cm)] for various body regions. Values from both German surveys based on mean values for E and DLP

	Shrimpton[a]	Italy (2006)[b]	EUR16262[c]	Germany (1999)[d]	Germany (2002)[e]	EU 2004[f, g]
Head and neck	0.0031	–	–	0.0039	0.0038	–
Head	0.0021	0.0024	0.0023	0.0028	0.0028	0.0023
Neck	0.0059	0.0052	0.0054	0.0098	0.0061	–
Chest	0.014	0.0163	0.017	0.0154	0.0016	0.019
Abdomen and pelvis	0.015	0.0149	0.015	0.0174	0.0186	0.017
Lumbar spine	–	0.0166	–	0.0125	0.0185	–
Pelvis	–	0.0175	0.019	0.0171	0.0185	0.017
Trunk	0.015	–	–	–	0.0177	–

[a] Shrimpton et al. (2003)
[b] Origgi et al. (2006)
[c] European Commission (1999)
[d] Galanski et al. (2001)
[e] Brix et al. (2003)
[f] CT Quality Criteria (2004)
[g] Cranium: acute stroke, chest: pulmonary embolism, abdomen/pelvis: rule out abscess

differ. This includes focus-to-axis distance, beam filtration and beam shaper.

The main limitation of surveys is the quality of the reported data. It is necessary to check the returned questionnaires for whether the scan parameters seem to be reasonable or not. In case of any doubts a validity check has to be made for the reported values of the scan parameters. The survey in Germany showed that the more complex the task of the survey, the more difficulties arise with the data quality. While the 1999 survey on single-slice scanners was rather easy to set up and carry out, the MSCT survey in 2002 was much more complex. Therefore, it was necessary to distribute a manual on how to collect the necessary data. The survey on paediatric examinations that started in 2006 was once again very complex for the user as well as conductors of the survey. A lot of queries were necessary to improve the reported data. In future these tasks will become increasingly complex because scanning and scanner techniques are rapidly changing and the user interfaces of the different scanners are becoming more varied. This means that for large-scale surveys one has to supply "translation tables" for each scanner family in order to help the user to spot the relevant and necessary data.

Some limitations and main findings of the different surveys are summarized in the following short quotations.

The survey in Iceland (IRPI) (van Unnik et al. 1997) listed only five CT bases and found an approximately 93% increase in the number of CT examinations from 1993 until 1998. The main conclusion was that "…*efforts to reduce dose should include optimization of both how CT examinations are performed and the criteria for requesting them*". This statement, although deduced from a very small survey, holds for every survey and are discussed in Section 5.8.

The Nordic survey (presented at the IAEA meeting in Malaga, Spain) (Olerud et al. 2001) included only five sites from each of the five participating countries (Denmark, Finland, Iceland, Norway, Sweden) and found that "*This Nordic pilot project shows that the EC quality criteria can be used as a collaborative inspection tool. However, the radiologists work within their own reference frames. That introduces a bias, and the survey design is not suitable for ranking*". These findings show that small surveys are often not suitable to represent the mean values for a whole country.

The main difficulty when comparing different surveys is the variation in their setup. In some countries examination of the abdomen means the whole abdomen; in others it means just the upper abdomen. In addition, the definition of series varies. In Germany, for example, examinations of the abdomen are mostly carried out as biphasic examinations, while for the NRPB surveys only one series was taken into account.

Another difficulty is that in some surveys dose values are calculated on the basis of axial examinations while other surveys use spiral examinations. In the German 1999 survey (Galanski et al. 2001) we tried to compare our data with data from the 1999 NRPB survey (National Radiological Protection Board 1999). The differences found

could be accounted for by differences in scan ranges and spiral technique.

5.6 Surveys Comparing MDCT and SDCT

When the first 4-slice scanners were established in early 2000 the reported dose values increased by a factor of 4 compared with those of single-slice scanners. This behaviour and the dramatic increase in dose to the patient were mainly the result of inadequate user experience with these new techniques. New concepts introduced by the vendors, such as effective mAs and its influence on dose values, were not sufficiently communicated to the users. Combined with the possibility of acquiring more and thinner slices, this led to the reported increase in dose. Now users are more experienced and know how to deal with thin slices, and the post processing technique of image processing has improved; hence, modern MSCT scanners should deliver a patient dose that is comparable to that given by modern single-slice scanners.

One main point presented at the 2003 symposium on Radiation Protection of the North West RP Societies in Utrecht was as follows: "It has to be emphasized that the comparison of the dose data collected from the three time periods, reflecting the different CT scanner generations, is rough since the medical indications were not identical. The huge variation in doses for the same medical indications indicates a potential for optimization of CT protocols in Norwegian hospitals. The best parameters to report for dose comparison would be $CTDI_{vol}$ and the total DLP" (Olerud 2003). This statement shows one of the main difficulties when comparing dose values from SDCT and MDCT. With the introduction of MDCT the indications for examination change and sometimes the scan protocols are not adapted accordingly. If indications change with new scanner technology then patient exposures are really hard to compare. For example, if combined protocols are possible with MDCT, for example chest and abdomen or abdomen and pelvis or even chest and abdomen and pelvis, it is hard to compare these results with SDCT examinations of only one of the aforementioned regions. What is possible, however, is to check whether the local dose values in the specified regions are nearly the same. Therefore, the introduction of the $CTDI_{vol}$ as an average dose within a CT slice was important. This dose value reflects to some extent the scanner technology (detector efficiency) and the selected scan parameters (kVp, mAs, pitch, etc.). The total dose for an examination as represented by the DLP reflects the scan length and number of series taken. Thus only examinations for nearly the same combination of scan regions can be compared. Nevertheless DLP is good and quick estimate of patient dose.

Also the German 2002 survey on MDCT (Brix et al. 2003) showed that the introduction of new scanner technologies first led to an increase in patient dose. After users had realized the pitfalls and the potential of the new technique, dose values could be reduced to the same level as estimated in the 1999 survey of SDCT. This was mainly caused by new display modalities. Trading off the potential of MDCT means using thin slices whenever possible and/or rapid scanning of the selected region. Unfortunately thin slices always cause increased noise in the resulting images because fewer photons reach the detectors and hence signal-to-noise ratios decrease. With the introduction of MDCT this led to a pronounced increase in patient dose (a factor of 2 to 4 compared with reported dose values for SDCT). The viewing technique or post processing of the image data improved rapidly at the same time as the MDCT technique started to be used. This allowed new so-called display modalities for diagnosis. The availability of the thin slab technique allows for the combination of several adjacent slices, either by simple averaging or by more sophisticated processing such as MIP (maximum intensity projection). This processing reduces image noise while keeping spatial resolution nearly constant. This was the main improvement used to overcome the dose trap of thin slices. Thus, both the scanning and the image viewing techniques have been changed, and the user trained to acquire thin slices at a patient dose that is similar to that associated with SDCT. The ideal procedure is to scan the anatomical region with thin slices and to look at the resulting thin slice data set as a so-called secondary raw data set which is used for display.

Within the framework of the EU 2004 survey on MDCT (CT Quality Criteria 2004; Shrimpton 2004) only 53 questionnaires were evaluated. For examinations of the cranium the reported CTDI values and the 3rd quartile of the evaluated DLP were of the same order of magnitude as the RDL from EUR16242 ($CTDI_w$ = 60 mGy, DLP = 1050 mGy·cm, see Tables 5.10, 5.11).

For chest HR examinations the findings showed that "the observed ratio of 5.6 for 75-percentile and the 25-percentile of the effective dose indicates substantial interdepartmental variations in technique and suggests the potential for optimization" (Shrimpton 2004).

As a conclusion the survey suggested that evidence for optimization can be deduced if "a high ratio (>3) between 75-percentile and 25-percentile indicates substantial variations in scan parameters and technique among the departments and suggests the need for protocol optimization" (Shrimpton 2004).

In the German 2002 MDCT survey the reported increase in the local dose value $CTDI_{vol}$ was 17%–60% compared with the single- and dual-slice systems.

The scan length increased in examinations of the spine by up to 160%, mainly caused by scanning the whole lumbar or cervical spine region instead of only a few segments. "*In general, however, the danger of an uncontrolled increase of patient exposure due to CT procedures has to be limited by a clear medical justification in each individual case, independent of whether a standard examination is carried out or a new MDCT application such as coronary angiography, coronary calcium scoring or virtual colonoscopy*" (Brix et al. 2003).

5.7 Paediatric Issues

Only few efforts have been made to estimate dose values to paediatric patients and to establish separate RDL. This is a very important task because the dose children receive when using the same settings as for adults results in a twofold to fourfold higher dose and hence a higher risk for radiation-induced cancer (Brenner et al. 2001). The diameters of small patients, especially children, are much smaller than those of standard-sized adults. Also the dose-related risk is 2–3 times higher than that of an adult. A promising task would be to reduce dose (mAs settings of a specific scanner) by a factor that is either size or weight dependent. Some examples are given elsewhere (Sandstede; Shrimpton and Wall 2000; Brenner et al. 2001; Donnelly et al. 2000; Paterson et al. 2001; Chapple et al. 2002, Huda 2002; Khursheed et al. 2002; Suess and Chen 2002; Boone et al. 2003; Hollingsworth et al. 2003; Linton and Mettler 2003; Pages et al. 2003; Cody et al. 2004; Verdun et al. 2004; Vock 2005).

Table 5.13. Paediatric reference dose levels from UK 2003 (Shrimpton et al. 2003) survey

	$CTDI_w$ (mGy)	$CTDI_{vol}$ (mGy)	DLP (mGy·cm)	*E* (mSv)[a]
Head 0–1 year	35	35	270	2.5
Head 5 years	50	50	470	1.5
Head 10 years	65	65	620	1.6
Chest 0–1 year	23	12	200	6.3
Chest 5 years	20	13	230	3.6
Chest 10 years	26	20	370	3.9

[a] Mean values

While a lot of surveys have been carried out to establish reference dose values for adults, little effort has been made to determine RDL for children. The first survey to cover values for children in particular was the UK 2003 review published as NRPB-W67 (Shrimpton et al. 2003) (results for RDL values are presented in Table 5.13) and discussed at a national conference on dose reduction CT with emphasis on paediatric patients (Linton and Mettler 2003).

The assessment of an effective dose for paediatric CT is particularly complicated. The EU 2004 survey introduced the concept of geometric scaling factors, conversions factors and paediatric enhancement factors to calculate effective dose from DLP values. The 3rd quartile values for the estimated $CTDI_{vol}$, DLP and effective dose in head and chest examinations can be found in Table 5.14 together with the corresponding values for adults. "*Effective doses are of the same order of magnitude when compared to values for the adult CT head acquisition (acute stroke). It seems feasible to restrict effective dose to about 1 mSv. Chest: The observed variations in CTDI and effective dose are substantial and they suggest a realistic potential for dose reduction*" (CT Quality Criteria 2004; Shrimpton 2004).

The survey also showed that there is a good agreement between effective dose and dose length product: "The linear relationship is expressed as conversion coefficients for the calculation of effective dose from dose length product" (CT Quality Criteria 2004; Shrimpton 2004).

In Table 5.15 those normalized dose values are presented and compared with the values for an adult

Table 5.14. The 75th percentiles of dose values for children and adult; from Quality criteria (2004) at www.msct.info

Children	$CTDI_{vol}$ (mGy)	DLP (mGy·cm)	*E* (mSv)	Remarks
Head 1–12 months	31	333	2.6	
Head 4–6 years	47	374	1.8	
Chest 1–12 months	5,8	78	5.9	
Chest 4–6 years	6,2	76	3.4	
Adult				
Head	72	945	2.1	Acute stroke
Chest	14	549	8.4	Pulmonary embolism

Table 5.15. Normalized values of effective dose per dose length product [$f = E$/DLP in mSv/(mGy·cm)] for various body regions and patient ages (see also Fig. 5.5)

	(A)[a]	(B)[b]	(A)	(B)	(A)	(B)	(A)	(B)	(B)	(A)	EUR 16262	Germany (1999)
Age in years	0		1		5		10		15	adult	adult	adult
Head and neck	0.013	–	0.0085	–	0.0057	–	0.0042	–	–	0.0031	–	0.0039
Head	0.011	0.027	0.0067	0.008	0.004	0.004	0.0032	0.003	–	0.0021	–	0.0028
Neck	0.017	–	0.012	–	0.011	–	0.0079	–	–	0.0059	0.0054	0.0098
Chest	0.039	0.034	0.026	0.022	0.018	0.014	0.013	0.011	0.01	0.014	0.017	0.0154
Abdomen and pelvis	0.049	0.043	0.030	0.019	0.020	0.013	0.015	0.011	0.01	0.015	0.015	0.0174
Pelvis	–	0.037	–	0.027	–	0.018	–	0.017	0.01	–	0.019	0.0171
Trunk	0.044	–	0.028	–	0.019	–	0.014	–	–	0.015	–	–

[a] (A) Data from Shrimpton (2004), Shrimpton et al. (2003) and EU MDCT Quality Criteria (2004)
[b] (B) Data from Chapple et al. (2002)

(see also Table 5.12). To apply those values to dose estimation is rather simple and robust but does not include variations depending on scanner characteristics. The error when estimating dose values can be very large when the scanners have, for example, a different focus-axis distance or different filtration. Thus calculated values should serve only as a rough estimate.

The values of Shrimpton and Wall (2000) and Quality Criteria (2004) seem to be higher than those estimated by Chapple et al. (2002) (with the exception of values for the head for neonates). Thus values from Shrimpton and Wall (2000) can be regarded as conservative values to estimate the radiation dose using conversion factors. Values from Chapple et al. (2002) were derived from measurements using paediatric anthropomorphic phantoms (thermo-luminescent dosimeters, TLDs, loaded inside and on the surface of the five phantoms). There may be a large uncertainty related to the fact that there are only two scanners included in this estimation. A graphical representation of those normalized effective dose values [conversion factors *E*/DLP in mSv/(mGy·cm)] can be found in Figure 5.5; Figure 5.5a shows the values for head examination, Figure 5.5b for examination of the abdomen, together with the values for adults according the EUR16262 document and the results from the German 1999 survey.

In Germany the national authorities (BfS) initiated a survey at the end of 2005 to get reliable data on scan protocols for children, helping to establish RDL for children. This work started with a survey of age distribution and frequencies of paediatric CT examina-

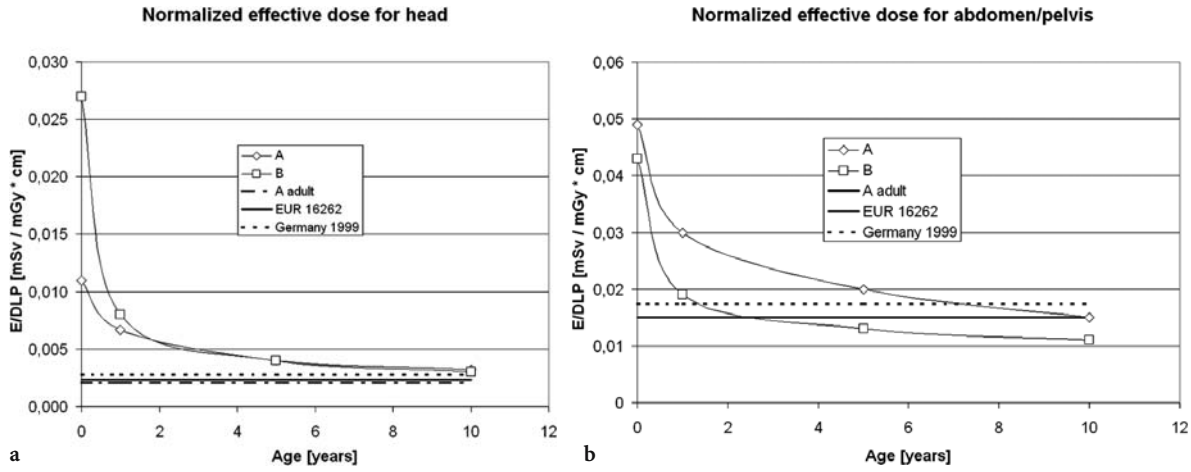

Fig. 5.5a,b. Normalized effective dose as a function of patient age for head (**a**) and abdomen/pelvis (**b**) region according Table 5.15 with curve (*A*) representing data from UK 2003 (Shrimpton 2004), Shrimpton et al. (2003) and EU MDCT Quality Criteria (2004) and (*B*) data from Chapple et al. (2002). Also included for reference are the values from the EUR16262 document and the German 1999 survey

tions. After identifying those institutes with at least 100 paediatric CT examinations per year, these institutes were included in a second survey to gather data for the scan protocols of the five most frequently carried out types of examinations. The first results show that the distribution of paediatric CT examinations is about 1%–2% of all CT examinations. This may be true only for Germany, so each country must check their annual rate of paediatric CT examinations. It also turned out that the main indications for paediatric CT are examinations of the head/brain, chest, abdomen, NHH (faces and sinuses) and spine.

A Nordic paediatric CT SURVEY is ongoing in 2005–2006, and the survey is focused on the following scan regions, brain, chest, abdomen and whole body; these are likely to be the main examinations carried out in paediatric CT, as shown by the preliminary results of the German paediatric survey.

Those surveys are absolutely necessary because we have only few reliable data on patient dose for paediatric CT examinations. There are a lot of suggestions on minimizing the radiation dose to children but those papers are not suitable for establishing RDL for children. Some strategies should be mentioned as follows:

Donnelly et al. (2001) suggested adapting the tube current for paediatric patients according the weight. Other authors (Boone et al. 2003; Verdun et al. 2004) recommended matching according the patient's circumference or diameter. Hollingsworth et al. (2003) focus on the kVp settings, which should and can be lowered to 100 kVp or even 80 kVp for small children: "*Kilo-voltage of 120 may not be the optimal level for examining infants*".

Suess and Chen (2002) suggest an adaptation of dose by changing the mAs settings in relation to settings for adults. For examinations of the head they propose a variation with age (< 6 month = 25%, > 6 years = 100%), while for body protocols the variation should be done according to patient weight (< 15 kg = 15%, > 54 kg = 100%). Also defining a patient-equivalent diameter can be used to set dose reduction factors (relative mAs-settings) with respect to a 28-cm patient diameter. According to Boone et al. (2003) this dose reduction factor may vary from 0.05 = 5% for a diameter of 12 cm (circumference = 38 cm) to 3.5 = 350% for a diameter of 35 cm.

The 16-cm CTDI phantom is not suitable for estimating/measuring CTDI for newborns and children. As the displayed $CTDI_{vol}$ and DLP values at the operator console are based on phantom values for a 16-cm and a 32-cm phantom, they are too high and cannot serve as a dose constraint with regard to RDL.

When looking at survey data from UK 2003 (Shrimpton et al. 2003) and the MDCT quality criteria 2004 (CT Quality Criteria 2004; Shrimpton 2004) there seems to be at least a factor of 2 between the RDL values for adults and children. Thus more sophisticated surveys are necessary to define those RDL and the corresponding image quality. Should the noise level for adults and children be the same when defining RDL, or do we have to deal with a lot

of examinations where the detection of low-contrast lesions is not of primary interest and importance?

5.8 Optimization Processes

The main question remaining is how to change scanning protocols to meet the requirements of RDL. As a result of the German 1999 survey the steps for an optimization process have been defined and reported (H.D. Nagel, Leitfaden zur Bewertung und Optimierung der Strahlenexposition bei CT-Untersuchungen, private communication).

This more practical guideline can serve as a first step to adjusting scan parameters.

CT is a radiological procedure that still has scope for dose reduction despite the progress already made. The 3rd quartile values deduced from the different surveys can only serve as a first attempt of dose optimization. Users of older single-slice scanners should redeem these values, while users of modern single-slice and multislice scanners should follow the 1st quartile values for an optimization process. So called ‚achievable doses mentioned in the 1999 NRBP vol. 10 document (National Radiological Protection Board 1999) are typically a factor of 2 or 3 lower than the RDL. Dose optimization with respect to $CTDI_w$ will be mainly based on a reduction of the mAs settings. With respect to DLP, the optimization has to be made on pitch factor and scan length or even on the number of series.

The starting point for dose optimization should be examination of the abdomen and pelvis. The first reason for this is that this examination has a high exposure, while requiring good image quality, in particular low contrast resolution.

Examinations with almost the same requirements for image quality and /or absorption should be done with the same values for $CTDI_w$/$CTDI_{vol}$; for example, liver and kidney or the abdominal aorta or head and neck.

The lower absorption in the chest region allows an obvious dose reduction compared to the values for the abdomen especially when using a wide window for image display (“lung/chest window”). To ensure adequate representation of the mediastinum and tips of the lung, the adaptation should not be lower than one-half of the values for the abdomen. This also holds true for examinations of the thoracic aorta and the pulmonary vessels. For distinct high-contrast examinations of the chest a reduction to one-tenth of the $CTDI_w$ value for the abdomen is possible, but this should be created as a special scanning protocol. Examinations of the pelvis also have a higher inherent contrast and allow a dose reduction to two-thirds of the $CTDI_w$ value of the abdomen. This also holds true for examinations of the whole trunk.

5.9 Conclusion

Surveys are necessary to define RDLs. They should be carried out on a large scale, because small-scale surveys just result in a snapshot of the current situation in the participating institutes. Also bias related to the limited number of scanners and manufacturers included in a small-scale survey can adulterate the findings. A comparison of different surveys should be made very carefully, taking into account different scanning techniques (number of series, slice thickness, pitch) as well as the different definitions of the region to be examined [upper and lower limit of scan region, different protocols for example in the head region (axial versus helical)].

An update of important surveys in order to define RDL in terms of new dose quantities such as $CTDI_{vol}$ seems to be necessary and has been reported in several surveys carried out recently. Our own experience suggests that the setup, the procedure and the evaluation of large-scale surveys will become more difficult in future because gathering all the relevant scan parameters will become an increasingly complex and time-consuming task. This is particularly true for those scanners using AEC or any other option for modulating the tube current. The technical development is rapid. This will unburden the users from having to carefully choose the scan parameters and adapting them for each patient more or less individually, but we are at the mercy of the technical developments. Verification of the dose estimates either displayed at the operator console or calculated retrospectively will become more and more difficult.

Special surveys have to be carried out to define RDL for children. This task is even more complex to accomplish. Those surveys have to take into account several age groups (at least four; namely <1 year,

< 5 years < 10 years and < 15 years) which means that the number of institutes executing a sufficient number of annual examination will be rather small (for example the ongoing survey in Germany listed only about 75 institutes carrying out at least 100 procedures each year).

References

Aroua A, Vader JP, Valley JF (1998) Survey on exposure by radiodiagnostics in Switzerland in 1998 (www.hospvd.ch/public/instituts/ira)

Bernhardt J, Veit R, Bauer B (1995) Erhebung zur Strahlenexposition der Patienten bei der Röntgendiagnostik. Z Med Phys 5:33–39

Boone JM, Geraghty EM, Seibert JA, Wootton-Gorges SL (2003) Dose reduction in pediatric CT: a rational approach. Radiology 228:352–360

Brenner DJ, Elliston CD, Hall EJ, Berdon WE (2001) Estimated risks of radiation-induced fatal cancer from pediatric CT. AJR Am J Roentgenol 176:289–296

Brix G, Nagel HD, Stamm G, Veit R, Lechel U, Griebel J, Galanski M (2003) Radiation exposure in multi-slice versus single.slice CT: results of a nationwide survey. Eur Radiol 13:1979–1991

Bundesamt für Strahlenschutz, Bekanntmachung der diagnostischen Referenzwerte für radiologische und nuklearmedizinische Untersuchungen vom 10 Juli 2003, Bundesanzeiger Nummer 143 vom 5.8.2003, 17503–17504

Chapple CL, Willis S, Frame J (2002) Effective dose in paediatric computed tomography. Phys Med Biol 47:7–115

Cody DD, Moxley DM, Krugh KT, O'Daniel CJ, Wagner LK, Eftekhari F (2004) Strategies for formulating appropriate MDCT techniques when imaging the chest, abdomen, and pelvis in pediatric patients. AJR Am J Roentgenol 182:49–859

Conway BJ, McCrohan JL, Antonson RG, Rueter FG, Slayton RJ, Suleiman OH (1992) Average radiation dose in standard CT examinations of the head: results of the 1990 NEXT Survey. Radiology 184:135–140

2004 CT Quality Criteria (A 6th Framework Research Project of the European Commission) at http://www.msct.info/CT_Quality_Criteria.htm

Donnelly LF, Emery KH, Brody AS (2001) Minimizing radiation dose for pediatric body applications of single-detector helical CT: strategies at a large children's hospital. AJR Am J Roentgenol 176:303–306

Einarsson G, Magnusson S (2001) Patient dose and examination frequency for diagnostic radiology in Iceland 1993–1998. In: Radiological protection of patients in diagnostic radiology, nuclear medicine and radiotherapy. Proceedings of an IAEA-CN-85 International Conference held in Malaga, Spain

European Commission (1999) European guidelines on quality criteria for computed tomography. Report EUR 16262 EN. Office for Official Publications of the European Communities, Luxembourg, pp 69–78, http://www.drs.dk/guidelines/ct/quality/`22.

Friberg EG (2003) Dual and multi slice CT – what about the doses. In: Proceedings of the Radiation Protection Symposium of the North West RP Societies, Utrecht 2003, pp 193–196

Galanski M, Nagel HD, Stamm G (2001) CT-Expositionspraxis in der Bundesrepublik Deutschland. Ergebnisse einer bundesweiten Umfrage im Jahre 1999. Fortschr Röntgenstr 173:R1–R66

Goddard CC, Al-Farsi A (1999) Radiation doses from CT in the Sultanate of Oman. Br J Radiol 72:1073–1077

Hart D, Wall BF (2001) Radiation exposure of the UK population from medical and dental X-ray exmaninations, NRBP-W4 (http://www.hpa.org.uk/radiation/publications/w_series_reports/2002/nrpb_w4.htm)

Hatziioannou K, Papanastassiou E, Delichas M, Bousbouras P (2003) A contribution to the establishment of diagnostic reference levels in CT. Br J Radiol 76:541–545

Hiles PA, Brennen SE, Scott SA, Davies JH (2001) A survey of patient dose and image quality for computed tomography in Wales. J Radiol Prot 21:345–354

Hollingsworth C, Frush DP, Cross M, Lucaya J (2003) Helical CT of the body: a survey of techniques used for pediatric patients. AJR Am J Roentgenol 180:401–406

Huda W (2002) Dose and image quality in CT. Pediatr Radiol 32:709–713

IEC International Electrotechnical Commission (2001) Medical electrical equipment – Part 2: particular requirements for the safety of X-ray equipment for computed tomography. IEC-Standard 60601-2-44 Ed. 2.0. International Elecrotechnical Commission, Geneva

Khursheed A, Hillier MC, Shrimpton PC, WALL BF (2002) Influence of patient age on normalized effective doses calculated for CT examinations. Br J Radiol 75:19–830

Linton AW, Mettler FA Jr (2003) National conference on dose reduction in ct, with an emphasis on pediatric patients. AJR Am J Roentgenol 181:21–29

Meeuwsen E, Brugmans M (2002) Gegevens over medische stralingstoepassingen: van ziekenhuisquêtes tot zorgverzekeraars. RIVM Rapport nr. 610059 009, Bilthoven http://www.rivm.nl/bibliotheek/rapporten/610059009.html

Meeuwsen E, Brugmans M (2003) Radiation exposure or the Dutch population from medical examinations. Proceedings Radiation Protection Symposium of the North West RP Societies, Utrecht, 2003, pp 273–278

National Radiological Protection Board (1999) Guidelines on patient dose to promote the optimisation of protection for diagnostic medical exposures. Documents of the NRPB, Vol 10, No. 1

Nowotny R. Entwicklung und Vergleich von Methoden zur Ermittlung und Überprüfung von Dosisreferenzwerten in der Röntgendiagnostik gemäss Patientenschutzrichtlinie EU 97/43 im Auftrag des Bundesministerium für Soziale Sicherheit und Generationen http://www.bmgf.gv.at/cms/site/detail.htm?thema=CH0343&doc=CMS1065194276970

Olerud HM (1997) Analysis of factors influencing patient doses from CT in Norway. Radiat Prot Dosimet 71:123–133

Olerud HM (2003) CT-dose surveys. In: Proceedings of the Radiation Protection Symposium of the North West RP Societies, Utrecht 2003, pp 178–192

Olerud HM, Torp CG, Einarsson G et al (2001) Use of the EC quality criteria as a common method of inspecting

CT laboratories – a pilot project by the Nordic radiation protection authorities. In: Radiological protection of patients in diagnostic radiology, nuclear medicine and radiotherapy. Proceedings of an IAEA-CN-85 International Conference held in Malaga, Spain

Origgi D, Vigorito S, Villa G, Bellomi M, Tosi G (2006) Survey of computed tomography techniques and absorbed dose in Italian hospitals: a comparison between two methods to estimate the dose-length product and the effective dose to verify fulfilment of the diagnostic reference levels. Eur Radiol 16:227–237

Pages J, Buls N, Osteaux M (2003) CT doses in children: a multicentre study. Br J Radiol 76:3–811

Papadimitriou D, Perris A, Manetou A et al (2003) A survey of 14 computed tomography scanners in Greece and 32 scanners in Italy. Examination frequencies, dose reference values, effective doses and doses to organs. Radiat Prot Dosimet 104:47–53

Paterson A, Frush DP, Donnelly LF (2001) Helical CT of the body: are settings adjusted for pediatric patients? AJR Am J Roentgenol 176:97–101

Sandstede J. Pediatric CT. At http://www.multislice-ct.com/www/

Scheck R, Coppenrath EM, Bäuml A, Hahn K (1998) Radiation dose and image quality in spiral computed tomography: results of a multicentre study at eight radiological institutions. Radiat Prot Dosimet 80:283–286

Shrimpton PC (2004) Assessment of patient dose in CT, NRPB-PE/1/2004. Chilton, NRBP. Also published as Appendix C or the 2004 CT Quality Criteria (MSCT, 2004) at http://www.msct.info/CT_Quality_Criteria.htm

Shrimpton PC, Wall BF (2000) Reference doses for paediatric CT. Radiat Prot Dosimet 90:249–252

Shrimpton PC, Jessen KA, Geleijns J, Panzer W, Tosi G (1998) Reference dose in computed tomography. Radiat Prot Dosimet 80:55–59

Shrimpton PC, Hillier MC, Lewis MA, Dunn M (2003) Doses from computed tomography (CT) examinations in the UK – 2003 review, NRPB-W67 (http://www.hpa.org.uk/radiation/publications/w_series_reports/2005/nrpb_w67.htm)

Suess Ch, Chen X (2002) Dose optimization in pediatric CT: current technology and future innovations. Pediatr Radiol 32:729–734

Szendrö G, Axelsson B, Leitz W (1995) Computed tomography practice in Sweden. Quality control, techniques and patient dose. Radiat Prot Dosimet 57:69–473

Thomson JEM, Tingey DRC (1997) Radiation doses from computed tomography in Australia, ARL/TR 123

Tsapaki V, Kottou S, Papadimitriou D (2001) Application of European Commission reference dose levels in CT examinations in Crete, Greece. Br J Radiol 74:836–840

UNSCEAR Report 2000 Annex D, Medical Radiation Exposure, New York (2000) United Nations

van Unnik JG, Broerse JJ, Geleijins J et al (1997) Survey of CT techniques and absorbed dose in various Dutch hospitals. Br J Radiol 70:367–371

Verdun FR, Lepori D, Monnin P, Valley JF, Schnyder P, Gudinchet F (2004) Management of patient dose and image noise in routine pediatric CT abdominal examinations. Eur Radiol 14:835–841

Vock P (2005) CT dose reduction in children. Eur Radiol 15:330–2340

Methods and Strategies for Radiation Dose

6

Optimization – and Reduction – in MDCT with Special Focus on the Image Quality

Denis Tack

CONTENTS

D. Tack, MD, PhD
Clinic of Cardiac Imaging, Department of Radiology, Hôpital Erasme, Université libre de Bruxelles, Route de Lennik 808, 1070 Brussels, Belgium

6.1 Introduction: Should We Optimize/Minimize the Patient's Radiation Exposure?

The danger of ionizing radiation is related to the potential long-term risk of carcinogenesis. In Chapters. 1 and 2 of this book, Chadwick and Cohen have detailed how this risk is evaluated and considered in the field of low-level radiation in which diagnostic imaging (including CT) in comprised. The linear no threshold (LNT) theory of carcinogenesis is based on the risk of hereditary mutations deriving from cellular effects in germ cells. This theory considers that the cancer risk is linearly proportional to the dose at high doses as well as at low doses, from zero dose up. On the other hand, failure of the LNT theory is based on series of investigations showing that there is substantial evidence that low-level radiation does not have any carcinogenic effect and may even be protective against cancer, a view known as "hormesis".

Important here is the fact that the Recommendations of the International Commission on Radiological Protection (ICRP), outlined in its Publication 60 (ICRP 1991), implicitly have adopted the LNT concept, because of the precautionary principle. ICRP considers that the risks estimated using the LNT concept are probably conservative. The concept has formed the basis for the development of a radiological protection philosophy including the ALARA (as low as readily achievable) principle. In 1991, the ICRP quantified the radiation risk by adopting a value of 5% for the nominal lifetime excess absolute risk per Sievert (Sv) for fatal cancer for a general population exposed to low-level radiations.

The radiation dose received by patients undergoing diagnostic radiological examinations by CT are generally in the order of 1–24 mSv per examination for adults (UNSCEAR 2000) and 2–6.5 mSv for children (Shrimpton et al. 2003). These effective doses can be classified as low even though they are invari-

ably larger than those from conventional diagnostic radiography. Typically, a chest radiographic examination (including two views) delivers between 0.08 and 0.30 mSv whereas a standard dose multidetector-row CT (MDCT) represents a 100 times higher risk, delivering 8 mSv. One fatal cancer should be expected for every 250,000 chest X-rays whereas this risk is 1/2,500 for a chest MDCT scan. More than one-half of the collective dose delivered for diagnostic imaging procedures is due to CT (Golding and Shrimpton 2002). Thus, particular attention has to be paid to dose optimization and reduction while using CT.

In this chapter, we will review the many faces of limiting the radiation dose from CT and in particular from MDCT. We will comment on the alternatives to using CT, on the CT parameters managed by the radiology team that have an impact on the radiation dose, and on how to minimize this dose per acquisition, per examination, and per patient. Finally, we will propose dose values suitable for an optimized use of MDCT.

6.2 Guidelines for Appropriate Use of Imaging

CT and in particular MDCT is a fabulous technique with regard to its liability, rapidity, and availability. The spatial resolution provided by MDCT with isotropic voxels makes radiologists and physicians highly confident in the diagnosis yielded by these examinations. As a practical result, the radiologists, the clinicians, and even the patients probably prefer dealing with CT than with other imaging methods or medical tests that could be more difficult to interpret. In addition, new indications of CT have been validated (i.e., ureteric stone disease, virtual colonoscopy, CT angiography including the coronary arteries, etc.). As modern MDCT scanners can now process 60–70 patients a day, as compared to 30–40 patients in the 1990s, the increase in the number of procedures can easily be overcome by modern radiology departments. Most importantly, image-based media now have a central role in our modern societies. CT scans, by showing directly "what is happening inside the patient", seem easy to read and are thus more attractive than conventional radiography, which often suggests the diagnosis through indirect signs. This evolution has already resulted in a huge increase in CT examinations and subsequently in collective dose.

To overcome some abuse in the use of CT, it should be kept in mind that alternative imaging techniques such as ultrasonography (US) and magnetic resonance imaging (MRI) are also widely available. Substitution of CT with US and MRI is an important factor in collective radiation dose reduction. As an example, a CT scan of the central nervous system (brain and spine) can be replaced by MRI in almost all patients except those with acute trauma. However, this would need a number of MR units approximately as high as that of CT units. There are equal numbers of MR and CT units in some countries, such as Japan, but in others the number of MR units is still three times lower than that of CT. This relative shortfall of MR compared to CT equipment contributes to the excess collective dose.

In order to define diagnostic strategies for clinicians in their consideration of patient radiation protection, guidelines for the prescription of imaging tests have been proposed by the Royal College of Radiology (Royal College of Radiologists 2006). Ideally, such guidelines should be evidence based.

As an example of an evidence-based study, diagnostic strategies including MDCT angiography of pulmonary arteries (CTPA) have been investigated by the group in Geneva (Perrier et al. 2004). These authors have documented the clinical potential of a diagnostic strategy for ruling out pulmonary embolism (PE) based on D-dimer dosage combined with lower-limb US before performing CT pulmonary angiography (CTPA) in outpatients. Such an approach led to a recurrence rate of PE of only 1% (95% confidence interval: 0.5%–2.1%), and CTPA was performed in only 593 out of 965 outpatients (61%). Perrier et al. (2004) concluded thus that a noninvasive diagnostic strategy combining clinical assessment, D-dimer dosage, lower-limb US, and helical CT scanning – necessary in approximately two-thirds of patients only – yields an accurate diagnosis in 99% of outpatients suspected of having PE.

Nowadays, it appears in clinical practice that CTPA is ordered for almost all patients suspected of having a PE. Indeed, in emergency departments of almost all community hospitals, MDCT has now become as available as D-dimer dosage. In addition, the results of CTPA are more rapidly obtained than those of D-dimer dosage and MDCT can deliver very important information on possible alternative

diagnoses. As a consequence, it has been recently reported that not more than 10% of CTPA ordered to rule out PE were actually positive for PE (Schaefer-Prokop and Prokop 2005) whereas this percentage ranged from 20% to 40% 10 years ago.

Other evidence-based studies have been conducted on patients presenting with acute abdominal pain. In such circumstance, the high diagnostic performance of CT for the diagnosis of various acute abdominal diseases – including trauma, small bowel obstruction, acute appendicitis, acute colon diverticulitis, pelvic inflammatory disease, and pyelonephritis – has been reported. This is extensively discussed in Chapter 10 by Keyzer et al. The success of CT in diagnosing acute abdominal disorders has resulted in the wide use of this technique with a subsequent decrease – from 40% to 20% – of the proportion of positive results (Chen et al. 1999). In other words, the collective radiation dose has been doubled for diagnosing a constant number of acute abdominal diseases. The risk versus benefit ratio of CT has thus been reduced. In addition, promising results collected in studies dealing with acute abdominal pain have been extended to subacute abdominal pain without any robust evidence. One possible reason for this extension is the ability of CT to demonstrate unsuspected diseases, as illustrated in Figure 6.1. However, the risk versus benefit ratio of CT in subacute abdominal pain remains unknown.

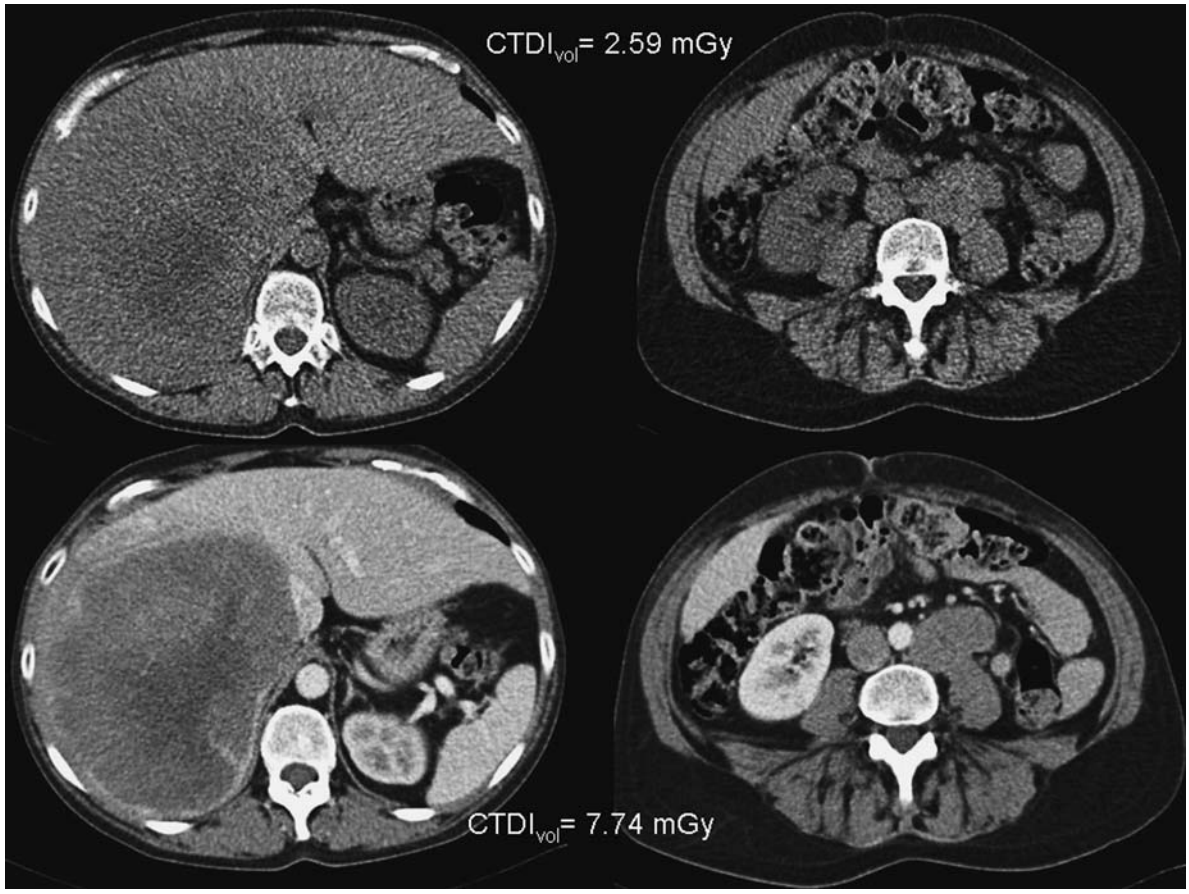

Fig. 6.1a–d. A 42-year-old woman 1.62 m tall and weighing 67 kg referred for an abdomino-pelvic CT complaining of chronic abdominal pain for 4 months. Unenhanced low-dose CT of the abdomen (**a**, **c**) and pelvis is obtained with a dose–length product (*DLP*) of 115 mGy·cm, equivalent to one-quarter of the mean value from the UK 2003 survey (NRPB 2005). This acquisition shows a focal hepatic mass (**a**) and retroperitoneal lymphadenopathies (**c**). Enhanced standard-dose CT confirms liver metastases and lymphadenopathies (**b**, **d**). Biopsy of the cervix confirmed adenocarcinoma. Enhanced CT delivered 300 mGy·cm, corresponding to less than one-half of the mean values from the NRPB 2003 survey study. The CT scanner was a Siemens Emotion 16® with 16×0.6 mm collimation, 130 kVp, an image quality index of 130 mAs (effective) and used an AEC device

In summary, it is of utmost important to remember that the most efficient way to limit a patient's radiation dose is to avoid imaging by CT, and whenever possible to substitute CT with MRI and/or US. If still needed, CT technique optimization is mandatory.

6.3 Optimization of the MDCT Technique

Once the clinical indication of CT is well established, the appropriate CT technique is then required in order to optimize the image quality with the lowest possible radiation dose. The influences of the numerous CT components and/or parameters on radiation dose are detailed in the present edition by Nagel (Chap. 4). We will therefore restrict our discussion to those that can be easily modified and adapted by the operator performing the examination. As a general rule, it should be noted that the use of standardized and fixed acquisition parameters leads to unnecessary overexposure of patients.

6.3.1 CT Parameters

6.3.1.1 Tube Potential (*U*)

The relationship between the dose and the tube potential (*U*) is not a straight and linear one, but rather exponential and varying according to the specific circumstances. The intensity of the radiation beam at the detector array, for example, varies with *U* to the power of 3.5. If the tube potential is increased, e.g., from 120 kVp to 140 kVp, the intensity of the electrical signal obtained from the detectors changes by a factor of 1.7.

Tube potential *U* is usually modified only through the kilovoltage (kVp) settings, which are restricted to a small number of possible levels. These kVp values differ from one manufacturer to another, as well as from one CT scanner to another, and vary from 80 kV to 140 kV. As the effect of increasing *U* has a huge influence on radiation dose, a general rule for selecting kVp could be the following:

- To avoid 140 kVp except for CT of the chest, the abdomen, and the pelvis in extremely obese patients [i.e., with a body mass index (BMI) greater than 35 kg/m^2], and for CT of the lumbar spine in obese patients (i.e., with BMI > 30 kg/m^2).
- To prefer 100–110 kVp for CT of the chest, the abdomen, and the pelvis in thin patients (i.e., with a BMI < 22 kg/m^2), and in 10- to 15-year-old children.
- To prefer 80–90 kVp for CT angiography and in children younger than 10 years old.
- In all other circumstances, to select 120–130 kVp.

6.3.1.2 Tube Current–Time Product (*Q*) and Adaptation to Patient's Size

As in conventional radiography, a straight linear relationship exists between the tube current–time product (*Q*) and the dose; i.e., all dose quantities will change by the same amount as the mAs setting applied. The settings for *Q* should be adapted to the characteristics of the scanner unit, the patient's size (see Chap. 4), and the dose requirements for each type of examination.

Examinations with high intrinsic contrasts (as of the chest and the skeleton), which are displayed with wide window width, can most often be carried out with strongly reduced mAs settings and no impairment of image quality.

Appropriate use of *Q* also depends on the patient's size, which is an important parameter to consider in dose optimization. Considerable reductions in *Q* are appropriate for slim patients, and particularly for children. In order to avoid unnecessary overexposure, *Q* should be intentionally adapted by the operator unless automatic exposure control (AEC) devices, or similar, are available. A detailed description of how AEC devices work and what they bring in terms of dose optimization is given in Chap. 7.

As a general rule, one should remember that the *Q* setting may be halved when the patient's trunk diameter – typically 30 cm – decreases by 4 cm without loss of image quality. For a CT scan of the adult trunk, if the CT unit is not equipped with an AEC device, the following settings may be proposed (with the effective mAs being defined as *Q* divided by the pitch factor):

- 1.0 mAs/kg (effective) for chest CT scan
- 1.5 mAs/kg (effective) for abdominal and pelvic CT scans.

In a patient weighting 70 kg and 1.70 m tall (i.e., representative of the typical Monte Carlo Model and

Rando Anthropomorphic Phantom used for effective dose calculations by ICRP), the dose–length product (DLP) delivered for a chest CT scan at 120 kVp and 70 mAs (effective) would be approximately 180 mGy·cm. Using 1.5 mAs/kg (effective), an abdomino-pelvic CT scan would deliver approximately 320 mGy·cm. These two DLP values correspond to approximately one-half of the reference values (i.e., the 75th percentile in survey studies) used in the European Union in 1999 (EUR 1999).

If the CT unit is equipped with an AEC device, the reference image quality has to be defined, according to the scanned body region, and/or the clinical indication. Recommendations for the appropriate value of *Q* in brain and neck CT studies as well as in CT examination of sinonasal cavities are discussed by Mulkens et al. in Chapter 8 of the present edition. Recommendations for appropriate use of *Q* in CT studies of the trunk are discussed below.

6.3.1.3 Slice Collimation

Detailed descriptions of the influence of slice collimation, slice thickness, overbeaming, and overranging on the radiation dose are given in Chapter 4. As modern MDCT scanners can provide isotropic voxel resolution, thin-slice collimations are now widely used. Radiologists have to keep in mind that the image noise represented by the graininess or mottle aspect of the images not only depends on the radiation dose but also on the algorithm used for reconstruction and on slice thickness. In order to reduce the image noise due to thin collimation, it is not appropriate to increase the dose (mainly by increasing *Q*). Indeed, adapted reconstruction algorithms generating little noise, slightly thickened sections, and multiplanar reformations (MPR) designed to erase most image noise from native images may be valuable alternatives. An example is given in Figure 6.2.

6.3.1.4 Pitch Factor

With single detector row CT (SDCT) scanners, increased pitch serves primarily to decrease the duration of the acquisition, but it also decreases the radiation dose proportionally. However, as a side-effect, the slice profile width, i.e., *z*-resolution, is impaired.

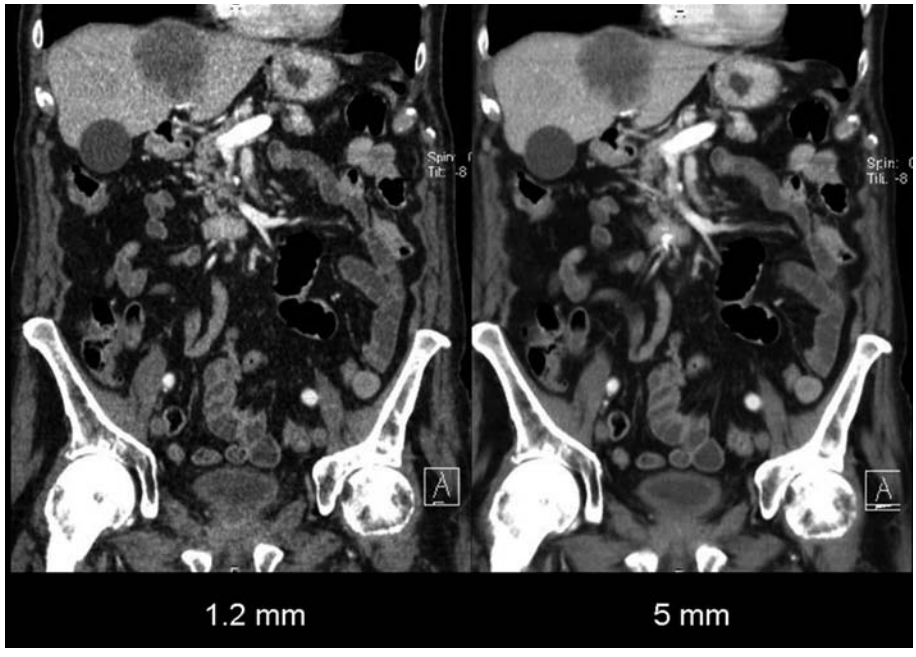

Fig. 6.2. Enhanced standard-dose MDCT of the abdomen showing a liver metastasis in a man with prostate carcinoma. Left CT image is reconstructed in the coronal orientation with a thickness of 1.2 mm and shows quite an important mottle aspect of the abdominal structures. Right CT images is reconstructed in an identical orientation but with a thickness of 5 mm. The mottle aspect seen in the thin-section coronal CT slice is no longer visible. The effect of image smoothing by thickening the CT slice is seen when the noise is due to low-dose scanning and when the noise is related to high-frequency reconstruction algorithms

With MDCT scanners, the spiral interpolation scheme is different than that on SDCT scanners. With MDCT, the slice profile width is unaffected by the pitch but the image noise is influenced by it (see Fig. 4.34a) unless the tube current is adapted accordingly. This adaptive process is named the "effective mAs" concept.

Scanners based on the effective mAs concept not only keep slice profile width constant, but also the image noise when the pitch is modified. In order to keep the slice profile width and image noise independent of pitch, the electrical mAs product supplied to the X-ray tube is automatically adapted through a straight linear relationship with pitch. As a consequence, the patient's dose – expressed as $CTDI_{vol}$ – and the slice profile are no longer modified with the pitch. On the other hand, MDCT scanners that are not based on the effective mAs concept still limit dose by increasing the pitch with, as a consequence, impaired image quality (i.e., increased noise) if mAs settings are not adapted manually by the operator.

With MDCT scanners, the pitch should be selected exclusively with respect to the scan speed, spiral artifacts, and tube power. Radiation dose considerations no longer play a role if MDCT scanners are based on the effective mAs concept or if the mAs setting can be adapted to pitch in order to achieve a constant image noise. Nevertheless, this simple rule has limitations with scanners that have more than 32 detector rows, because they have a large beam width such that the overranging effect generates an additional exposure that depends on the pitch. With such scanners, high pitch values can amount to 30% of the dose as compared to low pitch values (i.e., pitch of 1.75 with a 64-row MDCT scanner for an acquisition on the upper abdomen).

6.3.1.5 CT Dose Index and Dose–Length Product

Definitions of the CT dose index (CTDI) and DLP – the two most commonly used dose descriptors – are in Chapter 4. Newer scanners must be equipped with a dose display; at present, only display of the volume computed tomography dose index ($CTDI_{vol}$) is mandatory (IEC 2001). However, many scanners also show DLP, either just per scan series, or both per scan series and per exam. Such a dose display enables comparison with recommended values. In addition, changes in scan parameter settings and their effect on patient exposure are visible on the CT screen. Thus, these displays are appropriate for dose optimization. Finally, $CTDI_{vol}$ can also be used as a fair estimate of the dose delivered to the organs located within the scan range. The interpretation of dose values displayed on the scanner's console needs special attention in the following situations:

- Many dose recommendations are expressed in weighted CTDI ($CTDI_w$), in order to allow comparisons; therefore, the pitch correction involved in $CTDI_{vol}$ should be reverted by multiplying $CTDI_{vol}$ by the pitch factor.
- Until now, dose values used for body scanning have been based on body-CTDI, regardless of the patient's size. In pediatric examinations, the figures displayed should be multiplied by a factor of 2 for children and of 3 for infants in order to give a realistic estimate of the patient's dose.

6.3.1.6 Number of Acquisitions per Examination

The radiation dose depends linearly on the number of CT acquisitions performed. As an example of optimizing this parameter, one has to define the following:

- The need for unenhanced acquisition prior to enhanced acquisition (in many instances, unenhanced CT prior to enhanced CT is not mandatory).
- The number of acquisitions in dynamic CT scanning:
  - for the assessment of a pulmonary nodule, determining the enhancement patterns of a pulmonary nodule may require up to four acquisitions (Swensen et al. 2000);
  - for the detection of hepatocarcinoma, a multiphasic examination may include four acquisitions (Lim et al. 2002).

6.3.1.7 *Z*-coverage

Z-coverage is defined as the length of the acquisition and is expressed in centimeters. The radiation dose is grossly proportional to *Z*. The *Z*-coverage is included in DLP. In the daily practice, it is important to limit *Z*-coverage to what is strictly necessary. The risk of limiting *Z*-coverage is misdiagnosis.

An example of optimization of *Z*-coverage in abdominal CT performed to rule out acute appendicitis is given in Chapter 11. It has been proposed to limit *Z*-coverage to a height of 12 cm. However,

the proportion of alternative diagnoses that could be missed in the upper abdomen has not yet been quantified.

For the diagnosis of acute pulmonary embolism, SSCT proved to have a 98% negative predictive value (Tillie-Leblond et al. 2002). This technique included *Z*-coverage of approximately 15 cm, from the aortic arch to the diaphragm. Using MDCT, one has the possibility of extending *Z*-coverage to the whole chest by using a thinner collimation but with reduced duration of acquisition. With this MDCT technique, *Z*-coverage has been grossly doubled but the negative predictive value has not been modified (98.5% vs. 98.0%). Regarding alternative diagnosis, SSCT with 15 cm *Z*-coverage showed an alternative diagnosis in up to 40% of patients whereas MDCT is now reported to show an alternative diagnosis in 28% of patients (Weiss et al. 2006).

6.3.1.8 Patient Centering

CT users should be aware of the potential overexposure due to inadequate patient centering in the *Y*-axis, due to bow tie filters. A detailed description of this effect can be found in Chap. 8.

6.3.1.9 Automatic Exposure Control (AEC)

As explained in Section 6.3.1.2, dose requirements are strongly dependent on the patient's size, weight or diameter, and absorption. Chapter 4 shows how dose requirements can be expressed by Brook's formula. This formula has been studied on phantoms by Boone et al. (2003) and by Siegel et al. (2004). A reduction of 12 cm (i.e., from 32 to 20 cm) of the phantom diameter can be associated with a 71% reduction in mAs without any decrease in image quality. Newer CT scanners are equipped with AEC that can automatically adapt the mAs settings to the patient's size and shape. AEC are described and discussed in detail in Chapter. 7. Using an AEC device, the role of CT users is to define the expected image quality – and the subsequent radiation dose – suitable for the acquisition.

6.3.1.10 Intravenous Injection of Iodine Contrast Material

Compared to unenhanced CT, enhanced CT with intravenous iodine contrast injection does not require a higher tube current–time product. This can be easily demonstrated by comparing the DLP delivered by a CT scanner equipped with an AEC device between two consecutive acquisitions, one without and one with iodine injection. In such circumstances, the DLP delivered automatically – with unchanged CT parameters – varies by less than 1%.

6.3.2 Determination of a Standard of Reference for Image Quality

6.3.2.1 Definition and Methodology

Image noise, an important determinant of image quality, is inversely proportional to the X-ray beam energy. Although a decrease in tube current or in tube voltage results in a dose reduction, such a decrease is associated with an increase in image noise, which may compromise the image quality to a variable extent. Thus, while dose reduction is crucial because of the possible risks of radiation exposure, it is equally essential to realize the benefit of a "quality CT examination" that adequately addresses pertinent clinical issues affecting patient care (Rehani et al. 2000). Therefore, radiation dose reduction, although prudent when appropriate (i.e., in pediatric CT), must not compromise the diagnostic outcome of clinically relevant examinations. It is worthwhile remembering that, in most circumstances, strategies should be directed toward radiation dose optimization rather than dose reduction per se, so that the image quality maintains a diagnostic standard. For instance, a high radiation dose may not necessarily provide substantially improved image quality and increased lesion conspicuity in comparison with standard or even low-dose scanning.

As explained above, one of the most difficult parameters to account for in dose optimization is the patient's mass, weight, or BMI. If an AEC device is not available on the CT scanner used, one has to adapt the mAs setting for each patient. We suggest using 1.0 and 1.5 mAs (effective) per kg of weight, respectively for the chest and the abdomen.

As modern scanners are now equipped with AEC devices, they are thus able to deliver a homogeneous image quality throughout the acquisition regardless of the patient's diameter, weight, absorption, and shape. The parameters of such acquisitions are to be

set by the users and are thus not dependent on the patient's weight, rather only on the desired level of image quality. However, it remains extremely difficult to define the required image quality, as what is acceptable to one radiologist may be unacceptable to another, even with uncompromised diagnostic performance.

In order to optimize the dose by determining a "reasonable" image noise or a "reasonable" image quality, robust references could be considered as a starting point. Survey studies conducted through the US and EU may serve as such starting points. The reference levels elicited by theses surveys correspond to the 75% percentile of the delivered dose in participating CT departments. As these levels reflect very heterogeneous scanning methods and CT equipment, they are quite high. As a balance between diagnostic performance, diagnostic confidence, and radiation dose has not yet been critically defined, it is mandatory to proceed step by step in order to optimize the dose.

The aim of the following paragraphs is thus to comment on and illustrate a possible approach to achieving appropriate image quality and radiation dose using modern scanners equipped with AEC devices. This can be applied to adults only. Pediatric CT scanning is discussed by in Chapter 15.

6.3.2.2 Optimization of Standard-Dose MDCT Acquisitions

In our approach to dose optimization, we considered the results of clinical research conducted by our group on low-dose CT (Tack et al. 2003a–c; Keyzer et al. 2004; Tack et al. 2005a, b), and the mean or median dose values (instead of reference dose values) from survey studies (Brix et al. 2003; NRPB 2005) recently conducted in Germany and UK. Survey studies reflect the dose delivered in hospitals using a wide range of CT scanners, including SDCT, MDCT with two, four, and eight detector rows. In general, the CT dose tends to decrease with a constant image quality when using newer generations of MDCT scanners. In addition, as the survey studies cover a large variety of CT scanners, it should be noted that dose optimization with MDCT should aim to reach approximately the 25% percentile of dose as reported in the surveys. This is detailed in Chapter 5.

6.3.2.2.1 Brain CT Examination

Based on their personal experience and on published data, Mulkens et al. (Chap. 9) recommend the use of a $CTDI_w$ of 30 mGy (equivalent to $CTDI_{vol}$ if the pitch factor is set at 1), a 50% reduction as compared to reference values obtained from a 1999 survey (EUR 1999). A comparison of two CT acquisitions of the brain obtained with $CTDI_{vol}$ values of 40 mGy, and 31 mGy is shown in Figure 6.3. No clinically relevant loss of image quality is detectable at 31 mGy as compared to 40 mGy. It should be noted that there is no need to apply AEC when scanning the brain, as the differences in attenuation between orientations and/or between slices are minimal. Therefore, modern scanners equipped with AEC devices do not apply them when in head mode.

6.3.2.2.2 Chest CT Examination

Unhenhanced CT of the Lung Parenchyma and Mediastinum

Naturally high contrasts between thoracic structures, particularly in the lung parenchyma where air is abundant, reduce the need for high doses to produce excellent image quality. Using MDCT equipped with an AEC device, the user has to set the required image quality. This image quality is expressed by indexes varying from manufacturer to manufacturer. Siemens expresses this quality by a "reference mAs value". Figure 6.4 shows images acquired on such an MDCT scanner at 120 kVp, with 32×0.6 mm beam collimation, and 90 mAs (effective) as reference quality mAs. The AEC device automatically reduced the tube current–time product to 61 mAs, as the patient was thin (BMI = 21 kg/m^2).

$CTDI_{vol}$ and DLP were, respectively, 4.67 mGy and 176 mGy·cm, corresponding to 50% of the reference dose (P75) reported in the German survey (Brix et al. 2003), and to less than 50% of the mean dose value reported in the UK survey (NRPB 2005).

How AEC devices react to obese patients is illustrated in Figure 6.5. The image quality of Figure 6.5a was set to the same reference quality mAs as in Figure 6.4 [90 mAs (effective)]. As this woman was obese (BMI = 35 kg/m^2), the automatically adjusted $CTDI_{vol}$ was 10.5 mGy, a value corresponding to the mean dose reported in the UK survey (NRPB 2003) and to 80% of that reported in the German survey

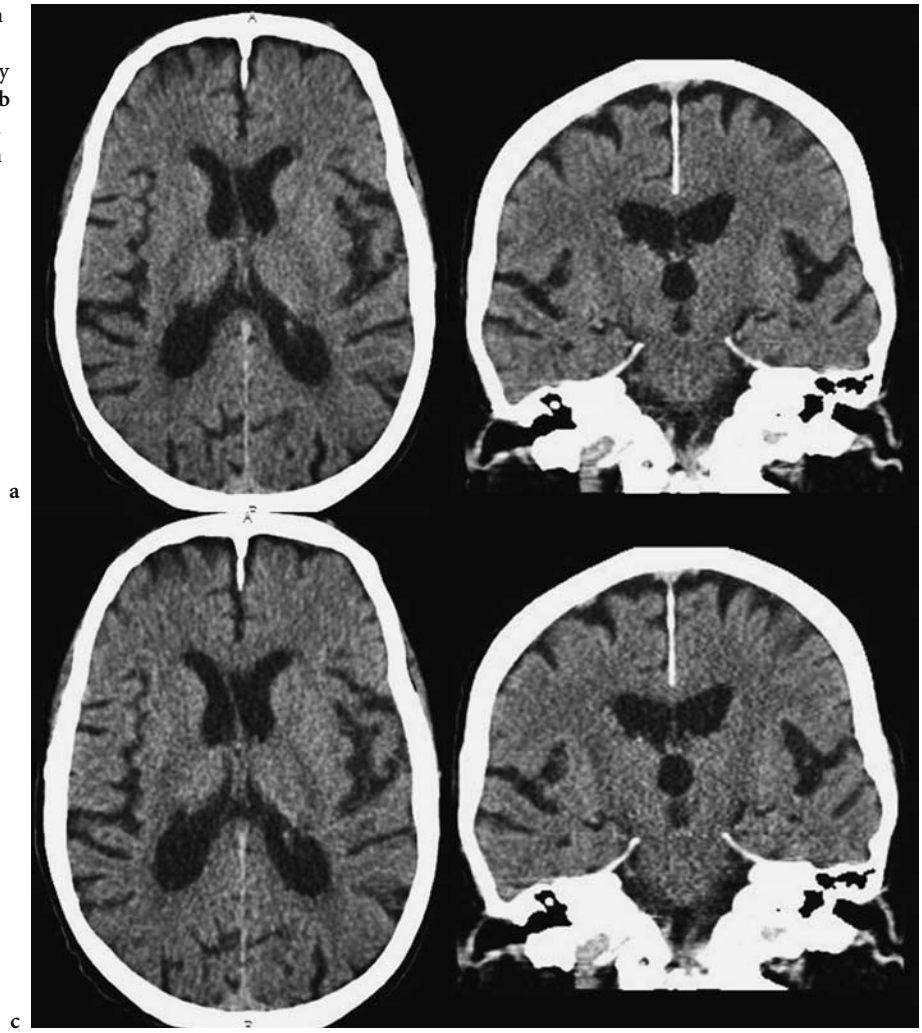

Fig. 6.3a–d. CT of the brain obtained with two acquisitions at a $CTDI_{vol}$ of 40 mGy (**a** in axial orientation and **b** in coronal orientation) and at a $CTDI_{vol}$ of 31 mGy (**c** in axial orientation and **d** in coronal orientation). Scans in **a** and **c**, and in **b** and **d** show comparable image quality

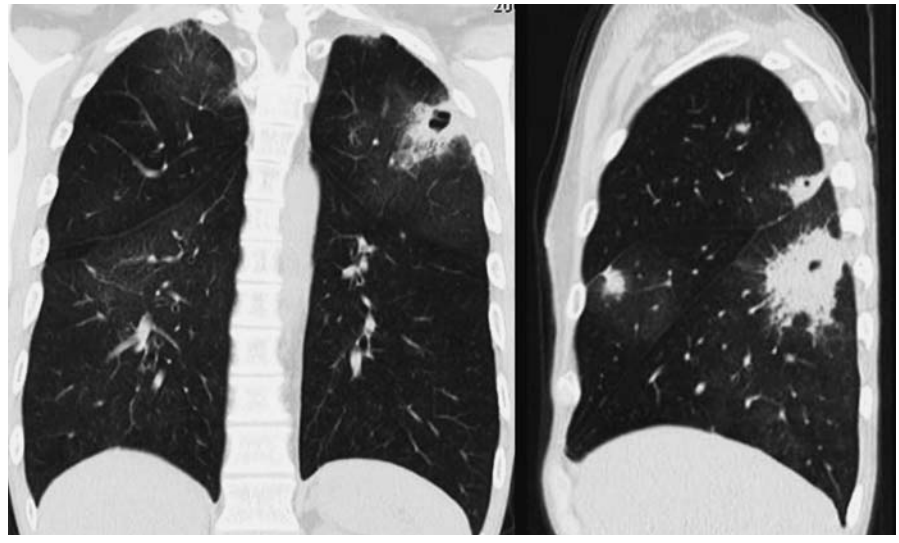

Fig. 6.4. A 38-year-old man 1.79 m tall and weighing 67 kg complains of mild fever and dyspnea. Multiple irregular excavated pulmonary nodular consolidations are demonstrated by MDCT and correspond to infections due to *Legionella*. MDCT parameters are displayed at the bottom of each coronal and sagittal reconstruction. In this thin patient, the AEC device reduced the mAs from 90 to 61 mAs

(Brix et al. 2003). On this particular woman, a second acquisition was obtained with 60 mAs (effective) as the reference quality mAs (Fig. 6.5b). This 33% dose reduction did not affect the image quality, as illustrated by comparing Figure 6.5a with Figure 6.5b, which appear very similar.

Another example comparing image quality index at 90 and at 60 mAs is shown in Figure 6.6 in a thin patient. In this example, the delivered dose resulted in $CTDI_{vol}$ values of respectively 4.4 and 2.9 mGy only. In this patient with a tumor infiltrating the carina, mediastinal images at 90 and 60 mAs (effective) as reference of image quality (Figs. 6.6a, b) illustrate similar and clinically acceptable image quality.

CT Angiography of Pulmonary Arteries

Dose optimization of CT angiography of pulmonary arteries (CTPA) relies more on reduction of *U* than on reduction of *Q*. As discussed in Chapter 10, the use of low, or very low mAs settings is associated with a huge amount of noise (Tack et al. 2005b). Even if pulmonary emboli are still visible in noisy images, the effect of noise on overall diagnosis of pulmonary embolism and alternative diagnoses remains unknown. A low tube potential setting has been validated in clinical practice (Sigal-Cinqualbre et al. 2004) at 80 kVp, at least in patients weighing less than 75 kg. This study was conducted with a CT scanner that was neither equipped with an AEC device nor able to scan at 100 kVp. As shown in Chapter 4, the signal of iodine at 80 kVp is much higher than that at the standard kVp setting (120 kVp). Newer scanners are now able to modulate the mAs setting at 100 kVp. Figures 6.7 and 6.8 show CTPA acquisitions at 110 kVp (16×0.6 mm beam collimation scanner) and 100 kVp (32×0.6 mm beam collimation scanner), respectively, in a thin and in an obese patient with acute and chronic pulmonary embolism.

The DLP values delivered by these CTPA acquisitions were respectively 99 and 163 mGy·cm, a very low dose as compared to the mean value from the UK (400 Gy·cm) and German (331 mGy·cm) surveys.

6.3.2.2.3 Abdominal CT

Standard dose abdominal MDCT scans require a higher dose than standard dose chest MDCT because the abdominal cavity contains solid organs that absorb much more the X-rays than the lungs. As explained above, if the MDCT scanner is not equipped with an AEC device, the operator should chose 120 kV and 1.5 mAs/kg weight. For patients of a normal weight, an abdomino-pelvic MDCT scan obtained with these parameters would deliver a DLP of 320 mGy·cm, corresponding to one-third of the

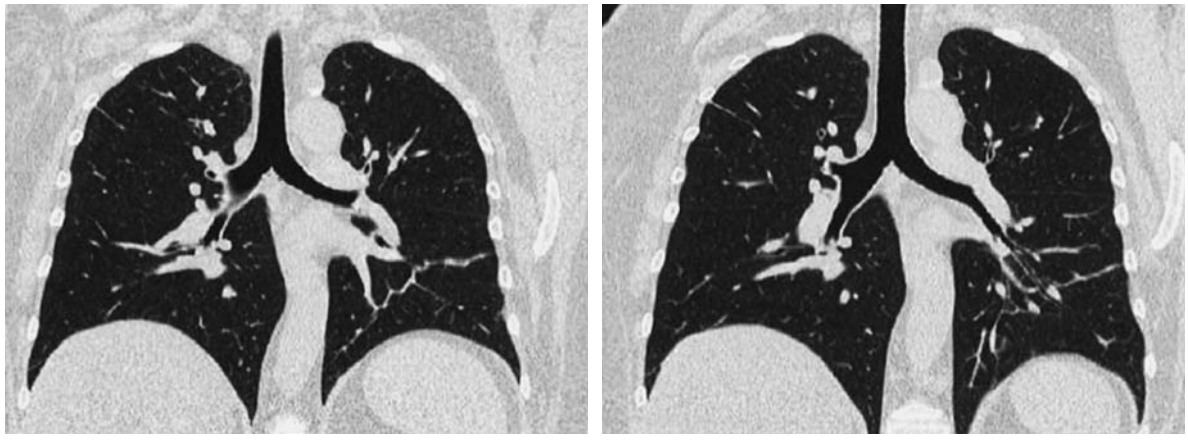

a b

Fig. 6.5a,b. A 45-year-old woman 1.68 m tall and weighing 95 kg (BMI = 35 kg/m^2) is referred for CT for follow-up of breast carcinoma and opacity in the left bases at chest radiography. Two CT acquisitions were performed, both using AEC. The first one (**a**) was obtained while the reference quality mAs was set at 90 mAs (effective). The second one (**b**) was obtained with a reference mAs reduced to 60 mAs (effective). Dose descriptors ($CTDI_{vol}$ and DLP) are displayed. Compared to Fig. 6.4 obtained from a thin patient, the dose for **a** obtained in this obese patient was doubled automatically by the AEC device in order to maintain the image quality constant

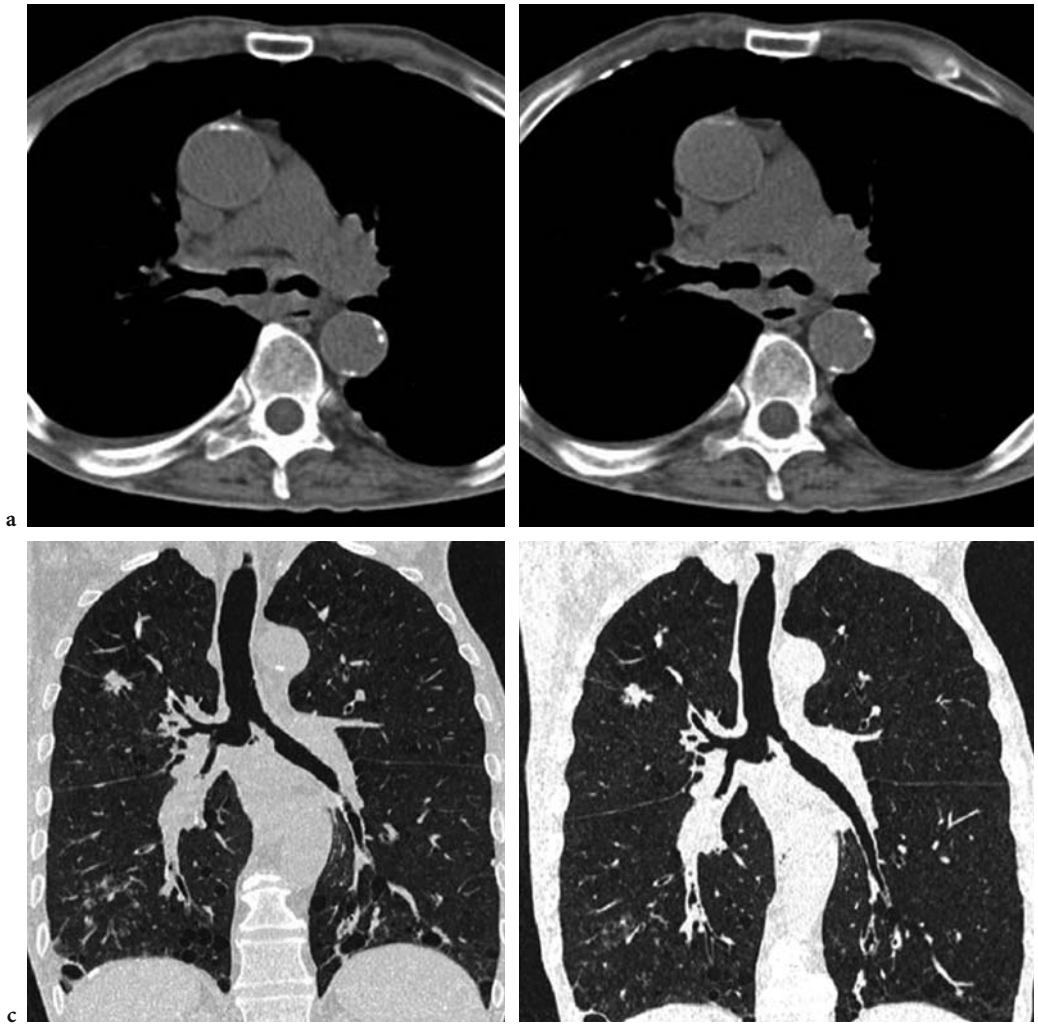

Fig. 6.6a–d. A 67-year-old man 1.83 m tall and weighing 69 kg (BMI = 20 kg/m^2) is referred for CT for cough and fever. MDCT chest acquisitions with parameters displayed at the bottom of the figure are obtained using an AEC device and a 32×0.6 mm beam collimation, at 120 kVp. A nodule is seen in the right upper lobe, centrilobular ill-defined nodules are seen in the right lower lobe and a tumor infiltrating the carina is seen in the mediastinal window. **a, c** Obtained with a reference quality mAs set at 90 mAs; **b, d** obtained with a reference quality mAs set at 60 mAs (effective). Delineation of mediastinal structures is not modified by the 33% dose reduction applied between **a** and **b**, and **c** and **d**

European reference value (EUR 1999), and to two-thirds of the mean dose reported by the UK survey (NRPB 2005). With modern scanners equipped with an AEC, the dose varies according to the patient's weight by a factor ranging from 2 to 5 as illustrated in Figures 6.9 and 6.10.

Compared to the doses reported by survey studies, these examples illustrate that one can select CT settings that enable one to perform standard acquisitions with a dose not higher than one-fifth to four-fifths of the European reference values (EUR 1999).

6.3.2.2.4 Spine

Cervical Spine

Optimizing the dose for CT of the cervical spine seems difficult to achieve as this segment of the spine is very close to the skull base and to the shoulders, two regions where dose requirements are high. As a consequence, only well-designed AEC devices are able to adapt the dose while maintaining the image quality constant.

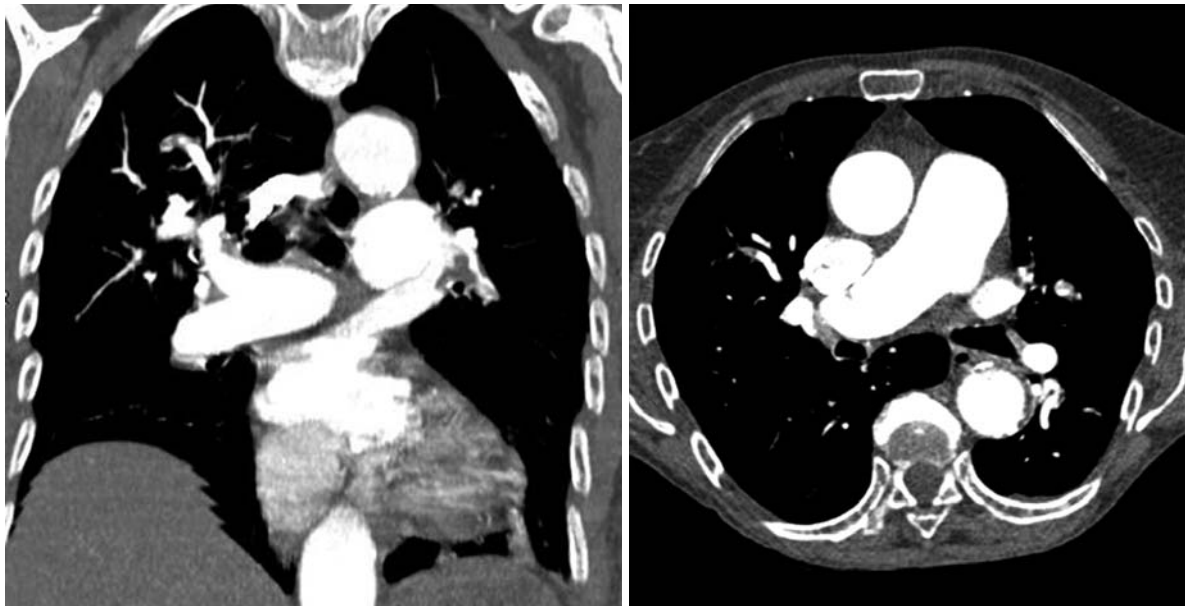

Fig. 6.7. An 84-year-old woman with dyspnea and a BMI of 21.6 kg/m^2, referred for CTPA. CTPA shows patterns of acute and chronic pulmonary embolism. Acquisition was obtained with a 16×0.6 mm beam collimation, 110 kVp and an AEC device. The reference effective mAs value reflecting the desired image quality is set at 100 mAs. The AEC device reduced this value to 44 mAs. The DLP for the entire acquisition was 99 mGy·cm, and the corresponding effective dose was 1.5 mSv, a dose no higher than that of a chest CT for screening for lung cancer

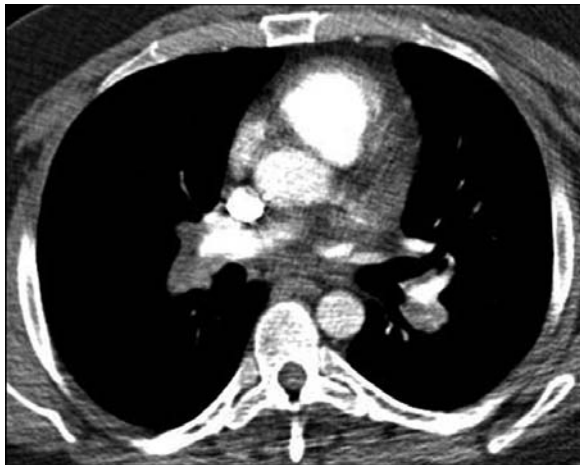

Fig. 6.8. A 58-year-old man with dyspnea and a BMI of 38.8 kg/m^2, referred for CTPA. CTPA shows patterns of acute and chronic pulmonary embolism. Acquisition was obtained with a 32×0.6 mm beam collimation, 100 kVp and an AEC device. The reference effective mAs value reflecting the desired image quality was set at 100 mAs. The AEC device has added 44 mAs to the 100 mAs, which was suggested in order to compensate for the noise generated by the patient's obesity. $CTDI_{vol}$ values were however only 6.6 mGy and a DLP of 163 mGy·cm

Lumbar Spine

As for the cervical spine, high image quality is required for distinguishing a herniated disk from nerve roots. Consequently, dose reduction obtained by decreasing the mAs setting is limited as it results in increased image noise. Similar finding have been shown for CT of the lumbar spine. As shown by Bohy et al. (2007), if the CT radiation dose is adapted to the patient's weight (i.e., using AEC), the potential to reduce the mAs setting was shown to be limited to a 35% reduction. Larger reductions in the mAs setting have a significant effect on image analysis. Thus, the most important determinants of limiting the radiation-related risks induced by scanning the lumbar spine are reducing the height of the scanned region and modulating both *U* and mAs settings according to the patient's weight, as illustrated in Figure 6.11.

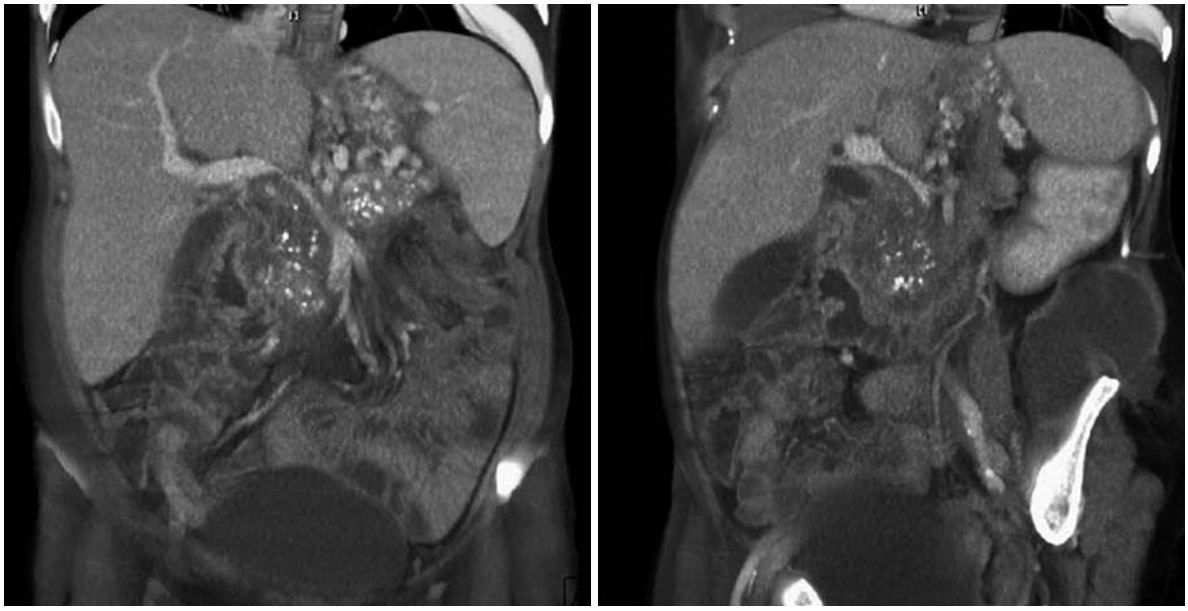

Fig. 6.9. A 44-year-old woman with known chronic pancreatitis due to alcohol abuse is referred to CT for pain and tender mass in the left flank. Her BMI is 23.6 kg/m^2. Enhanced MDCT of the abdomen with one phase was obtained during the portal vein phase. Pancreatic calcifications, portal vein stenosis, and gastric varicose are demonstrated on a coronal VRT reformation (*left image*) and an abscess is demonstrated in the left flank (*right image*). The acquisition was performed with 16×0.6 mm collimation, 110 kVp, and a reference effective mAs (representing the image quality index) of 90 mAs. This image quality index is 30% lower than that recommended by the vendor for standard MDCT. For this acquisition, AEC has automatically reduced the mean mAs setting to 53 mAs. The entire abdomen was scanned with a resulting DLP of 167 mGy·cm, which corresponds to one-seventh the reference dose for CT for EUR 1999, and less than one-half of the mean dose from the UK 2003 survey

The left image was obtained from an obese patient (BMI > 35 kg/m^2), and the right image was obtained from a patient of normal weight (BMI = 24 kg/m^2). The DLP delivered to the obese patient was three times higher than that to the patient of normal weight, but the image quality was higher in the right image than in the left.

In terms of optimizing CR dose parameters, the most significant factor is to avoid the use of a high tube potential, and 120 kVp should be sufficient in almost all patients unless they are obese.

6.3.2.3 Optimization of Low-Dose CT Scanning

The expression "low-dose CT" is not clearly defined. Reducing the dose recommended by the manufacturer could be considered as achieving a low dose, whatever the magnitude of reduction. In the literature, the concept of low dose is quite heterogeneously interpreted, and the same value can be considered as low by some authors and as standard by others. As a mater of fact, the so-called low-dose CT pro-

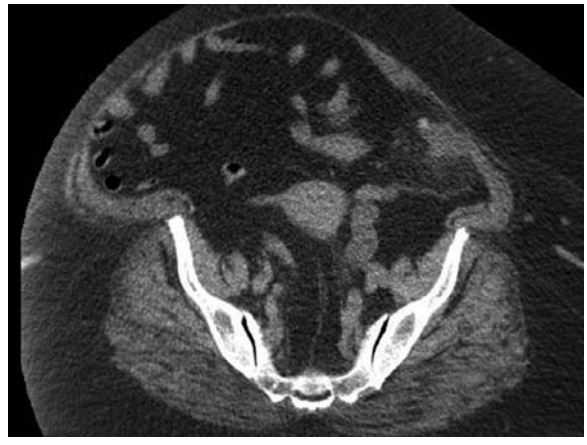

Fig. 6.10. A 64-year-old woman with left iliac fossa pain. This extremely obese patient has a BMI of 46.1 kg/m^2. Unenhanced MDCT was obtained using 130 kVp (the maximum possible for the MDCT), 16×0.6 mm collimation and a reference mAs (index of image quality) set at 110 mAs. The AEC device automatically elevated the mAs to 168 mAs. The resulting DLP for this unenhanced acquisition was 757 mGy·cm, which is nearly 5 times the dose delivered to the patient in Figure 6.8. The figure shows peritoneal fat infiltration around the descending colon in the left iliac fossa indicating acute diverticulitis

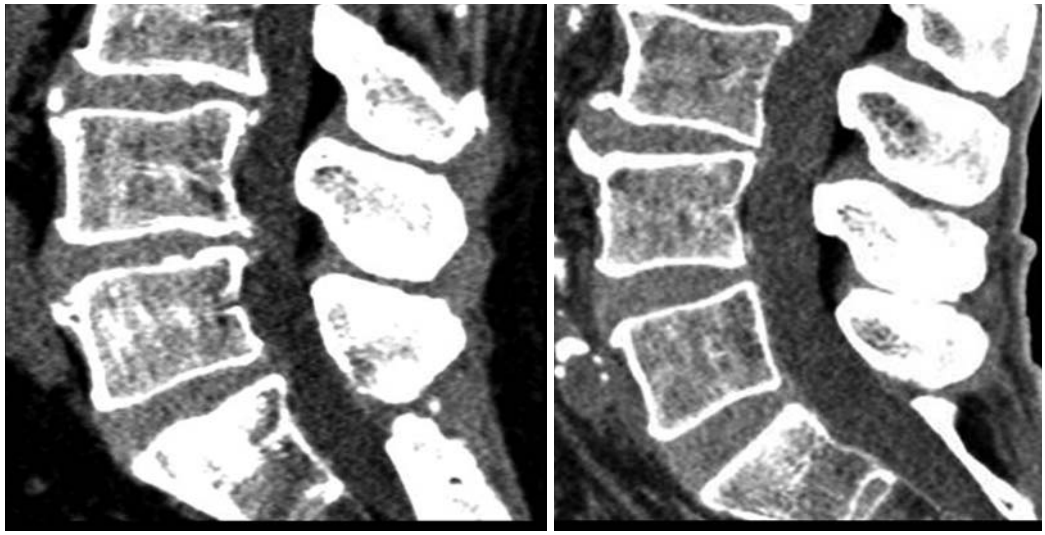

Fig. 6.11. Sagittal reconstructions in an obese patient (*right image*) with a BMI of 54.2 kg/m^2, and in a thin patient (*left image*) with a BMI of 21.5 kg/m^2 are shown. Automatic exposure-controlled acquisitions were obtained with tube voltage settings respectively of 140 and 120 kVp and with indexes of image quality expressed in effective mAs respectively of 350 and 280 mAs. The resultant $CTDI_{vol}$ values were 33.8 and 9.8 mGy. Despite a five times higher dose, the image noise seen in the obese patient's image on the *right* is greater than that obtained from the thin patient on the *left*. These dose levels are lower than the mean reference values from surveys of CT scans of the lumbar spine

tocols still deliver a high dose, since they use high kVp values.

A more appropriate use of the expression "low-dose CT" may be based on the fact that low-dose CT corresponds to a substantial dose reduction as compared to an optimized standard-dose CT, where optimized standard-dose CT corresponds to the lowest possible dose for an image quality ranging from good to excellent. Examples of optimized standard-dose CT scans are given in Figures 6.3–6.11.

With such definition, the radiation dose related to "low-dose CT" should be approximately at the level of radiographic examinations of identical body regions. As a general rule, low-dose CT should produce images of reduced photographic quality but with unchanged diagnostic quality. Low-dose CT scans have been used increasingly and were applied to early lung cancer screening programs (see Chap. 17.1), and the detection of colon polyps (see Chap. 17.2). Such low-dose CT protocols were also proposed in clinical practice for the diagnosis of chronic sinusitis (see Chap. 9), parenchymal lung diseases and CT pulmonary angiography (see Chap. 10), and most importantly for abdominal diseases as detailed in Chapter. 11.

6.3.2.3.1 The Sinonasal Cavities

As shown in Chapter 9, the radiation dose reached by low-dose MDCT is at the same level or even lower than that delivered by conventional radiographic examinations. Low-dose CT should thus be recommended in the clinical assessment of chronic sinusitis, with standard-dose CT, which delivers a dose approximately five times higher than that given by low-dose CT, only being recommended in cases of facial trauma.

6.3.2.3.2 The Thorax

As detailed in Chapter 10, low-dose CT of the lung parenchyma has been proposed since the early 1990s. However, low-dose CT is rarely applied in routine chest CT examination. The major reason for that is probably related to the low life expectancy of most patients referred for chest CT examinations, particularly in the case of thoracic or extrathoracic malignancies. Low-dose MDCT delivering less than 1 mSv per examination is thus almost always only used in screening of patients

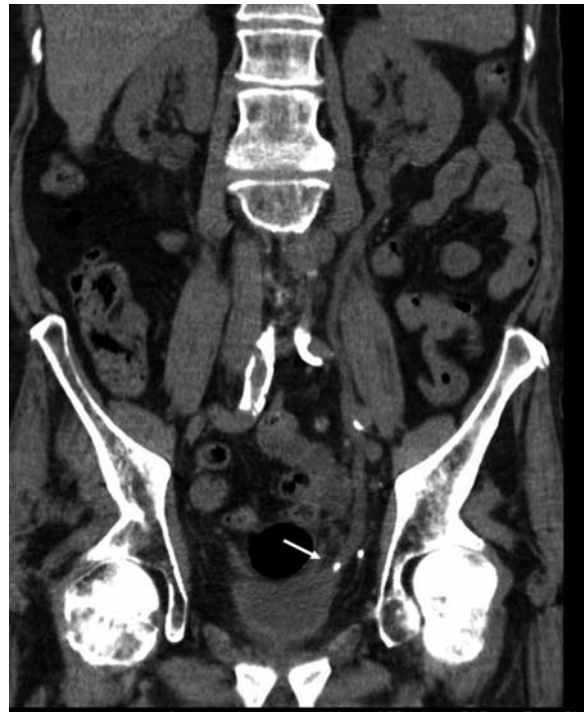

Fig. 6.12. Curved coronal reconstruction delineating the left ureter and showing a left ureteral stone in the lower pelvis. Low-dose CT acquisition with an AEC device, 110 kVp, 16×0.6 mm collimation and an image quality reference index of 50 mAs (effective). As the patient has a normal BMI of 24.6 kg/m^2, the AEC has reduced the current–time product to 33 mAs (effective). DLP of the entire examination was of 112 mGy·cm. This dose represents 20%–25% of the mean reference values from recent CT surveys

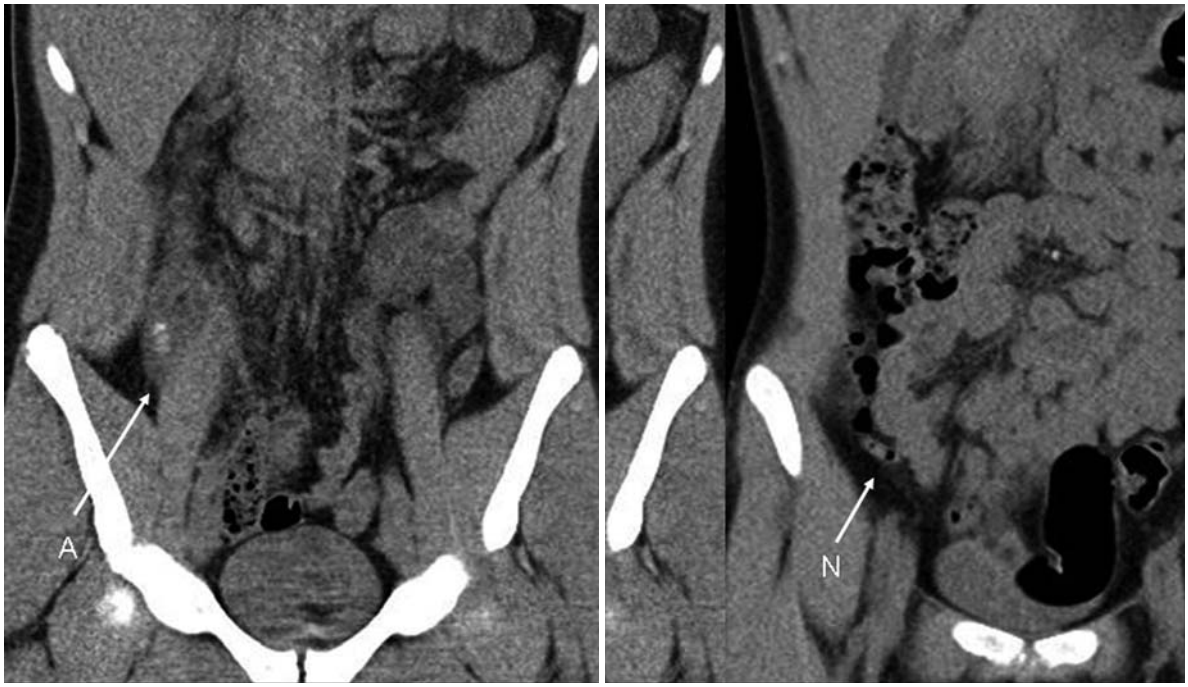

Fig. 6.13. Two patients with suspected appendicitis have undergone a low-dose MDCT of the abdomen and pelvis using an AEC device with the reference image quality effective mAs value set at 50 mAs. The patient on the *left* has a BMI of 24.4 kg/m^2, received a dose of 110 mGy·cm and has an acute appendicitis without abscess (*A* and *arrow*). The patient on the *right* has a BMI of 22.1 kg/m^2 and weighed 70 kg. He received a dose of 73 mGy·cm and had a normal appendix (*N* and *arrow*). The patient on the *left* has a BMI of 28 kg/m^2 , and weighed 85 kg. He had an acute appendicitis and received a radiation dose of 110 mGy·cm. As in Figure 6.12, the hereby delivered radiation dose represents 20%–25% of the mean reference values from recent CT surveys. This dose is equivalent to the dose of a radiographic examination of the abdomen including three views and is no higher than one-tenth of the reference values for abdomino-pelvic CT scanning

at risk of lung carcinoma, as detailed in Chapter 16.1.

6.3.2.3.3 The Abdomen

Low-dose CT has great potential in clinical investigations of the abdomen. As detailed in Chapter 11, low-dose abdominal CT should be used in young patients complaining of acute or subacute abdominal pain, with suspected benign diseases that may eventually recur, such as acute appendicitis, colon diverticulitis, renal colic, and Crohn's disease. An example of a low-dose CT protocol is shown in Figures 6.12 and 6.13 showing low-dose MDCT scans obtained while using an AEC device in patients suspected of having renal colic and acute appendicitis. This example illustrates the fact that low-dose MDCT of the abdomen can be achieved with a dose not higher than a radiographic examination of the abdomen with three views (1.9 and 1.2 mSv respectively). These doses are less than one-tenth of the references levels for abdomen-pelvis CT examinations, and one-quarter of the mean dose observed in the German survey study. For low-dose MDCT using an AEC device, the index of image quality expressed in effective mAs can be set at 50.

6.3.2.4 Optimized Radiation Doses for MDCT: In Summary

The most recent reference levels for MDCT of the chest and the abdomen are listed in Table 6.1. The optimized dose levels for imaging these two regions by low-dose MDCT as well as the corresponding validated dose levels are summarized in Table 6.2.

Table 6.1. Reference radiation doses for standard helical MDCT of the trunk (per scan series)

Body region	Dose reference	Survey 2003 Germany		Survey 2003 UK	
		CTDIvol (mGy)	DLP/series (mGy·cm)	CTDIvol (mGy)	DLP/series (mGy·cm)
Chest	Mean	13.2	398	12	400
	P75	14.7	442	14	580
Abdomen and pelvis	Mean	10	395	11	470
	P75	12.9	515	14	560

Table 6.2. Optimized radiation doses for helical MDCT of the trunk (per scan series)

Body region	Body weight	Standard-dose Multidetector CT (MDCT)		Low-dose Multidetector CT (MDCT)	
		CTDIvol (mGy)	DLP/series (mGy·cm)	CTDIvol (mGy)	DLP/series (mGy·cm)
Chest	Thin patient	4.5	135±20%	2	40–70
	Normal patient	7	210±20%	3	70–120
	Obese patient	11	330±20%	5	140–180
Abdomen and pelvis	Thin patient	4–6	150–270	3	80–120
	Normal patient	7–10	280–400	5	150–200
	Obese patient	11–15	450–600	7–10	350–400

Note: Acquisitions obtained using an automatic exposure control device

6.4 Comments

Images illustrating this chapter were selected from our daily practice because they are a reflection of optimized CT protocols based on data reported in peer-reviewed journals. The subsequent dose delivered is lower than mean or median doses reported in survey studies. The dose delivered by such acquisition protocols is indeed in the same range of magnitude as the 25th percentile reported in these survey studies. As the image quality obtained with such a reduced dose is still very high, further dose reduction should be investigated in terms of diagnostic accuracy.

Dose optimization has some limitations. The dose recommended by radiologists who can accept image noise in CT images may not be tolerated by others, despite the fact that several published reports have demonstrated that the diagnostic performance was not compromised by low-dose and even very low-dose MDCT.

Radiologists play a very important role in dose optimization. He or she indeed determines the number of acquisitions, *Z*-coverage, mAs and kVp settings, etc. As a matter of debate, should the CT protocol used in a radiology department have to satisfy radiologists and clinicians, as the use of CT cannot be restricted to one single person but has to be interpreted and managed by a multidisciplinary team? Thus, CT protocols should provide an image quality sufficient to address the patient's clinical issue through an accurate diagnosis obtained with an appropriate radiation dose.

6.5 In Summary

Reducing the collective as well as the individual radiation dose requires the following factors:

- Avoiding unnecessary examinations
- Substituting CT examinations with MRI or US examinations
- Using an optimized CT technique including
  - *Z*-coverage
  - An appropriate number of acquisitions
  - Appropriate CT settings adapted to the patient, and to the clinical context.

When scanning the chest, the abdomen or the sinonasal cavities, once the image quality has been optimized for the standard settings and results in mean dose values no higher than one-quarter to one-half of the reference values, further dose reductions can be applied for really low-dose scanning, with radiation doses no higher than those of a plain film examination. These scanning conditions have been validated in numerous indications, i.e., for the acute abdomen, follow-up of chest diseases and chronic sinusitis.

References

Boone JM, Geraghty EM, Seibert JA et al (2003) Dose reduction in pediatric CT: a rational approach. Radiology 228:352–360

Bohy P, Tack D, Rocquigny A et al (2007) Multidetector-row CT in patients with suspected lumbar disc herniation: Comparison of standard-dose and simulated low-dose techniques. Radiology 2007, (in press)

Brix G, Nagel HD, Stamm G et al (2003) Radiation exposure in multi-slice versus single-slice spiral CT: results of a nationwide survey. Eur Radiol 13:1979–1991

Chen MY, Zagoria RJ, Saunders HS et al (1999) Trends in the use of unenhanced helical CT for acute urinary colic. AJR Am J Roentgenol 173:1447–1450

EUR – European Union (1999) European guidelines on quality criteria for computed tomography. EUR 16262 EN (http://www.drs.dk/guidelines/ct/quality/htmlindex.htm) access on 31 May, 2006

Golding SJ, Shrimpton PC (2002) Radiation dose in CT: are we meeting the challenge? Br J Radiol 75:1–4

ICRP 1991 (1990) Recommendations of the International Commission on Radiological Protection. ICRP Publication 60. Annals of the ICRP 21:1–3

IEC (International Electrotechnical Commission) (2001) Medical electrical equipment – Part 2: Particular requirements for the safety of X-ray equipment for computed tomography. IEC-Standard 60601-2-44 Ed. 2.0. IEC, Geneva

Keyzer C, Tack D, de Maertelaer V et al (2004) Acute appendicitis: comparison of low-dose and standard-dose unenhanced multi-detector row CT. Radiology 232:164–172

Lim JH, Choi D, Kim SH, Lee SJ et al (2002) Detection of hepatocellular carcinoma: value of adding delayed phase imaging to dual-phase helical CT. AJR Am J Roentgenol 179:67–73

NRPB (National Radiological Protection Board) (2005) Doses from computed tomography in the UK – 2003 review. NRPB-W67. ISBN 0 85951 556 7

Perrier A, Roy PM, Aujesky D et al (2004) Diagnosing pulmonary embolism in outpatients with clinical assessment, D-dimer measurement, venous ultrasound, and helical computed tomography: a multicenter management study. Am J Med 116:291–299

Rehani MM, Bongartz G, Kalender W et al (2000) Managing X-ray dose in computed tomography: ICRP Special Task Force report. Ann ICRP 30:7–45

Royal College of Radiologists (2006) Making the best use of a department of clinical radiology guidelines for doctors, 5th edn. On line publication at http://www.rcr.ac.uk/index.asp?PageID=310&PublicationID=71 (access on 26 May, 2006)

Schaefer-Prokop C, Prokop M (2005) MDCT for the diagnosis of acute pulmonary embolism. Eur Radiol 15 [Suppl 4]: D37–D41

Shrimpton PC, Hillier MC, Lewis MA et al (2003) Data from computed tomography (CT) examinations in the UK – 2003 review. NRPB – 67, National Radiological Protection Board, Chilton

Siegel MJ, Schmidt B, Bradley D et al (2004) Radiation dose and image quality in pediatric CT: effect of technical factors and phantom size and shape. Radiology 233:515–522

Sigal-Cinqualbre AB, Hennequin R, Abada HT et al (2004) Low-kilovoltage multi-detector row chest CT in adults: feasibility and effect on image quality and iodine dose. Radiology 231:169–174

Swensen SJ, Viggiano RW, Midthun DE et al (2000) Lung nodule enhancement at CT: multicenter study. Radiology 214:73–80

Tack D, Widelec J, De Maertelaer V et al (2003a) Comparison between low-dose and standard-dose multidetector CT in patients with suspected chronic sinusitis. AJR Am J Roentgenol 181:939–944

Tack D, De Maertelaer V, Gevenois PA (2003b) Dose reduction in multidetector CT using attenuation-based online tube current modulation. AJR Am J Roentgenol 181:331–334

Tack D, Sourtzis S, Delpierre I et al (2003c) Low-dose unenhanced multidetector CT of patients with suspected renal colic. AJR Am J Roentgenol 180:305–311

Tack D, Bohy P, Perlot I et al (2005a) Suspected acute colon diverticulitis: imaging with low-dose unenhanced multidetector row CT. Radiology 237:189–196

Tack D, De Maertelaer V, Petit W et al (2005b) Multi-detector row CT pulmonary angiography: comparison of standard-dose and simulated low-dose techniques. Radiology 236:318–325

Tillie-Leblond I, Mastora I, Radenne F et al (2002) Risk of pulmonary embolism after a negative spiral CT angiogram in patients with pulmonary disease: 1-year clinical follow-up study. Radiology 223:461–467

UNSCEAR (2000) Sources and effects of ionizing radiation. United Nations Scientific Committee on the Effects of Atomic Radiation Report to the General Assembly. United Nations, New York

Weiss CR, Scatarige JC, Diette GB et al (2006) CT pulmonary angiography is the first-line imaging test for acute pulmonary embolism: a survey of US clinicians. Acad Radiol 13:434–446

Automatic Exposure Control in Multidetector-Row Computed Tomography

7

Mannudeep K. Kalra

CONTENTS

"Confusion now hath made his masterpiece!"

William Shakespeare

"Confusion is a word we have invented for an order which is not yet understood."

Henry Miller

William Shakespeare might have accidentally explained the premise for development of automatic exposure control (AEC) techniques, although Henry Miller might have summarized the issues related to the heterogeneous nomenclature of these techniques!

This chapter attempts to explore the rationale behind development of AEC for multi-detector-row CT scanners and to describe the mechanisms, clinical evidence and pitfalls of AEC techniques for radiation dose reduction or optimization.

M. K. Kalra, MD, DNB
Department of Radiology, Massachusetts General Hospital, 55 Fruit Street, Boston, MA 02114, USA

7.1 Definition

AEC techniques have been defined as automatic adjustment of tube current in the x–y plane (angular AEC), along the z-axis (z-axis AEC) or both (combined AEC), according to the size and attenuation characteristics of the body region being scanned in order to achieve constant computed tomography (CT) image quality with lower radiation dose (Kalra et al. 2004b,e). The temporal automatic tube current modulation or the electrocardiography (ECG)-controlled (pulsed) dose modulation is also a type of AEC technique used for cardiac and coronary CT angiography.

In simple terms, AEC techniques used for CT scanning behave like photo-timing used in conventional radiography (Kalra et al. 2005a,b). The photo-timing technique terminates exposure once it has been adequately achieved. In this way, photo-timing attempts to limit dose while making sure that adequate quality has been achieved, regardless of patient size and body region assessed. Thus, it allows longer exposure time for X-ray projection of a larger, thicker and denser body part or patient, and shorter exposure time for thinner, smaller and less dense portion. However, CT scanning requires continuous exposure to X-rays, so instead of terminating exposure, the AEC techniques change tube current (mA) for different X-ray projections to maintain constant image quality (generally noise). Thus, AEC will decrease tube current for projections through smaller, less dense body regions (such as anterior–posterior projection at the level of the shoulders or chest) and will increase it for projections through larger, denser regions (such as lateral projection at the shoulder or abdomen). The ultimate objective of both techniques, AEC and photo-timing, is to ensure that no more and no less exposure is given to patients in order to acquire images with constant quality (Kalra et al. 2004e).

7.2 Rationale

Until recently, most CT studies were performed using a fixed tube current technique (Kalra et al. 2004b). These fixed tube current values may be selected by technologists based on their arbitrary judgment or as per department protocols set by technologists, radiologists and/or medical physicists based on patient age and size, or study indication (Kalra et al. 2002, 2003a). However, the fixed tube current technique for multi-detector CT scanning may be associated with the following limitations:

- Lower dose efficiency: tube potential determines the photon energy, and tube current influences the photon fluence or the number of photons. The proportion of X-rays used for image creation to the amount of incident X-rays determines dose efficiency of the scanner. In contrast to the situation with a fixed tube current, AEC techniques can improve dose efficiency while maintaining constant image quality by modulating tube current to apply required amount of photons during a single X-ray rotation (for different X-ray beam projections) and from one rotation to the next (for different z-axis or section locations) (Althen 2005; Terada 2005).
- Standardization issues: fixed tube current values have to be adjusted for different generations of multi-detector-row CT scanners. Given the fact that on any given modern multi-detector-row scanner there are several ways to perform scanning, manual selection of fixed tube current may be difficult. In such circumstances, AEC techniques can automatically modulate mA to the selected combination of scanning parameters to obtain CT images of required quality. In this context, the AEC techniques are being increasingly used for dose optimization with multi-detector CT (Miyazaki et al. 2005).
- ECG controlled dose modulation or ECG pulsing: in contrast to fixed tube current, ECG pulsing can reduce tube current during ventricular systole and increase tube current during the relevant diastolic phase.

7.3 Nomenclature and Types of AEC Techniques

There is some confusion over the most appropriate nomenclature for the AEC technique (Kalra et al. 2004e). Both automatic exposure control and automatic tube current modulation have been used to describe the same technique. Although automatic tube current modulation may actually represent the technique more accurately, AEC may be the more commonly accepted term for the technique.

Similarly, several terminologies have also been used to describe different subtypes of AEC techniques (Kalra et al. 2004e). In order to avoid confusion, the most commonly used or described terminologies have been specified and used in this chapter (Table 7.1). Based on the scanning plane or direction in which AEC techniques are used for dose or tube current modula-

Table 7.1. Summary of mechanism of use of different automatic exposure control (AEC) techniques

AEC techniques	Mechanism of use
Angular AEC	Specify
Smart mA	mA
DOM	mAs/slice
CARE dose	Effective mAs
Z-axis AEC (Auto mA)	Specify noise index as well as minimum and maximum mA thresholds for tube current modulation
Z-axis AEC (ZEC)	Specify quality reference mAs value (rarely used without angular AEC also)
Z-axis AEC (Real EC)	Choose from four levels of image noise based on diagnostic requirement
Combined AEC (Auto mA 3D)	Specify noise index, minimum and maximum mA thresholds
Combined AEC (CARE Dose 4D)	Specify quality reference mAs value (modulation strength: weak, average, or strong, for small and large patients can be preset)

tion, AEC techniques may be classified as angular, z-axis, or combined techniques (Kalra et al. 2004e). The angular AEC techniques adapt tube current during each gantry rotation around the patient (Greess et al. 1999, 2001, 2002, 2004; Kopka et al. 1995). Thus, more than one tube current (mA) may be used during each gantry rotation. The angular AEC may estimate tube current during the first 180 degree gantry rotation and use this information for adapting tube current for the subsequent 180 degree rotation. This has been labeled as real-time or online angular AEC (CARE Dose, Siemens Medical Solutions, Forchheim, Germany; DOM, Philips Medical Systems, Netherlands) (Kalra et al. 2004e). The other type of angular AEC technique (Smart mA, GE Healthcare Technologies, Waukesha, Wisconsin, USA) uses a single localizer radiograph (the lateral projection) to obtain information for tube current modulation during the entire 360 degree rotation of X-ray tube around the patient.

In z-axis AEC, the tube current is adapted to maintain a constant specified image quality over the scan length. Thus, z-axis AEC techniques [Auto mA, GE Healthcare Technologies; z-exposure control (ZEC), Siemens Medical Solutions; Real EC, Toshiba Medical Solutions] change tube current from one table position to the other, based on information derived from a single lateral localizer radiograph (Kalra et al. 2005a).

Lastly, the combined AEC techniques (Auto mA 3D, GE Healthcare Technologies; CARE Dose 4D, Siemens Medical Solutions) include tube current modulation in both z-axis (z-axis AEC) and x–y plane (angular AEC) (Kalra et al. 2005b).

The different types of available AEC techniques on current multi-detector CT scanners are summarized in Table 7.2 (Kalra et al. 2005a).

7.4 AEC Mechanisms

Before moving on to the mechanism of AEC, it may be helpful to understand some basic physics nomenclature regarding CT. The three axes of CT scanner in relation to the patients are explained in Figure 7.1. Within each section position, there are

Table 7.2. Different types of automatic exposure control (AEC) techniques available on current multi-detector computed tomography (CT) scanners [Z-DOM is a combination of Automatic Current Setting (ACS) and DOM techniques]

Technique	GE	Philips	Siemens	Toshiba
Angular AEC	Smart mA	DOM	CARE Dose	–
Z-axis AEC	Auto mA	–	ZEC	Real EC
Combined AEC	Auto mA 3D	Z-DOM*	CARE Dose 4D	–

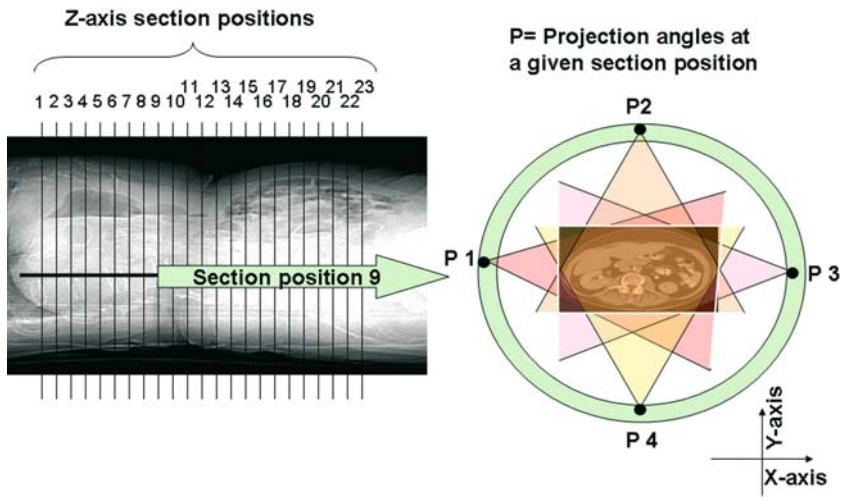

Fig. 7.1. The three axes of computed tomography (CT). The z-axis section position implies slice location or slice position. The x–y axes plane lies within each z-axis section position and represents the plane of X-ray beam projections during each gantry rotation

several hundred projection angles from which X-ray beams begin their journey from X-ray source to the detectors through the patient body. These projection angles lie in the x–y plane of the scanner. With table feed, there is change in the z-axis section position of the patient.

Image noise–mottle or graininess–an important determinant of image quality, depends on applied tube current and X-ray beam attenuation (Kalra et al. 2004b). The latter depends on patient size, shape and attenuation characteristics (profile) of the body region being scanned. An increase in the tube current results in lower noise, and a decrease in the tube current causes greater image noise. In general, an increase in attenuation profile results in greater image noise and vice-versa. Thus, in order to maintain constant image noise in the presence of changing attenuation profile, a region or projection with lower attenuation can be scanned with lower tube current than one with a high attenuation region or projection, which needs greater tube current. Although fixed tube current can be selected based on patient weight or size, use of fixed tube current does not allow adjustment of tube currents within a given study (Fig. 7.2) (Kalra et al. 2002, 2003a).

Angular AEC. The localizer radiograph-based angular AEC was the first AEC technique developed for radiation dose optimization in the early 1990s for single detector-row helical CT scanners (Kopka et al. 1995; Giacomuzzi et al. 1996; Lehmann et al. 1997). With the angular AEC technique, the tube current is modulated to decrease X-rays in projection angles (or in the x–y plane), which will have less beam attenuation and contribute less to the noise in the overall image (Kalra et al. 2004e). This is especially helpful in reducing radiation dose to the non-circular or asymmetric body regions, such as the shoulders, where "non-lateral" projections (such as anterior–posterior projections) have less X-ray beam attenuation than the lateral projection (which is typically the projection with greatest attenuation and noise contribution). Therefore, angular AEC will reduce mA and dose in the "non-lateral" projections without affecting overall image noise.

The Smart mA technique is a localizer radiograph-based, angular AEC technique, which determines the mA values from estimation of patient size, cross-sectional shape and regional attenuation information obtained from a single localizer radiograph (Fig. 7.3) (Kopka et al. 1995; Giacomuzzi et

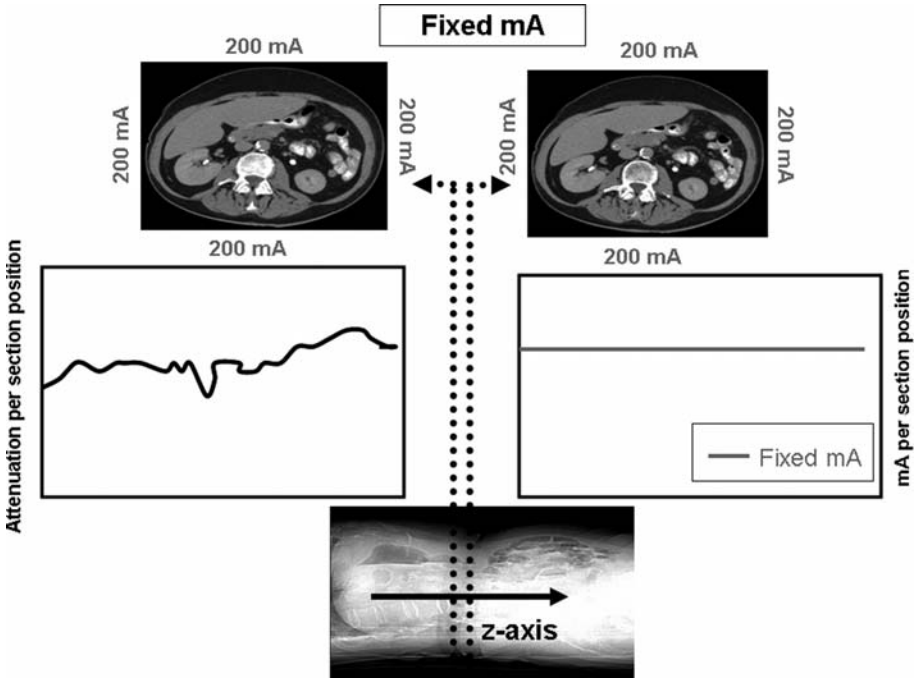

Fig. 7.2. With a fixed tube current, the scanner employs a single, specified mA value for all projections and section position for a given scan series acquisition. Although several computed tomography centers adapt this value with a fixed tube current technique based on patient size and study indication, this technique cannot take into account the variability of attenuation in a section at different beam projections and at different z-axis section positions

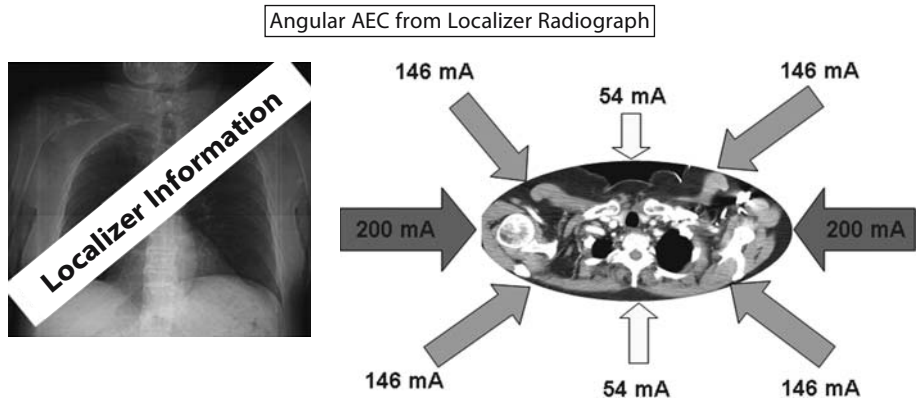

Fig. 7.3. Using a localizer radiograph-based angular automatic exposure control (AEC) technique, information about attenuation profile at different beam projections within each section position is collected from localizer radiograph. This information is used to modulate mA values at different beam projection angles during each X-ray tube revolution (the entire 360°). In an elliptical or asymmetric body cross-section, the technique will decrease mA values for beam projections in thinner portions or lower attenuation (such as in anterior–posterior or posterior–anterior projections) and increase them for those projections passing through regions with greater attenuation or thicker portion (such as lateral projections)

al. 1996; Lehmann et al. 1997). For this technique, the technologists specify a mA value and the software automatically adjusts tube current for different X-ray beam projection angles for the entire 360° tube rotation. The specified mA value provides information about the desired image noise for lateral projections and this information is then used to reduce mA for other "non-lateral" projections.

However, the CARE Dose technique is an on-line, angular AEC technique that adapts mA in real time or "on-the-fly" from projection data, which tails 180° behind the initial projection angles of X-rays and uses attenuation profile data from initial half rotation (180°) to modulate mA values in real time for the following half rotation (180°) (Fig. 7.4) (Greess et al. 1999, 2001, 2002, 2004; Kalra et al. 2004e). For this technique, the technologist selects an effective mAs value [product of tube current (mA) and gantry rotation time (s) divided by the pitch], and the scanner automatically adapts the tube current during each tube rotation while using a specified effective mAs value as a reference for desired image noise in the lateral projections of the first 180° rotation.

Regardless of its type, if used alone, all angular AEC techniques require specification of mA values and thus introduce an element of arbitrary or inappropriate selection of this initial value. For example, selection of a higher value for angular AEC will result in a higher dose than when selecting a lower value (Kalra et al. 2004e).

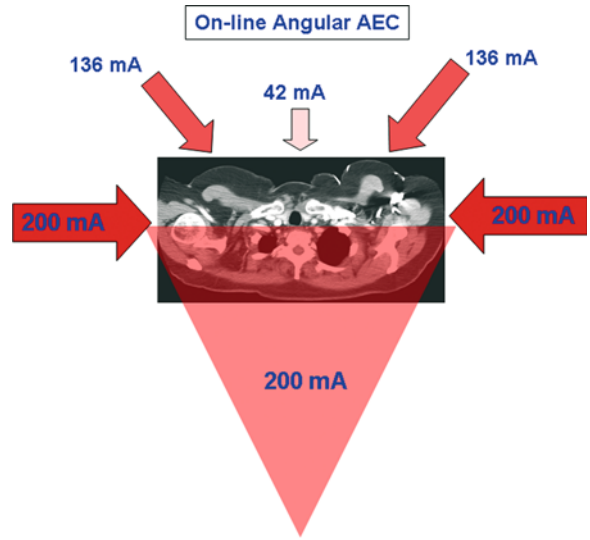

Fig. 7.4. Using an on-line, real-time angular automatic exposure control (AEC) technique, information about attenuation profile at different beam projections within each section position is collected during the first half rotation of X-ray tube around the patient. This technique assumes that the beam for subsequent half rotation is a mirror image of the first half rotation and modulates mA values for the second half according to attenuation data collected from the first half rotation. As a result, the on-line angular AEC modulates mA with a 180° lag. In an elliptical or asymmetrical body cross-section, the technique will use the same prescribed mA value (in present example 200 mA) in the first half rotation, and adapt the values for beam projections in the second half rotation based on beam attenuations

Z-axis AEC. The z-axis AEC techniques modulate mA for different z-axis section positions along the scanning direction based on the attenuation profile of the region being scanned (Fig. 7.5) (Kalra et al. 2004c,d; Campbell et al. 2005; Chapman et al. 2005; Namasivayam et al. in press). Contrary to the angular AEC, the z-axis AEC techniques adjust mA values to maintain image quality (noise index for Auto mA and quality reference mAs value for ZEC technique) specified by the user at all z-axis section positions and do not change tube current for different projections angles. Using a single localizer radiograph (generally the lateral radiograph), the software estimates mA values required to obtain images with a specified noise level (Kalra et al. 2005a).

For the Auto mA technique, the technologist selects a noise index (which approximates the image noise desired for the study) and an acceptable tube current range (minimum and maximum mA values, within which the technique will modulate the tube current) for the CT exam. Radiation dose with this technique depends on the specified noise index and patient size. A 5% decrease in noise index implies an approximate 10% increase in dose, whereas a 5% increment in noise index causes approximately 10% dose reduction (Kalra et al. 2005a). The minimum and maximum mA values also influence radiation dose associated with Auto mA by limiting the extent of decrease or increase in mA at any given noise index.

Although z-axis AEC represents a step forward from angular AEC techniques, as it requires technologists or radiologists to specify desired image quality rather than a tube current value, appropriate image quality requirements have not been completely defined. Furthermore, image quality requirements may differ for different studies and for different patients (small versus large). Thus, selection of high image quality can result in better image quality and higher dose exam that may not necessarily provide higher diagnostic yield. Conversely, lower image quality selection with z-axis AEC can cause inadvertently higher image noise

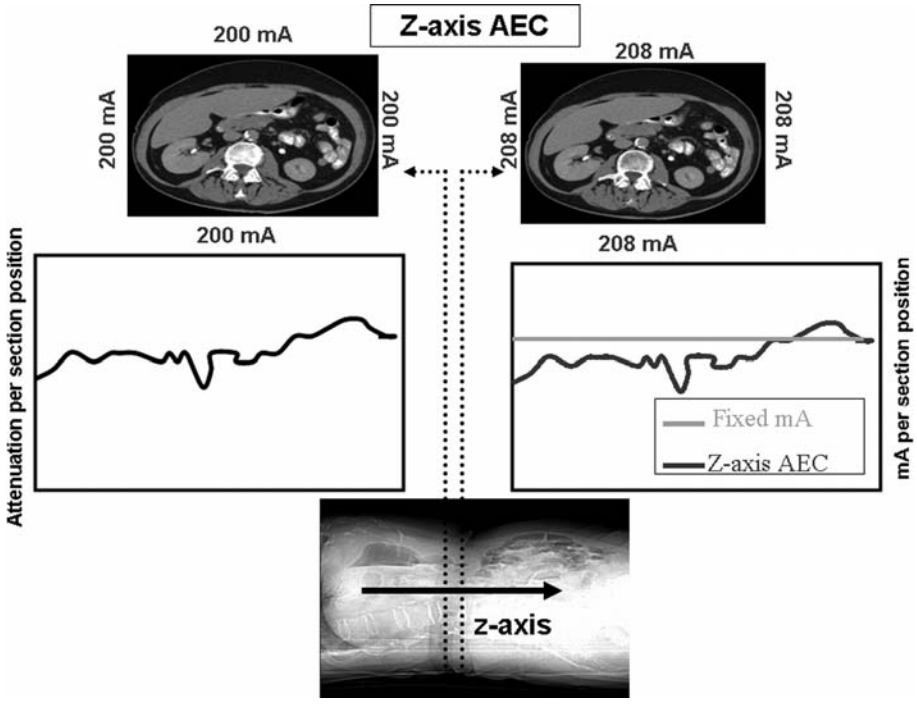

Fig. 7.5. Using a z-axis automatic exposure control (AEC) technique, attenuation for each z-axis section position is estimated from a single localizer radiograph. These data are used to estimate the mA value for each z-axis section position in order to generate images with specified image quality at all sections positions (as selected by the user in terms of quality reference mAs value or noise index). These values change from one section position to the other but not for different projection angles as in angular AEC techniques

and may compromise the diagnostic acceptability of the CT exam.

Combined AEC. These techniques modulate tube current for each z-axis section position (z-axis AEC component) and for different projection angles in each X-ray tube rotation (angular AEC component) (Fig. 7.6) (Kalra et al. 2005b; Rizzo et al. in press). The angular AEC component of the technique may be based on attenuation profile information obtained from the localizer radiograph or from online estimation of attenuation at different projection angles.

The Auto mA 3D technique uses a single localizer radiograph to derive information for modulating mA at each slice position (Auto mA) and for different projection angles (Smart mA). As required for the Auto mA technique, for this technique also, the user prescribes a noise index value with or without minimum and maximum mA limits (Kalra et al. 2004e).

CARE Dose 4D combines the on-line angular AEC (CARE Dose 4D) with the z-axis AEC technique (ZEC) (Rizzo et al. in press). This technique estimates size, shape and attenuation profile over the scan length (z-axis) in the direction of projection as well as in the perpendicular direction (in the x–y plane) using a mathematical algorithm. Axial mA values are determined by estimation of these attenuation profiles and are adapted, based on the patient size and attenuation profile. This adaptation is based on the user-specified quality reference mAs value for the z-axis AEC. Subsequently, these mA levels are used for on-line angular AEC according to the attenuation profile at different projection angles. The quality reference mAs values indicate the effective average for a "reference patient." The reference patient is defined as a "typical adult" weighing 70–80 kg (for adult CT studies) or as a "typical child" weighing 20 kg (for pediatric CT studies) (Rizzo et al. in press).

The diagnostic requirements of studies and radiologists' preferences determine the quality reference mAs value. Although the quality reference mAs value is not changed for patients of different size, for adjusting image quality or dose, the users can

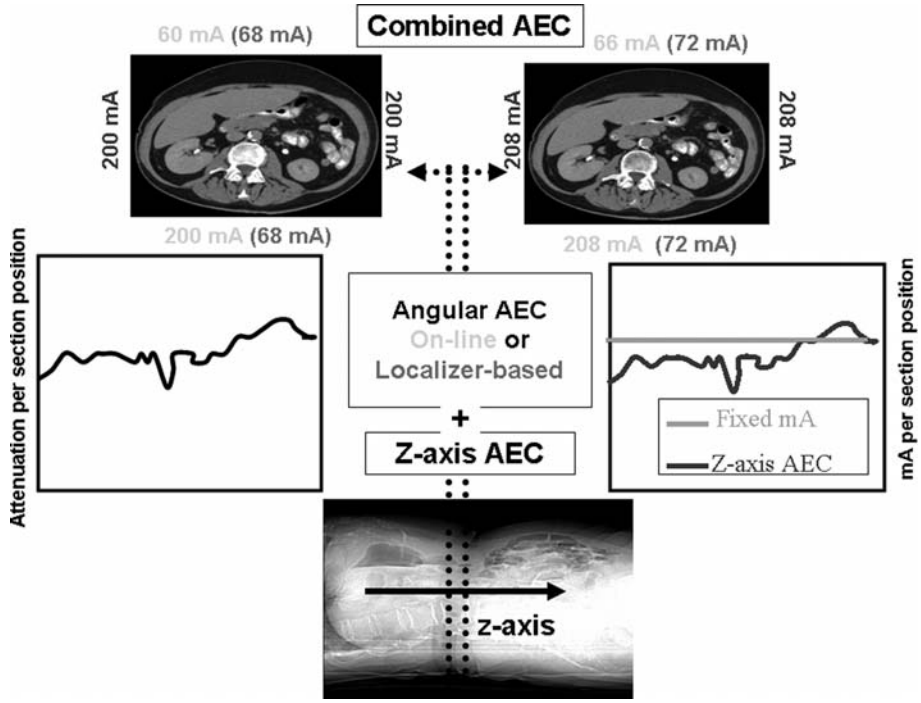

Fig. 7.6. The combined automatic exposure control (AEC) techniques initially use z-axis AEC to estimate mA values for each section position from a localizer radiograph. Subsequently, these values for angular AEC are also estimated based on mA values estimated from z-axis AEC and localizer radiograph (Auto mA 3D), or from z-axis AEC and on-line estimation of attenuation (CARE Dose 4D)

change the quality reference mAs value or strength of AEC. The technique classifies the patient as "slim" or "obese" from a single localizer radiograph and adapts the mA according to the user-specified modulation strength for "slim" or "obese." With CARE Dose 4D, effective mAs value is decreased for "slim" patients and increased for "obese" patients and the extent of mA modulation can be controlled using appropriate modulation strengths (weak, average or strong).

ECG dose modulation. For coronary CT angiography studies, most image data are reconstructed during ventricular diastole so that the influence of cardiac motion during systole can be reduced. The ECG pulsing decreases the tube current substantially during ventricular systole and increases it to the specified level during the diastolic phase, which is used for image reconstruction. This helps to reduce the overall dose to the patients. Thus, there will be no compromise in image quality in the diastolic phase reconstructed image data; whereas, during systole there will be more noise. With ECG pulsing, slower and regular heart rates allow greater and more precise dose modulation and reduction during ventricular systole, whereas faster and/or irregular heart rates will be associated with greater radiation dose to the patient.

7.5 Clinical Evidence for AEC Techniques

In the past 10 years, several clinical studies have shown a benefit of AEC techniques in managing radiation dose for single-detector row helical CT as well as multi-detector-row CT scanners (Kopka et al. 1995; Giacomuzzi et al. 1996; Lehmann et al. 1997; Greess et al. 1999, 2004; Tack et al. 2003; Kalra et al. 2004c,d; Mastora et al. 2004; Campbell et al. 2005; Chapman et al. 2005; Mulkens et al. 2005; Namasivayam et al. in press; Rizzo et al. in press). Compared with the fixed tube current technique, these techniques have been shown to reduce radiation dose for most patients without compromising diagnostic acceptability of CT studies and increase radiation dose in some large patients in order to maintain image quality at specified levels (Greess et al. 1999, 2001, 2002, 2004; Tack et al. 2003; Kalra et al. 2004c,d; Mastora et al. 2004; Campbell et al. 2005; Chapman et al. 2005; Mulkens et al. 2005; Namasivayam et al. in press; Rizzo et al. in press). The results of some clinical studies using AEC techniques are summarized in Table 7.3.

Several studies have shown benefits of ECG pulsing for cardiac CT studies (Poll et al. 2002). Phantom studies have shown that up to 37–44% dose reduction can be achieved using ECG pulsing, depending on the heart rate. A patient study indicated that, when compared with non-modulated coronary multidetector CT angiography, an average radiation dose reduction of 48% for males and of 45% for females can be achieved using ECG-controlled tube current modulation (Jakobs et al. 2002).

7.6 Trouble-shooting for AEC Techniques

- For all localizer radiograph-based AEC techniques (Smart mA, Auto mA, Auto mA 3D, Real EC, ZEC, CARE Dose 4D), the localizer radiograph must include the entire region being scanned with AEC. Beyond the localizer radiograph, these techniques will not adapt tube current appropriately.
- As some AEC techniques rely on localizer radiographs, it is important to avoid patient movement after acquisition of the first localizer radiograph (generally a single lateral localizer is used for most AEC techniques).
- AEC techniques will adapt tube current, taking into account all other relevant scanning parameters such as section profile, beam pitch, detector configuration, gantry rotation time and tube potential.
- Appropriate centering of patient in gantry isocenter, particularly in reference to table height, is extremely important in multi-detector CT scanners, as surface dose to the patient and image noise can increase with off-centering (Thomas L. Toth, GE Healthcare Technologies, personal communication).
- If arms are positioned by the side of the patient undergoing body CT, AEC techniques can increase the dose by as much as 30–35% (as they will compensate for increase in attenuation from arms) (Kalra et al. 2003). Thus, where possible, localizer radiographs must be acquired with appropriate positioning of the arms.

Table 7.3. Summary of reports on automatic exposure control techniques

Study	Technique	Region	Dose reduction
Greess et al. (1999)	CARE Dose	Shoulders	38%
Greess et al. (2001)	CARE Dose	Chest (pulmonary nodules)	21%
Greess et al. (2002)	CARE Dose	Neck	20%
		Chest	23%
		Abdomen	23%
Tack et al. (2003)	CARE Dose	Chest	17%
		Abdomen	20%
Mastora et al. (2004)	CARE Dose	Thoracic outlet	35%
Kalra et al. (2004c)	Auto mA	Abdomen	10–41%
Kalra et al. (2005b)	Auto mA	Chest	18–26%
Kalra et al. (2005a)	Auto mA	Abdomen (renal stones)	43–66%
Mulkens et al. (2005)	CARE Dose 4D	Chest	20%
		Abdomen-pelvis	32%
		Lumbar spine	37%
		Cervical spine	68%
Namasivayam et al. (*)	Auto mA	Neck	36%
Rizzo et al. (*)	CARE Dose 4D	Abdomen	41–43%

- Some AEC techniques ignore metallic implants when estimating attenuation profile and tube current (such as CARE Dose 4D) (Dalal et al. 2005), while others increase tube current in the region of metallic prosthesis as they cannot exclude the contribution of high attenuation from metallic prostheses (Rizzo et al. 2005). In the latter, a lower desired image quality should be set or the fixed tube current technique be used.
- Pediatric and adult settings for desired image quality usually differ and must be set as such (Kalra et al. 2004a,c).
- For a large patient, an increase in tube current with AEC techniques may be insufficient to obtain the desired or specified image quality (Kalra et al. 2004a,c). In such instances, the user must be attentive to other scanning parameters such as table feed, gantry rotation time and kVp.
- For low dose examinations, such as CT colonography and kidney stone CT, a lower "desired image quality" requirement for AEC techniques than with routine indications should be selected.
- CT dose index volume–CTDI vol displayed on the user interface of the scanner is the average CTDI vol over the scan length. This is crucial to understand as CTDI vol changes over the scan length and can be higher or lower at different section positions in the scan range. Thus, estimation of local or organ-based effective doses using these average values may not be accurate.
- Some AEC techniques may not be applicable or appropriate in all body regions, such as in head or extremities; therefore, user must inquire about applicability and accuracy of AEC techniques from their vendors.
- With ECG pulsing, image data during systolic phase will be noisy and may impair the cardiac cine or functional assessment as well as visualization of incidental extra-cardiac thoracic findings. In some cases, reconstructing these image data sets at thicker sections and/or smoother reconstruction kernel settings may help.

7.7 Pitfalls

Despite commendable advances and efforts of the vendors to optimize radiation dose associated with CT scanning, there are some issues associated with use of AEC techniques in routine clinical practice. Most importantly, there are substantial differences

between nomenclature and dose modulation with AEC techniques from different vendors. This implies that the scanning method used with one AEC technique cannot be used on a similar technique using a scanner from a different vendor. Furthermore, presently, most vendors recommend use of an "empirical" desired image quality for scanning. It is important to understand that AEC techniques will work only as efficiently as the specified or desired image quality. If a higher image quality is specified (for example, higher quality reference mAs value for CARE Dose 4D or lower noise index for Auto mA), then the system will use a higher dose. Likewise, different desired image quality thresholds must be specified for different clinical indications; for example, a lower quality reference mAs value must be used for a kidney stone protocol than for routine abdominal CT protocols. Selection of inadvertently low image quality can lead to excessive dose reduction using AEC techniques and compromise diagnostic acceptability of the study. To facilitate appropriate use of AEC techniques, there is a need to define threshold levels of "desired image quality" for different clinical indications and patient ages.

Although AEC techniques can automatically increase tube current and dose to large patients, it is important to realize that, in a large patient, an increase in applied peak kilovoltage, gantry rotation time or scan field of view, or a decrease in beam pitch may also be necessary to obtain desired diagnostic information.

As with any new technique, there is a learning curve that radiologists and technologists must overcome in order to use these AEC techniques appropriately.

7.8 Summary

- Most modern multi-detector-row CT scanners allow use of AEC techniques
- AEC techniques can aid in optimizing radiation dose for different patient sizes and clinical indications
- Constant image quality at lower radiation dose can be achieved using AEC techniques in most patients
- For different clinical indications, users must modify the scanning parameters for AEC in order to attain desired dose reduction or image quality

References

Althen JN (2005) Automatic tube-current modulation in CT–a comparison between different solutions. Radiat Prot Dosimetry 114:308–312

Campbell J, Kalra MK, Rizzo SMR, Maher MM, Shepard J (2005) Scanning beyond anatomic limits of thorax in chest CT: findings, radiation dose and automatic tube current modulation. AJR Am J Roentgenol 185:1525–1530

Chapman VM, Kalra MK, Grottkau BE, Albright M, Jaramillo D (2005) 16-Slice multidetector CT of the post-traumatic pediatric elbow: optimum parameters and associated radiation dose. AJR Am J Roentgenol 185:516–521

Dalal T, Kalra MK, Rizzo SM, Schmidt B, Suess C, Flohr T et al (2005) Metallic prosthesis: technique to avoid increase in CT radiation dose with automatic tube current modulation in a phantom and patients. Radiology 236:671–675

Giacomuzzi SM, Erckert B, Schopf T, Freund MC, Springer P, Dessl A et al (1996) The smart-scan procedure of spiral computed tomography: a new method for dose reduction. Rofo Fortschr Geb Rontgenstr Neuen Bildgeb Verfahr 165:10–16

Greess H, Baum U, Wolf H, Lell M, Nomayr A, Schmidt B et al (2001) Dose reduction in spiral-CT: detection of pulmonary coin lesions with and without anatomically adjusted modulation of tube current. Rofo 173:466–470

Greess H, Lutze J, Nomayr A, Wolf H, Hothorn T, Kalender WA et al (2004) Dose reduction in subsecond multislice spiral CT examination of children by online tube current modulation. Eur Radiol 14:995–999

Greess H, Nomayr A, Wolf H, Baum U, Lell M, Bowing B et al (2002) Dose reduction in CT examination of children by an attenuation-based on-line modulation of tube current (CARE Dose). Eur Radiol 12:1571–1576

Greess H, Wolf H, Baum U, Kalender WA, Bautz W (1999) Dosage reduction in computed tomography by anatomy-oriented attenuation-based tube-current modulation: the first clinical results. Rofo 170:246–250

Jakobs TF, Becker CR, Ohnesorge B, Flohr T, Suess C, Schoepf UJ et al (2002) Multislice helical CT of the heart with retrospective ECG gating: reduction of radiation exposure by ECG-controlled tube current modulation. Eur Radiol 12:1081–1086

Kalra MK, Prasad S, Saini S, Blake MA, Varghese J, Halpern EF et al (2002) Clinical comparison of standard-dose and 50% reduced-dose abdominal CT: effect on image quality. AJR Am J Roentgenol 179:1101–1106

Kalra MK, Maher MM, Prasad SR, Hayat MS, Blake MA, Varghese J et al (2003a) Correlation of patient weight and cross-sectional dimensions with subjective image quality at standard dose abdominal CT. Korean J Radiol 4:234–238

Kalra MK, Maher MM, Saini S (2003b) What is the optimum position of arms for acquiring scout images for whole-body CT with automatic tube current modulation? AJR Am J Roentgenol 181:596–597

Kalra MK, Maher MM, Kamath RS, Horiuchi T, Toth TL, Halpern EF et al (2004a) Sixteen-detector row CT of abdomen and pelvis: study for optimization of Z-axis modulation technique performed in 153 patients. Radiology 233:241–249

Kalra MK, Maher MM, Toth TL, Hamberg LM, Blake MA,

Shepard JA et al (2004b) Strategies for CT radiation dose optimization. Radiology 230:619–628

Kalra MK, Maher MM, Toth TL, Kamath RS, Halpern EF, Saini S (2004c) Comparison of Z-axis automatic tube current modulation technique with fixed tube current CT scanning of abdomen and pelvis. Radiology. 232:347–353

Kalra MK, Maher MM, Toth TL, Kamath RS, Halpern EF, Saini S (2004d) Radiation from "extra" images acquired with abdominal and/or pelvic CT: effect of automatic tube current modulation. Radiology 232:409–414

Kalra MK, Maher MM, Toth TL, Schmidt B, Westerman BL, Morgan HT et al (2004e) Techniques and applications of automatic tube current modulation for CT. Radiology 233:649–657

Kalra MK, Naz N, Rizzo SM, Blake MA (2005a) Computed tomography radiation dose optimization: scanning protocols and clinical applications of automatic exposure control. Curr Probl Diagn Radiol 34:171–181

Kalra MK, Rizzo SM, Novelline RA (2005b) Reducing radiation dose in emergency computed tomography with automatic exposure control techniques. Emerg Radiol 11:267–274

Kopka L, Funke M, Breiter N, Hermann KP, Vosshenrich R, Grabbe E (1995) An anatomically adapted variation of the tube current in CT: studies on radiation dosage reduction and image quality. Rofo Fortschr Geb Rontgenstr Neuen Bildgeb Verfahr 163:383–387

Lehmann KJ, Wild J, Georgi M (1997) Clinical use of software-controlled X-ray tube modulation with "SmartScan" in spiral CT. Aktuelle Radiol 7:156–158

Mastora I, Remy-Jardin M, Delannoy V, Duhamel A, Scherf C, Suess C et al (2004) Multi-detector row spiral CT angiography of the thoracic outlet: dose reduction with anatomically adapted online tube current modulation and preset dose savings. Radiology 230:116–124

Miyazaki O, Kitamura M, Masaki H, Nosaka S, Miyasaka M, Kashima K (2005) Current practice of pediatric MDCT in Japan: survey results of demographics and age-based dose reduction. Nippon Igaku Hoshasen Gakkai Zasshi 65:216–223

Mulkens TH, Bellinck P, Baeyaert M, Ghysen D, Van Dijck X, Mussen E et al (2005) Use of an automatic exposure control mechanism for dose optimization in multi-detector row CT examinations: clinical evaluation. Radiology 237:213–223

Namasivayam S, Kalra MK, Pottala K, Waldrop S, Hudgins PA (2006) Optimization of z-axis automatic exposure control for multidetector row CT evaluation of neck and comparison with fixed tube current technique for image quality and radiation dose. AJNR Am J Neuroradiol 27:2221–2225

Poll LW, Cohnen M, Brachten S, Ewen K, Modder U (2002) Dose reduction in multi-slice CT of the heart by use of ECG-controlled tube current modulation ("ECG pulsing"): phantom measurements. Rofo 174:1500–1505

Rizzo S, Kalra MK, Schmidt B, Suess C, Flohr TG, Blake MA et al (2006) Comparison of angular and combined automatic tube current modulation techniques with constant tube current CT scanning of the abdomen and pelvis. AJR Am J Roentgenol 186:673:679

Rizzo SM, Kalra MK, Maher MM, Blake MA, Toth TL, Saini S (2005) Do metallic endoprostheses increase radiation dose associated with automatic tube-current modulation in abdominal-pelvic MDCT? A phantom and patient study. AJR Am J Roentgenol 184:491–496

Tack D, De Maertelaer V, Gevenois PA (2003) Dose reduction in multidetector CT using attenuation-based online tube current modulation. AJR Am J Roentgenol 181:331–334

Terada M (2005) Optimization of image quality by CT scanner automatic exposure control systems. Nippon Hoshasen Gijutsu Gakkai Zasshi 61:1384–1386

Patient Centering in MDCT: Dose Effects

8

Mannudeep K. Kalra and Thomas L. Toth

CONTENTS

I have expressed some ideas that point to the center; I have saluted the dawn in my way, from my point of view. He who knows the way should do the same, in his way, and from his point of view.

Friedrich Von Schlegel

Although the contribution of CT scanning to radiation dose was recognized prior to the introduction of multidetector-row CT scanners, ever expanding applications of multidetector-row CT scanning in patient care and, of late, use of CT for screening have heightened concerns and awareness of radiation-induced cancer from CT radiation dose and prompted the development of strategies and techniques for dose reduction (Frush 2003; Kalra et al. 2004a; Tack and Gevenois 2004). Technological innovations for dose reduction and optimization include pre-patient beam collimation and beam-shaping filters as well as automatic exposure control techniques (Kalra et al. 2004b). To obtain appropriate benefits of these techniques in terms of dose reduction without compromising image quality, it is important to appropriately center the patients in the scanner gantry isocenter (Kalra et al. 2004b).

In this chapter, we will discuss the effects of and reasons for off-centering patients in the gantry isocenter, factors contributing to patient off-centering, rationale for precise patient centering, and strategies that can be adopted to obtain adequate patient centering prior to their CT examinations.

8.1 Patient Positioning and Centering

For the sake of simplicity, we have arbitrarily classified the process of patient placement on the gantry table into positioning and centering. Positioning alludes to proper placement of the patient on the gantry table in the z-axis or along the length of patient for scanning a particular portion or region of the body. Improper positioning of the patient may necessitate the acquisition of a localizer radiograph beyond the region of interest and perhaps acquisition of a repeat localizer radiograph (Namasivayam et al. 2006). A recent study analyzing localizer radiographs for abdominal CT examinations performed in a single institution have reported that localizer radiographs extended 13 cm (on average) beyond the defined region of interest (Namasivayam et al. 2006). With regards to patient positioning it is important to pay special attention to the position of the patient's arms, particularly when automatic exposure control techniques are being used for scanning. Automatic exposure control techniques employ tube current based on beam attenuation data obtained from the localizer radiographs and/or "on the fly" during initial tube rotation around the patient. Therefore, for body CT, if the arms are positioned by the patient's side, estimation of tube current

M. K. Kalra, MD, DNB
Department of Radiology, Massachusetts General Hospital, 55 Fruit Street, Boston, MA 02114, USA
T. L. Toth, MD
General Electric Healthcare Technologies, 3000 North Grandview Boulevard, Waukesha, WI 53188, USA

with automatic exposure control techniques will be erroneous and can lead to a substantial increment in radiation dose (Kalra et al. 2003).

On the other hand, centering alludes to appropriate placement of the patient with respect to the scanner gantry, so that the patient's center corresponds to the scanner gantry isocenter in the x-y plane or the transverse cross-section of the patient. A recent study evaluating scanning practice in a single tertiary health care center has reported that 95% of patients undergoing chest and abdominal CT examinations were off-centered relative to the superior–inferior direction in the gantry (Namasivayam et al. 2006).

8.2 Effects of Off-Centering

Image noise, mottle or graininess, a principle determinant of image quality, affects the low-contrast resolution of CT. A higher image noise may compromise low-contrast resolution and impair diagnostic confidence. Conversely, a lower image noise may improve low-contrast resolution at the cost of higher radiation dose.

As the X-ray tube revolves around the patient, X-ray beams traverse through the body region being scanned from several projections. Each image pixel generated from CT scanning is contributed by the attenuation of several X-ray projections. Image noise in an image pixel is derived from the noise of all X-ray projections responsible for the generation of that pixel. In general, less X-ray beam attenuation implies less image noise and vice versa. The beam attenuation is also directly related to the length of the path along which beams traverse through the portions of the body region being scanned. Therefore, a shorter beam path at the periphery will be associated with less image noise, compared to a longer beam path centrally. Bow-tie filters take advantage of the geometry of the patient's cross-section by reducing X-rays in projections with a short beam paths and improving the radiation dose efficiency of the scanner (Fig. 8.1) (Toth et al. 2005). In other words, these filters shape the X-ray beam to the body, restricting X-rays for the peripheral, less attenuating, portions, and allowing most X-rays for the central portions with greater attenuation and contribution to image noise.

Bow-tie filters presume that the center of the body region being scanned coincides or approximates with the gantry isocenter. However, with off-centering relative to the gantry isocenter, the bow-tie filters miss their target. As a result portions of the body region being scanned other than the peripheral portion receive fewer X-rays and contribute to higher image noise (compromising image quality). Conversely, peripheral portions receive more X-rays, resulting in higher peripheral and central radiation doses. These noise and dose effects assume importance in view of the availability and use of automatic exposure control techniques on most modern multidetector row CT scanners. When using a fixed tube current for scanning, there was a tendency to use a higher tube current for small patients and a relatively lower tube current for larger patients. With precise dose adaptation using automatic exposure control techniques, a substantial dose reduction was reported for small patients and a dose increment was documented for larger patients (Kalra et al. 2004c). Use of lower doses for smaller patients with automatic exposure control techniques implies

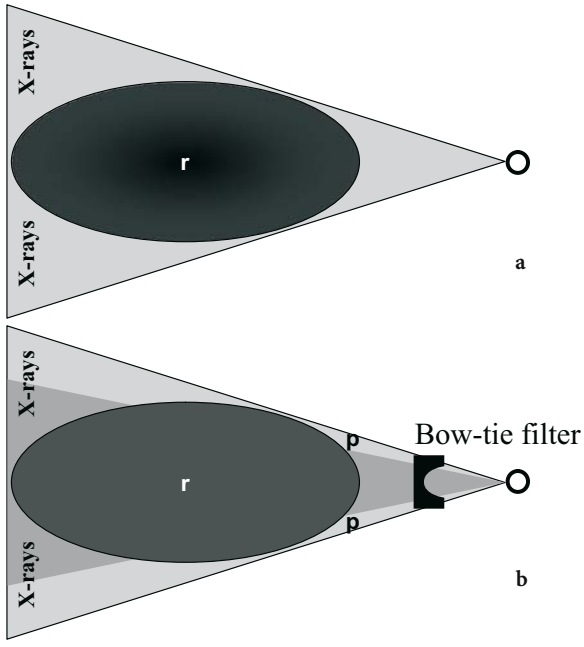

Fig. 8.1. a Without bow-tie filter, the homogeneous X-ray beam will lead to images with lower noise in the periphery and at the surface portions in the region being scanned (*r*). **b** With a bow-tie filter, the X-rays are reduced in the periphery (*p*) so that the peripheral and surface doses in the region being scanned increase and noise in these regions becomes similar to that in the central portions

that the off-centering of these patients can lead to a disproportionate increase in image noise as well as the surface and peripheral radiation doses. Unfortunately, compared to large patients, there is "more room" to off-center a small patient in the scanner gantry.

Prior phantom studies investigating causes of suboptimal image quality in smaller patients undergoing abdominal-pelvic CT with the automatic exposure control technique have shown that off-centering in the superior–inferior direction (*y*-axis of the gantry or table height related) with respect to the gantry isocenter increases image noise (Kalra et al. 2004d). Up to a 30% increase in image noise was noted when the phantom was scanned at a position that was 6 cm below the gantry isocenter. Therefore, in this chapter, all references to centering and off-centering are related to patient placement in the superior–inferior direction of the gantry isocenter.

Subsequent studies have documented that up to a 50% increase in surface and peripheral radiation dose can occur with 6-cm off-centering of a phantom (Li et al. 2006). Patient studies show about a 2%–30% increase in surface and peripheral radiation doses from chest and abdominal CT examinations performed with off-centering of patients relative to the gantry isocenter (Li et al. 2006). This increase in the surface radiation dose with off-centering can result in an increased radiation dose to radiosensitive body parts such as the breasts, thyroid, eyes, and gonads.

8.3 Reasons for Off-Centering

Although no formal study has evaluated the reasons for off-centering patients in the gantry isocenter, these may not be difficult to understand. Possible causes of off-centering patients undergoing CT scanning include:

- Awareness. Technologists and radiologists may not be aware of the importance of centering the patients appropriately in the gantry isocenter.
- Attention to details of centering. Inadequate attention to centering may be related to the training of the technologists and radiologists, suboptimal use of laser-assisted centering or the increasing workload of multidetector row CT scanners with expanding applications. This practice may be accentuated by the acquisition of two orthogonal localizer radiographs for planning and the ability to shift the display field of view (DFOV).
- Adjustment of DFOV. Modern scanners allow the technologists to shift the DFOV in all three planes (longitudinally or in the z-axis along scan length, and transversely or in the x–y axis for the section plane) on the localizer radiographs. Although this ability helps when displaying selected regions that are situated away from the gantry isocenter (for example, coronary CT angiography), it may also be responsible for the lack of attention to centering, as the DFOV can be shifted to accommodate off-centering without increasing the size of the DFOV.
- Patient-related factor. Patients seldom have a perfectly cylindrical shape. Thus, multi-region (such as neck, chest and abdomen) scanning in the same imaging session may make decisions related to patient centering difficult. Likewise, patients without a circular cross-section are also difficult to center, as are patients who cannot lie flat, those who cannot elevate their arms sufficiently above their heads (such patients are more likely to be centered below the gantry isocenter), and those who have spinal curvature abnormalities, or need to elevate their head or chest relative to caudal portions of their body. Similarly, patients on life support systems or those referred for emergent clinical indications may also be difficult to center optimally.
- Lack of automatic patient centering techniques. Such techniques may guide the users to center the patients correctly and inform them about off-centering and the possible dose and noise penalties associated with scanning patients who are not adequately centered in the gantry.

8.4 Strategies for Ensuring Appropriate Patient Centering

In view of the importance of optimal patient centering in the gantry isocenter prior to their CT scanning, it is important to devise strategies to minimize patient off-centering. These may include:

- Education. Education of technologists, radiologists, and medical physicists about the importance of patient centering and the implications of off-

centering will facilitate attention to the details of patient centering.

- Guidelines. Some guidelines can be given to the technologists for patient centering in the gantry isocenter. These may include the importance of adjusting patient centering in the gantry rather than adjustment of DFOV. Users must be instructed to pay particular attention to the centering of children and small adults, especially when automatic exposure control techniques are being used for CT scanning or a low-dose CT is being performed. For patients who cannot rest their arms above their heads, body CT can be performed in "feet first" alignment so as to avoid inferior off-centering in these patients.
- Automatic patient-centering software. This technique has not been commercially released at the time of writing this chapter. Initial assessment of this software (GE Healthcare Technologies, Waukesha, Wis.) has shown that this technique can help the users to center the patients with respect to the gantry (Li et al. 2006). For body CT, this software estimates the patient center from the mean projection area data obtained from the entire lateral localizer radiograph. It recommends a correction factor (in mm) for the patient table position which can be used to adjust table height in order to achieve appropriate patient centering. In addition, the technique also describes the surface and peripheral doses that can be saved with appropriate centering based on the recommended correction factor.

In summary, perhaps the quotation from Friedrich Von Schlegel, a German philosopher, at the beginning of this chapter aptly emphasizes the importance of recognizing the necessity of centering the patients for CT scanning, in light of findings that indicate increased surface and peripheral doses to patients who are off-centered relative to the gantry isocenter as well as increased image noise. In future, automatic centering techniques may help the technologists and/or radiologists to achieve precise patient centering for CT scanning.

References

Frush DP (2003) Responsible use of CT. Radiology 229:289–291

Kalra MK, Maher MM, Saini S (2003) What is the optimum position of arms for acquiring scout images for whole-body CT with automatic tube current modulation? AJR Am J Roentgenol 181:596–597

Kalra MK, Maher MM, Toth TL, Hamberg LM, Blake MA, Shepard JA et al (2004a) Strategies for CT radiation dose optimization. Radiology 230:619–628

Kalra MK, Maher MM, Toth TL, Schmidt B, Westerman BL, Morgan HT et al (2004b) Techniques and applications of automatic tube current modulation for CT. Radiology 233:649–657

Kalra MK, Maher MM, Toth TL, Kamath RS, Halpern EF, Saini S (2004c) Comparison of Z-axis automatic tube current modulation technique with fixed tube current CT scanning of abdomen and pelvis. Radiology 232:347–353

Kalra MK, Maher MM, Kamath RS, Horiuchi T, Toth TL, Halpern EF et al (2004d) Sixteen-detector row CT of abdomen and pelvis: study for optimization of Z-axis modulation technique performed in 153 patients. Radiology 233:241–249

Li J, Toth TL, Udayasankar U, Seamans J, Small WC, Kalra MK (2006) Automatic patient centering for MDCT: effect on radiation dose. Scientific paper at ARRS, Vancouver, Canada (in press)

Namasivayam S, Kalra MK, Mittal P, Small WC (2006) Can radiation exposure associated with abdominal and/or pelvic CT be minimized with better practice? Initial results. Scientific paper at ARRS, Vancouver, Canada (in press)

Tack D, Gevenois PA (2004) Radiation dose in computed tomography of the chest. JBR-BTR 87:281–288

Toth TL, Cesmelia E, Ikhlef A, Horiuchi T (2005) Image quality and dose optimization using novel X-ray source filters tailored to patient size. Proceedings of SPIE 5745:283–91 (Accessed at http://spiedl.aip.org/dbt/dbt.jsp?KEY=PSISDG&Volume=5745&Issue=1&bproc=year&scode=2005 on 16.3.2006)

Part II

Clinical Approaches of Dose Optimization and Reduction

Dose Optimization and Reduction in CT of the Head and Neck, Including Brain

9

Tom Mulkens, Rodrigo Salgado, and Patrick Bellinck

CONTENTS

9.1 Dose Optimization and Reduction in CT of the Head (Brain)

9.1.1 Introduction

Since its introduction in the 1970s, CT has played an increasingly important role in the imaging diagnosis of a variety of disorders. This is especially true in the field of neuroradiology, where CT made direct visualization of neurological anatomy possible for the first time, thereby revolutionizing diagnostic imaging.

T. Mulkens, MD
P. Bellinck, MD
Dept. of Radiology, Heilig Hart Ziekenhuis, Mechelsetraat 24, 2500 Lier, Belgium
R. Salgado, MD
Dept. of Radiology, Universitair Ziekenhuis, Wilrijkstraat 10, 2650 Edegem – Antwerpen, Belgium

However, it is well known that the CT-induced radiation dose is considered high compared with other (X-ray based) imaging techniques. For a CT examination of the same region, various authors have reported different dose values. This difference is due to variations in applied scan protocols, and the different choice of units of measurements in which they expressed the dose. This hindered comparison between studies and makes the correlation of CT with other radiological procedures difficult. In routine practice, about 30%–40% of all CT studies are studies of the head or brain, with a mean effective dose ranging from 1 mSv to 5 mSv (Van Unnik et al. 1997).

Although magnetic resonance imaging (MRI) was expected to reduce the overall frequency of CT (especially in neuroimaging), this has not been the case (Rehani and Berry 2000). Indeed, the advent of helical and multidetector helical CT (MDCT) with rapid acquisitions times and new diagnostic fields (e.g. CT angiography, perfusion CT) has led to a further increase in CT examinations: over the last 10 years CT has more than doubled its contribution and is now responsible for 47% of the collective dose from medical X-rays in the UK (Hart and Wall 2004). This evolution has spurred a growing interest in CT dose optimization and reduction in recent years.

MRI has superseded CT for examining the head, neck and spine, many parts of the musculoskeletal system and it offers an alternative to CT in the abdomen and pelvis. Nevertheless, the higher cost and the lesser availability of MRI remain a problem. Therefore, CT remains the method of choice for evaluation of post-traumatic injuries of the head, spine, thorax, abdomen and pelvis, for detection and characterization of parenchymal lung disease and for staging of almost all solid malignancies, including lymphomas. In the evaluation of cerebrovascular pathology, recent developments with diffusion and perfusion techniques have given MRI a higher sensitivity and specificity, although CT still plays a major role

in the evaluation of these disorders, due to its high sensitivity in the detection of intracranial haemorrhage, faster image acquisition, wider availability, lower cost, ease of use and fewer contraindications (Rehani and Berry 2000).

In CT, the effect of changing dose (e.g. by changing tube current or mAs settings) on image quality is sometimes difficult to assess, as CT is a digital technique in which image acquisition and display are not related, i.e. the "uncoupling effect". Thus, unlike conventional plain-film radiography, excessive exposure will not result in overexposure of images and degradation of image quality. As a result, significant variations have been observed between individual scanners in the typical patient doses for common CT examinations (Van Unnik et al. 1997; Clark et al. 2000). Multiple studies concentrating on dose reduction showed that low-dose CT is possible in high-contrast imaging, e.g. imaging of the lungs, without loss of diagnostic information (Zwirewich et al. 1991). It remains however unclear if dose reduction is also possible in areas with low contrast differences, such as the intracranial brain structures.

This is nevertheless an important issue, since patients who are examined or treated for complex or chronic brain disease (e.g. malformation, tumours, trauma and cerebrovascular disease) often undergo multiple CT studies over time. This also applies, for instance, to children with hydrocephalus with malfunctioning ventricular shunts. Although initial CT studies are oriented towards identification of subtle changes of intracranial structures, the main purpose of those control studies is to identify complications and gross morphological changes. As this often involves structures with high contrast or large structures (e.g. follow-up of haemorrhage or ventricular size), a reduction of "standard" scan parameters to lower dose settings seems possible in these CT studies (Cohnen et al. 2000).

9.1.2 Typical Dose Values in Head CT

Two large-scale surveys regarding the use of brain CT were undertaken in the late 1980s and early 1990s in the USA (McCrohan et al. 1987; Conway et al. 1992). These involved more than 250 CT scanners of different models. The average radiation dose in a standard CT brain examination in adults was hereby investigated at that time. Results showed that for brain CT examinations, the tube voltage (kV) was consistent at 120–140 kV for a given manufacturer and model. Slice thickness, slice spacing (increment) and total scan length and therefore the number of slices were also quite consistent and constant. However, tube current (mAs) was one of the most variable parameters between different CT systems and even for systems of the same manufacturer and model. For most systems, the minimum and maximum mAs values used for CT brain examinations differed by a factor of 3–4. This resulted in a dose variation of a factor of 2 or more for a typical ("standard") head examination for a given model of CT scanner. In these earlier surveys, the multiple-scan average dose (MSAD) was used as the dose descriptor. For most of the systems, the MSAD at the midpoint on the central axis of a standard dosimetry phantom varied between 22 and 68 mGy, but doses as high as 140 mGy were noted. Furthermore, the registered dose sometimes varied by a factor of 2 or more between identical CT units. The MSAD can be compared with the later introduced and now more commonly used CT dose index (CTDI), since both are based on the integral of a single-section dose profile, whereby CTDI may differ from MSAD with a variation of 10% up to 25%, depending on the used slice thickness and spacing. Both measurement units give a simple estimate of the dose delivered during the entire CT procedure to the region of the central section (Conway et al. 1992). The authors of these two large surveys concluded that these wide dose ranges indicated that dose has the potential to be reduced by careful selection of standard CT techniques.

Overall, variations in dose can result from differences in the user's choice of technique (desired image quality) or from actual differences in scanner performances (caused by differences in collimation, filtration or scan geometry). "Users of CT systems should be aware of radiation dose delivered with CT, dose ranges associated with different systems and doses delivered by their particular unit. This requires that dose performances of CT systems should be assessed by means of a protocol that allows comparison of data collected for identical and/or different units. To use CT appropriately, a facility should consider dose as well as image quality in selecting optimal techniques for typical modes of operation" (McCrohan et al. 1987; Conway et al. 1992).

In 1990, The International Commission on Radiological Protection introduced the dosimetric quantity "effective dose" that provides a direct relationship to the radiation hazard (ICRP 1991, report

60). In the context of regulations and radioprotection, this quantity of effective dose is probably the most relevant way in which to express and compare "the dose given to a patient" from different imaging procedures. It takes account of the distribution of dose amongst the radiosensitive organs in the body by summing the individual organ doses, having weighted each one according to the relative sensitivity of the organ to radiation-induced somatic or genetic effects. Effective dose is expressed in a special SI unit, Sievert (Sv). The risk for a given effective dose decreases with increasing patient age at exposure, since somatic effects, being delayed for many years or even decades after the exposure, will have a reduced opportunity for expression after X-ray exposure on the elderly. Furthermore, genetic effects are of no consequence for patients beyond their reproductive years (Wall and Hart 1997).

Although the main scan parameters, tube current time product (mAs) and tube voltage (kV), are relatively high in CT studies of the head in comparison with other CT studies, the effective dose associated with head CT scans is considerably less than that of abdominal or chest CT examinations (Van Unnik et al. 1997). Like the initial US surveys, similar surveys were done in the UK (Shrimpton et al. 1991), which showed that minimum and maximum doses for brain CT examinations could vary by a factor of up to 11-fold. Inherent differences in scanner design have been shown to contribute to this dose variation between models by up to a factor of 3 at most. Hence, much of the wider variation observed was caused by difference in local scanning technique and parameters employed. They conducted a survey in which the CTDI was measured in scanners of a large number of English hospitals and effective doses of various standard examinations were calculated using organ-dose conversion factors. A Dutch survey showed similar findings (Van Unnik et al. 1997) and confirmed that the greatest single variable that determines the patient dose is the way the scan is performed. They found mean effective doses in a CT brain examination ranging from 0.8 to 5 mSv, whereby the large dose distribution can be explained in part by the fact that a repeat scan with administration of iodine contrast doubles the dose. Although the reason for administration of contrast generally depends on the clinical situation, a large variation was shown, whereby in some hospitals nearly all patients were scanned without contrast and in others nearly all patients were scanned with contrast. Despite the clinical introduction of MRI more than 10 years ago, this Dutch survey showed that CT of the brain still represented about 35%–40% of all CT examinations in 1997.

This is comparable with a local survey in our department which showed in 1997 that 37% of all CT examinations were cranial ones. Nevertheless, the number cranial CT exams in our department is declining, comprising 41% and 39% of all CT examinations in 1991 and 1995, respectively. This further lowered to 31% and 30% in 2002 and 2003, after introduction of an MR unit. This declining trend in the use of CT of the head (in favour of MRI) is also reflected by the fact that in the first US survey of 1987, more than 50% of all CT examinations were brain CT's (McCrohan et al. 1987).

In 1998, the European Commission (EC) proposed reference dose quantities or levels for CT (EC Working Document, EUR 16262, 1998), based on the weighted CT dose index ($CTDI_w$, mGy) and dose length product (DLP, mGy·cm). These EC dose reference levels (DRL) for CT represent the third quartile values of mean CT dose recorded for an adequate sample of patients and have proved to be useful as reference dose levels in previous surveys. For CT of the head, these reference values are 60 mGy for the $CTDI_w$ and 1050 mGy·cm for the DLP. This corresponds to a "reference" effective dose for CT of the head of 2.2 mSv (Clark et al. 2000). The EC working document gives data that allow the values of DLP to be converted into effective dose by using conversion factors for broad regions of the body. For cranial CT this conversion value is 0.0021 mSv/(mGy·cm). These reference doses are, in effect, investigation levels related to average practice, since they are derived from mean doses and are not applicable to individual patients. It is accepted that the use of these levels should not interfere with good clinical practice, but that they can be useful for comparing samples of patients from different centres. The goal or rationale behind these reference levels is the following: by setting the reference level on the third quartile values, the 25% of hospitals or departments contributing to the highest dose would review their procedures and reduce their patient doses accordingly. This philosophy is now accepted in Europe. A local survey in Northern Ireland showed that comparison of effective dose was more useful than usage of the proposed EC reference levels for routine CT examinations of the head, chest, abdomen and pelvis. They concluded that revision of the mAs values will produce a significant reduction in patient dose, without compromising image quality (Clark et al. 2000).

9.1.3 Modalities for Dose Reduction in Cranial CT

Scan parameters of "standard" examination protocols in cranial CT are usually implemented by manufacturers, and are oriented toward attaining the best image quality in order to meet the highest diagnostic criteria. For decades, neuroradiologists have welcomed the advances in depicting neuroanatomy by new imaging techniques and accepted physics theories and vendor advice that high signal-to-noise ratio concerns justify using recommended CT dose rates (Fox 2004). Indeed, image conspicuity for brain structures such as grey and white matter is in the category of "low contrast". Nevertheless, many neuroradiologists do not pay attention to the doses used in their own CT suites. Their technologists usually receive training from the CT vendors, which do not like to demonstrate routine work at minimal dose, because images with more noise show a vendor's product to be inferior (Fox 2004).

Only a few studies have focused on the possibility of lowering the dose for CT of the head.

In a study (Cohnen et al. 2000) to assess image quality changes on CT scans of the head using a formalin-fixed cadaver, the radiation dose was reduced by lowering both tube current and kilovoltage, and this on two different CT machines, both in conventional sequential mode and (single-slice) helical scanning mode. Five experienced readers independently evaluated subjective image quality, whereby no observable differences in image quality between scans obtained with doses from 100% ("standard mode") to 60% of standard settings were noted. "Standard mode" for sequential mode was 135 kV–270 mAs and 130 kV–315 mAs for two different scanners, and 120 kV–185 mAs and 130 kV–157 mAs for helical scanning, with these two machines, respectively. Image noise was substantially higher in the cerebellar parenchyma (posterior fossa) than at the centrum semiovale (supratentorial level), suggesting the influence of petrous and facial bones. This was more obvious on low-dose images. In this study a linear inverse relation between image noise and dose was found. There was only a general assessment of subjective image quality of a cadaver head and no correlation with a clinical situation. Scans produced with a dose that was more than 50% reduced in comparison with "standard" settings were judged uninterpretable.

In a recent study (Mullins et al. 2004) of 20 elderly (> 65 years) patients with a 4-MDCT helical CT exam of the head for routine indications, with settings of 140 kV, 170 mAs, 1 s scan time and pitch factor of 0.75 ($CTDI_w$ of 65 mGy), the scan was repeated for a limited volume by covering four 5-mm-thick images at 90 mAs ($CTDI_w$ of 34 mGy, other scan parameters identical) at four levels: posterior fossa, middle cranial fossa, corona radiata and centrum semiovale, with a dose reduction of 47% (Fig. 9.1). The conspicuity between grey matter (GM) and white matter (WM) was not significantly different between the two dose groups. Main GM contrast-to-noise ratio (CNR) was 22% higher in the 170-mAs group, which was statistically significant, but all 90-mAs images (although somewhat noisier) were considered to be of acceptable diagnostic image quality and sufficient resolution, as rated by three experienced neurora-

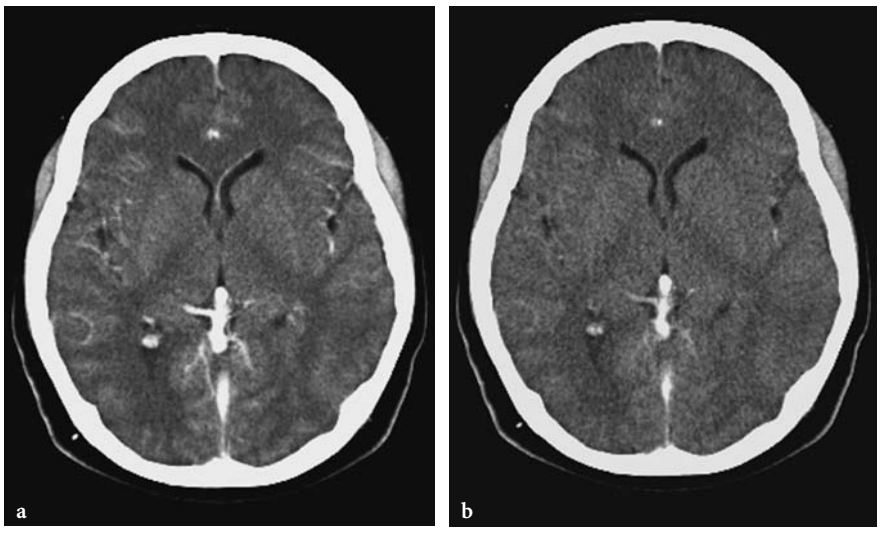

Fig. 9.1a, b. CT images of a 43-year-old woman with persistent headache for 3 weeks show normal brain struc-tures at the level of the basal ganglia. Standard brain CT after intravenous iodium contrast with a 6-MDCT at 130 kV, 280 mAs, 1 s rotation, CTDI = 61.2 mGy, comparable to the "EC reference level" and standard dose level of the study of Mullins et al. (2004). Calculated effective dose of the "standard" CT exam is 2.13 mSv; DLP = 820 mGy·cm. **a** A 5 mm axial image with "standard" dose at 280 mAs and **b** an additional 5 mm axial image at low dose at 140 mAs: with 50% dose reduction the image is somewhat noisier but there is a clear delineation of the anatomical structures

diologists. They indicate that in a hospital with an active neurological intensive care unit and a stroke unit, it is not unusual for some critically ill patients to receive multiple (sometimes daily) CT exams of the head for a period of some days or even weeks. The indications for these scans are frequently gross imaging findings, but which may change and affect management decisions: traumatic or non-traumatic haemorrhage (Fig. 9.2), aneurysm rupture, stroke and hydrocephalus (Fig. 9.3). For younger patients (and children) the difference between scans with a $CTDI_w$ of 65 mGy and of 34 mGy seems significant, especially when this is repeated several times in a short period. Recommendation of a low-dose technique for initial workup seems inappropriate (at present), since there is no scientific backup from other low-dose studies showing its potential to detect subtle pathology (e.g. lacunar infarctions) accurately. However, objective measurements showed no statistically significant difference in GM–WM conspicuity between standard and low-dose (about 50% less) images, which is a far more subtle distinction in terms of Hounsfield units than the conspicuity of most lesions (Mullins et al. 2004).

Another recent study (Britten et al. 2004) reached similar results: they added spatially correlated statistical noise to standard CT images of the head to simulate exposure reduction of up to 50% in 23 elderly patients (> 69 years). In this way, at 120 kV, starting from an initial scan at 420 mAs, they simulated images at 300, 260 and 210 mAs. They used the presence of periventricular low-density lesions as an

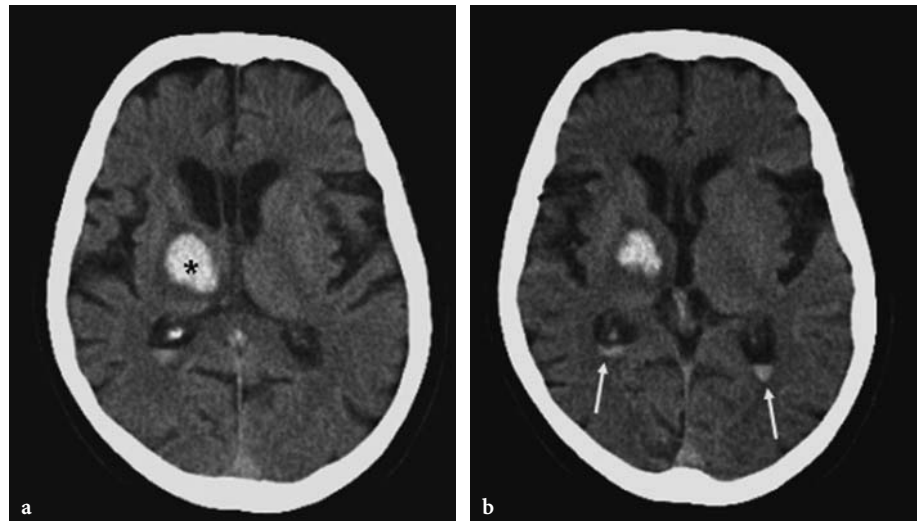

Fig. 9.2a, b. Control brain CT study with 50% dose reduction (CTDI of 30.6 mGy) in comparison with "standard" settings by halving tube current in a 69-year-old woman with right-sided thalamus haemorrhage, 1 day after admission to the intensive stoke unit because of progressive somnolentia (same scan protocol as in Fig. 9.1b). **a** Axial 5 mm images show clear visualization of haemorrhage (*asterisk*) and **b** the presence of an intraventricular extension with small blood-liquor levels (*arrows*) in both occipital horns. Calculated effective dose of low-dose CT exam is 1.12 mSv; DLP = 432 mGy·cm

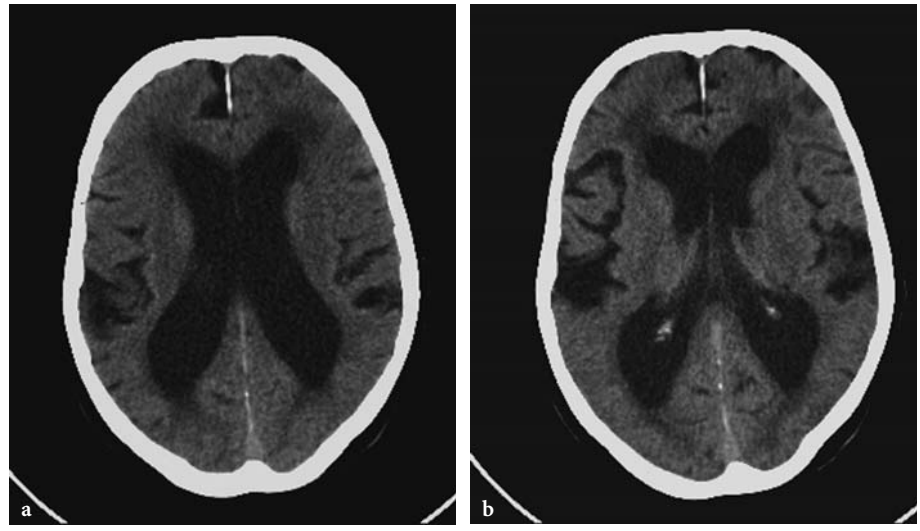

Fig. 9.3a, b. Follow-up brain CT study at low dose (CTDI of 30.6 mGy) in a 79-year-old woman with (normal pressure) hydrocephalus. Low-dose axial CT images are of sufficient quality to compare the dilatation of both lateral ventricles (**a** and **b**) with previous CT studies. Calculated effective dose of low-dose CT exam is 1.05 mSv; DLP = 405 mGy·cm

example of the effect of simulated dose reduction on diagnostic accuracy, which was not lowered significantly even with 210-mAs images (50% dose reduction), and used visualization of the internal capsule as a measurement of image quality, which was obviously lowered with low-dose images.

A drawback of these two low-dose cranial CT studies is the small number of patients that were studied: the question remains as to whether the same would be achieved in the total population. A reduction of sensitivity can be expected in the total population, given the extremely low number of patients (n= 22 and 23) studied.

A third recent study (Gündogdu et al. 2005) analysed the effect of various tube current settings in an attempt to optimize the image quality and dose for adult cranial CT in 60 patients. They examined three reference levels (posterior fossa, basal ganglia and centrum semiovale) and evaluated subjective image and noise quality scores and quantitative noise measurements. At 50% decreased dose protocol, starting from a CTDI of 58.2 mGy for the posterior fossa and 48 mGy supratentorially, there was no poor quality score at any level; at nearly 60% decreased dose protocol, poor quality scores were much higher, especially in the posterior fossa.

The importance of these three recent studies (Britten et al. 2004; Mullins et al. 2004; Gündogdu et al. 2005) is that they indicate that it is clinically feasible to lower the dose for "standard" cranial CT examinations and that a dose reduction up to 50% seems to give no significant image quality loss. Their limitation is that they evaluated only morphologically normal anatomical brain areas and the question remains as to how much the resolution of low-contrast lesions will be affected by low-dose protocols.

In CT of the brain, the lens of the eye is of particular concern as cataract formation is a well-documented result of radiation damage. The use of a different scan plane (different beam angulation by gantry angulation) to avoid the orbits has been shown to reduce the eye lens dose by 87% (Yeoman et al. 1992), without affecting the severity of posterior fossa artefacts (beam hardening by the petrous bones). An international questionnaire survey in this study in more than 180 hospitals in the UK, USA, Australia and Europe showed that only 32% of the hospitals routinely avoided the eye lens during cranial CT.

In 2001, Brenner et al. reported an estimated lifetime cancer mortality risk of 0.18% for paediatric abdominal CT and 0.07% for paediatric head CT, both of which were approximately 10 times higher than the same risks for adults. These results are debatable (they are estimations) and the authors stressed that these numbers still represent only a small increase in cancer mortality over the natural cancer background rate; nevertheless, their study indicates the importance of adapting radiation exposure in CT to a substantially lower level for children and not just applying adult scan parameters to the paediatric population, a method that was common practice until that period (Rogers 2001). Image quality in CT (e.g. CNR) depends primarily on the detected X-ray fluency; consequently, the technique factors used in paediatric CT can and should be reduced in comparison with adult technique factors, because smaller patients attenuate fewer X-rays. Thus, equivalent image quality can (and must) be produced at lower dose levels. Moreover, the values for energy imparted at CT in paediatric patients are generally lower than in adults, but the smaller mass of children (and the longer expected lifetime) causes the corresponding effective dose to be higher in children than in adults undergoing similar CT examinations (Huda et al. 1997).

Like in adults, cranial CT is the most common CT examination in children. In neonates and young children, about 25%–30% of the active bone marrow is present in the skull, whereby in adults this is only 5%–10%. The marrow-absorbed dose in a 6-year-old phantom for a paediatric cranial CT is reportedly higher than that for chest or abdominal CT (Fearon and Vucich 1987). In 1999, a paediatric brain CT study showed that a lower tube current can be used for children with no difference in image quality (Chan et al. 1999). They compared cranial CT at 120 kV with 250 or 200 mAs (age above or under 5 years; n = 53) with that at 150 or 125 mAs (according to age; n = 47) and found no difference in image quality scores at seven different anatomical areas, whereby a dose reduction of 37.5% and 40% was reached (Fig. 9.4). Similar results were shown by comparing paediatric cranial CT at 140 kV and 180–240 mA (according to age) with a lower dose at 90–130 mA (Shah et al. 2005): a 45%–50% tube current reduction was possible without any significant effect on image quality and reader confidence in the level of detail available to reach a diagnosis.

Wong et al. proposed using the maximum anteroposterior diameter (MAPD) of the child's head, measured on a lateral scout view at the start of the examination, as a good criterion for tube current selection (Wong et al. 2001). Another practical proposition is the use of CT technique charts (Boone et al. 2003)

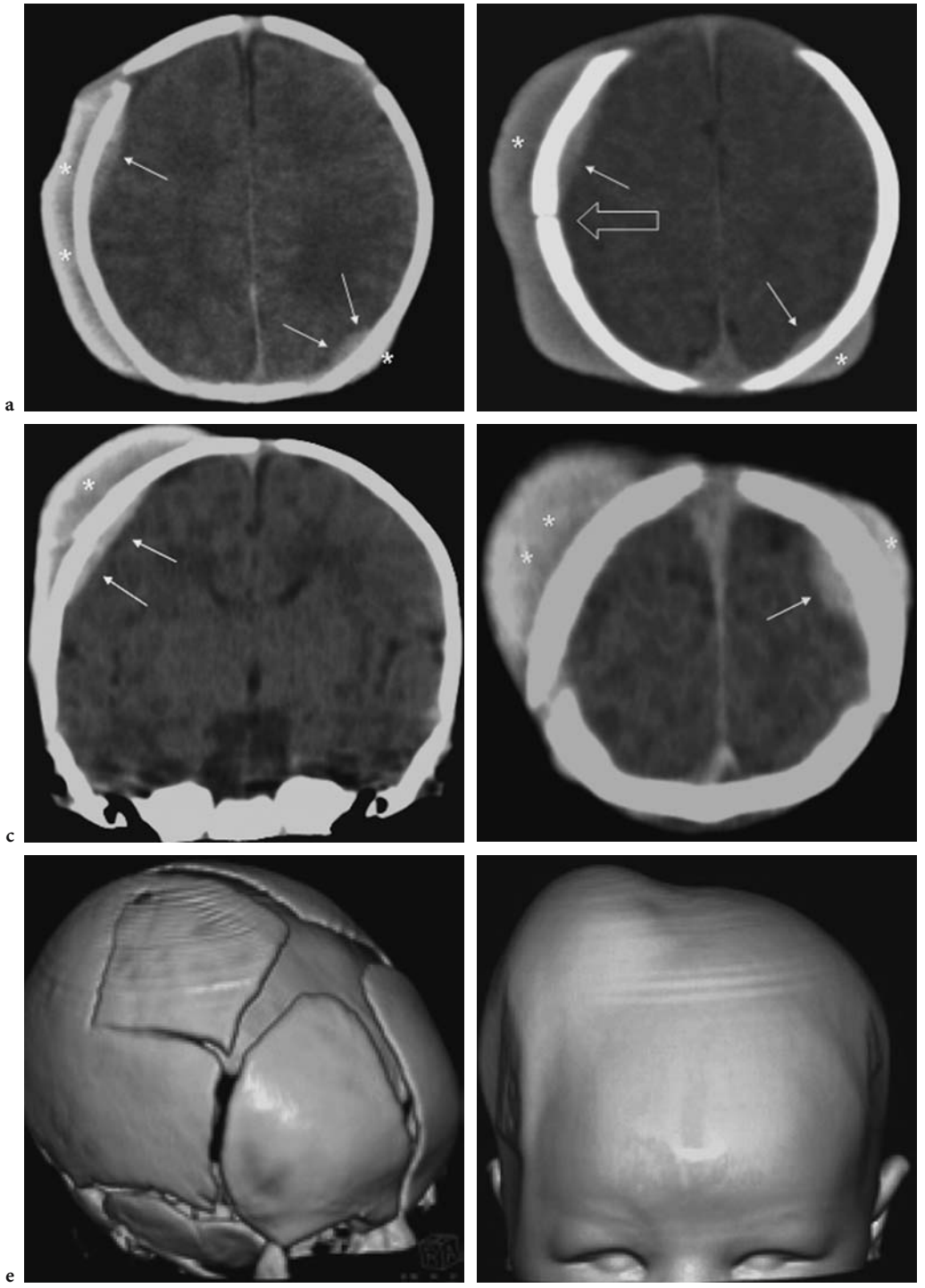

Fig. 9.4a–f. Male newborn with gradual soft-tissue swelling on the right side of the head after difficult delivery assisted with vacuum extractor. Standard skull X-ray showed linear parietal fracture. A 6-MDCT helical brain exam was performed with adapted paediatric protocol: 110 kV, 125 mAs, 1 s rotation, CTDI vol of 23.75 mGy, pitch factor of 1. Calculated effective dose was 5.9 mSv. **a**, **b** Axial 5 mm images showing bilateral epidural haematomas (*arrows*), skull fracture (*open arrow*) and large (right) and small (left) cephalhaematomas (*asterisks*). **c**, **d** A 5 mm coronal MPR image and 5 mm axial image showing communication of the right epidural haematoma with right cephalhaematoma trough skull fracture (*open arrow*); there is no brain oedema or important mass effect of the hematomas. **e**, **f** Volume rendering images with bone setting (**e**) show the extent of the linear, angle-shaped right parietal bone fracture and with soft-tissue settings (**f**) show nicely the extent of the cephalhaematomas

where, depending on the child's (head or trunk) diameter or circumference, a tube current reduction factor is given, starting from the tube current used in adults, reducing the radiation dose and preserving the contrast-to-noise ratio. These factors were calculated based on physically measured data in phantom cylinders of different diameter. Because of the exponential relationship between patient thickness and X-ray attenuation, very large dose reductions are proposed in the smallest children (Boone et al. 2003).

Since children have less thick and less dense (less calcified) bones, it seems logical to use a lower tube voltage to lower the dose; for example, lowering the tube voltage from 120 to 80 kV gives a dose reduction of 75%. Especially for young children and infants the use of 100 kV as the tube voltage in cranial CT seems sufficient (Chan et al. 1999).

9.1.4 Conclusion

The goal of radiology is accurate, timely and clinically relevant diagnosis. Reducing patient dose by limiting X-ray exposure has the inevitable consequence of increasing noise in CT images. The key question is to identify the minimum X-ray exposure, i.e. the "poorest" image quality, required for a given examination and pathology (Britten et al. 2004). Recent studies have shown the possibility of reducing the radiation in adult cranial CT up to 50%, without significant loss of image quality, but they mostly studied only normal anatomical brain images. The question remains as to whether this low-dose technique still holds for specific brain pathologies, which frequently give a "low contrast" difference in comparison with normal brain tissue. The ability to add noise by computer simulation to real CT studies offers the prospect of being able to perform large-scale studies to evaluate diagnostic accuracy as a function of reducing the dose: in this time of picture archiving and communication systems (PACS), every radiological site has access to a substantial archive of clinical pathological cases in order to study the potential of reaching an objectively judged minimum dose level.

In certain clinical circumstances and patient populations, a trade-off between reduced radiation dose and image quality may already be acceptable, without sacrificing diagnostic accuracy. Low-dose brain CT may be appropriate when routine follow-up of initial high contrast findings is required (e.g. hydrocephalus or haemorrhage). Also, hospitalized patients who require frequent serial CT scans for neurological or neurosurgical care may also benefit from this low-dose scanning. Finally, it is important to lower the dose parameters for paediatric head CT, since children are more sensitive to radiation-induced damage. Nowadays, all CT vendors offer specific paediatric scan protocols with adapted lower dose settings.

9.2 Dose Optimization and Reduction in CT of Head and Neck Region

9.2.1 Dose Optimization and Reduction in Sinus CT

9.2.1.1 Introduction

Sinusitis is a frequent disorder. The underlying cause can be viral, bacterial, allergic, vasomotor or reactive. It can occur as a complication of dental infection or tooth extraction. In acute sinusitis there is generally no need for imaging, except when there is suspicion of complication with intra-orbital or intracranial extension. About one-third of the patients develop a chronic sinusitis. Chronic sinusitis is defined as persistent (acute) inflammation or frequently recurrent episodes of (sub) acute sinusitis. In these patients imaging is indicated as follows: to visualize the grade and extent of the inflammatory sinus pathology, to identify an eventual underlying cause, to describe the site of pathology in the complex anatomy of the maxillofacial region and to guide endoscopic surgery. Better understanding of the physiopathology of sinusitis and the development of functional endoscopic sinus surgery (FESS) have changed the role of imaging: CT has become the "gold standard" in the evaluation of (chronic) sinusitis, and has largely replaced conventional radiography, as CT is excellent for studying key regions of interest, such as the osteomeatal complex and anterior ethmoid region (Zinreich et al. 1996; Eggesbö 2006).

Before the advent of helical CT, direct coronal CT was the method of choice for visualizing sinuso-nasal anatomy. Since the introduction of helical and multi-

detector CT, axial imaging with fine (sub)millimetre collimation and reformations in the axial, coronal and sagittal plane with thin slices has become the method of choice, due to the possibility of getting an (nearly) isotropic volume data set. Coronal reformations give equal or even better image quality, due to the absence of dental filling artefacts, which were frequently present in earlier direct coronal scanning (Eggesbö 2006).

While CT is superior at demonstrating fine bony anatomy, the extent and anatomic localization of inflammatory lesions and complications such as sclerotic bone thickening and bone destruction, it has limitations in the differentiation of soft tissue masses, such as distinguishing mucosal thickening from pus-filled areas and inflammatory lesions (such as retention cysts, polyps and mucocoeles) from neoplastic processes. MR is superior at soft tissue characterization and has the advantage of using no radiation: MR is useful when in advanced opacification of the sinuso-nasal cavities a distinction has to be made between "simple" sinusitis, pyocele, fungal sinusitis and neoplastic disease. It is also excellent for visualizing invasion of the orbit or intracranial compartments. If neoplasm or complications of inflammatory processes are to be ruled out, additional imaging with intravenous administered gadolinium is mandatory (Rao and El-Noueam 1998).

9.2.1.2 Low-Dose CT of the Sinuses

Low-dose CT for sinuso-nasal imaging has been available for a long time and together with low-dose CT of the lung, introduced the application of low-dose CT to radiology. In 1991, before the introduction of helical CT, two studies had already stressed the ability to image the sinuses at a much lower dose than was commonly used in clinical practice at that time. Scanning a head phantom with a constant tube voltage at 120 kV, six successive sets of axial and coronal examinations were obtained, whereby the mAs setting was consistently reduced by approximately 50% every time (Marmolya et al. 1991): from 451 mAs to 16 mAs in the axial plane and from 503 mAs to 23 mAs in the coronal plane (dose reduction by a factor of 28). The same systematic dose reduction was used in a subsequent prospective study of 60 patients in the same way: divided into six groups of ten patients, each group underwent scanning with one of the six combinations of axial and coronal scanning as in the head phantom study. Additionally, 30 patients received the lowest mAs settings. In both the phantom and the patient study the amount of visually perceived noise increased, somewhat more in the axial than in the coronal plane, but all images were considered as of diagnostic image quality: "On the coronal images of the lowest setting of 23 mAs, the osteomeatal complex was clearly identifiable and presence of air versus soft tissue or fluid could be confidentially diagnosed" (Fig. 9.5). Another study of the same

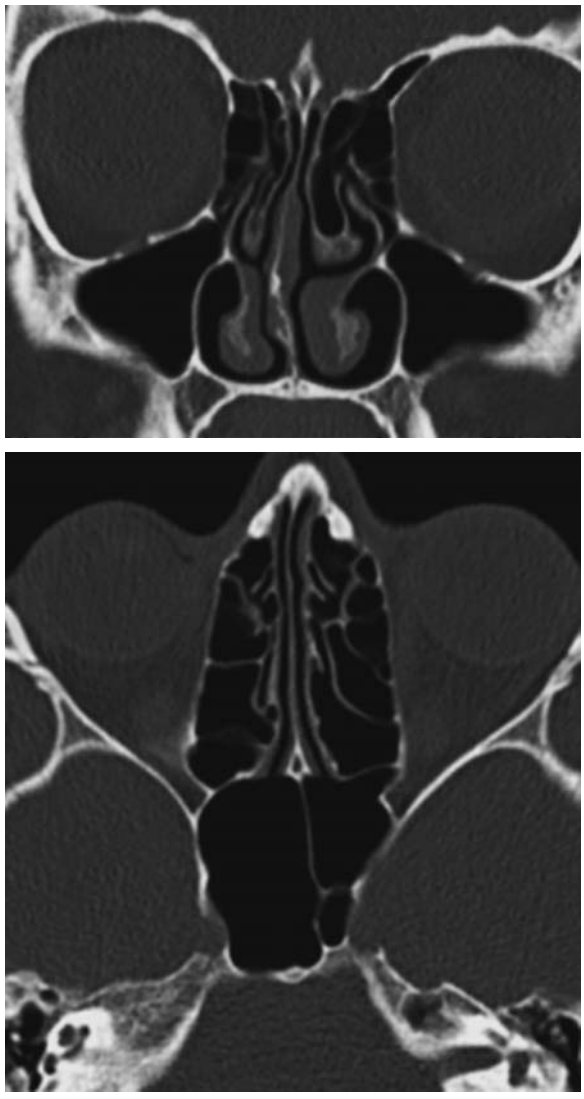

Fig. 9.5a, b. A 24-year-old woman with suspicion of chronic sinusitis. Low-dose 16-MDCT at 120 kV and 25 mAs ($CTDI_{vol}$ of 5.2 mGy) with 2 mm coronal (**a**) and axial (**b**) images show clearly the normal anatomy of the osteomeatal units and infundibulum with clear aeration of both maxillary, ethmoidal and sphenoidal sinuses. Calculated effective dose of CT exam is 0.10 mSv

year recommended a comparable dose reduction: in 44 patients with inflammatory sinus disease, the dose was reduced by lowering the tube current from 390 mAs to 180 mAs, and further to 90 mAs and finally to 60 mAs (Duvoisin et al. 1991). In all cases the exact extent of the disease was correctly assessed on each of the low dose settings, with no false negatives: "although the less pleasant appearance to the eyes, the increased noise in the low dose images seemed not to induce errors of interpretation". They reported that in cases of extensive sinus disease the thickness and integrity of the fine bony (ethmoid) septa are sometimes difficult to evaluate on low-dose CT images (Fig. 9.6).

Several more recent studies confirmed these initial observations of the early 1990s: both with conventional incremental CT (Czechowski et al. 2001) and single-detector helical CT (Suojanen and Regan 1995; Kearny et al. 1997; Sohaib et al. 2001; Hein et al. 2002). They all proposed scan protocols with lower tube current settings of 40 or 50 mAs at 120 kV tube voltage as an alternative to many existing protocols which employed high mAs (up to 200 mAs – in the belief that this necessarily improves scan image quality). However, modern CT scanners are able to deliver excellent image quality at much lower dose levels (Kearny et al. 1997). Also the natural high contrast between the structures of interest (bone, air and soft tissue) in sinus CT enables using lower mAs settings and gives a correspondingly lower dose (Sohaib et al. 2001). The problem with these low-dose sinus CT studies is that they did not deliver additional dose descriptors, such as CTDI or effective dose, so that comparisons between different scanners is difficult: mAs values can vary by a factor of 2–3 for the same dose with different scanners. Therefore, directly comparing mAs values alone, across studies with different scanners, has limitations (Shrimpton et al. 1991).

Tack et al. (2003) calculated the effective dose of these previously reported low-dose CT studies of the sinuses (both incremental and single-detector helical CT studies), by using a commercially available software program on a PC (CT Expo, Hanover, Germany). For a mean scanned region of 12 cm length in their study they calculated a range of 0.11–0.24 mSv (mean: 0.17 mSv) for men and a range of 0.12–0.26 mSv (mean: 0.18 mSv) for women. In their own multidetector CT study, low-dose CT was compared with standard-dose CT on a 4-MDCT machine in the same 50 patients, who underwent both protocols. For standard-dose CT the scan protocol was 120 kV, 150 mAs, 4 × 1 mm collimation, pitch factor of 0.75, which gave a mean effective dose of 0.70 mSv for men and 0.76 mSv for women. For low-dose CT, 120 kV, 10 mAs, 4 × 1 mm collimation and a pitch

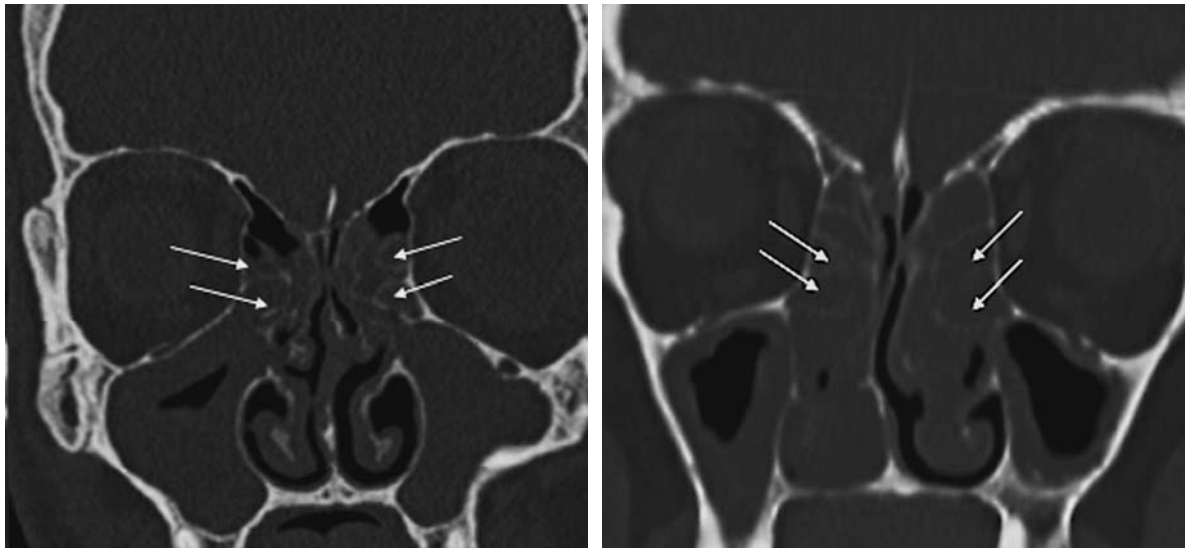

a b

Fig. 9.6a, b. In cases of extensive sinus disease it is difficult to evaluate the integrity of the fine bony (ethmoid) septa (*arrows*), especially at low-dose CT. This can be due to bony erosion, partial volume effect or lack of contrast at low dose. **a** Coronal 2 mm image of a low-dose 16-MDCT (same scan protocol as in Fig. 9.5) with effective dose of 0.12 mSv in a 56-year-old man; **b** comparable extensive sinus pathology in a 36-year old man at standard-dose 16-MDCT with 120 kV, 100 mAs, ($CTDI_{vol}$ of 21.4 mGy) and effective dose of 0.55 mSv, with bony erosion of the ethmoid septa (*arrows*)

factor of 2 were used, which gave a mean effective dose of 0.047 mSv in men and 0.051 mSv in women, which is comparable with the radiation dose used in a four-view standard radiographic examination (Tack et al. 2003). They analysed mucosal abnormalities at eight different sinuso-nasal anatomic landmarks and two bony abnormalities and found greater variation in analysing cases of significant discrepancies in observations between three reviewers than between findings obtained at different dose levels: "in other words, observational variations associated with the decrease in radiation dose (by use of the low dose protocol) were fewer than those variations than can contributed to the reviewers themselves". They concluded that low-dose MDCT should be considered the imaging method of choice in the evaluation of chronic sinusitis.

A local DRL study in our department of low-dose CT of the sinuses in 100 adult patients in 2005 gave a mean effective dose of 0.13 mSv and 0.15 mSv on two different MDCT machines, a 6-MDCT and 16-MDCT, respectively (unpublished data). For 6-MDCT ($n = 50$), we used 80 kV, 60 mAs, 6×0.5 mm collimation, pitch factor of 1, which gives a $CTDI_{vol}$ of 5.04 mGy, and got a mean DLP of 54.8 mGy·cm. For the 16-MDCT ($n = 50$), we used 120 kV, 25 mAs, 16×0.75 mm collimation, which gives a $CTDI_{vol}$ of 5.22 mGy, and got a mean DLP of 60.2 mGy·cm. In comparison with the scan protocols proposed by the manufacturer for scanning of the sinuses, this gives a dose reduction with a factor of 4: for the 6-MDCT they recommend the use of 130 kV, 70 mAs, 6×1 mm collimation with a pitch of 0.83, which gives a $CTDI_{vol}$ of 19.4 mGy; for the 16-MDCT they propose 120 kV, 100 mAs, 16×0.75 mm collimation, pitch of 0.55, which gives a $CTDI_{vol}$ of 21.3 mGy.

A recent study with a limited scan protocol of a non-contiguous incremental CT examination of the sinuses with ten 1-mm-thick coronal slices (interslice gap varied from 5 to 15 mm) at 120 kV and 40 mAs reached a very low mean effective dose of only 0.02 mSv, which is lower than the effective dose of standard radiography (Hagtvedt et al. 2003). Since this is only a limited exam in the coronal plane, small key anatomic landmarks with clinical importance might not have been able to be identified (Tack et al. 2003). Multidetector CT has the advantage of three-dimensional imaging, whereby all structures are better visualized in one of the three different anatomic planes: e.g. the sphenoethmoidal recess is better visualized in the axial plane and the nasofrontal duct and periodontal spaces are better visualized in the sagittal plane.

Infections of the upper respiratory system are by far the most common cause of illness in infancy and childhood, accounting for approximately 50 percent of all illness in children younger than 5 years of age, and 30 percent in children between the ages of 6 and 12 years: the large majority of these upper respiratory infections are viral rhinitis or pharyngitis and are self-limiting diseases, also known as 'common cold'. About 10% of these upper respiratory infections are complicated by sinusitis, which a common problem in the paediatric population (George and Huges 1990). According to the American College of Radiology, acute sinusitis is a clinical diagnosis that may not need imaging (McAlister et al. 2000). Although the use of radiography is not indicated in these patients and should be discouraged, it is still frequently used for diagnosis: the physical examination alone can give difficulties in the diagnosis of acute bacterial sinusitis, because of the similarity of physical findings in the patient with uncomplicated viral rhinosinusitis. Also the clinical findings of recurrent or chronic sinusitis are often not specific, especially in younger children (Kronemer and McAlister 1997; McAlister et al. 2000). Plain radiography of the sinuses in children is technically demanding and difficult to perform, particularly in very young children, since correct positioning may be difficult to achieve. Therefore, the radiographic images may over- or underestimate the presence of abnormalities within the sinuses. Furthermore, the interpretation of sinus radiographs in children is difficult: there is a lack of accuracy (low specificity and sensitivity), largely related to the small size of the sinuses, the angulation of the X-ray beam and nasal secretions (Kronemer and McAlister 1997; McAlister et al. 2000).

The American Academy of Pediatrics (2001) therefore advises to reserve the use of imaging of sinusitis for situations in which the patient does not recover or worsens during the course of appropriate antimicrobial therapy or in cases of recurrent disease. The use of CT is restricted to children who have very persistent or recurrent sinus infections, who are not responsive to medical management and whereby surgery is considered an option as a management strategy and to those who present with complications of acute sinusitis. CT scan images give a much better detailed image of the sinus anatomy, and, when taken in conjunction with the clinical findings, remain a useful adjunct to guide (surgical) treatment.

Previous studies have already shown the lack of accuracy of sinus radiographs for the diagnosis of

sinusitis in children in comparison with CT. In up to 75% of the patients the findings of the radiographs did not correlate with those on CT scans: in about 40% of the patients with normal radiographs, there were signs of pathology on CT scans and, vice versa, when there was an abnormality suspected on radiographs in 35% of the patients the CT scan showed normal findings (McAlister 1989). Another disadvantage of sinus radiographs is the great variability in their interpretation between radiologists: there is a low inter-observer agreement in the evaluation of these radiographs. This inter-observer agreement between radiologists is much better with CT (Kronemer and McAlister 1997; McAlister et al. 2000). However, there used to be an important threshold for use of CT in children for sinus evaluation: first of all, the radiation dose of CT is much higher than that of radiographs and, secondly, the use of sedation was frequently necessary (in young children) to perform a good CT exam. With the advent of spiral CT and MDCT, CT became the imaging modality of choice for the diagnosis of sinus disease in adults, whereby it is possible not only to lower the radiation dose, but also to shorten the examination time substantially. A recent study in 125 children showed that the effective dose of low-dose sinus MDCT can be lowered to a level of 0.05 mSv, which was comparable with the level of effective dose measured from standard radiographs in 69 other children (Mulkens et al. 2005a). In a scan protocol with 80 kV and with a mAs range of 15–25 mAs (according to age) on a 6- and 16-MDCT, a $CTDI_{vol}$ of 1.28 to 2.1 mGy was reached with preservation of diagnostic image quality (Fig. 9.7). Scan time was very short with a mean of 2.1 s and 9 s (16-and 6-MDCT, respectively), whereby there was no need for sedation for any CT exam. Compared to the "default" examination protocols for sinus CT in children as proposed by the manufacturer, the radiation using low-dose protocols, expressed in $CTDI_{vol}$, was 5–7 times lower. The large majority of the children (85%) were referred for CT for evaluation of chronic or recurrent sinus complaints (Fig. 9.8); only about 15% of the children were referred to CT for evaluation of an acute history with fever, sinus discomfort or headache or for evaluation of fever of unknown origin. This study shows another advantage of the use of low-dose CT in these children: CT permits the simultaneous visualization of the pharyngeal tonsils (adenoids), middle ear and mastoids, which are displayed in the same scan volume as the sinuses. In this way, CT displays the whole ear, nose and throat region in one examination, which is not possible with radiographs. The presence of adenoid hypertrophy and fluid in the middle ears ("glue ear") and mastoids (Fig. 9.8) is frequently seen in these children with recurrent upper respiratory infections and this can be accurately diagnosed at the same time with the same low dose (Mulkens et al 2005a).

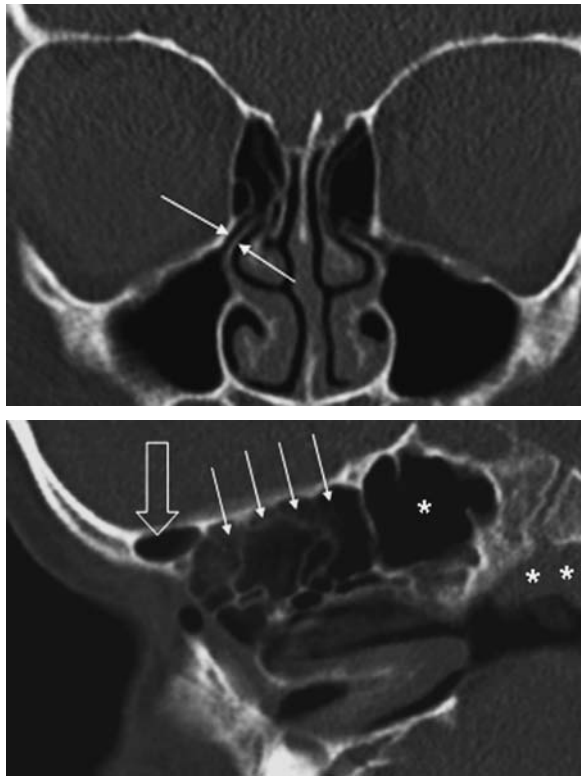

Fig. 9.7a, b. Normal findings in low-dose CT exam of the sinuses in a 6-year-old girl (6-MDCT, $CTDI_{vol}$ of 1.68 mGy, effective dose of 0.035 mSv). **a** Coronal 2 mm image shows normal maxillary and ethmoidal sinuses with clear depiction of infundibulum, medially bordered by the uncinate process (*arrows*). **b** Sagittal 2 mm image shows normal frontal sinus (*open arrow*), ethmoidal cells (*small arrows*), sphenoid sinus (*asterisk*) and adenoids (*double asterisks*)

A disadvantage in imaging of sinusitis (both of adults and children) is the high incidence of soft tissue changes found in the sinus cavities in radiographic, CT and MRI exams in patients who undergo medical imaging for other reasons and who have no clinical evidence of sinus disease. This incidence is reported to be 33%–45% (Glasier et al. 1989; Gordts et al. 1997). A common cold or other upper airway infection acutely produces mucosal abnormalities in the sinuses in the majority of adults and children, and this is reflected in imaging, especially

in patients who had a "cold" in the 2 weeks preceding imaging. Therefore, the diagnosis of acute and chronic or recurrent sinusitis should not be made on the imaging findings alone: the diagnosis of acute or chronic sinusitis should be made clinically, with confirmation with laboratory and imaging findings (Gordts et al. 1997; McAlister et al. 2000).

9.2.1.3 Conclusion

With modern multidetector CT, low-dose CT has become the method of choice to evaluate inflammatory pathology of the sinuses, especially in patients with chronic or recurrent sinusitis complaints. In patients with acute sinusitis, there is generally no need for imaging. Both in adults and children low-dose CT can be done with a mean effective dose that approaches or is comparable with the range of effective doses of standard radiography: 0.05–0.15 mSv. One has to keep in mind that with every imaging technique mucosal abnormalities in the sinus cavities are frequently found in patients referred for other reasons and who do not have clinical signs of sinus pathology. This lack of specificity, together with the lack of soft-tissue contrast, of low-dose CT is a disadvantage: when there is suspicion of complications of sinus disease with intra-orbital or intracranial extension (Fig. 9.9) or of underlying tumour pathology, the use of standard-dose CT with intravenous iodine contrast with additional soft window settings or MRI should be considered first.

9.2.2 Other Options for CT Dose Optimization in the Head and Neck Region

Since almost all other anatomical structures of interest in the head and neck region are soft tissues (pharynx and larynx, tongue and salivary glands, thyroid and parathyroid glands, muscles), the use of low-dose CT for imaging is not possible, since sufficient contrast (and dose) is necessary to distinguish between sometimes low-contrast lesions and normal soft tissue. Nevertheless, there are some options for optimizing the patient's dose and some specific indications whereby low-dose CT can be used.

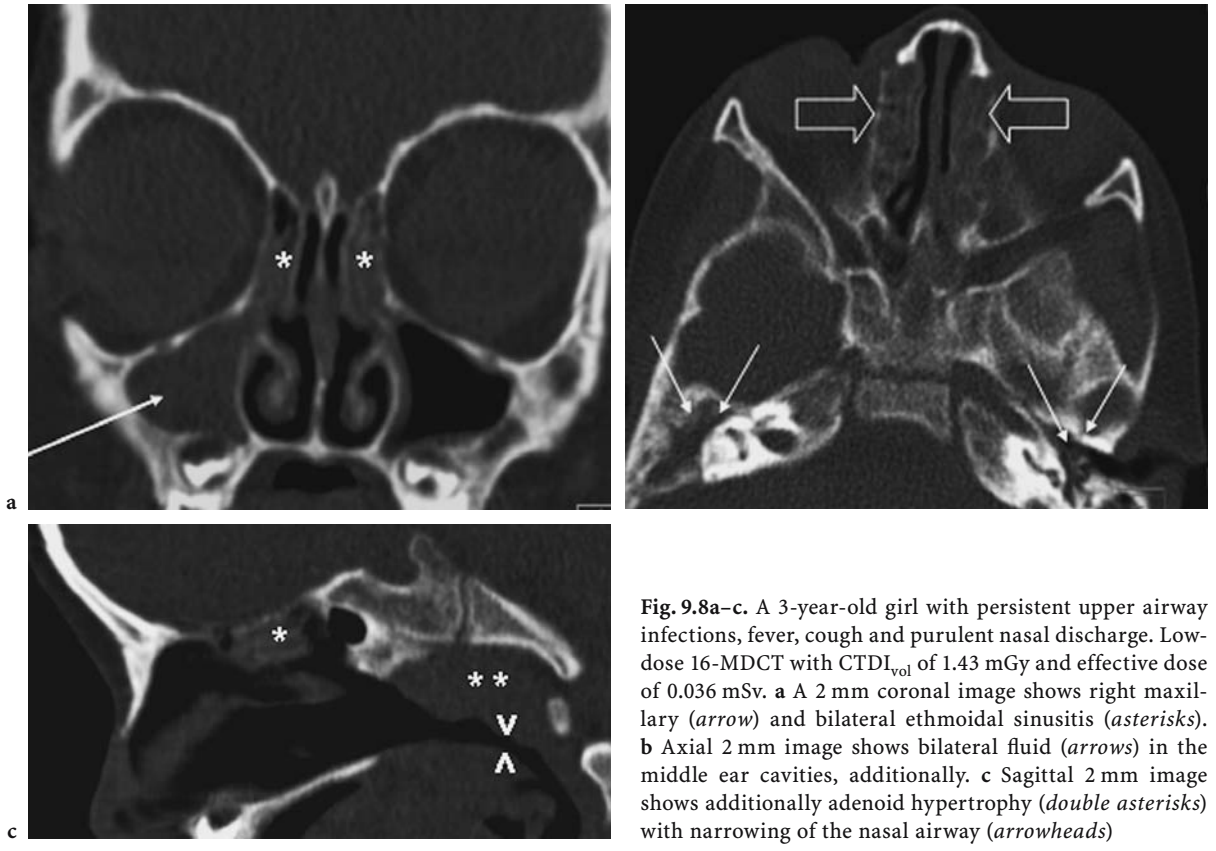

Fig. 9.8a–c. A 3-year-old girl with persistent upper airway infections, fever, cough and purulent nasal discharge. Low-dose 16-MDCT with $CTDI_{vol}$ of 1.43 mGy and effective dose of 0.036 mSv. **a** A 2 mm coronal image shows right maxillary (*arrow*) and bilateral ethmoidal sinusitis (*asterisks*). **b** Axial 2 mm image shows bilateral fluid (*arrows*) in the middle ear cavities, additionally. **c** Sagittal 2 mm image shows additionally adenoid hypertrophy (*double asterisks*) with narrowing of the nasal airway (*arrowheads*)

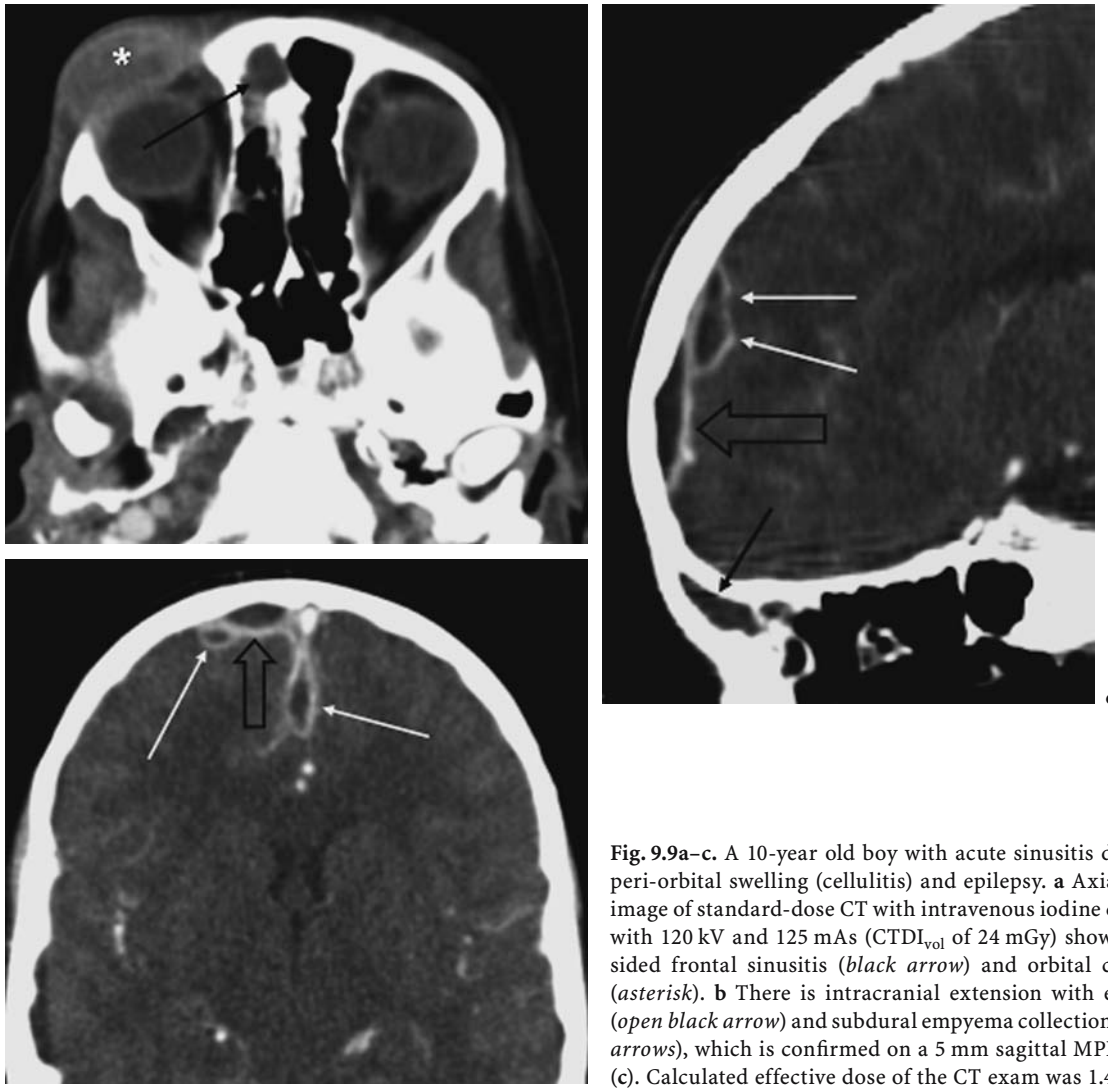

Fig. 9.9a–c. A 10-year old boy with acute sinusitis develops peri-orbital swelling (cellulitis) and epilepsy. **a** Axial 5 mm image of standard-dose CT with intravenous iodine contrast with 120 kV and 125 mAs ($CTDI_{vol}$ of 24 mGy) shows right-sided frontal sinusitis (*black arrow*) and orbital cellulitis (*asterisk*). **b** There is intracranial extension with epidural (*open black arrow*) and subdural empyema collections (*white arrows*), which is confirmed on a 5 mm sagittal MPR image (**c**). Calculated effective dose of the CT exam was 1.4 mSv

The use of tube current modulation systems in modern multidetector CT have been shown to optimize and reduce a patient's dose with different ranges, depending on the body region examined (McCollough et al. 2006). Automatic tube current modulation in CT is analogous to the automatic exposure control or photo timing technique for automatically terminating radiographic exposure in conventional radiography, once the predetermined radiographic density has been obtained. Automatic tube current modulation in CT is based on the principle that X-ray attenuation and quantum image noise are determined by the size of the object and its tissue density. The tube current can thereby be adjusted (and reduced) with the changing regional attenuation during the continuous scanning process of helical CT, while maintaining image quality and increasing dose efficiency (Kalra et al. 2004). Modern modulation systems adjust tube current along the three different scan planes (angularly around the patient and along the long axis of the patient) constantly during the time of the scan process, and reach a substantial dose reduction with a range of 20% to more than 60%, depending on the anatomical region (Kalra et al. 2004; Mulkens et al. 2005b; McCollough et al. 2006). In the head and neck region, the use of tube current modulation has been shown to reduce the dose with a mean of 20%, both in adults (McCollough et al. 2006) and in children (Greess et al. 2004).

In dental radiology, CT is used in the preoperative planning of dental implant surgery, evaluating the bony anatomy of the mandibular and/or maxilla, measuring bone thickness and evaluating its

integrity. Dedicated dental CT software packages are available to visualize the bone in parasagittal and "panoramic" reconstructions. Several studies have reported the possibility of reducing the dose for dental CT imaging, by reducing the tube current and increasing the pitch, both on single detector helical CT (Rustemeyer et al. 2004) and multidetector helical CT (Loubele et al. 2005). The dose can thereby be reduced by a factor of 8–9, with an effective dose in the range of 0.10–0.20 mSv, without sacrificing diagnostic image quality (Fig. 9.10): "the dose reduction with acceptable image quality was possible because only the bony anatomy is of interest for indications of maxillofacial surgery and dental implant planning, and not the contrast of the different soft tissues" (Loubele et al. 2005).

In analogy with low-dose CT of the abdomen for detection of urinary lithiasis, low-dose CT of the head and neck region can be used for detection of sialolithiasis, i.e. lithiasis of the salivary glands (Fig. 9.11).

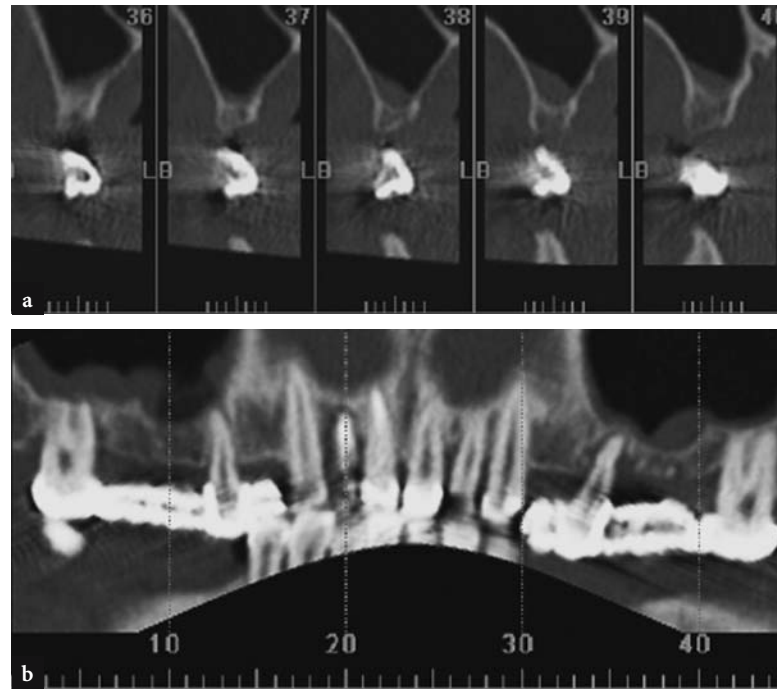

Fig. 9.10a, b. Low-dose dental CT exam for planning of dental implant surgery in a 38-year-old woman: 16-MDCT with 120 kV, 40 mAs and CTDI of 8.5 mGy. **a** Parasagittal 1.5-mm-thick reconstruction images and **b** "panoramic" 2-mm-thick reconstruction. Calculated effective dose of the CT exam was 0.11 mSv

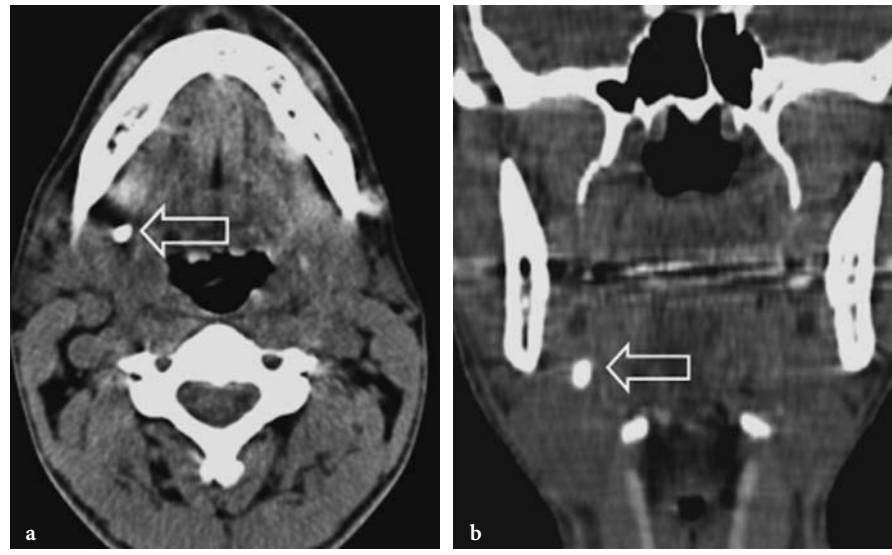

Fig. 9.11a, b. A 53-year-old man with pain and swelling of the right submandibular region during eating. Low-dose 6-MDCT with 110 kV, 50 mAs and $CTDI_{vol}$ of 4 mGy. **a** The 4 mm thick axial and **b** coronal images show large lithiasis (*open arrowhead*) at the junction of the gland with the ductus of Wharton. Calculated effective dose of the CT exam was 0.34 mSv

In this way the effective dose range was lowered from 1.5–2 mSv in our "standard" head and neck protocol to a range of 0.3–0.5 mSv by using both a lower kV (100 or 110 kV) and lower mAs (50 mAs) on both our 6- and 16-MDCT machines (unpublished data). We use the same low-dose MDCT protocol for preoperative planning of patients with thyroid surgery: to evaluate the size of the thyroid goitre, its contour and its relationship with the trachea, the great vessels and its extension in the upper mediastinum.

References

American Academy of Pediatrics (no authors listed) (2001) Subcommittee on management of sinusitis and Committee on quality improvement: clinical practice guideline: management of sinusitis. Pediatrics 108:798–808

Boone JM, Geraghty EM, Seibert JA et al (2003) Dose reduction in pediatric CT: a rational approach. Radiology 228:352–360

Brenner DJ, Elliston CD, Hall EJ et al (2001) Estimated risks of radiation-induced fatal cancer from pediatric CT. AJR Am J Roentgenol 176:289–296

Britten AJ, Crotty M, Kiremidjian H et al (2004) The addition of computer simulated noise to investigate radiation dose and image quality in images with spatial correlation of statistical noise: an example application to X-ray CT of the brain. Br J Radiol 77:323–328

Chan CY, Wong YC, Yu SK et al (1999) Radiation dose reduction in paediatric cranial CT. Pediatr Radiol 29:770–775

Clark J, Cranley K, Robinson J et al (2000). Application of draft European Commission reference levels to a regional CT dose survey. Br J Radiol 73:43–50

Cohnen M, Fisher H, Hamacher J et al (2000) CT of the head by use of reduced current and kilovoltage: relationship between image quality and dose reduction. Am J Neuroradiol 21:1654–1660

Conway BJ, McCrohan JK, Antonsen RG et al (1992) Average radiation dose in standard CT examinations of the head: results of the 1990 NEXT survey. Radiology 184:135–140

Czechowski J, Janeczek J, Kelly G et al (2001) Radiation dose to the lens in sequential and spiral CT of facial bones and sinuses. Eur Radiol 11:711–713

Duvoisin B, Landry M, Chapuis et al (1991) Low-dose CT and inflammatory disease of the paranasal sinuses. Neuroradiology 33:403–406

Eggesbö HB (2006) Radiological imaging of inflammatory lesions in the nasal cavity and paranasal sinuses. Eur Radiol 16:872–888

European Community (1998) Quality criteria for computed tomography. EC Working Document EUR 16262, Brussels, EU, 1998

Fearon T, Vucich J (1987) Normalized pediatric organ-absorbed doses from CT examinations. AJR Am J Roentgenol 148:171–174

Fox AJ (2004) Use of the lowest necessary radiation dose (editorial). Am J Neuroradiol 25:519

George P, Huges J (1990) Respiratory system. In: Summitt RL (ed) Comprehensive pediatrics. Mosby, New York

Glasier CM, Mallory GB, Steele RW (1989) Significance of opacification of the maxillary and ethmoid sinuses in infants. J Pediatr 114:45–50

Gordts F, Clement PA, Destryker A et al (1997) Prevalence of sinusitis signs on MRI in a non-ENT pediatric population. Rhinology 35:154–157

Greess H, Lutze J, Nomayr A et al (2004) Dose reduction in subsecond multislice spiral CT examination of children by online tube current modulation. Eur Radiol 14:995–999

Gündogdu S, Mahmutyazicioglu K, Ozdemir H, Savranlar A, Asil K (2005) Assessment of image quality of a standard and three dose-reducing protocols in adult cranial CT. Eur Radiol 5(9):1959–1968

Hagtvedt T, Aalokken TM, Notthellen J et al (2003) A new low-dose CT examination compared with standard-dose CT in the diagnosis of acute sinusitis. Eur Radiol 13:976–980

Hart D, Wall BF (2004) UK population dose from medical X-ray examinations. Eur Radiol 50:285–291

Hein E, Rogalla P, Klingebiel R et al (2002) Low-dose CT of the paranasal sinuses with eye lens protection: effect on image quality and radiation dose. Eur Radiol 12:1693–1696

Huda W, Atherton JV, Ware DA et al (1997) An approach for the estimation of effective radiation dose at CT in pediatric patients. Radiology 203:417–422

International Commission on Radiological Protection (1991) Recommendations of the International Commission on Radiological Protection. ICRP report 60. Ann ICRP 21 (1–3), 1991

Kalra MK, Maher MM, Toth TL et al (2004) Techniques and applications of automatic tube current modulation. Radiology 233:649–657

Kearny SE, Jones P, Meakin K et al (1997) CT scanning of the paranasal sinuses – the effect of reducing mAs. Br J Radiol 70:1071–1074

Kronemer KA, McAlister WH (1997) Sinusitis and its imaging in the pediatric population. Pediatr Radiol 27:837–846

Loubele M, Jacobs R, Maes F et al (2005) Radiation dose vs. image quality for low-dose CT protocols of the head for maxillofacial surgery and oral implant imaging. Radiat Prot Dosimet 117:211–216

Marmolya G, Wiesen EJ, Yagan R et al (1991) Paranasal sinuses: low-dose CT. Radiology 181:689–691

McAlister WH, Lusk R, Muntz HR (1989) Comparison of plain radiographs and coronal CT scan in infants and children. AJR Am J Roentgenol 153:1259–1264

McAlister WH, Parker BR, Kushner DC et al (2000) Sinusitis in the pediatric population. American College of Radiology. ACR Appropriateness Criteria, 1999. Radiology 215 [Suppl]:811–818

McCollough CH, Bruesewitz RT, Kofler JM (2006) CT dose reduction and dose management tools: overview of available options. Radiographics 26:503–512

McCrohan JL, Patterson IF, Gagne RM et al (1987) Average radiation doses in standard head examination for 250 CT systems. Radiology 163:263–268

Mulkens TH, Broers C, Fieuws S et al (2005a) Comparison of effective doses for low-dose MDCT and radiographic examination of sinuses in children. AJR Am J Roentgenol 184:1611–1618

Mulkens TH, Bellinck P, Baeyaert M et al (2005b) Use of an automatic exposure control mechanism for dose optimization in multidetector-row CT examinations: clinical evaluation. Radiology 237:213–223

Mullins ME, Lev MH, Bove P et al (2004) Comparison of image quality between conventional and low-dose nonenhanced head CT. Am J Neuroradiol 25:533–538

Rao VM, el-Noueam KI (1998) Sinonasal imaging. Anatomy and pathology. Radiol Clin North Am 36:921–939

Rehani MM, Berry M (2000) Radiation doses in computed tomography. Br Med J 320:593–594

Rogers LF (2001) Taking care of children: check out the parameters used for helical CT (editorial). AJR Am J Roentgenol 176:287

Rustemeyer P, Streubuhr U, Suttmoeller J (2004) Low-dose dental computed tomography: significant dose reduction without loss of image quality. Acta Radiol 45:847–853

Shah R, Gupta AK, Rehani MM et al (2005) Effect of reduction in tube current on reader confidence in paediatric computed tomography. Clin Radiol 60:224–231

Shrimpton PC, Jones DG, Hillier MC et al (1991) Survey of CT practice in the UK, NRPB-R249. National Radiological Protection Board, Chilton

Sohaib SA, Peppercorn PD, Horrocks JA et al (2001) The effect of decreasing mAs on image quality and patient dose in sinus CT. Br J Radiol 74:157–161

Suojanen JN, Regan F (1995) Spiral CT scanning of the paranasal sinuses. Am J Neuroradiol 16:787–789

Tack D, Widelec J, De Maertelaer V et al (2003) Comparison between low-dose and standard-dose multidetector CT in patients with suspected chronic sinusitis. AJR Am J Roentgenol 181:939–944

Van Unnik J, Broerse JJ, Geleijns J et al (1997) Survey of CT techniques and absorbed dose in various Dutch hospitals. Br J Radiol 70:367–371

Wall BF, Hart D (1997) Revised radiation doses for typical X-ray examinations. Br J Radiol 70:437–439

Wong ETH, Yu SK, Lai M et al (2001) MAPD – an objective way to select mAs for paediatric brain CT. Br J Radiol 74:932–937

Yeoman LJ, Howarth L, Britten A et al (1992) Gantry angulation in brain CT: dosage implications, effect on posterior fossa artifacts, and current international practice. Radiology 184:113–116

Zinreich SJ, Benson ML, Oliveiro PJ (1996) Sinusonasal cavities: CT normal anatomy, imaging of the osteomeatal complex, and functional endoscopic sinus surgery. In: Harnsberger HR (ed) Head and neck imaging, 3rd edn. St. Louis, Mosby

Zwirewich CV, Mayo JR, Müller NL (1991) Low-dose high resolution CT of lung parenchyma. Radiology 180:413–417

Dose Reduction and Optimization in Computed Tomography of the Chest

10

Pierre Alain Gevenois and Denis Tack

CONTENTS

10.1 Introduction

Since the late 1980s, helical computed tomography (CT) has revolutionized diagnostic imaging of the chest. Single-detector CT scanners (SDCT) and, more recently, multi-detector CT scanners (MDCT) have markedly increased the number of indications of CT. As a result, the number of CT examinations performed has increased dramatically, as have the average scanned volume per patient and the number of acquisitions per examination. The subsequent increase in collective radiation dose has been of concern to radiologists, medical physicists and governmental regulatory authorities and it has been suggested that the radiation dose used for CT was excessive (Rogers 2001a, b).

The radiation dose received by patients undergoing diagnostic radiological examinations by CT is generally in the order of 1–24 mSv per examination for adults (UNSCEAR 2000) and 2–6.5 mSv for children (Shrimpton et al. 2003). These effective doses can be classified as low even though they are invariably greater than those from conventional radiography. Typically, a chest radiographic examination with two views delivers a dose ranging from 0.08 to 0.30 mSv. In contrast, a standard-dose MDCT delivers 8 mSv, i.e. a 100-fold risk of death by cancer. In other words, one death by cancer is expected every 250,000 chest X-rays and every 2,500 MDCT examinations. Most importantly, more than one-half of the collective radiation dose delivered for diagnostic imaging procedures is due to CT examinations (Golding and Shrimpton 2002). Consequently, particular attention has to be paid to dose optimization and dose reduction, and radiologists and medical physicists should be aware of their responsibility in achieving the appropriate balance between the image quality necessary for diagnostic purposes and the amount of radiation dose delivered to patients (Golding and Shrimpton 2002). In the rapidly evolving field of MDCT, the quest for the highest image quality supposed to lead to the greatest diagnostic efficacy has obscured possible issues regarding the radiation dose. In this chapter we review the interactions between image quality, diagnostic performances and radiation dose. We specifically focus on clinical advances in dose reduction in chest CT.

Although CT is an imaging technique that uses relatively high radiation doses, it should be noted that it has replaced other techniques – such as pulmonary angiography and bronchography – that delivered even higher doses. Nevertheless, a further step in reducing the radiation dose is needed as CT has become the main source of the radiation delivered by medical procedures.

P. A. Gevenois, MD, PhD
Professor of Radiology, Clinic of Chest Imaging, Department of Radiology, Hôpital Erasme, Université libre de Bruxelles, Route de Lennik 808, 1070 Brussels, Belgium
D. Tack, MD, PhD
Clinic of Cardiac Imaging, Department of Radiology, Hôpital Erasme, Université libre de Bruxelles, Route de Lennik 808, 1070 Brussels, Belgium

10.2 Routine Chest CT

The concept of reducing the radiation dose in chest CT was first introduced by Naidich et al. (1990), who reduced the tube current on incremental 10-mm-collimation CT, and demonstrated that with low tube current settings (i.e. 20 mAs), the image quality is sufficient for assessing the lung parenchyma. While these images are sufficient for assessing lung parenchyma, the increased noise results in marked degradation of the quality of images photographed with mediastinal window settings. Because of this, these authors recommended that such low-dose techniques should be most suitable for children and for screening. As such, these recommendations have been implemented and further studied in lung cancer screening programs (Henschke et al. 1999; Itoh et al. 2000; Swensen et al. 2002).

Similar dose reduction strategies have been applied to thin-section CT, in which no significant difference in lung parenchyma structures was detectable between low doses (i.e. 40 mAs) and high doses (i.e. 400 mAs) (Lee et al. 1994; Zwirewich et al. 1991). Although observed differences were not statistically significant, changes in ground-glass opacity were difficult to assess at low-dose CT because of the increased noise. Therefore, it was recommended that 200 mAs should be used for initial thin-section CT and lower doses (i.e. 40–100 mAs) for follow-up examinations. An example of a tree-in-bud patter demonstrated at 10 mGy ($CTDI_{vol}$) and 1 mGy is shown in Figure 10.1.

The relationship between radiation exposure and image quality at mediastinal and pulmonary window settings has been evaluated on conventional 10-mm-collimation CT images on a single model of CT scanner with mAs settings ranging from 20 to 400 mAs (Mayo et al. 1987). Although this study showed a consistent increase in image quality with radiation dose, no difference in detection of mediastinal and lung abnormalities could be detected. These findings were confirmed on MDCT by Dinkel et al. (2003), who showed that a 90% reduction in dose compared with standard-dose techniques was not associated with impaired detection of suspicious lesions of malignant lymphoma and extrapulmonary tumours.

In order to investigate the effect of dose reduction without scanning patients several times at several dose levels, it is now possible to use computed simulation of dose reduction by adding random noise to the image obtained at standard dose. In a validation trial, it has been shown that experienced chest radiologists were unable to distinguish CT images obtained with simulated reduced doses from those obtained with really reduced doses (Mayo et al. 1997). This technique of simulated reduced doses

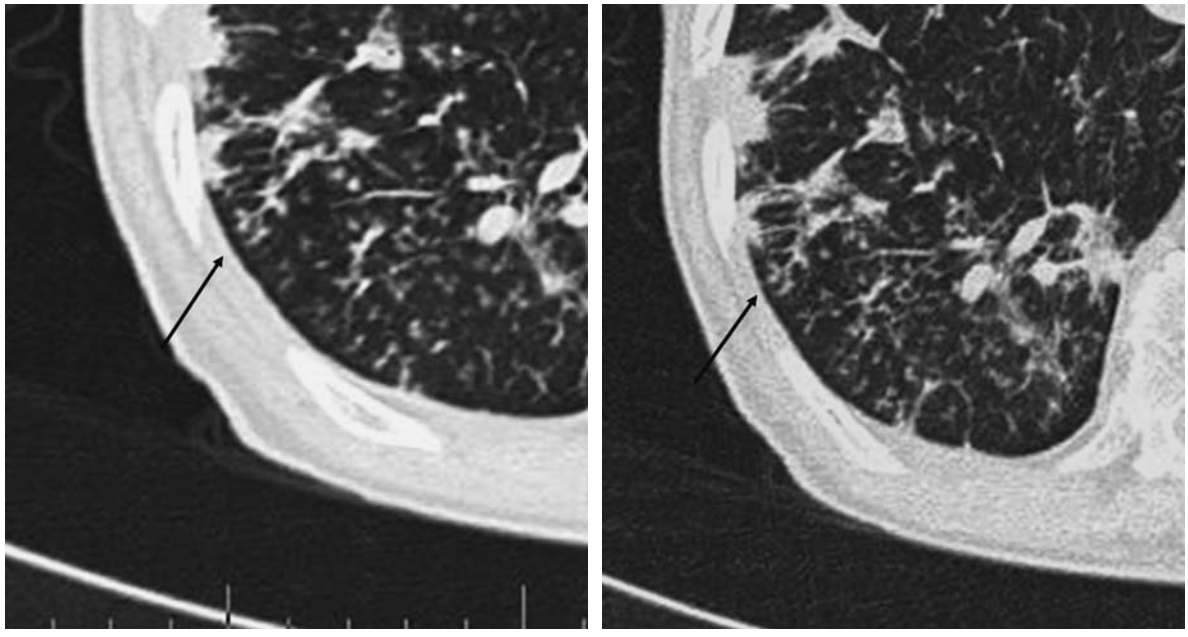

a b

Fig. 10.1a,b. High-resolution MDCT performed with a $CTDI_{vol}$ at **a** 10 mGy and **b** at 1 mGy in a patient with a tuberculous bronchiolitis. A tree-in-bud pattern (*arrow*) is identified in the right lower lobe at both radiation doses

allows investigators to determine the impact of dose reduction on the diagnostic performances without exposing patients to additional radiations and/or several injections of iodinated contrast material.

10.3 CT Pulmonary Angiography

The simulated low-dose technique has been used to evaluate the effect of dose reduction on CT pulmonary angiography. A group of 21 individuals that showed at least one filling defect within a pulmonary artery were used to simulate CT pulmonary angiography with reduced radiation doses, at 60, 40, 20 and 10 mAs. This study showed that frequencies of positive and inconclusive results of the branching order of the most distal artery with a filling defect were not changed when the tube current–time product was reduced from 90 to 10 mAs. This is illustrated in Figure 10.2. On the other hand, the quality of intravascular contrast enhancement decreased when the time current–time product setting was lower than 40 mAs. Thus, this study suggests that the reduction of the tube–current time product setting to 40 mAs to achieve a reduced radiation dose at CT pulmonary angiography appears acceptable (Tack et al. 2005).

Sigal-Cinqualbre et al. (2004) have assessed the feasibility of low kilovoltage in CT pulmonary angiography protocols and have evaluated the effect of such protocols on image quality. These authors have simultaneously reduced the tube potential and increased the mAs settings. They have shown that in patients weighing less than 75 kg, 80 kV (and 135 or 180 mAs respectively in patients weighing less than 60 or 75 kg) is sufficient to obtain the same image quality as in patients larger than 75 kg and scanned at 120 kV and 90 mAs. These results need to be confirmed and verified in indications other than CT pulmonary angiography, but this study has already suggested that reducing the tube potential could be a valid method, and an alternative to decreasing the mAs settings, of reducing the radiation dose.

As shown by H.D. Nagel in Chapter 4 of the present edition, the signal of iodine is higher at 80 kV as compared to 120 or 100 kV (Fig. 4.29). This may explain the good image quality as reported by Sigal-Cinqualbre et al. (2004) during in CT pulmonary angiography. CT pulmonary angiography images acquired at 100 and 110 kV are illustrated in Figures 6.7 and 6.8 of Chapter 6, in obese and small patients respectively.

10.4 Air Trapping and Expiratory CT

By demonstrating air-trapping, expiratory thin-section CT is able to detect a disease earlier than functional tests. This makes this technique an essential part of the diagnosis of bronchiolitis of various origins. As expiratory CT is most often obtained after inspiratory CT, this additional acquisition exposes patients to a supplementary radiation dose. This is of concern in patients with bronchiolitis, because they often can be young, and, despite their relatively favourable prognosis, have a high risk of recurrence resulting in repeated follow-up examinations and repeated exposure to CT radiation. In order to investigate the possible effect of dose reduction on the visual quantification of air trapping, we considered the "bronchiolitis obliterans syndrome" (BOS) after lung transplantation as a model for bronchiolitis (Bankier et al. 2006). In this model, we applied the simulated low-dose technique on expiratory thin-section CT examinations in patients with possible BOS. In 27 lung transplant recipients, expiratory thin-section CT was performed at 140 kVp and 80 mAs eff. Dose reduction corresponding to 60, 40, and 20 mAs eff. was simulated. This study showed that a simulated dose-equivalent to 25% of the standard dose, i.e. 20 mAs, had no substantial effect on the visual quantification of air trapping. An illustrative example is shown in Figure 10.3. Because its radiation dose approximated that of incremental thin-section CT with 10-mm section intervals performed with a standard dose, expiratory low-dose MDCT could thus be used in the assessment of air trapping in patients with suspected bronchiolitis. This model could be extended to other origins of bronchiolitis.

10.5 CT Quantification of Pulmonary Emphysema

Pulmonary emphysema is a chronic obstructive pulmonary disease (COPD) defined as a permanent distal airway enlargement with alveolar wall destruc-

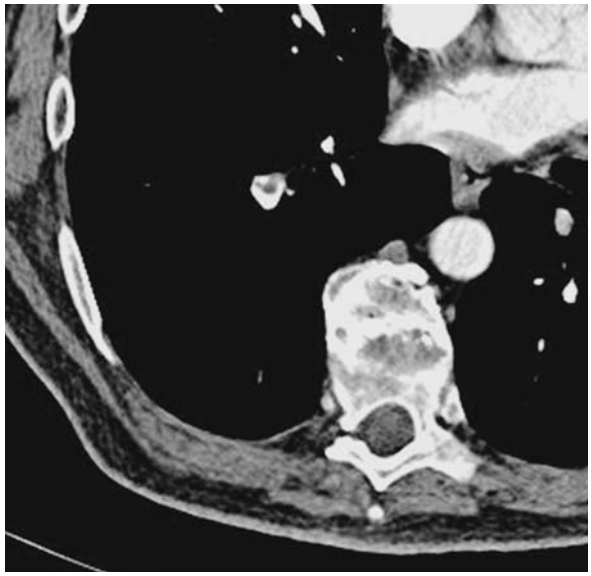
a

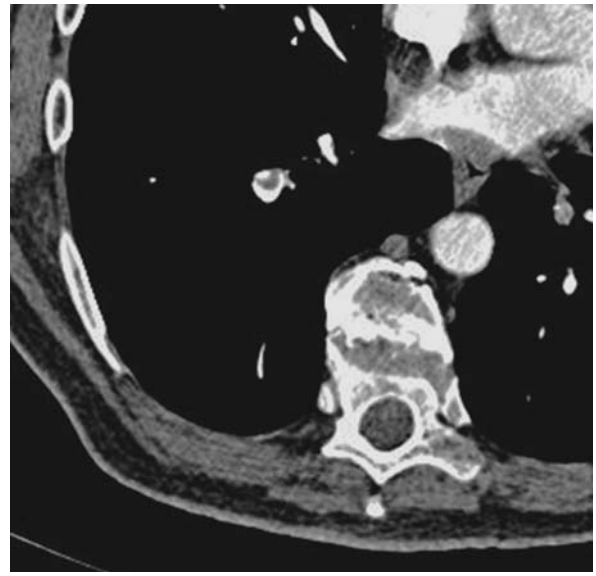
b

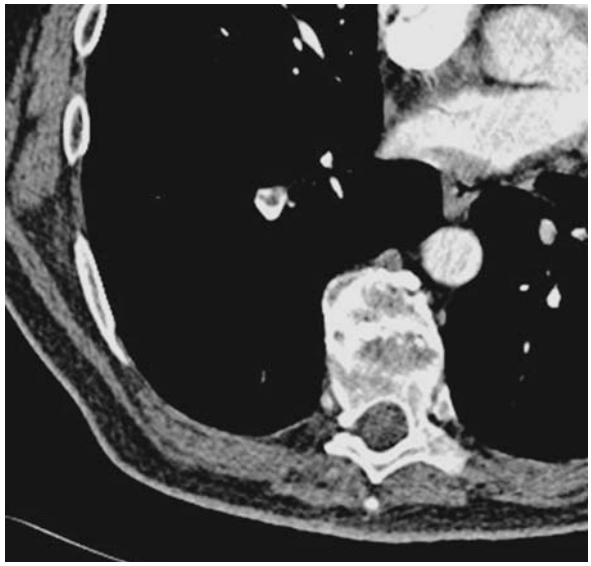
c

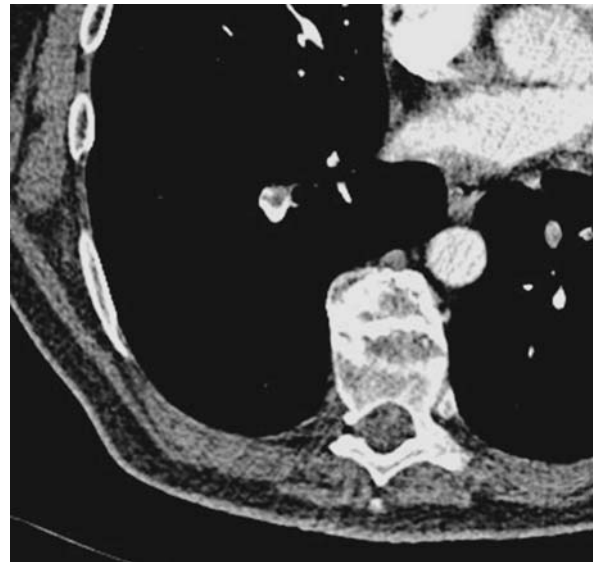
d

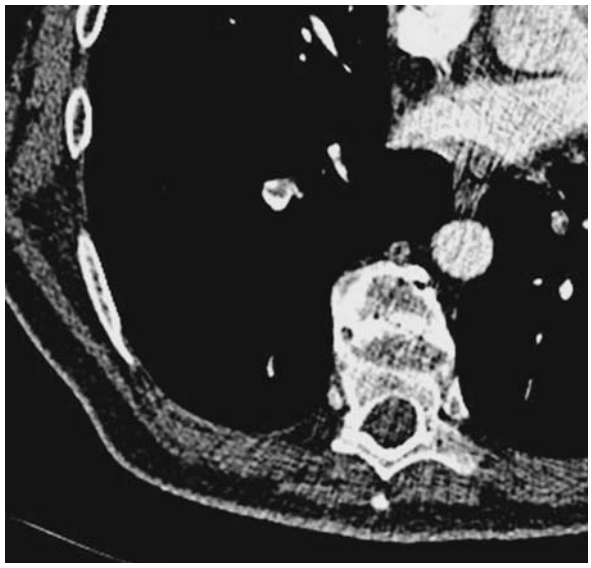
e

Fig. 10.2. a CT pulmonary angiography acquired with 120 kV and 90 mAs eff. Simulated low mAs scans at **b** 60, **c** 40, **d** 20 and **e** 10 mAs eff. are shown. An intravascular filling defect corresponding to a pulmonary embolus in a right lower lobe segmental artery is identified. Images reproduced with permission of Denis Tack and the Radiological Society of North America [Tack et al. (2005) *Radiology* 236:318–325]

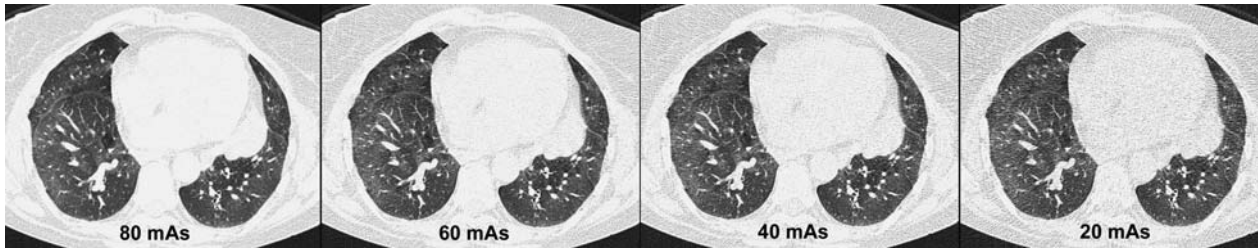

Fig. 10.3. Expiratory MDCT 140 kV and 80 mAs eff. Simulated low-mAs scans at 60, 40, and 20 mAs eff. Areas of air trapping are equally detectable at each dose. Images are courtesy of Alexander A. Bankier, Vienna, Austria

tion but without fibrosis (Snider et al. 1985). In the world, COPD is the 6th most common cause of mortality and the 12th most common cause of morbidity (Rennard et al. 2002). The severity of COPD can be, at least in part, assessed by pulmonary function tests (PFT). These tests are widely available but are unspecific. As CT yields densitometric measurements that are highly reproducible and highly correlated with morphometric measurements of alveolar wall destruction, it can be complementary to PFT in order to assess the extent and/or the severity of pulmonary emphysema. As a result, this technique has been recommended in follow-up studies, particularly in the evaluation of therapeutic interventions (Bae et al. 1997; Dirksen et al. 1999; Gierada et al. 2001; Newell et al. 2004). The recently introduced multi-detector row CT (MDCT) is of interest in the quantification of pulmonary emphysema – a heterogeneously distributed disorder – because MDCT is able to image the entire lung parenchyma. On the other hand, as this technique increases the radiation dose by an additional 300% per examination compared to incremental single-detector row CT (Studler et al. 2005), it would be important to reduce the radiation dose as patients with pulmonary emphysema can be young and may have a favourable prognosis. The level of radiation that these patients are exposed to with these examinations is compounded by repeated follow-up examinations throughout their life.

As specific drugs able to stop lung parenchyma destruction or even restore the lung growth have been elaborated and tested in animal models, it is important that individuals included in clinical trials can be imaged with the lowest possible radiation dose that provides valid measurements. We have investigated the effect of radiation dose on quantitative indexes of MDCT in pulmonary emphysema (Madani et al. 2006). In 70 patients referred for surgical resection of a lung tumour who underwent unenhanced MDCT with 4×1 mm collimation, 120 kVp, and 20 and 120 mAs eff., we compared relative areas (RA) of lung with attenuation coefficients lower than nine thresholds and eight percentiles of the distribution of attenuation coefficients with the pathological extent of emphysema. This was measured macroscopically and microscopically. We observed that radiation dose does not substantially influence the strength of the correlation between RAs (or percentiles) and pathologic references. This suggests that reducing the dose to 20 mAs eff. is safe and should be recommended in CT quantification of pulmonary emphysema, especially in patients who face repeated follow-up examinations. Nevertheless, comparisons between examinations, such as in follow-up studies, require that the dose should be kept constant.

10.6 Optimized MDCT Acquisitions Using Automatic Exposure Control

Automatic modulation of the tube current as a function of the patient's absorption is now available on all modern CT scanners. Differences still exist between manufacturers regarding the methods used for this modulation, and the dose reductions subsequently delivered. Detailed description, limitations and the results of the different automatic exposure control devices are presented and discussed by M. Kalra in Chapter 7 of the present edition. The most important feature of these devices is that the radiation dose is adapted to the patient's weight and absorption. Consequently, the role of the CT user is now restricted to select an image quality appropriate to the clinical indication of the CT examination. A rational approach for selecting this image quality is presented in Chapter 6 of the present edition.

10.7 Recommendations and Proposals

Recommendations from regulatory authorities such as the European Union are based on a balance between the theoretical radiation risk and the medical benefit expected from the CT examination. In addition, reference values for the upper limits of dose are only based on surveys studies. In this book, D. Tack has detailed these values in Tables 6.1 and 6.2 of Chapter 6. The reference value approximates 14 mGy for $CTDI_{vol}$ and ranges between 446 and 580 mGy·cm for dose–length product. However, lowering these dose values is still possible and, depending on the patient's weight, $CTDI_{vol}$ may be lowered down to 4–11 mGy (see Table 6.2 in Chap. 6). Using modern MDCT scanners and automatic exposure control devices, it is now possible to produce CT images of very high standard quality with a dose representing less than one-half of the reference values derived from survey studies. Furthermore, low-dose CT images (as for screening of lung nodules) can be obtained with doses that are 5–10 times lower than these doses considered as references (see Chap. 16.1).

10.8 Conclusion

Even if the clinical benefit of MDCT of the chest is expected to be much higher than the potential risks from radiation, reduction and optimization of the radiation dose delivered by MDCT are highly recommended in accordance with the ALARA principle. As the chest in composed of organs and structures that are characterized by high differences in attenuation values with a subsequently high spontaneous contrast, it is expected that dose could be dramatically reduced. It has indeed been documented that in numerous clinical circumstances, radiation dose cannot be higher than 10%–20% of the standard doses recommended by the scanner manufacturers (i.e. 0.6–2.5 mSv as compared to 8–14 mSv). This is of particular concern in patients with long life expectancy and can be achieved by automatic exposure control in conjunction with either reduced tube current–time product or reduced tube potential. Further investigations should be conducted in order to investigate the possible benefit of combined reduction of both tube potential and current–time product.

References

Bae KT, Slone RM, Gierada DS, Yusen RD, Cooper JD (1997) Patients with emphysema: quantitative CT analysis before and after lung volume reduction surgery. Radiology 203:705–714

Bankier AA, Schaefer-Prokop C, De Maertelaer V, Tack D, Jaksch P, Klepetko W, Gevenois PA (2006) Air trapping on thin-section CT examinations: comparison of standard-dose and simulated low-dose techniques. Radiology (in press)

Dinkel HP, Sonnenschein M, Hoppe H, Vock P (2003) Low-dose multislice CT of the thorax in follow-up of malignant lymphoma and extrapulmonary primary tumors. Eur Radiol 13:1241–1249

Dirksen A, Dijkman JH, Madsen F et al (1999) A randomized clinical trial of α1-antitrypsin augmented therapy. Am J Respir Crit Care Med 160:1468–1472

Gierada DS, Yusen RD, Pilgram TK et al (2001) Repeatability of quantitative CT indexes of emphysema in patients evaluated for lung volume reduction surgery. Radiology 220:448–454

Golding SJ, Shrimpton PC (2002) Radiation dose in CT: are we meeting the challenge? (Commentary). Br J Radiol 75:1–4

Henschke CI, McCauley DI, Yankelevitz DF et al (1999) Early Lung Cancer Action Project: overall design and findings from baseline screening. Lancet 354:99–105

Itoh H, Ikeda M, Arahata S et al (2000) Lung cancer screening: minimum tube current required for helical CT. Radiology 215:175–183

Lee KS, Primack SL, Staples CA, Mayo JR, Aldrich JE, Müller NL (1994) Chronic infiltrative lung disease: comparison of diagnostic accuracies of radiography and low- and conventional-dose thin-section CT. Radiology 191:669–673

Madani A, De Maertelaer V, Zanen J, Gevenois PA (2006) Pulmonary emphysema: impact of radiation dose and section thickness on objective quantification at multidetector row CT – comparison with macroscopic and microscopic morphometry. Radiology (in press)

Mayo JR, Webb WR, Gould R et al (1987) High-resolution CT of the lungs: an optimal approach. Radiology 163:507–510

Mayo JR, Whittall KP, Leung AN et al (1997) Simulated dose reduction in conventional chest CT: validation study. Radiology 202:453–457

Naidich DP, Marshall CH, Gribbin C, Arams RS, McCauley DI (1990) Low-dose CT of the lungs: preliminary observations. Radiology 175:729–731

Newell JD, Hogg JC, Snider GL (2004) Report of a workshop: quantitative computed tomography scanning in longitudinal studies of emphysema. Eur Respir J 23:769–775

Rennard S, Decramer M, Calverley PM, Pride NB, Soriano JB, Vermeire PA, Vestbo J (2002) Impact of COPD in North America and Europe in 2000: subjects' perspective of

Confronting COPD International Survey. Eur Respir J 20:799–805
Rogers LF (2001a) Radiation exposure in CT: why so high? AJR Am J Roentgenol 177:277
Rogers LF (2001b) Serious business: radiation safety and radiation protection. AJR Am J Roentgenol 177:1
Shrimpton PC, Hillier MC, Lewis MA et al (2003) Data from computed tomography (CT) examinations in the UK – 2003 review. NRPB – 67, National Radiological Protection Board, Chilton
Sigal-Cinqualbre AB, Hennequin R, Abada HT, Chen X, Paul JF (2004) Low-kilovoltage multidetector row chest CT in adults: feasability and effect on image quality and iodine dose. Radiology 231:169–174
Snider GL, Kleinerman JL, Thurlbeck WM et al (1985) The definition of emphysema. Report of a national Heart, Lung, and Blood Institute, Division of Lung Disease Workshop. Am Rev Respir Dis 132:182–185
Studler U, Gluecker T, Bongartz G et al (2005) Image quality from high-resolution CT of the lung: comparison of axial scans and of sections reconstructed from volumetric data acquired using MDCT. AJR 185:602–607
Swensen SJ, Jett JR, Sloan JA et al (2002) Screening for lung cancer with low-dose spiral computed tomography. Am J Respir Crit Care Med 165:508–513
Tack D, De Maertelaer V, Petit W, Scillia P, Muller P, Suess C, Gevenois PA (2005) Comparisons of standard-dose and simulated low-dose multi-detector-row CT pulmonary angiography. Radiology 236:318–325
UNSCEAR (2000) Sources and effects of ionizing radiation. United Nations Scientific Committee on the Effects of Atomic Radiation Report to the General Assembly. United Nations, New York
Zwirewich CV, Mayo JR, Müller NL (1991) Low-dose high-resolution CT of lung parenchyma. Radiology 180:413–417

Dose Optimization and Reduction in MDCT of the Abdomen

11

Caroline Keyzer, Pierre Alain Gevenois, and Denis Tack

CONTENTS

11.1 Introduction

Computed tomography is nowadays widely used in abdominal imaging in various circumstances including acute abdominal pain. This use is explained by the fact that this technique is highly reproducible, very rapid, highly sensitive and specific, quite easy to perform, and it causes little discomfort to the patient. With multi-detector row CT (MDCT) scanners, rapid volume acquisition became possible and examination of the whole abdomen is more and more frequently performed as a screening test in patients suspected of abdominal disorder. Such examinations of the whole abdomen are justified by the ability to detect alternative and/or additional diagnoses. However, since the abdomen contains sensitive organs, the radiation dose delivered to patients becomes a particular concern, especially in young patients and in those with chronic diseases who undergo repeated CT studies. Strategies to reduce the radiation dose delivered by CT have been developed and clinical investigations have shown that in several abdominal disorders the diagnostic performance of CT is not decreased by dose reduction. Reducing the dose was first investigated in conditions characterized by intrinsic high contrast between structures, such as ureteral stones, and later on in conditions characterized by intrinsic low contrast between structures, such as acute appendicitis.

C. Keyzer, MD
Department of Radiology, CHU of Charleroi, Boulevard Janson 92, 6000 Charleroi, Belgium
P. A. Gevenois, MD, PhD
Professor of Radiology, Clinic of Chest Imaging, Department of Radiology, Hôpital Erasme, Université libre de Bruxelles, Route de Lennik 808, 1070 Brussels, Belgium
D. Tack, MD, PhD
Clinic of Cardiac Imaging, Department of Radiology, Hôpital Erasme, Université libre de Bruxelles, Route de Lennik 808, 1070 Brussels, Belgium

11.2 Usual Radiation Dose and Reference Levels

Ideally, the dose delivered to the patient should be at the level below which the image quality would be insufficient to yield an accurate diagnosis. Practically, the delivered dose should be adapted first to the patient's size and second to the clinical indication. As evidence-based recommendations do not exist, guidelines have been derived from survey studies reporting the large-scale distribution of the delivered dose. The arbitrary fixed recommended dose threshold corresponds to the third quartile of the distribution observed in these surveys (Shrimpton et al. 2005), doses higher than the upper third quartile being considered as of unacceptable practice

(EUROPEAN COMMISSION 1999). Detailed results of these survey studies, conducted mainly in United Kingdom and in Germany, are reported and discussed in Chapter 5.

The guidelines established by the Commission of the European Union have proposed that reference levels for routine abdominal CT examination (from the top of the liver to the aortic bifurcation) should be, respectively for the weighted CT dose index (CTDIw) and dose–length product (DLP), 35 mGy and 780 mGy·cm. For CT examinations of the liver and the spleen, the corresponding values should be 35 mGy and 900 mGy·cm. For the pelvis, they should be 35 mGy and 570 mGy·cm (EUROPEAN COMMISSION 1999). More recently, the National Radiological Protection Board (NRPB) has reported a snapshot of doses delivered in United Kingdom in 2003 (Shrimpton et al. 2005). In this report, the third quartile value of dose distribution, expressed in DLP, was 559 mGy·cm for routine abdominal CT examination obtained with MDCT. The corresponding value for liver examination in patients with possible metastases was 472 mGy·cm. These doses are clearly lower than those proposed in 1999 by the Commission of the European Union. This lowering probably reflects the increasing concern in reducing the dose as observed recently as well as technological advances in CT technology (i.e. the introduction of solid-state detectors).

The indication of each examination is very important to consider in order to select the required image quality and subsequently the lowest acceptable radiation dose. As an example, the dose delivered when searching for metastases or for imaging trauma can be higher than that for imaging acute abdominal pain. Nevertheless, as the minimum radiation doses needed for accurate diagnosis are unknown in most abdominal disorders, many examinations are actually performed with unnecessarily elevated radiation doses.

Furthermore, with MDCT scanners, the ability to rapidly scan large volumes tempts the operator to increase this volume along the z-axis, and/or to use multiple-pass CT instead of single-pass CT. Therefore *z*-coverage should be adapted to the clinical indication and to the possible alternative diagnoses. Unjustified screening the entire abdomen because of a "you never know" policy should thus be banished. Such policy is unacceptable in young patients who are at a low risk of having an incidental associated disease. Similarly, repeated acquisitions should not be performed in circumstances where they do not specifically yield additional information.

Automatic exposure control (AEC) devices that are nowadays available in modern equipment modulate the tube current as a function of the table position along the z-axis and of the image quality requested by the radiologist. Such devices reduce the tube current in thin patients and increase it in obese and overweight patients, tending to maintain the image quality constant. Therefore, radiologists using these devices should think in terms of image quality and not of tube current. Mulkens et al. (2005) showed that systems based on both angular and z-axis modulation reduce the mean tube current by 20%–68% when applied to standard MDCT protocols at constant tube current. With such systems, these authors also showed a good correlation between the mean effective tube current and the patient's body mass index (BMI), with an adaptation in obese and overweight patients leading to the reference tube current level being exceeded. These devices, which are only a partial response to the issue of the radiation dose, are extensively described in Chapter 7.

11.3 Dose Reduction in Acute Abdominal Disorders

11.3.1 High Contrast Between Structures

Unenhanced CT has been validated for the diagnosis of ureteral stones and it has been shown to be superior to intravenous urography (IVU) (Smith et al. 1995; Katz et al. 2000; Liu et al. 2000; Hamm et al. 2001). It also has the advantage of avoiding intravenous administration of iodine contrast material and may provide the basis for suggesting or establishing alternative and/or additional diagnoses (Sourtzis et al. 1999). On the other hand, CT scanning exposes the patient to radiation doses higher than that delivered by IVU and patients with ureteral stone may be young, will have repeated control examinations, and are at risk of recurrence.

With single detector row CT (SDCT), dose reduction can be achieved by increasing the pitch and by increasing the X-ray beam width. Such modulation provides thick transverse sections that could theoretically predispose smaller stones to be missed. Nevertheless, it has been shown that the number of ureteral stones missed by using such sections is not

substantially higher than that detected by IVU. On the other hand, ureteral stones smaller than 5 mm in diameter are detected at CT but not at IVU (Liu et al. 2000). Diel et al. (2000) showed that increasing the pitch up to 2.5 or 3.0 is an effective method of reducing the radiation dose even if the image quality decreases with a pitch of 3.0. With these methods of reducing the dose, these authors delivered an effective dose ranging from 2.8 to 5.7 mSv, which is higher than doses delivered by IVU (Tack et al. 2003). Using the SDCT scanner, Hamm et al. (2002) have both reduced the tube current and increased the pitch on SDCT, resulting in a lower radiation dose than IVU. These authors showed that, except in obese patients, unenhanced SDCT has a sensitivity and specificity of 96% and 97%, respectively, for the diagnosis of ureteral stone.

Dose reduction by increasing the pitch is possible on SDCT and MDCT scanners constructed by GE and Toshiba, but not on MDCT scanners by Philips and Siemens. These two manufacturers have introduced the concept of "effective mAs"; the scanner automatically increases the tube current proportionally with the table speed, i.e. the tube current is doubled if the table speed or the pitch doubles. With these scanners, the dose and the slice profile are thus independent from the pitch. However, on the newest MDCT scanners with 16 or more detector rows, increasing the pitch factor has a negative effect on the radiation dose, because of overranging. Overranging elongates the scan length and corresponds to the dose delivered by additional rotations at the beginning and the end of the helical scan that are required for data interpolation. The amount of additional dose due to overranging depends on the pitch and the beam width, and is higher on 64 MDCT scanners than on 16 MDCT scanners. This is extensively discussed in Chapter 4.

Since MDCT scanners have been equipped with solid-state detectors, it has become possible to reduce the tube current as compared to SDCT. Using an MDCT scanner and acquisitions performed with a beam collimation of 4×2.5 mm, 120 kVp, and 30 mAs eff., Tack et al. (2003) have reported accuracy higher than 93% and excellent intra- and interobserver agreements in the detection of ureteral stone. The higher agreement reported by Tack et al. as compared to SDCT could be explained by thinner collimation with higher *z*-resolution and by the use of cine-viewing, multiplanar, and curved reformations as illustrated in Figure 11.1. The mean effective dose delivered by these authors – 1.2 mSv in men, and 1.9 mSv in woman – was approximately the same as that delivered by a three-film IVU (approximately 1.5 mSv). However, in this study performed without an AEC device, additional images obtained at 60 mAs were required to complement those at 30 mAs. This requirement could be explained by

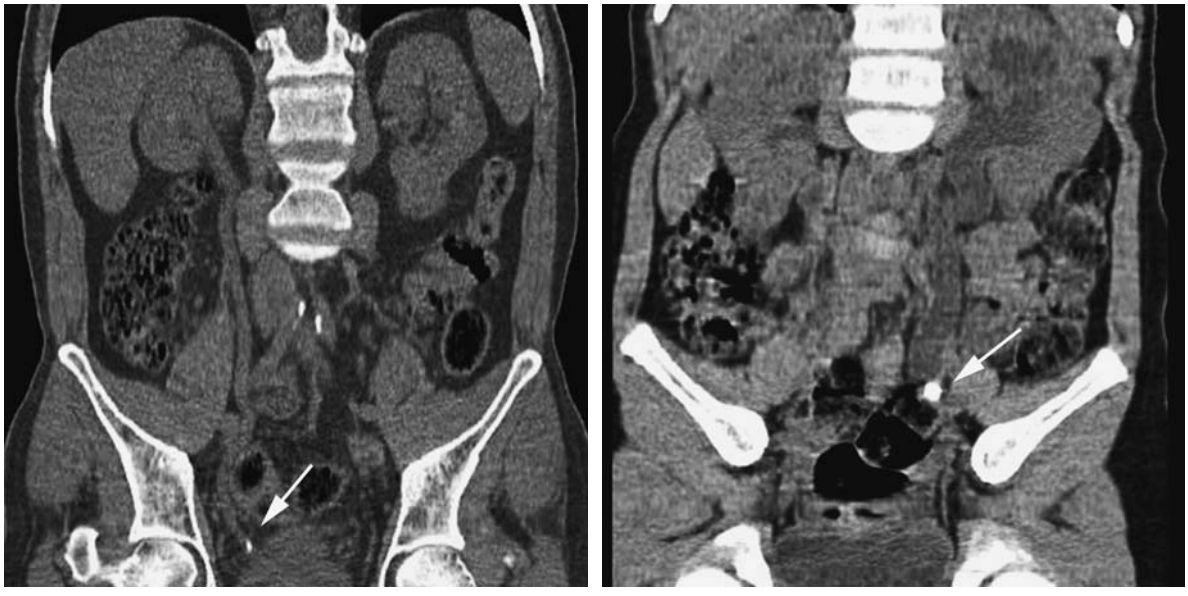

Fig. 11.1. a Ureteral stone (*arrow*). A 3 mm curved MPR from a low-dose acquisition performed with MDCT (4×2.5 mm, 120 kVp) at 30 mAs eff., without automatic exposure control (*AEC*). **b** Ureteral stone (*arrow*). A 3 mm curved MPR from a low-dose acquisition performed with MDCT (4×2.5 mm, 120 kVp) at 30 mAs eff., without AEC

greater image noise in the pelvis than in the abdomen at the same tube current due to the pelvic bones. In such circumstances, the AEC technique, unlike the fixed tube current technique, offers the opportunity to select the desired image quality in order to automatically reduce or increase the tube current according to the patient's size ("light" versus "heavy" patients) and body attenuation (abdomen versus pelvis). Kalra et al. (2005) showed that AEC along the z-axis can be used in patients suspected of urinary stone with 43%–66% dose reduction without compromising stone detectability. A recent report mentioned that ultra-low-dose MDCT – 120 kVp, 6.9 mAs eff. – delivering an effective radiation dose equivalent to one conventional abdominal X-ray view (approximately 0.5 mSv) achieved a sensitivity and specificity of, respectively, 97% and 95% for this diagnosis (Kluner et al. 2006).

Most importantly, it has been extensively demonstrated that low-dose unenhanced CT can also provide alternative diagnoses (Diel et al. 2000; Liu et al. 2000; Tack et al. 2003; Keyzer et al. 2004; Kluner et al. 2006). This will be discussed in the following paragraphs.

11.3.2 Low Contrast Between Structures

Reduction in radiation dose was first investigated in diagnostic conditions characterized by high intrinsic contrast between structures, such as lung nodule screening (Rusinek et al. 1998), CT colonography (van Gelder et al. 2002), and ureteral stones (Diel et al. 2000; Liu et al. 2000; Hamm et al. 2002; Tack et al. 2003; Kalra et al. 2005). In these early studies, it was suggested that alternative diagnoses can be made despite the reduced dose. Indeed, periureteric and perinephric fat stranding is still visible at low-dose CT (Heneghan et al. 2003), suggesting that any intra-abdominal fat stranding, as in numerous acute abdominal conditions, could also be detectable. These low intrinsic contrast conditions – characterized by peritoneal and retroperitoneal fat stranding – are visible in acute colon diverticulitis and acute appendicitis.

11.3.2.1 Acute Colon Diverticulitis

CT is known to be the optimal method for diagnosis and severity grading in patients suspected of having acute colon diverticulitis (Rao et al. 1998). In addition, CT is a fast technique and enables possible alternative and/or additional diagnoses (Birnbaum and Balthazar 1994). With the recently introduced MDCT technology, repeated acquisitions, extended z-axis coverage and thin collimations contribute to increase the radiation dose per examination as compared with that delivered with SDCT. This is especially of concern in patients with diverticulitis as they can be young and have a high risk of recurrence (Ferzoco et al. 1998).

Tack et al. (2005) compared unenhanced low-dose MDCT (30 mAs, 120 kVp) and enhanced standard-dose MDCT (120 mAs, 120 kVp) in patients suspected of acute diverticulitis. These authors showed that sensitivity and specificity are similar regardless of dose, and that CT has the potential to depict alternative disease. For the diagnosis of acute diverticulitis, the sensitivity and specificity of low-dose unenhanced MDCT range respectively from 85% to 100% and from 92% to 99%, depending on the reader, and are associated with good to excellent reader agreements. In this study, the final diagnosis was achieved without intravenous injection of iodinated contrast medium and with an effective radiation dose corresponding to that of a three-view conventional radiographic examination of the abdomen (Wall and Hart 1997). Indeed, the effective dose of low-dose CT scans obtained with the parameters used by Tack et al. was calculated at 1.6 mSv in women and 1.2 mSv in men. Fat stranding, known as an excellent sign of acute colon diverticulitis (Kircher et al. 2002), was demonstrated as the most predictive sign of this diagnosis regardless of the dose. In addition, this study revealed that low-dose MDCT enables the correct assessment of the presence of abscess and air collections distant to the colon (Fig. 11.2). Subsequently, dose reduction has no effect on the severity grading.

11.3.2.2 Acute Appendicitis

Because of its high sensitivity and specificity in the diagnosis of acute appendicitis – even without intravenous injection of iodinated contrast material (Lane et al. 1999; Ege et al. 2002) – CT has been used more and more frequently in the past decade in order to increase the accuracy of clinical diagnosis. CT, especially without any contrast material, is rapid and causes little discomfort to the patient. Nevertheless, as many individuals suspect-

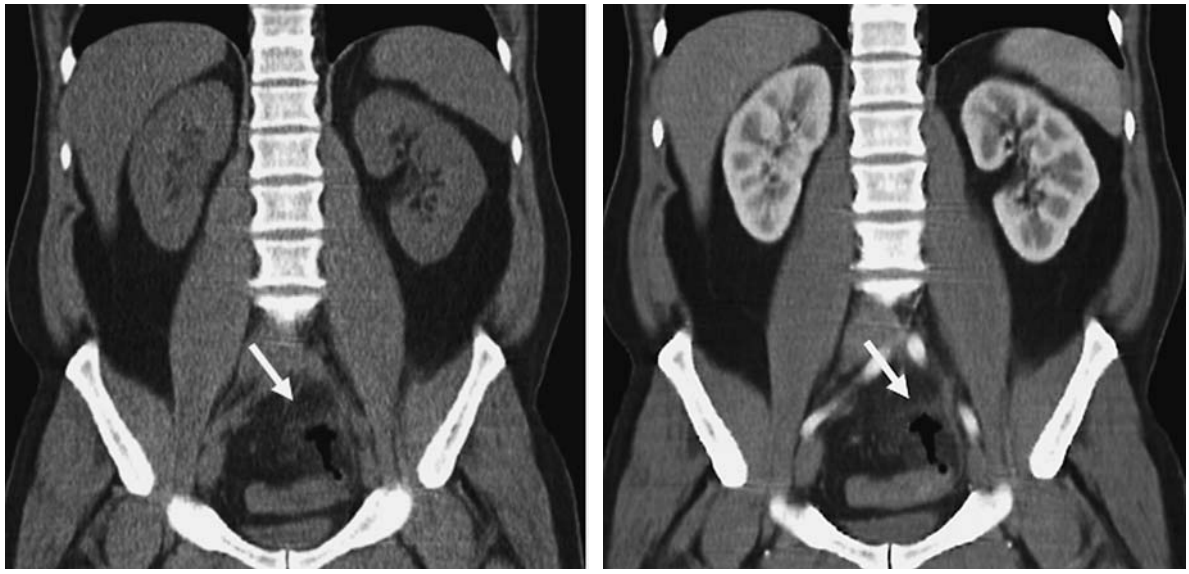

Fig. 11.2. a Acute sigmoid diverticulitis with a gaseous collection (*arrow*). Acquisition performed with MDCT (4×2.5 mm, 120 kVp) at 30 mAs eff., without AEC and without any contrast material. **b** Acute sigmoid diverticulitis with a gaseous collection (*arrow*). Acquisition performed with MDCT (4×2.5 mm, 120 kVp) at 120 mAs eff., without AEC, with intravenous iodine contrast material

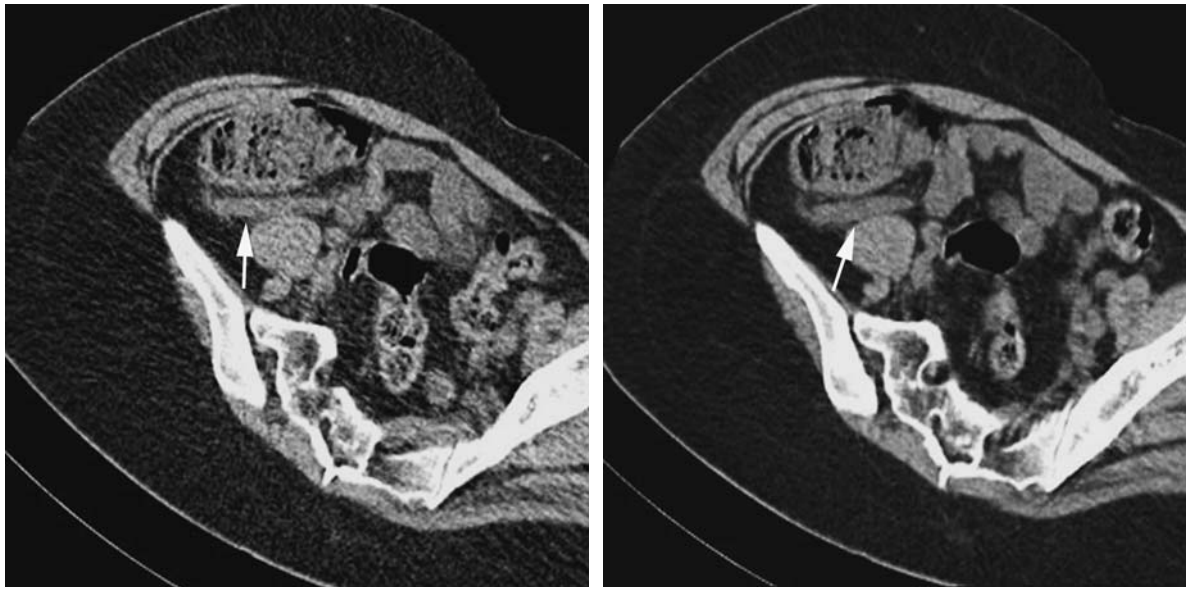

Fig. 11.3. a Acute appendicitis (*arrow*). Enlarged appendix with periappendiceal fat stranding. A 3 mm oblique reformation. Acquisition performed with MDCT (4×2.5 mm, 120 kVp) at 30 mAs eff., without AEC and without any contrast material. **b** Acute appendicitis (*arrow*). Enlarged appendix with periappendiceal fat stranding. A 3 mm-oblique reformation. Acquisition performed with MDCT (4×2.5 mm, 120 kVp) at 100 mAs eff., without AEC and without any contrast material

ed of acute appendicitis are young – with a mean age of 30 years (Flum et al. 2001) – the radiation dose should be reduced. Keyzer et al. (2004) compared unenhanced low-dose (30 mAs, 120 kVp) and standard-dose (100 mAs, 120 kVp) MDCT in patients with suspected acute appendicitis. The frequency of visualization of the appendix and the diagnostic performance were similar regardless of the radiation dose (Fig. 11.3). Unenhanced MDCT achieves sensitivity and negative predictive values of 98% or

even more. These two characteristics are the most important in patients suspected of acute appendicitis as this condition is potentially life-threatening and can be easily treated by a very efficient surgical procedure (Krieg et al. 1975). Specificity and positive predictive values are lower than sensitivity and negative predictive values but they are not different between doses. These values range respectively between 80%–94% and 69%–88%. As in acute colon diverticulitis, fat stranding – i.e. periappendiceal fat stranding – is the most predictive sign of acute appendicitis whatever the dose. Finally, the ability to propose a correct alternative diagnosis is not influenced by the dose (Fig. 11.4a, b). Another example of alternate diagnosis is illustrated in Figure 6.1 of Chapter 6 by D. Tack in the present edition.

These results could not be extended to children. Indeed, in a study performed with a phantom-based simulation technique, diagnostic performances of simulated low-dose CT (20 mAs) were reported as significantly lower than those of standard-dose CT (median, 126 mAs) (Fefferman et al. 2005). Sen-

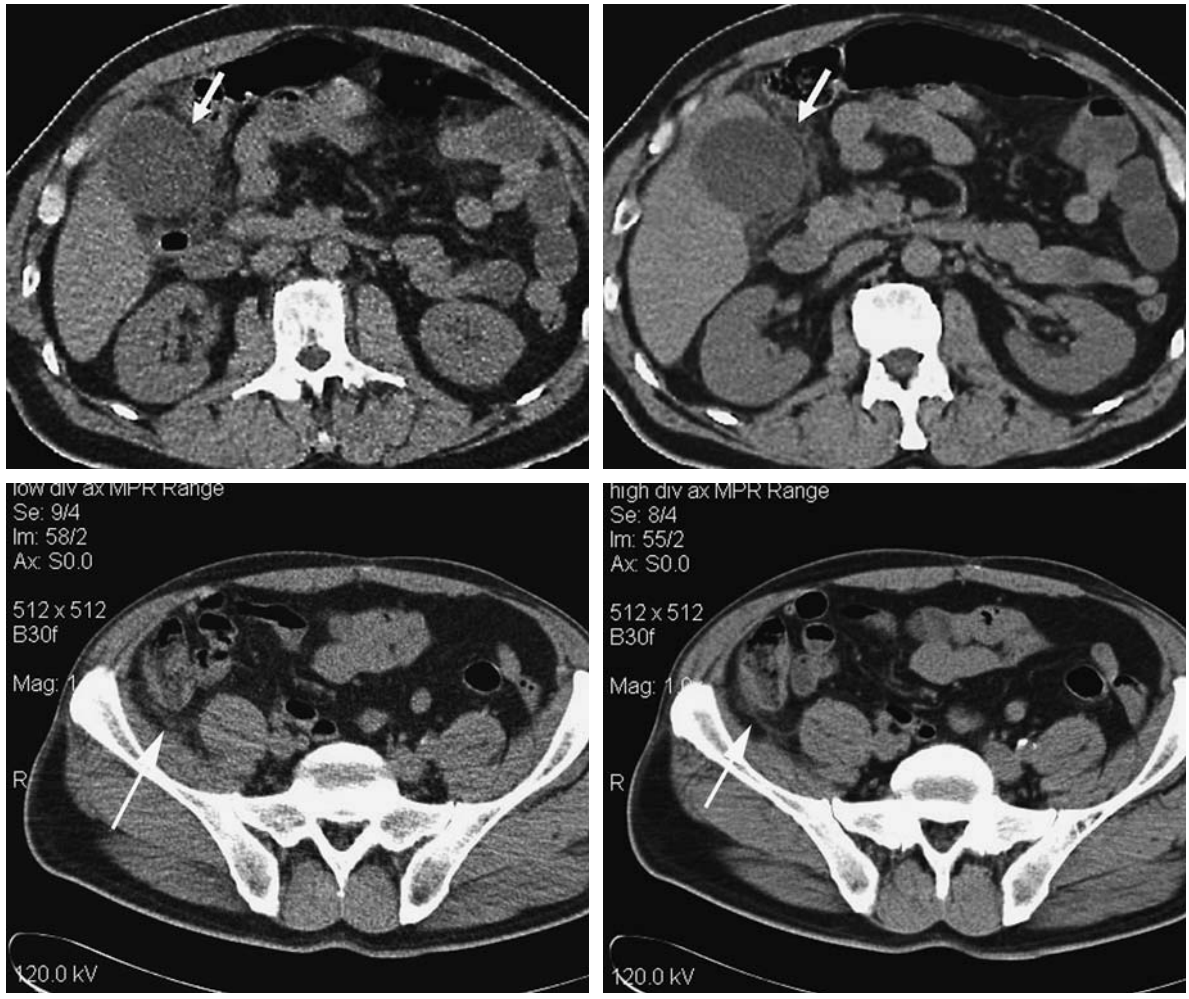

Fig. 11.4. a Patient with suspected acute appendicitis. Definite diagnosis of acute cholecystitis (*arrow*) that was visible at MDCT; 3 mm axial reconstructions. Acquisition performed with MDCT (4×2.5 mm, 120 kVp) at 30 mAs eff., without AEC and without any contrast material. **b** Patient with suspected acute appendicitis. Definite diagnosis of acute cholecystitis (*arrow*) that was visible at MDCT; 3 mm axial reconstructions. Acquisition performed at 100 mAs eff. (4×2.5 mm, 120 kVp), without AEC and without any contrast material. **c** Patient with suspected acute appendicitis. Definite diagnosis of acute caecal diverticulitis (*arrow*) that was visible at MDCT; 3 mm axial reconstructions. Acquisition performed at 30 mAs eff. (4×2.5 mm, 120 kVp), without AEC and without any contrast material. **d** Patient with suspected acute appendicitis. Definite diagnosis of acute caecal diverticulitis (*arrow*) that was visible at MDCT; 3 mm axial reconstructions. Acquisition performed at 100 mAs eff. (4×2.5 mm, 120 kVp), without AEC and without any contrast material

sitivity, specificity and accuracy are 77% versus 91%, 94% versus 93%, and 86% versus 92%, respectively, at low-dose and at standard-dose CT. It must be noted that this study was performed on SDCT and that these results have not been confirmed on MDCT.

11.4 Dose Reduction in Chronic Abdominal Disorders

In chronic disorders, repeated abdominal CT investigation are performed, even in young patients, in various conditions such as inflammatory bowel disease, pancreatitis and postoperative complications. Of course, in cases of cancer, dose reduction is of minor importance for the patient as he or she is at higher risk of dying of the existing cancer than of developing 20 years later another cancer induced by the radiation.

Most follow-up investigations need the use of intravenous contrast enhancement but no published study has evaluated the diagnostic performance of enhanced low-dose CT in chronic abdominal disorders. Studies have only compared image quality between CT at standard tube current and reduced tube current. Kalra et al. (2002) have addressed the possibility of reducing CT radiation dose in relatively thin patients (i.e. with small abdominal dimensions) with an acceptable image quality. This quality was achieved with a DLP of 550 mGy·cm (140 kVp, 120–150 mA). On the other hand, Nakayama et al. (2005) have proposed to reduce the tube voltage from 120 kVp to 90 kVp with a constant tube current of 300 mAs. These authors have shown that, despite increased noise and streak artefacts, the image quality is acceptable and that these artefacts rarely affect the diagnostic. Interestingly, with such reduction in tube voltage, the amount of contrast material can be reduced by at least 20% without degradation of image quality and organ enhancement, or sacrifice of low-contrast detectability (Funama et al. 2005). Such tube voltage reduction results in a dose reduction of 57% with CTDIw of 13.2 mGy and 5.7 mGy, at respectively 120 and 90 kVp (with a high tube current of 300 mAs). This is also of potential interest in CT angiography, which is discussed separately in Chapter 12.

11.5 Effect of Body Mass Index

Image noise increases with body size and the noise can be of huge importance in obese patients, particularly in the pelvis. Early studies were first performed on scanners that were not equipped with AEC. In these studies, mAs presets were maintained constant whatever the patient's size. With 30 mAs eff., Keyzer et al. (2004) showed that for the visualization of the appendix and the diagnosis of acute appendicitis, standard-dose and low-dose CT have equivalent diagnostic performance in patients with a BMI greater than 30 kg/m^2. This observation can be explained by the fact that the negative effect of an increase in BMI could be, at least in part, balanced by the accumulation of intra-abdominal fat around the appendix. On the other hand, for scanners not equipped with an AEC device, it has been proposed that in patients with a BMI greater than 30 kg/m^2 who are suspected of having ureteral stone or acute colon diverticulitis, the tube current should be increased up to 60 mAs eff., but maintained below the usual standard dose (Tack et al. 2003, 2005).

As detailed by H.D. Nagel in Chapter 4, the Brooks formula enables us to predict that mAs settings may be divided by a factor of 2 if the patient's diameter is reduced by 4 cm, with unchanged image quality. Thus, 60 mAs eff. in obese patients provides similar image quality to 30 mAs eff. in patients of normal mass. As the effective dose is higher in thin patients as compared to obese patients with constant CT parameters, the radiation risk for an obese patient scanned at 60 mAs eff. is similar to that of a normal-mass patient at 30 mAs eff. Using modern scanners equipped with AEC devices, the image quality and radiation risks are thus both kept constant regardless of the patient's size.

With modern scanners equipped with AEC devices, an image quality index corresponding to 50 mAs eff. is grossly equivalent to the previously investigated 30 mAs eff. (in normal-mass patients) and 60 mAs eff. (in obese patients) on 4-detector-row scanners with no AEC. Examples of optimized standard-dose and low-dose acquisitions acquired with AEC are shown in Figures 6.8–6.12 in Chapter 6 by D. Tack in the present edition.

If the dose reduction is achieved by decreasing the tube voltage from 120 to 90 kVp, the signal-to-noise ratio is decreased, implying that noise has a greater effect on images obtained at 90 kVp than on those

at 120 kVp (Nakayama et al. 2005). Therefore, the use of the low-voltage technique could be restricted to normal and underweight patients or compensated by a higher tube current. Simultaneous reduction of tube voltage and tube current needs to be investigated.

11.6 Proposals of Presets and Doses

In this paragraph, doses appropriate for abdominal MDCT will be proposed. Such proposals are still a matter of debate. They are based on published references, if there are any; if there are none, we suggest reasonable doses as used in our clinical routine.

The presets, z-axis coverage and repeated exposure before and after intravenous administration of iodinated contrast material should always be adapted to the suspected diagnosis.

The standard presets recommended by the manufacturers with regard for the guidelines from the Commission of the EU and the NRPB should only be used in patients with suspected neoplasia and/or metastasis, old patients and those with severe trauma.

In suspected diagnoses such as ureteral stone, acute appendicitis and acute diverticulitis, reducing the dose is recommended by adapting the presets to the patient's size – i.e. patient's BMI – especially in those who are young and who could have repeated follow-up CT examinations. When one of these three diseases is clinically suspected, unenhanced low-dose MDCT is recommended as a first-line examination because it can confirm the clinical suspicion as well as demonstrate alternative diagnoses. If unenhanced low-dose examination is insufficient, one acquisition at standard dose after intravenous injection of iodinated contrast material can be focused on the abnormality detected at unenhanced CT. Suggestions of presets and the effective resulting dose are listed in Table 6.2 of Chapter 6 by D. Tack in the present edition. If the equipment includes an AEC device, the image quality can even be reduced in order to ensure an additional dose reduction.

For all other suspected diagnoses for which there are no published reports, we recommend the following general guidelines. First, a tube voltage of 120 kVp can be used in clinical routine and reduced to 100 kVp in thin or underweighted patients (without any subsequent decrease in image quality). Second, 140 kVp should not be used unless in extremely obese patients, as an increase from 120 to 140 kV will increase the radiation dose by 45% to 50%. Third, an AEC device should be used. Fourth, if the reconstructed images appear too noisy, multiplanar reformation with increased slice thickness can be used (Fig. 11.5).

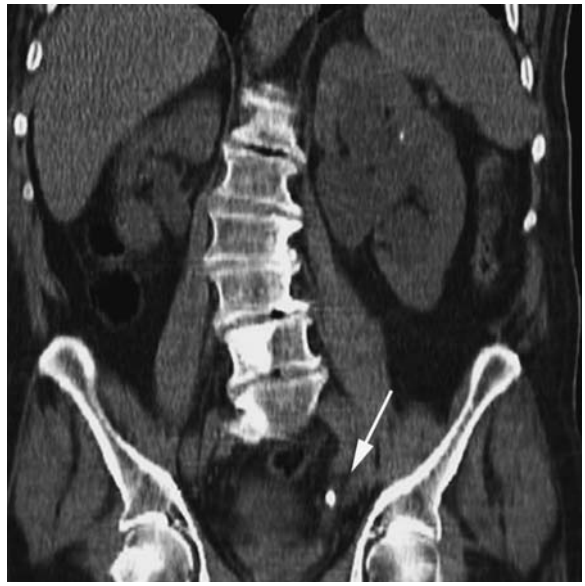

Fig. 11.5. Ureteral stone (*arrow*) 5 mm coronal MPR from a low-dose acquisition performed with MDCT (4×2.5 mm, 120 kVp) at 30 mAs eff., without AEC, in an obese patient with a BMI of 39.7 kg/m^2

11.7 Perspectives

The "as low as reasonably achievable" principle asserts that the radiation dose should be kept to a minimum while giving an image of sufficient quality to make a correct diagnosis possible. This minimal dose should be evaluated for all specific clinical circumstances. In order to investigate the relationships between the radiation dose and the diagnostic performance without repeated acquisitions (with the subsequent increased dose delivered to the patients included in such clinical investigations), noise simulation techniques could be used. Such noise simulation techniques are obviously useful in clinical trials but also in day to day routine,

as they can be used to determine the mAs settings needed to obtain the requested image quality. Such functionality is already available with some recent MDCT scanners.

In the near future, further studies are needed to investigate simultaneous tuning of tube current and tube voltage and should pay particular attention to anthropometric measurements in order to minimize the radiation dose without compromising diagnostic performance.

From a technological point of view, noise-reducing filters should be developed as a tool for imaging with very thin collimation. Indeed, thin sections are acquired with higher radiation dose than thick images, because of narrower beam collimation, slower table feed, lower scanner dose efficiency and higher tube current. Kalra et al. (2004) and Rizzo et al. (2005) have indeed demonstrated that such filters reduce the image noise quantitatively and visually, without affecting the attenuation values of both normal and abnormal tissues.

11.8 Conclusion

Survey studies have shown that collective doses have increased as MDCT has replaced SDCT. However, the radiation dose has been optimized over the last decade, mainly through AEC devices and reasonable use of tube current and tube voltage presets. This was achieved thanks to technological improvements and the willpower of several study groups to investigate the effect of dose reduction in terms of image quality and diagnostic performance. Nevertheless, as both the number of examinations and the number of clinical indications for CT increase, a major effort should be made in order to optimize the radiation dose. In addition, as survey studies have shown that great variations in doses among institutions remain, a supplementary effort should be made in order to recommend standardized acquisition protocols.

References

Birnbaum BA, Balthazar EJ (1994) CT of appendicitis and diverticulitis. Radiol Clin North Am 32:885–898

Diel J, Perlmutter S, Venkataramanan N, Mueller R, Lane MJ, Katz DS (2000) Unenhanced helical CT using increased pitch for suspected renal colic: an effective technique for radiation dose reduction? J Comput Assist Tomogr 24:795–801

Ege G, Akman H, Sahin A, Bugra D, Kuzucu K (2002) Diagnostic value of unenhanced CT in adult patients with suspected acute appendicitis. Br J Radiol 75:721–725

European Commission (1999) European Guidelines on Quality Criteria for Computed Tomography, Report EUR 16262. Brussels

Fefferman NR, Bomsztyk E, Yim AM, Rivera R, Amodio JB, Pinkney LP, Strubel NA, Noz ME, Rusinek H (2005) Appendicitis in children: low-dose CT with a phantom-based simulation technique – initial observations. Radiology 237:641–646

Ferzoco LB, Raptopoulos V, Silen W (1998) Acute diverticulitis. N Engl J Med 338:1521–1526

Flum DR, Morris A, Koepsell T, Dellinger EP (2001) Has misdiagnosis of appendicitis decreased over time? A population-based analysis. J Am Med Assoc 286:1748–1753

Funama Y, Awai K, Nakayama Y, Kakei K, Nagasue N, Shimamura M, Sato N, Sultana S, Morishita S, Yamashita Y (2005) Radiation dose reduction without degradation of low-contrast detectability at abdominal multisection CT with a low-tube voltage technique: phantom study. Radiology 237:905–10

Hamm M, Wawroschek F, Weckermann D, Knopfle E, Hackel T, Hauser H, Krawczak G, Harzmann R (2001) Unenhanced helical computed tomography in the evaluation of acute flank pain. Eur Urol 39:460–465

Hamm M, Knopfle E, Wartenberg S, Wawroschek F, Weckermann D, Harzmann R (2002) Low dose unenhanced helical computerized tomography for the evaluation of acute flank pain. J Urol167:1687–1691

Heneghan JP, McGuire KA, Leder RA, DeLong DM, Yoshizumi T, Nelson RC (2003) Helical CT for nephrolithiasis and ureterolithiasis: comparison of conventional and reduced radiation-dose techniques. Radiology 229:575–580

Kalra MK, Prasad S, Saini S, Blake MA, Varghese J, Halpern EF, Rhea JT, Thrall JH (2002) Clinical comparison of standard-dose and 50% reduced-dose abdominal CT: effect on image quality. AJR Am J Roentgenol 179:1101–1106

Kalra MK, Maher MM, Blake MA, Lucey BC, Karau K, Toth TL, Avinash G, Halpern EF, Saini S (2004) Detection and characterization of lesions on low-radiation-dose abdominal CI images postprocessed with noise reduction filters. Radiology 232:791–797

Kalra MK, Maher MM, D'Souza RV, Rizzo S, Halpern EF, Blake MA, Saini S (2005) Detection of urinary tract stones at low-radiation-dose CT with z-axis automatic tube current modulation: phantom and clinical studies. Radiology 235:523–529

Katz DS, Scheer M, Lumerman JH, Mellinger BC, Stillman CA, Lane MJ (2000) Alternative or additional diagnoses on unenhanced helical computed tomography for suspected renal colic: experience with 1000 consecutive examinations. Urology 56:53–57

Keyzer C, Tack D, De Maertelaer V, Bohy P, Gevenois PA, Van Gansbeke D (2004) Acute appendicitis: comparison of low-dose and standard-dose unenhanced multi-detector row CT. Radiology 232:164–172

Kircher MF, Rhea JT, Kihiczak D, Novelline RA (2002) Fre-

quency, sensitivity, and specificity of individual signs of diverticulitis on thin-section helical CT with colonic contrast material: experience with 312 cases. AJR Am J Roentgenol 178:1313–1318

Kluner C, Hein PA, Gralla O, Hein E, Hamm B, Romano V, Rogalla P (2006) Does ultra-low-dose CT with a radiation dose equivalent to that of KUB suffice to detect renal and ureteral calculi? J Comput Assist Tomogr 30:44–50

Krieg AF, Gambino SR, Galen RS (1975) Why are clinical laboratory tests performed? When are they valid? J Am Med Assoc 233:76–78

Lane MJ, Liu DM, Huynh MD, Jeffrey RB, Mindelzun RE, Katz DS (1999) Suspected acute appendicitis: nonenhanced helical CT in 300 consecutive patients. Radiology 213:341–346

Liu W, Esler JS, Kenny BJ, Goh RH, Rainbow AJ, Stevenson GW (2000) Low-dose nonenhanced helical CT of renal colic: assessment of ureteric stone detection and measurement of effective dose equivalent. Radiology 215:51–54

Mulkens TH, Bellinck P, Baeyaert M, Ghysen D, Van Dijck X, Mussen E, Venstermans C, Termote JL (2005) Use of an automatic exposure control mechanism for dose optimization in multi-detector row CT examinations: clinical evaluation. Radiology 237:213–223

Nakayama Y, Awai K, Funama Y, Hatemura M, Imuta M, Nakaura T, Ryu D, Morishita S, Sultana S, Sato N, Yamashita Y (2005) Abdominal CT with low tube voltage: preliminary observations about radiation dose, contrast enhancement, image quality, and noise. Radiology 237:945–951

Rao PM, Rhea JT, Novelline RA et al (1998) Helical CT with only colonic contrast material for diagnosing diverticulitis: prospective evaluation of 150 patients. AJR Am J Roentgenol 170:1445–1449

Rizzo SMR, Kalra MK, Schmidt B, Raupach R, Maher MM, Blake MA, Saini S (2005) CT images of abdomen and pelvis: effect of nonlinear three-dimensional optimized reconstruction algorithm on image quality and lesions characteristics. Radiology 237:309–315

Rusinek H, Naidich DP, McGuinness G, Leitman BS, McCauley DI, Krinsky GA, Clayton K, Cohen H (1998) Pulmonary nodule detection: low-dose versus conventional CT. Radiology 209:243–249

Shrimpton PC, Hillier MC, Lewis MA, Dunn M (2005) National Radiological Protection Board. Doses from computed tomography (CT) examinations in the UK – 2003 Review. NRPB-W6

Smith RC, Rosenfield AT, Choe KA, Essenmacher KR, Verga M, Glickman MG, Lange RC (1995) Acute flank pain: comparison of non-contrast-enhanced CT and intravenous urography. Radiology 194:789–794

Sourtzis S, Thibeau JF, Damry N, Raslan A, Vandendris M, Bellemans M (1999) Radiologic investigation of renal colic: unenhanced CT compared with excretory urography. AJR Am J Roentgenol 172:1491–1494

Tack D, Sourtzis S, Delpierre I, De Maertelaer V, Gevenois PA (2003) Low-dose unenhanced multidetector CT of patients with suspected renal colic. AJR Am J Roentgenol 180:305–311

Tack D, Bohy P, Perlot I, De Maertelaer V, Alkeilani O, Sourtzis S, Gevenois PA (2005) Suspected acute colon diverticulitis: imaging with low-dose unenhanced multidetector row CT. Radiology 237:189–196

van Gelder RE, Venema HW, Serlie IWO, Nio CY, Determann RM, Tipker CA, Vos FM, Glas AS, Bartelsman JFW, Bossuyt PMM, Laméris JS, Stoker J (2002) CT colonography at different radiation dose levels: feasibility of dose reduction. Radiology 224:25–33

Wall BF, Hart D (1997) Revised radiation doses for typical X-ray examinations: report on a recent review of doses to patients from medical X-ray examinations in UK by NRPB. Br J Radiol 70:437–439

Optimization of Radiation Dose in Cardiac and Vascular Multirow-Detector CT

12

Jean-François Paul and Hicham T. Abada

CONTENTS

J.-F. Paul, MD
Radiologie, Centre Chirurgical Marie Lannelongue, 133 avenue de la Résistance, 92350 Le Plessis-Robinson, France
H. T. Abada, MD
Clinical Associate Professor, Dept. of Radiology, Vascular and Interventional Section, University of Iowa Hospitals and Clinics, 200 Hawkins Drive, 3897 JPP, Iowa City, IA 52242, USA

12.1 Optimization of Radiation Dose in Cardiac Detector Row CT

12.1.1 Introduction

The radiation dose is becoming a major issue for contrast-enhanced cardiac CT (coronary CT angiography), because the radiation level associated with ECG-gated acquisition is generally higher than that with other CT acquisitions. However, multiphasic acquisitions of other organs (for example liver) may also be associated with a comparable or even higher total radiation, so this large radiation dose is not specific to cardiac CT.

The radiation dose delivered for coronary CT angiography is necessarily high, because only part of the total radiation delivered is used for the reconstruction of the image. The "useful" radiation corresponds to a temporal window of one phase of the cardiac cycle (for example mid-diastole). This temporal window is determined by the rotation time of the machine: its value is about half the rotation time for a monophasic reconstruction. This temporal window may be shortened in multisegment reconstruction (by a factor of 2 if data are provided from two different cycles). Nevertheless, on average, only 20% of the radiation burden is used to reconstruct one phase of the cardiac cycle (Fig. 12.1).

This is the main reason for the high radiation levels associated with coronary CT angiography. CTDI for coronary CT angiography may reach or pass 100 mGy, which is a very high radiation dose, with a dose length product (DLP) of up to 2000 mGy·cm(100 mGy × 20 cm) if the entire thorax is scanned. For a thoracic acquisition, a DLP of 2000 corresponds to a radiation dose of 33 mSv (male patients) to 40 mSv (female patients). This may be required in cases of bypass patency evaluation or ascending aorta evaluation associated with coronary artery studies. Due to these high radiation

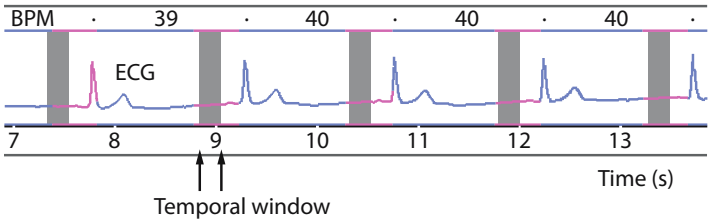

Fig. 12.1. ECG-gated acquisition: the temporal window is represented by the *grey* area. This window corresponds to the "useful" radiation exposure time

levels, it seems essential to optimize radiation dose as far as possible for cardiac CT examinations.

The various technical factors influencing radiation dose will be reviewed in the first part of this chapter. These factors vary according to the choices of the equipment manufacturer. The second part of the chapter addresses the different ways to reduce radiation dose without substantial loss of image quality, by the judicious use of the available tools and adaptation to the patient's individual anatomy. Finally, the particular issues associated with paediatric cardiac CT will be considered in the third part of this chapter.

12.1.2 Parameters which Influence Radiation Dose in Cardiac CT

12.1.2.1 General Parameters

12.1.2.1.1 Tube Power

The latest generation of CT scanners has higher tube power than earlier machines, due to the need to deliver more energy in less time for cardiac acquisitions. For example, a new dual-source CT system using two tubes has recently become available from Siemens. This new system allows delivery of a dose of at least 20% more radiation than the previous 64-slice CT scanner from the same manufacturer. The maximal CTDI of the earlier 64-slice machine was 84 mGy (using 140 kV and 700 mAs), whereas the new dual-source system gives a maximal CTDI above 100 mGy. The maximal power of machines from other manufacturers is also generally above 100 mGy. This power is useful for scanning obese patients, but on the other hand, it may be a source of unnecessarily high radiation dose in thinner patients if the settings are not modified. Consequently, individual optimization according to the patient's morphology is essential.

12.1.2.1.2 Detector Width

The efficiency of X-rays is lower at the periphery of the detector. The larger the detector, the lower the efficiency due to the wider angle of incidence of X-rays on the detector. Thus, larger detectors tend to give higher radiation doses, to provide enough radiation at the periphery of the detectors.

12.1.2.1.3 Size of the Detector

Coronary arteries are small, making sub-millimetre collimation essential for depiction of the coronaries. Thinner detectors require higher dose due to noise, growing exponentially with higher resolution. At present, detector width currently ranges from 0.5 to 0.75 mm. Resolution on the z-axis may be as low as 0.4 mm using flying spot technology (Flohr et al. 2005). This new technology has great potential because it enhances spatial CT resolution without increasing radiation dose.

12.1.2.1.4 X-Ray Filtration

"Soft X-rays" are X-rays which do not reach the detector and therefore do not contribute to the image, but nevertheless contribute substantially to the amount of radiation received by the patient. Filtration of X-rays is necessary to minimize soft X-rays. Bow-tie or beam-shaping filters are more effective than flat filters for this type of reduction of radiation dose. They are currently used in cardiac CT and are generally associated with a smaller field of view.

12.1.2.1.5 Automatic Modulation of Tube Current

This technique modulates the dose according to the patient's morphology in the x,y plane or in the z-axis, or in both, allowing substantial reduction in radiation exposure. However, this sparing-dose

technique is not fully compatible with the ECG-modulation technique used in priority in the ECG-gated protocols. The modulation in the z-axis does not work at present with ECG modulation. Although combined modulation is feasible, making possible the obtention of low-dose ECG-gated CT angiograms of the chest in routine clinical practice, using 3-mm-thick slices (D'Agostino et al. 2006), this combined modulation has not been evaluated yet for coronary arteries. Thus, it is not possible to fully modulate X-rays to the anatomical conditions automatically; consequently, individual optimization by the radiologist or CT technician is essential. This point will be developed below.

12.1.2.1.6
Rotation Time

Gantry rotation time can be up to 0.33 s. A faster rotation time results in a lower radiation dose if the current (mA) is constant. Thus, to maintain the same image quality, the tube current may have to increase, requiring much more tube power.

12.1.2.1.7
Scan Coverage

The scan coverage is set up visually on the topogram. As the total radiation dose delivered is directly proportional to scan coverage, precise adjustment of scan coverage is important for optimization of dose length product (DLP). With the new capabilities of Multidetector CT (MDCT) systems, there is a general tendency to increase the area of coverage. If the scan length is too long, for example if the scan range includes the upper part of the abdomen, unnecessary radiation will be delivered to abdominal organs. However, if the scan length is too short, for example if a portion of the coronary tree is not included in the scan range, the examination would not be complete, such that repeat scans would be required, resulting in additional radiation doses to patients. For coronary artery imaging (except for bypass imaging), starting scanning at the level of the bifurcation of the trachea is often judicious. However, the scanning start level can vary according to individual anatomy. For example, if the left ventricle is dilated, the left anterior descending coronary artery may be positioned over the plane of the bifurcation of the trachea. In contrast, in thin patients with a small, vertically oriented heart, scanning may start lower than the level of the bifurcation of the trachea, without risk of missing the proximal part of the coronary artery tree.

It is important to be able to stop the scan during the acquisition, precisely adjusting heart scanning, just after the base of the heart (if it is a cranio-caudal acquisition), so as to avoid unnecessary irradiation of the upper abdomen. However, not all machines currently used allow manual interruption of CT acquisition. Adjustment of scan length requires careful attention by the CT technicians to optimize radiation dose. Scan length optimization from the topogram may be difficult because heart position may vary with breathing.

12.1.2.1.8
Pitch

The pitch is defined by the ratio of table feed per gantry rotation to the nominal width of the X-ray beam. An increase in the pitch decreases radiation exposure, as time of exposure is shorter. For cardiac CT, pitch is usually fixed by the manufacturer, for optimization of cardiac synchronization. Users are generally not allowed to change this parameter. With the latest CT system (Definition from Siemens), pitch may vary automatically with the heart rate. Using automated table speed adaptation, this new CT increases pitch with higher heart rates, resulting in a faster table speed and a corresponding reduction of radiation exposure. This new feature makes it possible to decrease dose with higher heart rates, which was not possible with previous systems. Thus, this new generation machine allows two ways of reducing dose according to the patient's heart rate: either by ECG modulation at heart rates below 70 beats per minute, or by increasing pitch at higher heart rates.

12.1.2.2
Specific Cardiac Parameters

12.1.2.2.1
Prospective or Retrospective Acquisition

The first cardiac CT system was the electron-beam CT, available since the 1980s. Very fast acquisition times (100 or even 50 ms) were already available in the early 1980s, making it possible to obtain images free from heart motion artefacts. These images are scanned prospectively using electron-beam technology. The ECG can trigger a sequential image. However, images were acquired with a low spatial resolution (3 mm thickness), and the total time of acquisition

was long, depending on the heart rate. For example, 40 s was required to create 40 3-mm-thick images at the heart rate of 60 beats per minutes.

In a prospective mode, one image is acquired sequentially during the same phase of the cardiac cycle. The whole exposure time is used for one image: there is no unnecessary radiation exposure in any other phase of the cardiac cycle. Consequently, prospective acquisition requires a much shorter exposure time than retrospective acquisition: radiation exposure is about 4 times less (Hunold et al. 2003). Note that with the recent Multidetector CT (MDCT) system, it is still possible to obtain prospective gated images. This mode is currently used for calcium scoring, but not usually for contrast-enhanced coronary imaging. Prospective acquisition with Multidetector CT (MDCT) systems is associated with lower radiation doses (2–3 mSv for a whole heart) (Hunold et al. 2003).

12.1.2.2.2 ECG-dependant Dose Modulation

All recent coronary CT angiography studies are acquired using retrospective acquisitions. The tube current ECG-dependant modulation is currently the most effective technical tool for radiation dose reduction during retrospectively gated acquisitions, without loss of image quality, if the cardiac rhythm is regular. The irradiation may be reduced by up to 50% by application of a simple principle: radiation dose is decreased by up to 80% during the systolic phase, and the full dose is delivered only during the diastolic phase (Fig. 12.2). Thus, in principle, dose reduction is applied only during the phases that are not necessary for interpretation of coronary arteries (phases associated with heart motion), and there is no loss for the "useful" phases (phases when the heart is still).

ECG modulation is activated prospectively, based on the previous cardiac beats. There is a major drawback with the ECG modulation technique: it is not satisfactory in cases of arrhythmia or of premature contraction of the heart, because the systolic or diastolic phases are then not correctly predicted. In these cases, there is a large risk of reconstruction during a low radiation dose phase, with consequent substantial loss of image quality (images being very noisy due to insufficient current). Thus, in cases of cardiac arrhythmia, it is not recommended to activate the ECG-modulation tool because there is a high probability of reduction of tube current during the diastolic phase. New algorithms will soon be provided by the manufacturers to detect premature contraction of the heart automatically and thereby stop ECG modulation in a real-time mode during the acquisition. These technical advances in ECG modulation are to be welcomed, because they may facilitate the generalization of the use of these tools in daily practice.

There is another important drawback of ECG modulation: some end-systolic phases allow a better analysis of the coronary arteries than any reconstruction during the diastolic phase. This is common when the heart rate is above 65 beats per minute, and the diastolic phase is therefore too short to create a reconstruction free of motion artefacts. For this reason ECG modulation should not be used systematically for heart rates above 65 beats per minute; it is nevertheless recommended for regular cardiac rhythms below 65 beats per minute. It is important that the users can themselves adjust the temporal amplitude of the modulation. For example, if the heart rate is above 70 beats per minute, it may be

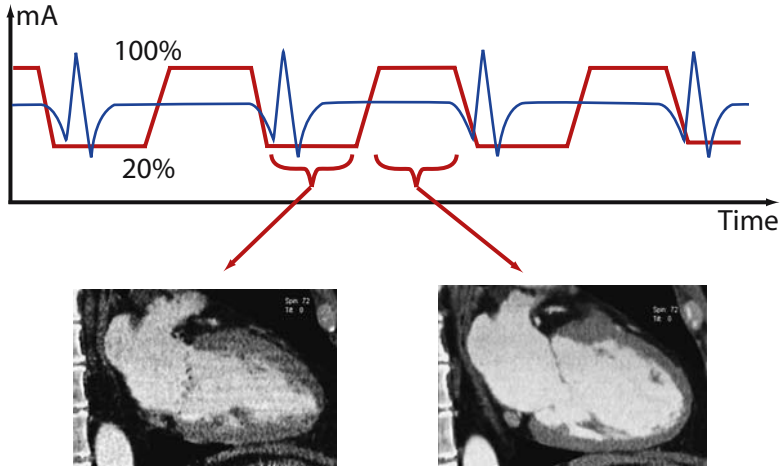

Fig. 12.2. Using ECG modulation, the tube current may be lowered at 20% of the nominal tube current value in the systolic phase, responsible for a noisy systolic image (*left*). However, full dose is applied during the diastolic phase, responsible for high-quality images when the heart is still (*right*)

valuable to have the mid-diastolic and end-systolic images at full dose. In contrast, a regular low heart rate may be scanned with a full dose period limited to diastole, favouring overall dose reduction.

In clinical routine, authors report ECG modulation use in 82% of cases (Hausleiter et al. 2006) without substantial impairment of image quality. However, in some rare cases, an unexpected premature heart beat may occur, causing partial image degradation related to dose modulation. In our experience, this is rare, and should not prevent systematically attempting to use this powerful dose-reducing tool.

It is important to underline that the efficiency of the ECG modulation varies with the cardiac rhythm: the lower rhythm, more efficient is the modulation, because the full dose phase is proportionally shorter within the cardiac cycle. Consequently, the use of beta-blockers enhances radiation dose efficiency if ECG modulation is active, by lowering cardiac rhythm and thereby lengthening the diastolic phase.

12.1.3 Radiation Dose Strategies in Cardiac CT

12.1.3.1 Judicious Use of ECG Modulation

With 64-slice CT from some manufacturers (for example the Lightspeed 64 from General Electric), it is possible to set the period of dose modulation and to adjust the current level at the full and the reduced doses. These tools are very beneficial for optimal use of ECG modulation; for example, if the cardiac rhythm is regular, sinusal and below 65 beats per minute, the best reconstruction will be round 75% with a high probability. In such cases it is possible to adjust the full dose to between 70% and 80% of the RR interval. If the current is reduced to 20% of the tube current during the modulation, the total reduction of dose would be 64%. For a heart rate higher than 70 beats per minute, the correct time for reconstruction may vary from 30% to 80%. It is advisable to set the full dose period from 30% to 80% for patients with a high heart rate: in these cases the overall reduction of dose over a cardiac cycle would be 40%.

12.1.3.2 Individual Optimization

Generally, standard CT protocols lead to higher radiation doses for slim than for normal or over-weight patients, because attenuation of X-rays is lower in slim patients. This is particularly true for coronary CT imaging, and adaptation of the parameters (mAs and kilovoltage) is essential for radiation dose optimization. Many studies show that mAs can be lowered without impairment of image quality according to the patient's body mass index (BMI) or weight. For coronary CT angiography, individually weight-adapted protocols have been successfully applied, by adjusting mAs to the patient's weight (Jung et al. 2003). Reduction of dose was 17.9% for men, and 26.3% for women, keeping noise constant. More recently, use of a lower kilovotage setting has been shown to be possible with an additional benefit on iodine dose (Sigal-Cinqualbre et al. 2004), because iodine attenuation is higher at lower kilovoltage settings. Settings of 100 kV and 80 kV have been successfully used for thoracic and even cardiac studies, especially in slim patients and children. Because radiation dose is proportional to the square of the kilovoltage, a reduction from 120 kV to 80 kV at the same current setting allows a 65% decrease in radiation dose.

12.1.3.2.1 A Simple Method: Small, Medium or Large

The simplest method for an individually adapted approach to dose reduction is to divide patients into three categories: slim, normal and over-weight. Each category has its own set parameters. This method allows a substantial reduction of the radiation dose in slim patients, for example by using 100 kV settings (Hausleiter et al. 2006). However, this classification is rather subjective unless using weight or BMI for classification. For routine thoracic imaging, 80 kV acquisitions have been successfully used for patients weighing less than 75 kg (Sigal-Cinqualbre et al. 2004). There are obviously considerable differences in chest attenuation, especially between men and women, because of the breasts. Also, there are large differences in fat distribution between individuals. Consequently, the impact of this approach, with its inaccuracies, is limited.

12.1.3.2.2 The Noise Approach

To improve individually adapted parameters, we are developing a noise-based approach in our centre using an image from the pre-control CT acquisition. This concept is applicable for CT machines, but the

values would be specific for each. With the Siemens Sensation 64, the pre-control image is set at 120 kV and 20 mAs. An image of the heart is acquired to define the region of interest (ROI) over the aorta. The principle is to calculate the noise on this image, and thereby predict the sufficient and necessary radiation level for each individual. Because there is a substantial difference in attenuation between the upper and the lower parts of the heart, we use the bottom part of the heart for the pre-control scan, to find the region with maximal attenuation as the reference.

We trace a ROI over the left ventricle and the noise corresponds to the value of the standard deviation within the ROI (Fig. 12.3). In women with large breasts, causing substantial attenuation, we recommend fixing the breast as high as possible using adhesive tape. This has two advantages. First, the mammary gland is not directly in the field of the X-rays delivered during the acquisition, massively decreasing breast radiation exposure – a major concern during cardiac or thoracic CT. Second, due to the reduced attenuation in the region of scanning when the breast is up, a lower radiation dose may be delivered without affecting image quality.

Table 12.1 indicates the values for kV and mAs we use currently, according to noise on the pre-control scan. Eight different settings have been defined. These values have been chosen step-by-step from the results of hundreds of coronary CT examinations. We calculate that the radiation dose using this protocol varies from 2 to 30 mSv, depending on whether or not ECG modulation is employed, and depending on the scan length. Image quality, based on signal-to-noise evaluation in the aorta and coronary arteries, was found similar in all groups (Fig. 12.4), resulting from an analysis of 120 consecutive patients. By attempting ECG modulation whenever possible, the overall mean radiation level was 9.3 mSv in this study.

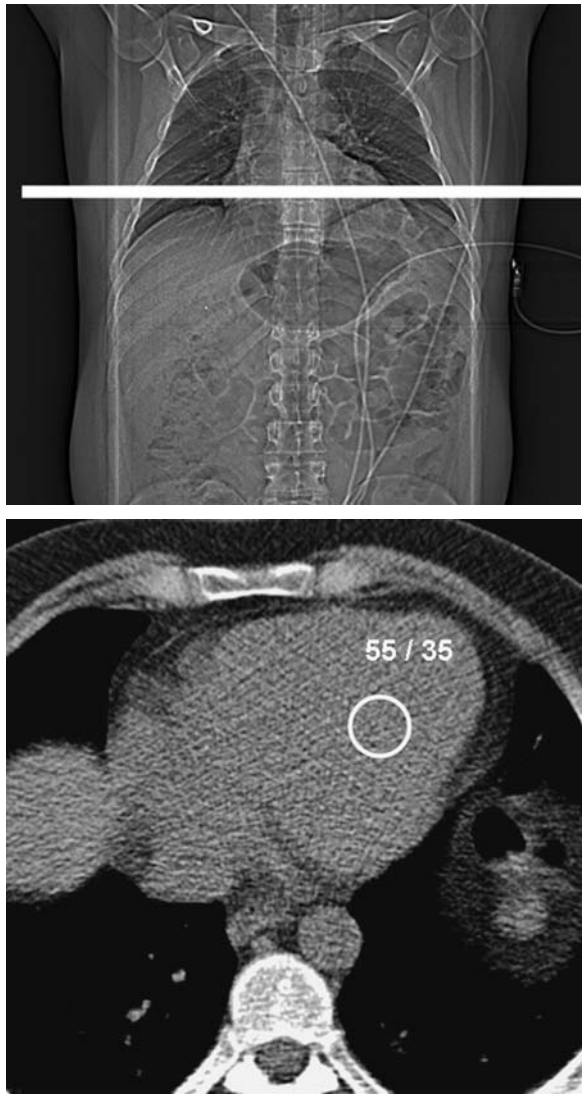

Fig. 12.3. a Using the topogram, a slice is positioned on the basis of the heart. **b** Slice is acquired at the level defined in **a**, the noise is measured in the left ventricle as the standard deviation of the value of the pixels within the region of interest (*circle*). Here the standard deviation was found to be 35 HU, leading to set radiation dose parameters at 120 kV and 900 mAS (see Table 12.1) for the subsequent contrast-enhanced coronary CT

Table 12.1. Adaptation of the mAs and kV settings depending on the noise measured on a pre-control image realized at 120 kV and 20 mAs, on a Sensation 64 CT. In our population, this rule leads to a mean radiation dose of 9.3 mSv, by combination with the ECG modulation technique. Image quality was found to be similar in the eight different groups

Noise (HU)	Tube current–time product (mAs)	Tube power (kVp)	$CTDI_{vol}$ (mGy)
<15	700	80	14
15–19	700	100	32
20–24	500	120	39
25–29	700	120	54
30–34	800	120	62
35–39	900	120	70
40–44	600	140	72
>44	700	140	84

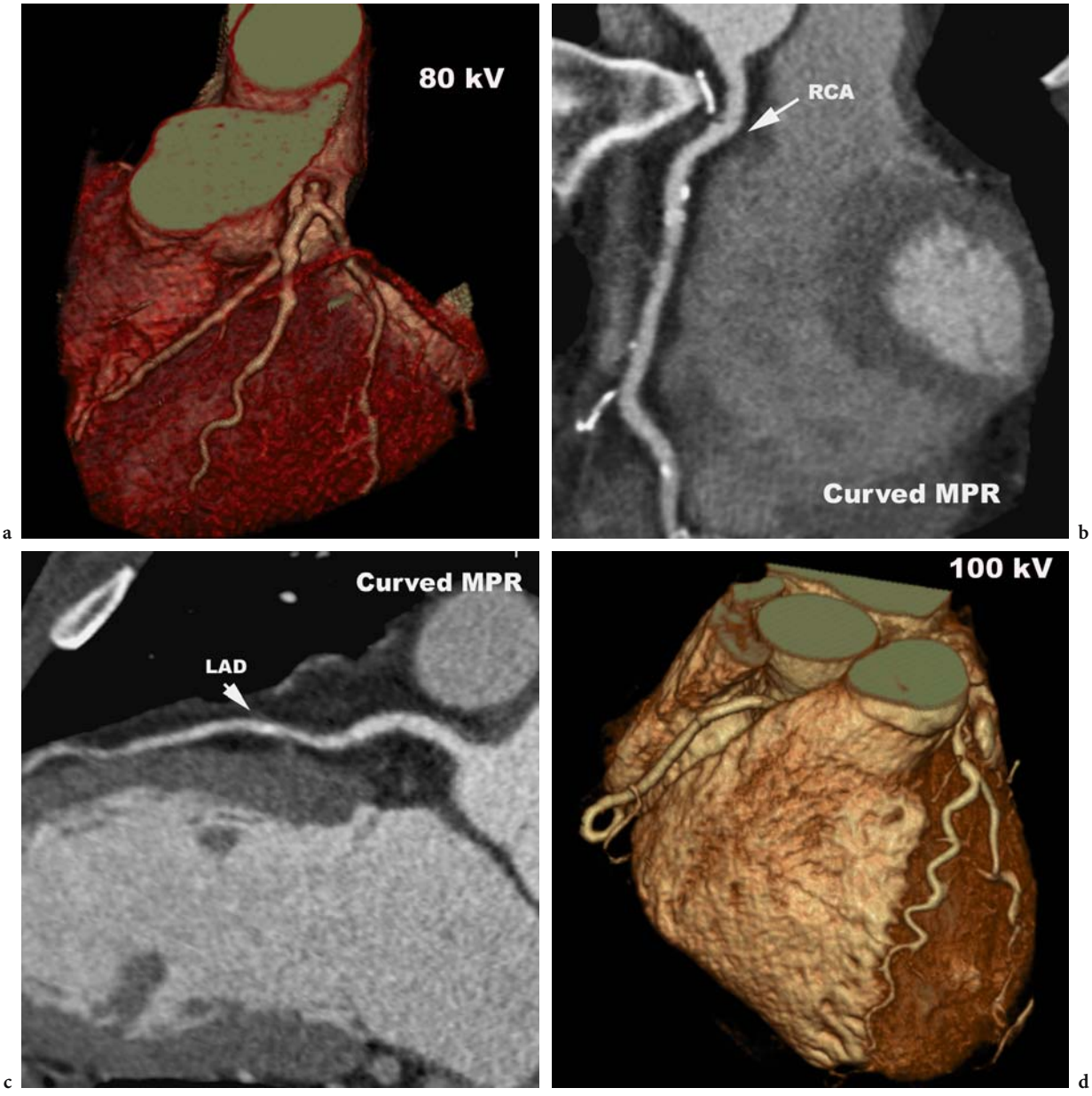

a b c d

Fig. 12.4a–d. Example of curved multiplanar reformatted images (**b**,**c**)and 3D coronary image (**a**) in a 36-year old heart transplant patient obtained at 80 kV and 700 mAs, using a 64-slice CT. Patient was 60 kg with a noise measured at 12 Hounsfield Units (HU) on the pre-control image. DLP of contrast-enhanced acquisition was 148 mGy·cm, accounting for an estimated dose of 2.5 mSv. **d** Example of a 3D coronary image in a woman presenting with atypical chest pain: noise was found at 18 HU and images were acquired at 100 kV and 700 mAs, using a 64-slice CT. Patient was 55 kg. DLP was 246 mGy·cm corresponding to a radiation dose of 5 mSv. In both cases image quality was found satisfactory for diagnosis

12.1.4 Literature Review

ECG modulation and individual adaptation are different approaches, and therefore they are complimentary and have an additive effect on dose reduction. We have shown that it is possible to scan down to 2 mSv in selected, slim patients, using this combined approach (Abada et al. 2006). Using 100 kV in addition to ECG modulation, Hausleiter and colleagues (2006) report radiation dose levels of 5 mSv for coronary CT angiograms. This has important implications because this dose is equal to or even lower than the mean radiation dose associated with conventional angiography.

All published studies addressing radiation dose during cardiac Multidetector CT (MDCT) were performed on Siemens CT scanners. There might be, however, substantial differences in radiation dose between different makes of machine, but no specific study has yet been published for the other manufacturers, to the best of our knowledge.

Using 4-slice coronary CT, the radiation dose for coronary CT angiography was reported to be 7.7 mSv in men (Poll et al. 2002): in this study, ECG pulsing was responsible for a dose reduction of between 37% and 44%. Another comparative study from three protocols included the recommended protocol from Siemens. The reported radiation dose (without ECG modulation) varied from 6.7 to 10.9 mSv for male patients, and from 8.1 to 13 mSv for female patients respectively. The manufacturer-recommended protocol yielded the highest effective doses overall (Hunold et al. 2003). Doses were found to be about 5 times higher than those delivered with electron-beam CT or conventional angiography.

More studies are available for the 16-slice CT. For coronary CT angiography, radiation estimates vary from 8.1 to 14.7 mSv without the use of ECG modulation (Coles et al. 2006; Gerber et al. 2005; Trabold et al. 2003). ECG pulsing reduces the dose by 28% (Gerber et al. 2005) to 47% (Trabold et al. 2003).

A larger number of detectors is associated with higher radiation dose: Coles et al. (2006) found a significantly higher dose with 16 (14.5±2.2 mSv) than with 12 (13.5±2 mSv) detectors on the same machine. A recent study comparing 16-slice and 64-slice CT in the same centre confirms this tendency. The overall effective dose estimates of cardiac CT angiography were 6.4±1.9 and 11±4.1 mSv with 16- and 64-slice CT, respectively, using ECG modulation for both in most cases (Hausleiter et al. 2006). Thus, radiation exposure has nearly doubled from 16- to 64-slice CT. Radiologists should be increasingly careful about radiation dose levels, and should attempt to use dose-savings algorithms whenever possible. Indeed, it is possible to reach up to 40 mSv if ECG-gated acquisition using maximal settings is used over the whole thorax (for example, in the case of bypass imaging, without ECG modulation).

Recently, delayed enhancement imaging has been proposed using cardiac CT (Gerber et al. 2006; Lardo et al. 2006; Mahnken et al. 2005; Paul et al. 2005). These late enhancement protocols do not require high spatial resolution and are best performed at low kilovoltage, to enhance contrast uptake in the myocardium (Paul et al. 2005). The radiation dose at 80 kV is about 2–4 mSv, roughly one-third of that required for coronary CT imaging.

12.1.5 Specific Protocols in Cardiopaediatrics

12.1.5.1 Specific Issues in Cardiopaediatrics

Compared to earlier helical CT, Multidetector CT (MDCT) allows more rapid acquisition, thinner slices and eventually ECG-gated acquisition, making it appropriate for congenital heart disease studies (Gilkeson et al. 2003; Paul et al. 2002; Westra et al. 1999a). Compared to MRI, Multidetector CT (MDCT) provides much higher spatial resolution, using much quicker and safer procedures. In particular anaesthesia is not required for Multidetector CT (MDCT) examinations .

The first issue is to decide whether ECG-gated acquisition should be used in congenital heart disease patients, and the second is which protocol is best suited: the radiation dose delivered should be estimated for each protocol to minimize radiation exposure. In our centre, the first criterion we consider for the choice of the protocol is whether or not apnoea is possible during the acquisition. Generally, it is only possible for children over the age of 6 or 7 years.

For infants between ages 6 and 12, we usually test the breath-hold 2 or 3 times before the acquisition, to ensure thoracic immobility is possible during the scanning process. If apnoea is not possible, ECG-

gated acquisitions are in principle not recommended, because these acquisitions are much longer than non-gated acquisitions: longer scan time, larger respiratory artefacts and lower image quality.

It is not possible to make neonates or young infants hold their breath. The cardiac rhythm of babies with cyanotic congenital heart disease is very high, generally between 140 and 180 beats per minute, making total motion-free cardiac images impossible to obtain. In addition, ECG-gated cardiac retrospective acquisition requires a much higher radiation dose than non-gated thoracic CT, because only a part of the dose (the dose delivered during diastole) is used for creating images. Organ sensitivity to radiation is much higher in babies than in adults, and the risk increases with radiation dose.

The second issue is clinical. Gated acquisitions are generally not necessary for evaluation of pulmonary arteries or the aorta, except the aortic root, which is subject to substantial heart motion artefacts. For example, patients with pulmonary atresia with ventricular septal defect are evaluated in our centre by fast, non-gated acquisition. Coronary origins may be frequently clearly visualized in babies using a non-gated protocol (80% of cases in our experience, in agreement with reported values; Goo et al. 2005).

Despite all these reasons, in some specific cases for some babies it may be beneficial to use ECG-gated acquisitions to look for an anomalous origin of the coronary arteries (Fig. 12.5). Even with heart rates above 140 beats per minute, ECG-gated acquisitions may improve visualization of coronary arteries in our experience.

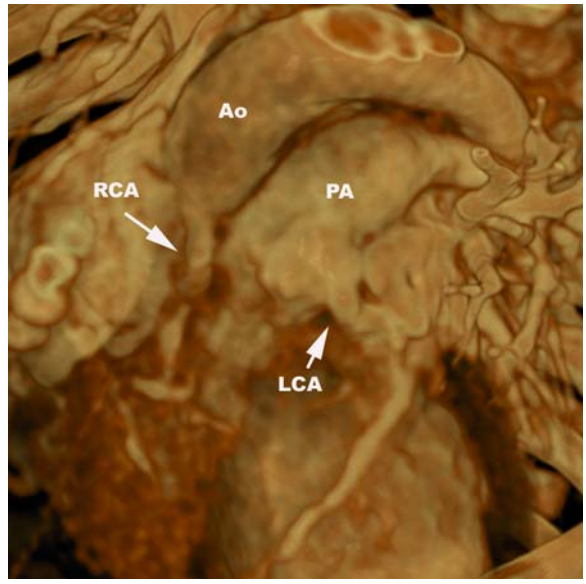

Fig. 12.5. Nine-month-old boy with dilatation of the left ventricle and signs of anterior myocardial ischaemia on ECG: an anomalous origin of the left coronary was suspected. ECG-gated coronary angiography was performed for confirmation of diagnosis. Despite a very fast heart rate (140 beats per minute) a very low dose ECG-gated protocol was performed, using 80 kV and 150 mAs, accounting for a DLP of 27. Estimated radiation dose for this baby, after correction due to body size, was estimated close to 1 mSv. Note that the coronary origins are well depicted, with a left main coronary artery originating from the left side of the pulmonary artery. (*Ao* Aorta, *LCA* left coronary artery, *PA* pulmonary artery, *RCA* right coronary artery)

12.1.5.2 Protocols

The principle of "going as fast as possible" allows good image quality in neonates with congenital heart disease, and furthermore short acquisition times minimize respiratory artefacts. Very short acquisition times (2 s or less) allow apnoea in intubated babies, and the images obtained are free of respiratory artefacts. With the 64-slice CT, the thorax of a baby can be scanned in about 1.5 s using 0.6 mm collimation.

The thorax is a low attenuation region, though substantial dose reduction during chest CT is feasible because of the high inherent contrast. In August 2001, the ALARA Conference of the Society for Paediatric Radiology considered the issue of dose reduction by the reduction of kilovoltage. In our centre, we decided to apply the ALARA principle as far as possible to neonates and babies with congenital heart disease, and then apply some systematic rules:

- Systematic use of 80 kV settings (Paul et al. 2004)
- Adaptation of the mAs to the child's weight (starting from 17 mAs)
- Only one phase acquisition when possible
- Protection of non-scanned organs (shield)

80 kVp setting is sufficient for good quality images, as long as the mAs setting is adjusted according to the child's weight. The other advantage of using only 80 kV is that the amount of contrast medium injected can also be reduced, because iodinated contrast is more attenuated at low kilovoltage settings (iodine has a high atomic number) than higher settings.

For thoracic imaging, current exposure is adapted to the body weight in neonates and babies, using the following scale:

Weight (kg)	kV	mAs
3	80	25
4	80	30
5	80	35
6	80	40

Using this protocol, the radiation exposure for a neonate was estimated to be less than 1 mSv; this dose is equivalent to about 6 months of natural radiation. Even lower doses may be used in premature babies or when high-quality images are not required for diagnosis. The minimum exposure setting allowed with the 64-slice CT from Siemens (Sensation 64) is 80 kV and 17 mAs. A previous study compared radiation dose with electron-beam CT and conventional angiography in babies with pulmonary atresia: the authors estimated that electron-beam CT was associated with 25–50 times less skin exposure than conventional angiography (Westra et al. 1999b). Anatomical data acquired from CT may be judiciously used to limit the number of views acquired with angiography, and sometimes replace conventional angiography altogether. Thus, CT can contribute to reducing the overall radiation exposure in congenital heart disease patients.

12.1.6 Conclusion

Because the radiation exposure is high and tends to increase for patients investigated with the latest generation of cardiac CT, it is essential to use radiation dose-reduction tools whenever possible. These tools should be judiciously used to avoid jeopardizing image quality. In addition, individually adapted protocols, including a low kilovoltage approach for slim patients, are beneficial because they have an independent impact on radiation dose reduction without substantial loss of image quality. New efforts from manufacturers are expected in the near future, to further decrease radiation associated with coronary CT angiography.

12.2 Radiation Dose Optimization in CTA for Aorta and Peripheral Vessels

12.2.1 Introduction

Computed angiography (CTA) of aorta and peripheral vessels has gained widespread use for screening patients with peripheral aortic occlusive disease (PAOD). Scanning patients with PAOD requires taking into account two different regional body anatomies that confer two levels of attenuation: the abdomen, in order to image abdominal aorta and renal arteries with high attenuation level, and the extremities, in order to image run-off vessels with low attenuation level. An important shift from a region of high attenuation to a region of low attenuation, as illustrated by the imaging of peripheral vascular vessels, leads us to consider that a standard protocol that maintains constant kV and mAs is inappropriate regarding radiation dose exposure. From the different approaches that contribute to radiation saving, four appear crucial for imaging the aorta and peripheral vessels:

- Automatic techniques
- Reduction of tube current
- Reduction of tube voltage (the kV approach)
- The pitch

12.2.2 Automatic Techniques

Continuous improvements in multislice technology increased the need to obtain the lowest radiation dose exposure possible. Different automatic approaches are now available on various recent CT scanners that challenge the concerns about unnecessary dose exposition. These techniques emerged on the basis that current fixed-tube methods subject patients to greater radiation dose exposure because they do not differentiate, in their settings, shifts in patients' size and anatomy from one region to another. Our concern when imaging the aorta and peripheral vessels is to optimize radiation dose exposure in the abdomen, which represents a region of high attenuation.

The concept of on-line, attenuation-adapted tube current modulation was first introduced with single-slice technology (Kalender et al. 1999). This tech-

nique is based on the principle that the tube current is automatically adjusted regarding different X-ray beam projection angles (in which only x- and y-axes are considered). A pre-specified level of image noise is determined according to the anatomical region scanned, and each adjustment of the tube current is then performed. The system provides a dose reduction of 23%.

This technique allowed an ever-growing set of automatic technological advances.

Indeed, another automatic tube current modulation technique considers the z-axis as well. z-axis modulation considers a level of noise that is selected by the operator regarding the desired image quality of the scanning region (Kalra et al. 2004). This level of noise represents the reference at which the system will regulate tube current values throughout the scanning time. Actually, the modulation follows information provided by scout scan projections that draw the attenuation and shape of the patient scanned. The system uses a noise index coefficient that is estimated at the preselected kV initially performed by the operator. The tube current modulation technique using the z-axis technique is then strongly linked to image noise.

Recently, a combination of both abovementioned approaches to radiation saving has been proposed in the system provided by Siemens (the CARE Dose 4D), which includes on-line tube current modulation for each tube rotation and determines a tube current value for each slice position. This system takes into account simultaneously the z-axis as well as the x- and y-axes (Rizzo et al. 2006). Rizzo et al. (2006) demonstrated that using the CARE Dose 4D to scan the abdomen and pelvis results in a reduction of radiation dose of 42%–44% when compared to maintaining constant tube current settings. This technique did not result in a dramatic impairment in image quality, as the concept of diagnostic acceptability stated by the authors fit the requirements for such a diagnostic purpose. Overall, the great advantage of these techniques is that they offer the operator the opportunity to reduce radiation dose exposure automatically on daily, routine CT exams.

12.2.3 Reduction of Tube Current

Before the introduction of automatic techniques, the primary approach to decreasing radiation was restricted to the reduction of the tube current. One reason for this is that it was more straightforward to decrease radiation empirically, on a step-by-step basis, because a wide range of settings was available. Because any decrease in tube current should affect image noise and image quality, one had to decrease radiation cautiously to prevent obscuring diagnostic demands. Several studies reported advantages of tube current reduction for radiation saving in body imaging for both adults and children (Diederich et al. 1999; Fefferman et al. 2005; Kalra et al. 2002; Sohaib et al. 2001; Tack et al. 2005). Only one study, to our knowledge, has been made for PAOD (Fraioli et al. 2006). Indeed, in order to achieve a substantial reduction in X-ray exposition to evaluate peripheral arterial disease, Fraioli et al. (2006) used different tube current settings at 50 mAs, 100 mAs and 130 mAs. Data analysis showed absence of impairment in diagnostic accuracy. The corresponding approximation of radiation dose exposure was 3.7 mSv for 50 mAs, and, respectively, 8.2 mSv and 13.7 mSv for 100 mAs and 130 mAs. Image quality was graded as excellent when weight did not exceed 85 kg. This approach highlights that radiation saving for imaging PAOD could be achieved with a decrease in tube current settings at constant value during the scan duration. However, because the performance of the on-line automatic tube current modulation technique achieved with CARE Dose 4D is better, fixed lowering of tube current settings should be addressed when automatic tools are lacking in some non-upgraded CT scanners that are still in use.

12.2.4 The kV Approach

The relationship between tube voltage and radiation exposure is not linear. Thus, reducing tube voltage induces an exponential reduction of radiation exposure. A magnitude of 65% of radiation saving could be attempted if tube voltage is reduced from 120 kV to 80 kV while tube current is maintained with the same settings.

The drastic decrease of radiation dose obtained with the kV approach is attractive; however, it needs to be performed cautiously because of concern about image quality. Signal-to-noise ratio, contrast-to-noise ratio and vessel density are the main factors of diagnostic relevance for CTA of aorta and peripheral vessels. Low kV settings allow an increase in vessel density because the photoelectric effect of X-ray attenuation is increased at lower

tube voltages with structures of high atomic number, such as iodine. Our approach to lowering kV for studies of aortic and renal arteries is a weighted, adaptive protocol that uses a tube voltage of 100 kV. A cut-off of 80 kg delineates the limit at which that protocol should be applied on a routine CTA of the aorta. The 100-kV protocol is of great value when assessment of peripheral vessels is also attempted with the same CT scan. Indeed, the higher scan coverage, which increases the radiation dose exposure, is counterbalanced by the saving attempt of a low-kV protocol. Our experience shows that an optimal enhancement of the aorta and femoro-popliteal arteries is always met with a mean enhancement of 380 HU when a biphasic iodine injection protocol is performed (20 ml iodine at 5 ml/s and 100 ml iodine at 3.5 ml/s and 50 ml saline at 2 ml/s). Wintersperger et al. (2005) demonstrated the effective use of a 100-kV protocol for aorto-iliac arteries when compared to a 120-kV protocol, with constant tube current settings in both protocols. The authors found that even though the noise increased in the 100-kV group, the signal-to-noise ratio and the contrast-to-noise ratio remained at the same magnitude because of the abovementioned effect of kV lowering, which increased the contrast. The 100-kV protocol allowed a reduction of radiation dose exposure from 10 mSv to 6.1 mSv, corresponding to a radiation saving of 37% (Wintersperger et al. 2005).

One consideration when imaging patients with PAOD is that we need to image aorta, renal arteries, iliac, arteries, femoral arteries, and run-off vessels in a single CT examination. Imaging aorta, renal and iliac arteries requires dealing with abdominal tissue, which could result in high differences of attenuation from one patient to another. In addition, the abdomen represents an area of low contrast and it contains important structures such as the liver, which must not be misinterpreted in a vascular CT study. Lowering tube voltage in that region induces an increase in image noise as a consequence of reduction in photon flux in an area of low attenuation. Recent studies have shown that we can perform kV lowering in the abdomen, taking into account the diagnostic capability of the CT exam regarding the hepatic parenchyma. The well-known concept of low contrast detectability (Baron 1994) was used by one group of investigators to show that the tumour-to-liver contrast could be reached. They stressed that CT capabilities with low kV could be clinically relevant for screening hepatic parenchyma. Funama et al. (2005) demonstrated in a phantom study that the use of 90 kV in the abdomen instead of 120 kV can reduce radiation dose as much as 35% without obscuring low contrast detectability. Furthermore, Nakayama et al. (2005) also stressed the impact of kV lowering on a clinical study using 90 kV in the abdomen. This protocol allowed a radiation saving of up to 57% compared to the 120-kV protocol (Nakayama et al. 2005). In addition, a reduction of contrast amount of 20% was realized with images at 90 kV, which were enhanced more highly than those at 120 kV. The reduction of contrast volume with low kV in the chest was also previously reported (Sigal-Cinqualbre et al. 2004) and remains applicable to the abdomen. Because low-kV protocols yield images with better enhancement, their use for vascular purposes is recommended when patients' size and morphology requirements are met.

12.2.4.1 Combined Approach of Automatic Techniques (x-, y-, and z-axis Tube Current Modulation) and kV Lowering

Combined angular and z-axis modulation (CARE Dose 4D), the ultimate automatic system for radiation dose optimization, has been recently reported regarding different tube voltage settings. Goo and Suh (2006) studied phantoms of different levels of attenuation to determine how the CARE Dose 4D system is influenced when 80-kV, 100-kV and 120-kV settings are applied. They found that on larger attenuation regions, appropriate tube current modulation is obtained at 120 kV and 100 kV, but could not be achieved at 80 kV. Actually, at 80 kV, in regions of high attenuation, tube current was not modulated and was constant at 180 mAs. Authors assume that 180 mAs might be the maximal tube current setting in high attenuation regions using 80 kV with the Siemens CARE Dose 4D system (Goo and Suh 2006). These findings show how a good understanding of the system used is mandatory in the prevention of miscalculation in the selection of CT parameters.

While no clinical study has investigated the scope of a combined 100-kV protocol and CARE Dose 4D for CTA of aorta and peripheral vessels, the results of Goo and Suh (2006) show that such a protocol might be applicable. Further studies are needed to attest to this statement.

12.2.5 Pitch

Pitch is defined as the ratio of table feed to the width of the X-ray beam per gantry rotation. Thus, an increase of the pitch results in a decrease of the time of exposure to the X-ray beam. Based on the above definition of the pitch, any attempt to raise the pitch should save radiation exposure. However, this statement becomes non-applicable with manufacturers that use effective milliampere-second settings. The milliampere-second, which is expressed as milliampere-second divided by pitch, remains constant even if the pitch is changed. In fact, any modification of the pitch performed by the operator makes the system adjust tube current proportionally and automatically in order to maintain the same value of noise. In this way, image quality cannot be hampered by the operator and remains at the same magnitude (Mahesh et al. 2001). Under such conditions, decreasing the pitch has no effect on saving radiation exposure because of the manufacturer's intervention.

The recent development of CT technology enables us to shorten scan duration. Indeed, using 64 detectors allows an increase in z-axis coverage, which might be interesting when performing CTA of peripheral vessels. However, the use of such CT scanners requires radiologists to readjust their protocols regarding time acquisition and their injection protocols. One issue to face is obtaining the optimal balance between scan duration (slice thickness and pitch) and the contrast medium bolus time necessary to reach calf arteries. Consequently, one option to overcome such requirements is to increase the pitch in order to have a time of acquisition that matches the bolus time of contrast medium in the target area. CT scanners that use milliamperes-second enable us to decrease the pitch but induce automatic adjustments of mAs. Hence, eventually the radiation exposure is maintained at the same value. Using higher pitch in such circumstances, and with scanners that use mAs, would enable us to cut down the scan duration without decreasing radiation dose exposure. Depending on the CT scanner used, one must know whether variation of the pitch affects the radiation dose; again we see the importance of radiologists being aware of the capabilities and properties of their machine.

12.2.6 Conclusion

The introduction of multidetector CT technology, along with improvements in workstations dedicated to display 3D and multiplanar reconstruction of vascular structures, has led to the widespread use of CTA of aorta and peripheral vessels. The large scan coverage represents a concern regarding radiation dose exposure that requires optimization techniques. The rapid development of automatic techniques represents a robust approach to saving radiation exposure.

Despite these automatic techniques, the role of the radiologist is not undermined because a comprehensive knowledge of CT capabilities is of utmost importance. Before each CT examination, the operator should keep in mind that any attempt to increase radiation dose exposure would be undertaken in order to improve diagnostic performance. Imaging aorta and peripheral vessels leads to dealing with abdomen regions, where low-contrast areas might be deeply affected by increasing image noise. The radiologist is the only one who can assess the clinical purpose of the examination and determine the best approach to be undertaken for achieving the ALARA principle.

References

Abada HT, Larchez C, Daoud B, Sigal-Cinqualbre A, Paul JF (2006) MDCT of the coronary arteries: feasibility of low-dose CT with ECG-pulsed tube current modulation to reduce radiation dose. AJR Am J Roentgenol 186: S387–390

d'Agostino AG, Remy-Jardin M, Khalil C, Delannoy-Dekan V, Flohr T, Duhamel A, Remy J (2006) Low-dose ECG-gated 64-slices helical CT angiography of the chest: evaluation of image quality in 105 patients. Eur Radiol 16(10):2137–2146

Baron RL (1994) Understanding and optimizing use of contrast material for CT of the liver [review]. AJR Am J Roentgenol 163(2):323–331

Coles DR, Smail MA, Negus IS et al (2006) Comparison of radiation doses from multislice computed tomography coronary angiography and conventional diagnostic angiography. J Am Coll Cardiol 47:1840–1845

Diederich S, Lenzen H, Windmann R et al (1999) Pulmonary nodules: experimental and clinical studies at low-dose CT. Radiology 213:289–298

Fefferman NR, Bomsztyk E, Yim AM et al (2005) Appendicitis in children: low-dose CT with a phantom-based simulation technique – initial observations. Radiology 237(2):641–646

Flohr TG, Stierstorfer K, Ulzheimer S, Bruder H, Primak AN, McCollough CH (2005) Image reconstruction and image quality evaluation for a 64-slice CT scanner with z-flying focal spot. Med Phys 32:2536–2547

Fraioli F, Catalano C, Napoli A et al (2006) Low-dose multidetector-row CT angiography of the infra-renal aorta and lower extremity vessels: image quality and diagnostic accuracy in comparison with standard DSA. Eur Radiol 16(1):137–146

Funama Y, Awai K, Nakayama Y et al (2005) Radiation dose reduction without degradation of low-contrast detectability at abdominal multisection CT with a low-tube voltage technique: phantom study. Radiology 237(3):905–910

Gerber TC, Kuzo RS, Morin RL (2005) Techniques and parameters for estimating radiation exposure and dose in cardiac computed tomography. Int J Cardiovasc Imaging 21:165–176

Gerber BL, Belge B, Legros GJ et al (2006) Characterization of acute and chronic myocardial infarcts by multidetector computed tomography: comparison with contrast-enhanced magnetic resonance. Circulation 113:823–833

Gilkeson RC, Ciancibello L, Zahka K (2003) Pictorial essay. Multidetector CT evaluation of congenital heart disease in pediatric and adult patients. AJR Am J Roentgenol 180:973–980

Goo HW, Suh DS (2006) The influences of tube voltage and scan direction on combined tube current modulation: a phantom study. Pediatr Radiol 36(8):833–840

Goo HW, Park IS, Ko JK et al (2005) Visibility of the origin and proximal course of coronary arteries on non-ECG-gated heart CT in patients with congenital heart disease. Pediatr Radiol 35:792–798

Hausleiter J, Meyer T, Hadamitzky M et al (2006) Radiation dose estimates from cardiac multislice computed tomography in daily practice: impact of different scanning protocols on effective dose estimates. Circulation 113:1305–1310

Hunold P, Vogt FM, Schmermund A et al (2003) Radiation exposure during cardiac CT: effective doses at multidetector row CT and electron-beam CT. Radiology 226:145–152

Jung B, Mahnken AH, Stargardt A et al (2003) Individually weight-adapted examination protocol in retrospectively ECG-gated MSCT of the heart. Eur Radiol 13:2560–2566

Kalender WA, Wolf H, Suess C, Gies M, Greess H, Bautz WA (1999) Dose reduction in CT by on-line tube current control: principles and validation on phantoms and cadavers. Eur Radiol 9(2):323–328

Kalra MK, Prasad S, Saini S et al (2002) Clinical comparison of standard-dose and 50% reduced-dose abdominal CT: effect on image quality. AJR Am J Roentgenol 179(5):1101–1106 [Erratum in: AJR Am J Roentgenol 2002 Dec;179(6):1645]

Kalra MK, Maher MM, Toth TL et al (2004) Strategies for CT radiation dose optimization. Radiology 230:619–628

Lardo AC, Cordeiro MA, Silva C et al (2006) Contrast-enhanced multidetector computed tomography viability imaging after myocardial infarction: characterization of myocyte death, microvascular obstruction, and chronic scar. Circulation 113:394–404

Mahesh M, Scatarige JC, Cooper J, Fishman EK (2001) Dose and pitch relationship for a particular multislice CT scanner. AJR Am J Roentgenol 177(6):1273–1275

Mahnken AH, Koos R, Katoh M et al (2005) Assessment of myocardial viability in reperfused acute myocardial infarction using 16-slice computed tomography in comparison to magnetic resonance imaging. J Am Coll Cardiol 45:2042–2047

Nakayama Y, Awai K, Funama Y et al (2005) Abdominal CT with low tube voltage: preliminary observations about radiation dose, contrast enhancement, image quality, and noise. Radiology 237(3):945–951. Epub 2005 Oct 19

Paul JF, Lambert V, Losay J et al (2002) Three-dimensional multislice CT scanner: value in patients with pulmonary atresia with septal defect. Arch Mal Coeur Vaiss 95:427–432

Paul JF, Abada HT, Sigal-Cinqualbre A (2004) Should low-kilovoltage chest CT protocols be the rule for pediatric patients? AJR Am J Roentgenol 183:1172; author reply 1172

Paul JF, Wartski M, Caussin C et al (2005) Late defect on delayed contrast-enhanced multi-detector row CT scans in the prediction of SPECT infarct size after reperfused acute myocardial infarction: initial experience. Radiology 236:485–489

Poll LW, Cohnen M, Brachten S, Ewen K, Modder U (2002) Dose reduction in multi-slice CT of the heart by use of ECG-controlled tube current modulation („ECG pulsing“): phantom measurements. Rofo 174:1500–1505

Rizzo S, Kalra M, Schmidt B, Dalal T et al (2006) Comparison of angular and combined automatic tube current modulation techniques with constant tube current CT of the abdomen and pelvis. AJR Am J Roentgenol 186(3):673–679

Sigal-Cinqualbre AB, Hennequin R, Abada HT, Chen X, Paul JF (2004) Low-kilovoltage multi-detector row chest CT in adults: feasibility and effect on image quality and iodine dose. Radiology 231:169–174

Sohaib SA, Peppercorn PD, Horrocks JA, Keene MH, Kenyon GS, Reznek RH (2001) The effect of decreasing mAs on image quality and patient dose in sinus CT. Br J Radiol 74:157–161

Tack D, Bohy P, Perlot I et al (2005) Suspected acute colon diverticulitis: imaging with low-dose unenhanced multi-detector row CT. Radiology 237(1):189–196. Epub 2005 Aug 26

Trabold T, Buchgeister M, Kuttner A et al (2003) Estimation of radiation exposure in 16-detector row computed tomography of the heart with retrospective ECG-gating. Rofo 175:1051–1055

Westra SJ, Hill JA, Alejos JC, Galindo A, Boechat MI, Laks H (1999a) Three-dimensional helical CT of pulmonary arteries in infants and children with congenital heart disease. AJR Am J Roentgenol 173:109–115

Westra SJ, Hurteau J, Galindo A, McNitt-Gray MF, Boechat MI, Laks H (1999b) Cardiac electron-beam CT in children undergoing surgical repair for pulmonary atresia. Radiology 213:502-512

Wintersperger B, Jakobs T, Herzog P et al (2005) Aorto-iliac multidetector-row CT angiography with low kV settings: improved vessel enhancement and simultaneous reduction of radiation dose. Eur Radiol 15(2):334–341. Epub 2004 Dec 21

Dose Optimization and Reduction in CT of the Musculoskeletal System Including the Spine

13

Alain Blum, Alain Noël, Daniel Winninger, Toufik Batch, Thomas Ludig, Gilles Ferquel, and Benoît Sauer

CONTENTS

13.1 Introduction

Since its introduction in the 1970s, computerized tomography (CT) has played an important role in the diagnosis of musculoskeletal disorders. It rapidly became the examination of choice for the diagnosis of disc herniation, fractures, bone tumours and some developmental abnormalities. Although the image quality was altered by streak artefact associated with medical devices, CT was also indicated in postoperative imaging (Blum et al. 2000; Iochum et al. 2001; Cotten et al. 2002; Fayad et al. 2005a, 2005b).

However, the performance of CT was hampered by its relatively low contrast resolution, which led to poor soft tissue evaluation compared with magnetic resonance imaging (MRI). Intra-articular lesions are almost impossible to detect without the administration of intra-articular contrast medium, and soft tissue masses are frequently misdiagnosed. CT is also the largest single source of medical exposure to radioactivity. For all these reasons, MRI has superseded CT as the first-line investigation in many situations.

Nevertheless, tremendous interest is now being expressed in CT due to its increased availability, low cost compared with MRI, and improved performance thanks to the advent of multidetector row CT (MDCT). With MDCT, images can be produced with submillimetre acquisition, thus providing true isotropic high-resolution volume data sets. Multiplanar reconstructions and 3D imaging improve the evaluation of bone and soft tissue disorders. The short acquisition speed (a few seconds) eliminates the need for sedation, minimizes dependence on patient cooperation and fits the technique perfectly for use in the complete evaluation of polytraumatized patients. Finally, the possibility of retrospectively modifying reconstruction parameters improves the overall performance without increasing the dose exposure. For example, large and small field of view reconstructions can be obtained from a single acquisition, simultaneously providing an overview and a detailed analysis of different anatomical regions. The slice thickness can be retrospectively increased, enhancing the signal-to-noise ratio and improving the soft tissue analysis (Blum 2002; Walter et al. 2003; Fayad et al. 2005a, 2005b).

Assessing and reducing dose is an important issue because some patients are very young and may undergo repeated CT examinations; furthermore, radiosensitive organs may be exposed to high doses.

A. Blum, MD; T. Batch, MD; T. Ludig, MD; G. Ferquel, MD; B. Sauer, MD
Hôpital Central, Service d'Imagerie Guilloz, CHU Nancy, 29, av du Mal de Lattre de Tassigny, 54035 Nancy Cedex, France
A. Noël, MD
Unité de radiophysique médicale, CRAN UMR 7039 CNRS, Centre Alexis Vautrin, Av de Bourgogne, Vandoeuvre-les-Nancy 54 511, France
D. Winninger, MD
Direction des ressources médico-techniques, CHU Nancy, av de Lattre de Tassigny, 54000 Nancy, France

In most situations, CT examinations are performed for the evaluation of high-contrast structures and low doses can be recommended.

13.2 Typical Dose in Musculoskeletal CT Examinations

The International Commission on Radiological Protection (1991) recommends the establishment of agreed levels for use in investigations; when greater exposure is proposed, the need for it, and the implications of its use, should be examined. The Council Directive of June 30, 1997 requires the member states of the European Community to promote the establishment and use of diagnostic reference levels that are expected not to be exceeded during standard procedures (European Community 1997). The European Commission suggests reference doses, defined by the weighted CT dose index ($CTDI_w$) and dose–length product (DLP), to be used in various CT examinations (European Commission 1999).

For the lumbar spine, the proposed reference levels are a $CTDI_w$ of 35 mGy and a DLP of 800 mGy·cm. For the osseous pelvis, the proposed reference levels are a $CTDI_w$ of 25 mGy and a DLP of 520 mGy·cm (European Commission 1999). However, these doses are based on survey data from the late 1980s and early 1990s, prior to the widespread introduction of spiral CT and MDCT (Shrimpton and Edyvean 1998; Hidajat et al. 2001). Since that time, MDCT has changed practice dramatically, and guidelines should be reviewed accordingly (Hidajat et al. 2001; Bongartz et al. 2004).

Some surveys have been conducted recently, but most focus on the chest and abdomen, and very few data are available concerning musculoskeletal examinations (Tables 13.1–13.3) (Galanski et al. 2001; Hidajat et al. 2001; Brix et al. 2003; Hatziioannou et al. 2003). New guidelines (March 2004) resulting from the work of a European study group of radiologists and physicists involved in diagnostic CT recommend that the volume CT dose index ($CTDI_{vol}$) should remain below 40 mGy for exploration of the cervical spine, below 20 mGy for limb and peripheral joint examinations, and below 15 mGy for the lumbar spine, pelvic skeleton and the shoulder (Bongartz et al. 2004).

CT scanning plays an increasing role in the management of musculoskeletal disorders, particularly with the advent of 16-section multidetector CT, which has numerous advantages. First, most studies are completed in under 10 s, which helps minimize the need for patient cooperation. The speed of image acquisition with MDCT is particularly advantageous compared with MRI. Second, isotropic volume image data are acquired, allowing retrospective reconstruction of multiple high-resolution image sets from the original raw data – thereby enabling 3D CT images to be produced in numerous planes from only one acquisition. Third, the slice thickness and reconstruction algorithm can be retrospectively modified in order to improve the signal-to-noise ratio, and thereby the soft tissue analysis, without increasing the dose of radiation. Fourth, when used correctly, 3D CT volume imaging can help minimize the dose. Finally, although its high-contrast resolution means that MRI is undoubtedly superior to CT in detecting and defining soft tissue and bone marrow abnormalities, MDCT is essential in several settings, as follows. In postoperative cases, metal artefact typically prohibits MRI evaluation, but volume rendering of a MDCT axial database virtually eliminates streak artefact associated with hardware. In the evaluation of masses, CT, unlike MRI, allows for the detection and characterization of calcification, cortical disruption, and periosteal reaction. In the setting of trauma, fracture lines are exquisitely defined, as is the extent of fracture. Large anatomical areas (such as in patients with congenital thoracic deformities or skeletal dysplasias), and areas not easily evaluated by MRI (such as the ribs and skull), are clearly delineated using MDCT (Iochum et al. 2001; Walter et al. 2003; Fayad et al. 2005a, 2005b).

In our institution, CT is indicated in the following situations: complex fracture, fracture with vascular impairment, dislocation with fracture, occult fracture (other than hip and scaphoid), skeletal and soft tissue tumours, postoperative follow-up, bone dysplasia, disc herniation, and joint evaluation. CT arthrography of the shoulder, elbow, wrist, first metacarpophalangeal joint, hip, knee and ankle may be preferred to MRI or MR arthrography for preoperative evaluation.

We retrospectively evaluated the $CTDI_w$ and the DLP for the types of CT examination most commonly carried out for musculoskeletal disorders in our institution. CT was performed using 16-row MDCT (Sensation 16, Siemens, Erlangen).

All images, plus dose values ($CTDI_{vol}$ and PDL) as displayed on the scanner, were sent to the picture archiving and communications (PACS) system (Impax V5, Agfa, Belgium). Five anatomical regions were selected for the study: cervical spine, lumbar spine, pelvic skeleton, shoulder and knee. For the cervical spine and the pelvic skeleton, acquisitions were performed with a collimation of 16×0.75 mm. The tube voltage was generally equal to 120 kV and the mAs product was usually set to 250. For the lumbar spine, the acquisitions were performed with a 16×0.75 mm collimation, 120 kV and generally 350 or 400 mAs. For the shoulder, the acquisitions were performed with a 16×0.75 mm collimation, 120 kV and generally 300 mAs. For the knee, collimations of 12×0.75 mm or of 2×0.6 mm (for ultra-high resolution) were used. The tube voltage was 120 kV and mAs values ranged from 150 to 350. In all cases, the pitch factor was between 1 and 1.8. The automatic exposure control (AEC) was not used.

Significant variations in $CTDI_{vol}$ and DLP were observed for each type of examination (Tables 13.4, 13.5). This can be explained by the adjustment of exposure parameters according to patient size. Exposure parameters were also lower when the examination was focused on bony structures, whereas the mAs product was higher when a precise soft tissue evaluation was necessary. The major influence on dose was probably the extent of the target volume, which was increased when multiple lesions were suspected.

Table 13.1. Weighted computed tomography dose index (*$CTDI_w$*) in CT examinations in some recent surveys. Data in *parentheses* are the minimum and maximum. (*NA* Not available)

Author, year of publication	Type of CT scan	Cervical spine $CTDI_w$ (mGy)	Lumbar spine $CTDI_w$ (mGy)	Pelvis and pelvic skeleton $CTDI_w$ (mGy)[b]	Extremities $CTDI_w$ (mGy)
Galanski et al. (2001)	Single-slice CT	33.9	37.1	26	NA
Hidajat et al. (2001)	Conventional	NA	32.8 (12.7–62.7)[a]	32.7 (23.7–47.5)	NA
	Spiral CT	NA	24.8[a]	16.4 (12.6–25.3)	NA
Hatziioannou et al. (2003)	Conventional and spiral CT	49.2 (14.9–103.2)	29.6 (10.6–53.3)	22.4 (8.7–43.7)	NA
Brix et al. (2003)	Dual-slice and quad-slice CT	26.0	30.3	21.8[b]	14.8

[a] CT scan performed for disk evaluation
[b] Only the survey reported by Galanski and Brix concerns CT scan performed specifically for the pelvic skeleton

Table 13.2. DLP in CT examinations in some recent surveys. Data in *parentheses* are the minimum and maximum. (*NA* Not available)

Author, year of publication	Type of CT scan	Cervical spine DLP (mGy·cm)	Lumbar spine DLP (mGy·cm)	Pelvis and pelvic skeleton DLP (mGy·cm)[b]	Extremities DLP (mGy·cm)
Galanski et al. (2001)	Single-slice CT	129	216	487	NA
Hidajat et al. (2001)	Conventional	NA	391 (130–980)[a]	845 (504–2018)	NA
	Spiral CT	NA	270[a]	306 (168–488)	NA
Hatziioannou et al. (2003)	Conventional and spiral CT	295 (56–760)	203 (63–508)	336 (131–676)	NA
Brix et al. (2003)	Dual-slice and quad-slice	277	445	440	171

[a] CT scan performed for disc evaluation
[b] Only the survey reported by Galanski and Brix concerns CT scan performed specifically for the pelvic skeleton

Table 13.3. Effective dose in CT examinations in some recent surveys. Data in *parentheses* are the minimum and maximum. (*NA* Not available)

Author, year of publication	Type of CT scan	Cervical spine (mSv)	Lumbar spine (mSv)	Pelvis and pelvic skeleton (mSv)[a]	Extremities (mSv)
Galanski et al. (2001)	Single-slice CT	2.1	2.7	8.8	NA
Hidajat et al. (2001)	Conventional spiral CT	NA	NA	NA	NA
Hatziioannou et al. (2003)	Conventional and spiral CT	1.59 (0.30–4.10)	NA	6.38 (2.49–12.85)	NA
Brix et al. (2003)	Dual-slice and quad-slice	2.9	8.1	8.2	NA

[a] Only the survey reported by Galanski and Brix concerns CT scan performed specifically for the pelvic skeleton

Table 13.4. $CTDI_{vol}$ in musculoskeletal examinations in the present authors' institution

	$CTDI_{vol}$ (mGy)					
	Cervical spine	Lumbar spine	Pelvis, skeleton	Shoulder	Knee	Knee (ultra-high resolution)[a]
Mean	21	32	21	25	18	17
Range	18.5–45.2	23.4–56.4	15.6–33.4	23.4–35.0	10.9–31.2	14.6–32.2
3rd quartile	21.4	35.0	23.4	27.3	21.8	17.3

[a] Acquisition with a collimation of 2 × 0.6 mm

Table 13.5. Dose–length product (*DLP*) in musculoskeletal examinations in the present authors' institution

	DLP (mGy·cm)					
	Cervical spine	Lumbar spine	Pelvis, skeleton	Shoulder	Knee	Knee (ultra-high resolution)[a]
Mean	411	782	602	332	425	263
Range	321–766	399–1527	366–1359	253–688	195–757	174–539
3rd quartile	455.2	825.5	680.2	349.2	555	287.5

[a] Acquisition with a collimation of 2 × 0.6 mm

With the advent of MDCT, and more specifically 16-section MDCT, the possible applications of CT scanning in musculoskeletal disorders have dramatically increased, and major changes have been made to scanning protocols. The entire spine can be explored for fractures (Fig. 13.1). Whole-body CT has been recommended for the diagnosis of multiple myeloma (Horger et al. 2005). Musculoskeletal explorations can be combined with CT angiography for the diagnosis of post-trauma vascular lesions, evaluation of musculoskeletal tumours, and diagnosis of artery entrapment syndromes (Fig. 13.2) (Karcaaltincaba et al. 2004; Fayad et al. 2005b). CT of the lumbar spine may be combined with sacroiliac joint evaluation when a spondyloarthropathy is suspected. All these new applications lead to an extended target volume or to multiphasic explorations.

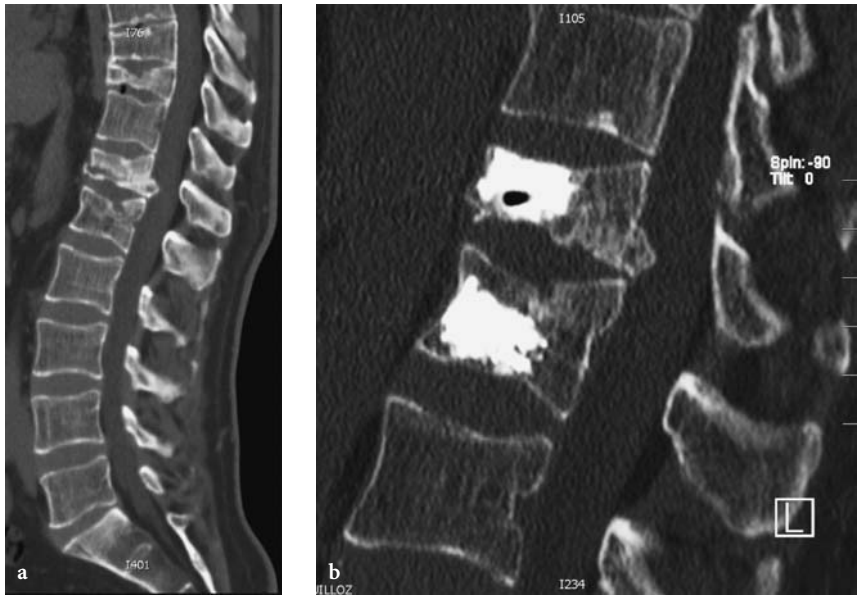

Fig. 13.1a, b. Vertebral fractures in a 38-year-old man. **a** Sagittal multiplanar reformation (*MPR*) with low-dose MDCT of the thoraco-lumbar spine. **b** Follow-up after kyphoplasty

13.3 Motion Studies

With improved temporal resolution, MDCT permits cinematic evaluation of the joints. Due to the limited width of the detectors (no more than 4 cm), only rotational motion can be explored at present. However, this technique could help in kinesiology studies and in the diagnosis of occult instabilities. Batch et al. (2004a) conducted a study involving a rotational phantom and patients undergoing shoulder arthrography with 16-section MDCT. Using a 12 × 1.5 mm collimation (18 mm), a partial scanning technique and a rotation time of 0.5 s, a structure located 3 cm away from the centre of rotation could rotate at the speed of one revolution in 15.8 s without significant artefact. With two motion acquisitions, one each in the upper and lower portions of the gleno-humeral joint, it is possible to evaluate the most important parts of the joint. With low-dose acquisitions (120 kV and 50 mAs) lasting 10 s, the total $CTDI_{vol}$ and DLP are respectively 144.4 mGy and 260 mGy·cm. Therefore, this technique could replace acquisitions obtained in different positions. The image quality obtained with such acquisitions also suggests that low-dose protocols could be applied to shoulder CT arthrography (Batch et al. 2004b). Finally, it is probable that with the advent of large detectors, CT motion studies will gain importance.

13.4 Modalities for Dose Reduction in Musculoskeletal CT

CT scanner manufacturers have made significant efforts to reduce radiation doses while maintaining good image quality. All the technical approaches to dose reduction are described in detail in the literature (Linton and Mettler 2003; Kalra et al. 2004; Althen 2005). Radiologists and radiographers are now aware of the need for ALARA (as low as reasonably achievable) protocols, but they sometimes appear reluctant to reduce the dose. Another issue is that new CT applications lead to an extended volume of exploration and multiphasic acquisitions, again resulting in increased doses of radiation.

Various investigators have focused on the possibility of lowering the dose used for CT without altering its diagnostic capabilities. Their work concerns pulmonary nodule detection, CT colonography, renal colic, acute appendicitis, chronic sinusitis and screening (Rusinek et al. 1998; van Gelder et al. 2002; Tack et al. 2003a, 2003b; Keyzer et al. 2004). A recent study by Horger et al. (2005) showed that whole-body low-dose MDCT is appropriate for the diagnosis of lytic bone changes and for the assessment of fracture risk in multiple myeloma patients – among whom it represents a serious alternative to current standards. A 16 × 1.5 mm collimation was

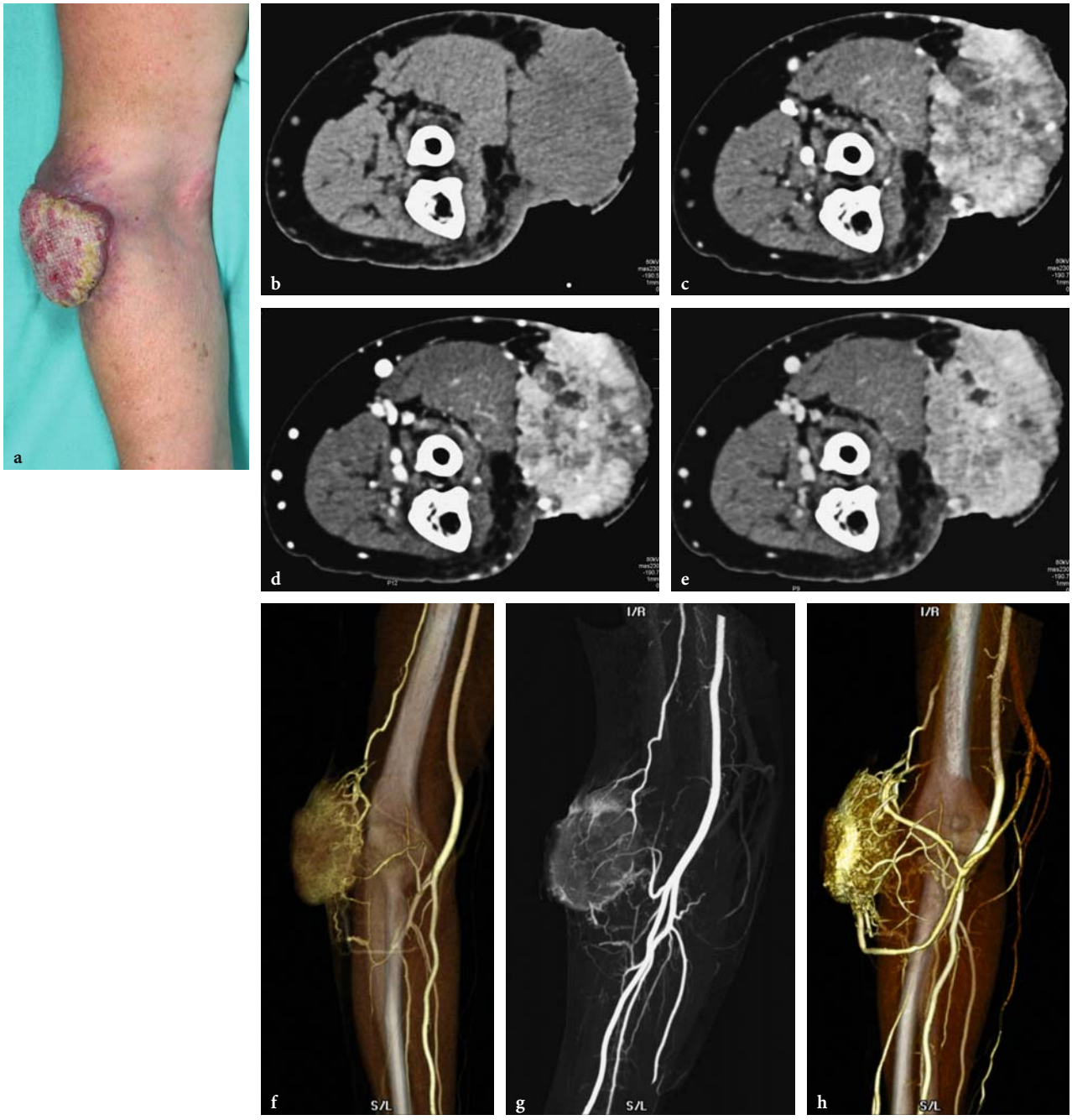

Fig. 13.2a–h. Multiphasic exploration with CT in a case of Merkel cell tumour of the elbow. Four acquisitions were performed with 80 kV and 230 mAs: before IV injection of contrast media and at the arterial, venous and equilibrium phases. **a** Photography of the elbow showing a large hypervascularized tumour. **b–e** Axial slices obtained at the different phases showing a large mass with a rapid initial enhancement followed by sustained late enhancement and some areas of necrosis highly suggestive of a malignant tumour. **f, g** Volume rendering technique (*VRT*) and maximum intensity projection (*MIP*) obtained from the arterial acquisition highlighting the three arteries feeding the tumour. **h** VRT obtained from the venous phase demonstrating the vascular relationship of the tumour as well as rapid venous opacification. In such cases, multiphasic MDCT provides a precise topographic and compartmental analysis of the tumour, a vascular map of the anatomical region and a dynamic evaluation of the lesion

used with a tube voltage of 120 kV and a tube current time product ranging from 40 to 70 mAs. The effective radiation dose of MDCT calculated at a tube current time product of 40 mAs was 1.7-fold higher than the mean radiation dose associated with conventional X-ray (4.1 mSv versus 2.4 mSv) (Horger et al. 2005).

Due to the high contrast of bony structures, low-dose protocols should be enthusiastically recommended for their evaluation. Such protocols are particularly suited for the diagnosis and evaluation of fractures or of bone tumours and lytic processes. However, doses should not be reduced when exploring the cervicothoracic junction as the noise from the shoulder degrades the image quality. Low-dose protocols are also well adapted to CT arthrography (with the exception of the shoulders of large patients), as the intra-articular contrast medium produces a high contrast interface between intra-articular structures. No study has yet determined whether low-dose protocols would be of value when soft tissue evaluation is also necessary. With regard to disc evaluation, a good signal-to-noise ratio is necessary in order to detect subtle changes, for example in cases of disc sequestration or facet joint synovial cyst.

One of the main advantages of MDCT in evaluating musculoskeletal disorders is the possibility of retrospectively modifying the slice thickness. The acquisition can be performed with the thin slices best suited for bony structure evaluation. Reconstructing thicker slices with a standard convolution filter produces images with a better signal-to-noise ratio, thus improving soft tissue evaluation (Fig. 13.3). Thicker slices can also be obtained using multiplanar reconstruction software.

Some authors recommend modulating tube current in order to decrease the dose. When evaluating the cervicothoracic junction, Schaefer-Prokop et al. (2003) favours automatic current modulation, and increasing the maximum mAs setting by a factor of 1.5–2 to ensure sufficient exposure during the lateral projection while significantly reducing the dose on the AP projections. Automatic current modulation can also be used for pelvic examinations. A dose reduction of 23%–45% is possible with no significant difference in subjective assessments of image quality (Iball et al. 2006). Mastora et al. (2001) found that online tube current modulation resulted in a 35% reduction in the product of mean tube current and time with no loss in image quality when exploring the thoracic outlet for suspected thoracic outlet syndrome.

Finally, the classic recommendations concerning patient positioning remain crucial in order to reduce the noise and streak artefacts and to minimize exposure. The region of interest has to be placed as close as possible to the centre of the gantry in order to improve the spatial resolution and the signal-to-noise ratio. The explored volume has to be as thin as possible to limit scattered radiation and beam hardening artefacts. That is why shoulder girdles are placed on different levels when exploring the shoulder.

With MDCT, the isotropic volume allows multiplanar reformation (MPR) to be performed in any plane of interest, including traditional axial, coronal, sagittal and oblique planes. The plane of choice for the acquisition is the one which offers a minimal width of the explored region, in order to improve the signal-to-noise ratio and to limit beam hardening artefacts. Therefore, the spine is explored without tilting the gantry. Using a four-row MDCT, Ludig et al. (2000) compared the radiation dose between two protocols on the same patients, using the same collimation (4×1 mm), slice thickness (1.25 mm), MPR thickness, pitch factor, tube voltage, tube current time product and convolution filter. With the first protocol, three helical acquisitions were obtained. They were localized on L3–L4, L4–L5 and L5–S1 discs from the level of the pedicle of the upper vertebra to the level of the pedicle of the lower vertebra, with gantry tilting in order to obtain slices parallel to the disc planes. In the second protocol, one single acquisition was performed in the axial plane from the level of L3 pedicles to S1 and secondary MPR were obtained in the disc planes. Skin dose was compared for 12 patients. Thermoluminescent dosimeters were placed on the right antero-superior iliac process, the omphalus, the sternum and L4 spinous process. The average skin dose with the first protocol was 101 mGy on the right antero-superior iliac process, 82 mGy on the omphalus, 129 mGy on the L4 spinous process and less than 1 mGy on the sternum. The average skin dose with the second protocol was 74 mGy on the right antero-superior iliac process, 88 mGy on the omphalus, 83 mGy on the L4 spinous process and less than 1 mGy on the sternum. Although the target volume was about 40% greater with the second protocol, the effective dose was slightly reduced and the signal-to-noise

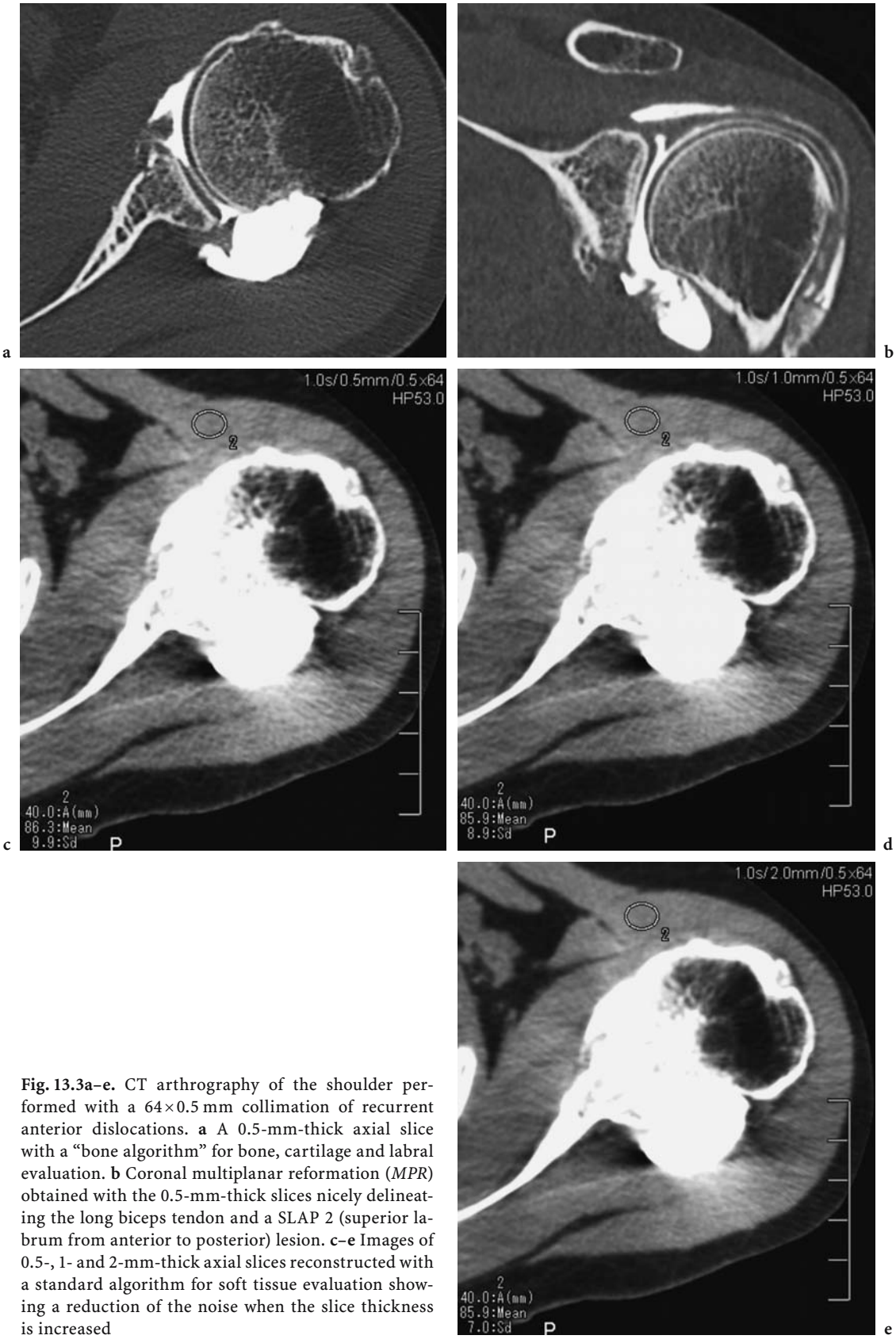

Fig. 13.3a–e. CT arthrography of the shoulder performed with a 64×0.5 mm collimation of recurrent anterior dislocations. **a** A 0.5-mm-thick axial slice with a "bone algorithm" for bone, cartilage and labral evaluation. **b** Coronal multiplanar reformation (*MPR*) obtained with the 0.5-mm-thick slices nicely delineating the long biceps tendon and a SLAP 2 (superior labrum from anterior to posterior) lesion. **c–e** Images of 0.5-, 1- and 2-mm-thick axial slices reconstructed with a standard algorithm for soft tissue evaluation showing a reduction of the noise when the slice thickness is increased

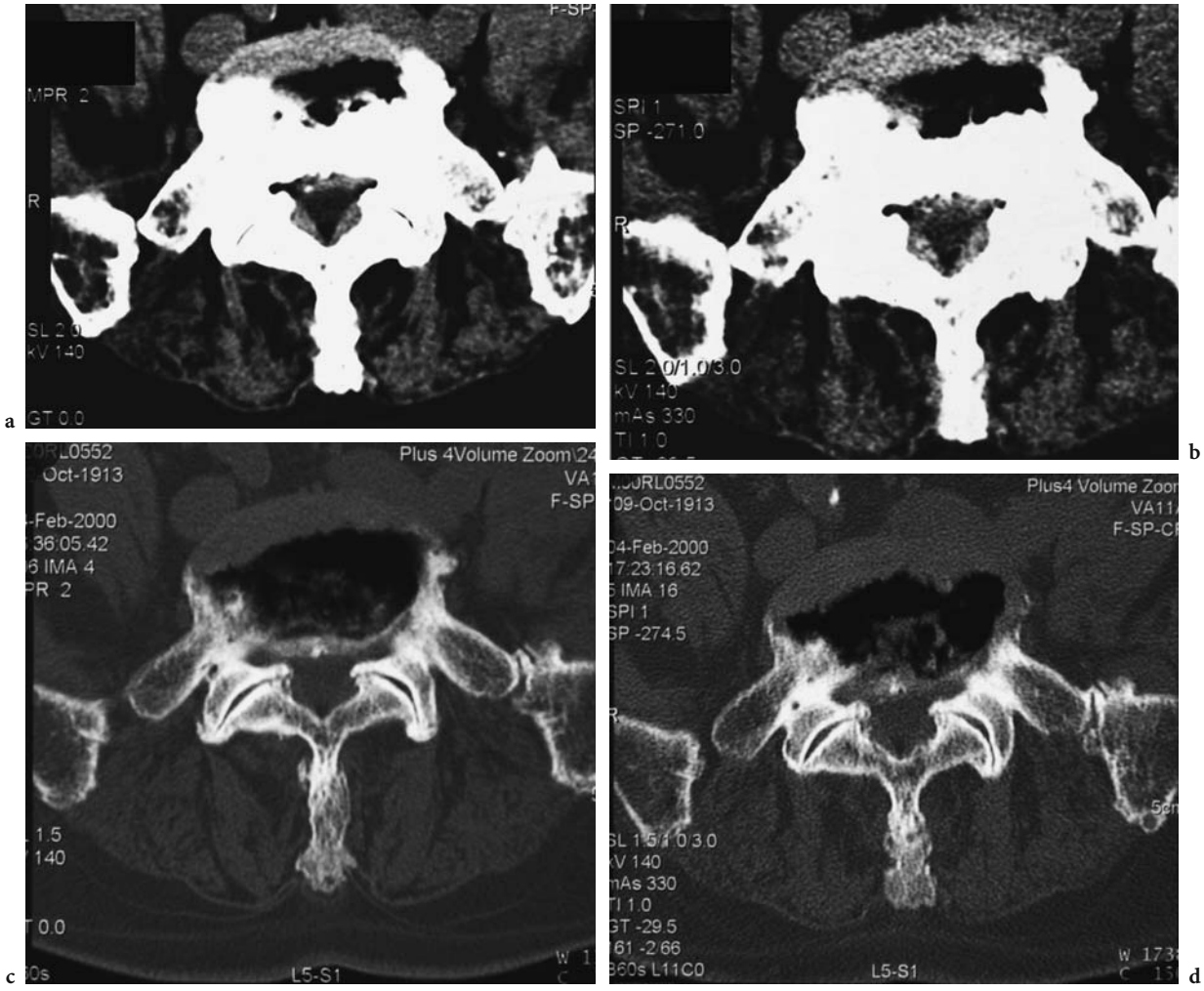

Fig. 13.4a–d. Comparison of oblique MPR obtained with an axial MDCT acquisition and oblique native slices from a tilted MDCT acquisition for the evaluation of L5–S1 vertebrae. The collimation is 4 × 1 mm. The inclination of the gantry is 29.5° for the tilted acquisition. MPR and native slices acquisition and reconstruction parameters are identical for soft tissue evaluation and bony analysis. **a**,**b** A 2-mm-thick MPR and native slice with a soft tissue algorithm showing a significant reduction of the noise of the MPR image with a better delineation of the disc compared to the native oblique slice. **c**,**d** A 1.5-mm-thick MPR and native slice with a bone algorithm showing equivalent in-plane spatial resolution

ratio was improved (up to 25%, depending on the gantry tilting) (Fig. 13.4).

13.5 Conclusion

MDCT is widely used in the diagnosis of musculoskeletal disorders. Few data are available on radiation dose for musculoskeletal CT examinations. New CT applications lead to extended volume exploration and multiphasic acquisitions, resulting in increased dose of radiation. However, most examinations should be performed with low-dose protocols.

References

Althen JN (2005) Automatic tube-current modulation in CT – a comparison between different solutions. Radiat Prot Dosimet 114:308–312

Batch T, Winninger D, Guerra R, Raffray L, Barbara K, Zhu X, Blum A (2004a) Mise au point des protocoles d'acquisition pour l'étude cinésiologique des articulations: Etude sur fantôme (abstract). J Radiol 85:1456

Batch T, Sirveaux F, Henrot P, Zhu X, Iochum-Duchamp S, Molé D, Coudane H, Blum A (2004b) Principe d'exploration cinésiologique de l'épaule en scanner dynamique volumique multicoupe (abstract). J Radiol 85:1368

Blum A (2002) Scanner volumique multicoupe: principes, applications et perspectives. JBR-BTR 85:82–99

Blum A, Walter F, Ludig T, Zhu X, Roland J (2000) Multislice CT: principles and new CT-scan applications. J Radiol 81:1597–1614

Bongartz G, Golding SJ, Jurik AG et al (2004) European Guidelines for Multislice Computed Tomography. Funded by the European Commission (Contract number FIGM-CT2000-20078-CT-TIP). March 2004

Brix G, Nagel HD, Stamm G, Veit R, Lechel U, Griebel J, Galanski M (2003) Radiation exposure in multi-slice versus single-slice spiral CT: results of a nationwide survey. Eur Radiol 13:1979–1991

Cotten A, Iochum S, Blum A (2002) 3D imaging in musculoskeletal system. In: Baert AL, Caramella D, Bartolozzi C (eds) 3D image processing. Techniques and clinical applications. Springer, Berlin Heidelberg New York, pp 247–255

European Commission (1999) European guidelines on quality criteria for computed tomography. Report EUR 16262. Luxembourg, 1999

European Community (1997) Council Directive 97/43/EURATOM, 30 June 1997, on health protection of individuals against the dangers of ionizing radiation in relation to medical exposure (repealing Directive 84/466/Euratom). Off J Eur Commun L180 40:22–27

Fayad LM, Bluemke DA, Fishman EK (2005a) Musculoskeletal imaging with computed tomography and magnetic resonance imaging: when is computed tomography the study of choice? Curr Probl Diagn Radiol 34:220–237

Fayad LM, Johnson P, Fishman EK (2005b) Multidetector CT of musculoskeletal disease in the pediatric patient: principles, techniques, and clinical applications. Radiographics 25:603–618

Galanski M, Nagel HD, Stamm G (2001) CT radiation exposure risk in Germany. Rofo 173:R1–R66

van Gelder RE, Venema HW, Serlie IWO et al (2002) CT colonography at different radiation dose levels: feasibility of dose reduction. Radiology 224:25–33

Hatziioannou K, Papanastassiou E, Delichas M, Bousbouras P (2003) A contribution to the establishment of diagnostic reference levels in CT. Br J Radiol 76:541–545

Hidajat N, Wolf M, Nunnemann A, Liersch P, Gebauer B, Teichgraber U, Schroder RJ, Felix R (2001) Survey of conventional and spiral CT doses. Radiology 218:395–401

Horger M, Claussen CD, Bross-Bach U, Vonthein R, Trabold T, Heuschmid M, Pfannenberg C (2005) Whole-body low-dose multidetector row-CT in the diagnosis of multiple myeloma: an alternative to conventional radiography. Eur J Radiol 54:289–297

Iball GR, Brettle DS, Moore AC (2006) Assessment of tube current modulation in pelvic CT. Br J Radiol 79:62–70

International Commission on Radiological Protection (1991) Recommendations of the International Commission on Radiological Protection. ICRP Publication 60. Pergamon, Oxford

Iochum S, Ludig T, Walter F, Fuchs A, Henrot P, Blum A (2001) Value of volume rendering in musculo-skeletal disorders. J Radiol 82:S221–S230

Kalra MK, Maher MM, Toth TL, Schmidt B, Westerman BL, Morgan HT, Saini S (2004) Techniques and applications of automatic tube current modulation for CT. Radiology 233:649–657

Karcaaltincaba M, Aydingoz U, Akata D, Leblebicioglu G, Akinci D, Akhan O (2004) Combination of extremity computed tomography angiography and abdominal imaging in patients with musculoskeletal tumours. J Comput Assist Tomogr 28:273–277

Keyzer C, Tack D, De Maertelaer V, Bohy P, Gevenois PA, Van Gansbeke D (2004) Acute appendicitis: comparison of low-dose and standard-dose unenhanced multi-detector row CT. Radiology 232:164–172

Linton OW, Mettler FA Jr (2003) National Council on Radiation Protection and Measurements. National conference on dose reduction in CT, with an emphasis on pediatric patients. AJR Am J Roentgenol 181:321–329

Ludig T, Marchal C, Noel A, Bresler F, Corruble B, Blum A (2000) Lumbar spine: the influence of acquisition mode using multislice helical CT on patient radiation dose (abstract). Radiology 217 (P):271

Mastora I, Rémy-Jardin M, Seuss C, Scherf C, Guillot JP, Rémy J (2001) Dose reduction in spiral CT angiography of thoracic outlet syndrome by anatomically adapted tube current modulation. Eur Radiol 11:590–596

Rusinek H, Naidich DP, McGuinness G et al (1998) Pulmonary nodule detection: low-dose versus conventional CT. Radiology 209:243–249

Schaefer-Prokop C, von Smekal U, van der Molen AJ (2003) Musculoskeletal system. In: Prokop M, Galanski M (eds) Spiral and multislice computed tomography of the body. Thieme, Stuttgart, pp 929–997

Shrimpton PC, Edyvean S (1998) CT scanner dosimetry. Br J Radiol 71:1–3

Tack D, Sourtzis S, Delpierre I, De Maertelaer V, Gevenois PA (2003a) Low-dose unenhanced multidetector CT of patients with suspected renal colic. AJR Am J Roentgenol 180:305–311

Tack D, Widelec J, De Maertelaer V, Bailly JM, Delcour C, Gevenois PA (2003b) Comparison between low-dose and standard-dose multidetector CT in patients with suspected chronic sinusitis. AJR Am J Roentgenol 181:939–944

Walter F, Ludig T, Iochum S, Blum A (2003) Multi-detector CT in musculo-skeletal disorders. JBR-BTR 86:6–11

Dose Reduction in CT Fluoroscopy

14

Nico Buls, J. de Mey

CONTENTS

14.1 Introduction

Computed tomography fluoroscopy (CTF) is a technique that provides the physician immediate feedback via the reconstruction and display of CT images in real time and overcomes the classic limitations of ultrasound imaging and conventional fluoroscopy. It matches the advantages of CT quality images to be matched with the speed of fluoroscopic guidance. CTF images: (1) have a wide dynamic range for imaging air, soft tissue and bone, (2) do not superimpose anatomical structures in the same way as conventional fluoroscopy does, and (3) they provide acceptable image quality relatively unaffected by the patient's breathing and motion (Kato et al. 1996; Froelich et al. 1998; Nickoloff et al. 2000). These characteristics allow immediate correction for the depth and direction of a needle during a percutaneous procedure. The obvious benefits of obtaining CT images in real time has made CTF a popular image guiding tool for various types of non-vascular and therapeutic interventions. Reported procedures using CTF guidance are, amongst others, precise needle placement, core biopsies, fluid collection aspirations, catheter insertion and drainage, local drug injections, radiofrequency ablations, placement of marking coils before stereotactic radiotherapy, lumbar nerve root blocks, vertebroplasty, jejunostomy tube insertion, arthrodesis of the spine and arthrography. The term "fluoroscopy" in CTF is only used by analogy with its conventional radiology counterpart; the only common thing is that both techniques are based on X-ray imaging to give the impression of a real-time imaging display. In this paper, the use of real-time CT is referred to as CT fluoroscopy.

N. Buls, MSc
J. de Mey, MD, PhD
AZ-VUB, Laarbeeklaan 101, 1090 Brussels, Belgium

14.1.1 Radiation Risk

A drawback of CTF is the potential for significantly high patient and staff doses. This is reported by several authors and also by competent bodies such as UNSCEAR in their 2000 report and ICRP in their report "Managing patient dose in computed tomography" (ICRP 2000). The interventional nature of CTF requires specific radiation protection considerations compared to conventional CT.

First of all, the patient skin dose is of concern. Since the scanning plane is kept constant during the entire procedure, the same skin area is repeatedly exposed and cumulative patient skin doses can be substantial, which may reach deterministic thresholds for radiation injuries. Maximum patient skin dose is therefore the risk-related quantity of concern, rather than the effective dose received by the patient. Effective dose from CTF is usually in the same order of magnitude as doses from diagnostic CT scans due to the small patient volume irradiated. With CTF, the user can select high exposure settings in terms of high tube potentials (120 kVp) and high tube currents (90 mA). These are high values when compared to the exposure factors used in, for example, vascular interventional radiological (IR) procedures. This results in substantial skin dose rates. Also, prolonged CT scanning times can be necessary in cases of small lesions that are difficult to access.

In contrast to conventional CT where the operator is protected behind the lead screen of the console, CTF procedures require the presence of the staff in the examination room during CT scanning (Fig. 14.1). As a result, the operator is exposed to an intense scatter radiation field. For such IR procedures it is standard practice for the medical staff to protect themselves by wearing a lead apron. A lead apron efficiently shields most important organs, reducing the effective dose received by the individual. However, surface doses to the parts of the body that are not shielded by the apron can be substantial. These are in particular the doses to both hands and the dose to the head (eyes). Also, information about these doses is often unavailable, as they are not monitored routinely. The dose to the hands is of particular concern due to its proximity to the scanning plane, and although it is unacceptable and every effort must be made to keep the hands out of the primary beam, the risk exists and it has been reported (Fig. 14.2). A CT room is usually

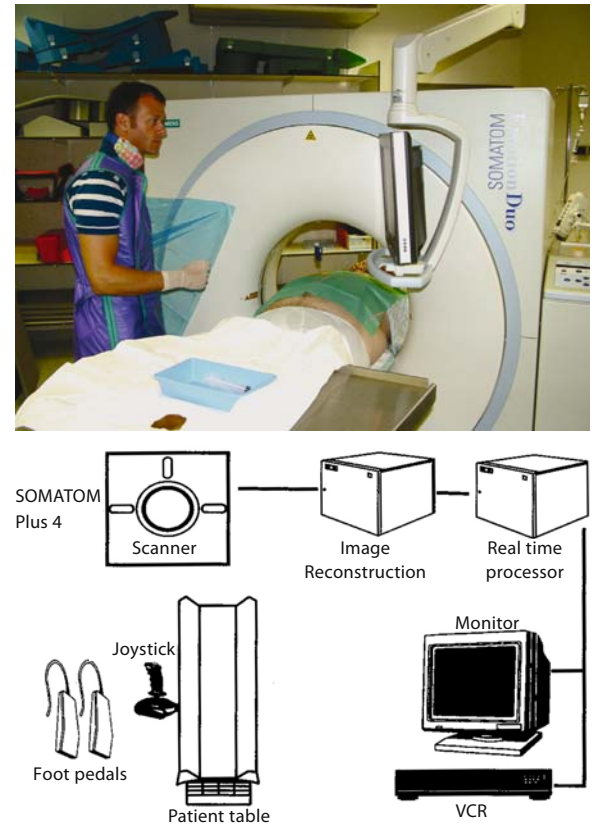

Fig. 14.1a,b. The presence of staff in the examination room during CT scanning can lead to their exposure to an intense scatter radiation field, especially of body parts not protected by the lead apron.

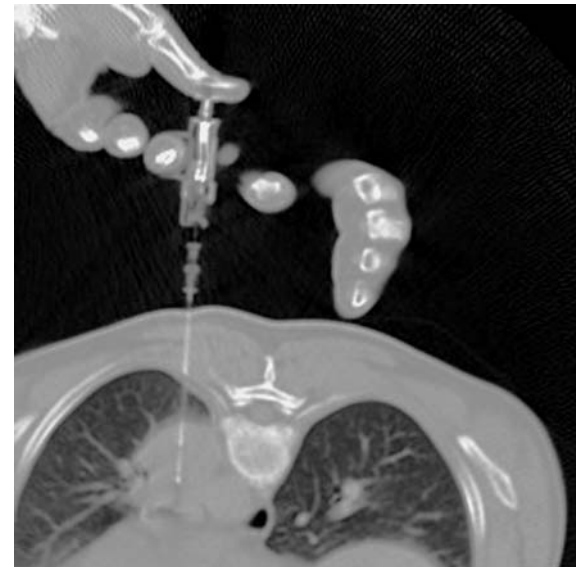

Fig. 14.2. The hand of the operator entering the primary beam during a CTF procedure

not as well equipped regarding radiation protection devices as compared to X-ray equipment that is used in, for example, vascular IR, where mobile lead shields or other barriers are often available. Also, as in many IR procedures, physicians may be involved of specialities other than radiology. Although it is a requirement of the Euratom 97/43 directive (EURATOM 1997) that staff performing practical aspects of a medical exposure should have received adequate training in radiation protection, a non-radiologist (e.g., pneumonologist) may not have had in-depth training in radiation management using diverse forms of fluoroscopic equipment such as CTF. Also the learning process involved with a new technology such as CTF will have a profound impact on both patient and staff doses. It is clear that CTF is another advancement in radiology with additional challenges in radiation management (Wagner 2000).

14.2 Technical Development

Since its introduction in radiology about 30 years ago, CT has been used as a guidance tool for various percutaneous interventions in both adults (Haaga and Alfidi 1976; Moran et al. 1979) and children (Baran et al. 1984). Since 1980, CT technology has made rapid progress with the development of slip ring technology, X-ray tubes with improved heat capacity, sub-second rotation times, fast array processors, and the development of partial reconstruction algorithms. These advantages contributed to the development of a real-time CT scanning system or CTF system that was introduced by Katada et al. (1994). They modified a third-generation CT scanner by adding a high-speed array processor (real-time reconstruction unit) to increase the image reconstruction speed (Katada et al. 1996) of the CT images. The first image is created from the initial 360° of raw data acquired during scanning. Subsequently, the corresponding data of the next 60° scanning are processed by the real-time reconstruction unit and replace the first 60° data set of the previous image. This technique of synchronous addition of new, and subtraction of old, 60° data sets allows the image to be updated at a rate of six frames per second and provides the operator a nearly real-time display of CT images. The system uses a reduced image matrix of 256×256 in order to achieve a higher response rate, which results in a delay time of 0.17 s.

Figure 14.1 shows the configuration of a typical CTF system (de Mey et al. 2000). The physician can operate the equipment entirely from in-room controls. He or she can run the CT scanning from the tableside during a procedure by pressing a foot pedal alongside the table, similar to in an angiography suite. The obtained real-time images are displayed on an in-room monitor located next to the table. A joystick attached to the couch can be used to control the patient's position.

Recent multi-detector row CT scanners can acquire multiple sections (usually three) that are displayed simultaneously on multiple monitors at increased frame rates (between 6 and 13 frames/s). Multiple-image CTF has the potential to increase the likelihood of localizing the tip of the needle in the *z*-direction during a single shot exposure due to the larger coverage (Katoaka et al. 2006). This could be especially helpful in angulated access routes.

Today, CTF is available from most CT manufacturers. The CTF packages are usually sold as upgrade options, usually consisting of an exposure foot pedal, tabletop control mechanism, in-room monitor(s), and sometimes including hardware to enable rapid image reconstruction (Keat 2001).

14.3 Scanning Techniques: Real-Time Method and Quick-Check Method

There are two common CT fluoroscopic guidance methods: the initial real-time method and the quick-check method developed by Silverman et al. (1999). Both are also often called the continuous method and the intermittent method respectively. The distinction between both is whether the system is operated continuously in real-time during needle manipulation or whether it is operated intermittently between interventional actions. Real-time CTF shows the exact needle trajectory during advancement or manipulation and requires the use of a standoff needle holder in order to increase distance to the scanning plane. With the quick-check method single fluoroscopic spot images are acquired to check the needle location after manipu-

lation and to confirm alignment with the puncture tract. During these spot images, the physician can retract his or her hands from the scanning plane. This reduces scatter exposure to the hands due to the increased distance to the scanning plane, and also prevents entering the primary beam with the hands (Fig. 14.2).

It is well acknowledged that the quick-check method reduces CT scanning time, and thus both patient and staff exposure. It is advocated to be used whenever possible, reserving the use of the real-time mode only in selected cases in which respiratory motion is a problem (Silverman et al. 1999; Carlson et al. 2001; Paulson et al. 2001).

14.4 Interventional Techniques: Clinical Procedures

Non-vascular diagnostic and therapeutic interventions with CTF are becoming more and more important in patient work up. This evolution is seen in spite of the improving performance of diagnostic imaging (CT, MR, ultrasound and nuclear medicine) and the improvement of surgical techniques. There are four main reasons for the shift to a more invasive diagnostic and therapeutic approach in radiology.

Due to the technical evolution, CT-fluoroscopy proves to be an accurate, safe and fast technique in guiding interventional procedures. Besides the evolution in imaging techniques, the development of new biopsy needles has made it possible to obtain core biopsy samples under image guiding in an accurate way. New drainage catheters and new ablation techniques have opened a broad spectrum of therapeutic options in non-vascular interventional radiology. A second reason is the evolution in oncology. A few decades ago major surgery was often the only option in oncology and it was obvious that a percutaneous biopsy before surgery was not useful in the patient work up. During the last few decades a broad spectrum of new therapeutic options have been developed in radiotherapy, oncology and surgery. Optimal morphological tumour staging (TNM classification) and anatomopathological staging (cancer type) in combination with biological tumour staging (receptors, etc.) are indispensable in modern oncological treatment. A third reason is the general trend towards a less invasive treatment. Percutaneous abscess drainage, pleural fluid drainage and percutaneous hepatobiliary interventions can sometimes be an alternative to open surgery. Percutaneous techniques are also economically attractive. A percutaneous biopsy of a suspected mass can often be done without the need for hospitalization or general anaesthesia. It is the fastest way to get information about the cancer type, without the need for complex and time-consuming examinations to characterize the primary tumour.

14.4.1 Diagnostic Percutaneous Biopsy

Image-guided biopsy can be performed with fine needles or with cutting core biopsy needles. CT-guided fine needle aspiration or core biopsy is generally regarded as a safe procedure with limited morbidity and extremely rare mortality even in difficult interventions (Zech et al. 2002). Even in children it is reported as a safe and accurate procedure that obviates open surgical biopsy in most patients (Cahill et al. 2004). Fine needle aspiration biopsy is sensitive to the detection of tumoral lesions (90%) but often does not allow adequate sub-typing of carcinoma and seldom yields specific pathologic diagnoses in cases of benign disease. The combined use of fine needle aspiration and core biopsy can improve the diagnostic ability of CTF-guided lung biopsy, even in small lesions (Yamagami et al. 2003).

In the thorax, pneumothorax remains the most frequent complication and tube thoracostomy is sometimes required. Fatal complications after thoracic fine needle aspiration due to systemic air embolism, haemorrhage, or pericardial tamponade have been reported but are rare. The use of fine needles (> 19 G) reduces bleeding complications and pneumothorax rate (Geraghty et al. 2003).

Passage through the caudal part of the costodiaphragmatic sinus is accepted to be safe. In difficult lesion localization, gantry tilt, angulated needle placement or an alternative approach (trans-sternal, through an iatrogenic pneumothorax, transcaval or transaortic) can be valuable options. Salinization is the injection of a saline solution through a small needle and can open a window for a bigger biopsy needle (Klose 1993). A coaxial biopsy technique is an extra manipulation, but has the advan-

tage of more needle stability and gives the possibility of taking more additional biopsies without the need for multiple skin passages. Even in lung biopsy samples this coaxial technique is reported to be safe (Laurent et al. 1999).

The assistance of an in-room anatomopathologist can be an aid to ensure that the biopsy sample is accurate for a correct diagnosis. However, this is still time consuming, and would have a major impact on workflow, since image-guided biopsy has become a routine procedure with short in-room times (around 15 min).

In most cases diagnostic interventional procedures are performed under local anaesthesia with lidocaine and require no sedation. In nearly all the recent studies diagnostic biopsy is performed on an outpatient basis.

14.4.2 Therapeutic Percutaneous Interventions

Percutaneous drainage (fluid collections, biliary and urinary), tissue ablation, nerve block and lesion marking before surgery with image guidance are well-established methods developed during the last three decades.

Percutaneous drainage of abscesses and fluid collections have been performed with ultrasound and CT guidance for more than 25 years. This technique has proven to be highly effective, with low morbidity. CTF on the other hand has been shown to be a practical clinical tool, in the more complex or difficult procedures as well (Meyer et al. 1998). Percutaneous biliary drainage procedures are often performed with fluoroscopic monitoring. The combination of CTF and C-arm fluoroscopy can be advantageous (Laufer et al. 2001). Percutaneous catheter biliary or abscess drainage may require substantial dilatation through the abdominal and back musculature and often results in placement of large catheters (> 10 F), these interventions are more painful and higher levels of sedation or even general anaesthesia can be necessary. In guiding a peripheral nerve block, CTF again offers major advantages, such as real-time viewing during needle progression and evaluating the diffusion of the injected solution if contrast is added. Even a transaortic approach with small 21-gauge needles has proven to be safe (Lee 2000).

There are a lot of possible strategies for obtaining tissue ablation. Chemical ablation or tissue instillation with agents such as ethanol has become less popular since the development of thermal ablation techniques. These latter techniques, such as radiofrequency ablation, laser ablation, microwave ablation, ultrasound ablation and cryoablation, use a large number of potential energy sources. A lot of different strategies are used for applications under different image-guiding modalities. Radiofrequency ablation under CT or ultrasound guidance is the technique most often used in the last 10 years and has proved to be an effective method (Rosenthal et al. 2003).

14.4.3 Typical CTF Procedure

The following section describes the course of a typical CTF biopsy procedure (Fig. 14.3). A CT scan prior to the CTF procedure is usually not required as most patients have a recently documented lesion. The CTF procedure starts with the selection of the technical scan parameters by the operator. The applied tube current depends on the scan region and patient size (see Tables 14.2 and 14.7) and should be selected to be as low as possible to allow adequate image quality. After scan parameter selection, the puncture tract is determined and the skin is marked for the approach. In some cases a contrast medium can be administered to opacify vessels or to retrieve a better delineation of soft tissue lesions (liver, kidneys, spleen and pancreas). After sterile preparation of skin and draping, local anaesthesia is applied. The anaesthetic's syringe needle can be bent to increase the radiologist's hand access to the scanning plane (Fig. 14.3a). CTF can be performed to check the anaesthetic needle tract. After local anaesthesia, a short guiding needle can be placed through the skin (Fig. 14.3b) and its position is checked with CTF. A needle holder is used to increase the distance to the scanning plane. Finally, a biopsy needle is placed through the guiding needle and is advanced towards the lesion (Fig. 14.3c) by applying intermittent fluoroscopy. Thanks to the presence of the guiding needle through the skin, there is less resistance during the needle's introduction and the biopsy itself. It also provides sufficient support for the biopsy needle, allowing the hands to be removed from the scan plane during fluoroscopy. When the biopsy needle is positioned into the lesion, a control fluoroscopy is necessary. Final CTF is applied after the techni-

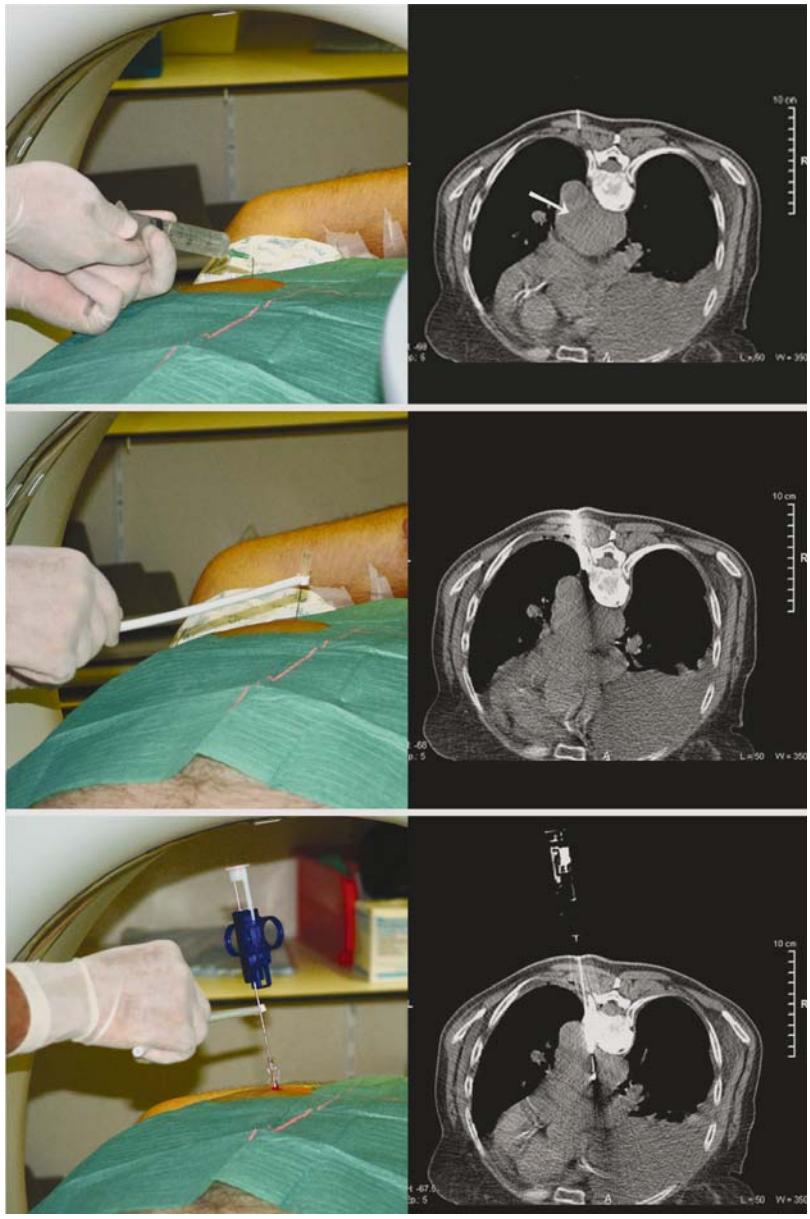

Fig. 14.3a–c. The course of a typical CTF biopsy procedure

cal procedure to check for bleeding, pneumothorax or other related complications.

Drainages of collections are performed following the same general technique. In more difficult procedures a short guiding needle can be applied. In a second step a guide-wire can be slid into the collection, followed by dilatation and placement of a drainage catheter. For larger lesions, direct puncture can be performed. Minimal table movements make it possible to follow the tip of the drainage catheter during placement.

14.4.4 Some Clinical Cases

The main advantage of doing interventional procedures under CTF is that the needle or catheter tract can be monitored at any time. Some clinical possibilities in diagnostic and therapeutic procedures are discussed in the following cases. The choice of technical material and of the puncture can differ; monitoring the needle during the intervention however is indispensable.

1. To guaranty accurate lung nodule biopsy it is necessary to view and follow the needle tip going into the lesion. Figure 14.4 shows a lesion adjacent to the anterior pleural wall. After performing a biopsy the small lesion is pushed into the lung and without CTF imaging during the procedure this would result in a non-diagnostic biopsy (Fig. 14.4b).
2. Access in a non-axial plane and changing the patient's position is one way to access lesions in difficult locations such as a lung lesion adjacent to the rib (Fig. 14.5).
3. Every mediastinal mass or lymph node can be accessed under CTF guidance. Paravertebral access is possible in combination with salinization of the paravertebral subpleural space (Fig. 14.6a, b). Anterior access is possible parasternally (Fig. 14.6c) or even trans-sternally. Access to a lymph node anterior to the trachea can be done through an intentionally created pneumothorax and with a transtracheal puncture (Fig. 14.6d).
4. Vertebral biopsy can be done in a transpedicular way (Fig. 14.7a) or a lateral way (Fig. 14.7b).
5. Access to a surrenal mass is possible by liver passage (Fig. 14.8a) or costodiaphragmatic sinus passage (Fig. 14.8b). Passage through the costodiaphragmatic sinus of the lung is safe if lung passage is limited to 2 cm.
6. In this case drainage of an abdominal collection was performed with a 10-gauge locked pigtail (Fig. 14.9).
7. Radiofrequency ablation is mostly used for liver lesions and can be done under ultrasound or CTF guidance. In cases of ablation of smaller bone lesions, CTF is preferred (ablation of osteoid osteoma Fig. 14.10a, b). Ablation of small long nodules is not always the first therapeutic choice but can also easily be done under CTF guidance (Fig. 14.10c, ablation, and Fig. 14.10d control 3 weeks after ablation).
8. Coeliac block under CTF guidance, with an anterior approach, is demonstrated in Figure 14.11a,b. Another way to perform a coeliac block is posteriorly, shown in Figure 4.11c (paravertebral) and Figure 14.11d (with passage through the aorta). Aortic passage is safe with smaller needles, in this case a 20-gauge needle.
9. Lung lesions can be marked to optimize radiotherapy. This is shown in Figure 14.12, where a small vascular coil is placed in a lung nodule adjacent to the mediastinum.

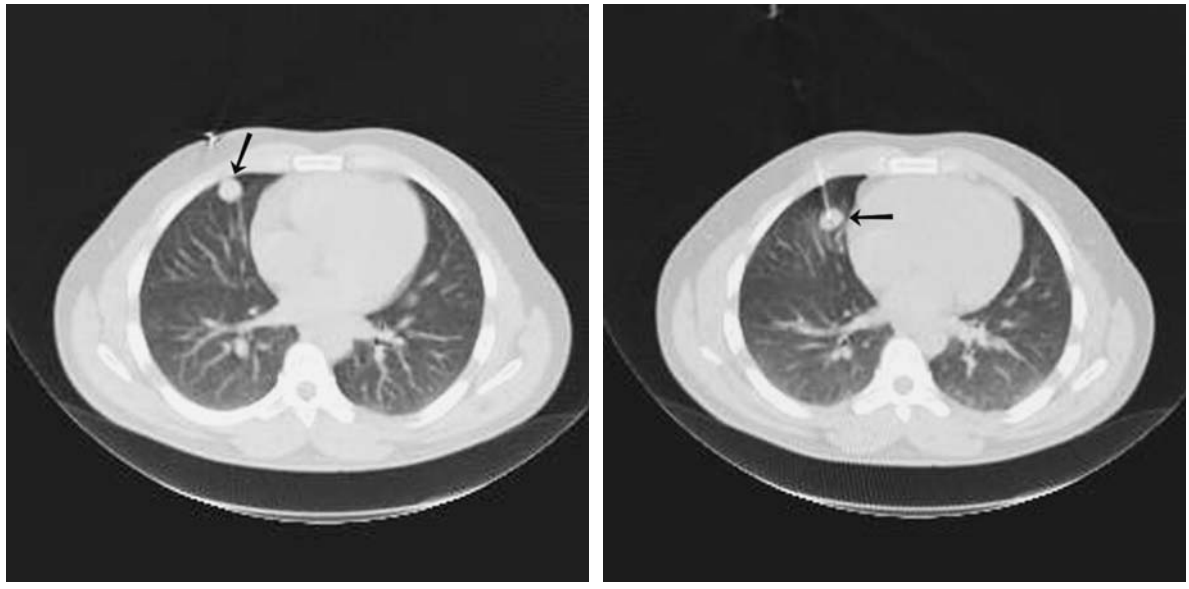

a b

Fig. 14.4a,b. Case 1: lung nodule pushed away during biopsy

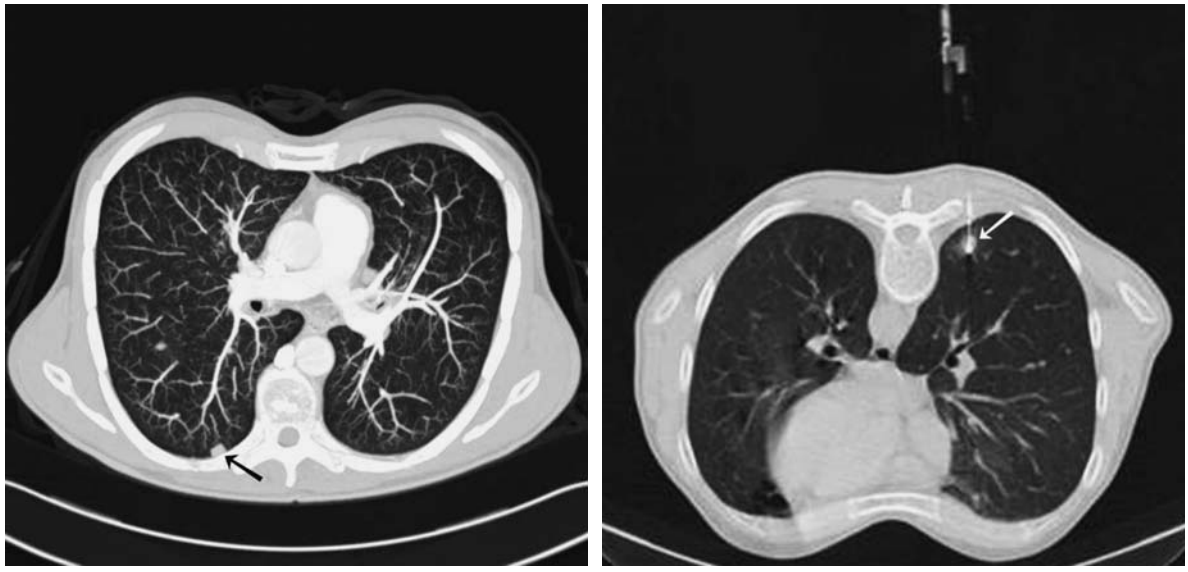

Fig. 14.5a,b. Case 2: lung nodule biopsy in locations of difficult access

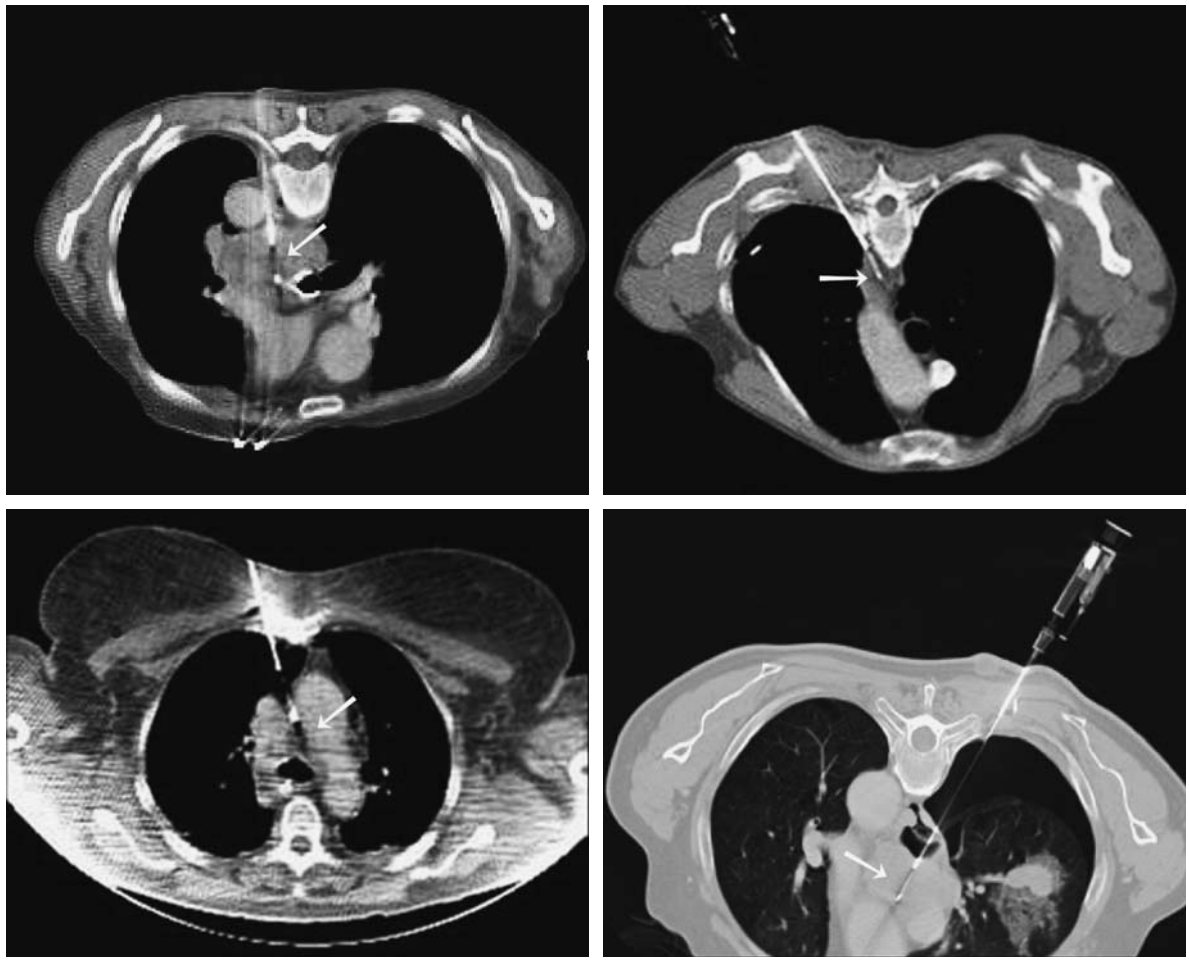

Fig. 14.6a–d. Case 3: biopsy of mediastinal mass by paravertebral access (**a**,**b**), anterior access (**c**) and transtracheal access with intentionally created pneumothorax (**d**)

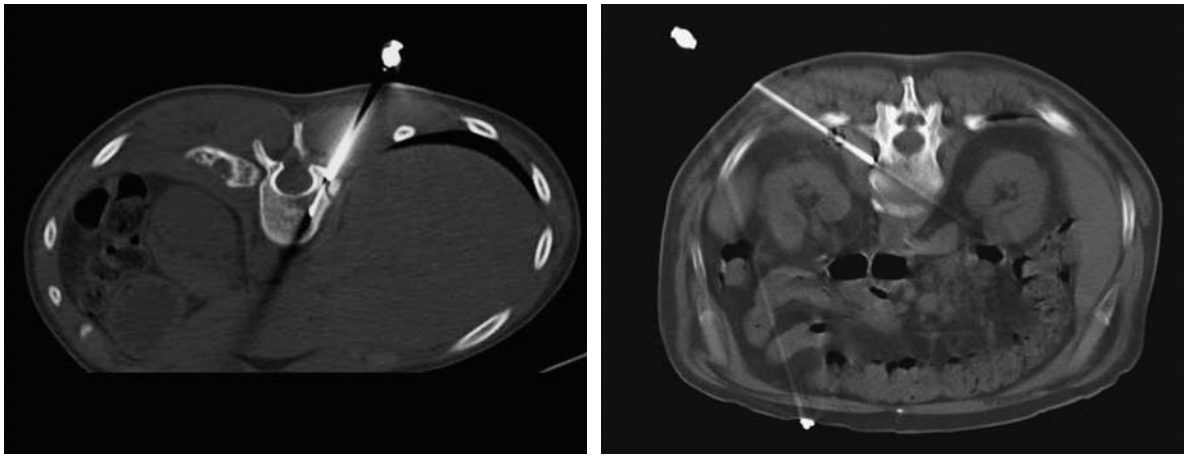

a b

Fig. 14.7a,b. Case 4: vertebral biopsy in a transpedicular (**a**) and lateral (**b**) way

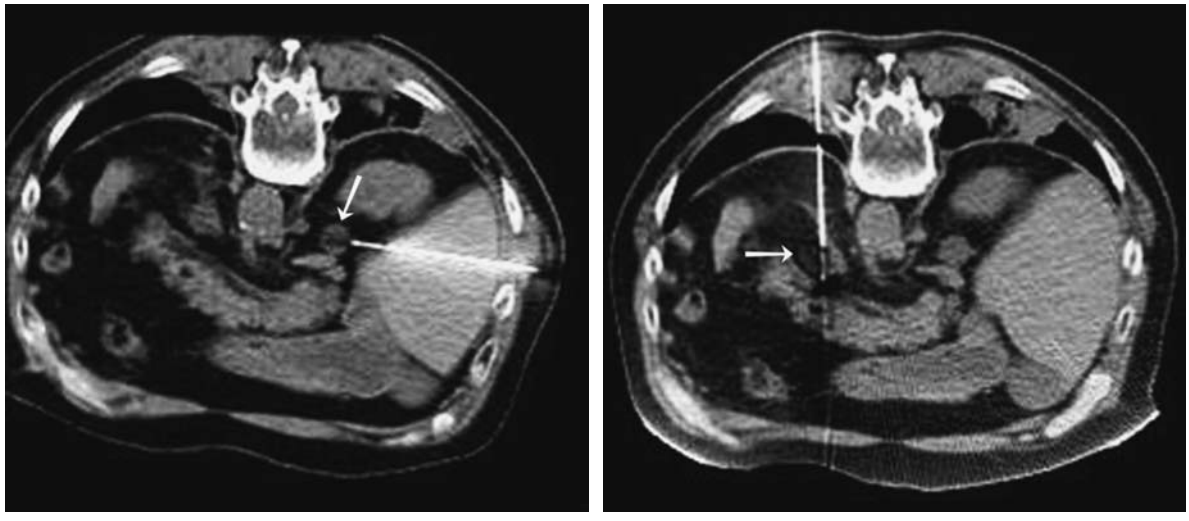

a b

Fig. 14.8a,b. Case 5: surrenal biopsy by liver passage (**a**) and costodiaphragmatic sinus passage (**b**)

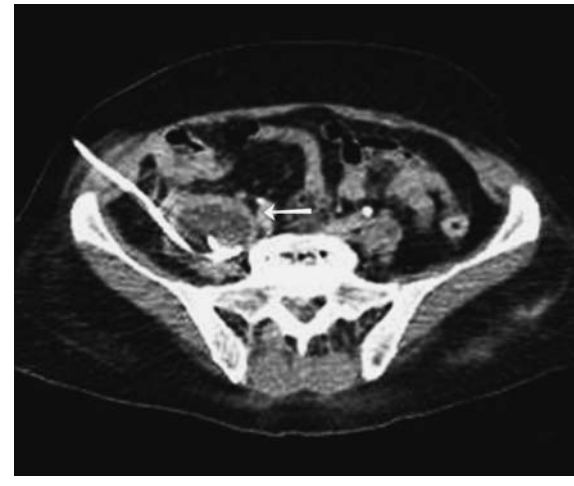

Fig. 14.9. Case 6: drainage of abdominal collection

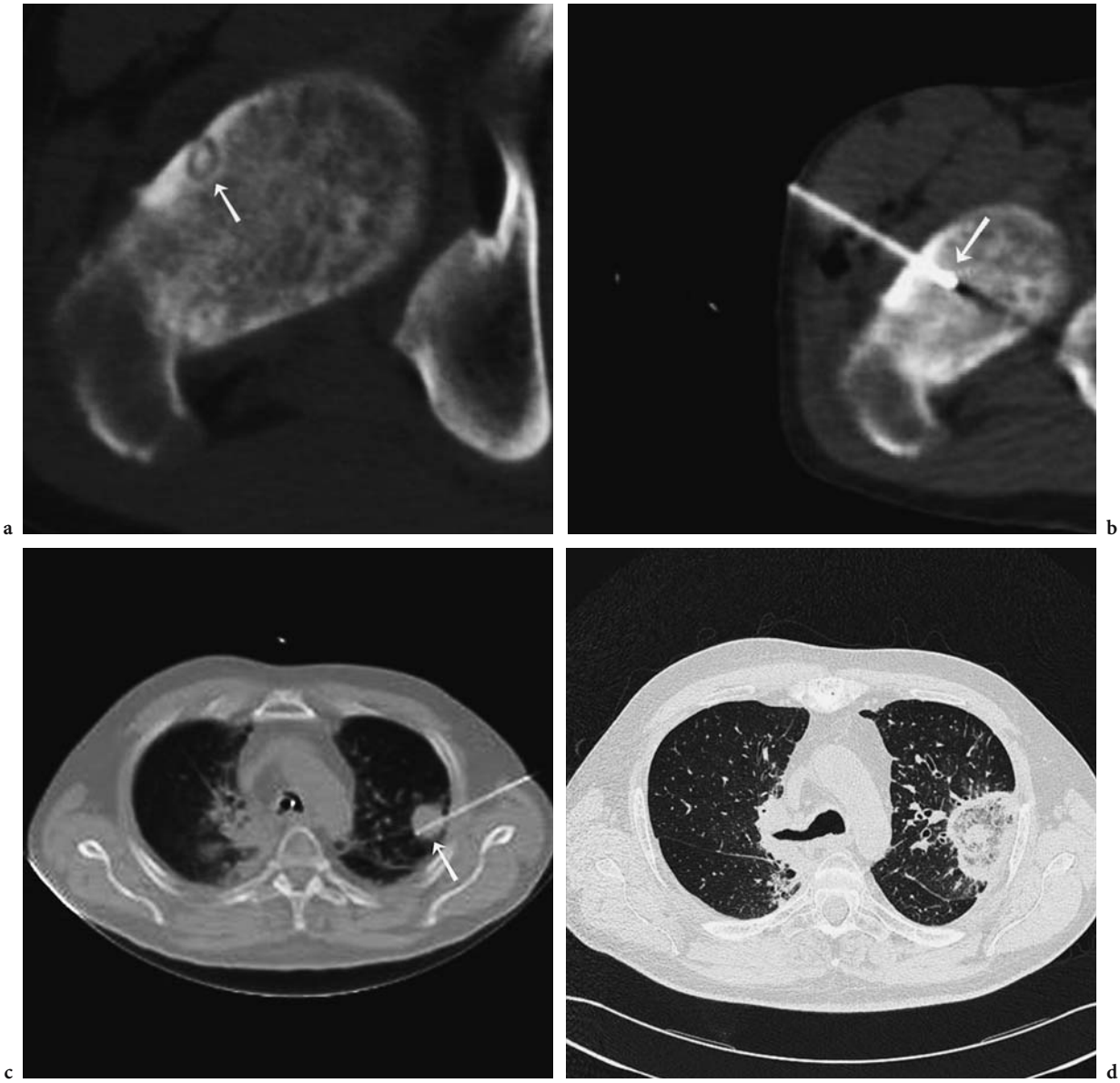

Fig. 14.10a–d. Case 7: radiofrequency ablation of osteoid osteoma (**a**,**b**) and lung nodule (**c**) with a control image 3 weeks after ablation (**d**)

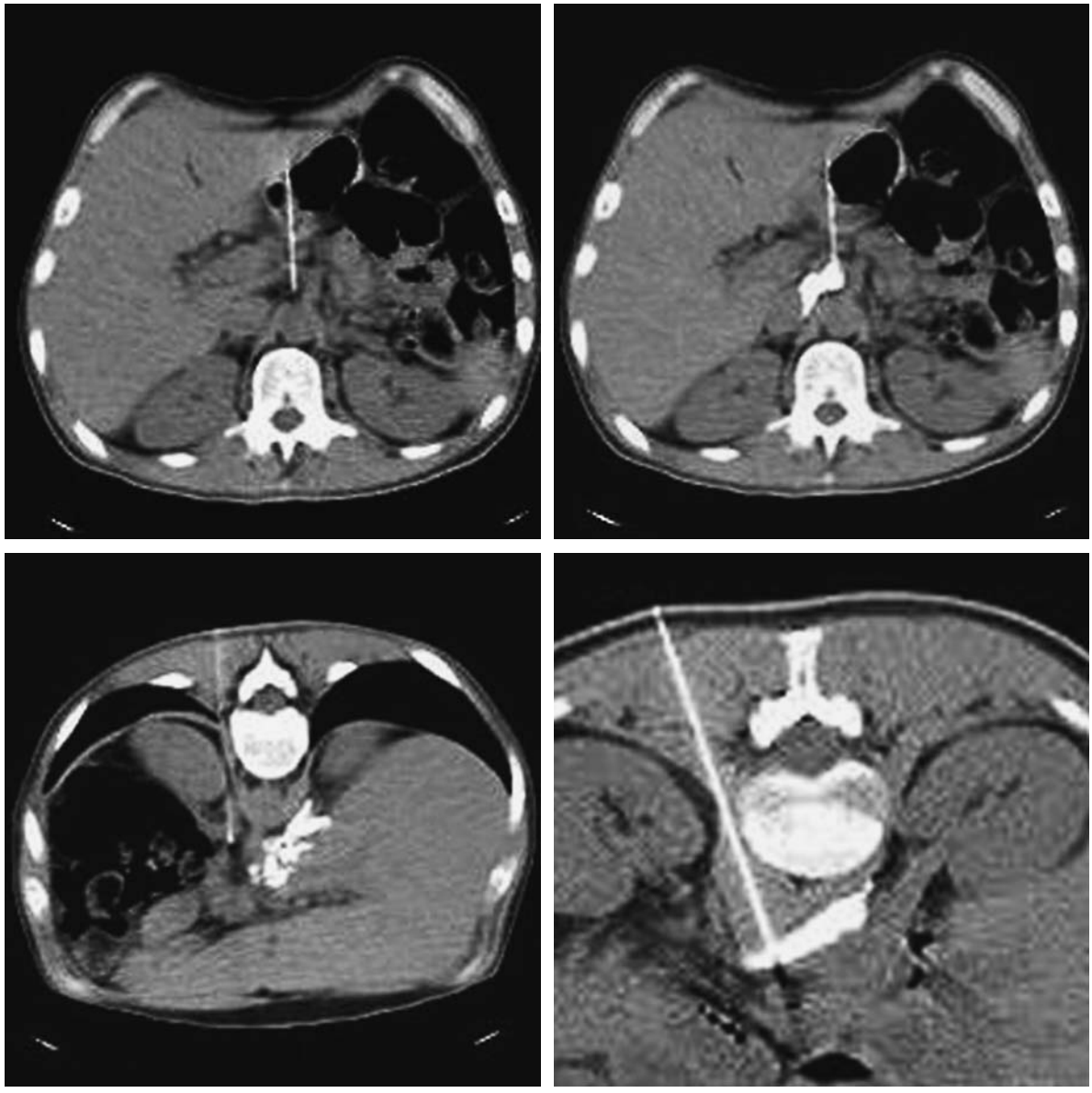

Fig. 14.11a–d. Case 8: coeliac block with anterior approach (**a**,**b**) and posterior approach paravertebrally (**c**) and with passage through the aorta (**d**)

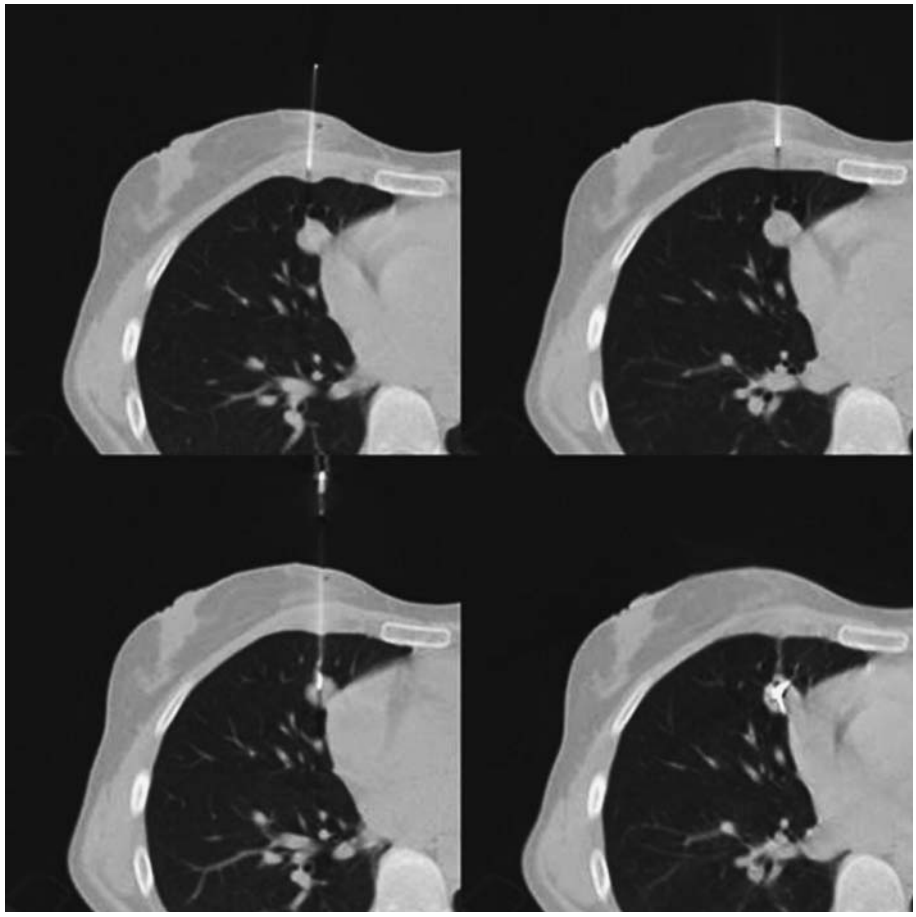

Fig. 14.12. Case 9: coil (*marker*) placement in lung lesions to optimize radiotherapy

14.5 Dose to the Patient

Since the scanning plane is mostly kept constant during a CTF procedure, the same skin area is repeatedly exposed and cumulative patient skin doses can be substantial. Maximum patient skin dose is therefore the risk-related quantity of concern in CTF, rather than the effective dose as in conventional CT. Effective dose from CTF is usually in the same order of magnitude as doses from diagnostic CT scans due to the small patient volume irradiated.

14.5.1 Deterministic Effects – Skin Injuries

In the field of IR, specific concern exists about radiation-induced skin injuries. Skin changes such as erythema, ulcers, telangiectasia and dermal atrophy are potential deterministic effects (Koenig et al. 2001). Such effects occur only when the radiation dose exceeds a certain threshold, and their severity increases rapidly with dose. The single-fraction threshold dose for these deterministic effects (transient erythema) is generally accepted to be 2 Gy (Wagner et al. 1994). Table 14.1 summarizes single-fraction threshold skin entrance doses for various reported injuries (from Koenig et al. 2001). Fluoroscopy-induced injuries can be recognized by the location of the injury as being congruent with the entrance of the X-ray beam. The injury often shows well-defined borders. Some patients may be at greater risk of injury because of pre-existing health conditions such as collagen vascular disease, diabetes mellitus, or telangiectasia, or because of a high radiation dose from a previous procedure. During the last 10 years, more than 70 cases of skin injuries have

Table 14.1. Threshold skin entrance doses for various skin injuries (from Koenig et al. 2001)

Effect	Dose (Gy)	Onset
Early transient erythema	2	Hours
Main erythema	6	~10 days
Temporary epilation	3	~3 weeks
Permanent epilation	7	~3 weeks
Dry desquamation	14	~4 weeks
Moist desquamation	18	~4 weeks
Secondary ulceration	24	>6 weeks
Late erythema	15	~8–10 weeks
Ischemic dermal necrosis	18	>10 weeks
Dermal atrophy (1st phase)	10	>12 weeks
Dermal atrophy (2nd phase)	10	>1 year

been reported in the reference literature (Koenig et al. 2001). Most of the reported cases are involved with cardiac interventions that use prolonged exposure times with a high dose rate combination. None of the reported cases are due to CTF. In 1994, the United States Food and Drug Administration issued a public health advisory concerning the avoidance of skin injuries induced during fluoroscopically guided procedures (US FDA 1994). Also, the United Nations Scientific Committee on Effects of Atomic Radiation specifically expresses their concern about the potential for high patient and staff doses with CTF in their 2000 report (UNSCEAR 2000).

14.5.2 Skin Dose Characteristics in CT

The main determinants of patient skin dose in CT are not only the technical exposure factors (beam width, tube potential and tube current), but also the location of the patient inside the gantry.

14.5.2.1 Influence of Patient Size and Position Inside the Gantry

Avilés et al. (2001) studied extensively the relation between skin dose in CT and both the position and size of the patient. They found that, for phantoms simulating adult patients, the skin dose is independent of phantom size and varies mainly with phantom position along the vertical axis of the CT plane. The maximum surface dose is reached at the isocentre of the scanner and decreases as the surface moves vertically away. The design of the bow-tie filter determines the shape of this variation. This effect of patient position on skin dose is illustrated by Figure 14.13, which shows the normalized peak surface dose as a function of the vertical position in the gantry for two phantom sizes. The data were obtained by measuring the surface dose with thermoluminescent dosimeters (TLD) on the surface of both 32-cm- and 16-cm-diameter phantoms for various vertical positions in the gantry of a Siemens Somatom Emotion Duo scanner (Siemens Medical Systems, Erlangen, Germany). As can be observed, surface doses are independent of phantom size. However, patient size has an indirect effect on skin dose

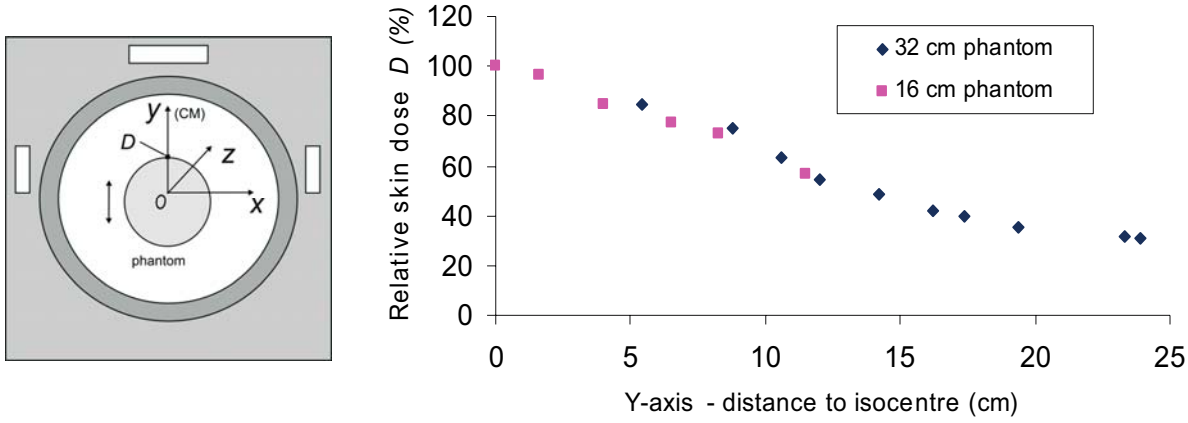

Fig. 14.13. Relative skin dose as a function of its distance to the isocentre, for two phantom sizes (after Avilés et al. 2001)

because it determines the location of the patient's surface in the gantry. As a consequence, skin doses will be higher for smaller patients (smaller equivalent diameter), for children, and also for patients where the table is placed in the lowest position inside the gantry. In this position, the shortest distance between the isocentre and the anterior skin surface is likely to be reached. The data of Figure 14.13 shows that, when both phantoms are placed in the isocentre, the skin dose rate is almost double for the 16-cm phantom compared to the 32-cm phantom, and that the skin dose rate at the isocentre is almost 3 times as high as the skin dose rate at a distance of 16 cm from the isocentre. The strong effect of patient size and position warrants knowledge of both when estimating patient skin dose in CT, especially when using phantoms.

14.5.2.2 Influence of Technical Scan Settings – Dose Optimization

With CTF, the operator can select tube potential (kVp), tube current (mA), tube rotation time (s) and slice thickness (mm). Scanner technique settings play an important role in both patient and staff dose since the relative X-ray tube output is roughly proportional to the product of the tube current (mA) with the power of 2.5 of the tube potential ($kVp^{2.5}$) and the exposure time (s). A low kVp-mA-s technique will thus result in a significant decrease in patient and staff dose. Reported scan parameters for CTF vary depending on the scanner type and model used. Tube potential can typically range between 80 and 130 kVp, but is often reported fixed at 120 kVp for CTF as is the case in conventional CT. Reported tube current settings usually vary between 20 and 90 mA. Slice thickness should be sufficiently wide to monitor the puncture tract and is usually set between 5 and 10 mm.

The most important adjustable parameter in CTF that affects dose is the tube current. CTF does not apply automatic tube current modulation as modern systems do in conventional CT. Tube current has to be intentionally adapted by the user according to the size of the anatomical region of interest. As in conventional CT, there is a linear relationship between tube current (mA) or tube current–time product (mAs) and dose, and an inverse proportional relationship between image noise and the square root of dose. Within the ALARA concept, the lowest possible tube current values should be used that allow an adequate image quality in the anatomical region of interest. As CTF procedures require less diagnostic image quality, tube currents can be drastically reduced when compared to conventional CT. Also, procedures in low attenuating regions such as the thorax allow a tube current reduction in comparison to higher attenuating regions such as the abdomen. Table 14.2 shows technical CTF settings that are

Table 14.2. Technical CTF scan settings that are reported in the literature

Author	Scanner model	Tube potential (kVp)	Tube current (mA)	Slice thickness (mm)
Buls et al. (2003)	Siemens Somatom plus 4	120	90	8
Buls et al. (2004)	Siemens Emotion duo	120	38	5
Kataoka et al. (2006)	GE HiSpeed CT/I	120	30–80	7
Kataoka et al. (2006)	Toshiba Aquilion 16	120	30–80	8
Stoeckelhuber et al. (2005)	Toshiba Aquilion multi	120	50	n.a.
Meleka et al. (2005)	Toshiba Aquilion 16	120	50	n.a.
Yamagami et al. (2003)	Toshiba X Vigor Laudator	120	30–50	3
Gianfelice et al. (2000)	GE Prospeed	120	50	10
Froelich et al. (1998)	Siemens Somatom plus 4	120	50	n.a.
Paulson et al. (2001)	GE HiSpeed CT/I	140	13	5
Silverman et al. (1999)	Siemens Somatom plus 4	120	50–90	10

reported in the literature. Tube currents normally range from 10 to 90 mA, and are often set at 50 mA.

There are no real guidelines for tube current settings as there are in conventional CT. A study by Carlson et al. (2001), from data on 203 consecutive CTF procedures, reported following typical applied tube current values: 10 mA for paediatric patients, 10–40 mA for chest cases, 40–50 mA for abdominal cases and 30–50 mA for bone cases. A further reduction could be obtained by using even lower current values when possible, particularly when lesions are large, fluid or cystic (good inherent contrast), superficial, or easily accessible. This encourages greater radiologist involvement in setting up the scan so the lowest current value is used.

It should be noted, however, that tube current settings that are established with one specific CT scanner model might not be applied generally. Often, *dose* in CT is characterized by tube current due to their linear relationship, but tube output (mGy/mA) may differ a lot depending on the CT scanner's hardware components such as the X-ray tube and beam shape filtration. Selected dose values should be specified in physical measurable dose quantities such as CTDIw, rather than as mA values.

14.5.3 Reported Patient Doses from CTF

Comparing reported patient doses from CTF is not straightforward, as several variables should be taken into account such as the type of included procedures (biopsies, aspirations, etc.), type of scanner, exposure settings (kVp, mA and collimation), exposure time, CTF technique (intermittent or real-time) and patient's position inside the gantry. Also, the applied method of patient skin dose estimation might vary. Some authors use the periphery CTDI of the standard 32-cm-diameter dosimetric body phantom as a metric for patient surface dose (Nickoloff et al. 2000; Teeuwisse et al. 2001), others apply a correction factor to convert peripheral CTDI to skin dose (Nawfel et al. 2000), and also, humanoid Alderson phantoms (The Phantom Laboratory, New York) are used to measure surface dose rate (Paulson et al. 2001). With phantoms, patient size is standardized, which allows investigation of the influence of parameters such as tube current and beam collimation independently. Usually, the measured surface dose rate data are extrapolated according to the length of exposure to the CTF procedure. A drawback of such a method is that it may not include important factors that influence skin dose, such as the movement of the patient in relation to the thin beam slice, and the influence of the patient's position (and size) in the gantry. These factors are included when in vivo skin dose monitoring is applied (Buls et al. 2003).

14.5.3.1 Reported Patient Skin Dose Rates

Reported patient surface dose rates that are measured by phantom are shown in Table 14.3. For comparison, the surface dose rate that is observed for typical conventional angiography equipment is also included. The last column estimates the exposure time that is required to reach the 2 Gy threshold dose for deterministic radiation skin effects.

Depending on technical settings, reported surface dose rates might vary from 10 cGy/min up to about 60 cGy/min. For equal technical settings, reported surface doses tend to be higher for smaller phantom sizes (data expressed per mAs). This is congruent with the fact that surface dose decreases as the surface moves further away from the isocentre, as discussed in Section 14.5.2.1. With a dose rate of 62.4 cGy/min, the 2 Gy threshold skin dose for transient erythema would be reached as quickly as after 3.2 min of scanning. Such scanning times could be reached for one patient when difficult procedures are involved. Mean reported exposure times are usually below 1 min (Table 14.4), but maximum CT scanning times for one case of 9.1 min (Silverman et al. 1999) and 13.6 min (Buls et al. 2003) are also reported. Such exposure times could clearly result in skin doses above 2 Gy when high exposure settings are used.

As stated before, tube current has a nearly linear relationship with dose under equal exposure conditions. This is illustrated by the data of Nawfel et al. (2000) who reported a dose rate of 32.4 cGy/min with 50 mA, compared to 62.4 cGy/min with 90 mA. Paulson et al. (2001) intentionally applied a low tube current of 10 mA, which resulted in a surface dose rate of only 10.8 cGy/min.

Surface dose rates from CTF can also be compared to the observed skin dose rates for conventional fluoroscopy. For C-arm angiography X-ray equipment the surface dose rate measured on a 20-cm PMMA phantom is typically below 2 cGy/min during fluoroscopy. This is roughly a factor of 30 less than the surface dose rate observed during CTF with maximal exposure settings of 120 kVp and 90 mA.

Table 14.3. Reported patient skin dose rates in CTF, determined by phantom measurements

Method	Author	Tube potential (kVp)	Tube current (mA)	Dose rate (cGy/min)	Exposure time (min) required to reach 2 Gy threshold
Periphery CTDI of 32-cm-diameter PMMA phantom					
	Nickoloff et al. (2000)	120	30	23.9	8.4
	Teeuwisse et al. (2001)	120	25	12.6	15.9
	Teeuwisse et al. (2001)	140	25	17.4	11.4
	Nawfel et al. (2000)	80	135	27.6	7.2
	Nawfel et al. (2000)	120	50	32.4	6.2
	Nawfel et al. (2000)	120	90	62.4	3.2
Periphery CTDI of 20-cm-diameter PMMA phantom					
	Silverman et al. (1999)	Varying	Varying	18.6–82.8	10.8–2.4
Periphery CTDI of 16-cm-diameter PMMA phantom					
	Nickoloff et al. (2000)	120	30	46.3	4.3
	Teeuwisse et al. (2001)	120	25	20.4	9.8
	Teeuwisse et al. (2001)	140	25	28.2	7.1
TLD on Alderson Humanoid phantom					
	Paulson et al. (2001)	140	10	10.8	18.5
Typical conventional fluoroscopy: TLD on 20 cm PMMA					
	Angiography abd	80	3	typ. 1.0–2.0	200–100

In consequence, patient skin doses accumulate very rapidly in CTF compared to conventional fluoroscopy. Whereas with conventional fluoroscopy the 2 Gy threshold dose is reached after 100–200 min of fluoroscopy, it can be reached in CTF after only 3–10 min of scanning.

14.5.3.2 Reported Skin Doses

Table 14.4 shows reported patient skin doses from CTF for various types of CTF procedures, together with their respective scan settings and applied CTF technique. Doses are expressed per procedure and vary from about 30 mGy up to 800 mGy. For comparison, reported skin doses from typical conventional fluoroscopy angiography and IR procedures are also included.

The reported mean exposure times from CTF vary from 15 to 150 s and are usually below 60 s. Some authors reported very short exposure times that were achieved for various types of procedures. Paulson et al. (2001) reported a mean exposure time of only 18 s for 189 various procedures. Also, Carlson et al. (2001, 2005) reported very short exposure times for various types of procedures with median values in the range of 16–22 s.

The combination of such short exposure times with a low tube current technique results in strongly reduced patient doses. Paulson et al. (2001) and Carlson et al. (2001) and reported skin doses of only 32 mGy and 43 mGy per procedure respectively. The fact that these values were reported for various types of CTF procedures shows that a technique using a low tube current and short exposure time can be achieved in clinical routine.

Table 14.4. Reported patient entrance skin doses per procedure during CTF. (*PTA* Percutaneous transluminal angioplasty)

Author	Procedures	CTF technique	Technical settings (kVp)/(mA)	Exposure time (s)	Skin dose (mGy)
Silverman et al. (1999)	Biopsies (61), aspirations/drainages (34)	Quick-check (19%) Real-time (71%)	120/50–90	79	740
Paulson et al. (2001)	Biopsies (85), aspirations/drainages (78), injections (57)	Quick-check (87%) Real-time (2%) Combination (11%)	140/10	18	32
Teeuwisse et al. (2001)	Biopsies (35)	Quick-check	120–140/25	28	130
Nickoloff et al. (2000)	Biopsies (78)	n.a.	120/30	97	400
Buls et al. (2003)	Biopsies (46), aspirations/drainages (22), ablations (14)	Quick-check	120/90	151	346
Buls et al. (2004)	Biopsies (48)	Quick-check	120/38	73	111
Carlson et al. (2001)	Biopsies (146), aspirations/drainages (57)	Quick-check (97%) Combination (3%)	120/10–50	21	43
Carlson et al. (2005)	Biopsies (56) bellows	Quick-check	120/10–50	16	38
	Biopsies (57)	Quick-check	120/10–50	22	51
Nawfel et al. (2000)	Biopsies		120/90	80	832
Typical IR conventional fluoroscopy					
McParland (1998)	Hepatic angiography				340
McParland (1998)	Renal angiography				100
Miller et al. (2003)	Carotid stent				597
Miller et al. (2003)	Renal PTA with stent				1812

14.6 Dose to the Staff

Unlike diagnostic CT, the physician enters the room during CTF scanning and stands next to the patient while manipulating the interventional device (Fig. 14.1a). Also other staff members such as nurses or anaesthetists can be present in the room during scanning and are also subjected to scattered radiation. The doses to the hands and the eyes are of particular concern as they are usually unshielded.

14.6.1 Scattered Radiation

The main source of radiation to the radiologist is the scattered radiation that exits the patient. For all radiographic procedures except mammography, most photon interactions in soft tissue produce scattered X-ray photons. Scattered photons are detrimental in radiographic imaging because they violate the basic geometric premise that photons travel in straight lines (Bushberg et al. 2002). Compton scattering (also called inelastic scattering) is the predominant interaction of X-ray photons in the diagnostic energy range. Compton scattering results in the ionization of an atom and a division of the incident photon energy between the scattered photon and an ejected electron. The Compton scattered photon may traverse the medium (patient) without interaction or may undergo subsequent interactions. The majority of the incident photon energy (120 keV_p) is transferred to the scattered photon, which results in scattered photons with relatively high energies and about equal penetrability as the primary beam.

The scatter interaction fraction is proportional to the primary photon fraction and the probability of interaction increases as the incident photon energy

increases. In general, the scatter radiation field per unit of time around a CT scanner is more intense and energetic than the scatter field encountered in conventional fluoroscopy (e.g. angiography room). This is due to the use of both more intense (due to increased mA and kVp) and higher energy (increased kVp) beams in CTF. Interventional procedures with conventional fluoroscopy usually operate with beam energies at around 80 kVp and tube currents between 1 and 10 mA, compared to 120 kVp and 30–90 mA with CTF. These elevated scatter radiation fields involved with CTF result in an elevated risk for the operator and require adequate radiation protection management.

Another concern in CTF is the direction of the scattered radiation field. In radiography, the direction of scattered radiation is mainly directed back towards the X-ray tube. This is a well-known effect and has already been documented by several authors (Trout and Kelley 1972) and reports (ICRP 2001). For this reason, an under-table X-ray tube geometry is generally applied in IR, which directs the scatter radiation towards the floor, and prevents the upper body of the worker (head and neck) from receiving a large fraction of scattered radiation. With CTF, the operator cannot control the scatter direction as in IR due to the continuous rotation of the X-ray beam around the patient. The scatter field in CT is nearly symmetrical in both horizontal and vertical directions, apart from absorption of nearby components such as the gantry or the table stand. Figure 14.14 shows the scatter radiation direction of a conventional fluoroscopy C-arm X-ray system and a CT scanner system. The under-table tube geometry of the C-arm system causes the scattered radiation to be directed towards the floor, reducing operator exposure. Such a dose-reducing method is not possible with CTF.

14.6.2 Personal Protection – Radiation Dose Monitoring

For CTF, it is standard practice for the medical staff to protect themselves from scattered radiation by wearing a lead apron. An apron with 0.5 mm lead equivalent efficiently shields most radiosensitive organs (lungs, red bone marrow, stomach, gonads, colon, etc.), limiting the effective dose received by the individual. For interventions where scattered radiation is directed towards the upper part of the body, such as with CTF, it is also recommended to use additional lead collar protection. The use of an additional collar results in high organ dose reductions for all organs at risk in the neck region (thyroid, oesophagus). In particular, the dose to the thyroid is of interest as it presents a significant contribution (5%) to the effective dose. Appropriate personal protection limits the effective dose to the worker; however, surface doses to unshielded parts of the body can be substantial.

According to legislation, classified radiation workers are subjected to annual dose limits and they should be monitored by a radiation badge. For workers that systematically wear a lead apron as in CTF, the use of two radiation badges is recommended (ICRP 1982). One dosimeter should be worn

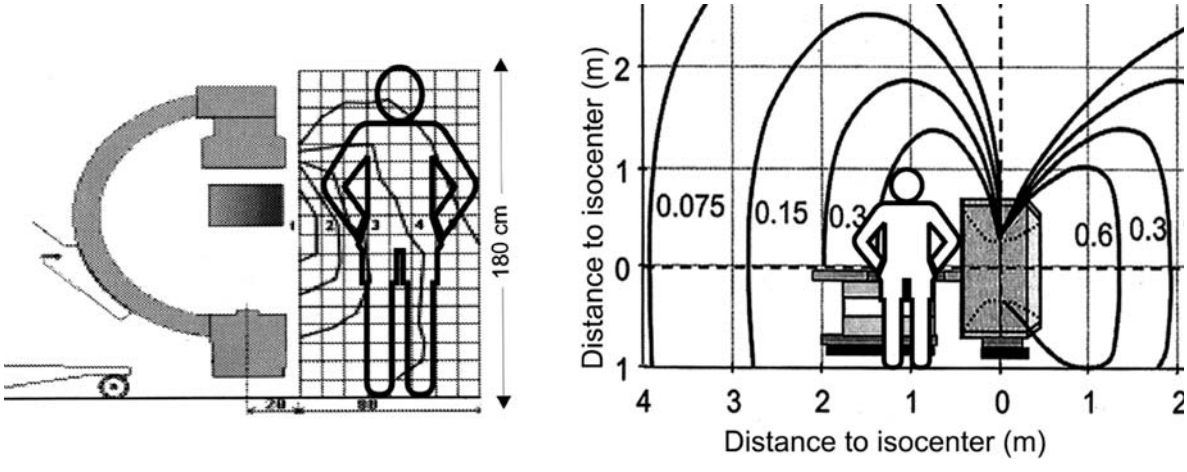

Fig. 14.14. Isoexposure contours of a conventional fluoroscopy C-arm equipment and a CT scanner (*left image* from Philips Medical Systems, *right image* from Bushberg et al. 2002)

under the apron (shielded) and a second one should be worn outside (unshielded) the apron. A single dosimeter worn under the apron will underestimate the effective dose of the worker as it does not take into account the dose to the unshielded parts of the body, and neither does it provide information about the dose to the eyes, which is of special interest in CTF.

14.6.3 Reported Scattered Dose Rates from CTF

Several authors evaluated scattered exposure rates from a phantom during CTF by measuring ambient dose rates at various distances with dose monitoring equipment. The dose to the operator during CTF can be estimated from these data by multiplying the dose rate that is observed at a specific distance by the time the operator spends at that location during scanning. Usually, the dose rates at two distances to the scanning plane are considered: the level of the hand (5–25 cm) and the level of the body/head (~100 cm). Such data often provide useful information concerning the influence of several parameters (e.g. distance, tube current, etc.) on scatter dose rate but they do not include the actual variation of the position of the staff during the procedure. Table 14.5 shows reported scattered dose rates at two positions from the scanning plane: the considered position of the hand and the body of the operator. As with patient dose rates, several phantom sizes are used.

Table 14.5. Reported scattered dose rates from CTF, determined by measuring ambient dose rates from phantoms

Method	Author	Technical settings (kVp)/(mA)	Scattered dose rate at the level of the			
			Hand		Body–head	
			(μGy/s)	@ (cm) from plane	(μGy/s)	@ (cm) from plane
Scattered exposure from 32-cm-diameter PMMA phantom						
	Nickoloff et al. (2000)	120/30	17	@ 20 cm	0.93	@ 100 cm
	Kato et al. (1996)	80/30	1140	@ 0 cm		
	Kato et al. (1996)	80/30	19	@ 4 cm		
Scattered exposure from 20-cm-diameter PMMA phantom						
	Silverman et al. (1999)	120/50	29.5	@ 10 cm	0.97	@ 100 cm
	Nawfel et al. (2000)	120/50	23.6	@ 10 cm		
Scattered exposure from Alderson humanoid phantom						
	Stoeckelhuber et al. (2005)	120/50	39.5	@ 15 cm		
	Paulson et al. (2001)	140/10	0.06	@ 25 cm	0.03	@ 60 cm
Scattered exposure, not specified						
	Gianfelice et al. (2000)	120/50	18	@ 10 cm		
Scattered exposure from Alderson humanoid phantom with a lead drape						
	Stoeckelhuber et al. (2005)	120/50	3.2	@ 15 cm		
Scattered exposure from Alderson humanoid phantom with 30 cm needle holder						
	Stoeckelhuber et al. (2005)	120/50	13.2	@ 30 cm		
Scattered exposure from 20-cm-diameter PMMA phantom with a lead drape						
	Nawfel et al. (2000)	120/50	6.8	@ 10 cm		

The second part of the table shows reported scattered dose rates when radiation protection methods are applied, such as using a lead drape or prolonged standoff needle devices.

Reported scatter dose rates at the level of the hand of the operator usually vary between 20 and 40 μGy/s, depending on the scanner type, technical scan settings and the distance to the scanning plane of the measurement. Lower dose rates can be achieved by: (1) reducing exposure settings, (2) increasing distance to the scanning plane with the use of needle holders, or (3) by using a lead barrier. The dose rate inside the primary beam itself can be over 1000 μGy/s, even with reduced scan settings. Entering the primary beam leads to unacceptably high doses.

At the level of the head (eyes), dose rates are reduced due to the increased distance to the area where the primary beam enters the patient. For the dose at the level of the head, two authors reported a similar dose rate of about 1 μGy/s at a distance of 100 cm.

14.6.4 Reported Doses to the Staff from CTF

The actual dose to the operator will depend on the time that he or she spends at specific distances from the scatter source during the CTF procedure. Besides estimated doses that are derived from ambient dose rate data (indirect measurements), doses are also reported from direct in vivo measurements that are performed during CTF procedures. Direct measurements tend to be more accurate as they include the actual variation of individual staff positioning during each CTF procedure. They are usually performed with personalized ring badges containing TLDs. Table 14.6 shows reported doses to the operator, both from indirect and direct measurements. The first part of the table shows reported doses from indirect measurements based on ambient dose rates; the second part shows data from direct in vivo measurements by using TLDs. Reported doses to the hands from the literature are partly given as radiation doses, expressed in Gy, and partly as the superficial dose equivalent $H_s(0.07)$ in soft tissue, expressed in Sv. For exposures with X-rays of the diagnostic energy range, both unities yield comparable values. For CT X-ray energies, a conversion factor of 1.1 can be applied to transfer dose (Gy) to dose equivalent (Sv) in soft tissue. The data in Table 14.6 are expressed as radiation doses (mGy) unless stated otherwise.

When no specific radiation protection methods are applied, reported doses to the dominant hand in CTF vary between 0.46 mGy and 2.2 mGy per procedure, depending on the technical settings, the exposure time and the method of dose estimation.

14.6.5 Staff Effective Dose

When appropriate personal protection is used, the effective dose to the worker remains limited in CTF. Teeuwisse et al. (2001) evaluated effective doses (E) to both the physician and the assisting radiographer by placing electronic personal dosimeters (EPD) outside the lead apron (unshielded). They estimated that the average dose per CTF procedure to the radiologist was well below 10 μSv and the average dose to the assisting radiographer was below 1 μSv. Actual effective dose values would be even lower as the attenuation of the lead apron is not included in the above data. For a radiologist performing 70% of the CTF procedures at their hospital, they estimated an annual effective dose less than 0.1 mSv. Also, Paulson et al. (2001) measured a limited mean effective dose to the physician of 25 μSv per procedure.

14.6.6 Reducing Dose to the Staff

14.6.6.1 By Reducing Patient Dose

The main source of radiation to the radiologist is the scattered radiation that exits the patient. Decreasing patient dose will decrease scatter radiation, as is true with other radiological procedures. In radiology, both tube current and exposure time have a linear relationship with patient and staff dose. Reducing the exposure to the patient by controlling the tube current and exposure time results in an equal reduction of the dose to the staff. Paulson et al. (2001) reported a negligible dose to the operator by applying a low tube current – exposure time technique (Tables 14.5, 14.6). Also slice thickness influences scatter radiation. A reduction in slice thickness from 10 to 5 or 2 mm can result in personnel exposure reductions of 50%–80% (Nawfel et al. 2000).

Table 14.6. Reported staff doses per procedure from CTF

Author	Method of dose Measurement	CTF technique Method	Technical settings (kVp)/(mA)	Exposure time (s)	Dose at the level of	
					Hand (mGy)	Head (mGy)
Nickoloff et al. (2000)	Indirect (20–100 cm)	20 cm needle holder	120/30	100	1.70	0.09
[a] Kato et al. (1996)	Indirect (4 cm)	4 cm needle holder	80/30	59	1.50	
Nawfel et al. (2000)	Indirect (10–100 cm)		120/50	80	2.2	0.1
[a] Paulson et al. (2001)	Indirect (25–60 cm)		140/13	18	0.001	0.0006
Gianfelice et al. (2000)	Indirect (10 cm)	10 cm needle holder	120/50	50	0.90	
Gianfelice et al. (2000)	Indirect (10 cm)	10 cm needle holder	120/50	26	0.46	
Nawfel et al. (2000)	Direct by TLD		120/50	n.a.	1.70	
[a] Irie et al. (2001a)	Direct by TLD	7 cm needle holder	120/30	38	0.76	
[a] Irie et al. (2001a)	Direct by TLD	7 cm needle holder and lead plate	120/30	50	0.41	
[a] Irie et al. (2001a)	Direct by TLD	15 cm needle holder and lead plate	120/30	41	0.06	
Buls et al. (2003)	Direct by TLD		120/90	151	0.70	0.21
Buls et al. (2004)	Direct by TLD	Under-table tube exposure	120/38	73	0.29	0.14

[a] Data expressed as dose equivalent (mSv)

14.6.6.2 Distance

Distance is a very efficient and costless radiation protection tool. The exposure rate from a point source of radiation decreases by the square of the distance to the source. For example, the dose rate from a source would be 4 times lower when the distance is doubled. This *inverse square law* is the result of the geometric relationship between the surface area and the radius of a sphere (Bushberg et al. 2002). This relationship is only valid for point sources (i.e. sources whose dimensions are small with respect to the distance from the source). Thus, the *inverse square law* would not be strictly valid in CTF where the radiation source size (patient) is large with respect to the distance between staff member and patient. However, experimental data from Nawfel et al. (2000) show that scatter exposure rate is approximated by the inverse square law at distances greater than 30 cm from the scanning plane.

14.6.6.3 Needle Holders – Robotically Driven Interventions

Since the introduction of CTF, standoff needle devices have been developed to increase the distance of the physician's hand to the scanning plane (Kato et al. 1996; Daly et al. 1998; Irie et al. 2001b). Figure 14.3b,c shows a picture of an abdominal CTF procedure with a 15-cm needle holder. Besides reducing the scatter radiation level to the hand due to the larger distance, they also prevent the hand from entering the primary beam directly. They should always be used when the real-time scanning method is applied. Irie et al. (2001b) developed three devices, 7 cm, 10 cm and 15 cm in length, that yielded markedly reduced doses to the physician's hand (see Table 14.6). Stoeckelhuber et al. (2005) reported a scatter dose rate reduction from 39.5 µGy/s to 13.2 µGy/s by using a 35-cm needle holder compared to a 15-cm needle holder (Table 14.5). Besides dedicated tools, less expensive but sometimes also less efficient objects such as sponge forceps or towel

clamps are also applied (Daly et al. 1998; Paulson et al. 2001). Although it has been shown that needle holders reduce the dose to the hand, there are some reported drawbacks due to reduced tactile feedback. Although Kato et al. (1996) and Irie et al. (2001a) concluded that dedicated needle holders did not cause any artefacts that interfered with the biopsy procedure, Carlson et al. (2001) did not advocate the use of holders due to their decreased tactile feedback and difficulties when penetrating resistant tissue planes. Also, Silverman et al. (1999) reported that there were times when the needle became dislodged from the holder, and at other times it was difficult to exert sufficient inward force. The use of needle holders requires training in order to prevent a prolonged exposure time due to reduced tactile feedback.

The ultimate way of reducing staff exposure is a CTF procedure that does not require the staff members to be present in the CT room. Solomon et al. (2002) developed a robot that could hold, orient and advance a needle, with CTF guidance. This robot could be either computer or joystick controlled. In an evaluation with 23 biopsy interventions no complications were encountered and dose to the physician was eliminated. Although they do not report fluoroscopic screening times in their study, they claim that patient exposure could also be reduced since the computer can advance the robot's needle to the target without the need for continuous imaging. The main drawbacks of such system are the extra preparation time to install the robot and the cost. Solomon et al. (2002) estimated that a commercial unit might cost in the range of $20,000.

14.6.6.4 Using a Lead Drape

An efficient and easy to use method of reducing scatter exposure is to place a lead drape on the patient caudal from the cutaneous access side, adjacent to the scanning plane (Fig. 14.15). This lead barrier absorbs scattered photons that leave the patient's body directed towards the operator and reduces scatter dose considerably (see also Table 14.5). Several authors have reported the use of a lead drape (Silverman et al. 1999; Irie et al. 2001b; Nawfel et al. 2000; Stoeckelhuber et al. 2005). Nawfel et al. 2000 investigated scatter exposure to the hand by measuring ambient dose rates at specific distances to a phantom. According to their results, a 0.5-mm lead drape reduced the scattered exposure by approximately 70% at a distance of 10 cm from the scanning plane. Irie et al. (2001b) conducted a similar study by placing a small lead plate directly under the hand of the physician. They measured a hand dose of 0.41 mSv per case with the lead plate compared to 0.76 mSv per case without the lead plate (Table 14.6). The small lead plate was easy to sterilize and caused little discomfort for the patients. Also, scatter dose reductions up to 97% are reported by using two lead drapes, one placed above and one placed below the patient (Stoeckelhuber et al. 2005).

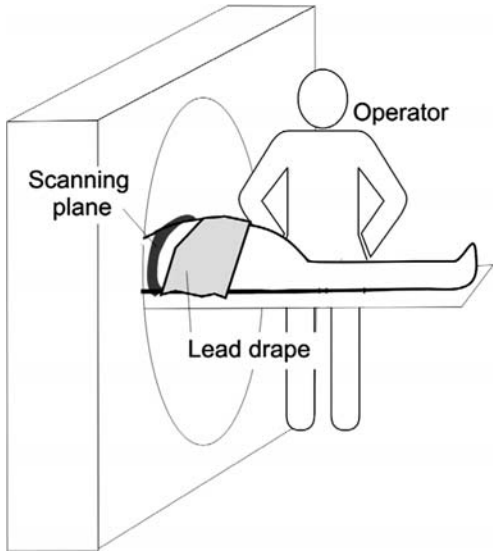

Fig. 14.15. A lead drape placed caudal from the scanning plane reduces scattered radiation towards the operator

14.6.6.5 Leaded Gloves

Using leaded gloves can also protect the hands of the operator. However, the lead equivalent of gloves that are thin enough to permit an adequate sense of touch is often limited with high energy X-rays beams that are used with CTF (120 kVp). Nickoloff et al. (2000) evaluated the protection of three different types of thin leaded gloves, which permitted an adequate sense of touch to direct biopsy needles. The leaded gloves provided only a 15%–33% reduction in the radiation dose to the hands at a tube potential of 120 kVp. This is low compared to the protection of a lead drape (95%), which has more lead content.

14.6.6.6 Under-Table Tube Geometry

When performing interventions that require fluoroscopy it is common to use X-ray systems with the tube positioned under the table. Such an under-table setup reduces the amount of backscatter radiation that is directed towards the upper body part of the staff standing next to the patient (see Sect. 14.6.1). In CTF, this principle is applied by one manufacturer (HandCARE™ option, Siemens, Erlangen, Germany). The system reduces the scattered radiation exposure to the physician by interrupting X-ray exposure when the tube rotates above the patient (between the 10:00 and 2:00 o'clock position), while maintaining the integrated mAs per rotation. As a result, the scatter radiation that leaves the anterior part of the patient will be limited, thus reducing the exposure that is directed towards the operator. A recent study demonstrated that the dose to the operator's hand could be halved by using such system (Buls et al. 2004).

However, while reducing exposure to the staff, such systems can increase patient's skin doses as the same dose is delivered to a smaller skin area in comparison to 360° CT scanning. Figure 14.16 shows the relative patient dose distribution with and without a CTF system that interrupts exposure. The data are obtained by measuring the normalized periphery CTDI in a 32 cm phantom for various angular positions with a 10° increment (Buls et al. 2004). With continuous scanning, the surface dose is more or less equally distributed around the patient whereas with the beam interruption device, the surface dose is concentrated in the posterior part of the patient. As a result, the peak skin dose rate is about 1.5 times increased in that part compared to continuous scanning.

14.6.6.7 Learning Curve

With acquisition of any new image-guided interventional apparatus, there is inevitably a period of time during which learning is necessary to acquire expertise and perform the procedures efficiently (Gianfelice et al. 2000). This becomes more important as the spectrum of CTF procedures expands to complex types of interventions, which may require longer exposure times due to the lack of expertise. Gianfelice et al. (2000) studied the effect of the learning process for biopsy procedures on exposure times. They observed a significant reduction from 50.3 to 25.8 s per patient after a 2-year period or 250 consecutive patients. The learning process associated with CTF technology impacts on procedure parameters by decreasing both mean procedure and fluoroscopy times, thereby increasing patient turnover and decreasing radiation exposure to the patient and the operator.

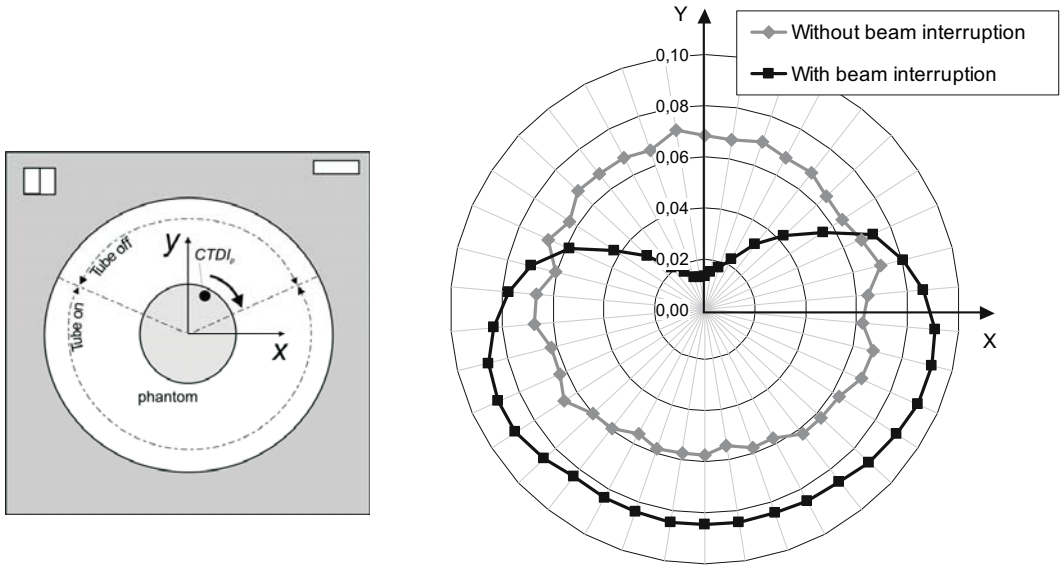

Fig. 14.16. Patient surface dose distribution, with and without a beam interruption CTF device. Image shows relative peripheral CTDI for different angular positions

Also other methods could be used to decrease exposure time. A study by Carlson et al. (2005) reported a mean exposure time reduction from 18.0 to 12.6 s by using a breath-hold monitoring and feedback system with biopsies of the lung and the upper abdomen.

14.7 Regulatory Dose Limits

Today, the annual regulatory dose limits for classified workers are: 20 mSv for the effective (total body) dose, 500 mSv for the equivalent dose to the skin, and 150 mSv for the equivalent dose to the eyes (ICRP 1990). Dose limits to the eyes and skin are both set in order to prevent deterministic effects. For the staff in CTF, the dose to the hands or the eyes will be the critical factor with regard to regulatory dose limits, not the effective dose.

The number of CTF procedures before exceeding regulatory dose limits can be estimated from the data in Table 14.6. At a maximal permissible dose of 500 mSv to the hands per year, about 230 CTF procedures would be allowed when using the highest reported dose of 2.2 mGy per procedure (Nawfel et al. 2000). This number increases rapidly when more dose-saving CTF methods are applied by either using reduced exposure settings, or by using standoff needle devices or other methods to reduce the scattered dose to the hands. For example, using the reported data of Gianfelice et al. (2000) with 120 kVp, 30 mA and 26 s exposure time, over 1000 CTF procedures could be performed before exceeding dose limits. The combination with using a lead drape could increase this number even further up to over 8000 procedures.

For patients, no legal dose limits apply but it is mandatory to respect Diagnostic Reference Levels (DRLs). DRLs are dose levels in diagnostic practices for typical examinations that are expected not to be exceeded for standard procedures when good practice is applied (EURATOM 1997). In contrast to standard CT examinations where DRLs are well established in terms of CTDI and DLP, they do not yet exist for CTF. In a strict sense, CTF is not a diagnostic investigation so DRLs would not apply. However, typical dose levels for interventional procedures using conventional fluoroscopy do exist. These are usually expressed as Dose Area Product (DAP) values. DRLs for CTF could indicate whether the levels of patient dose are unusually high for a specific procedure. If so, a local review should be initiated to determine whether protection has been adequately optimized or whether corrective action is required (ICRP 1996).

14.8 Conclusions

Non-vascular diagnostic and therapeutic interventions are becoming more and more important in patient work up. This shift to a more invasive diagnostic and therapeutic approach in radiology is seen in spite of the improving performance of imaging techniques and the improvement of surgical techniques. CTF has proven to be an effective modality for guiding diagnostic and therapeutic radiological interventions. With CTF, the physician can follow the exact trajectory of needle placement from the skin surface to the targeted lesion due to the display of CT images in real time, and it can be applied in soft tissue, fluid- and air-filled cavities and bones. CTF-guided procedures are particularly challenging in uncooperative patients or in organs that are prone to respiratory motion such as the lung or liver.

A drawback of CTF is the potential for significantly high patient and staff doses. For the patient, the same skin area is repeatedly exposed and the physician is exposed to scattered radiation as he or she enters the CT room while scanning. If CTF is used improperly by a combination of a high current and prolonged exposure times, it has a potential for patient skin injuries. Whereas with conventional fluoroscopy the 2-Gy threshold dose for deterministic skin effects is reached after 100–200 min of fluoroscopy, it can be reached in CTF after only 3–10 min of scanning when a high tube current is applied. For the physician, doses to the hand have been reported up to 2.2 mGy per procedure and dose rates at the level of the hand vary between 20 and 40 μGy/s when no radiation protection measures are applied. Operators need to be aware of different methods of CTF guidance and the factors that determine radiation exposure for both patient and staff. This becomes more important as the spectrum of CTF procedures might expand to more complex procedures that may require longer fluoroscopy times.

Table 14.7 summarizes the factors that affect patient and staff doses in CTF and their risk potential, and proposes measures to be taken for dose optimization.

Although CTF has the potential to deliver high doses to both patients and staff, radiation doses can be reduced to acceptable levels. This can be achieved by proper radiation management that uses a combination of manually selecting low tube currents and by using the quick-check or intermittent CTF method that limits fluoroscopy time as much as possible. Literature data indicate that such a method can be easily applied in clinical routine.

Table 14.7. Factors that affect both patient and staff doses in CTF

Parameter	Potential risk	Measures
Compared to conventional CT, the position of the scan plane stays constant with CTF	The same patient skin area is repeatedly exposed, resulting in high accumulated skin doses that may reach 2 Gy. Risk for radiation-induced skin injuries	Operators must be aware of the potential for skin injuries and recognize the characteristics of skin doses in CTF
Compared to conventional fluoroscopy, CTF allows high exposure settings in terms of tube current (mA) and tube potential (kVp). Automated tube current modulation is not available with CTF	As a result, patient surface (skin) dose rates are much higher in CTF. They can vary from 10 cGy/min up to 60 cGy/min. Also, scattered radiation dose rates towards the operator are much more intense and energetic	The lowest possible tube current values should be used that allow an adequate image quality in the anatomical region of interest. Reported values are typically 10–30 mA for chest cases, and 30–50 mA for abdominal cases. Tube currents above 50 mA should be avoided
Exposure time or CT scanning time (s)	Prolonged exposure times can be necessary in cases of small and poorly accessible lesions or cases with increased patient motion. Both patient skin dose rate and scatter dose rate increase linearly with exposure time	Limit exposure time as much as possible by using the quick-check method. Typical reported exposure times are below 60 s per procedure. Very short exposure times, in the range of 20 s, are also reported in clinical routine for various types of procedures
CTF technique: real-time method or quick-check method	Real-time method increases exposure time considerably and therefore also patient and staff doses	Avoid real-time scanning. Use the standard quick-check method and reserve real-time method only for limited cases with increased patient motion
Patient size and children	Skin dose rate increases for smaller patients due to the shorter distance between skin and isocentre	Give special attention to tube current reduction for smaller patients. For paediatric patients typical tube current values of 10 mA are reported
Position of the patient inside gantry	Surface dose rate decreases when the surface moves away from isocentre. The maximal skin dose rate is reached at the isocentre	Position the centre of the patient in the isocentre, thus maximizing the distance between skin surface and isocentre to minimize skin dose. Avoid the patient surface being positioned at isocentre
In contrast to conventional CT, the operator stands next to the patient during CT scanning	The operator is exposed to scattered radiation	Staff members should always wear appropriate lead aprons complemented with a thyroid collar. Simultaneous dose monitoring by two radiation badges (over and under the apron) is recommended
The CT tube rotates continuously around the patient during exposure	The direction of the scattered radiation field is nearly symmetrical and is not as controllable as in conventional fluoroscopy (e.g. angiography). It is also more intense as in conventional fluoroscopy	See below → →

Table14.7. Continued

Parameter	Potential risk	Measures
Slice thickness (mm)	Both patient skin dose and scattered exposure increase with slice thickness	Select the smallest possible slice thickness as a function of the puncture access route. Usually 5–10 mm. Too small a selected slice thickness may influence CTF efficiency and may increase exposure time
Standoff needle device	These usually have a length of 10–30 cm. They prevent the hands entering the primary beam and reduce scatter dose at the level of the hand due to the larger distance to scanning plane	Should be always used during real-time scanning. Is not required when the quick-check method is applied. Could result in reduced tactile feedback and, hence, may influence CTF efficiency and exposure time
Lead drape placed on the patient caudal from scanning plane	A 0.5-mm lead equivalent drape reduces scattered exposure to the hands (up to 95%) and upper part of operator's body	Lead drapes are reported to be very efficient and very easy to use. They should always be applied with CTF
Thin leaded gloves	Reduces scattered exposure to hands	Dose reduction not as significant as a lead drape. May reduce tactile feedback
Interruption of CT exposure when tube rotates above table	Reduces scattered exposure considerably to hands and upper part of operator's body, but increases patient's skin dose rate by 1.5	Should only be used with reduced tube current settings to limit patient skin dose
Physicians of various specialties perform CTF procedures	Non-radiologist operators may not have had in-depth training in radiation management. Risk of using non-optimized exposure settings or increased exposure times	Provide dedicated training for all CTF operators
Several staff members can be present in CT room	Several staff members are exposed to scattered radiation	Limit number of staff personnel in CT room, provide dedicated training and clear guidelines. Increase distance to patient as much as possible
CTF is a relatively new technique and its spectrum could expand to more complex interventions	Risk of prolonged exposure times due to learning curve	Provide dedicated training

References

Avilés LP, Castellano IA, Dance DR, Vañò E (2001) Analysis of surface dose variation in CT procedures. Br J Radiol 74:1128–1136

Baran GW, Haaga JR, Shurin SB, Alfidi RJ (1984) CT-guided percutaneous biopsies in pediatric patients. Pediatr Radiol 14:161–164

Buls N, Pages J, de Mey J, Osteaux M (2003) Evaluation of patient and staff doses during various CT fluoroscopy guided interventions. Health Phys 85(2):165–173

Buls N, de Mey J, Vandenbroucke F, Vanderdood K, Osteaux M (2004) Dose reduction in CT fluoroscopy. Abstract Proceedings of the Sixteenth European Congress of Radiology, 5–9 March 2004, Vienna, Austria. http://www.ecr.org/pages/past-meetings/ecr-2004.php?sub=2

Bushberg JT, Seibert JA, Leidholdt EM, Boone JM (2002) The essential physics of medical imaging. Lippincott Williams & Wilkins, Philadelphia, Pa.

Cahill AM, Baskin KM, Kaye RD, Fitz CR, Towbin RB (2004) CT-guided percutaneous lung biopsy in children. J Vasc Interv Radiol 15:955–960

Carlson SK, Bender CE, Classic KL, Zink FE, Quam JP, Ward EM, Oberg AL (2001) Benefits and safety of CT fluoroscopy in interventional radiologic procedures. Radiology 219:515–520

Carlson SK, Felmlee JP, Bender CE, Ehman RL, Classic KL, Hoskin TL, Harmsen WS, Hu HH (2005) CT fluoroscopy-guided biopsy of the lung or upper abdomen with a breath-hold monitoring and feedback system: a prospective randomized controlled clinical trial. Radiology 237:701–708

Council Directive 97/43/Euratom on health protection of individuals against the dangers of ionising radiation in

relation to medical exposure (1997) Official Journal of the European Community L180:22
Daly B, Templeton, Krebs TL,Carroll K, Wong-You-Cheong JJ (1998) Evaluation of biopsy needles and prototypic needle guide devices with CT fluoroscopic guidance in simulated organ tissue. Radiology 209:850–855
De Mey J, Op de Beeck B, Meysman M, Noppen M, De Maeseneer M, Vanhoey M, Vincken W, Osteaux M (2000) Real time CT-fluoroscopy: diagnostic and therapeutic applications. Eur Radiol 34:32–40
European Commission (1999) European guidelines on quality criteria for computed tomography. Office for Official Publications of the European Communities, Luxembourg. EUR 16262 EN, pp 63–66
Froelich JJ, Saar B, Hoppe M, Ishaque N, Walthers EM, Regn J, Klose KJ (1998) Real-time CT-fluoroscopy for guidance of percutaneous drainage procedures. J Vasc Interv Radiol 9(5):735–740
Geraghty PR, Kee ST, McFarlane G, Razavi MK, Sze DY, Dake MD (2003) CT-guided transthoracic needle aspiration biopsy of pulmonary nodules: needle size and pneumothorax rate. Radiology 229:475–481
Gianfelice D, Lepanto L, Perreault P, Chartrand-Lefebvre C, Milette PC (2000) Effect of the learning process on procedure times and radiation exposure for CT fluoroscopy-guided percutaneous biopsy procedures. J Vasc Interv Radiol 11:1217–1221
Haaga JR, Alfidi RJ (1976) Precise biopsy localisation by computed tomography. Radiology 118:603
International Commission on Radiation Protection (1982) General principles of monitoring for radiation protection of workers. ICRP Publication 35
International Commission on Radiological Protection (1991) Recommendations of the International Commission on Radiological Protection [ICRP Publication 60]. Pergamon; Oxford
International Commission on Radiological Protection (1996) Reference details missing
International Commission on Radiological Protection (2000) Managing patient dose in computed tomography [ICRP Publication 87]. Ann ICRP 30(4)
International Commission on Radiological Protection (2001) Avoidance of Radiation injuries from medical interventional procedures [ICRP Publication 85]. Ann ICRP 30(2)
Irie T, Kajitani M, Yoshioka H, Matsueda K, Inaba Y, Arai Y, Nakajima K, Nozawa K, Itai Y (2000) CT fluoroscopy for lung nodule biopsy: a new device for needle placement and phantom study. J Vasc Interv Radiol 11:359–364
Irie T, Kajitani M, Matsueda K, Arai Y, Inaba Y, Kujiraoka Y, Itai Y (2001a) Biopsy of lung nodules with use of I-I device under intermittent CT fluoroscopy guidance: preliminary clinical study. J Vasc Interv Radiol 12:215–219
Irie T, Kajitani M, Itai Y (2001b) CT fluoroscopy-guided intervention: marked reduction of scattered radiation dose to the physician's hand by use of a lead plate and an improved I-I device. J Vasc Interv Radiol 12:1417–1421
Katada K, Anno H, Koga S (1994) Initial trial with CT fluoroscopy. Radiology 190:662
Katada K, Kato R, Anno H, Ogura Y, Koga S, Ida Y, Sato M, Nonomura K (1996) Guidance with real-time CT fluoroscopy: early clinical experience. Radiology 200:851–856
Kataoka ML, Raptopoulos VD, Lin PJ, Siewert B, Goldberg SN, Kruskal J (2006) Multiple-image in-room CT imaging guidance for interventional procedures. Radiology 239:863–868
Kato R, Katada K, Anno H, Suzuki S, Ida Y, Koga S (1996) Radiation dosimetry at CT fluoroscopy: physician's hand dose and development of needle holders. Radiology 201:576–578
Keat N (2001) Real-time CT and CT fluoroscopy. Br J Radiol 74:1088–1090
Klose KC (1993) CT-guided large-bore biopsy: extrapleural injection of saline for safe transpleural access to pulmonary lesions. Cardiovasc Intervent Radiol 16:259–261
Koenig TR, Wolff D, Mettler FA, Wagner LK (2001) Skin injuries from fluoroscopically guided procedures. Part 1: Characteristics of radiation injury. AJR Am J Roentgenol 177:3–11
Laufer U, Kirchner J, Kickuth R, Adams S, Jendreck M, Liermann D (2001) A comparative study of CT fluoroscopy combined with fluoroscopy versus fluoroscopy alone for percutaneous transhepatic biliary drainage. Cardiovasc Intervent Radiol 24:240–244
Laurent F, Michel P, Latrabe V, Tunon de Lara M, Marthan R (1999) Pneumothoraces and chest tube placement after CT-guided transthoracic lung biopsy using a coaxial technique: incidence and risk factors. AJR Am J Roentgenol 172:1049–1053
Lee JM (2000) CT-guided celiac plexus block for intractable abdominal pain. J Korean Med Sci 15:173–178
McParland BJ (1998) Entrance skin dose estimates derived from dose-area product measurements in interventional radiological procedures. Br J Radiol 71:1288–1295
Meleka S, Patra A, Minkoff E, Murphy K (2005) Value of CT fluoroscopy for lumbar facet blocks. Am J Neuroradiol 26:1001–1003
Meyer CA, White CS, Wu J, Futterer SF, Templeton PA (1998) Real-time CT fluoroscopy: usefulness in thoracic drainage. AJR Am J Roentgenol 171:1097–1101
Miller DL, Balter S, Cole PE, Lu HT et al (2003) Radiation doses in interventional radiology procedures: the RAD-IR study. J Vasc Interv Radiol 14:977–990
Moran CJ, Naidich TP, Gado MH, Marchosky JA (1979) Central nervous system lesions biopsied or treated by CT-guided needle placement. Radiology 131:681–686
National Radiological Protection Board (1999) Guidelines on patient dose to promote the optimisation of protection for diagnostic medical exposures, Vol 10, no. 1. NRPB, HMSO
Nawfel RD, Philip F, Judy PF, Silverman SG, Hooton S, Tuncali K, Adams DF (2000) Patient and personnel exposure during CT fluoroscopy-guided interventional procedures. Radiology 216:180–184
Nickoloff EL, Khandji A, Dutta A (2000) Radiation doses during CT fluoroscopy. Health Phys 79(6):675–681
Paulson EK, Sheafor DH, Enterline DS, McAdams HP, Yoshizumi T (2001) CT fluoroscopy-guided interventional procedures: techniques and radiation dose to radiologists. Radiology 220:161–167
Rosenthal DI, Hornicek FJ, Torriani M, Gebhardt MC, Mankin HJ (2003) Osteoid osteoma: percutaneous treatment with radiofrequency energy. Radiology 229:171–175
Silverman SG, Tuncali K, Adams DF, Nawfel RD, Zou KH, Judy PF (1999) CT fluoroscopy-guided abdominal interventions: techniques, results and radiation exposure. Radiology 212:673–681

Stoeckelhuber BM, Leibecke T, Schulz E, Melchert UH, Bergmann-Koester CU, Helmberger T, Gelissen J (2005) Radiation dose to the radiologist's hand during continuous CT Fluoroscopy-guided interventions. Cardiovasc Intervent Radiol 28:589–594

Teeuwisse WM, Geleijns J, Broerse JJ, Obermann WR, Van Persijn Van Meerten EL (2001) Patient and staff dose during CT guided biopsy, drainage and coagulation. Br J Radiol 74:720–726

Trout ED, Kelley JP (1972) Scattered radiation from a tissue equivalent phantom for X-rays from 50 to 300 kVp. Radiology 104:161–169

United Nations Scientific Committee on the Effects of Atomic Radiation (UNSCEAR) (2000) Sources and effects of ionizing radiation, Vol 1 Sources. United Nations, New York

United States Food and Drug Administration. Public Health Advisory (1994) Avoidance of serious x-ray-induced skin injuries to patients during fluoroscopically-guided procedures. Center for Devices and Radiological Health, United States Food and Drug Administration, Rockville, Maryland.

Wagner AL (2004) Selective lumbar nerve root blocks with CT fluoroscopic guidance: technique, results, procedure time, and radiation dose. Am J Neuroradiol 25:1592–1594

Wagner LK (2000) CT fluoroscopy: another advancement with additional challenges in radiation management. Radiology 216:9–10

Wagner LK, Eifel PJ, Geise RA (1994) Potential biological effects following high x-ray dose interventional procedures. J Vasc Interv Radiol 5:71–84

Yamagami T, Iida S, Kato T, Tanaka O, Nishimura T (2003) Combining fine-needle aspiration and core biopsy under CT fluoroscopy guidance: a better way to treat patients with lung nodules? AJR Am J Roentgenol 180:811–815

Zech CJ, Helmberger T, Wichmann MW, Holzknecht N, Diebold J, Reiser MF (2002) Large core biopsy of the pancreas under CT fluoroscopy control: results and complications. J Comput Assist Tomogr 26:743–749

Suggested Reading

Amoretti N, Hovorka E, Dausse F, Chevallier P, Brunner P, Boileau P, Bruneton JN (2005) Posterior arthrodesis of the spine by percutaneous CT-guided application of screws: preliminary report. J Clin Imaging 29:231–234

Avilés LP, Dance DR, Castellano IA, Vañò E (2004) Monte Carlo simulations in CT for the study of the surface air kerma and energy imparted to phantoms of varying size and position. Phys Med Biol 49:1439–1454

Daly B, Templeton PA (1999) Real-time CT fluoroscopy: evolution of an interventional tool. Radiology 211:309–315

De Mey J, Op de Beeck B, Freson M, Osteaux M (1999) Ponction diagnostique sous contrôle tomodenitométrique en pathologie abdominale. J Radiol 80:11–16

Heyer CM, Lemburg PS, Kagel T, Mueller K, Nuesslein TG, Rieger C, Volkmar N (2005) Evaluation of chronic infectious interstitial pulmonary disease in children by low-dose CT-guided transthoracic lung biopsy. Eur Radiol 15:1289–1295

Layton K, Thielen K, Wald JT (2006) Percutaneous sacroplasty using CT fluoroscopy. Am J Neuroradiol 27:356–358

Nagel HD (2000) Radiation exposure in computed tomography, 2nd edn. Offizin Paul Hartung Duck, Hamburg, pp 5–13

Schweiger DG, Yip VY, Brown PB (2000) CT fluoroscopic guidance for percutaneous needle placement into abdominopelvic lesions with difficult access routes. Abdom Imaging 25:633–637

Sherif M, Ajanta P, Evan M, Kieran M (2005) Value of CT fluoroscopy for lumbar facet blocks. Am J Neuroradiol 26:1001–1003

Vañò E, Gonzalez L, Ten JI, Fernandez JM, Guibelalde E, Macaya C (2001) Skin dose and dose-area product values for interventional cardiology procedures. Br J Radiol 74:48–55

Dose Optimization and Reduction in CT of Children

15

Peter Vock and Rainer Wolf

CONTENTS

Radiation risks based on biology and physics have been covered in previous chapters and are, of course, also valid for children. In the same way, clinical approaches to dose optimization and reduction are similar in paediatric and adult CT examinations (Huda et al. 2000). This chapter will not repeat what has been said but concentrate on the fact that children are not just adults with smaller dimensions, thus it will rather point out what is different in children.

P. Vock, MD
R. Wolf, MD
Department of Radiology, University Hospital Inselspital, 3010 Bern, Switzerland

15.1 Why Dose Optimization and Reduction in CT is Even More Important in Children than in Adults

Several independent arguments clearly justify an even more careful use of the "as low as reasonably achievable" (ALARA) principle in children than in adults (Frush et al. 2003; Vock 2002) (Table 15.1):

- Children are indeed – depending on their stage of growth – *smaller* than adults, and this means that the physical laws of radiation interaction and absorption have to be respected during protocol definition (Boone et al. 2003; Chapple et al. 2002; Frush 2002; Huda 2002; Huda and Gkanatsios 1997). Usually, a decreased number of photons is required, which translates into a lower tube output (mAs). Often the use of a lower X-ray energy (kV) is appropriate as well in children. These facts – though known for over decades for radiography – were not realized for computed tomography (CT) by many radiologists until the early years of the new millennium (Paterson et al. 2001).
- At the same physical exposure to ionizing radiation, the *biological effects* are *more severe* in children than adults (Brenner 2002; Brenner et al. 2001, 2003; Frush et al. 2003; Pierce and Preston 2000); the risk of lethal cancer is multiplied by a factor of 2.5 on average, as compared to adult people, starting at around 10 in neonates and approaching adult values during adolescence. This is mostly explained by the fact that proliferating tissues are more vulnerable to the effects of radiation and that proliferation is much more active during the growth period than later in life. Furthermore the distribution of tissues is different in childhood: e.g. red bone marrow will hardly be irradiated during a CT extremity exam in adults whereas it will partly be included in the volume of primary radiation exposure in a child.

Table 15.1. Why children need specific CT planning

Difference	Cause, consequence
1. Smaller dimensions	Adapt protocol according to physics
2. Higher biologic sensitivity	Growth, cell proliferation, tissue distribution
3. Long life expectancy	Increased risk of tumor manifestation
4. Less fatty tissue	Adapt protocol to maintain contrast
5. Cooperation may not be possible	Prepare patient, immobilize, scan fast
6. Alternative imaging test equivalent	Ultrasound, MRI more often equivalent
7. Different pathology in children	Requires different justification/approach

- Children have a *longer life expectancy* than the average adult population studied by CT. Their natural life time left at the moment of CT scanning is in the range of 70 years whereas it is more often 10–20 years than 30–40 years in the adult CT population. Of course, since it is likely that the risk of radiation-induced carcinogenesis persists during the entire life span and since the delay of cancer manifestation is more often decades than years, more children than adults will be alive at the end of the latency period of radiation-induced cancers, and a significant percentage among them will die from cancer.
- Children usually have *less fatty tissue* between visceral organs than adults. To keep the contrast needed to differentiate structures with only tiny fatty layers in between, the signal-to-noise (*S*/*N*) ratio, and thus the dose, has to be increased, or the contrast has to be improved by other modifications of the protocol, such as by using a lower X-ray energy (kV).
- *Cooperation* is not as easy for children as it is for adults. This means that the combined contributions of trained personnel, patient preparation, the atmosphere in the examination room and sometimes the presence of a parent are all needed to reach an optimal result using minimal radiation exposure.
- *Alternatives* to CT exist in children – in contrast to multiple applications in adults. Children are excellent candidates for *ultrasound* imaging, and – unlike in adults – many more details in more regions of the body can be shown. Cerebral ultrasound in the neonate is just one prominent example. Similarly, *magnetic resonance imaging* (*MRI*), another alternative to CT without ionizing radiation, has an excellent accuracy in children; most contraindications to MRI, such as cardiac pacemakers, neurostimulators, ferromagnetic foreign bodies, or claustrophobia, are rarely a problem in children.
- *Pathology is different* in children than in adults. While congenital and inflammatory disorders are more frequently seen, degenerative and neoplastic diseases are clearly less abundant during the growth period. A different spectrum of pathology means a different diagnostic approach. Above all, justification follows the specific pathology and does not just ask for the best technical method for one organ but rather for weighing the advantages and risks of all methods in the specific situation.

15.2 Impact of New CT Scanners on Paediatric Patients

As medical aspects and the biologic impact of CT scanning are different in children than in adults, the impact of the recent technical development of CT scanners is special in children and requires some consideration (Table 15.2). Many new options come up, but these advantages have to be balanced with the disadvantages that are often tightly combined. In a phase of fast development there are of course major differences between the scanners of different manufacturers. Because these will level out, mostly within a few years, we will concentrate on the issues that all multi-row detector scanners have in common.

Table 15.2. Impact of modern CT scanners on paediatric CT

Technical feature of modern CT	Consequence
1. Faster scanning	Less cooperation/immobilization needed, new applications (e.g. vascular, multi-phasic), larger volume covered per time
2. Better *z*-axis resolution	Isotropic geometric resolution, noise
3. Slice thickness	Correct slice profile, more noise on thin slices (or increased radiation exposure)
4. Dose shaping (bow tie) filters	Useful for object with small dimensions
5. Dose modulation	Constant *S*/*N*, dose reduction (if used appropriately)
6. Geometric detector efficiency	*z*-axis overbeaming (collimation), non-detector area (element spacing)
7. Additional rotation in spiral mode needed for interpolation	Additional dose outside planned volume

- *Faster scanning*: this is obviously the single most important factor for the growing number of applications of CT in paediatrics (Mettler et al. 2000; Nickoloff 2002; Nickoloff and Alderson 2001). Children no longer need to stay immobile for 10–15 min, and often CT scanning is possible without sedation or with sedation instead of intubation anaesthesia. Motion artefacts have mostly disappeared, and the body volume studied during one session is no longer limited by the maximal period of cooperation of a child. Vascular applications of CT in children have only become available with modern scanners, thanks to the fact that the first or second pass of contrast agents can be used to get a high intravascular contrast before diffusion to the interstitial space occurs. Similarly, multiphasic examinations essentially have only been introduced with the arrival of the modern generation of CT scanners. New medical applications indeed are the most important reason for an important rise in the number of CT examinations performed in children during the last 10 years.
- *Better z-axis resolution*: the smaller dimensions of children basically require a high geometric resolution, with ideally isotropic voxels. The *z*-axis size of a voxel, a major problem with single detector rows, can be reduced to even submillimetric dimensions on scanners with multiple detector rows, without compromising the volume coverage of the scan. This is a major advantage, particularly for avoiding partial volume effects and secondarily for multiplanar 2D reformations and for 3D analysis of data.
- *Slice thickness*: thinner collimation in multi-row detector CT scanners produces raw data of an intrinsically high geometric resolution. However, the smaller submillimetric voxel volume necessarily causes a major signal drop and, thus, a drop of the *S*/*N* unless the X-ray flux is increased proportionally. This phenomenon has had an impact on the clinical application of four-detector-row scanners, where radiation exposure has risen in relation to single-row scanners. To handle this physical fact, most experts now suggest scanning at a thin collimation and a low dose but then reconstructing thicker images of 3–6 mm with a much better *S*/*N* for diagnosis. Thus, thin noisy slices are just consulted in cases of partial volume problems, and they are used for post-processing. In conclusion, it is useful to have the submillimetric slices available but to rely mostly on thicker ones for routine work, even in children. Another problem with slice thickness and single-row scanners has occurred: using an elevated pitch (1.5–3), as needed for faster scanning and for dose reduction, has caused a major widening of the slice profile. With multi-row scanners – thanks to more data available for interpolation – the slice profile is close to the nominal value, and the pitch factor has lost most of its critical influence.
- *Dose shaping filters (bow tie filters)*: dose shaping filters are used to adapt the X-ray profile. Obviously, objects with a diameter much less than the diameter of the gantry do not require the same X-ray flux in the periphery of the field of view compared to thick objects. Specific filters are used by most manufacturers to adapt the beam profile to the smaller dimension of an adult head, an extremity or a child, and they help to control radiation exposure.

- *Dose modulation*: the introduction of dose modulation in CT corresponds practically to automatic exposure control as used in fluoroscopy systems to keep the *S*/*N* at the detector constant during an examination. Body areas with smaller diameters and moderate bony components do not require the same X-ray flux as thick areas with a lot of bony structures. Dose modulation in the *xy*-plane and the *z*-axis is therefore a major step forward that should be used generally. However, let us keep in mind that it is not perfect at all. Depending on the modulation rules used by the manufacturer, modulation may even increase exposure beyond the nominal value, e.g. when the scan starts at a level with a thin body diameter, or when local organ shielding is used for the thyroid or the breast gland. The degree of adaptation of exposure to the local physical absorption (in order to maintain a constant *S*/*N* at the detector) also depends on the relation between the length of the detector and the length of the scan. When a scan covers only a small distance, as appropriate in scanning one anatomical region of a child, and when the detector – due to many rows (e.g. 64) – becomes long in the *z*-axis, the best modulation of tube output will fit the needs of the central detector elements whereas the elements above and below may receive too many or too few photons. In other words, the efficacy of dose modulation intrinsically decreases with an increasing number of detector rows. This is true, independently of the type of modulation, whether based on absorption measurements from localizer scans or interactively on the data on the previous rotation.
- Geometric detector efficiency: geometric efficiency of modern CT scanners is mostly determined by two factors, the z-axis geometric efficiency and the detector array geometric efficiency. To avoid penumbral effects in the outer portions of the detector array, collimation of the X-ray beam is usually set wider than the length of the detector array in multi-row scanners; this means a decreased z-axis geometric efficiency and, consecutively, an increase in exposure due to X-rays that will not hit the detector. The effect is most severe with four-row scanners and with narrow submillimetric slices; in this extreme condition, dose may be doubled (Chap. 4 by H.D Nagel) whereas the increase is rather in the range of 5%–20% with 8- to 64-row scanners (impact scan). As for dose modulation, this phenomenon is physically the same in children and in adults but again – due to the small dimension of a child's body – the effects beyond the planned and properly detected proportion of X-rays may easily extend to critical organs not to be studied in children, such as the thyroid in chest exams or the testes in abdominal exams.

  Detector array geometric efficiency is defined by the proportion of the overall detector area that contains active detector material. The proportional area of septa between active elements generally increases with the number of detector elements in the *xy*-plane and as well as with the number of rows in the *z*-axis. Again this effect is not unique in children but has to be considered in paediatric CT.
- *Additional rotations for interpolation in spiral mode*: projections outside the reconstructed *z*-axis range are needed in spiral (helical) mode at each end of the scan. Since spiral scanning has become the standard in most CT applications, this phenomenon must not be forgotten. The relative contribution to radiation exposure is more important the shorter the scan length. It also increases with multi-slice scanners since these usually have a larger total collimation (i.e. the sum of all detector elements in the *z*-axis). Again, in paediatric CT we have to be aware of radiation exposure beyond the planned scan range, e.g. with 64 rows of 0.6 mm detector length, half an additional rotation at pitch 1 will cover nearly 2 cm more both at the top and the bottom, whereas with a pitch of 2, nearly 4 cm of the body will be scanned outside the volume of interest. As for *z*-axis geometric efficiency, important organs outside our scanning volume might be exposed to direct instead of scattered radiation and receive a significant dose.

15.3 Justification

The "as low as reasonably achievable" (ALARA) principle may mean that an imaging study using ionizing radiation has to be cancelled when there is an equivalent test available that does not need radiation exposure: the global sum of its advantages has to be greater than the sum of its disadvantages in order to justify a specific test. Indeed, justification is the single most effective step in radiation protection. No other step discussed later will reduce

exposure by 100%, and even when a CT exam is replaced by another X-ray study, this usually means a major reduction of exposure since most other X-ray examinations cause a much smaller effective dose than CT studies (Shrimpton et al. 2005; Ware et al. 1999). However, justification is also the most difficult step since the risk of immediately not doing the examination cannot be directly compared with the long-time risk of inducing cancer (Vock 2005). What may be good for an elderly patient in internal medicine may not be an appropriate approach for a paediatric patient. Imaging studies not only involve ionizing radiation but also a number of other risks and chances, and they are often quite expensive. Depending on the specific medical infrastructure of a country, there is still a lack of high-tech equipment, and doing the study on the wrong patient may exclude another patient from getting the same CT examination that may be critical for his or her treatment or even the survival.

Slovis (2002) estimated around 40% of all paediatric CT examinations as not clearly indicated. All these reasons together underscore the importance of justification. Several countries have developed guidelines in using imaging procedures: in the US, the *appropriateness criteria* defined by a panel of experts (using a score of 1–9) have been introduced by the American College of Roentgenology (2006). For instance, appropriateness of CT of the brain in suspected physical child abuse will be low (2, mostly inappropriate) or very high (9, most appropriate), depending on the age, the results of physical examination and laboratory exams. The European Union (European Commission 2000b) has issued *referral criteria for imaging* that have been translated into many languages. In the referral criteria, paediatrics makes up an entire section that is further classified by anatomical areas and, within each area, by important clinical entities. Except for trauma, CT is rarely mentioned and the conditions for its use are further commented. It is obvious that major efforts are still needed to differentiate the diagnostic decision trees in specific clinical situations, including the age, the pathology, the body region as well as the urgency and the availability of alternative diagnostic tools.

Head trauma is also an example for clinical criteria helping to decide about the individual need for CT evaluation (Oman et al. 2006). Hardly ever is medical diagnostic imaging justified just for demonstrating morphology; as is true for any other diagnostic tests it is expected to detect disease, to differentiate between different pathologies, to stage disease or to provide information about the effects of treatment. However, all this information is not helpful unless it helps in the further management of the patient and is obtained with an appropriate "cost". Cost clearly includes both the financial cost of the examination and its medical risk. In paediatric CT, although there are risks with anaesthesia and intravenous contrast medium injection, the main two risks usually are the inaccuracy of the test (false-negative, false-positive findings) and the risk of radiation exposure, which is more important than in adult patients, even at the same nominal effective dose.

Before any imaging examination with x-rays is considered, alternatives must therefore be evaluated: ultrasound is the first-line imaging test in children since the slim body usually favours the access even to deep organs without any radiation exposure, combining morphological with real-time motional and even flow information. In experienced hands, it can provide a lot of essential information, thus avoiding CT. When ultrasound and radiography are unlikely to answer – or have not answered – the specific medical question, the choice is often between MRI and CT. In this situation severity of suspected disease, study duration, radiation exposure, side-effects of contrast agents and anaesthesia, volume of interest and the specific information required have to be considered in addition to the availability of the method. While there is no general answer, a disease concentrated in one organ or one limited region of the body, and situations requiring detailed information about soft tissues, the nervous system, the cardiovascular system or the bone marrow are often best approached by MRI. On the other hand, a large volume of the body, time and anaesthetic restrictions and emergency conditions, such as multiple trauma, as well as the need for information about cortical bone and calcification, or the combination with image-guided intervention all favour CT. Malignant disease with a poor prognosis will decrease the weight of radiation exposure; however, with an increasing chance of curative treatment – e.g. in malignant lymphoma – the added risk of many follow-up studies under and after treatment must be considered.

Follow-up CT scans are often performed too early, e.g. at a moment when the biology of the disease does not yet allow any treatment effects to be visible. Justification has to be as restrictive as for the first examination, and alternatives may be adequate for observing known manifestations of disease. Justifi-

cation as the first step of diagnostic imaging means a close cooperation between the referring doctor and the radiologist since it cannot be done by the clinician alone or by the radiologist alone. Both need education to adequately perform this important task; it is obvious that subspecialized paediatric radiologists will have a significant advantage of knowledge and experience in the pathology of a child and/or a specific diseased organ.

15.4 Patient Preparation

Patient preparation for CT of adult patients usually means obtaining informed consent, checking renal function and, for the gastrointestinal tract, instructing the patient about oral bowel contrast application or contrast enema. In children, preparation is usually more complex and is an important prerequisite for a successful examination (Table 15.3). Older children often want to be considered as individuals whereas in young children the preparation – beyond the patient herself/himself – often involves the physician, the nurse and the parents. They usually have a better approach to the child and are essential in convincing the child about the need for the examination, in informing about the procedure and its possible discomfort but also in staying with the child during the examination, or in calming by hand contact or conversation. Specially trained staff will site the intravenous line well in advance, will address the children properly and make them feel comfortable; an environment without machines and noise may meet the child's perceptions of the world and trigger trust. All actions avoiding pain and excitement and, thus, motion artefacts or even repeated scans should be considered to improve the quality of the examination and to control radiation exposure. Depending on the individual, medication, fixation for painless positioning, sedation, anaesthetic supervision or general anaesthesia may be appropriate. Many specialized centres, ours included, prefer propofol as medication; to avoid local pain at the injection site, it has to be preceded by injection of another local anaesthetic drug. General anaesthesia, while still used for young, retarded or handicapped children, is nowadays tolerated well, but it is increasingly possible to avoid it thanks to the speed of modern scanners. Exercising cooperation and respiratory apnoea within the scanner but without radiation is a useful, risk-free procedure that avoids repeated scans. Apnoea can mostly be achieved at the age of 5–7 years, and elder children can even cooperate with inspiratory apnoea. Below 5 years it is often wise to accept superficial continuous respiration. The test before the use of radiation will allow for individual adaptation of these age limits. And even in the same patient, depending on the mood and the atmosphere, cooperation may be possible one time and no longer achievable the next time.

Local, superficial, protective absorbing devices deserve special mention. They are available for the lenses of the eyes, the thyroid gland, the breast glands and the testes, and they are an efficient shield against external scatter radiation when the organ is outside the scanned area of the body (Beaconsfield et al. 1998; Brnic et al. 2003; Hidajat et al. 1996; Hohl et al. 2005; Price et al. 1999); of course, internal scatter will hardly be affected. Protecting organs located superficially within the area scanned is an alternative approach and must be used carefully since it might cause artefacts and lower the diagnostic quality (Fricke et al. 2003; Hopper et al. 1997). In our own experience, breast protection in adult women has not been as effective as suggested

Table 15.3. Patient preparation for paediatric CT

1. Decrease anxiety	– Inform where appropriate – Have an accompanying person in room – Provide calm environment
2. Avoid pain	– Site intravenous line well in advance – Immobilize – Sedate/anaesthetize/(intubate)
3. Exercise cooperation	In scanner, without radiation, exercise respiration, any specific cooperation expected
4. Apply local protection device	– Outside scanned volume (thyroid, breast, testes, lenses) – Organ protection within scanned volume (lenses, thyroid, breast, testes)

initially by Hopper, and it is rarely used in clinical routine. Fricke's group has reported better success in girls, keeping the absorbing material at a distance of around 2–3 cm from the skin by interposing a layer of foam, thus avoiding severe degradation of image quality. Testicular capsules are highly appropriate in shielding from indirect and direct exposure, and usually important information is not lost at the level of the testes. In contrast, the deep location of the ovaries basically excludes any local protection by an absorbing material.

15.5 Protocol Definition

15.5.1 Accept Noise as Long as the Scan is Diagnostic

The referring doctor and the radiologist basically want the best for the patient. Images at higher dose look nicer than those obtained at low dose, and if one equates nice to good one tends to prefer the beautiful higher dose images. This mechanism has favoured higher-dose practice over many years. Nowadays, radiologists and clinicians have to realize that *image quality cannot be the only criterion* when biological facts tell us that ionizing radiation may indeed induce cancer at a dose very close to the dose of one CT scan (in around 1‰ of small children). Unfortunately, it is not easy to balance an actual medical need with a rare statistical (stochastic) risk evident only within decades. Since we cannot easily quantify the risk, we should at least try to diminish it. Bringing the dose down to 50% mostly will not affect the diagnosis although the images will be slightly inhomogeneous. Often – of course depending on the organ and the medical question – a greater dose reduction will be tolerable. It is the radiologist's important task to go to the limits, i.e. to accept as much noise as the specific medical task allows (Cody et al. 2004; Ravenel et al. 2001; Shah et al. 2005; Vock 2005). The practical ways of simultaneously achieving dose reduction and *controlling the noise level* are discussed under points 2 and 3 (Table 15.4). The acceptable noise level can be defined by guidelines on *quality criteria* for specific medical imaging tasks, as initiated by the European Commission (European Commission 2000a). Whether post-processing using noise-reducing filters can be used in this situation without loss of sensitivity is still an open question (Kalra et al. 2004).

There is another way of reducing the dose and still maintaining the *S*/*N* ratio by post-processing. With modern scanners, while one usually does not want to lose *z*-axis resolution by prospectively scanning thicker slices, one can easily *acquire noisy thin slices* of 0.5–1.5 mm but simultaneously calculate *thicker images* of 2–6 mm, *used primarily for interpretation*. The thicker images have a good *S*/*N* ratio; the thin images still are used to look at critical details and to get 2D reformation and 3D analysis.

15.5.2 Optimize Scan Parameters Within the Axial Plane

Different scanners have different geometry and tube filtration, and slightly differing efficiencies of the detectors and data acquisition system, factors that usually cannot be influenced by the radiologist or technician. It is likely that the market competition will minimize these differences soon. It is also probable that *additional filtration* will be available for thin patients, decreasing the range of photon energies and therefore reducing the proportion of low-energy photons absorbed almost completely in the body, similar to the current experience in radiography and fluoroscopy. We are free to choose the kVp, the rotation time and mA settings. The *kVp* value needed goes with the diameter of the patient (Frush et al. 2002), and paediatric protocols provided by the manufacturer may suggest the appropriate kVp, mostly following the arguments discussed in Section 15.1 above. Figure 15.1 demonstrates that a lower tube voltage often allows improved image quality at the same or a lower dose. The shortest *rotation time* is mostly appropriate in paediatric CT; since with small objects the capacity of the tube and the acquisition system are not critical, this serves to minimize motion artefacts. Exceptions requiring slower rotation are the same as in adult patients but should be used restrictively. Defining the *tube current* (*mA*) needed is clearly the most critical and difficult choice. Again, general physical rules apply, and scanner-specific suggestions for different regions and ages have been proposed (Table 15.5). In practical work it may be important to realize that for every reduction of the patient diameter by 3.5 cm there is roughly 50% less absorption, and the current can be reduced accordingly in children.

Table 15.4. Protocol definition for dose reduction in CT of children

1	**Accept noise as long as the scan is diagnostic**
	– realize that in digital X-ray imaging noise reduction requires higher exposure – reduce mAs (and possibly kV) – reconstruct additional thick noise-reduced slices without increase of exposure
2	**Optimize scan parameters within the axial plane**
	– increase tube filtration (if available) – use maximal slice thickness appropriate for specific diagnosis – decrease kVp for thin objects – use shortest rotation time available (only few exceptions in children) – decrease baseline mA (CTDI) according to body diameter and composition – use *xy*-plane dose modulation to minimize CTDI
3	**Optimize scan parameters for volume coverage**
	– use representative volume sample when entire volume is not needed (by sequential scans with gaps) to reduce DLP – use spiral scan with pitch >1 (e.g. 1.5) to reduce DLP – use thicker collimation with overlapping reconstruction when thin slices are not needed – use *z*-axis dose modulation to decrease DLP – in the near future, use noise-defined automatic exposure control
4	**Scan minimal length**
	– be restrictive in defining uppermost and lowermost limits to keep DLP low – use localizing projection scan extending just minimally beyond scan limits
5	**Minimize repeated scanning of identical area**
	– avoid major overlap when scanning adjacent areas with different protocols – avoid non-enhanced scans unless specifically justified (e.g. for densitometry) – optimize the protocol to obtain all the information requested during one scan (e.g. contiguous 5-mm images and 1-mm HRCT images every 10 mm) – minimize number of scans in multiphase scanning to decrease DLP – in case of multiphase scanning, use shorter scan length for additional scans – use lower CTDI for non-enhanced or repeat scans unless high quality is needed – use minimal number of additional sequential functional scans to keep DLP low – minimize length of scans and fluoroscopy time in interventional applications – replace test bolus / bolus triggering by standard scan delay unless timing is very critical

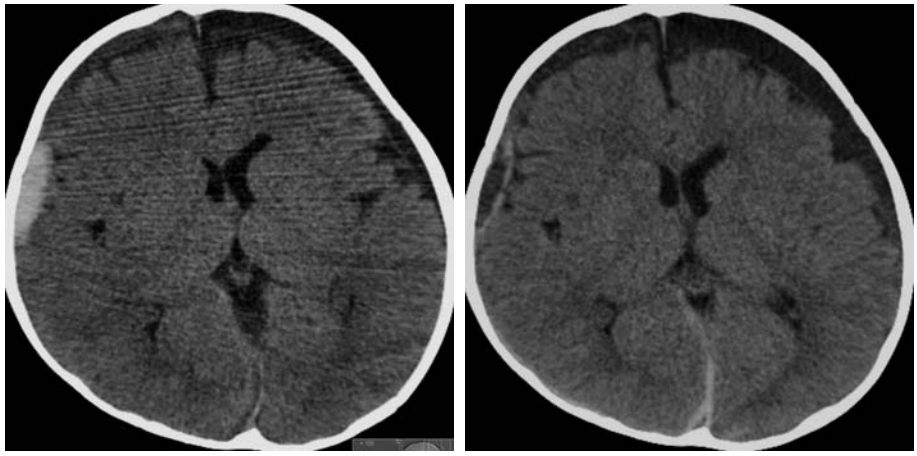

a **b**

Fig. 15.1a, b. Influence of decreasing the voltage on the quality of a brain CT in a 1-year-old child with subdural haematomas of variable age. **a** Scan at 120 kV, 250 mAs, $CTDI_{Vol}$ of 45 mGy, DLP of 688 mGy·cm, estimated effective dose of 4.8 mSv. **b** Scan 2 days later at 100 kV, 330 mAs, $CTDI_{Vol}$ of 43 mGy, DLP of 613 mGy·cm, estimated effective dose of 4.3 mSv. Note the markedly improved contrast in this follow-up scan despite a slightly lower effective dose

Table 15.5. Suggested paediatric CT protocols

Weight (kg)	$CTDI_{Vol}$	kV	mAs	Rows	Comment	Reference
4.5–<9/9–<18			40/50	4	chest	Donnelly et al. (2001) Frush et al. (2002)
18–<27/27–<36			60/70		abdomen	
36–45			80			
>45–69			100–120			
>70			•140			
2.5–5 (<2 years)	6.7 (5.6)	80	72	4 × 2.5	abdomen	Verdun et al. (2004)
5–15 (2–6 years)	9.4 (12)	100	56		pitch 0.75	
15–30 (6–14 years)	15.9 (14)	120	64			
30–50 (14–18 years)	24.5(23.5)	120	96			
<15		120[a]	14/25	4	chest/abdomen	Suess and Chen (2002)
15–24			23/41			
25–34			32/66			
35–44			45/99			
45–54			68/132			
>54			90/165			
<15		120[a]	17	16	chest	Fishman (2006)
15–24			20–40		abdomen	
25–34			30–50			
35–44			50–80			
45–54			70–100			
<15			30–40			
15–24			50–65			
25–34			65–80			
35–44			90–110			
45–54			120–140			
	$CTDI_w$	DLP	eff. dose		DRL brain/chest	Shrimpton and Wall (2000)
<1	40/20	300/200	2.7/6.4[b]			
5	60/30	600/400	2.4/7.2[b]			
10	70/30	750/600	2.3/7.8[b]			
<1	20/20	330/170	12.5/5.4[b]		upper/lower abdomen	
5	25/25	360/250	7.2/4[b]			
10	30/30	800/500	12/7[b]			

Dimensions – $CTDI_{Vol}$, $CTDI_w$: mGy; DLP: mGy·cm; eff. Dose: mSv.
[a] At 80 kV same *S/N* ratio at 50% mAs. [b] Eff.dose: Shrimpton et al. (2005).

Furthermore, based on the minimal risk of modern contrast agents, it might be appropriate in children to replace a native scan by a contrast-enhanced scan, using a lower mAs setting in view of the improved contrast. Unfortunately, no standards of *acceptable noise* with a specific reconstruction algorithm needed in different medical indications have yet been described. Definition of the desired noise level will facilitate scan protocol selection in the near future thanks to interactive *dose modulation* mechanisms that are currently being used in their first generation; since these options for automatic dose reduction are mostly effective in spiral volumetric scanning they will be discussed below with the approach to volume coverage.

$CTDI_w$, the CT dose index (CTDI) weighted for central and peripheral locations, is the entity that reflects the selection of parameters during one rota-

tion, such as used in sequential axial scanning, but also one of the most important parameters in spiral scanning. It is most helpful for comparing the relative exposure due to different protocols. However, it is clearly based on a round phantom and neither respects the diameter, the shape or the composition of the individual patient.

15.5.3 Optimize Scan Parameters for Volume Coverage

The way we scan the volume to be studied is the single most important determinant of radiation exposure in CT protocol definition. The term used to characterize volume exposure is the *dose–length product* (*DLP*), a parameter directly derived from the product of the $CTDI_w$ and the length of the scan. DLP has the same restrictions as $CTDI_w$ in being a physical parameter not adapted to the individual patient's body. But DLP and $CTDI_w$ have the important advantage of being measurable and, thus, offered by the scanner at the end of a study or even earlier for prospective planning. Since the literature gives factors to translate DLP values into effective dose (Chapple et al. 2002; Shrimpton et al. 2005), DLP as the only practical risk parameter must be checked regularly by both the radiologist and the technician; CT doses can therefore be estimated both for the individual patient (Table 15.6) and the population (Pages et al. 2003).

Historically, with *sequential CT* contiguous slices were usually measured, giving a more or less homogeneous dose distribution that we define as 100%. To improve *z*-axis resolution, one had to use some overlap; an overlap of 20% (e.g. slice 5 mm, distance between slices 4 mm) increased exposure to 120%. On the other hand, for HRCT in diffuse interstitial disease of the lung, scanning a sample of 10% of the organ (1 mm slice, distance between slices 10 mm), often considered adequate, reduces exposure to 10%. The introduction of *spiral CT scanning* with a *single row of detectors* avoided overlapping scanning, leaving exposure at 100% in the example cited, even when images were reconstructed at smaller distances of 1–4 mm; of course, this was only true with identical parameters and when table movement during one rotation was exactly the value of the slice collimation; this basic condition was defined as a *pitch* of 1 and, in consequence, a movement of twice the collimation was called a pitch of 2. For this type of scanner, it was therefore attractive to increase the pitch in order to reduce radiation exposure (Donnelly et al. 2001), with the only restriction that high pitch values caused a major thickening of the resulting slice above the collimation. Although not important for long *z*-axis volume scans, spiral scanning means a small additional exposure outside the defined volume during the first and the last rotation of the gantry since data are incomplete and have to be discarded partially.

Current *multirow detector scanners* have increased the options for protocols enormously but also share a disadvantage in performing the HRCT protocol of the lung and other applications where partial sampling of a volume would be medically adequate. They may have to scan two or four slices instead of the single one needed, and collimation at the detector may cause a loss of signal. Aside from this restriction, however, they are mostly used in the spiral mode and have enhanced the speed and the resolution of CT scanning, avoiding the problem of tube heating and offering real *isotropic data* for 3D analysis. The new scan geometry needs more complex image calculation to correct for the diverging beam of the outer detectors but the operator does not have to take care of this modification. Also, the pitch factor has become less important since the increased speed offers other ways to cover a large volume and still to control exposure; similarly, combining the information of different detector rows for the reconstruction of one image has overcome the problem of slice thickening, as seen with early spiral scanners and higher pitch factors.

Table 15.6. Effective dose estimated from dose–length product

Age (years)	Head	Neck	Chest	Abdomen/ Pelvis
0	0.011/0.027	0.017/–	0.039/0.034	0.049/0.040
1	0.007/0.008	0.012/–	0.026/0.021	0.030/0.024
5	0.004/0.004	0.011/–	0.018/0.014	0.020/0.016
10	0.003/0.003	0.008/–	0.013/0.011	0.015/0.014
15			–/0.015	0.015/0.009
Adult	0.002/0.003	0.006/–	0.014/0.009	0.015/–

Numbers give normalized effective dose per dose–length product (mSv per mGy·cm).
First number from Shrimpton et al. (2005)/second number from Chapple et al. (2002).

The increased power of modern scanners has mostly eliminated hardware restrictions of older generations and made it easy to define protocols with a high radiation exposure, reaching the range of complex angiographic or fluoroscopic studies. This has increased the pressure of using any solution available to reduce radiation exposure. Current CT scanners offer one or several of the following options:

XY-plane dose modulation: this option was introduced to overcome the physical problem that the human body is neither round nor of homogeneous density (Greess et al. 2004). To achieve the same *S*/*N* ratio, less radiation is required in the direction of the smaller diameter (anteroposterior at the level of the shoulders, *y*-axis) than in the direction of the larger diameter (left to right at the same level, *x*-axis), and this difference is exaggerated by the presence of more bony mass in the *x*-axis. Modulation of the tube current according to the angle of the tube position around the patient is the logical solution; it is achieved either by estimating the global absorption at all *z*-axis positions from an anteroposterior and a lateral localizing projectional view, or by using the information obtained during one rotation to interactively adapt the tube current for the same angle during the next rotation (Suess and Chen 2002). *xy*-plane dose modulation reduces the nominal mAs by around 20%–40%, depending on the body region, and it is generally appropriate to use it. Specific new applications of *xy*-dose modulation are appropriate for the heart and, maybe, the breast gland. This means prospectively ECG-triggered lower mA values during the phases of the heart that are not used for reconstruction and higher mA values during important phases, such as mid- to late diastole. A similar approach might be used to decrease the radiation exposure of the breast gland in chest CT of young women by decreasing mA when the tube is located in front of the patient and – for compensation – by increasing mA when the tube is at their back.

z-*axis dose modulation*: as for the axial plane, physically in the longitudinal axis of the body (*z*-axis) the radiation needed for an adequate *S*/*N* ratio will vary with the diameter and density of the patient. For example, in cervicothoracic scanning, the cervical area and the lower chest require much less of a dose for a given image quality than the thoracic inlet and shoulder area. Similarly, until recently, one had to interrupt scanning at a level between physically different adjacent body areas; e.g. to use a lower radiation exposure for the upper than the lower abdomen, one had to stop the upper scan at the pelvic rim and to start another scan with modified parameters for the pelvis, often with a significant technical delay. Modern scanners allow for adapting the tube output during one single scan in this and other clinical applications. The option of *z*-axis-dependent dose modulation is steered again either from the localizing view or interactively; it is clearly welcome to reduce radiation exposure and should be used generally (Tack et al. 2003).

It must be mentioned that dose modulation is an important step towards the final goal of *noise-defined automatic exposure control*, and that the solutions implemented in current scanners may have rules for adaptation not easily understood by the user; one therefore has to be careful not to run into dose augmentation, e.g. by starting the scan at a level with low dose requirement at a nominal mAs value selected for the thickest scan level to be covered. Software tools will simplify the choice in the near future, e.g. by offering a selection of images with different noise.

Control of noise in the image is one approach whereas observation of the DLP per examination is another practical approach. Since in CT examinations the DLP is a good representative of effective dose to a specific area of the body, *diagnostic reference levels* (*DRL*) indicating an upper DLP not to be exceeded in typical clinical tasks are the practical solution (Shrimpton and Wall 2000; Wall 2001). DRLs correspond to the third quartile (75% lower values obtained from a population with the same examination). They do not represent an absolute barrier; however, they should be defined for specific body areas, according to the weight and the medical task. Since the DLP is available immediately during the study, each radiologist can prospectively plan the DLP to stay within the specific DRL or, exceptionally and with an appropriate justification, to exceed it for a concrete reason.

15.5.4 Scan Minimal Length

This rule applies both for the scout view and the rotational scan since there is really no value in going beyond the tissue volume where pathology is suspected. It has to be followed at two levels: the referring physician and the radiologist have to find

a compromise about the minimal *body areas to be investigated*; the radiologist and the technician have to fine-tune the *upper and lower end of the examination* (Donnelly et al. 2001). In a lung scan, there is no reason to include the entire thoracic inlet with the thyroid gland as well as the upper half of the abdomen with multiple radiosensitive organs (Campbell et al. 2005). In a pelvic scan of a boy, there is hardly ever a medical reason to include the testes. Independent of the organs included, any increase in scan length will proportionally increase energy deposition and the biological effects of ionizing radiation. While other rules are the primary responsibility of the radiologist, the technician and her/his experience are most critical for this rule. In routine scanning, it is simply not justified to extend the length beyond the minimum required. For example, a chest scan has to cover the lowest part of the costophrenic sulcus and – in neoplastic disease – the adrenal glands; any inclusion of more abdominal structures will induce non-justified radiation exposure to sensitive organs.

For two reasons, the rule should be used less strictly for the localizing than for the sectional scan. First, radiation exposure – although often neglected in dose estimation – is small during a localizing projectional view, usually contributing a very low percentage to the global exposure. Second, the localizer has to include the starting and ending levels of the spiral scan and is a prerequisite for properly limiting the scan length to the minimum needed in the specific medical situation.

15.5.5 Avoid Non-Justified Multiple Scans of the Same Area

Numerous opportunities exist with the current powerful scanners to scan the same volume of the body twice or even several times. Since there is no longer a technical restriction, multiphase studies can be performed without tube heating or data overflow.

Perhaps the most frequent neglect of this rule happens when two adjacent body areas are scanned with different protocols and a large overlap. The obvious example for this may be cervicothoracic scanning in malignant lymphoma; while the head and neck scan is planned on a lateral localizer, the scan of the trunk is planned on an anteroposterior localizer, and large overlaps at the thoracic inlet often cause multiple scanning of sensitive organs, such as the thyroid gland.

A number of *medical reasons* may require different types of repeat scans of the same area:

- correct timing of scans, using a test bolus or repetitive scanning of one plane at low dose for bolus triggering of the proper diagnostic scan
- dynamic enhancement studies including arterial, parenchymal, venous and/or excretion phases of organs, such as the kidney or liver
- functional lung scans to detect air trapping in inspiration and expiration (in young children unable to cooperate this may also be achieved by scanning in right and left lateral decubitus position)
- supine and prone scans for demonstrating positional gravitational effects
- CT-guided intervention, with or without fluoroscopy
- screening with thick slices and subsequent detailed analysis with thin slices
- exceptionally in childhood: native and contrast-enhanced scan after intravenous bolus injection.

Some but by no means all of these technical possibilities are justified in medical problem solving, and it is probably the most difficult task of the resident in radiology to think of all these potential options and not to overuse them in view of radiation exposure. For example, renal CT may often be adequately performed with a single scan after a two-phase injection of the contrast agent, showing both the parenchyma and the pelvicalyceal systems. It is quite clear that *double scanning* means *twice the radiation exposure* as long as the same parameters are used, and even more scans will increase exposure proportionally. Aside from medical experience, a few general guidelines may help to appropriately select the number of scans. First of all, and again, the individual *situation of the current patient* must be checked. Will any of the repeat scans help this patient? Will it influence the management or even the outcome? Is it cost-efficient when we add radiation exposure to the financial cost? Second, *repeat scans* can often be *limited to a smaller volume* or performed at *lower dose* that will not hide the additional information expected. Third, fixed standard scan timing can often replace individual triggering or a test bolus unless cardiovascular disease is present and timing very critical. Fourth, while CT fluoroscopy is a very helpful tool in cases of difficult access, other biopsy methods or drainages can often be done under CT image control

or even under ultrasound guidance. Fifth, in the lung one single scan can usually be used to obtain all the information needed: using thin detector rows of around 1 mm will allow one to calculate both thin HRCT sections at any *z*-axis level and thick 5-mm scans, as needed for tumour search or mediastinal analysis; for reformations and 3D post-processing, continuous and overlapping images can be prepared from the same raw data.

In conclusion, CT is characterized by a significantly higher radiation exposure than radiography. Based on its excellent diagnostic potential in a range of medical situations its use has significantly increased in children. However, due to the increased biological impact of radiation exposure in children, paediatric CT examinations should follow a strict justification and optimization by careful selection of protocol parameters as well as the range. The steps discussed above help the radiologist to apply the ALARA principle when scanning children (Slovis 2003).

Acknowledgement
The authors thank Barbara Le Blanc for typing the manuscript.

References

American College of Radiology ACR (2006) Appropriateness criteria topic list. Available online at www.acr.org/s_acr/sec.asp?CID=1847&DID=16052 (24 October 2006)

Beaconsfield T, Nicholson R, Thornton A, Al-Kutoubi A (1998) Would thyroid and breast shielding be beneficial in CT of the head? Eur Radiol 8:664–667

Boone JM, Geraghty EM, Seibert JA, Wootton-Gorges SL (2003) Dose reduction in pediatric CT: a rational approach. Radiology 228:352–360

Brenner DJ (2002) Estimating cancer risks from pediatric CT: going from the qualitative to the quantitative. Pediatr Radiol 32:228–231

Brenner DJ, Elliston CD, Hall EJ, Berdon WE (2001) Estimated risks of radiation – induced fatal cancer from pediatric CT. AJR Am J Roentgenol 176:289–296

Brenner DJ, Doll R, Goodhead DT, Hall EJ, Land CE, Little JB, Lubin JH, Preston DL, Preston RJ, Puskin JS, Ron E, Sachs RK, Samet JM, Setlow RB, Zaider M (2003) Cancer risks attributable to low doses of ionizing radiation: assessing what we really know. Proc Natl Acad Sci USA 100:13761–13766

Brnic Z, Vekic B, Hebrang A, Anic P (2003) Efficacy of breast shielding during CT of the head. Eur Radiol 13:2436–2440

Campbell J, Kaira MK, Rizzo S, Maher MM, Shepard JA (2005) Scanning beyond anatomic limits of the thorax in chest CT: findings, radiation dose, and automatic tube current modulation. AJR Am J Roentgenol 185:1525–1530

Chapple CL, Willis S, Frame J (2002) Effective dose in paediatric computed tomography. Phys Med Biol 47:107–115

Cody DD, Moxley DM, Krugh KT, O'Daniel JC, Wagner LK, Eftekhari F (2004) Strategies for formulating appropriate MDCT techniques when imaging the chest, abdomen, and pelvis in pediatric patients. AJR Am J Roentgenol 182:849–859

Donnelly LF, Emery KH, Brody AS, Laor T, Gylys-Morin VM, Anton GA, Thomas SR, Frush DP (2001) Minimizing radiation dose for pediatric body applications of single-detector helical CT: strategies at a large children's hospital. AJR Am J Roentgenol 176:303–306

European Commission (2000a) European guidelines on quality criteria for computed tomography, EUR 16262EN. Office for Official Publications of the European Communities, Luxembourg. Available online at www.drs.dk/guidelines/ct/quality/index.htm (24 October 2006)

European Commission (2000b) Referral guidelines for imaging, EUR Radiation protection 118. Office for Official Publications of the European Communities, Luxembourg. Available online at www.ec.europa.eu/energy/nuclear/radioprotection/publication/118_en.htm (24 October 2006)

Fishman EK (2006) Pediatric spiral CT scanning protocol. Available online at www.ctisus.org/mdct16ped/ (28 October 2006)

Fricke BL, Donnelly LF, Frush DP, Yoshizumi T, Varchena V, Poe SA, Lucaya J (2003) In-plane bismuth breast shields for pediatric CT: effects on radiation dose and image quality using experimental and clinical data. AJR Am J Roentgenol 180:407–411

Frush DP (2002) Pediatric CT: practical approach to diminish the radiation dose. Pediatr Radiol 32:714–717

Frush DP, Soden B, Frush KS, Lowry C (2002) Improved pediatric multidetector CT using a size-based color-coded format. AJR Am J Roentgenol 178:721–726

Frush DP, Donnelly LF, Rosen NS (2003) Computed tomography and radiation risks: what pediatric health care providers should know. Pediatrics 112:951–957

Greess H, Lutze J, Nömayr A, Wolf H, Hothorn T, Kalender WA, Bautz W (2004) Dose reduction in subsecond multislice spiral CT examination of children by online tube current modulation. Eur Radiol 14:995–999

Hidajat N, Schroder RJ, Vogl T, Schedel H, Felix R (1996) The efficacy of lead shielding in patient dosage reduction in computed tomography (German). Rofo 165:462–465

Hohl C, Mahnken AH, Klotz E, Das M, Stargardt A, Mühlenbruch G, Schmidt T, Günther RW, Wildberger JE (2005) Radiation dose reduction to the male gonads during MDCT: the effectiveness of a lead shield. AJR Am J Roentgenol 184:128–130

Hopper KD, King SH, Lobell ME, TenHave TR, Weyver JS (1997) The breast: in-plane x-ray protection during diagnostic thoracic CT – shielding with bismuth radioprotective garments. Radiology 205:853–858

Huda W (2002) Effective dose to adult and pediatric patients. Pediatr Radiol 32:272–279

Huda W, Gkanatsios NA (1997) Effective dose and energy imparted in diagnostic radiology. Med Phys 24:1311–1318

Huda W, Scalzetti EM, Levin G (2000) Technique factors and image quality as functions of patient weight at abdominal CT. Radiology 217:430–435

Kalra MK, Maher MM, Blake MA, Lucey BC, Karau K, Toth TL, Gopal A, Halpern EF, Saini S (2004) Detection and characterization of lesions on low-radiation-dose abdominal CT images postprocessed with noise reduction filters. Radiology 232:791–797

Mettler FA, Wiest PW, Locken JA, Kelsey CA (2000) CT scanning: patterns of use and dose. J Radiol Prot 20:353–359

Nickoloff E (2002) Current adult and pediatric CT doses. Pediatr Radiol 32:250–260

Nickoloff EL, Alderson PO (2001) Radiation exposures to patients from CT. Reality, public perception, and policy. AJR Am J Roentgenol 177:285–287

Oman JA, Cooper RJ, Holmes JF, Viccellio P, Nyce A, Ross SE et al for the NEXUS II investigators (2006) Performance of a decision rule to predict need for computed tomography among children with blunt head trauma. Pediatrics 117:238–246

Pages J, Buls N, Osteaux M (2003) CT doses in children: a multicentre study. Br J Radiol 76:803–811

Paterson A, Frush DP, Donnelly LF (2001) Helical CT of the body: are settings adjusted for pediatric patients? AJR Am J Roentgenol 176:297–301

Pierce DA, Preston DL (2000) Radiation-related cancer risks at low doses among atomic bomb survivors. Radiat Res 154:178–186

Price R, Halson P, Sampson M (1999) Dose reduction during CT scanning in an anthropomorphic phantom by the use of a male gonad shield. Br J Radiol 72:489–494

Ravenel JG, Scalzetti EM, Huda W, Garrisi W (2001) Radiation exposure and image quality in chest CT examinations. AJR Am J Roentgenol 177:279–284

Shah R, Gupta AK, Rehani MM, Pandey AK, Mukhopadhyay (2005) Effect of reduction in tube current on reader confidence in paediatric computed tomography. Clin Radiol 60:224–231

Shrimpton PC, Wall BF (2000) Reference doses for paediatric computed tomography. Radiat Prot Dosim 90:249–252

Shrimpton PC, Hillier MC, Lewis MA, Dunn M (2005) Doses from computed tomography (CT) examinations in the UK – 2003 review. UK Health protection agency, NRPB-W67

Slovis TL (2002) The ALARA (as low as reasonably achievable) concept in pediatric CT intelligent dose reduction. ALARA conference proceedings. Pediatr Radiol 32:219–220

Slovis TL (2003) Children, computed tomography radiation dose, and the as low as reasonably achievable (ALARA) concept. Pediatrics 112:971–972

Suess C, Chen X (2002) Dose optimization in pediatric CT: current technology and future innovations. Pediatr Radiol 32:729–734

Tack D, De Maertelaer V, Gevenois PA (2003) Dose reduction in multidetector CT using attenuation-based online tube current modulation. AJR Am J Roentgenol 181:331–334

Verdun FR, Lepori D, Monnin P, Valley JF, Schnyder P, Gudinchet F (2004) Management of patient dose and image noise in routine pediatric CT abdominal examinations. Eur Radiol 14:835–841

Vock P (2002) CT radiation exposure in children: consequences of the American discussion for Europe (German). Radiologe 42:697–702

Vock P (2005) CT dose reduction in children. Eur Radiol 15:2330–2340

Wall BF (2001) Diagnostic reference levels – the way forward. Commentary. Br J Radiol 74:785–788

Ware DE, Huda W, Mergo PJ, Litwiller AL (1999) Radiation effective doses to patients undergoing abdominal CT examinations. Radiology 210:645–650

Radiation Risk Management in Low Dose MDCT Screening Programs

16

16.1 Lung Cancer Screening Including Pulmonary Nodule Management

Emmanuel Coche

CONTENTS

16.1.1 Introduction

Lung cancer is the leading cause of cancer-related mortality in the world, with almost one million deaths annually (Parkin et al. 1999). There are more deaths from lung cancer in the United States (US) than from the three next most common cancer-related causes of death (colorectal, breast, and prostate). It was estimated that in 2005, in the US alone, there would be more than 170,000 new cases of lung cancer, with approximately 163,000 related deaths (Jemal et al. 2005). Given these discouraging statistics, it is paramount to try to find the means of decreasing the mortality from this disease.

The reason why lung cancer is so frequently lethal is that most of the patients are diagnosed in the later stages of the disease, when their malignancy has grown beyond cure. By contrast, outcome is significantly improved in patients diagnosed at an earlier, resectable stage, with 5-year survival rates for stage I disease approaching 70% (Williams et al. 1981; Mountain 1986; Mountain et al. 1987; Martini 1990; Shah et al. 1996). Thus, earlier detection of the disease would enhance the chances of a curative resection and thereby reduce lung cancer mortality.

The possibility of producing non-superimposed, cross-sectional images with low-dose computed tomography (CT) places this technique and multidetector CT (MDCT) in strong positions as ideal tools for lung cancer screening. However, the radiation dose delivered to the patient due to baseline CT screening, repeated CT and lung nodule management represents one of the most important issues of this type of screening.

E. Coche, MD, PhD
Department of Medical Imaging, Cliniques Universitaires St-Luc, Avenue Hippocrate 10, 1200 Brussels, Belgium

16.1.2 Imaging Techniques Used for Early Lung Cancer Detection

16.1.2.1 Chest Radiography and Sputum Cytology

The first screening test for lung cancer used to be chest radiography. In the 1960s and 1970s there were large randomized trials conducted both in the US and Europe in which volunteers underwent either periodic chest radiography or a simple clinical follow-up as baseline examination (Brett 1969; Fontana et al. 1986). Although these studies found a higher incidence of resectable disease in the screened population, none of them showed a lung cancer mortality reduction with screening.

Large randomized trials conducted mainly in the US over recent decades have addressed the role of chest radiography and sputum cytology examination in screening for lung cancer. The Memorial-Sloan Kettering and John Hopkins University studies compared lung cancer detection rates using annual chest radiography alone (control arm) and annual radiography plus sputum cytology analysis every 4 months (intervention arm) (Flehinger et al. 1984; Frost et al. 1984). The Memorial-Sloan Kettering study enrolled 4,968 men to chest radiography and 5,072 to dual (chest radiography and sputum cytology) screen. There were 144 lung cancers detected in each group. The investigators found no significant difference in stage distribution, resectability, survival or disease-specific mortality between groups and concluded that the addition of sputum cytology examination offered no advantage over annual screening with chest radiography (Melamed et al. 1984). In the Johns Hopkins study, 5,161 men were randomized to chest radiography and 5,226 to dual screening. Screening resulted in the detection of 202 cases of lung cancer in the chest radiography group and 194 cases in the dual screening group (Tockman 1986).

The Mayo Lung Project (Fontana et al. 1984) enrolled over 10,900 subjects. Participants were offered chest radiography and sputum cytology at enrolment. They were then randomly assigned to a close-surveillance group, which underwent 4-monthly chest radiography and sputum cytology, or to a control group, which was advised to have the standard surveillance of yearly chest radiography and sputum analysis. There were no statistically significant differences in either survival or lung cancer-related mortality between the two groups.

Since those disappointing results, lung cancer screening with chest radiography has been abandoned.

16.1.2.2 Spiral CT and MDCT

16.1.2.2.1 Past Trials

Recent advances in technology have prompted new trials for early detection of lung cancer using spiral CT. The first trials were non-randomized screening studies performed in Japan, using a combination of chest radiography and CT (Kaneko et al. 1996; Sone et al. 1998). The authors demonstrated that low-dose CT was very effective in detecting early-stage lung cancer.

In 1993, the Early Lung Cancer Action Project (ELCAP) was started at Cornell Medical Center (Henschke et al. 1999). In that study, the baseline screening of 1,000 persons (smokers, over the age of 60 years) produced 27 screen-diagnosed (Henschke et al. 1999) lung cancers. Among the discovered lung cancers with low-dose CT, 23 out of 27 were stage I. The authors concluded that low-dose CT may increase the chances of detecting lung cancer at an earlier and potentially more curable stage. The authors demonstrated also that low-dose CT was superior to chest radiography at detecting early lung cancer (Fig. 16.1.1).

The results of other similar studies performed in Europe and in North America (Henschke et al. 1999; Diederich et al. 2002; Sobue et al. 2002; Swensen et al. 2002; Mahadevia et al. 2003; Pastorino et al. 2003; Swensen et al. 2003b; Bastarrika et al. 2005, Gohagan et al. 2005, MacRedmond et al. 2006) have demonstrated that the vast majority of lung cancers detected by screening, both at baseline and annual review, are stage I at diagnosis (Leong et al. 1999). The study by Swensen et al. (2002, 2003b) enrolled 1520 subjects, aged 50 years or more, who underwent annual sputum cytology and also DNA analysis. A total of 26 lung cancers were diagnosed at baseline CT, of which 2 were detected by sputum cytology only. Stage I disease was reported in 19 patients and the lung cancer detection rate was 1.7%. Then 2 years after baseline low-dose CT scanning, a further 588 non-calcified nodules were identified

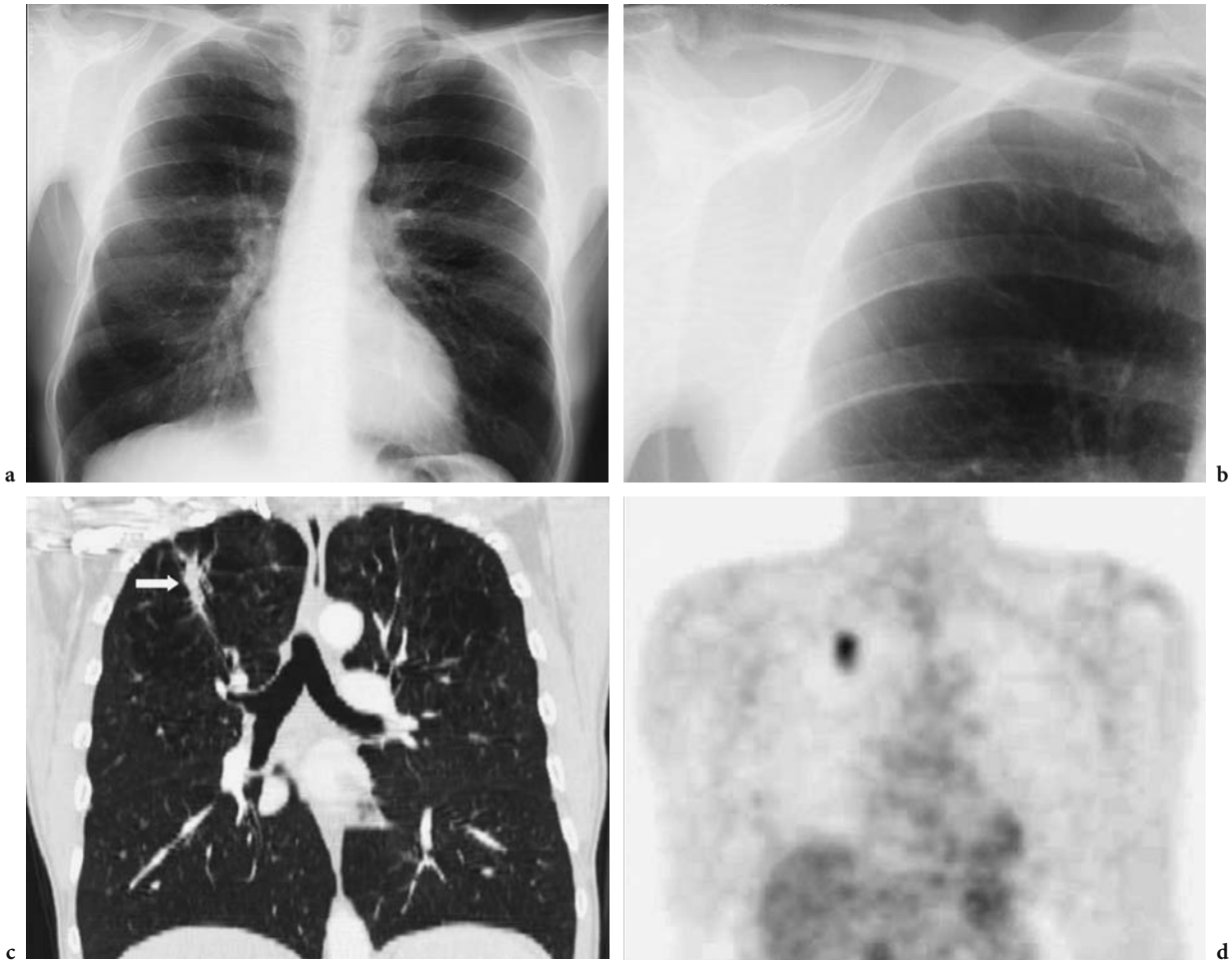

Fig. 16.1.1a–d. MDCT is more sensitive than chest radiography at detecting early lung cancer. ^{18}F-Deoxyglucose positron emission tomography (FDG-PET) can be used as an additional tool for lung nodule characterization. A 70-year old man, heavy smoker, underwent a chest radiograph and MDCT for lung cancer screening. **a** Postero-anterior chest radiography did not reveal any suspicious lung nodule. **b** A close-up of the right upper lobe did not show any lung lesion even retrospectively. **c** Frontal reformatted chest CT revealed a spiculated lung nodule (*arrow*) consistent with lung cancer. No mediastinal enlarged lymph node was present. **d** FDG-PET demonstrated an intense uptake in the right upper mass consistent with a lung tumour. The TNM staging was $T_1N_0M_0$ at the time of diagnosis

(incidence), of which 10 were lung cancer (9 stage I) (Swensen et al. 2002, 2003b).

Diederich et al. (2002) screened 817 smokers above 40 years of age using annual low-dose CT. The team detected 858 non-calcified nodules, of which 12 were lung cancers (12 at stage I) in 43% (350 of 817) of individuals. Follow-up of non-calcified nodules present at baseline low-dose CT demonstrated growth in 11 cases and 7 were lung cancers. Following re-screening, a further 174 new nodules were found of which 3 were lung cancers. Of the ten screen-detected lung cancers, six were at stage I.

MacRedmond et al. (2006) reported data concerning 449 smokers above 50 years of age. Screening with low-dose CT resulted in the finding of 155 non-calcified nodules, among which 2 were lung cancers with a prevalence of 0.46%.

Table 16.1.1 summarizes the main low-dose CT screening trials for lung cancer.

16.1.2.2.2 Current Trials

Some prospective randomized controlled trials comparing lung cancer mortality in a screening arm (with low-dose CT screening) and a control arm (without CT screening) have been initiated. At the end of those large studies, scientists hope to be able

Table 16.1.1. Summary of the main clinical trials using low-dose CT for early lung cancer detection

Author/modality	No. of cases	Age (years)	% of cancer	% of stage I
Henschke et al. 1999; Rx-CT	1,000	>60	2.7	83
Diederich et al. 2002; CT	817	40–78	1.3	63
Sobue et al. 2002; CT	1,611	40–79	0.87	78
Swensen et al. 2002; CT	1,520	50–85	1.7	73
Pastorino et al. 2003; CT + PET	1,035	≥50	1.1	100
Bastarrika et al. 2005; CT +PET	911	>40	1.5	84
Gohagan et al. 2005; Rx or CT	1660	55–74	1.8 (CT)	53 (CT)
	1658	55–74	0.4 (X-ray)	85 (X-ray)
MacRedmond et al. 2006; CT	449	50–74	0.46	NA

to see if low-dose CT screening is able to reduce lung cancer mortality. The US National Lung Screening Trial has recently randomized nearly 50,000 current or former smokers to undergo either an annual screening with low-dose CT or a chest radiograph for 3 years. The trial should be completed in 2009. It is designed to have a 90% power to detect a mortality reduction of 20% (National Lung Cancer Screening Trial, available online at: http://www.cancernet.nci.nih.gov/nlst). Other studies, currently underway, will assess the value of low-dose CT as a screening tool. In the Netherlands, the "Dutch Lung Cancer Screening Trial" plans to include 24,000 subjects and the French "Depiscan" project is hoping to study 21,000 subjects.

16.1.2.2.3 CT Scanning Protocols for Lung Nodule Detection and Lung Cancer Screening

The use of CT for lung cancer screening is based on the fact that low-dose CT can be used for reliable identification of anatomy and pathology when there is a large contrast between a structure (nodule) and its surroundings (lungs). The detectability of pulmonary nodules was studied by Diederich et al. (1996). The authors compared the performance of low-dose CT versus standard-dose CT to detect lung nodules. Low-dose CT was performed with a spiral technique using 120 kVp, 50 mAs per rotation, a slice thickness of 10 mm and pitch of 1.0. Standard-dose CT was generally conducted at 120 kVp, 250 mAs per rotation, a slice thickness of 10 mm and a pitch of 1.0. The authors were able to demonstrate that all soft-tissue nodules greater than 5 mm in diameter were clearly detectable with low-dose CT, regardless of dose reductions by a factor 5–10 (Fig. 16.1.2). Even nodules between 3 and 4 mm in diameter could be found in the vast majority of cases. Similar results were obtained by Nitta et al. (1998). They performed scans at 120 kVp, 10 mm slice thickness, pitch of 2.0 and a 5-mm reconstruction increment, with tube current-time product settings of 50, 6 and 3 mAs. Even at 6 mAs, no statistically significant difference was found in the detectability of artificial soft-tissue lesions of 5 and 10 mm in size, except for those in the upper fields of the lungs. These results confirm early findings on low-dose applications for chest CT that were previously reported in 1990 (Naidich et al. 1990).

The first studies (Kaneko et al. 1996) performed for the purpose of lung cancer screening used single-detector CT at 120 kVp, 50 mA, 10 mm collimation and pitch of 2.0. The International Early Lung Cancer Action program (I-ELCAP) (Henschke et al. 1999) performed baseline CT using 140 kVp, 40 mA, 10 mm collimation and a pitch of 2.0. Thereafter, modifications have been made in the framework of the international conferences (International Collaboration to Screen for Lung Cancer; http://ICScreen.med.cornell.edu) organized by this group and in their resultant international consortium on screening for lung cancer (I-ELCAP, see online at: www.IELCAP.org). I-ELCAP has adopted a common protocol (Henschke et al. 2002). In this regimen (Henschke et al. 2003), the initial low-dose test is identical at both baseline and repeated screenings. A multi-slice helical CT scanner [General Electric (GE) Lightspeed, Milwaukee, Wis., USA; Siemens Volume Zoom, Erlangen, Germany; or equivalent]

is preferably used, at a low-dose setting (120 kVp, 40 mA with 1.5:1 pitch, 1.25 mm slice thickness and 0.5 s rotation; Siemens: 120 kVp, 20 mA with a 1.75:1 pitch at 1 mm slice thickness and 0.5 s rotation). In a single breath-hold, contiguous slices from the thoracic inlet to the adrenal glands are obtained. A consensus statement of the Society of Thoracic Radiology (Aberle et al. 2001) recommends screening with a multi-detector row CT so that high-resolution scans can be performed retrospectively, without the need to use additional radiation. The use of contrast material is not involved. The general trend is to perform annual CT scanning in a high-risk population (at least 10- or 20-pack years of cigarette smoking) aged between 50 and 80 years.

The screening protocols will vary with the available imaging technology. The different CT scanning protocols used for lung cancer screening in main

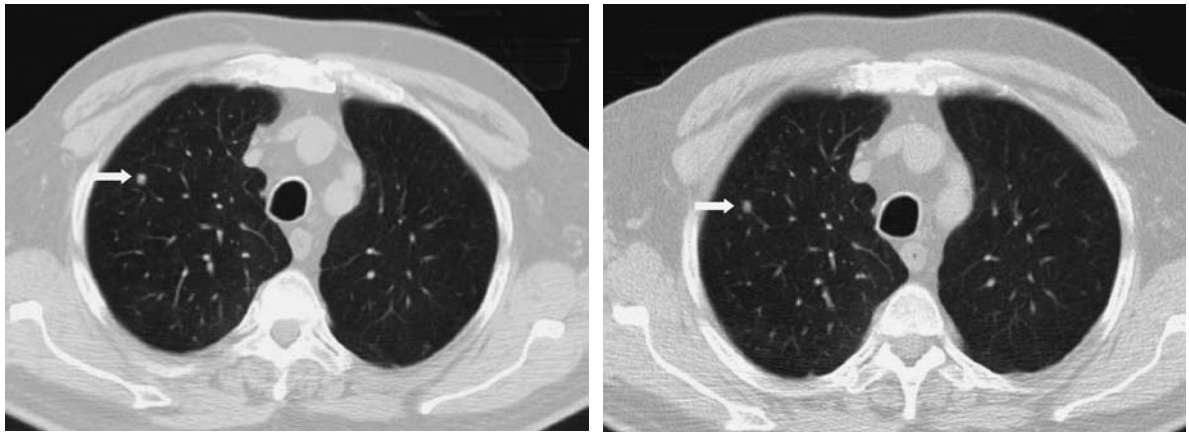

a b

Fig. 16.1.2a,b. Lung nodule (*arrow*) assessed with CT performed at 120 kV, 130 mA (**a**) and at 120 kV, 15 mA per rotation (**b**). There is increased noise in the CT image performed with lower parameters but the nodule detection (*arrows*) remains unchanged

Table 16.1.2. Scan parameters and effective dose per CT scan for various lung cancer screening studies

Author/modality	Type of CT	CT parameters	Effective dose (in mSv)	
			In men	In women
Henschke et al. 1999; CT	High-speed advantage, GE	140 kVp, 40 mA, 10-mm collimation	0.8	0.9
Diederich et al. 2002; CT	SR 7000, Philips	120 kVp, 50 mAs, 5-mm collimation, 5-mm recon interval, pitch: 2	0.6	1.1
Sobue et al. 2002; CT	TCT-900S Superhelix, Toshiba	120 kVp, 50 mA, 10-mm collimation, 10-mm recon interval, pitch: 2	0.6	0.7
Swensen et al. 2002; CT	Lightspeed model Qx/i, GE	120 kVp, 40 mA, 5-mm collimation, 3.75-mm recon interval	0.6	0.8
Pastorina et al. 2003; CT + PET	Single-slice CT	140 kVp, 40 mA, 10-mm collimation, 5-mm recon interval, pitch: 2	0.6 for CT	0.8 for CT
	Hispeed model, GE		NA for PET	NA for PET
Bastarrika et al. 2005; CT +PET	Single-slice CT, Somatom plus 4, Siemens	140 kVp, 43 mAs, 8-mm collimation, recon interval NA, pitch: 1.5	1.0	1.3
	4-row multislice CT, Somatom Volum Zoom, Siemens	120 kVp, 20 mAs, 1.25-mm collimation	0.9	1.1

clinical trials are displayed in Table 16.1.2 and the related radiation doses calculated with CT Expo software (Dr Stamm, Hannover, Germany).

16.1.3 Imaging Techniques for Lung Nodule Management

16.1.3.1 Background

With the improved quality of CT examinations and increasing use of MDCT, small pulmonary nodules are frequently detected on CT scans. This is not an insignificant problem since such nodules are small and thus difficult to biopsy using minimally invasive techniques. In the near future, diagnostic and therapeutic issues with small pulmonary nodules are likely to increase quantitatively because of sub-millimetre slice acquisition in routine MDCT examinations.

Screening projects using CT for early detection of lung cancers found pulmonary nodules in 23%–74% of populations at risk (Henschke et al. 1999; Swensen 2003a, Swensen et al. 2003b, 2005). In the Mayo Clinic study, almost 70% of the volunteers had non-calcified pulmonary nodules. Only a fraction of these required further invasive follow-up, including resection of benign lesions in eight patients (Swensen 2003a, Swensen et al. 2003b). The false-positive rates in that study ranged from 92.9% for nodules larger than 4 mm in diameter to 96% for all nodules (Swensen et al. 2005). By contrast, only 23% of the volunteers at baseline screening in the I-ELCAP study had non-calcified nodules that needed further evaluation (Henschke et al. 1999). In order to try to minimize the number of invasive procedures required to confirm (or exclude) malignancy and the inherent risk for complications, Libby et al. (2004) created an algorithm based on the ELCAP data and the medical literature from 1993–2003 for nodules discovered incidentally on CT. They based it upon the size, number and density of the nodule(s), as well as patient characteristics such as age, gender, smoking history, occupational history, and any antecedent granulomatous disease. An additional advantage of this approach is that it can be used for a wider population than that typically enrolled in CT screening programs.

Lung nodule management remains difficult and highly variable among clinicians. A survey conducted in Austria revealed a large variation of nodule management among radiologists, pneumologists and thoracic surgeons (Prosch et al. 2006). In order to help radiologists and clinicians to assess lung nodules, guidelines for management of small pulmonary nodules have been published by the Fleischner Society (MacMahon et al. 2005).

16.1.3.2 Characterization of Lung Nodule on Baseline CT

In evaluating a solitary pulmonary lung nodule detected by chest radiography or chest CT, it is helpful to review old chest radiographs or CT scans to determine if the lesion was present before. If the lesion remains stable for 2 years or more, it is classified as benign and does not require any further evaluation. If the nodule remains undetermined, the next step is to perform thin-section spiral CT using 1- to 3-mm collimation. The length coverage is greater than the nodule size to compensate for slight differences in patient inspiratory volumes and thus ensure inclusion of the entire region of interest within the scanning volume (Leung 1997).

If the thin-section CT identifies fat in a nodule, calcification in a benign pattern, no further work-up is needed (Erasmus et al. 2000). Eccentric calcifications may occur in malignant nodules and require further evaluation. Recently, small adenocarcinomas of the lung showing ground-glass opacity (GGO) on CT have been reported (Nambu et al. 2005; Shimizu et al. 2006).

16.1.3.3 CT Follow-Up

Small nodules are usually monitored by means of serial CT examinations, with the aim of detecting an increase in size suggestive of malignancy. The ELCAP group (Henschke et al. 1999) recommends that follow-up CT be performed 3 months after initial identification of nodules between 5 and 10 mm in diameter. If no growth is detected, CT should be repeated 6, 12, and 24 months later. Biopsy is indicated if growth is detected. Recent review of nodules measuring less than 5 mm on

baseline CT screening in the ELCAP study (Henschke et al. 2004) demonstrated that non-calcified nodules smaller than 5.0 mm in diameter do not justify immediate work-up but only annual repeat CT screening to determine whether interim growth has occurred.

For nodules detected incidentally on CT scans performed outside a lung cancer screening program, the Fleishner Society has edited new guidelines (MacMahon et al. 2005) (Table 16.1.3).

Researchers (Revel et al. 2004a) have demonstrated that two-dimensional (2D) CT measurements were not reliable in the evaluation of small non-calcified pulmonary nodules. They found that both intra- and inter-reader agreement for 2D measurement of nodule size on CT scans were poor. The same team of researchers (Revel et al. 2004b) demonstrated that 3D volumetric evaluation of nodule growth was more accurate than 2D diameter measurement. Furthermore, Yankelevitz et al. (2000), in a study of segmentation techniques for assessing the growth rate of pulmonary nodules in three dimensions, found that some malignant nodules showed asymmetric growth that was not detected by using 2D techniques. The doubling time for most malignant nodules is between 30 and 400 days (Hartman 2005). At present, many manufacturers have developed computer-assisted detection (CAD) and 3D measurement tools that allow easy comparison of nodule size on routine CT examinations (Fig. 16.1.3).

16.1.3.4 Nodule Enhancement at Dynamic CT

Over the past decade, there has been considerable research interest in the enhancement of indeterminate lung nodules with spiral CT. The hypothesis in most studies was that malignant lung nodules enhance substantially more than benign nodules (Swensen et al. 1995, 1996). Swensen et al. (1995) initially evaluated patterns of contrast uptake in a total of 163 patients with solitary nodules measuring less than 4 cm in size using a single detector CT scanner. Following a bolus of 100 ml of intravenous contrast medium injection, injected at a rate of 2 ml/s, six serial thin-section 3-mm images were obtained through the nodules at 30-s intervals up to 2 min, beginning 60 s after the onset of the injection. In each case, a representative CT number was then obtained for user-determined regions of interest (ROI) in order to derive a measurement of peak nodule enhancement (Fig. 16.1.3). Using this technique, the authors found that malignant neoplasms (median, 40 HU) enhanced to a greater extent than benign lesions (median, 12 HU). Furthermore, using 20 HU as a threshold for identifying a malignant nodule, sensitivity reached 100%, specificity 77%, positive predictive value 90%, negative predictive value 100% and accuracy 93%. More recently, this same approach has been validated in a larger multi-institutional trial (Swensen et al. 2000). Using 15 HU as a threshold, CT reached

Table 16.1.3. Recommendations for follow-up and management of nodules smaller than 8 mm detected incidentally at non-screening (MacMahon et al. 2005)

Nodule size (mm)[a]	Low-risk patient[b]	High-risk patient[c]
≤4	No follow-up needed[d]	Follow-up CT at 12 months; if unchanged, no further follow-up[e]
>4–6	Follow-up CT at 12 months; if unchanged, no further follow-up[e]	Initial follow-up CT at 6–12 months then at 18–24 months if no change[e]
>6–8	Initial follow-up CT at 6–12 months then at 18–24 months if no change	Initial follow-up CT at 3–6 months then at 9–12 and 24 months if no change
>8	Follow-up CT at around 3, 9, and 24 months, dynamic contrast-enhanced CT, PET, and/or biopsy	Same as for low-risk patient

Note: newly detected indeterminate nodule in persons 35 years of age or older.

[a] Average of length and width.

[b] Minimal or absent history of smoking and of other known risk factors.

[c] History of smoking or of other known risk factors.

[d] The risk of malignancy in this category (< 1%) is substantially less than that in a baseline CT scan of an asymptomatic smoker.

[e] Nonsolid (ground-glass) or partly solid nodules may require longer follow-up to exclude indolent adenocarcinoma.

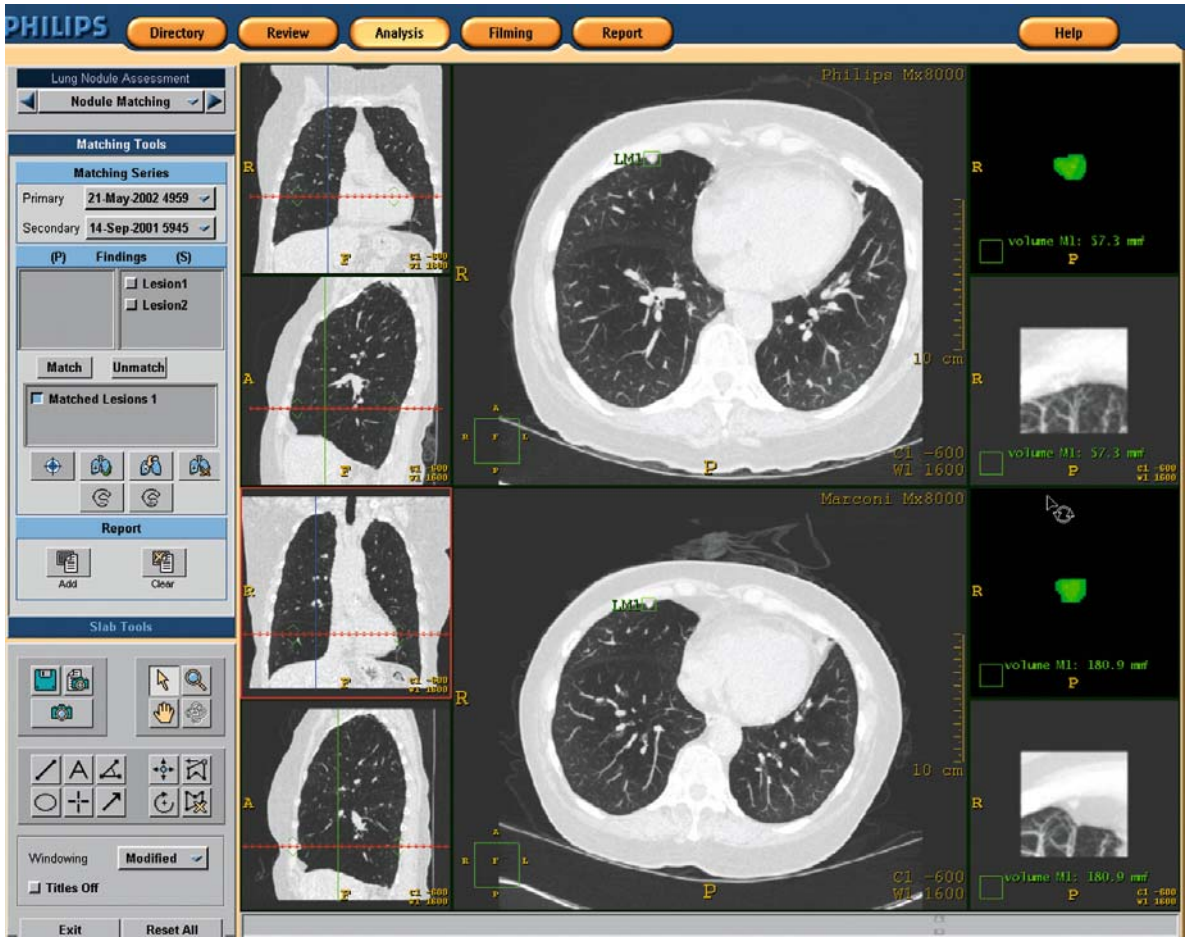

Fig. 16.1.3. Many manufacturers propose computer-assisted detection (CAD) and nodule segmentation for nodule growth and comparison on serial CT scanners. At baseline CT, the nodule volume was measured at 57 mm^3. Then 8 months after, the nodule volume was measured at 180 mm^3. The nodule growth was consistent with malignancy

a sensitivity of 98%, a specificity of 58%, a positive predictive value of 68%, a negative predictive value of 96% and an accuracy of 77%. Another team of researchers (Yi et al. 2004; Jeong et al. 2005) has proposed evaluating dynamic enhancement of lung nodules with multi-detector row CT (4-and 16-detector row CT). With 30 HU or more of net enhancement as a cut-off value in differentiation of malignant from benign nodules, Yi et al. (2004) found a sensitivity for malignant nodules of 99%, a specificity of 54%, a positive predictive value of 71%, a negative predictive value of 97%, and an accuracy of 78%.

16.1.3.5 PET and Integrated PET-CT

Positron emission tomography (PET) can generate functional images of tumour tissues based on the increased glucose metabolism by cancerous cells. Numerous studies have shown that PET is effective for differentiating between benign and malignant pulmonary nodules (Patz et al. 1993; Gupta et al. 1996, 1998). Since its clinical introduction in 2001, integrated PET-CT has allowed the fusion of the morphological CT and functional PET images, enabling a better localization of the fluorodeoxyglucose- (FDG-) avid lesions. These integrated systems offer improved image quality, shorter imaging times (by about 30%) and increased patient convenience. In one study (Yi et al. 2006) PET-CT was shown to be

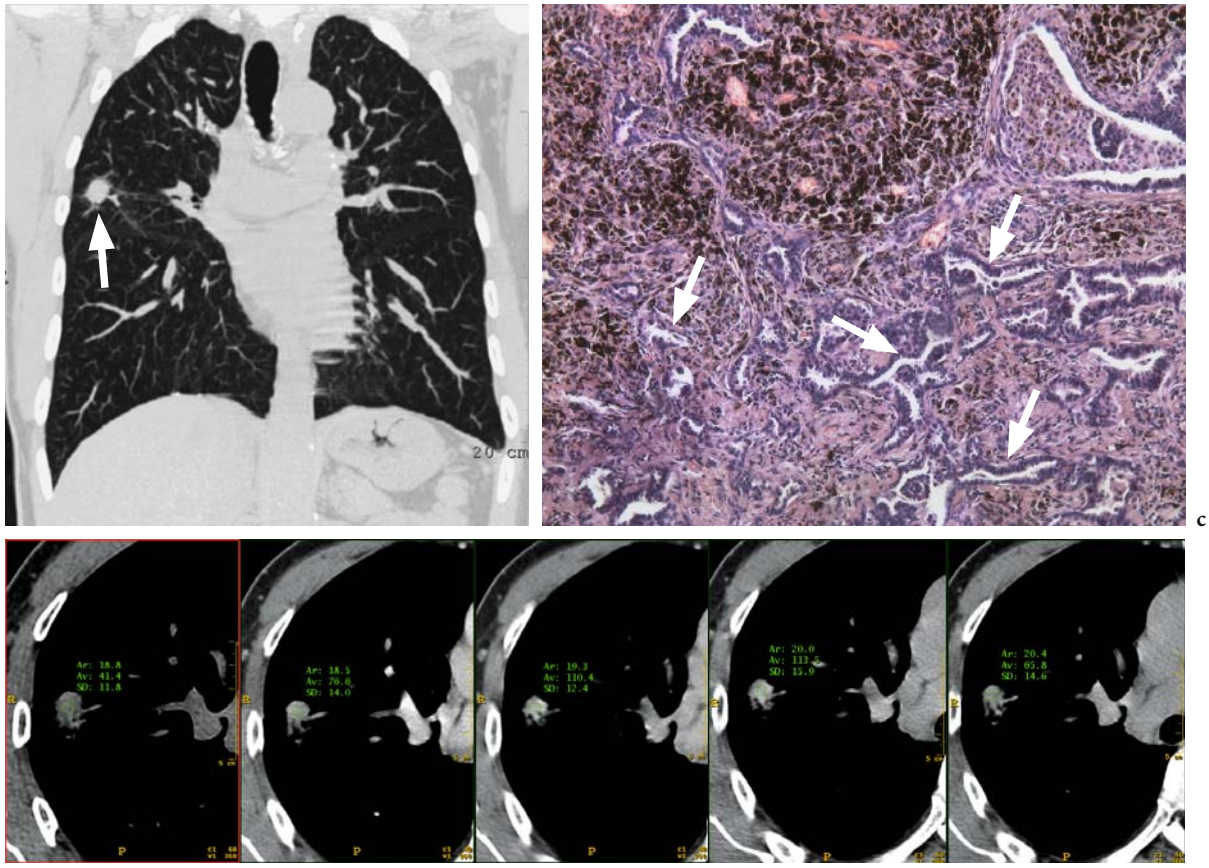

Fig. 16.1.4a–c. A 64-year old man with previous tuberculosis and indeterminate nodule in the right lung. **a** Frontal reformatted MIP showed an irregular non-calcified nodule measuring 18 mm × 16 mm in the right upper lobe (*arrow*). **b** Serial CT acquisitions performed at 120 kV, 145 mAs before and after injection of 100 ml of contrast medium at 60, 120, 180, 240 s. The maximal contrast enhancement was reached after 120 s (113 HU). The difference between maximal enhancement (113 HU) and baseline density (41 HU) of the nodule (72 HU) was suggestive of malignancy. **c** Surgical resection specimen. Well differentiated adenocarcinoma made of numerous atypical glandular structures (*white arrows*) in a fibrotic background containing abundant black pigment (H and E staining, objective: 10×)

more sensitive and accurate in the characterization of single pulmonary nodules than helical CT, even when using state-of-the-art dynamic CT acquisition protocols.

The current limited availability and cost of PET make it an unsuitable screening investigation tool. However, PET has shown promising results in the differentiation between benign and malignant nodules and may therefore have a role in the investigation of indeterminate nodules discovered on low-dose CT (Fig. 16.1.1) avoiding unnecessary surgical biopsy (Patz et al. 1993; Scott et al. 1994; Gupta et al. 1996, 1998; Gambhir et al. 1998). However, false positives due to granulomas or pneumonia (Fig. 16.1.5) (Mortensen et al. 2000; Jemal et al. 2005) are reported, and nodules less than 1 cm identified on low-dose CT may be below the resolving power of PET.

Researchers (Pastorino et al. 2003; Bastarrika et al. 2005) have shown that low-dose spiral CT combined with selective use of PET can effectively detect early lung cancer. The addition of FDG-PET to the decision algorithm for nodules of 10 mm and more or for smaller (> 7 mm), growing nodules may reduce unnecessary invasive procedures to a minimum without resulting in missed cancers.

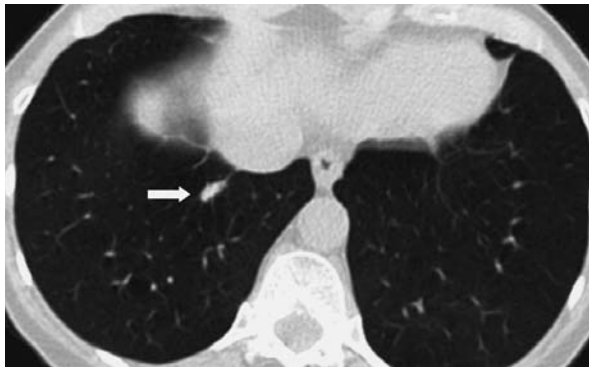

a

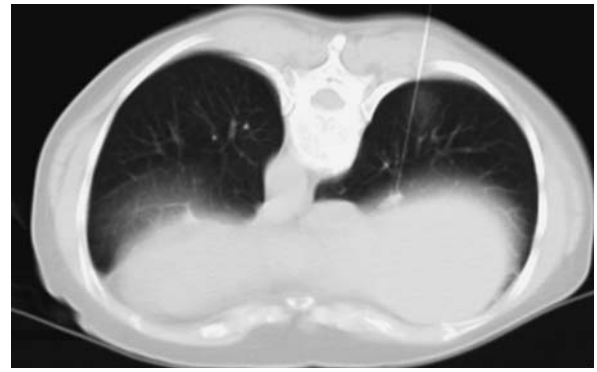

c

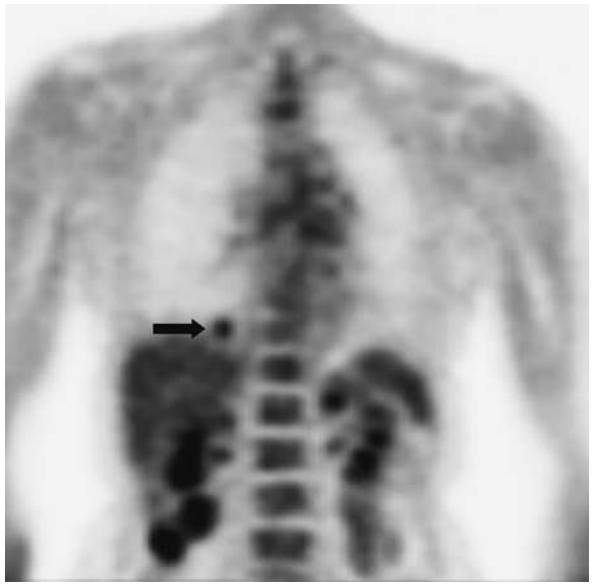

b

Fig. 16.1.5a–c. A 64-year woman, heavy smoker (36 pack-years) involved in a lung cancer screening program. **a** A low-dose CT was performed with the following parameters: 120 kVp, 30 mA, 4 × 2.5 mm collimation. An elongated non-calcified nodule (*arrow*) is present in the right lower lobe. **b** FDG-PET demonstrated a moderate uptake within the suspicious lung nodule (*arrow*). **c** CT-guided percutaneous biopsy was performed with the patient placed in prone position. Pathology revealed giant inflammatory cells consistent with tuberculous granulomatosis

16.1.3.6 Lung Biopsy

For nodules that have clinical and imaging features suspicious of malignancy, a tissue sample is required. There are many methods of obtaining tissue from a solitary pulmonary nodule, such as video-assisted thoracoscopic or open surgical biopsy. Three main imaging modalities, CT, fluoroscopy and CT-fluoroscopy-guided needle biopsies, can be used for this procedure. CT allows better planning of the needle path and safe biopsy (Fig. 16.1.5) of lesions located next to vascular or mediastinal structures. Fluoroscopy allows real-time monitoring of the needle course and is often easier in patients who are less cooperative with respect to breath-holding, since the needle can be directed into the lesion even if the patient is breathing. Real-time fluoroscopy-CT-guided fine needle aspiration combines the advantages of CT and fluoroscopy. This new technique provides high diagnostic accuracy comparable to that of conventional CT-guided procedures, with a low rate of complications, even for small tumours (Heck et al. 2006).

16.1.4 Delivered Radiation Dose

An important issue related to lung cancer screening with MDCT is the risk of radiation exposure (cumulative doses) received during the whole screening procedure including baseline CT, repeated CT examinations and during the different assessments performed for lung nodule management. Lung cancer screening and lung nodule management

will increasingly play a major role in the dramatic increase in patient radiation. In the UK, radiation associated with CT scanning contributed 40% of the total radiation exposure in 1999 (Crawley et al. 2001).

16.1.4.1 During Baseline CT Examination

CT scanning is associated with significantly higher radiation exposure compared to other radiation-based medical examinations such as conventional radiography (Bier 1990). In the literature, the effective dose equivalent from a single CT examination of the chest is reported to range from 2 to 25 mSv, depending on the CT scanner and the examination protocol used (Nishizawa et al. 1991; Geleijns et al. 1994; Poletti 1996; Kaul et al. 1997; Van Unnik et al. 1997; Wade et al. 1997; Wall and Hart 1997).

A substantial reduction at chest CT is possible because of its high intrinsic contrast and because of the low radiation absorption of the lungs (Naidich et al. 1990; Zwirewich et al. 1991; Ambrosino et al. 1994; Lee et al. 1994; Mayo et al. 1995, 1997). Modern low-dose protocols of CT expose the patient to a significantly lower radiation dose (0.65 mSv) than the traditional standard-dose protocols (2–25 mSv), with only a minimal reduction in sensitivity (Fig. 16.1.2.).

The radiation dose to the lungs from a low-dose CT lung examination depends strongly on the protocol used for the examination, and primarily on the product of the current and exposure time (the mAs setting) (Table 16.1.2). Brenner (2004) calculated the lung radiation doses to be expected from the various techniques reported in the literature from low-dose CT. They estimated the doses to vary from approximately 2.5 to 9.0 mGy.

16.1.4.2 During CT Follow-Up

The delivered radiation dose during serial CT follow-up is highly variable from subject to subject and related to the selected CT parameters and the total number of CT acquisitions. Follow-up CT examination is usually performed at standard dose with thin sections (1–3 mm). Ko et al. (2003) demonstrated in an experimental study that simulated lung nodules in a phantom were more accurately measured with a high-frequency algorithm, 1-mm sections and 120 mAs compared to low-dose CT. Dose estimation of nodule follow-up has been performed in a lung cancer screening program in Italy (Italung-CT trial) (Mascalchi et al. 2006). The delivered radiation dose for nodule work-up performed on single-slice CT at 140 kVp and 171 mAs with a scan length of 20 mm ranged from1.2 to 2.2 mGy. The delivered radiation dose decreased between 0.5 to 1 mGy when CT acquisition was performed at 4-MDCT with 1-mm collimation, 120 kVp, 80 mAs, scan length of 20 mm.

16.1.4.3 During Nodule Uptake Study at CT

Different protocols concerning nodule uptake at CT exist in the literature. In the study performed by Swensen et al. (2005), a spiral series of scans through the chest is obtained after a delay of 20 s from the onset of injection. Then, at 1 min after the onset of injection, 3-mm-collimation spiral imaging through the nodule with a 1-mm reconstruction interval is performed for 5 s. Finally, spiral sections through the nodule are obtained at 2, 3, and 4 min. In the paper published by Yi et al. (2004), a series of 13 images was obtained throughout the nodule for 30 mm along the *z*-axis with 2.5-mm collimation, 120 kVp, 170 mA, 0.8-s gantry rotation time, and a table speed of 3.75 mm/s over 8 s. Thereafter, an additional nine series of images were obtained at 20-s intervals for 3 min after contrast medium injection with a power injector with the same parameters used for the initial pre-enhancement series (10 total series of images obtained at 0, 20, 40, 60, 80, 100, 120, 140, 160, and 180 s). The delivered radiation doses during the above-mentioned protocols were not reported.

The delivered radiation dose during dynamic nodule uptake at CT was detailed in the paper written by Jeong et al. (2005). The authors evaluated dynamic enhancement of pulmonary nodules at 4- and 16-detector row CT in 130 patients. The researchers first studied thin-section helical CT. The measured total organ dose at thin-section, dynamic, and staging CT ranged from 98 to 115 mGy at the nodule site and ranged from 35 to 40 mGy elsewhere in the lungs. This dose at nodule location is about five times larger than that used for single-detector row CT (18–19 mGy with 1- to 10-mm collimation, 120 kVp, 300 mAs; McNitt-Gray 2002). However

this organ dose applies only to the band-like area (approximately 3 cm in length in the *z*-axis) of the nodule location. For this reason, this technique is not appropriate in young women because of breast interposition with a low pretest probability of malignancy or T_1N_0 lung cancer.

16.1.4.4 During PET and Integrated PET-CT

The injection of radioactive substances during PET or PET-CT exposes the patient and the nuclear technicians to radiation. It has been shown that the radiation exposure of PET technologists was higher than that of technologists performing general nuclear medicine studies (Roberts et al. 2005). The estimated dose per PET procedure was 4.1 μSv (11 nSv/MBq). Injection of ^{18}F-FDG contributed to the highest radiation exposure.

Brix et al. (2005) investigated radiation exposure of patients undergoing whole-body ^{18}FDG PET-CT examinations at four hospitals equipped with different tomographs. The effective radiation dose for patients undergoing whole-body ^{18}FDG PET-CT has been estimated at 25 mSv (Brix et al. 2005). The delivered radiation dose is increased in comparison with an individual CT or PET examination (Wu et al. 2004).

16.1.4.5 During Lung Biopsy

CT fluoroscopy provides real-time guidance of the biopsy specimens from pulmonary masses or nodules. This technique decreases procedure time and requires fewer needle passes than CT-guided biopsies without fluoroscopic guidance (Daly and Templeton 1999; Silverman et al. 1999; Gianfelice et al. 2000; Froelich et al. 2002; Kirchner et al. 2002).

CT has furthermore been shown to significantly reduce radiation doses to the patient, but it exposes the radiologist to radiation, as the operator is in the room at the time (Carlson et al. 2001; Froelich and Wagner 2001). Carlson et al. (2001) have calculated the patient's absorbed dose per procedure and the median procedure time with CT fluoroscopy in 203 consecutive percutaneous intervention procedures with use of CT fluoroscopic guidance and 99 consecutive procedures with conventional CT guidance. The estimated maximum skin dose was significantly lower for all CT-fluoroscopy-guided biopsies, with a median of 41 mGy versus a median of 772 mGy for conventional CT ($p < 0.05$).

16.1.5 Risk Induced from Lung Cancer Screening Programs

The radiation risk may be not negligible in a general screening population. The risk from CT screening is generally high when compared to the risk from screening with imaging modalities, since the latter use lower doses such as chest radiography. The risk from CT cancer screening strongly depends on age, sex, organ system, dose per examination, number of examinations and time interval between examinations (Beir 2005; Prokop 2005). For example, screening from the age of 40 years with annual chest radiographs yields an excess lifetime risk of only 0.003% in comparison to 0.79% with CT (Buls et al. 2005). The lifetime risk of fatal cancer for a screened population can be estimated by integrating the product of the effective dose and the corresponding age-dependent lifetime cancer mortality risk factor for all scans during the screening program (Le Heron 2003; Buls et al. 2005).

Previously published reports have suggested radiation risks even with a low-dose CT scan as a part of a regular screening program (Brenner 2004) and also a possible synergistic interaction between the risk from smoking and radiation exposure (Neugut et al. 1994; Tokarskaya et al. 2002; Gilbert et al. 2003; Pierce et al. 2003). We have also to take into consideration that the lung doses delivered during low-dose CT are within the range for which there is evidence of increased carcinogenic risk in atomic bomb survivors (Little 1999). The risk of very low doses is based on radiobiological models as well as on fitting curves to existing risk data (Beir 2005). Detailed information concerning methods used for risk evaluation are given in Chapter 2 by K.H. Chadwick and H.P. Leenhouts, and in Chapter 3 by L. Cohen of the present edition.

In a recent analysis, Brenner (2004) suggested that if half of the high-risk population in the US was screened with low-dose CT scans annually for 20–25 years, there would be an estimated 36,000 new lung cancers solely as a result of radiation exposure

over that 20-year period, an increase of 1.8%. The International Commission on Radiological Protection predicts that the CT scanning techniques used in 2001 would induce 5 cancers per 100,000 examinations (Diederich et al. 2001). However, Lenzen et al. (1996) suggested that, with helical CT, it was possible to reduce the equivalent dose of radiation close to that of a conventional chest radiograph in two projections, thereby further decreasing the risk of malignancy. Notwithstanding this lower exposure, the risk for lung cancer in the tobacco-exposed, older individual is significantly higher than the theoretical risk of radiation-induced lung cancer. Although every effort must be taken to minimize exposure to radiation, the lethal effects of tobacco are substantial. Also, the lethality of lung cancer in individuals being followed with annual spiral CT scans is likely to be considerably less than diagnosis in the absence of screening, so this is a dynamic issue that must be seen in perspective (Goodman 2002).

16.1.6 Reduction of Dose in CT Screening Programs

The radiologist has the responsibility to limit the patient dose by applying strict and systematic medical indications for each examination and by selecting lower dose settings whenever appropriate from the diagnostic point of view. A decrease in radiation dose through changes in technique would be expected to result in a corresponding decrease in risk. However, the lowest settings possible in CT screening programs have yet to be definitively established. Itoh et al. (2000) have evaluated the lowest tube current required for lung cancer screening with helical CT in normal volunteers. The detectability of nodules was not significantly degraded by reducing the tube current to 20 mA in the upper zone of the lung, to 12 mA in the middle zone, or to 18 mA in the lower zone. They concluded that the minimum tube current required for screening helical CT differs for different locations in the lung and an ideal CT protocol for the lung should permit the tube current to be changed during helical scanning. Among all major technical developments for radiation reduction, automatic exposure control represents the most promising technique, which significantly reduces the radiation dose from CT scanning (Kalra et al. 2003). Doses as low as 0.12 mSv have been suggested (Gergely et al. 2005), which would reduce cancer risks by a factor of more than 10. Itoh et al. (2001) designed a new filter made of aluminium with a concave shape with a thickness of 5.8 mm at the centre and evaluated radiation dose and lung nodule detection in 35 patients. The authors demonstrated that very-low-dose helical CT performed at a tube current of 30 mA with the new filter was able to depict all the pathological lesions greater than 5 mm in diameter detected by standard helical CT.

Scout view of the chest can be avoided in lung cancer screening programs in order to decrease the radiation dose. However, the delivered radiation dose during a scout view of the chest is minimal. Coche et al. (2006) measured the delivered radiation dose during a scout view of the chest on a 4-slice CT and anthropomorphic phantom. The investigators obtained a mean radiation dose of 0.17 mGy. Mascalchi et al. (2006) estimated the effective dose of 0.05 mSv for a scout view performed during the Italung-CT trial.

MDCT may help reduce the radiation dose in such a way that, compared to conventional or single-slice helical CT, comparable image quality is achieved albeit with a lower radiation dose (Vlassenbroek et al. 2005). This fact is mainly due to a better dose utilization and reduced penumbra overlap with MDCT. Italian researchers demonstrated that the cumulative effective doses per 1,000 subjects were 3.3 Sv using an MDCT and 5.8 or 7.1 Sv using a single-detector CT scanner (Mascalchi et al. 2006). The advantages of MDCT include both improved nodule detection and nodule characterization on lung cancer screening programs, because the entire lung can be scanned with thin slices in a single breath-hold without an intersection gap.

16.1.7 Conclusions

Lung cancer screening with low-dose CT appears to be an interesting technique for detecting lung cancer at an early stage. However, its benefits in terms of reduction of specific lung cancer-related mortality remain to be proven in large, well-designed multicentre prospective trials. The main limitations for CT reside in the high numbers of incidental nodules which necessitate multiple serial CT control or a

minimally invasive technique for nodule work-up. The delivered radiation dose during CT screening and nodule management is highly variable depending on the parameters selected, the interval of CT controls and the duration of screening. The potential of radiation to induce neoplasia during lung cancer screening remains hypothetical but has to be taken into account when screening programs and follow-up strategies are instituted on a large scale.

References

Aberle DR, Gamsu G, Henschke CI, Naidich DP, Swensen SJ (2001) A consensus statement of the Society of Thoracic Radiology: screening for lung cancer with helical computed tomography. J Thorac Imaging 16:65–68

Ambrosino MM, Genieser NB, Roche KJ, Kaul A, Lawrence RM (1994) Feasibility of high-resolution, low-dose chest CT in evaluating the pediatric chest. Pediatr Radiol 24:6–10

Bastarrika G, Garcia-Velloso MJ, Lozano MD, Montes U, Torre W, Spiteri N, Campo A, Seijo L, Alcaide AB, Pueyo J, Cano D, Vivas I, Cosin O, Dominguez P, Serra P, Richter JA, Montuenga L, Zulueta JJ (2005) Early lung cancer detection using spiral computed tomography and positron emission tomography. Am J Respir Crit Care Med 171:1378–1383

Bier V (1990) Board on radiation effects research council, health effects of exposure to lows of ionizing radiation. Academy Press, Washington

Beir VII (2005) National research council committee on the biological effects of ionizing radiation, health effects of exposure to low levels of ionizing radiation. National Academy Press, Washington

Brenner DJ (2004) Radiation risks potentially associated with low-dose CT screening of adult smokers for lung cancer. Radiology 231:440–445

Brett GZ (1969) Earlier diagnosis and survival in lung cancer. Br Med J 4:260–262

Brix G, Lechel U, Glatting G, Ziegler SI, Munzing W, Muller SP, Beyer T (2005) Radiation exposure of patients undergoing whole-body dual-modality ^{18}F-FDG PET/CT examinations. J Nucl Med 46:608–613

Buls N, de Mey J, Covens P, Stadnik T (2005) Health screening with CT: prospective assessment of radiation dose and associated detriment. JBR-BTR 88:12–16

Carlson SK, Bender CE, Classic KL, Zink FE, Quam JP, Ward EM, Oberg AL (2001) Benefits and safety of CT fluoroscopy in interventional radiologic procedures. Radiology 219:515–520

Coche E, Vynckier S, Octave-Prignot M (2006) Pulmonary embolism: radiation dose with multi-detector row CT and digital angiography for diagnosis. Radiology 240(3):690–697

Crawley MT, Booth A, Wainwright A (2001) A practical approach to the first iteration in the optimization of radiation dose and image quality in CT: estimates of the collective dose savings achieved. Br J Radiol 74:607–614

Daly B, Templeton PA (1999) Real-time CT fluoroscopy: evolution of an interventional tool. Radiology 211:309–315

Diederich S, Lenzen H, Puskas Z, Koch AT, Yelbuz TM, Eameri M, Roos N, Peters PE (1996) Low dose computerized tomography of the thorax. Experimental and clinical studies. Radiologe 36:475–482

Diederich S, Wormanns D, Heindel W (2001) Low-dose CT: new tool for screening lung cancer? Eur Radiol 11:1916–1924

Diederich S, Wormanns D, Semik M, Thomas M, Lenzen H, Roos N, Heindel W (2002) Screening for early lung cancer with low-dose spiral CT: prevalence in 817 asymptomatic smokers. Radiology 222:773–781

Erasmus JJ, Connolly JE, McAdams HP, Roggli VL (2000) Solitary pulmonary nodules: Part I. Morphologic evaluation for differentiation of benign and malignant lesions. Radiographics 20:43–58

Flehinger BJ, Melamed MR, Zaman MB, Heelan RT, Perchick WB, Martini N (1984) Early lung cancer detection: results of the initial (prevalence) radiologic and cytologic screening in the Memorial Sloan-Kettering study. Am Rev Respir Dis 130:555–560

Fontana RS, Sanderson DR, Taylor WF, Woolner LB, Miller WE, Muhm JR, Uhlenhopp MA (1984) Early lung cancer detection: results of the initial (prevalence) radiologic and cytologic screening in the Mayo Clinic study. Am Rev Respir Dis 130:561–565

Fontana RS, Sanderson DR, Woolner LB, Taylor WF, Miller WE, Muhm JR (1986) Lung cancer screening: the Mayo program. J Occup Med 28:746–750

Froelich JJ, Wagner HJ (2001) CT fluoroscopy: tool or gimmick? Cardiovasc Intervent Radiol 24:297–305

Froelich JJ, Ishaque N, Regn J, Saar B, Walthers EM, Klose KJ (2002) Guidance of percutaneous pulmonary biopsies with real-time CT fluoroscopy. Eur J Radiol 42:74–79

Frost JK, Ball WC Jr, Levin ML, Tockman MS, Baker RR, Carter D, Eggleston JC, Erozan YS, Gupta PK, Khouri NF (1984) Early lung cancer detection: results of the initial (prevalence) radiologic and cytologic screening in the Johns Hopkins study. Am Rev Respir Dis 130:549–554

Gambhir SS, Shepherd JE, Shah BD, Hart E, Hoh CK, Valk PE, Emi T, Phelps ME (1998) Analytical decision model for the cost-effective management of solitary pulmonary nodules. J Clin Oncol 16:2113–2125

Geleijns J, Van Unnik JG, Zoetelief J, Zweers D, Broerse JJ (1994) Comparison of two methods for assessing patient dose from computed tomography. Br J Radiol 67:360–365

Gergely I, Neumann C, Reiger F, Dorffner R (2005) Lung nodule detection with ultra-low-dose CT in routine follow-up of cancer patients. Rofo 177:1077–1083

Gianfelice D, Lepanto L, Perreault P, Chartrand-Lefebvre C, Milette PC (2000) Value of CT fluoroscopy for percutaneous biopsy procedures. J Vasc Interv Radiol 11:879–884

Gilbert ES, Stovall M, Gospodarowicz M, Van Leeuwen FE, Andersson M, Glimelius B, Joensuu T, Lynch CF, Curtis RE, Holowaty E, Storm H, Pukkala E, van't Veer MB, Fraumeni JF, Boice JD Jr, Clarke EA, Travis LB (2003) Lung cancer after treatment for Hodgkin's disease: focus on radiation effects. Radiat Res 159:161–173

Gohagan JK, Marcus PM, Fagerstrom RM, Pinsky PF, Kramer BS, Prorok PC, Ascher S, Bailey W, Brewer B, Church T, Engelhard D, Ford M, Fouad M, Freedman M, Gelmann E, Gierada D, Hocking W, Inampudi S, Irons B, Johnson CC, Jones A, Kucera G, Kvale P, Lappe K, Manor W, Moore A, Nath H, Neff S, Oken M, Plunkett M, Price H, Reding D, Riley T, Schwartz M, Spizarny D, Yoffie R, Zylak C, The lung screening study research group (2005) Final results of the Lung Screening Study, a randomized feasibility study of spiral CT versus chest X-ray screening for lung cancer. Lung Cancer 47:9–15

Goodman PC (2002) Radiation risk in CT screening for lung cancer. Radiology 225:233

Gupta NC, Maloof J, Gunel E (1996) Probability of malignancy in solitary pulmonary nodules using fluorine-18-FDG and PET. J Nucl Med 37:943–948

Gupta NC, Gill H, Graeber G, Bishop H, Hurst J, Stephens T (1998) Dynamic positron emission tomography with F-18 fluorodeoxyglucose imaging in differentiation of benign from malignant lung/mediastinal lesions. Chest 114:1105–1111

Hartman TE (2005) Radiologic evaluation of the solitary pulmonary nodule. Radiol Clin North Am 43:459–65, vii

Heck SL, Blom P, Berstad A (2006) Accuracy and complications in computed tomography fluoroscopy-guided needle biopsies of lung masses. Eur Radiol 16:1387–1392

Henschke CI, McCauley DI, Yankelevitz DF, Naidich DP, McGuinness G, Miettinen OS, Libby DM, Pasmantier MW, Koizumi J, Altorki NK, Smith JP (1999) Early Lung Cancer Action Project: overall design and findings from baseline screening. Lancet 354:99–105

Henschke CI, Yankelevitz DF, Smith JP, Miettinen OS (2002) Screening for lung cancer: the early lung cancer action approach. Lung Cancer 35:143–148

Henschke CI, Yankelevitz DF, McCauley DI, Libby DM, Pasmantier MW, Smith JP (2003) Guidelines for the use of spiral computed tomography in screening for lung cancer. Eur Respir J Suppl 39:45S–51S

Henschke CI, Yankelevitz DF, Naidich DP, McCauley DI, McGuinness G, Libby DM, Smith JP, Pasmantier MW, Miettinen OS (2004) CT screening for lung cancer: suspiciousness of nodules according to size on baseline scans. Radiology 231:164–168

Itoh S, Ikeda M, Arahata S, Kodaira T, Isomura T, Kato T, Yamakawa K, Maruyama K, Ishigaki T (2000) Lung cancer screening: minimum tube current required for helical CT. Radiology 215:175–183

Itoh S, Koyama S, Ikeda M, Ozaki M, Sawaki A, Iwano S, Ishigaki T (2001) Further reduction of radiation dose in helical CT for lung cancer screening using small tube current and a newly designed filter. J Thorac Imaging 16:81–88

Jemal A, Murray T, Ward E, Samuels A, Tiwari RC, Ghafoor A, Feuer EJ, Thun MJ (2005) Cancer statistics, 2005. CA Cancer J Clin 55:10–30

Jeong YJ, Lee KS, Jeong SY, Chung MJ, Shim SS, Kim H, Kwon OJ, Kim S (2005) Solitary pulmonary nodule: characterization with combined wash-in and washout features at dynamic multi-detector row CT. Radiology 237:675–683

Kalra MK, Maher MM, Saini S (2003) Multislice CT: update on radiation and screening. Eur Radiol 13:M129–M133

Kaneko M, Eguchi K, Ohmatsu H, Kakinuma R, Naruke T, Suemasu K, Moriyama N (1996) Peripheral lung cancer: screening and detection with low-dose spiral CT versus radiography. Radiology 201:798–802

Kaul A, Bauer B, Bernhardt J, Nosske D, Veit R (1997) Effective doses to members of the public from the diagnostic application of ionizing radiation in Germany. Eur Radiol 7:1127–1132

Kirchner J, Kickuth R, Laufer U, Schilling EM, Adams S, Liermann D (2002) CT fluoroscopy-assisted puncture of thoracic and abdominal masses: a randomized trial. Clin Radiol 57:188–192

Ko JP, Rusinek H, Jacobs EL, Babb JS, Betke M, McGuinness G, Naidich DP (2003) Small pulmonary nodules: volume measurement at chest CT-phantom study. Radiology 228:864–870

Le Heron J (2003) CT screening patient doses and risks from radiation. Proceedings of the world congress on medical physics and biomedical engineering

Lee KS, Primack SL, Staples CA, Mayo JR, Aldrich JE, Muller NL (1994) Chronic infiltrative lung disease: comparison of diagnostic accuracies of radiography and low- and conventional-dose thin-section CT. Radiology 191:669–673

Lenzen H, Roos N, Diederich S, Meier N (1996) Radiation exposure in low dose computerized tomography of the thorax. Radiologe 36:483–488

Leong SS, Rocha Lima CM, Sherman CA, Green MR (1999) The 1997 International Staging System for non-small cell lung cancer: have all the issues been addressed? Chest 115:242–248

Leung AN (1997) Spiral CT of the thorax in daily practice: optimization of technique. J Thorac Imaging 12:2–10

Libby DM, Smith JP, Altorki NK, Pasmantier MW, Yankelevitz D, Henschke CI (2004) Managing the small pulmonary nodule discovered by CT. Chest 125:1522–1529

Little JB (1999) Induction of genetic instability by ionizing radiation. CR Acad Sci III 322:127–134

MacMahon H, Austin JH, Gamsu G, Herold CJ, Jett JR, Naidich DP, Patz EF Jr, Swensen SJ (2005) Guidelines for management of small pulmonary nodules detected on CT scans: a statement from the Fleischner Society. Radiology 237:395–400

MacRedmond R, McVey G, Lee M, Costello RW, Kenny D, Foley C Logan PM (2006) Screening for lung cancer using low dose CT scanning: results of 2 year follow-up. Thorax 61:54–56

Mahadevia PJ, Fleisher LA, Frick KD, Eng J, Goodman SN, Powe NR (2003) Lung cancer screening with helical computed tomography in older adult smokers: a decision and cost-effectiveness analysis. J Am Med Assoc 289:313–322

Martini N (1990) Surgical treatment of lung cancer. Semin Oncol 17:9–10

Mascalchi M, Belli G, Zappa M, Picozzi G, Falchini M, Nave RD, Allescia G, Masi A, Pegna AL, Villari N, Paci E (2006) Risk-benefit analysis of X-ray exposure associated with lung cancer screening in the Italung-CT trial. AJR Am J Roentgenol 187:421–429

Mayo JR, Hartman TE, Lee KS, Primack SL, Vedal S, Muller NL (1995) CT of the chest: minimal tube current required for good image quality with the least radiation dose. AJR Am J Roentgenol 164:603–607

Mayo JR, Whittall KP, Leung AN, Hartman TE, Park CS, Primack SL, Chambers GK, Limkeman MK, Toth TL, Fox SH (1997) Simulated dose reduction in conventional chest CT: validation study. Radiology 202:453–457

McNitt-Gray MF (2002) AAPM/RSNA physics tutorial for residents: topics in CT. Radiation dose in CT. Radiographics 22:1541–1553

Melamed MR, Flehinger BJ, Zaman MB, Heelan RT, Perchick WA, Martini N (1984) Screening for early lung cancer. Results of the Memorial Sloan-Kettering study in New York. Chest 86:44–53

Mortensen J, Enevoldsen H, Friberg L et al (2000) Preliminary findings of a prospective study of FDG-PET in patients with possible lung cancer. Clin Positron Imaging 3:158

Mountain CF (1986) A new international staging system for lung cancer. Chest 89:225S–233S

Mountain CF, Lukeman JM, Hammar SP, Chamberlain DW, Coulson WF, Page DL, Victor TA, Weiland LH (1987) Lung cancer classification: the relationship of disease extent and cell type to survival in a clinical trials population. J Surg Oncol 35:147–156

Naidich DP, Marshall CH, Gribbin C, Arams RS, McCauley DI (1990) Low-dose CT of the lungs: preliminary observations. Radiology 175:729–731

Nambu A, Araki T, Taguchi Y, Ozawa K, Miyata K, Miyazawa M, Hiejima Y, Saito A (2005) Focal area of ground-glass opacity and ground-glass opacity predominance on thin-section CT: discrimination between neoplastic and non-neoplastic lesions. Clin Radiol 60:1006–1017

Neugut AI, Murray T, Santos J, Amols H, Hayes MK, Flannery JT, Robinson E (1994) Increased risk of lung cancer after breast cancer radiation therapy in cigarette smokers. Cancer 73:1615–1620

Nishizawa K, Maruyama T, Takayama M, Okada M, Hachiya J, Furuya Y (1991) Determinations of organ doses and effective dose equivalents from computed tomographic examination. Br J Radiol 64:20–28

Nitta N, Takahashi M, Murata K, Morita R (1998) Ultra low-dose helical CT of the chest. AJR Am J Roentgenol 171:383–385

Parkin DM, Pisani P, Ferlay J (1999) Global cancer statistics. CA Cancer J Clin 49:33–64

Pastorino U, Bellomi M, Landoni C, De Fiori E, Arnaldi P, Picchio M, Pelosi G, Boyle P, Fazio F (2003) Early lung-cancer detection with spiral CT and positron emission tomography in heavy smokers: 2-year results. Lancet 362:593–597

Patz EF Jr, Lowe VJ, Hoffman JM, Paine SS, Burrowes P, Coleman RE, Goodman PC (1993) Focal pulmonary abnormalities: evaluation with F-18 fluorodeoxyglucose PET scanning. Radiology 188:487–490

Pierce DA, Sharp GB, Mabuchi K (2003) Joint effects of radiation and smoking on lung cancer risk among atomic bomb survivors. Radiat Res 159:511–520

Poletti JL (1996) Patient doses from CT in New Zealand and a simple method for estimating effective dose. Br J Radiol 69:432–436

Prokop M (2005) Cancer screening with CT. Dose controversy. Eur Radiol 15:D55–D61

Prosch H, Strasser G, Oschatz E, Schober E, Schneider B, Mostbeck GH (2006) Management of patients with small pulmonary nodules: a survey of radiologists, pulmonologists, and thoracic surgeons. AJR Am J Roentgenol 187:143–148

Revel MP, Bissery A, Bienvenu M, Aycard L, Lefort C, Frija G (2004a) Are two-dimensional CT measurements of small noncalcified pulmonary nodules reliable? Radiology 231:453–458

Revel MP, Lefort C, Bissery A, Bienvenu M, Aycard L, Chatellier G, Frija G (2004b) Pulmonary nodules: preliminary experience with three-dimensional evaluation. Radiology 231:459–466

Roberts FO, Gunawardana DH, Pathmaraj K, Wallace A, Pl U, Mi T, Berlangieri SU, O'Keefe GJ, Rowe CC, Scott AM (2005) Radiation dose to PET technologists and strategies to lower occupational exposure. J Nucl Med Technol 33:44–47

Scott WJ, Schwabe JL, Gupta NC, Dewan NA, Reeb SD, Sugimoto JT (1994) Positron emission tomography of lung tumors and mediastinal lymph nodes using [18F]fluorodeoxyglucose. The Members of the PET-Lung Tumor Study Group. Ann Thorac Surg 58:698–703

Shah R, Sabanathan S, Richardson J, Mearns AJ, Goulden C (1996) Results of surgical treatment of stage I and II lung cancer. J Cardiovasc Surg (Torino) 37:169–172

Shimizu K, Ikeda N, Tsuboi M, Hirano T, Kato H (2006) Percutaneous CT-guided fine needle aspiration for lung cancer smaller than 2 cm and revealed by ground-glass opacity at CT. Lung Cancer 51:173–179

Silverman SG, Tuncali K, Adams DF, Nawfel RD, Zou KH, Judy PF (1999) CT fluoroscopy-guided abdominal interventions: techniques, results, and radiation exposure. Radiology 212:673–681

Sobue T, Moriyama N, Kaneko M, Kusumoto M, Kobayashi T, Tsuchiya R, Kakinuma R, Ohmatsu H, Nagai K, Nishiyama H, Matsui E, Eguchi K (2002) Screening for lung cancer with low-dose helical computed tomography: anti-lung cancer association project. J Clin Oncol 20:911–920

Sone S, Takashima S, Li F, Yang Z, Honda T, Maruyama Y, Hasegawa M, Yamanda T, Kubo K, Hanamura K, Asakura K (1998) Mass screening for lung cancer with mobile spiral computed tomography scanner. Lancet 351:1242–1245

Swensen SJ, Brown LR, Colby TV, Weaver AL (1995) Pulmonary nodules: CT evaluation of enhancement with iodinated contrast material. Radiology 194:393–398

Swensen SJ, Brown LR, Colby TV, Weaver AL, Midthun DE (1996) Lung nodule enhancement at CT: prospective findings. Radiology 201:447–455

Swensen SJ, Viggiano RW, Midthun DE, Muller NL, Sherrick A, Yamashita K, Naidich DP, Patz EF, Hartman TE, Muhm JR, Weaver AL (2000) Lung nodule enhancement at CT: multicenter study. Radiology 214:73–80

Swensen SJ, Jett JR, Sloan JA, Midthun DE, Hartman TE, Sykes AM, Aughenbaugh GL, Zink FE, Hillman SL, Noetzel GR, Marks RS, Clayton AC, Pairolero PC (2002) Screening for lung cancer with low-dose spiral computed tomography. Am J Respir Crit Care Med 165:508–513

Swensen SJ (2003a) Screening for cancer with computed tomography. Br Med J 326: 894–895

Swensen SJ, Jett JR, Hartman TE, Midthun DE, Sloan JA, Sykes AM, Aughenbaugh GL, Clemens MA (2003b) Lung cancer screening with CT: Mayo Clinic experience. Radiology 226:756–761

Swensen SJ, Jett JR, Hartman TE, Midthun DE, Mandrekar SJ, Hillman SL, Sykes AM, Aughenbaugh GL, Bungum AO, Allen KL (2005) CT screening for lung cancer: five-year prospective experience. Radiology 235:259–265

Tockman M (1986) Survival and mortality from lung cancer in a screened population: the John Hopkins study. Chest 89:325S–326S

Tokarskaya ZB, Scott BR, Zhuntova GV, Okladnikova ND, Belyaeva ZD, Khokhryakov VF, Schollnberger H, Vasilenko EK (2002) Interaction of radiation and smoking in lung cancer induction among workers at the Mayak nuclear enterprise. Health Phys 83:833–846

Van Unnik JG, Broerse JJ, Geleijns J, Jansen JT, Zoetelief J, Zweers D (1997) Survey of CT techniques and absorbed dose in various Dutch hospitals. Br J Radiol 70:367–371

Vlassenbroek A, Coche E, Denis JM, Octave-Prignot M, Vynckier S, De Wilde O (2005) Radiation dose and image quality with multi-slice CT: comparison of 2, -4, -16, and 40-slice CT. RSNA 91st Scientific assembly and annual meeting, 267

Wade JP, Weyman JC, Goldstone KE (1997) CT standard protocols are of limited value in assessing actual patient dose. Br J Radiol 70:1146–1151

Wall BF, Hart D (1997) Revised radiation doses for typical X-ray examinations. Report on a recent review of doses to patients from medical X-ray examinations in the UK by NRPB. National Radiological Protection Board. Br J Radiol 70:437–439

Williams DE, Pairolero PC, Davis CS, Bernatz PE, Payne WS, Taylor WF, Uhlenhopp MA, Fontana RS (1981) Survival of patients surgically treated for stage I lung cancer. J Thorac Cardiovasc Surg 82:70–76

Wu TH, Huang YH, Lee JJS et al (2004) Radiation exposure during transmission measurements: comparison between CT- and germanium-based techniques with a current PET scanner. Eur J Nucl Med Mol Imaging 31:38–43

Yankelevitz DF, Reeves AP, Kostis WJ, Zhao B, Henschke CI (2000) Small pulmonary nodules: volumetrically determined growth rates based on CT evaluation. Radiology 217:251–256

Yi CA, Lee KS, Kim EA, Han J, Kim H, Kwon OJ, Jeong YJ, Kim S (2004) Solitary pulmonary nodules: dynamic enhanced multi-detector row CT study and comparison with vascular endothelial growth factor and microvessel density. Radiology 233:191–199

Yi CA, Lee KS, Kim BT, Choi JY, Kwon OJ, Kim H, Shim YM, Chung MJ (2006) Tissue characterization of solitary pulmonary nodule: comparative study between helical dynamic CT and integrated PET/CT. J Nucl Med 47:443–450

Zwirewich CV, Mayo JR, Muller NL (1991) Low-dose high-resolution CT of lung parenchyma. Radiology 180:413–417

Radiation Risk Management in Low Dose MDCT Screening Programs

16

16.2 Dose Reduction in Screening Programs: Colon Cancer Screening

Jaap Stoker, Henk W. Venema, and Rogier E. van Gelder

CONTENTS

16.2.1 Colorectal Cancer Screening

16.2.1.1 Disease Prevalence

In Western countries colorectal cancer is one of the leading causes of cancer-related mortality. In the European Union in 2002, 142,505 individuals died of this disease and in the USA 59,345 individuals (Globoscan 2002). Most colorectal cancers are thought to develop from adenomas through the so-called adenoma-carcinoma sequence. Despite improvements in the treatment of colorectal cancer, mortality is not decreasing noticeably. The most important reason for this is the presence of extensive disease at the time of diagnosis. Prevention and early detection of colorectal cancer and precursors of colorectal cancer (adenomatous polyps) by screening is possible and at this moment seems to be the only way to substantially reduce the incidence and mortality of colorectal cancer (Pignone et al. 2002).

16.2.1.2 Screening Tests

Currently, screening for colorectal cancer is performed in several countries and considered in other countries. Several screening techniques are avail-

J. Stoker MD
Professor of Radiology, Department of Radiology, Academic Medical Center, University of Amsterdam, PO Box 22700, 1100 DE Amsterdam, The Netherlands
H. W. Venema PhD
Physicist, Departments of Radiology and Medical Physics, Academic Medical Center, PO Box 22700, 1100 DE Amsterdam, The Netherlands
R. E. van Gelder MD
Resident in Radiology, Dept. of Radiology, Academic Medical Center, PO Box 22700, 1100 DE Amsterdam, The Netherlands

able, including the fecal occult blood test, sigmoidoscopy, barium enema and colonoscopy. However, the fecal occult blood test has limited sensitivity and specificity for colorectal cancer and even more for adenomatous polyps. Sigmoidoscopy is not a full colon examination, although the results for detection of colorectal cancer and polyps are considerably better than those of the fecal occult blood test. Barium enema has been studied as a screening test, but it has considerable limitations in sensitivity and specificity. Colonoscopy has the highest sensitivity and specificity, but this is a burdensome procedure, as an extensive bowel preparation is required and the colonoscopy procedure is arduous as well, with limited acceptance by participants and not without complications. Computed tomography (CT) colonography (also named virtual colonoscopy) using the multi-slice CT technique is considered as a valuable alternative. CT colonography is a dedicated colorectal multi-slice CT examination in which the distended colon is evaluated for the presence of colorectal cancer and/or polyps.

16.2.2 CT Colonography Procedure

CT colonography is performed after bowel preparation as otherwise colorectal cancer and polyps will be obscured by stool. Distension is required to differentiate between collapsed bowel and colorectal cancer as well as to visualize the bowel surface.

16.2.2.1 Bowel Preparation

Until recently, CT colonography examinations were performed after extensive bowel preparation as is used in colonoscopy. This bowel preparation cleanses the colon although often some fluid or fecal residue will remain. The amount of fluid/residue will be influenced by the cathartic regimen used and individual factors. As polyps beneath the fluid level will not be detected because there are usually no attenuation differences between lesions of the bowel wall and the fluid, the use of fluid tagging has been introduced. This concerns the addition of an iodine or barium contrast agent to the bowel preparation. Tagging facilitates the identification of cancer or polyps covered by fluid or stool, because it results in an increase in the CT value of the fluid or stool. In general no intravenous contrast medium is administered for polyp detection as the beneficial effect is limited, certainly as tagging has become routine. In symptomatic individuals often intravenous contrast medium will be used to detect possible metastatic disease.

The disadvantage of extensive bowel preparation is that it is burdensome. Therefore, research has been performed into alternative approaches and has led to the combination of limited bowel preparation schemes and an oral tagging agent. The optimal limited bowel preparation scheme has not been determined yet, but in general a low fiber diet is combined with an iodine and/or barium contrast agent, while stool softeners can be used for better homogeneity of the tagged stool. This limited bowel preparation leads to improved acceptance, while the sensitivity of CT colonography does not seem to be negatively influenced (Lefere et al. 2002; Iannaccone et al. 2004).

16.2.2.2 CT Colonography Procedure

CT colonography is performed in both the supine and the prone position, as some bowel segments may be collapsed in one position and distended in the other position. Thereby, movement of residual fluid and stool between both positions facilitates the evaluation of an otherwise obscured bowel surface and polyps submerged in untagged fluid and stool. Although not a firm criterion, it might also help to differentiate between a polyp (in general no significant change in position) and stool (Laks et al. 2004). Room air or carbon dioxide (better patient acceptance than room air) are used for distension.

CT scan parameters are discussed in Section 16.2.4.

16.2.2.3 CT Colonography Evaluation and Computer-Aided Detection

CT colonography examinations are read using a combination of two-dimensional (2D) reading, including multiplanar reformatting (MPR), and three-dimensional (3D) reading. There is no consensus whether a primary 2D reading method (3D only

used for problem solving) or primary 3D reading method (2D only used for problem solving) should be used, but it is clear that a combination of 2D and 3D is mandatory.

When limited bowel preparation is used in combination with fecal tagging, and the images are evaluated with 3D reading, it is necessary to remove the tagged substances from the image beforehand. Otherwise polyps that are covered by fluid or stool remain invisible while stool might be read as a polyp or cancer. The removal of tagged material is done by a procedure usually known as electronic cleansing (Zalis et al. 2004; Franaszek 2006).

Colorectal cancer can present as an obstructing mass or as a polypoid or flat lesion. Sessile polyps are recognized as focal elevations of the colonic wall. Some polyps have another morphology: pedunculated or flat. Flat lesions are more difficult to identify than sessile or pedunculated polyps as flat lesions concern slight elevations or (less frequently) depressions of the colonic surface. Rarely flat lesions do not have an elevated or depressed morphology and are in plane with the colonic mucosa. These latter lesions cannot be identified at CT colonography and are often even hard to identify at colonoscopy without specific measures (e.g., dye spray facilitating identification of a disturbance of the normal colonic surface pattern by a flat lesion).

Differentiation between polyp and untagged stool is done primarily by evaluating the internal structure of the lesion: polyps have a homogeneous morphology while stool is heterogeneous and can have air inside the lesion. In tagged examinations the main discriminating factor is the contrast between tagged material and colorectal cancer and polyps. Helpful but a less reliable feature is the lack of change of relative position of a potential lesion between the two scans. This feature is indicative of a polyp, although bowel segments are mobile and especially pedunculated polyps can change position. The opposite may occur as well, as sticky stool can be adherent to the colonic wall without being influenced by the effect of gravity.

Computer-aided detection has been introduced in CT colonography. Based on shape features and internal characteristics colorectal cancer and polyps are identified. Computer-aided detection schemes have been designed for application in situations where extensive bowel preparation has been applied, as well as for tagged examinations (Summers et al. 2005a, 2005b). For tagged examinations usually electronic cleansing is used before the computer-aided detection scheme is used.

16.2.3 CT Colonography Performance

CT colonography can identify colorectal cancer and polyps. However, adenomatous polyps – precursors of colorectal cancer – cannot be differentiated from other polypoid lesions at CT colonography (e.g., hyperplastic polyps). Polyp size (diameter) is for this reason an important criterion for the differentiation between types of polyps. Large polyps other than adenomas are rare. Malignancy in adenomatous polyps is present in over 10% of polyps with a diameter ≥10 mm and in approximately 1% of the polyps <10 mm. Polyps 6–9 mm and especially polyps ≥10 mm are therefore considered relevant lesions. Many lesions <6 mm are not adenomas and thereby in adenomatous polyps <6 mm the chance of malignancy is approximately 0.1%. Therefore, small polyps can be disregarded irrespective of histopathology.

CT colonography should have a good performance for the detection of colorectal cancer and for polyps with a diameter ≥10 mm. Polyps in the intermediate size range 6–9 mm cannot be neglected although relevance is less than for larger polyps. As CT colonography will be used to select patients for colonoscopy, the test characteristics (i.e., sensitivity, specificity and predictive values) *per patient* are of primary importance. This is because patients will be selected for colonoscopy based on the presence of at least one relevant lesion and therefore the number of lesions is less important. Colonoscopy will be performed for polyp removal by biopsy with subsequent histopathology of the lesion. In colorectal cancer biopsy is performed for histopathology. The per-polyp test characteristics are, for this reason, less relevant than the per-patient characteristics.

16.2.3.1 Detection of Colorectal Cancer and Polyps

In three systematic reviews of the literature CT colonography has been shown to have good test characteristics for the findings important at colorectal cancer screening: detection of participants with colorectal cancer and large (often adenomatous) polyps (diameter ≥10 mm) (Sosna et al. 2003; Halligan et al. 2005; Mulhall et al. 2005). These systematic reviews primarily concern studies in symptomatic populations. For colorectal cancer

the sensitivity is high, namely 95.9%, and specificity is > 99%. For larger polyps (diameter ≥ 10 mm) sensitivity is 85%–92.5% and specificity 95%–97.4%. For polyps ≥ 6 mm the per-patient sensitivity is reported as 70%, 84% and 86.4%, with a specificity of 86.1% and 93%.

At the moment of writing (May, 2006) three multi-center studies have been published concerning larger series with participants with average risk or increased risk (Pickhardt et al. 2003; Cotton et al. 2004; Rockey et al. 2005). The largest series (1233 participants) concerns a study in an average risk population aged 50 years or older (Pickhardt et al. 2003). In this study in a screening population a state of the art CT colonography technique was used leading to a sensitivity of CT colonography for screening participants with one or more adenomatous polyps ≥ 10 mm of 94% and a specificity of 96%. The other studies report inferior results, with differences in several study characteristics such as CT colonography technique, use of tagging, evaluation method and reader experience. Disease spectrum with differences in polyp number, polyp size and polyp morphology will also influence results. For example, the presence of primarily large lesions in a large number of participants will lead to more favorable results while on the other hand flat lesions can be more difficult to detect than polypoid and pedunculated lesions (van Gelder et al. 2004b).

More research in larger screening populations is necessary to determine the test characteristics of CT colonography, the cost-effectiveness of CT colonography as a screening technique and the effect on mortality.

Initial studies on computer-aided detection in small numbers are promising: approximately 80%–90% per-polyp sensitivity for polyps ≥ 10 mm and a limited number of false positives (Summers et al. 2005a). These results were confirmed in the first study with a larger number of individuals (Summers et al. 2005b). This concerned a study population of 792 screening participants originating from the CT colonography screening study of 1233 participants described before (Pickhardt et al. 2003). The per-polyp and per-patient sensitivity of computer-assisted detection for adenomas were good: both 89.3% with 2.1 false positive per patient.

16.2.3.2 Extracolonic Findings

Apart from colorectal lesions, also extracolonic findings may be present. The frequency and relevance will depend on the population studied (Gluecker et al. 2003; Pickhardt et al. 2003). In populations with symptoms of colorectal cancer the chance of extracolonic findings will be highest. In a recent systematic review of the literature extracolonic findings were observed in almost 40% of individuals with symptoms of colorectal cancer (Xiong et al. 2005). In one-quarter of the patients these concerned relevant findings, although many were already known prior to the CT colonography examination. The prevalence of new, relevant findings was relatively low.

In a screening setting the number of extracolonic findings most likely will be lower than in symptomatic individuals. In the previously cited CT colonography study with 1233 asymptomatic people being screened a finding of potentially high clinical importance was found in 56 persons (4.5%) (Pickhardt et al. 2003). Unsuspected extracolonic cancer was in the end proven in only five persons (0.4%). It is noteworthy that more extracolonic cancers ($n = 5$) than colon cancers ($n = 2$) were detected in this study. Two patients underwent successful repair of unsuspected abdominal aortic aneurysms. A higher number of extracolonic findings of moderate clinical importance were found, including nephrolithiasis in 98 patients (7.9%) and gallstones in 69 patients (5.6%). The proportions of patients that required follow-up for extracolonic and intracolonic findings (polyps of 10 mm and larger) were approximately similar: 4.5% and 7.5%, respectively. These facts emphasize that extracolonic information resulting from CT colonography screening will have considerable consequences.

The frequency of extracolonic findings depends also on the dose level of the CT colonography examination, as will be discussed later.

The encouraging results make CT colonography a potential valuable screening method for colorectal cancer. However, while further studies are undertaken to more extensively study CT colonography as a screening method, an important drawback of CT should be considered. The use of ionizing radiation – with the risk of induction of cancer and genetic damage – has to be weighed against the potential benefits of screening with CT colonography.

16.2.4 Possibilities for Dose Reduction in CT Colonography

The choice of CT colonography scan parameters has a direct effect on radiation exposure. First an overview is given on the factors influencing radiation dose and image quality at CT colonography. This is followed by a discussion on the possibilities of the adjustment of the dose to the posture of the patient and dose modulation, possibilities for noise reduction by smoothing of the raw data and by the use of noise reduction filters, a recent survey on the CT colonography scan parameters that are used by different groups, a section on experimental studies in dose reduction using simulation methods and phantoms, and finally the results of some clinical studies using reduced radiation dose CT protocols.

16.2.4.1 Scan Parameters and CT Colonography

CT colonography scan parameters were initially based on clinical abdominal CT protocols, and later on were adjusted to lower dose settings. This lowering of the dose was possible because essential differences exist between the two examinations with regard to the kind of details that have to be visualized. In clinical abdominal CT subtle contrasts between the different soft tissues are important that may be obscured when the images are too noisy. Therefore, a relatively high dose is required in order to reduce the noise. In CT colonography examinations, on the other hand, the large difference in attenuation between bowel wall and the intraluminal air leads to a much higher contrast, which remains visible in much noisier images. This made it possible to reduce the radiation exposure.

It is obvious that the introduction of tagging in CT colonography examinations which has taken place recently will necessitate a higher dose than that required for examinations where the colon is perfectly clean, at least when one requires that a high percentage of the polyps immersed in the tagged material are detected as well. After all, in this last situation the contrast between polyps and surroundings may be considerably reduced. More on this topic in Section 16.2.4.3.

16.2.4.2 Factors Influencing CT Radiation Dose

The effective dose of a CT examination is a measure of the radiation risk associated with the examination. It depends in the first place on the amount of radiation used in the examination, which is directly related to the effective mAs level: the tube current (in mA) times the rotation time (in s) divided by the pitch, and the tube voltage (kV) of the examination. It also depends on the construction of the CT scanner (geometry, amount of filtration of the X-ray beam, presence or absence of a shaped filter), the number of detector arrays and the collimation, as discussed hereafter.

Reduction of radiation exposure at CT can be achieved in several ways. The most simple approach is to reduce the effective mAs level – by reducing the tube current or the rotation time or by increasing the pitch – which leads to a proportional decrease in radiation dose. The choice of the tube voltage is also an important factor. A tube voltage of 120 kV is generally used, although the use of higher tube voltages (140 kV), or lower ones (80 or 100 kV), can be considered in specific situations. The choice of the tube voltage has a marked effect on the effective dose: compared with the 120 kV situation, the use of 140 kV leads to an increase in effective dose by a factor in the order of 1.3–1.6, the use of 100 kV to a reduction in dose by a factor 1.5–1.7, and the use of 80 kV even to reduction in the order of a factor 3–4. All these figures depend somewhat on the type of CT scanner used in the examination. The reduction of radiation dose leads to a reduction of the radiation used in the imaging process, and therefore to an increase in noise and a decrease in image quality (see Sect. 16.2.4.3).

The introduction of multidetector-row scanners initially produced a slight increase in effective dose, because of a reduced efficiency of the use of ionizing radiation compared with single-slice scanners, due to the penumbra effect. This is especially the case in four-slice scanners, for which typical increases of 10%–30% in effective dose have been reported for the same protocols (Kalender 2005). For scanners with more detector arrays this effect is of less importance (Kulama 2004; Kalender 2005). Another source of dose inefficiency is the fact that in spiral CT an additional layer of tissue is irradiated adjacent to the volume to be depicted, because the reconstruction of the first and last slices requires data beyond the boundaries of this volume (Prokop 2005; Tzedakis

et al. 2005). This effect of z-overscanning is most pronounced for CT scanners with a large beam collimation, notably in 64-slice CT scanners, where the total beam width can be up to 40 mm.

In the near future the introduction of CT scanners with more detector rows, for example 256 or 512, can be expected in clinical practice. At the time of writing a prototype 256-slice CT scanner is being evaluated (Mori et al. 2005, 2006). With these scanners the loss of dose efficiency due to the penumbra effect will be low (Mori et al. 2004). The above-mentioned loss of dose efficiency due to z-overscanning, however, will be substantial, at least when these scanners are operated in the spiral mode. At present these scanners are operated for a number of applications in the axial mode, where z-overscanning is not present. However, for CT colonography the z-coverage of 100 mm, which is available in this mode at present (Mori et al. 2005), will not be sufficient.

16.2.4.3 Image Quality of CT Colonography: Noise, Contrast, Sharpness

The image quality of a CT colonography examination is determined by noise, contrast and sharpness.

16.2.4.3.1 Image Quality of CT Colonography: Noise

The noise in a CT colonography examination is primarily dependent on the amount of radiation, or the number and energy of the photons, used in the CT scan. As discussed in Section 16.2.4.2, the number of photons depends on the effective mAs setting and the kV of the scan. Reducing the effective mAs level by a factor 4 will double the noise in the CT images.

At a lower tube voltage fewer photons are produced, and these photons will have less penetrating power due to their decreased energy. Therefore, the noise will increase with decreasing kV. However, the detrimental effect of an increase in noise is counteracted by an increase in contrast, as discussed below. An increase in kV leads to the opposite effect.

The number of photons that reach the detectors of the CT scanner is the decisive factor for the noise level in CT colonography images; therefore, it is clear that, other things being equal, the size of the patient is a very important factor as well, and the noise level may become extremely high in scans of very obese persons. This point is addressed in Section 16.2.4.4.

16.2.4.3.2 Image Quality of CT Colonography: Contrast

The important contrast in a CT colonography examination is the contrast between the lesions in the colon wall and their surroundings. In a perfectly cleansed colon the lumen is filled with air, but when limited bowel preparation is used in combination with oral tagging, the lesions may be immersed in tagged material (Fig. 16.2.1). In this situation the contrast may be reduced considerably; in the example shown in Figure 16.2.1 by a factor of nearly 3.

This reduction of contrast will impair the visibility of these polyps when the lowest mAs values are used. Consider, for example, the polyp in Figure 6.2.1 with a CT number of 30 HU, surrounded by tagged material with a CT number of 400 HU. When we compare this situation with the same polyp surrounded by air (–1000 HU), the mAs value has to be increased by a factor of nearly 8 ($1030^2/370^2$) to obtain the same image quality. This example stresses the importance of using a bowel preparation scheme that produces tagging with sufficient contrast.

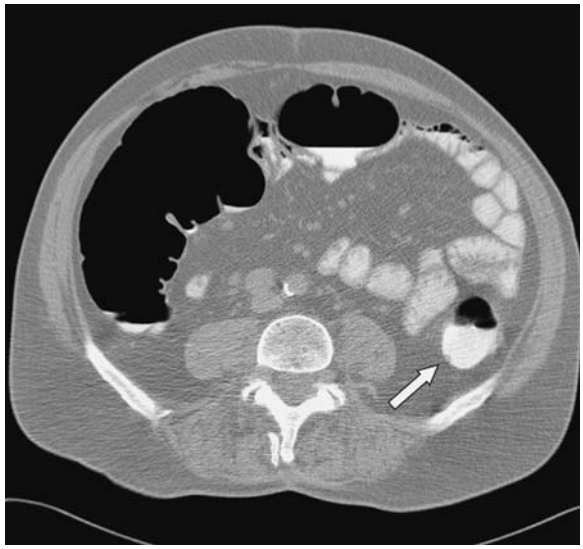

Fig. 16.2.1. Example of a polyp (*arrow*) shown by CT colonography (level –100, window 1200) submerged in tagged fluid. The CT value of soft tissue is in the order of 30 HU; in the tagged fluid the CT value is in the order of 400 HU. Therefore, the contrast is only 370 HU, considerably less than when the polyp is surrounded by air or carbon dioxide. In that case the contrast is 1030 HU, or nearly a factor of 3 higher

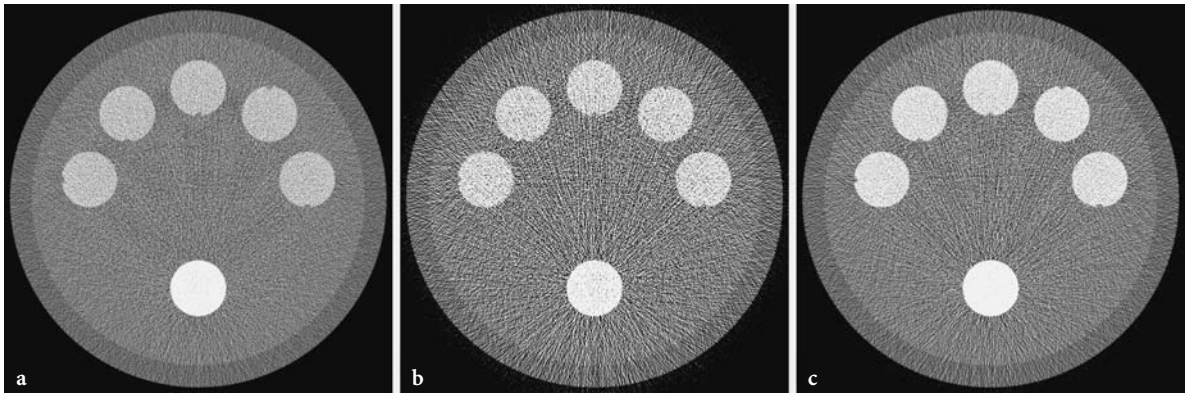

Fig. 16.2.2a–c. Simulated CT images (level 0, window 1600) of a mathematical phantom mimicking an abdominal cross-section (diameter 34 cm) containing five cross-sections of the colon, each one containing a 6-mm polyp, and a stylized vertebra in the lower part of the image. The colon is filled with iodine-tagged water. The simulation on the *left* (**a**) was made with 120 kV, 25 mAs; in the *middle* (**b**) with 80 kV, 25 mAs; on the *right* (**c**) with 80 kV, 75 mAs. The slice thickness for all images is 2.5 mm. This simulation shows the effect of reduction of tube voltage from 120 to 80 kV on the contrast and the noise level. The dose of the simulated CT scan on the *right* (**c**) is slightly lower than that of the simulated CT scan on the *left* (**a**), yet the signal-to-noise ratio (and the visibility of the polyps) is better

When tagging is used the contrast between a lesion and its surrounding will depend on the tube voltage that is used in the CT colonography examination. For lower tube voltages, the contrast between tissue and the materials with high atomic numbers that are used in the tagging, such as iodine ($Z = 53$) and barium ($Z = 56$), will increase. This phenomenon counteracts the increase in noise that also occurs at lower tube voltages. Thus for the same dose, a reduction in kV may give a better contrast-to-noise ratio (Fig. 16.2.2). This potential for dose reduction by using lower tube voltages needs further investigation.

16.2.4.3.3 Image Quality of CT Colonography: Sharpness

Irrespectively of whether a primary 3D or a primary 2D reading method is used (Sect. 16.2.2.3), it is clear that optimal visualization of the lesions in 3D is of utmost importance. This optimal visualization is achieved when the images that are used have an isotropic resolution, i.e., the *same* resolution in all directions, and preferentially, of course, the same *high* resolution in all directions. This was not the case in the early years of CT colonography. The in-plane resolution for the CT colonography images, by which we mean the full width at half maximum (FWHM) of the point spread function (PSF), is customary in the order of 1 mm or slightly less, depending on the scanner mode and the kernel used in the reconstruction, whereas in the early years values of the FWHM of the PSF in the longitudinal direction (equivalent to the slice thickness) of 5 or 3 mm were used, due to limitations of the CT scanners at that time. With the widespread use of multi-slice CT scanners the slice thickness has dropped, and reconstructions can be made now of sub-millimeter slices. An important point is that the noise in the images increases with the reciprocal of the square root of the slice thickness. This can be counteracted by reconstructing (somewhat noisy) images with a thin slice thickness, so that an isotropic resolution is obtained, and by viewing multiplanar reconstruction (MPR) images with a somewhat increased thickness in the viewing direction, where the lack of sharpness matters least. Also for 3D viewing isotropic resolution is advantageous.

16.2.4.4 Dose Adjustment to Posture; Dose Modulation

Until recently nearly always the same CT protocols were applied to all patients and care was taken that a good image quality was obtained in (almost) all these patients. Although this is well understandable from a pragmatic point of view, this may lead to more than necessary radiation exposure in slim or average posture individuals. Moreover in very obese patients the CT settings might be insufficient for an adequate diagnostic quality because of the very high

noise level. A more individualized protocol prevents this problem (Wilting et al. 2001). Use of posture-linked CT scan protocols (e.g., slim, average, obese) is a simple approach and selection of the technique factors can be based on visual impression of the posture of the patient as well as measurement of the girth (van Gelder et al. 2004b). In a study where the circumference of the waist was measured in 50 consecutive persons undergoing CT colonography, it was shown that a simple relationship exists between the waist circumference and the mean standard deviation (SD) of the noise at the colon surface (Fig. 16.2.3) (Venema et al. 2002). This relationship could be used to adjust the mAs level to the size of the patient in order to obtain a more uniform image quality.

More recently, automatic mAs selection based on measurements of the body size has become available, as has dose modulation. In this last option the tube current is modulated during the rotation of the X-ray tube, reducing the tube current in areas where the patient is relatively transparent for the X-rays, while retaining higher mA values, for instance in lateral views of the pelvis, in order to reduce the noise. In this way a substantial dose reduction can be obtained, while retaining (or even improving) the image quality. Readers are referred to Chapter 6 for more information on tube modulation.

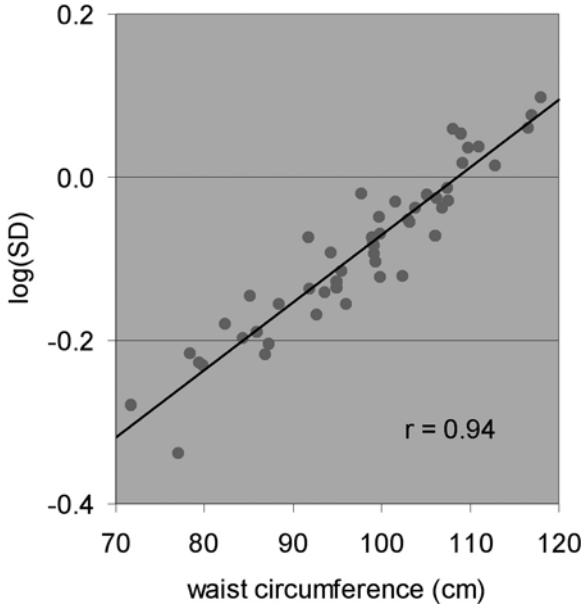

Fig. 16.2.3. For 50 consecutive persons undergoing CT colonography, the waist circumference was measured, and the mean standard deviation (*SD*) at the colon surface. The waist circumference is on the *horizontal axis*, the logarithm of the SD on the *vertical axis*. The level of the SD is taken to be arbitrary. Higher SD values correspond with a lower image quality. The logarithm of the SD is approximately linearly related to the waist circumference. At 120 cm waist circumference the mean SD is 2.6 times higher than at 70 cm

16.2.4.5 Noise Reduction by Smoothing of the Raw Data

The effectiveness of noise reduction by tube current modulation (see above) is caused by the fact that the noise in the measurements (*the raw data*) in the direction of the largest dimension of a cross-section contributes disproportionately to the noise in the reconstructed images. Therefore, an increase of the tube current for these measurements and a decrease of the tube current for measurements where the patient shows less attenuation is a very effective method to reduce the noise, for the same or even a reduced effective dose.

Another way to reduce the noise in the measurements where the X-ray beam is highly attenuated is to apply slight smoothing to these measurements. As these measurements usually make up only a small fraction of the total raw data set, this smoothing leads only to a minimal reduction of the sharpness of the images, while the noise can be reduced substantially (Hsieh 1998; Kachelriess et al. 2001; La Rivière 2005). In a study in which multi-slice CT scans were made of the pelvis of 50 patients with rectal or bladder cancer, the image quality improved considerably by use of this technique (Baum et al. 2003). Unfortunately this raw data smoothing technique is not available on all CT scanners.

16.2.4.6 Noise Reduction Filters

All other things being the same, the lowering of the dose of a CT examination inevitably does lead to an increase in the noise of the images, irrespectively of whether the dose reduction is obtained by reducing the mAs setting or the tube voltage. This noise can be reduced by different filtering procedures, and a number of studies have been executed to determine the effectiveness of such procedures.

Noise reduction can be obtained by linear and non-linear procedures. When linear procedures are used, the noise is reduced by smoothing, but the edges in the image, that may have clinical significance, are smoothed as well. Therefore, non-linear proce-

dures have been the most popular ones, as these procedures attempt to leave the relevant features of the images intact, while reducing the noise level.

Non-linear noise reduction filters were assessed in low-dose CT of the abdomen in a general setting, and not in the context of a CT colonography study (Kalra et al. 2003, 2004). In the original and the processed images the noise was measured, and the subjective image quality was assessed in observer studies. Although the noise was decreased in the processed images, it appeared that in some cases slight artifacts were present, and that the conspicuity of the lesions was compromised. The authors note that the procedure might be more successful in high-contrast settings, such as present in CT colonography. Another non-linear filter was recently tested in CT images of the abdomen and pelvis (Rizzo et al. 2005). Again the noise was reduced, and in this case the conspicuity of the lesions was not affected. It is doubtful, however, whether the image quality was improved, which of course is the ultimate goal of the application of these filters.

It thus appears that the effectiveness of the application of noise reduction filters for the improvement of image quality of 2D CT images has not yet been shown convincingly. We now consider the situation of 3D visualization, in which it has been shown that the use of filters is advantageous (van Gelder et al. 2004a). Apparently, the influence of noise is more detrimental in 3D viewing than it is in 2D viewing, especially for the very low (simulated) dose settings that were used in this study. In this case Gaussian (linear) filtering was applied.

Non-linear filtering techniques were applied in a CT colonography study in which 115 patients were examined at 10 mAs and presumably 120 kV (Cohnen et al. 2004; Vogt et al. 2004). They concluded that with this technique the sensitivity and specificity for the detection of polyps 5 mm or greater in size were excellent (94% and 84%, respectively).

16.2.4.7 Survey of CT Colonography Scan Parameters

For CT colonography different scan protocols have been used leading to a wide variation in dose. In 2006 a paper was published reporting on the spectrum of scan parameters based on an international literature search (literature 1996–2004) and a survey (2004) (Jensch et al. 2006). In this paper also an estimate was made of the associated risks for cancer induction. Effective radiation doses resulting from these different scan protocols were calculated by means of the ImPACT CT Patient Dosimetry Calculator (Jones and Shrimpton 1991). The relative accuracy of these figures is in the order of 10%–20%. As the effective dose values were determined using a mathematical androgynous phantom, these are mean values for men and women.

This inventory showed that the median effective dose in 2004 for a CT colonography examination was 5.1 mSv (range 1.2–11.7 mSv) per position (see Table 16.2.1). Most institutions (93%) scanned in both supine and prone positions, and for these institutions the median effective dose was 10.2 mSv for two positions. All institutions except one used a tube voltage of 120 kV. The median mAs value was 67 mAs (range 20–200 mAs), median collimation was 2.5 mm (range 0.75–5 mm). In concordance with the so-called linear non threshold model, a complete CT colonography examination with an effective dose of 10.2 mSv applied to a population aged 50 may result in a risk in the order of 1 fatal cancer in 4000 individuals (ICRP 1991). A recent study indicates that this estimate probably is too low; more on this in the discussion (Brenner and Georgsson 2005). A radiation-induced cancer may become manifest only after a long latent period, possibly tens of years. When individuals are to be examined more than once the risk will increase proportionally.

Table 16.2.1. Results of an international questionnaire on radiation exposure at CT colonography (Jensch et al. 2006)

	Number of simultaneously acquired slices				
	All	1	4	8	16
Number of institutions	28	1	18	4	5
Effective dose (mSv)	5.1 (1.2–11.7)	2.6	5.1 (1.2–11.7)	6.7 (2.7–9.9)	3.3 (2.6–5.8)
Effective tube charge (mAs)	66.8 (20–200)	70	65.3 (20–200)	83.6 (40–114)	55 (34–100)
Collimation per slice (mm)	2.5 (0.75–5.0)	5	2.5 (1.0–3.0)	1.9 (1.25–2.5)	1.1 (0.75–2.5)

When comparing the CT settings to the earlier used settings in these institutions published in the literature (1996 until 2004), a significant decrease in tube current and collimation ($P=0.006$, $P<0.0001$, respectively) was observed while the proportion of institutions that used a multislice scanner increased ($P<0.0001$) (Jensch et al. 2006). The effective dose had remained constant ($P=0.76$).

16.2.4.8 Experimental Studies in Dose Reduction: Simulation

Experimental dose reduction studies have demonstrated that dose reduction is possible beyond the median radiation exposure used in 2004. The mAs setting is the major factor influencing radiation exposure at fixed spatial resolution settings as long as the tube voltage is fixed at 120 kV.

Initially, tube current reduction from 100 mAs to 30 mAs was shown to be possible without a detrimental effect on polyp detection (van Gelder et al. 2002). This study concerned 50 individuals examined with 100 mAs CT colonography where 50- and 30-mAs CT colonographic examinations were simulated with controlled addition of noise to raw transmission measurements. It was demonstrated that, although image quality decreased, sensitivity and specificity were not affected. A further experimental study showed that dose reduction might be possible beyond the present-day lowest CT settings (van Gelder et al. 2004a). In CT colonography, examinations of 15 patients at 100 mAs were simulated to 25, 6.3, 1.6, and 0.4 mAs with controlled addition of noise to raw transmission measurements, cor-

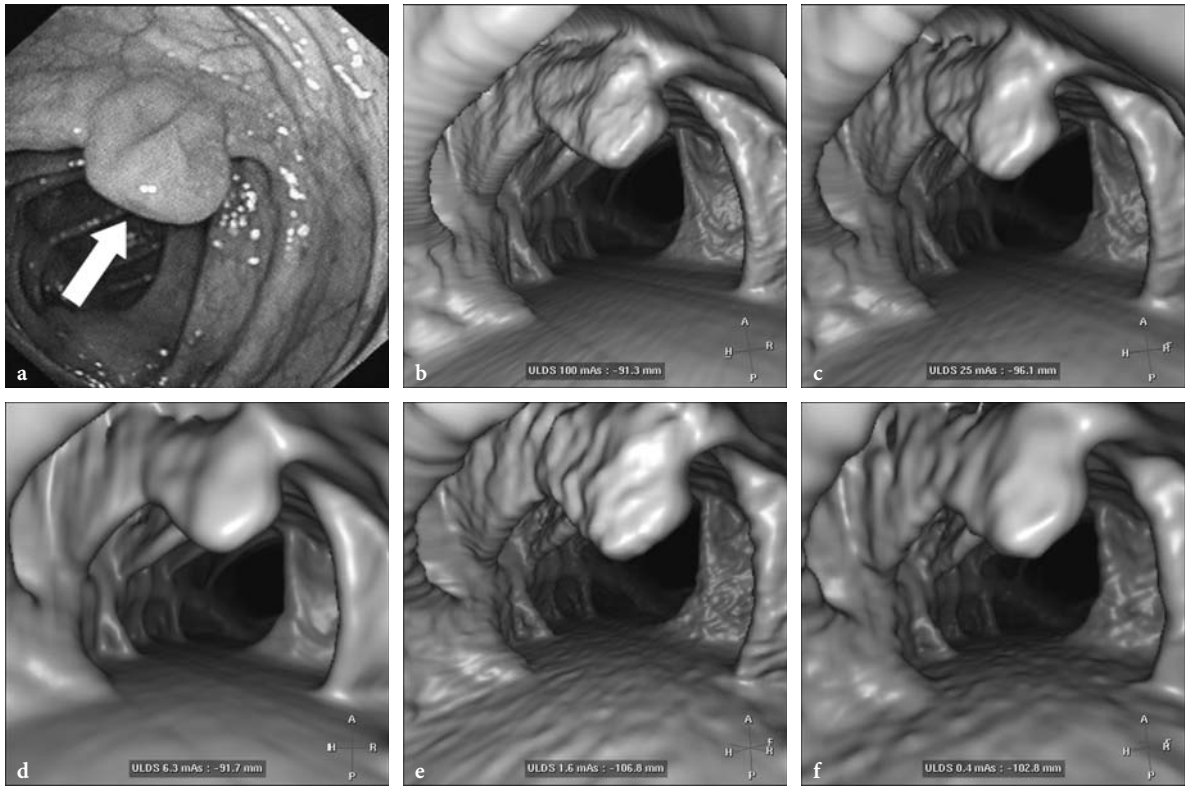

Fig. 16.2.4a–f. Images of a 15-mm polyp in a 60-year-old male patient at colonoscopy and at CT colonography with five doses. In the *top row*: **a** colonoscopic image shows 15-mm polyp in the ascending colon (*arrow*). **b** CT colonographic image obtained at 100 mAs. **c** CT colonographic image simulated at 25 mAs. In the *bottom row*: **d** CT colonographic image simulated at 6.3 mAs. **e** CT colonographic image simulated at 1.6 mAs. **f** CT colonographic image simulated at 0.4 mAs. Although the image quality decreases, polyp visibility is unimpaired. (Permission for reprint provided by the RSNA; van Gelder et al. (2004) CT colonography: feasibility of substantial dose reduction – comparison of medium to very low doses in identical patients. Radiology 232:611–620)

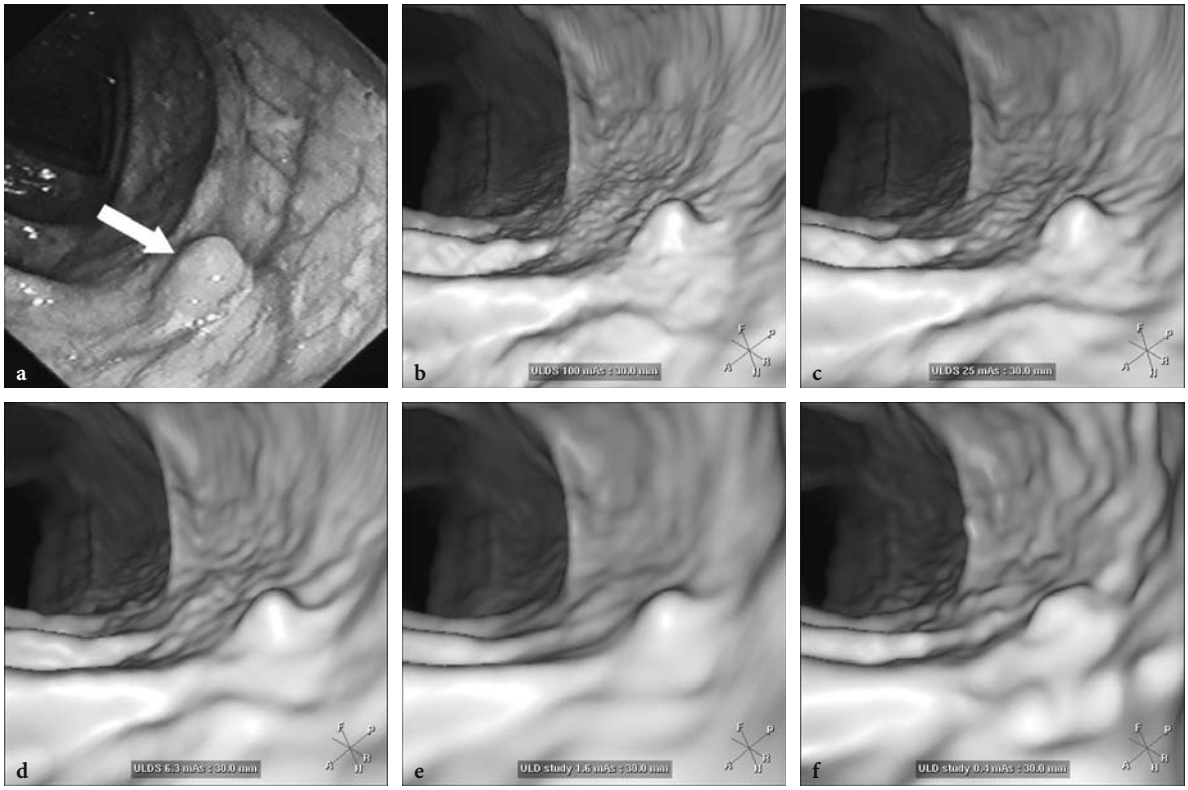

Fig. 16.2.5a–f. Images of a 5-mm polyp in a 57-year-old male patient at colonoscopy and at CT colonography with five doses. In the *top row*: **a** colonoscopic image shows 5-mm polyp (*arrow*) in the transverse colon. **b** CT colonographic image obtained at 100 mAs. **c** CT colonographic image at simulated 25 mAs. In the *bottom row*: **d** CT colonographic image simulated at 6.3 mAs. **e** CT colonographic image simulated at 1.6 mAs. **f** CT colonographic image simulated at 0.4 mAs. The image quality decreases and polyp visibility is affected at the lowest doses as a result of increased image noise and smoothing. (Permission for reprint provided by the RSNA; VAN GELDER et al. (2004) CT colonography: feasibility of substantial dose reduction–comparison of medium to very low doses in identical patients. Radiology 232:611–620)

responding to an effective dose of 3, 0.8, 0.2, and 0.05 mSv for two positions. For the lowest three simulations a Gaussian kernel was used to reduce the noise, which was mandatory at the lowest dose settings for the primary 3D visualization that was used in this study. Detection of polyps ≥5 mm was undisturbed to 1.6 mAs (0.2 mSv for two positions) (Figs. 16.2.4, 16.2.5).

The same simulation method was used in a study on the effect of the use of low mAs values on computer-assisted detection (DE VRIES et al. 2005). In all, 20 CT colonography examinations after extensive bowel preparation, made with 120 kV and 25 to 100 mAs (on average 70 mAs, with the mAs value dependent on waist circumference), were used. These patients had at least one colonoscopically proven polyp larger than 5 mm. Simulated ultra low dose scans were made at 6.3 mAs. The computer-assisted detection algorithm was identical for both dose levels, but the system was trained on data of the corresponding dose level only. Computer-assisted detection on the simulated ultra low dose data was feasible at the cost of only a slight increase in the number of false positives or a small drop in sensitivity as compared to the normal dose. At a sensitivity of 90% a median number of six false positives was detected at the normal dose and nine false positives at ultra low dose. When the operating point of the algorithm was moved to obtain six false positives at the ultra low dose setting the sensitivity dropped to 87%.

16.2.4.9 Experimental Dose Reduction Studies: Phantoms and Specimens

Phantom and specimen studies have been performed to study optimal CT settings including tube

current. A study of a colectomy specimen with 177 polyps demonstrated that tube current (50, 100 and 150 mA; effective dose 1.4–10.0 mSv per position, also depending on pitch and collimation) had no effect on polyp detection except for polyps < 5 mm (Taylor et al. 2003). A study using an anthropomorphic colon phantom showed that in the range of 10–140 mAs (effective dose for one position 0.7–11.6 mSv), tube current had no effect on the detection of polyps ≥ 8 mm irrespective of slice thickness and detector collimation studied (Wessling et al. 2003). Depiction of smaller polyps (6 and 2 mm) was less, but results improved with a collimation of 1 mm instead of 2.5 mm, and was only slightly influenced by the reduction in tube current.

A study with a borosilicate colon phantom containing 140 polyps (size 5–12 mm), which was scanned at a large range of mAs values (5–308 mAs) and a collimation of 1.25, 2.5 and 5 mm, showed that all polyps could be identified, except for 5 of the presumably 35 polyps of 5 mm in the 5-mAs scan with a collimation of 1.25 mm (Johnson et al. 2004).

A number of other phantom studies have been published (Laghi et al. 2003; Sundaram et al. 2003; Luz et al. 2004) that provide approximately comparable findings on the influence of dose on polyp visibility. Most studies agree on the fact that the use of thinner collimation helps in the visualization, especially for smaller polyps. Also noticeable is that polyp visibility appears to be better in the longitudinal than in the transverse direction of the colon (Johnson et al. 2004; Luz et al. 2004).

Unfortunately all these phantom studies provide data that are difficult to generalize, because of differences in methodology, and differences in basic scanning conditions such as the size and shape of the container in which the phantoms were scanned.

16.2.4.10 Clinical Decreased Radiation Dose Studies

Several clinical studies have reported on the use of low-dose scanning. In an initial study with extensive bowel preparation, 105 patients were studied using 120 kV, 50 mAs (effective dose for two positions 5.0 mSv for men and 7.8 mSv for women) (Macari et al. 2002) using 4 × 1 mm section collimation. Per-polyp sensitivity for polyps > 10 mm was 93% (13/14), for 6–9 mm polyps it was 70%. Another study reported on 27 patients using supine and prone 10-mAs CT colonography (effective dose for two positions 1.7 mSv for men and 2.3 mSv for women) (Iannaccone et al. 2003). In this study all colorectal cancers (9/9) and all polyps ≥ 6 mm (6/6) were detected. Recently, studies have reported on low-dose CT colonography in children (Anupindi et al. 2005; Capunay et al. 2005).

In a series of 137 patients with extensive bowel cleansing CT colonography was performed at 120 kV, 10 mAs (supine position only; effective doses 0.7 mSv for men and 1.2 mSv for women), 1.25 mm slice width; non-linear Gaussian filters were used for noise reduction (Cohnen et al. 2004). Combined 2D MPR and 3D endoluminal views were used. CT colonography detected 23 (82%) of 28 polyps ≥ 5 mm: 11 (78.6%) of 14 large polyps (> 10 mm), 12 (85.7%) of 14 medium polyps (9.9–5 mm). On a patient-by-patient basis, overall sensitivity was 70.3% and specificity 80.8%. These results are in the range of previous studies using higher tube current settings.

With the introduction of limited bowel preparation with tagging, the contrast between polyp and bowel content is reduced in case the polyp is surrounded by the tagged material instead of air. This impairs the visibility of these polyps when the lowest mAs settings are used, as discussed above (Sect. 16.2.4.3).

The use of limited bowel preparation and tagging (diatrizoate meglumine and diatrizoate sodium) at low dose (140 kV, 10 mAs; effective dose for two positions 1.8 mSv for men and 2.4 mSv for women) has been studied in 203 patients (Iannaccone et al. 2004). Using 3 mm slice thickness with primary 2D reading, computed tomographic colonography (CTC) had an average sensitivity of 95.5% for the identification of colorectal polyps ≥ 8 mm. The per-patient average sensitivity for all polyps was high: 89.9% and average specificity of 92.2% and for lesions ≥ 10 mm sensitivity and specificity were 100%. This study shows that good results are achievable with low- dose scanning in limited bowel prepped CTC examinations.

The fact that the results of this low-dose study are quite good, notwithstanding the problems pointed out earlier (Sect. 16.2.4.3.2), may have several explanations. In the first place it appears from the studies quoted earlier that, in the cleansed situation, virtually all polyps are seen, even at very low effective dose levels so that the polyps remain visible even if the image quality is somewhat more deteriorated. Secondly, only part of the polyps is surrounded by tagged material, so that an eventual reduced visibility for these polyps will lead to a much lower overall

reduction in visibility. The use of both supine and prone positions further increases the likelihood that a lesion in at least one position will not be covered by tagged material.

16.2.5 Discussion

The need to reduce the radiation dose of CT colonography examinations, especially when used in a screening setting, is dictated by the possible detrimental effects of X-rays on the human body. Unfortunately there is still controversy on the magnitude of the risks involved, and it is not very probable that these controversies will soon be resolved. Still, reduction of dose remains important; however, this must not be at the expense of the effectiveness of CT colonography as a screening tool. An adjunct of the reduction of radiation dose will be that the visualization of extracolonic findings will be affected. These issues will be discussed in this section. Most important is the effect on the detection of colorectal cancer and polyps, not only by human observers, but also by algorithms that are used in computer-assisted detection schemes.

16.2.5.1 Detection of Colorectal Cancer and Polyps

Both experimental and clinical studies (see above) have shown that radiation exposure can be reduced substantially without detrimental effect on the detection of colorectal cancer and polyps. We first discuss the situation of extensive bowel preparation. Present protocols often use settings of approximately 50 mAs at 120 kV (Jensch et al. 2006). Reduction seems to be possible to approximately 10 mAs, which is the lowest mAs setting for a number of CT scanners at present. Experimental studies have demonstrated the feasibility of CT colonography with even much lower radiation exposure. With simulated ultra low dose CT colonography detection of larger polyps (≥10 mm) was unimpaired at settings of 0.4–1.6 mAs, corresponding to effective doses of 0.05–0.2 mSv for two positions (van Gelder et al. 2004a). However, these settings are an order of magnitude lower than what can be realized with present-day scanners, and it is doubtful whether these extreme, low mAs settings will become available in the near future. When these low mAs settings eventually do become available, attempts should be made to determine whether the above-mentioned promising results of experimental ultra low radiation CT colonography can be reproduced in a clinical setting.

A substantial lower dose *can* be obtained with present-day scanners by using a lower tube voltage. Most CT scanners nowadays have a lowest setting of 80 kV, and, in comparison with the tube voltage that is customarily used of 120 kV, the choice of this lower tube voltage results in a dose reduction by a factor 3 or 4 (see Sect. 16.2.4.2). Again, the performance of ultra low dose CT achieved with this low tube voltage in combination with a low mAs setting should be verified in clinical practice.

The situation is more complicated when we consider CT colonography without extensive bowel preparation. In general one should realize that the possibilities of ultra low dose CT in the situation of limited bowel preparation and fecal tagging may be limited, because of the reduced contrast of the polyps relative to their surroundings (see Sect. 16.2.4.3.2). Therefore, it is important that a bowel preparation scheme is used that produces tagging with sufficient contrast. The choice of a lower tube voltage than the customary setting of 120 kV could be advantageous for CT colonography examinations with limited bowel preparation and fecal tagging. In these examinations one might choose a tube voltage of 80 kV (or 90 kV), as at these lower tube voltages the contrast-to-noise ratio for polyps embedded in material of higher atomic numbers, such as the tagging agents iodine and barium, may be increased. The magnitude of this effect will also depend on the size of the patient. As mentioned earlier, even in a situation of limited bowel preparation not all polyps will be covered by tagging material, and it is conceivable that one should be prepared to accept a slightly decreased visibility of these polyps, as long as the overall performance is not impaired to a significant degree. Clearly, further study is needed with respect to this point.

The use of thinner collimation (slice thickness less than 1 mm), which has become available with the newest generation of multi-slice CT-scanners, is advantageous for the visualization of polyps, especially of small polyps. Although the clinical relevance of detecting these small polyps (5 mm or less) is low, the increased spatial resolution might be important for detection of flat lesions. Whether sub-millimeter

collimation leads to substantial benefits for sensitivity and specificity has yet to be determined, but some beneficial effects can be expected. The truly isotropic resolution is advantageous for reconstructions and for computer-assisted detection because of the inherent 3D nature of the depicted volume of interest.

Of course, when the slice thickness is reduced without adjusting the other scan parameters, the noise in each slice will increase. This needs not be a problem, as this increase can be counteracted by viewing MPR images with a slightly increased thickness. For computer-assisted detection truly isotropic resolution will be advantageous as well, both for electronic cleansing of tagged examinations (see Sect. 16.2.2.3) and the detection of the polyps.

It is clear that all available means to obtain an optimal image quality for a given dose should be utilized. Thus, dose adaptation to the body size and/or dose modulation should be used, as the posture of a patient and the shape of their cross-section (e.g., of the pelvis) influence image noise to a large extent. By using these measures the differences in noise level in different parts of the patient, and between different patients, will be considerably reduced. Application of smoothing of the raw data (see Sect. 16.2.4.5) to reduce noise should be tried as well in low-dose CT colonography, when possible, as this is an effective means to reduce image noise, especially in eccentric cross-sections of the human body such as the pelvis. The value of the use of noise-reduction filters for CT colonography is still unclear with respect to its

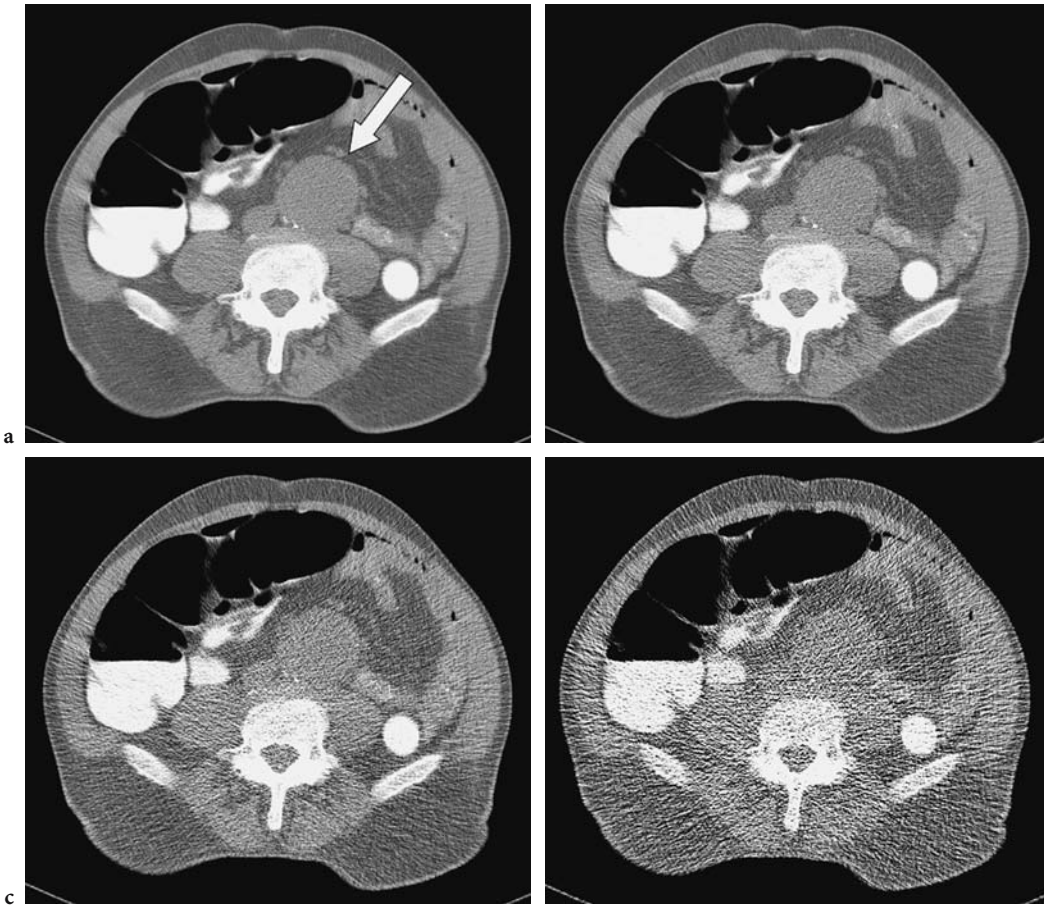

Fig. 16.2.6a–d. CT colonography in the supine position after extensive bowel preparation and tagging with iodine in a 76-year old man. **a** CT colonographic image obtained at 50 mAs; **b** CT colonographic image simulated at 25 mAs; **c** CT colonographic image simulated at 6.3 mAs; **d** CT colonographic image simulated at 1.6 mAs. The examination was performed for surveillance for colorectal cancer. As an incidental finding a 4.7-cm aneurysm of the distal abdominal aorta (*arrow*) was found, which was however already known prior to the examination. The aneurysm is still identifiable at the lowest dose

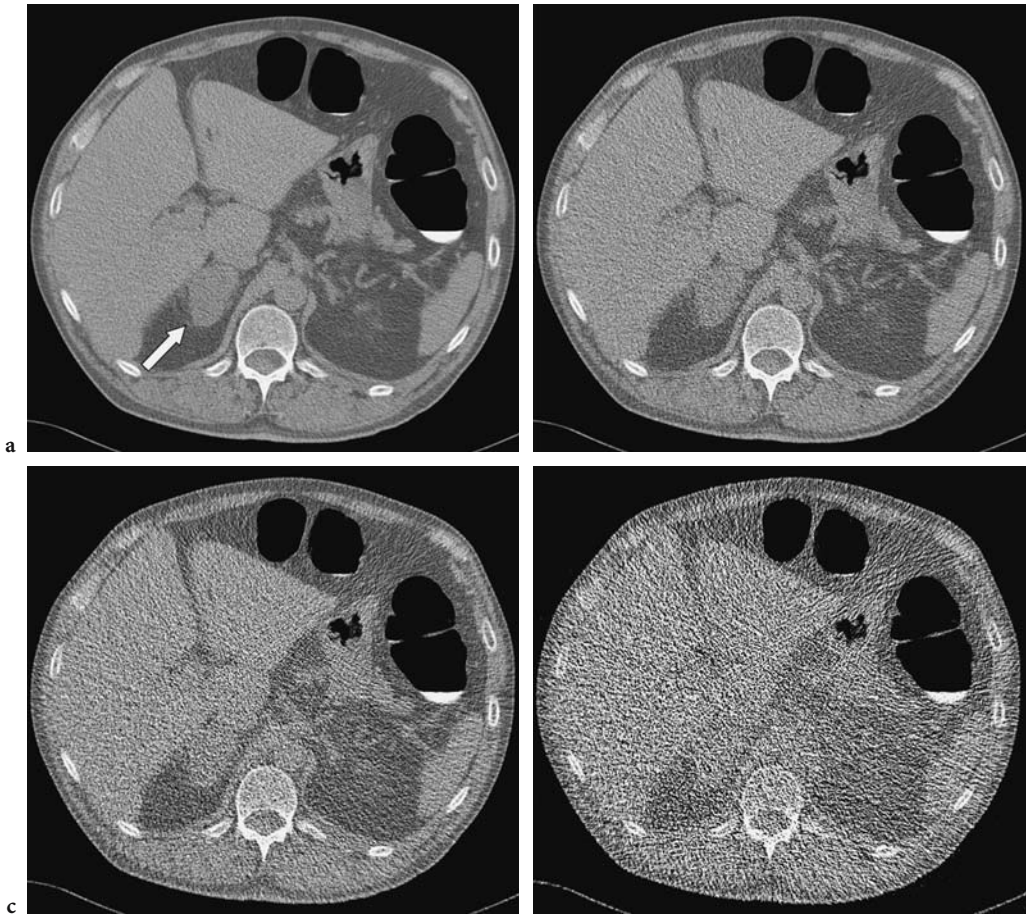

Fig. 16.2.7a–d. CT colonography in the supine position after extensive bowel preparation and tagging with iodine contrast medium in a 57-year old woman. **a** CT colonographic image obtained at 70 mAs; **b** CT colonographic image simulated at 25 mAs; **c** CT colonographic image simulated at 6.3 mAs; **d** CT colonographic image simulated at 1.6 mAs. The examination was performed for surveillance for colorectal cancer. As an incidental finding an enlarged right adrenal is visible (*arrow*) with CT features (size, density) suggestive of a metastasis. This finding was not known prior to the CT colonography and prompted further work up. The patient proved to have lung cancer with a metastasis in the right adrenal gland. The enlarged right adrenal is identifiable at 25 mAs and 6.3 mAs, but hardly identifiable at the lowest simulated dose of 1.6 mAs

potential to improve the image quality in 2D images. The use of noise reduction filters is important, however, for 3D visualization (see Sect. 16.2.4.6).

16.2.5.2 Extracolonic Findings

Extracolonic findings are relatively common at regular-dose CT colonography in symptomatic patients. Almost 40% of individuals with symptoms of colorectal cancer have extracolonic findings, although the prevalence of new, relevant findings is relatively low (Xiong et al. 2005). In a screening setting the number seems to be lower (Pickhardt et al. 2003).

Although some consider extracolonic findings a beneficial part of CT colonography – total body screening – this potentially is not the case. Many extracolonic findings are not relevant or are already known and some that may be relevant and new may concern untreatable disease (Figs. 16.2.6, 16.2.7). The anxiety of participants, additional diagnostic work up and possible treatment and use of resources are major disadvantages. Extracolonic findings may be an important factor determining whether CT colonography is a cost-effective screening method. Therefore, low radiation dose CT colonography may also be considered a boon in this respect as this will impair the detection of extra-colonic findings (Figs. 16.2.6, 16.2.7).

16.2.5.3 Risk Versus Benefit

The risks of a CT colonography examination (apart from rare complications such as perforation) are difficult to assess with certainty, as already mentioned in the introduction to this discussion. In a recent survey it was found that the effective dose of a CTC examination at present is in the order of 10 mSv, and that this corresponds with a risk of fatal cancer for a 50-year-old person in the order of 1 in 4000 (Jensch et al. 2006). This is in all probability an underestimate, as in a paper on the risks of screening with CT colonography a risk in the order of 1 in 700 was found for the risk of cancer (not *fatal* cancer), using a more involved, and probably more accurate, method (Brenner and Georgsson 2005). The risk for cancer mortality is of course considerably less than the risk for cancer itself, but this can explain only part of the discrepancy between these two risk estimates. More important than these differences is the fact that there is no direct statistically significant evidence for these risks, as these calculations are based on extrapolations from higher dose levels, and the estimates depend heavily on the assumptions that are made (Brenner and Georgsson 2005; Prokop 2005; Brenner and Sachs 2006; Friedl and Rühm 2006; Tubiana et al. 2006). Nevertheless, it is prudent to assume that exposure to the amount of radiation used in a CT colonography examination is accompanied by a small risk of induction of (fatal) cancer, and that this risk becomes smaller when the dose is reduced.

The benefit of CT colonography as a screening technique is not known yet. CT colonography has been shown to have potential as a screening technique (Pickhardt et al. 2003), although more studies are necessary to further study the performance of the technique and – with adequate performance – its cost-effectiveness (influenced amongst others by extracolonic findings) and effect on mortality. Low radiation dose CT colonography with tagging and an optimal dose–performance balance seems to be the optimal method for this research on the role of CT colonography in screening for colorectal cancer.

16.2.6 Conclusions

For CT colonography to be considered as a screening tool the benefit of its use must outweigh the risks/disadvantages. The benefit of CT colonography for reducing the mortality and morbidity of colorectal cancer has not been determined yet, although present data are encouraging. The risks and disadvantages include the possibility of the induction of cancer, as well as other factors such as false positives, extracolonic findings and costs. With regard to the induction of cancer, with the scan parameters used until now the risk seems to be relatively small, but cannot be completely neglected. Moreover, the risk will increase with the number of examinations performed. Although the frequency of screening for colon cancer with CT colonography most likely will be less than that for lung cancer or breast cancer, for instance, further reduction in radiation exposure associated with CT colonography is desirable. Apart from reducing the risk of cancer induction, reduction in radiation exposure also may be valuable for patient acceptance and adherence, for instance by reducing the fear of radiation exposure. Decreased radiation exposure will result in noisier images that at a certain level will preclude the evaluation of extracolonic findings. This might be an advantage when extracolonic findings might prove to be detrimental for cost-effective screening for colorectal cancer with CT colonography.

Low radiation dose CT colonography with acceptable to good sensitivity and specificity is feasible, even in combination with limited bowel preparation and tagging. Efforts should be made to further study the limits and pros and cons of low radiation dose CT colonography.

References

Anupindi S, Perumpillichira J, Israel EJ, Zalis ME, Jaramillo D (2005) Low-dose CT colonography in children: initial experience, technical feasibility, and utility. Pediatr Radiol 35:518–524

Baum U, Noemayr A, Reissig A et al (2003) Improvement of the image quality of msct of the pelvis with a raw data-based, multidimensional filter [in German]. Fortschr Röntgenstr 175:1572–1576

Brenner DJ, Georgsson MA (2005) Mass screening with CT colonography: should the radiation exposure be of concern? Gastroenterology 129:328–337

Brenner DJ, Sachs RK (2006) Estimating radiation-induced cancer risks at very low doses: rationale for using a linear no-threshold approach. Radiat Environ Biophys 44:253–256

Capunay CM, Carrascosa PM, Bou-Khair A, Castagnino N, Ninomiya I, Carrascosa JM (2005) Low radiation dose multislice CT colonography in children: experience after 100 studies. Eur J Radiol 56:398–402

Cohnen M, Vogt C, Beck A et al (2004) Feasibility of MDCT colonography in ultra-low-dose technique in the detection of colorectal lesions: comparison with high-resolution video colonoscopy. *AJR* Am J Roentgenol 183:1355–1359

Cotton PB, Durkalski VL, Pineau BC et al (2004) Computed tomographic colonography (virtual colonoscopy): a multicenter comparison with standard colonoscopy for detection of colorectal neoplasia. J Am Med Assoc 291:1713–1719

Franaszek M, Summers RM, Pickhardt PJ, Choi JR (2006) Hybrid segmentation of colon filled with air and opacified fluid for CT colonography. IEEE Trans Med Imag 25:358–368

Friedl AA, Rühm W (2006) LNT: a never-ending story. Radiat Environ Biophys 44:241–244

van Gelder RE, Venema HW, Serlie IWO et al (2002) CT colonography at different radiation dose levels: feasibility of dose reduction. Radiology 224:25–33

van Gelder RE, Venema HW, Florie J et al (2004a) CT colonography: feasibility of substantial dose reduction – comparison of medium to very low doses in identical patients. Radiology 232:611–620

van Gelder RE, Nio CY, Florie J et al (2004b) Computed tomographic colonography compared with colonoscopy in patients at increased risk for colorectal cancer. Gastroenterology 127:41–48

Gluecker TM, Johnson CD, Wilson LA et al (2003) Extracolonic findings at CT colonography: evaluation of prevalence and cost in a screening population. Gastroenterology 124:911–916

GLOBOSCAN (2002) Database. At http://www-dep.iarc.fr (accessed 1 May, 2006)

Halligan S, Altman DG, Taylor SA et al (2005) CT colonography in the detection of colorectal polyps and cancer: systematic review, meta-analysis, and proposed minimum data set for study level reporting. Radiology 237:893–904

Hsieh J (1998) Adaptive streak artifact reduction in computed tomography resulting from excessive x-ray photon noise. Med Phys 25:2139–2147

Iannaccone R, Laghi A, Catalano C, Mangiapane F, Piacentini F, Passariello R (2003) Feasibility of ultra-low-dose multislice CT colonography for the detection of colorectal lesions: preliminary experience. Eur Radiol 13:1297–1302

Iannaccone R, Laghi A, Catalano C et al (2004) Computed tomographic colonography without cathartic preparation for the detection of colorectal polyps. Gastroenterology 127:1300–1311

ICRP (1991) 1990 Recommendations of the International Commission on Radiological Protection. International Commission on Radiological Protection publication no. 60. In: Smith H, ed. Annals of the ICRP 21 (no. 1–3). Oxford, England: Pergamon

Jensch S, van Gelder RE, Venema HW et al (2006) Effective radiation doses in CT colonography: results of an inventory among research institutions. Eur Radiol 16:981–987

Johnson KT, Johnson CD, Anderson SM, Bruesewitz MR, McCollough CH (2004) CT colonography: determination of optimal CT technique using a novel colon phantom. Abdom Imag 29:173–176

Jones DG, Shrimpton PC (1991) Survey of CT practice in the UK: normalised organ doses for X–ray computed tomography calculated using Monte Carlo techniques. National Radiological Protection Board, Harwell. Available at: www.impactscan.org/ctdosimetry.htm

Kachelriess M, Watzke O, Kalender WA (2001) Generalized multi-dimensional adaptive filtering for conventional and spiral single-slice, multi-slice, and cone-beam CT. Med Phys 28:475–490

Kalender WA (2005) Computed tomography fundamentals, system technology, image quality, applications, 2nd edn (revised and enlarged). Publicis MCD, Munich

Kalra MK, Maher MM, Sahani DV et al (2003) Low-dose CT of the abdomen: evaluation of image improvement with use of noise reduction filters pilot study. Radiology 228:251–256

Kalra MK, Maher MM, Blake MA et al (2004) Detection and characterization of lesions on low-radiation-dose abdominal CT images postprocessed with noise reduction filters. Radiology 232:791–797

Kulama E (2004) Scanning protocols for multislice CT scanners. Br J Radiol 77:S2–S9

La Rivière PJ (2005) Penalized-likelihood sinogram smoothing for low-dose CT. Med Phys 32:1676–1683

Laghi A, Iannaccone R, Mangiapane F, Piacentini F, Iori S, Passariello R (2003) Experimental colonic phantom for the evaluation of the optimal scanning technique for CT colonography using a multidetector spiral CT equipment. Eur Radiol 13:459–466

Laks S, Macari M, Bini EJ (2004) Positional change in colon polyps at CT colonography. Radiology 231:761–766

Lefere PA, Gryspeerdt SS, Dewyspelaere J, Baekelandt M, Van Holsbeeck BG (2002) Dietary fecal tagging as a cleansing method before CT colonography: initial results polyp detection and patient acceptance. Radiology 224:393–403

Luz O, Schafer J, Dammann F, Vonthein R, Heuschmid M, Claussen CD (2004) Evaluation of different 16-row CT colonography protocols using a porcine model. Rofo 176:1493–1500

Macari M, Bini EJ, Xue X et al (2002) Colorectal neoplasms: prospective comparison of thin-section low-dose multidetector row CT colonography and conventional colonoscopy for detection. Radiology 224:383–392

Mori S, Endo M, Tsunoo T et al (2004) Physical performance evaluation of a 256-slice CT-scanner for four-dimensional imaging. Med Phys 31:1348–1356

Mori S, Obata T, Kishimoto R et al (2005) Clinical potentials for dynamic contrast-enhanced hepatic volumetric cine imaging with the prototype 256-MDCT scanner. AJR Am J Roentgenol 185:253–256

Mori S, Endo M, Obata T, Tsunoo T, Susumu K, Tanada S (2006) Properties of the prototype 256-row (cone beam) CT scanner. Eur Radiol Mar 28; Eur Radiol 16:2100-2108

Mulhall BP, Veerappan GR, Jackson JL (2005) Meta-analysis: computed tomographic colonography. Ann Intern Med 142:635–650

Pickhardt PJ, Choi JR, Hwang I et al (2003) Computed tomographic virtual colonoscopy to screen for colorectal neoplasia in asymptomatic adults. N Engl J Med 349:2191–2200

Pignone M, Rich M, Teutsch SM, Berg AO, Lohr KN (2002) Screening for colorectal cancer in adults at average risk: a summary of the evidence for the U.S. Preventive Services Task Force. Ann Intern Med 137:132–141

Prokop M (2005) New challenges in MDCT. Eur Radiol 15: E35–E45

Rizzo SM, Kalra MK, Schmidt B et al (2005) CT images of abdomen and pelvis: effect of nonlinear three-dimensional optimized reconstruction algorithm on image quality and lesion characteristics. Radiology 237:309–315

Rockey DC, Paulson E, Niedzwiecki D et al (2005) Analysis of air contrast barium enema, computed tomographic colonography, and colonoscopy: prospective comparison. Lancet 365:305–311

Sosna J, Morrin MM, Kruskal JB, Lavin PT, Rosen MP, Raptopoulos V (2003) CT colonography of colorectal polyps: a meta analysis. AJR Am J Roentgenol 181:1593–1598

Summers RM, Frananzek M, Miller MT, Pickhardt PJ, Choi JR, Schindler WR (2005a) Computer-aided detection of polyps on oral contrast-enhanced CT colonography. AJR Am J Roentgenol 184:105–108

Summers RM, Yao J, Pickhardt PJ et al (2005b) Computed tomographic virtual colonoscopy computer-aided polyp detection in a screening population. Gastroenterology 129:1832–1844

Sundaram P, Beaulieu CF, Paik DS, Schraedley-Desmond P, Napel S (2003) CT colonography: does improved z resolution help computer-aided polyp detection? Med Phys 30:2663–2674

Taylor SA, Halligan S, Bartram CI et al (2003) Multi-detector row CT colonography: effect of collimation, pitch, and orientation on polyp detection in a human colectomy specimen. Radiology 229:109–118

Tubiana M, Aurengo A, Averbeck D, Masse R (2006) Recent reports on the effect of low doses of ionizing radiation and its dose-effect relationship. Radiat Environ Biophys 44:245–251

Tzedakis A, Damilakis J, Perisinakis K, Stratakis J, Gourtsoyiannis N (2005) The effect of z overscanning on patient effective dose from multidetector helical computed tomography examinations. Med Phys 32:1621–1629

Venema HW, van Gelder RE, Determann RM, Laméris J, Stoker J (2002) Determination of the technique factors for CT colonography: adjustment of mAs value to the size of the patient for constant image quality. Radiology 225: S584–S584

Vogt C, Cohnen M, Beck A, vom Dahl S, Aurich V, Modder U, Haussinger D (2004) Detection of colorectal polyps by multislice CT colonography with ultra-low-dose technique: comparison with high-resolution videocolonoscopy. Gastrointest Endosc 60:201–209

de Vries A, Schoonenberg GA, Venema HW, Grigorescu S, Peters J, Stoker J (2005) Feasibility of automated detection of colon polyps on simulated ultra low dose CTC datasets. Proceedings 91st Scientific Assembly and Annual Meeting Radiological Society of North America 2005; Oak Brook, USA

Wessling J, Fischbach R, Meier N et al (2003) CT colonography: protocol optimization with multi-detector row CT-study in an anthropomorphic colon phantom. Radiology 228:753–759

Wilting JE, Zwartkruis A, van Leeuwen MS, Timmer J, Zwartkruis AG, Feldberg M (2001) A rational approach to dose reduction in CT: individualized scan protocols. Eur Radiol 11:2627–2632

Xiong T, Richardson M, Woodroffe R, Halligan S, Morton D, Lilford RJ (2005) Incidental lesions found on CT colonography: their nature and frequency. Br J Radiol 78:22–29

Zalis ME, Perumpillichira J, Hahn PF (2004) Digital subtraction bowel cleansing for CT colonography using morphological and linear filtration methods. IEEE Trans Med Imag 23:1335–1343

Subject Index

List of Contributors

Hicham T. Abada, MD
Clinical Associate Professor
Department of Radiology
Vascular and Interventional Section
University of Iowa Hospitals and Clinics
200 Hawkins Drive, 3897 JPP
Iowa City, IA 52242
USA

Toufik Batch, MD
Hôpital Central
Service d'Imagerie Guilloz
CHU Nancy
29, av. du Mal de Lattre de Tassigny
54035 Nancy Cedex
France

Patrick Bellinck, MD
Department of Radiology
Heilig Hart Ziekenhuis
Mechelsetraat 24
2500 Lier
Belgium

Alain Blum, MD
Hôpital Central
Service d'Imagerie Guilloz
CHU Nancy
29, av. du Mal de Lattre de Tassigny
54035 Nancy Cedex
France

Nico Buls, MSc
AZ-VUB
Laarbeeklaan 101
1090 Brussels
Belgium

Kenneth H. Chadwick, PhD, Retired
3 Ellerbank
Cowan Head, Kendal
Cumbria LA8 9HX
UK

Emmanuel Coche, MD, PhD
Department of Medical Imaging
Cliniques Universitaires St. Luc
Avenue Hippocrate 10
1200 Brussels
Belgium

Bernard L. Cohen, MD
Department of Physics
University of Pittsburgh
201-B Old Engineering Hall
Pittsburgh, PA 15260
USA

J. de Mey, MD, PhD
Department of Radiology
AZ-VUB
Laarbeeklaan 101
1090 Brussels
Belgium

Gilles Ferquel,MD
Hôpital Central
Service d'Imagerie Guilloz
CHU Nancy
29, av. du Mal de Lattre de Tassigny
54035 Nancy Cedex
France

Pierre Alain Gevenois, MD, PhD
Professor of Radiology
Clinic of Chest Imaging
Department of Radiology
Hôpital Erasme
Université libre de Bruxelles
Route de Lennik 808
1070 Brussels
Belgium

Stephen Golding, MD
Radiology Research Group
Nuffield Department of Surgery
University of Oxford, MRI Centre
John Radcliffe Hospital
Oxford OX3 9DU
UK

Mannudeep K. Kalra, MD, DNB
Department of Radiology
Massachusetts General Hospital
55 Fruit Street
Boston, MA 02114
USA

Caroline Keyzer, MD
Department of Radiology
CHU of Charleroi
Boulevard Janson 92
6000 Charleroi
Belgium

Hendrik P. Leenhouts, PhD, Retired
FredBantinglaan 6
6721 BC Bennekom
The Netherlands

Thomas Ludig, MD
Hôpital Central
Service d'Imagerie Guilloz
CHU Nancy
29, av. du Mal de Lattre de Tassigny
54035 Nancy Cedex
France

Tom Mulkens, MD
Department of Radiology
Heilig Hart Ziekenhuis
Mechelsetraat 24
2500 Lier
Belgium

Hans-Dieter Nagel, PhD
Science and Technology Group
Philips Medical Systems
Roentgenstr. 24
22335 Hamburg
Germany

Alain Noël, MD
Unité de radiophysique médicale
CRAN UMR 7039 CNRS
Centre Alexis Vautrin
Av de Bourgogne
Vandoeuvre-les-Nancy 54511
France

Rajesh Patel, MD
Radiology Research Group
Nuffield Department of Surgery
University of Oxford, MRI Centre
John Radcliffe Hospital
Oxford OX3 9DU
UK

Jean-François Paul, MD
Radiology
Centre Chirurgical Marie Lannelongue
133 avenue de la Résistance
92350 Le Plessis-Robinson
France

Benoit Sauer, MD
Hôpital Central
Service d'Imagerie Guilloz
CHU Nancy
29, av. du Mal de Lattre de Tassigny
54035 Nancy Cedex
France

Rodrigo Salgado, MD
Department of Radiology
Universitair Ziekenhuis, Antwerpen
Wilrijkstraat 10
2650 Edegem–Antwerpen
Belgium

Georg Stamm, PhD
Medizinische Hochschule Hannover
Diagnostische Radiologie/AB Exp. Radiologie
Carl-Neuberg-Strasse 1
30625 Hannover
Germany

Jaap Stoker, MD
Professor of Radiology
Department of Radiology, Academic Medical Center
University of Amsterdam
P.O.Box 22700
1100 DE Amsterdam
The Netherlands

Denis Tack, MD, PhD
Clinic of Cardiac Imaging
Department of Radiology
Hôpital Erasme
Université libre de Bruxelles
Route de Lennik 808
1070 Brussels
Belgium

Thomas L. Toth, MD
General Electric Healthcare Technologies
3000 North Grandview Boulevard
Waukesha, WI 53188
USA

Henk W. Venema, PhD
Physicist
Departments of Radiology and Medical Physics
Academic Medical Center
P.O.Box 22700
1100 DE Amsterdam
The Netherlands

Peter Vock, MD
Department of Radiology
University Hospital Inselspital
3010 Bern
Switzerland

Rogier E. Van Gelder, MD
Resident in Radiology
Department of Radiology
Academic Medical Center
P.O.Box 22700
1100 DE Amsterdam
The Netherlands

Daniel Winninger,MD
Direction des ressources médico-techniques
CHU Nancy
av de Lattre de Tassigny
54000 Nancy
France

Rainer Wolf, MD
Department of Radiology
University Hospital Inselspital
3010 Bern
Switzerland